

รายงานการวิจัยฉบับสมบูรณ์

โครงการ การพัฒนาวัสดุโครงร่างกระดูกเทียมสำหรับงานด้านทันตกรรมและสัตวภิบาล

โดย ศาสตราจารย์พิชญ์ ศุภผล และคณะ

กันยายน 2555

สัญญาเลขที่ DBG5280015

รายงานการวิจัยฉบับสมบูรณ์

โครงการ การพัฒนาวัสดุโครงร่างกระดูกเทียมสำหรับงานด้านทันตกรรมและสัตวภิบาล

คณะผู้วิจัย **สังกัด**

1. ศาสตราจารย์พิชญ์ ศุภผล วิทยาลัยปิโตรเลียมและปิโตรเคมี จุฬาลงกรณ์มหาวิทยาลัย

2. ศาสตราจารย์ประสิทธิ์ ภวสันต์ ภาควิชากายวิภาค คณะทันตแพทยศาสตร์ จุฬาลงกรณ์มหาวิทยาลัย

3. ศาสตราจารย์มงคล เตชะกำพุ ภาควิชาสูติศาสตร์ เธนุเวชวิทยาและวิทยาการสืบพันธุ์ คณะสัตวแพทยศาสตร์ จุฬาลงกรณ์มหาวิทยาลัย

4. ผู้ช่วยศาสตราจารย์กัมปนาท สุนทรวิภาต ภาควิชาศัลยศาสตร์ คณะสัตวแพทยศาสตร์ จุฬาลงกรณ์มหาวิทยาลัย

5. ดร.เกศกัญญา สัพพะเลข ภาควิชาศัลยศาสตร์ คณะทันตแพทยศาสตร์ จุฬาลงกรณ์มหาวิทยาลัย

6. ผู้ช่วยศาสตราจารย์ธีรวัฒน์ ธาราศานิต ภาควิชาสูติศาสตร์ เธนุเวชวิทยาและวิทยาการสืบพันธุ์ คณะสัตวแพทยศาสตร์ จุฬาลงกรณ์มหาวิทยาลัย

สนับสนุนโดยสำนักงานกองทุนสนับสนุนการวิจัย

(ความเห็นในรายงานนี้เป็นของผู้วิจัย สกว. ไม่จำเป็นต้องเห็นด้วยเสมอไป)

Executive summary

Bone Tissue Engineering is an emerging interdisciplinary field that seeks to address the needs by applying the principles of biology and engineering to the development of viable substitutes that restore and maintain the function of human bone tissues. There are many approaches to bone tissue engineering, but all involve one or more of the following key ingredients: harvested cells, recombinant signaling molecules, and three-dimensional (3D) matrices. One popular approach involves seeding highly porous biodegradable matrices (or scaffolds), in the shape of the desired bone, with cells and signaling molecules (e.g., protein growth factors), then culturing and implanting the scaffolds into the defect to induce and direct the growth of new bone. The goal is for the cells to attach to the scaffold, multiply, differentiate (i.e., transform from a nonspecific or primitive state into cells exhibiting the bone-specific functions), and organize into normal, healthy bone as the scaffold degrades. The signaling molecules can be adhered to the scaffold or incorporated directly into the scaffold material.

Polymer-ceramic (Hydroxyapatite or Silica) composites may be extremely prospective bone substitute material mainly through evidence with its given biocompatibility towards bone and demonstrated continuity between living bone and the composites. The composites are implanted into rectangular bone defect created by operation at the load-bearing area in dog. The changes of surface strain at the composite implantation are measured at week after implantation when the compressive stress was applied in the direction of long axis in order to clarify the mechanical behaviors of composite living bone complex.

The expected results are that the polymer-ceramic composite living bone complex should have been proven to have sufficient flexibility. The strain pattern on the surface of composite implant should develop quite similar to that of natural cortical bone. These characteristics suggest that it achieves normal skeletal function in the points of biomechanical properties in vivo.

Abstract

Development of Bone Scaffolds for Applications in Dentistry and Animal Care

Prof.Pitt Supaphol, Prof.Pavasant, Prof.Mongkol Techakumphu,
Assist.Prof.Kumpanart Soontornvipart, Dr.Keskanya Subbalekha,
Assist.Prof.Theerawat Tharasanit

Keywords: Tissue engineering, Scaffold, Polycaprolactone, Hydroxyapatite, Mesenchymal stem cells

Recently, organ and tissue loss or failures resulting from an injury or other types of damage become a major human health problem. Tissue engineering has emerged as a promising alternative approach to treat the loss or malfunction of a tissue or organ without the limitations of current therapies. Tissue engineering is an interdisciplinary technology that combines materials engineering, cellular biology and genetic engineering into developing biological substitutes for defected or damaged tissues. One popular approach in bone tissue engineering to the development of viable substitutes that restore and maintain the function of human bone tissues involves seeding highly porous biodegradable scaffolds, in the shape of the desired bone, with cells and signaling molecules then culturing and implanting the scaffolds into the defect to induce and direct the growth of new bone. In this research work, not only the dentistry care is the main application of the scaffolds but also the animal care is the other application of them. Therefore the isolation techniques and differentiation potentials of canine mesenchymal stem cells derived from bone marrow and adipose tissue the specific markers for bone marrow derived MSCs have been compared. The cellular interaction of canine mesenchymal stem cells and polycaprolcatone/hydroxyapatite composite scaffold and the effect of canine mesenchymal stem cells combined with polycaprolcatone/hydroxyapatite(PCL/HA) composite scaffold on the healing of ulnar defects in dogs have been examined for *in vitro* and *in vivo* study, respectively. Mesenchymal stem cells (MSCs) have increasingly become an attractive aspect for tissue engineering. However, limitation of cell numbers at isolation and culture has restricted the clinical exploitations. Bone marrow contents were collected from 7 dogs and then submitted to 3 different MSC isolation techniques (direct plating, red blood cell lysis treatment and gradient density). The number of cells, expression of MSC markers and in vitro differentiation obtained

from each technique were examined. In conclusion, this study revealed that MSCs can be derived from bone marrow. The *in vitro* demonstrated a good biocompatibility between canine MSCs and PCL/HA scaffolds. Despite a promising result from an *in vitro* study, neither bone nor callus formation was observed in canine ulnar defects that implanted with PCL/HA and PCL/HA scaffolds. Defects in these two groups were healed with fibrovascular tissue which infiltrated through the pore of the scaffold.

บทคัดย่อ

ชื่อโครงการ : การพัฒนาวัสดุโครงร่างกระดูกเทียมสำหรับงานด้านทันตกรรมและสัตวภิบาล

ผู้ทำงานในโครงการ : ศ.ดร.พิชญ์ สุภผล, ศ.ดร.ประสิทธิ์ ภวสันต์, ศ.ดร.มงคล เตชะกำพุ,
ผศ.ดร.กัมปนาท สุนทรวิภาต, ดร.เกศกัญญา สัพพะเลข, ผศ.ดร.ธีรวัฒน์ ธาราศานิต

คำสำคัญ : วิศวกรรมเนื้อเยื่อ, โครงร่างเนื้อเยื่อเทียม, พอลิคาโพรแลคโตน, เซลล์ต้นกำเนิดมีเซนไคมอล

ในปัจจุบัน ปัญหาที่สำคัญอย่างหนึ่งของมนุษย์คือ การสูนย์เสียอวัยวะหรือเนื้อเยื่อของร่างกายของมนุษย์จากอุบัติเหตุ วิศวกรรมเนื้อเยื่อ คือ เทคโนโลยีแบบสหวิทยาการที่มีการบูรณนาการความรู้ด้านวิศวกรรม วิศวกรรมวัสดุ และชีววิทยา เพื่อพัฒนาทดแทน ซ่อมแซม หรือปรับปรุงการทำงานของเนื้อเยื่อหรืออวัยวะที่สูญเสียหรือบาดเจ็บ ซึ่งเป็นหนึ่งในวิธีการแก้ปัญหาที่เกิดขึ้น หนึ่งในกระบวนการที่สำคัญของวิศวกรรมเนื้อเยื่อ คือการพัฒนาวัสดุโครงร่างเนื้อเยื่อเทียมที่มีศักยภาพในการกระตุ้นการเกาะ การเพิ่มจำนวน และการสร้างเนื้อเยื่อกระดูก ในการทดลองที่เหมาะสม ถึงแม้ว่าเป้าหมายหลักของงานวิจัยนี้ คือการพัฒนาวัสดุโครงร่างกระดูกเทียมเพื่อสามารถนำไปใช้งานในด้านทันตกรรม อย่างไรก็ตาม การนำวัสดุโครงร่างกระดูกเทียมไปทดสอบในสัตว์ทดลอง(สุนัข) เพื่อใช้ในการรักษาสุนัขที่ต้องการการปลูกถ่ายเนื้อเยื่อกระดูกสามารถเป็นเป้าหมายรองในงานวิจัยนี้ได้อีกทางหนึ่งด้วย ดังนั้นในงานวิจัยนี้จึงได้มีการศึกษาการพัฒนาเซลล์ต้นกำเนิดที่ได้จากไขกระดูกและเนื้อเยื่อไขมัน และนำความรู้มาผสมผสาน เพื่อนำมาทดลองเพาะเลี้ยงกับวัสดุโครงร่างกระดูกเทียมที่ได้มีการพัฒนาขึ้นมาในสภาวะที่เหมาะสม และ ศึกษาความเป็นไปได้ในการใช้วัสุโครงร่างเทียมร่วมกับเซลล์ต้นกำเนิดจากการทดสอบในจานทดลองและทดลองกับสัตว์ทดลอง(สุนัข) จากการทดลองปลูกถ่ายเซลล์ต้นกำเนิดชนิดมีเซนไคมอลที่แยกได้จากไขกระดูกลงบนวัสดุโครงร่างเซลล์ซึ่งใส่อยู่ในตำแหน่งวิการของกระดูกอัลนา เพื่อศึกษาผลของการรักษาภาวะกระดูกต่อไม่ติดในสุนัข โดยทำการเก็บไขกระดูกในสุนัขจำนวน 7 ตัว ไขกระดูกของสุนัขแต่ละตัวนำมาแบ่งเพื่อคัดแยกเซลล์ต้นกำเนิดชนิดมีเซนไคมอลเป็น 3 วิธี ได้แก่ density gradient, RBC lysis buffer และ direct plating ทำการเพาะเลี้ยงในภาวะที่ควบคุมเดียวกันและ subculture ในวันที่ 7 เพื่อหาจำนวนเซลล์ทั้งหมดและเปอร์เซ็นต์เซลล์

ที่มีชีวิตที่ได้จากแต่ละวิธี การพิสูจน์คุณสมบัติของเซลล์ต้นกำเนิดชนิดมีเซนไคมอลทำได้โดยอาศัยการเกาะบนจานเพาะเลี้ยงพลาสติก การแสดงออกของโปรตีนบนผิวเซลล์และคุณสมบัติในการเปลี่ยนแปลงไปเป็นเซลล์ชนิดอื่น พบว่าเซลล์ต้นกำเนิดชนิดมีเซนไคมอลที่คัดแยกได้มีคุณสมบัติในการเปลี่ยนแปลงไปเป็นเซลล์กระดูก ปริมาณมีเซ็นไคมอลเสต็มเซลล์ที่รอดชีวิตภายในโครงร่างเซลล์พอลิคาโพรแลคโตนไฮดรอกซีอะพาไทต์มีความสำคัญเนื่องจากเซลล์ที่รอดชีวิตจะสามารถเพิ่มจำนวนและเปลี่ยนแปลงตัวเองไปเป็นเซลล์ที่มีความสามารถในการสร้างกระดูก ตัวอย่างโครงร่างเซลล์หลังการฉีดเซลล์ต้นกำเนิดไม่พบการเปลี่ยนแปลงใดๆที่รอยต่อของกระดูกอัลนากับวัสดุปลูกถ่ายทั้งทางด้านบนและด้านล่าง รวมทั้งไม่พบการสร้างแคลลัสที่บริเวณวิการของกระดูก เมื่อเปรียบเทียบผลการเอกซเรย์หลอดเลือดของขาหน้าบริเวณที่มีโครงร่างเซลล์ก่อนและหลังการฉีดเซลล์ต้นกำเนิดเข้าสู่โครงร่างเซลล์ พบแขนงของเส้นเลือดในบริเวณที่ตรงกับตำแหน่งที่ทำการใส่โครงร่างเซลล์และพบการแตกแขนงของเส้นเลือดในบริเวณที่ตรงกับตำแหน่งที่ทำการใส่โครงร่างเซลล์เพิ่มมากขึ้น

สัญญาเลขที่ DBG5280015

โครงการ: การพัฒนาวัสดุโครงร่างกระดูกเทียมสำหรับงานด้านทันตกรรมและสัตวภิบาล

รายงานการวิจัยฉบับสมบูรณ์ ของศาสตราจารย์พิชญ์ ศุภผล

==========

ชื่อหัวหน้าโครงการวิจัยผู้รับทุน : ศาสตราจารย์พิชญ์ ศุภผล

รายงานในช่วงตั้งแต่วันที่ 10 กันยายน 2552 ถึงวันที่ 9 กันยายน 2555

1. การดำเนินงาน ☑ **ได้ดำเนินงานตามแผนที่วางไว้ทุกประการ**

☐ **ได้ดำเนินงานล่าช้ากว่าแผนที่วางไว้**

☐ **ได้เปลี่ยนแผนงานที่วางไว้ดังนี้**

2. สรุปผลการดำเนินงาน

2.1 Hydroxyapatite/ovalbumin composite particles as model protein carriers for bone tissue engineering: I. Synthesis and characterization

Experimental procedures
1. Materials and material synthesis
The chemical reagents, e.g., nitric acid (HNO3, A.R. grade), phosphoric acid (H3PO4, A.R. grade), 2-amino-2-hydroxymethyl-propane-1,3-diol (tris-base, A.R. grade), and chicken egg white ovalbumin (OVA,grade II), were purchased from Sigma-Aldrich (USA). These were used without further purification. In the synthesis process, calcium oxide(CaO) was first synthesized from discarded egg shells [16]. Briefly, the egg shells were cleaned with distilled water at 80 °C and dried in vacuo. They were then calcined at 1000 °C in a Lindberg LBF799C oven, in two heating stages (i. 25 to 700 °C for 2 h to eliminate organic substances and ii. 700 to 1000 °C for another 2 h to eliminate CO2 to finally obtain CaO powder). Then, 2.5 g of the CaO powder was dissolved in 25 mL of 1 MHNO3 under gentle stirring at 70 °C for 3 h. Subsequently, 3.0 g of conc. H3PO4 (85 wt.-%) was added dropwise into the solution to adjust the Ca/P ratio to 1.67. The pH of the mixed solution was maintained at 2.0 and the whole system was continuously stirred at room temperature. Precisely 2.0 g of OVA was then added into
500 mL of the obtained solution under vigorous stirring for 1 h. Precipitation was achieved after 200 mL of 1, 1.5, or 2 M tris-base had been added into the solution to impart the buffering effect to the solution
at the pH of 7, 8, or 9, respectively. The mixture was vigorously stirred. The precipitates were filtered, washed several times with deionized water, and lyophilized for 48 h. The procedure was repeated to obtain the precipitates that did not contain OVA for comparative purposes.

2. Characterization

A Rigaku D/MAX 2000 X-ray diffractometer (XRD) was used to investigate the crystalline nature of the obtained powdery precipitates,using Cu Kα (1.54 Å) radiation over the 2θ range of 5–60° with 0.02° scanning step. The crystalline phase of the powder was identified with JCPDS standard (9-432). A Nicolet NEXUS 670 Fourier-transform infrared spectroscope (FT-IR), operating at a resolution of 4 cm−1 over a wavenumber range of 4000 to 400 cm−1, was used to examine the chemical functionalities of the powdery products. A Perkin-Elmer TGA-7 thermogravimetric analyzer (TGA) was used to investigate the thermal degradation behavior of the powder at a heating rate of 10 °C·min−1 in air. Some of the powdery products, after having been subjected to the thermal treatment in TGA, were reanalyzed by XRD. Microscopic morphology of the powder was observed by a JEOL JEM-2100 transmission electron microscope (TEM), operating at 200 kV. Surface morphology of the obtained products was investigated by a JEOL JSM-5410LV scanning electron microscope (SEM). Particle size distribution (PSD) of the powder was collected by a Mastersizer 2000 Malvern particle size analyzer (PSA). The powder was dispersed ultrasonically in water during the measurement. The pore characteristics and the Bruaauer–Emmett–Teller (BET) specific surface area of the obtained powdery products were determined based on the physisorption of N2 at a temperature of 77 K using a Quantachrome AS-1 autosorb-1 instrument. Lastly,the ζ potentials of the powdery products were measured by electrophoresis, using a Zeta-meter 3.0+ analytical system. Briefly, a suspension of 100 mg of the HAp or the HAp/OVA particles in 20 mL of deionized water was filled in an electrophoresis cell. Once energized, the powder was aroused to move towards one of the electrodes.The unit automatically converted the electrophoretic mobility of the particles into the ζ values using the Smoluchowski equation.

3. Results and discussion

Because of the similarity of the results obtained for the HAp particles that had been obtained at pHs 7, 8, and 9, only those of the particles that had been obtained at pH 9 were extensively reported and discussed. As shown in Fig. 1, all of the crystalline peaks as observed in the XRD patterns of the precipitated powdery products that had been obtained, both in the absence and the presence of OVA, at pH 9 could be assigned to those of HAp [i.e., the hexagonal P63/m space group with the lattice constants of a=b=0.9418 nm and c=0.6884 nm (cf. JCPDS No. 09-0432)]. The average crystallite sizes, as estimated from the width of the (002) reflection peaks using the Scherrer's equation [17], were around 17.3–20.9 nm and 16.8–19.8 nm for the HAp and the HAp–OVA particles, respectively (see Table 1). In particular, the average value of the crystallite size decreased with an increase in the pH used during the precipitation process. As the pH increased, more tris-base molecules, in their free form, would be available to nucleate the HAp crystalline entities (cf. the pKa of tris-base=8.06), hence the observed decrease in the crystallite size. At the same pH, the presence of OVA resulted in a slight reduction in the average value of the size of the obtained HAp crystals. The presence of OVA could retard the influx of Ca^{2+} and PO_4^{3-} into the growth face, as OVA would adsorb readily onto the HAp crystallites during the crystal growth.

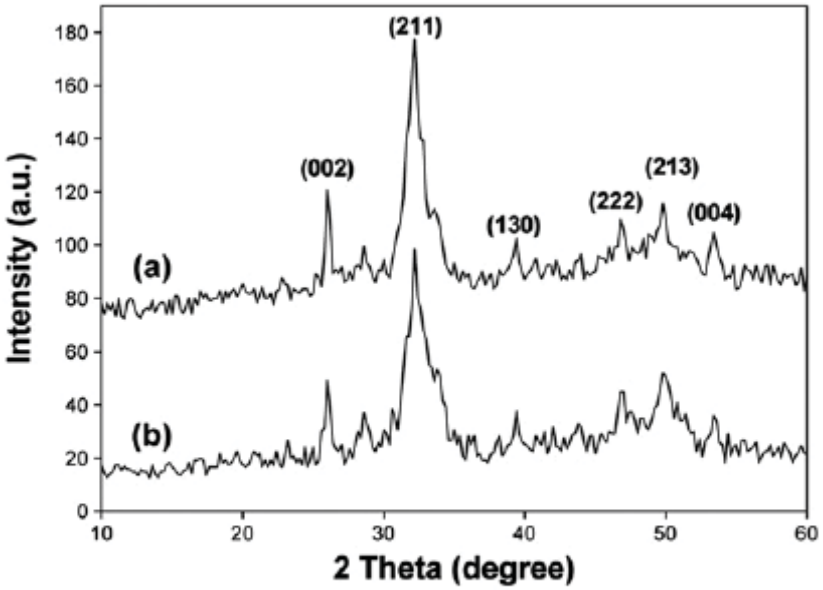


Fig. 1. XRD patterns of (a) pure HAp and (b) HAp–OVA particles that had been obtained at pH 9.

The FT-IR spectra of the HAp and the HAp–OVA particles that had been obtained at pH 9 as well as that of the as-received OVA in its dry state are shown in Fig. 2. For the HAp particles, the adsorption bands centering at 3569 and 1630 cm−1 could be assigned to the OH stretching and the OH vibration of the apatitic group [18]. The bands centering at 1035, 601, and 563 cm−1 should correspond to PO4 3− ions in the HAp structure. However, the band centering at 1384 cm−1 was thought to belong to the carbonate functionality, which might be a result of the contamination from the reaction with CO2 in the atmosphere[11]. As for the as-received OVA, the characteristic absorption peaks at 3299, 1652, 1539, and 1457 cm−1 could be ascribed to the N–H stretching, the carbonyl, the C–N, and the C–H stretching vibrations, respectively [19]. For the HAp–OVA particles, the presence of the absorption bands centering at 1654 and 1539 cm−1 confirmed the presence of OVA within the obtained HAp particles.

The HAp and the HAp–OVA particles that had been obtained at pH 9 were evaluated thermogravimetrically and the results are shown in Fig. 3a. For the HAp particles, three main stages in the loss of their mass were observed. The first stage, over the temperature range of 60–160 °C, should correspond to the loss of adsorbed water. The second stage, with the onset temperature at about 240 °C, should relate to the loss of tris-base from the HAp structure. The last stage at the onset temperature of about 740 °C was thought to relate to the loss of the remaining organic residues within the HAp structure. As for the HAp–OVA particles, all of the three stages were evident. However, the presence of an additional step at the onset temperature of about 330 °C should correspond to the loss of the incorporated OVA. After the TGA analysis, these HAp and the HAp–OVA particles were reanalyzed by XRD (Fig. 3b). Apparently, the crystalline peaks associated with HAp became much sharper (cf. Fig. 1), indicating further crystallization of HAp during the thermal treatment. Additionally, crystalline peaks that belong to other calcium-based chemical species such as CaO and carbonate apatite became much more evident (cf. Fig. 1).This suggests that parts of the imperfectly-formed HAp entities may undergo thermal decomposition or solid state chemical reaction at high temperatures. Notwithstanding, both

the FT-IR and the TGA results confirmed the presence of OVA within the structure of the obtained HAp–OVA particles.

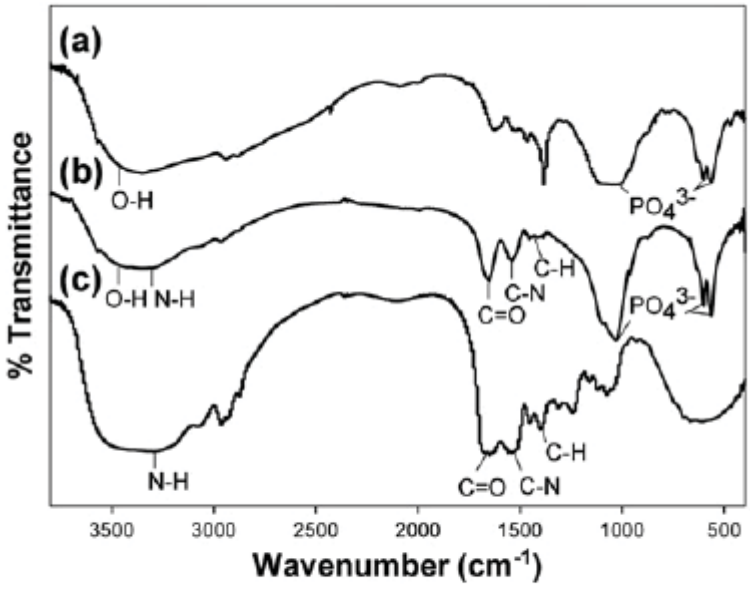


Fig. 2. FT-IR spectra of (a) pure HAp and (b) HAp–OVA particles that had been obtained at pH 9 as well as that of (c) as-received OVA in its dry state.

Table 1
Textural parameters of pure HAp and HAp–OVA particles that had been obtained at different pH conditions.

Type of HAp	Crystallite size (nm) ($n=3$)	Average size of primary particles (nm) ($n=3$)	Pore diameter (nm) ($n=2$)	BET Specific surface area ($m^2\,g^{-1}$) ($n=2$)	Pore volume ($cm^3 \cdot g^{-1}$) ($n=2$)	ζ potential (mV) ($n=10$)
HAp (pH 7)	20.9 ± 0.06	59.3 ± 0.25	8.9 ± 0.2	17.2 ± 0.7	0.079 ± 0.006	−31.6 ± 2.4
HAp (pH 8)	19.2 ± 0.08	57.7 ± 0.43	8.3 ± 0.1	16.1 ± 0.5	0.053 ± 0.003	−32.7 ± 1.6
HAp (pH 9)	17.3 ± 0.11	56.5 ± 0.28	8.1 ± 0.2	15.6 ± 0.3	0.029 ± 0.004	−36.9 ± 2.5
HAp–OVA (pH 7)	19.8 ± 0.09	50.4 ± 0.27	15.5 ± 0.4	21.3 ± 0.3	0.089 ± 0.002	−19.7 ± 1.3
HAp–OVA (pH 8)	18.4 ± 0.05	49.1 ± 0.41	14.4 ± 0.2	19.5 ± 0.4	0.058 ± 0.002	−20.2 ± 0.7
HAp–OVA (pH 9)	16.8 ± 0.06	46.2 ± 0.36	14.1 ± 0.3	16.6 ± 0.7	0.036 ± 0.003	−23.2 ± 1.1

The particle size distribution (PSD) curves of the HAp and the HAp–OVA particles that had been obtained at pH 9 are shown in Fig. 4. Based on the PSD results, the HAp and the HAp–OVA primary particles had the average sizes of around 56–59 nm and 46–50 nm, respectively. The average sizes of the HAp and the HAp–OVA primary particles that had been obtained at all pH levels investigated were measured and summarized in Table 1. Apparently, the presence of OVA resulted in significant reduction in the sizes of the obtained HAp primary particles. On the contrary, the average value of the primary particle size decreased slightly with an increase in the pH used during the precipitation process. Both of these should be a result of the increase in the number of nucleation sites, i.e., owing to the presence of OVA in the former and the more availability of the free tris-base molecules in the latter [20]. As for the effect of tris-base, the greater the amount of tris-base used, the greater the number of nuclei, hence the observed reduction in the sizes of the HAp primary particles.

The nano-crystalline structure of the HAp and the HAp–OVA particles that had been obtained at pH 9 was investigated by TEM (see Fig. 5). The rod-like morphology of the obtained HAp crystals, both in the absence and in the presence of OVA, was evident. The TEM results were consistent with the results obtained from the particle size analyzer (i.e., the PSD results), which revealed that the primary particles were in the nanometer range and the presence of OVA led to the reduction in the size of the primary particles. Despite the nano-crystalline nature of the individual primary particles, representative SEM images of the precipitated HAp and HAp–OVA powder that had been obtained at pH 9 (see Fig. 6) revealed the existence of large agglomerates and the extent of the agglomeration was accented by the presence of OVA. In addition, the HAp particles obtained at higher pH values existed as larger aggregates, owing possibly to the increase in the overall crystallization rate (viz. due to the increase in the nucleation rate, earlier mentioned) [21]. Notwithstanding, the existence of such agglomerates could easily be a result of lyophilization during the drying of the powdery products.

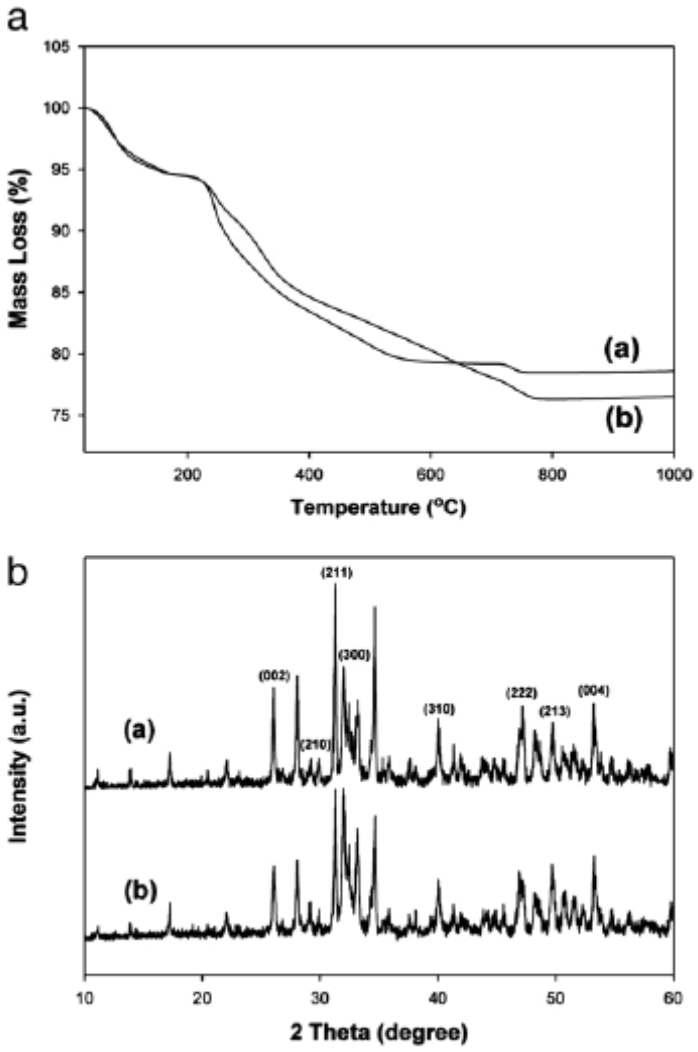


Fig. 3. (a) TGA curves of (a) pure HAp and (b) HAp–OVA particles that had been obtained at pH 9 and (b) XRD patterns of these particles after having been subjected to the TGA analysis.

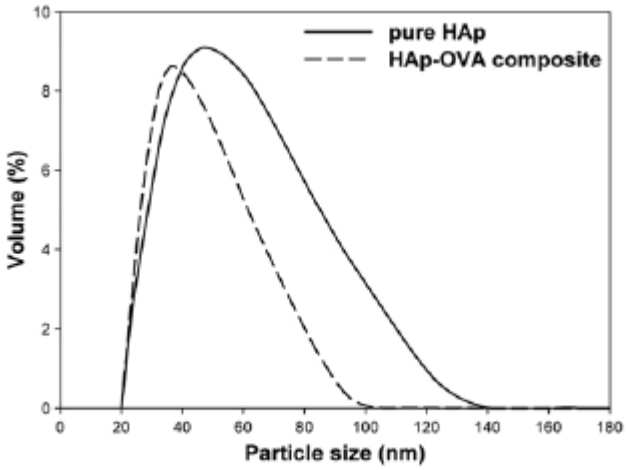


Fig. 4. PSD curves of pure HAp and HAp–OVA particles that had been obtained at pH 9.

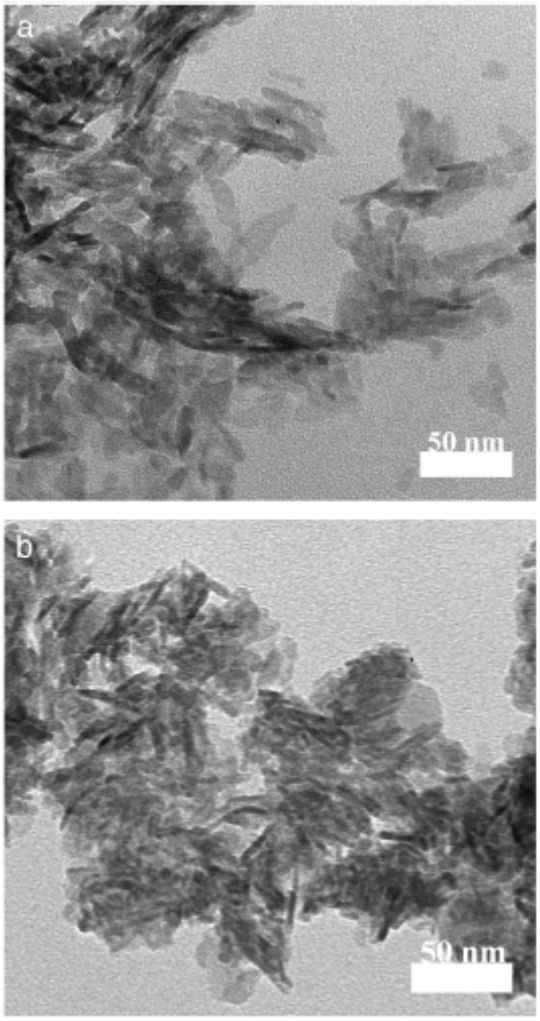


Fig. 5. TEM micrographs of (a) pure HAp and (b) HAp–OVA particles that had been obtained at pH 9.

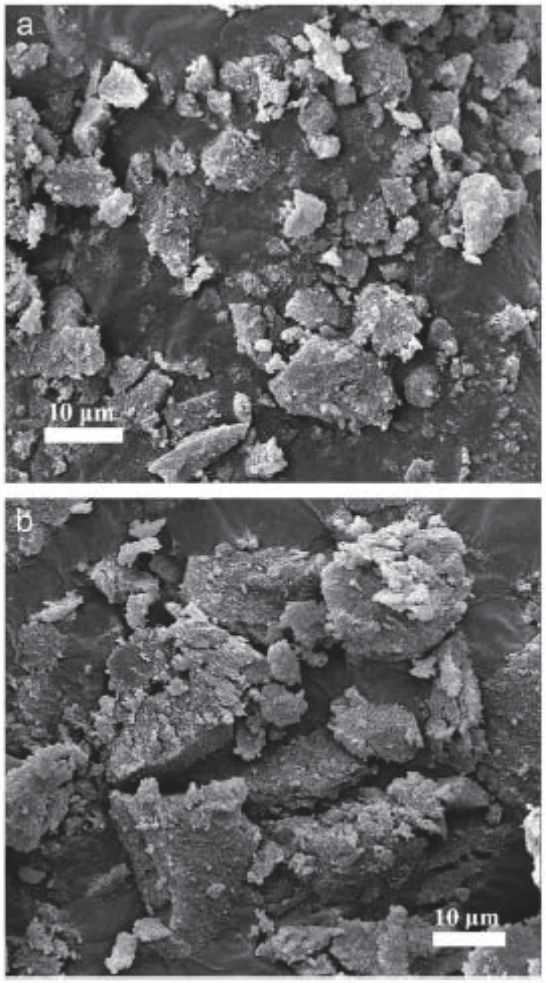


Fig. 6. SEM images of (a) pure HAp and (b) HAp–OVA particles that had been obtained at pH 9.

The N2 adsorption–desorption isotherms and the pore size distribution as calculated from the adsorption branch of the isotherms based on the Bopp–Jancsó–Heinzinger (BJH) model for the Hap and the HAp–OVA particles that had been synthesized at pH 9 are shown in Fig. 7 and in the inset of the figure, respectively. The isotherms can be categorized as type IV, which can be further categorized into H1-hysteresis loops of mesoporous materials [22]. The average pore sizes of the HAp and the HAp–OVA particles were determined to be about 8.1 nm and 14.1 nm, respectively. The isotherms and the pore size distribution of these two cases were slightly different. For the HAp–OVA particles, the isotherm exhibited a slightly steeper slope with a greater pore volume and the pore size distribution was narrower, owing to the more uniform pore sizes. This indicates that the aggregation of OVA within the HAp structure affected slightly the basic pore structure of the obtained mesoporous HAp particles. The pore diameter and the BET specific average surface area for each of the obtained products are summarized in Table 1. In the absence of OVA within the HAp structure, the pore sizes were 8.1–8.9 nm. Larger pore sizes were observed for the OVA-incorporated HAp particles (i.e., 14.1–15.5 nm). These correspond to the BET specific average surface area values of 15.6–17.2 and 16.6–21.3 $m^2 \cdot g^{-1}$, respectively, and the pore volume values of 0.029–0.079 and 0.036–0.089 $cm^3 \cdot g^{-1}$, respectively. These pores were thought to be generated upon the sublimation of the ice crystals formed during the lyophilization step [23,24]. The presence of OVA resulted in hypothetical increases in the

values of all of the pore parameters of the resulting HAp particles, while the increase in the pH during the precipitation process led to opposing trends. Furthermore, since the characteristic FT-IR bands associated with both HAp and OVA components were not shifted, it is expected that the mesopores may be present as the voids located at the grain boundaries of the aggregates of the rod-like HAp particles. The ζ potentials of the HAp and the HAp–OVA particles were finally measured based on the electrophoretic mobilities of these particles in deionized water. The average values for the HAp particles were in the range of −31.6 to −36.9 mV, while those for the HAp–OVA particles were in the range of −19.7 to −23.2 mV. Evidently, an increase in the pH during the precipitation process caused the ζ potentials of the HAp and the HAp–OVA particles to become more negative. It was reported that the ζ potentials of commercial Hap particles depended strongly on the pH of the suspending medium[25], in which the values varied from −5 to −37 mV as the pHincreased from 5.0 to 8.0. Over the pH levels of 7.0–8.0 however,the ζ potentials varied within a small range of −35 to −37 mV.Such a value for commercial HAp particles in phosphate buffer solution(pH=7.4) was determined to be −36 mV [26]. Clearly, thevalues of the ζ potentials for the HAp particles, as obtained here,agreed particularly well with those reported in the literature.

Upon the addition of OVA, which is an acidic protein (cf. isoelectricpoint=4.7 [26]) during the precipitation process to obtain theHAp–OVA particles, the ζ potentials decreased by about 12 mV on average. This reduction is a clear indication of the adsorption of the protein on the surface of the Hap crystallites. Marginal reduction in the values of the ζ potentials of the HAp particles was observed when their surfaces were covered with acidic and neutralproteins, while more significant reduction was observed when their surface was covered with basic proteins [25,26].

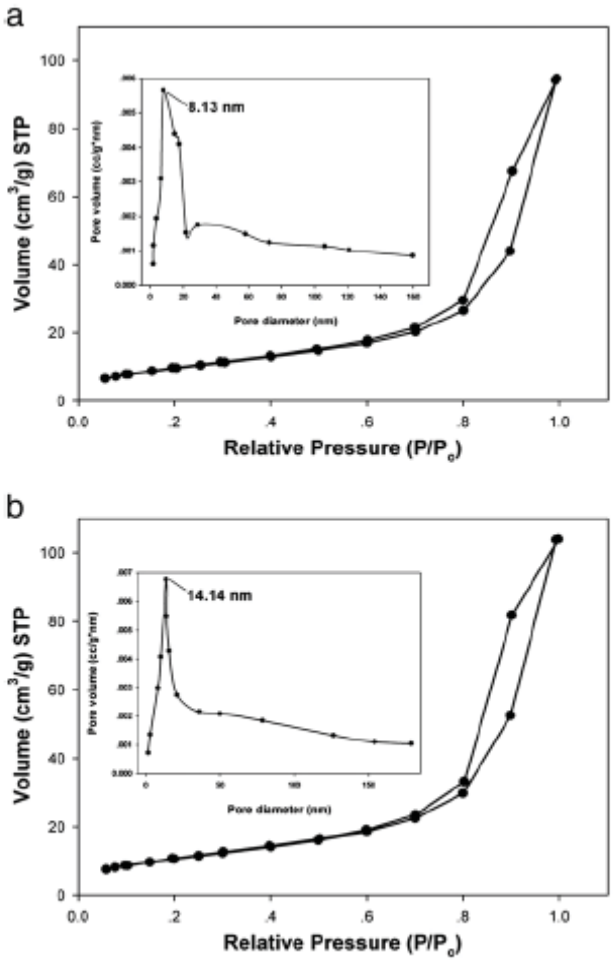


Fig. 7. Adsorption–desorption isotherms of N_2 within the pore structures of (a) pure HAp and (b) HAp–OVA particles that had been obtained at pH 9. The size distribution of the pores as determined based on the Bopp–Jancsó–Heinzinger (BJH) model is shown as the inset.

4. Conclusions

An economical and simple synthetic route for HAp–OVA particles from discarded egg shells and OVA, as the model incorporating protein, by co-precipitation method was proposed. Both XRD and FT-IR results confirmed the formation of HAp, while PSD and TEM results indicated the formation of discrete HAp nanocrystals, which were rod-like in nature. Both the crystallite sizes (as calculated from breadth of the (002) reflection peak) and the sizes of the individual nanocrystalline particles decreased in the presence of OVA. Electrophoretic analysis indicated that OVA adsorbed readily on the surfaces of the HAp nano-crystallites and this was responsible for their agglomeration into larger particles, as revealed by SEM analysis. The knowledge obtained from the preparation of these HAp–OVA materials could be used as a promising archetype for synthesizing composite particles of HAp and another functional protein for biomedical applications or bone tissue engineering purposes in particular.

2.2 Comparative Study of Protein Carriers Based on Hydroxyapatite Particles for Bone Tissue Engineering

Experimental procedure

1. Materials

All chemical reagents including Calcium hydrogen phosphate dihydrate ($CaHPO_4.2H_2O$, A.R. grade, Fluka), Calcium carbonate ($CaCO_3$, A.R. grade, Carlo Erba), Nitric acid (HNO_3, A.R. grade, Labscan), Phosphoric acid (H_3PO_4, A.R. grade, Labscan), Tris (hydroxymethyl)-aminomethane (tris-base, A.R. grade, Sigma), and Egg albumin (OVA, grade II, Sigma) were used without further purification. CaO from egg shells was prepared following the previous report of Rivera *et al.* [19].

2. Synthesis of hydroxyapatite

HAp was prepared by co-precipitation method. In the typical procedure, 2.00 g of $CaHPO_4.2H_2O$ (as a phosphorous source) and 0.79 g of $CaCO_3$ (as a calcium source) were dissolved in 1 M HNO_3 25 ml under gentle stirring at 70 ˚C for 2 h and the pH of the solution was kept to 2. OVA, subsequently, was added in the amount of 0, 1, 2, and 3 g/ 500 ml of the mixed solution at room temperature. 200 ml of 1 M and 2 M tris-base solution were then poured into the mixture generating the precipitation at pH 7 and pH 9, respectively. The precursor solution was stirred vigorously to yield a homogeneous product. The product was then filtered off and washed several times with deionized water. After centrifugation, the resulting material was freeze-dried for 48 h to obtain the fine powder products. The similar process with the use of 1.25 g of CaO and 1.50 g of H_3PO_4 as calcium and phosphorous sources respectively was performed for comparison. With many synthetic conditions above, the sample names were specified as shown in Table 1.

3. Release kinetics of OVA from HAp particles

About 20 mg of HAp-OVA particles were immersed in 10 ml phosphate buffer solution at pH 7.4, in which matches the normal body and blood system of a human being. The controlled release systems were shaken in the water bath with a stirring rate of 70 rpm at 37 ˚C. The amount of released OVA in the supernatant was measured at various times by UV-VIS spectrophotometer (UV-1800) at the wavelength of 280 nm through the use of a pre-determined standard calibration curve. Furthermore, the gravimetric analysis was used to confirm the amounts of OVA loss again after 21 days.

4. Characterization

The crystallographic phases of the HAp-OVA particles were analyzed by X-ray diffractometer (WDXRD, D/MAX 2000 series Rigaku) with an incident X-ray wavelength of 1.54 Å (Cu Kα line) at the scanning rate of 0.02° per minute over a range of 2θ from 5° to 60° with JCPDS database (9-432). Fourier transform infrared (FT-IR) spectrograph carried out on a Nicolet Nexus spectrometer (NEXUS 670, Nicolet) was performed using the KBr pellet technique, working in the wavelength from 4000 to 400 cm^{-1}. The structural morphology images were recorded on a transmission electron microscope (TEM, JEM-2100, JEOL) with an acceleration voltage of 200 kV. Energy dispersive X-ray (EDX) element analysis of the samples was also investigated with scanning electron microscope (SEM, JSM-5410LV, JEOL) operated at 15 kV. The average pore diameters of the obtained particles were

taken on autosorb-1 instrument (AS-1, Quantachrome) using physisorption of nitrogen at temperature of 77 K. Thermogravimetric analysis (TGA, TGA7, Perkin Elmer) was carried out on the dried samples (5 mg) to examine the relative amount of OVA associated with HAp particles with a heating rate of 10 ˚C /min under a flowing air atmosphere.

2.5. Statistical Analysis

All quantitative examinations were collected in triplicate and the results were presented as means and standard deviations. Significance between the mean values was determined by ANOVA one-way analysis using Tukey's test for variances at a 95% confidence level.

Results and discussion

1. Material characterization

The formation of HAp particles was ascertained by X-ray diffraction (XRD) analysis. The XRD patterns of the HAp-OVA particles with particular peaks ascribed to the lattice constant of HAp according to the JCPDS database (9-432) were given in the comparative chart of Fig. 1. From these results, the presence of the OVA during the synthesis does not have an influence on the structural development of HAp. Besides, no difference in HAp-OVA characteristic diffraction peaks was perceived for all synthetic cases given above. These XRD data also show poorly-crystallized traces of the powders due to water sublimation in the freeze-drying process [20], resulting in estimated crystallite sizes. Calculations of the crystallite size using the Scherrer equation were performed for the (002) reflection peak corresponding to $2\theta = 26^{\circ}$ because of well resolved characteristics [21]. The mean sizes of crystallites are within the range of 16-20 nm.

Table 1

Experimental conditions of HAp and HAp-OVA particles

Starting materials	Initial amounts of OVA (g)	pH conditions	Sample names
$CaCO_3$	-	7	0D-7
+	1	7	1D-7
$CaHPO_4.2H_2O$	2	7	2D-7
	3	7	3D-7
	-	9	0D-9
	1	9	1D-9
	2	9	2D-9
	3	9	3D-9
CaO (Egg shells)	-	7	0E-7
+	1	7	1E-7
H_3PO_4	2	7	2E-7
	3	7	3E-7
	-	9	0E-9
	1	9	1E-9
	2	9	2E-9
	3	9	3E-9

Fig. 2 exhibits the FT-IR spectra of the HAp-OVA particles. The IR spectra of pure OVA and HAp are also shown for comparison. The OVA spectrum displayed the typical bands at 3299 cm^{-1}, 1652 cm^{-1}, 1539 cm^{-1}, and 1457 cm^{-1} represented to the nitrogen-hydrogen stretch (N-H), the carbonyl vibration (C=O), the carbon-nitrogen vibration (C-N), and the stretching vibration of carbon-hydrogen (C-H), respectively [15]. The spectrum of pure HA demonstrates the adsorption bands at 3569 cm^{-1} assigned to OH stretching, 1630 cm^{-1} assigned to OH vibration of the apatitic group, 1035 cm^{-1} assigned to PO_4^{3-} stretching vibration, as well as 601 cm^{-1} and 563 cm^{-1} assigned to PO_4^{3-} deformation vibration [22,23]. The bands at 1654 cm^{-1} and 1539 cm^{-1} of HAp-OVA spectra, therefore, ascertained that OVA was incorporated in HAp particles.

EDX analysis was performed to give further confirmation of a molar Ca/P ratio of the samples. The EDX characteristic peaks indicated the existence of calcium (Ca), phosphorous (P), and oxygen (O) with proportional counts (Fig. 3). The molar Ca/P ratio of all samples revealed that the obtained samples synthesized by using the chemical starting material have the Ca/P ratio of 1.67-1.68 very close to the ideal one of 1.67 for HAp in human bone, while the Ca/P ratio measured for the obtained samples synthesized from the natural starting
material are within the range 1.62-1.65. On the other hand, there were not statistically significant differences for the Ca/P ratio of both starting materials ($p > 0.05$).

The HAp-OVA particles were also examined by transmission electron microscopy (TEM). The TEM micrographs of the samples synthesized from both natural and chemical substances at pH 7 and pH 9 with 1 g OVA show little difference in morphology (Fig. 4). In all obtained specimens, the primary particles have a rod-like shape with dimensions of 3-10 nm in diameter and 15-30 nm in length. However, it was noticed that the sizes of primary particle slightly increase with a higher OVA content and a lower pH condition.

2. Incorporation of OVA into HAp particles

The physi-sorption of nitrogen was performed to collect the average pore diameters of the pure HAp and HAp-OVA particles (see Table 2). The average pore sizes of HAp particles with the presence of OVA are larger than those of the absence ones, suggesting the incorporation of OVA within HAp particles by bond formation. The mechanism was that the carbonyl group and the phosphorous group of OVA have negative dipoles which could chelate the free Ca^{2+} ions; subsequently, the PO_4^{3-} ions may bond with OVA-associated calcium to generate HAp-OVA aggregates [18]. OVA, furthermore, could be adsorbed on the HAp surfaces by the crystal surface area available for growth [24]. When considering HAp-OVA particles, their average pore diameters at lower pH are bigger than those at higher pH. At the same pH, the chemical starting material shows the higher values of the average pore diameter compared with the natural one. The average pore diameters, nevertheless, are quite similar in cases of varying initial OVA contents. Therefore, it could be assumed that difference in these initial amounts of added OVA has a little influence on the average pore size. material are within the range 1.62-1.65. On the other hand, there were not statistically significant differences for the Ca/P ratio of both starting materials ($p > 0.05$).

The HAp-OVA particles were also examined by transmission electron microscopy (TEM). The TEM micrographs of the samples synthesized from both natural and chemical substances at pH 7 and pH 9 with 1 g OVA show little difference in morphology (Fig. 4). In all obtained specimens, the primary particles have a rod-like shape with dimensions of 3-10 nm in diameter and 15-30 nm in length. However, it was noticed that the sizes of primary particle slightly increase with a higher OVA content and a lower pH condition.

Table 2

Physico-chemical characteristics of HAp and HAp-OVA particles

Samples	Average pore diameter (nm)	Incorporated OVA amounts		Released OVA amounts	
		(%)*	(mg)*	(%)#	(mg)#
0D-7	9.43 ± 0.02	-	-	-	-
1D-7	16.4 ± 0.15	8.01 ± 0.92	0.40 ± 0.08	57.5 ± 3.71	0.92 ± 0.04
2D-7	16.8 ± 0.11	9.32 ± 0.37	0.47 ± 0.03	60.0 ± 4.10	1.12 ± 0.07
3D-7	16.9 ± 0.07	9.94 ± 0.96	0.49 ± 0.08	62.0 ± 3.82	1.23 ± 0.06
0D-9	8.69 ± 0.14	-	-	-	-
1D-9	13.7 ± 0.18	7.54 ± 0.83	0.38 ± 0.07	42.1 ± 2.73	0.63 ± 0.04
2D-9	14.2 ± 0.06	7.99 ± 0.68	0.40 ± 0.06	43.7 ± 2.90	0.70 ± 0.05
3D-9	14.8 ± 0.03	8.21 ± 0.74	0.41 ± 0.07	44.0 ± 1.95	0.72 ± 0.03
0E-7	8.91 ± 0.19	-	-	-	-
1E-7	15.0 ± 0.14	6.17 ± 0.45	0.31 ± 0.04	50.1 ± 3.06	0.62 ± 0.05
2E-7	15.3 ± 0.27	7.61 ± 0.33	0.38 ± 0.03	52.6 ± 2.81	0.80 ± 0.04
3E-7	15.6 ± 0.29	8.89 ± 0.87	0.44 ± 0.07	54.2 ± 3.66	0.96 ± 0.06
0E-9	8.18 ± 0.03	-	-	-	-
1E-9	13.5 ± 0.22	5.24 ± 0.72	0.26 ± 0.06	38.8 ± 1.13	0.41 ± 0.02
2E-9	13.9 ± 0.26	6.01 ± 0.79	0.30 ± 0.08	40.3 ± 2.09	0.48 ± 0.03
3E-9	14.3 ± 0.15	6.93 ± 0.44	0.35 ± 0.04	40.8 ± 1.84	0.56 ± 0.03

* based on around 5 mg of total weight of the particle analyzed from TGA

based on the incorporated OVA amounts into 20 mg of total weight of the particle

3. Incorporation of OVA into HAp particles

The physi-sorption of nitrogen was performed to collect the average pore diameters of the pure HAp and HAp-OVA particles (see Table 2). The average pore sizes of HAp particles with the presence of OVA are larger than those of the absence ones, suggesting the incorporation of OVA within HAp particles by bond formation. The mechanism was that the carbonyl group and the phosphorous group of OVA have negative dipoles which could chelate the free Ca^{2+} ions; subsequently, the PO_4^{3-} ions may bond with OVA-associated calcium to generate HAp-OVA aggregates [18]. OVA, furthermore, could be adsorbed on the HAp surfaces by the crystal surface area available for growth [24]. When considering HAp-OVA particles, their average pore diameters at lower pH are bigger than those at higher pH. At the same pH, the chemical starting material shows the higher values of the average pore diameter compared with the natural one. The average pore diameters, nevertheless, are quite

similar in cases of varying initial OVA contents. Therefore, it could be assumed that difference in these initial amounts of added OVA has a little influence on the average pore size. with the presence of higher initial OVA amount manifest a little higher OVA-release percentage, depending on the incorportaed OVA content, so the OVA release amount was not significantly dependent on the initial amount of added OVA ($p > 0.05$).

Conclusions

Protein carriers based on HAp were designed as potential devices for the controlled release system. HAp-OVA particles were obtained by the co-precipitation method with varying the starting material, pH value, and initial amount of OVA. The incorporated and released OVA amounts highly increased with lowering pH value to be neutral and slightly increased with increasing initial OVA content. A greater OVA incorporation and release were also observed in the HAp-OVA particles synthesized from the chemical starting material compared to those prepared from the natural one. All of the release kinetics exhibited a slow release in a sustained manner without initial OVA burst, resulting in prolonged release behavior. Consequently, it may be practicable to use these HAp particles with other protein drugs and growth factors as effective carries to achieve specific targets for bone tissue engineering applications.

3. **Polycaprolactone Fibrous Membranes Modified with Gelatin, Bovine Serum Albumin or Crude Bone Protein Extract and Their Potential for Use as Bone Scaffolds.**

EXPERIMENTAL SECTION

a. Materials

Materials used in the Fibrous Scaffolds Preparation and Surface Modification

- Poly(ε-caprolactone) (PCL) (M_n = 80,000 g/mol; Aldrich, USA)
- Dichloromethane (DCM; Lab-Scan (Asia), Thailand)
- *N*,*N*′-dimethylformamide (DMF; Lab-Scan (Asia), Thailand)
- 1,6-hexamethylenediamine (HMD; Aldrich, USA)
- *N*,*N*'-disuccinimidyl carbonate (DSC; Aldrich, USA)
- Ninhydrin (Aldrich, USA)
- Bovine serum albumin (BSA; Sigma, USA)
- Gelatin from porcine skin ,type A (Sigma, USA)
- Gelatin type-B (Sigma, USA)
- Triethylamine (TEA; Sigma, USA)
- Ethanol (J. T. Beaker, USA)

- Isopropanol (IPA; Fisher Sciencific (Asia), Thailand)
- 1,4-dioxane (Fisher Sciencific (Asia), Thailand)
- Dimethylsulfoxide (DMSO; Lab-Scan (Asia), Thailand)
- Phosphate buffer saline (PBS)

Materials used for cell culture

Model Cells

Model cells in this study were mouse calvaria-derived pre-osteoblastic cells (MC3T3-E1).

Medium for MC3T3-E1 cells

Minimum Essential Medium (with Earle's Balanced Salts) (MEM; Hyclone, USA), supplemented by 10% fetal bovine serum (FBS; Sorali, Campo Grande, Brazil), 1% L-glutamine (Invitrogen Corp., USA) and 1% antibiotic and antimycotic formulation [containing penicillin G sodium, streptomycin sulfate, and amphotericin B (Invitrogen Corp., USA)] was used as culture media for MC3T3-E1.

Material for Cell Culture Study

- 3-(4,5-dimethyl-thiazol-2-yl)-2,5-diphenyltetrazolium bromide (MTT; USB Corporation., USA)
- Trypsin-EDTA (GibThai Co.,Ltd.)
- Fetal Bovine Serum (Sorali, Campo Grande, Brazil)
- DMEM without phenol red (GibThai Co.,Ltd.)
- L-Glutamine (GibThai Co.,Ltd.)
- 50% Glutaraldehyde solution (Sigma, USA)
- Hexamethyl disilazane HMDS; Sigma, USA)
- p-nitrophenylphosphate (PNPP; Zymed Laboratories, USA)
- Bicinchoninic acid protein assay (BCA; Pierce Biotechnology, USA)
- L-ascorbic acid (Sigma, USA)
- β-glycerophosphate (Sigma, USA)
- Cetylpyridinium chloride (Sigma, USA)

b. Equipment

Equipment for Electrospinning Process

- High voltage power supply from Gamma High Voltage Research Inc. (Ormond Beach, Florida), model D-ES30PN/M692 DC
- Syringe with volume size of 25 ml
- Stainless steel needle with gauge number 20 (or the inner diameter of 0.91 mm)
- The rotating drum which covered with aluminum sheet has the width and OD about 14 and 15 cm, respectively.

Equipment for Characterization of Materials

- UV-Vis spectrophotometer (UV-1800; Shimadzu, Kyoto, Japan)
- quartz tube
- Fourier-transformed infrared spectrometer (FT-IR); attenuated total reflection (ATR-FTIR; Thermo Nicolet Nexus 670; resolution of 4 cm-1 and 128 scans)
- Contact angle goniometer (KRUSS Gmbh Germany; Model: DSA10-Mk2 T1C)
- Scanning electron microscope (SEM; A JEOL JSM 5200)
- X-ray Photoelectron Spectrometer (XPS; Thermo Fisher Scientific Thetaprobe; Monochromatic Al Kα X-ray, the analysis area was approximately 400 μm , while the maximum analysis depth lay in the range of ~4 to 8 nm.)

Equipment for Study of Cell Culture

- A Thermo Spectronic Genesis10 UV-vis spectrophotometer
- Laminar flow hood

c. Experimental Procedures

Preparation of Polycaprolactone Scaffolds

Preparation and Characterization of Fibrous Scaffolds

Electrospun Polycaprolactone fibrous scaffolds were prepared by electrospinning from a neat 12 % w/v PCL solution in 50:50 v/v DCM/DMF. The as-prepared PCL solution was contained in a glass syringe, the open end of which was connected to a blunt gauge-20 stainless steel hypodermic needle (o.d.0.91 mm) used as the nozzle. An Al sheet wrapped around a rotating cylinder (width and o.d. of the cylinder: 15 cm; rotational speed: 50 rpm) was

used as the collector. The distance from the tip of the needle to the surface of the Al sheet defining the collection distance was fixed at 10 cm. A gamma high-voltage research D-ES30PN/M692 power supply was used to generate a high dc potential (i.e., 21 kV). The spinning time was carried out continuously for 10 hours.

Morphological appearance and size of the individual fibers of the scaffolds were examined by a JEOL JSM-5200 scanning electron microscope (SEM). Fibrous scaffolds were dried in vacuum at 30 °C overnight to remove solvent. Each sample was plated in the stub and coated with a thin layer of gold by using a JEOL JFC-1100E ion sputtering device prior to SEM observation. The average diameters of as-spun fibers were determined by measuring the diameters. At least 100 readings of the fiber diameters from at least five SEM images are statistically analyzed using SemAphore 4.0 software, from which the arithmetic mean values of the individual fibers in the PCL fibrous scaffolds were determined to be 0.93 and 1.26 μm, respectively.

Preparation of Crude Bone Protein.

Crude bone protein (CBP) was extracted from the pork bone. In particular, bone was initially washed and cleaned thoroughly in tap water and then sectioned into small pieces with a high speed motor machine. Pieces of sectioned bones were further crushed into powder in liquid nitrogen. Then, the as-prepared powder was immersed in 0.6 N HCl at 4°C and shaken continuously on an orbital shaker. After three days, the bony solution was centrifuged and the supernatant was collected, dialyzed for 48 h and lyophilized. The dry CBP was kept in desiccators until use.

Surface Modification of PCL Scaffold via Aminolysis and Immobilization of Proteins

The scaffold was cut into disc shape with diameter 1.4 cm and immersed in ethanol/water (1:1, v/v) solution for 2 to 3 hours to clean oily dirt and then washed with a large amount of deionized water. The scaffold was subsequently immersed in various concentrations of 1,6-hexamethylene diamine (HMD) /isopropanol (IPA) solution (0.04, 0.06, 0.08, 0.10, 0.20 ,and 0.40 g/ml) for 2 hours at 30 °C. The resulting aminolyzed PCL scaffold was rinsed with deionized water for 24 hours at room temperature to remove free 1,6-hexamethylenediamine and dried under vacuum at 30 °C to constant weight. To determine the optimum concentration of HMD used for aminolysis using ninhydrin method, degreadation experiment, water retention experiment and SEM observation.

Aminolyzed PCL scaffold obtained using the optimum condition was immersed in 0.1 M *N,N'*-disuccinimidyl carbonate (DSC)/dimethylsulfoxide (DMSO) solution in the presence of 0.1 M triethylamine (TEA) for 1 hour at ambient temperature

followed by rinsing with large amount of deionized water. The scaffold was then directly transferred to 3 mg/ml of gelatin type-A, gelatin type-B, bovine serum albumin (BSA) or crude bone protein (CBP) in phosphate buffer saline (PBS) solution at ambient temperature for 24 hours. PCL scaffolds immobilized with proteins were rinsed by soaking in deionized water for 24 hours. The samples were dried under vacuum before surface characterization.

Characterization of Fibrous Scaffolds

Density, Porosity and Pore Volume

The density of the scaffolds ($\rho_{scaffolds}$) can be calculated using the following equation

$$\textbf{Apparent density } (\rho_{scaffold}, \textbf{g/cm}^3) = \frac{m}{txA} \quad \text{----------(3.1)}$$

where m is the mass of the scaffold (g), t is the thickness of the scaffold (cm) and A is the area of the scaffold (cm^2)

The porosity and pore volume of the scaffolds can be calculated using the following equation (Hou *et al*. 2003).

$$\textbf{Porosity (\%)} = \left(1 - \frac{\rho_{scaffold}}{\rho_{polymer}}\right) x100 \quad \text{---------(3.2)}$$

$$\textbf{Pore volume} = \left(\frac{1}{\rho_{scaffold}} - \frac{1}{\rho_{polymer}}\right) \quad \text{----------(3.3)}$$

where $\rho_{scaffold}$ is the apparent density of the fibrous scaffolds(g/cm^3) and $\rho_{polymer}$ is the density of the non-fibrous polymer ($\rho_{polymer}$ of PCL is 1.145 g/cm^3).

Water Retention Capacity

The dry scaffolds were weighed and then immersed in 5 mL of 0.1 M PBS solution at 37 °C within 48 hours. At the predetermined time point, scaffold were removed from the solution and carefully placed on glass for 5 seconds to remove the excessive water and weighed immediately. The water retention was calculated by using the following equation (Kothapalli *et al*., 2005).

$$\textbf{Water Retention (\%)} = \left(\frac{M_{wet} - M_{dry}}{M_{dry}}\right) x100 \text{ ----------(3.4)}$$

where M_{dry} and M_{wet} are the weight of the scaffold before and after immersion in 0.1 M PBS solution respectively. Five measurements were performed for the calculation of an average water retention value.

Degradation Study of Fibrous Scaffolds

In degradation study, the disc shape of the fibrous scaffolds with diameter 1.4 cm had been immersed in the 0.1 M PBS pH 7.4 at 37 °C within 48 hours. The fibrous scaffolds were then dried in the vacuum to constant weight.

The rate of degradation can be calculated using the following equation.

$$\textbf{Weight loss (\%)} = \left(\frac{Mf - Mi}{Mi}\right) x100 \text{ ----------(3.5)}$$

where M_i is the initial weight of the scaffolds and M_f and is the weight of the scaffold at the given degradation time point, immersed in 0.1 M PBS solution. Five measurements were performed for the calculation of an average water degradation rate value.

Determination of the Amino Groups on PCL Surface after Aminolysis and Protein Immobilization

The ninhydrin analysis method was carried out to quantitatively determine the amount of NH_2 groups on the aminolysed PCL and biomolecule-immobilized PCL scaffolds. The scaffold was immersed in 1 M ninhydrin/ethanol solution for 15 minutes. After the adsorbed ethanol had evaporated, 1,4-dioxane was added to dissolve the scaffold. When the scaffold surface turned blue, isopropanol (IPA) was then added to stabilize the blue compound. This mixture was transfered to quartz tube and measured the absorbance at the wavelength of 538 nm using a UV-vis spectrophotometer. A calibration curve was obtained with known concentration of 1,6-hexamethylenediamine in 1,4-dioxane/IPA (1:1, v/v) solution**.**

Surface Characterization

Water Contact Angle Measurements

*C*ontact angle goniometer (KRUSS Gmbh Germany; Model: DSA10-Mk2 T1C) were used for the determination of water contact angles. The measurements were carried out by the sessile drop method in air at room temperature. The reported angle was an average of 5 measurements on different area of each sample**.**

UV-Vis Spectrophotometer

UV-vis spectrophotometer Model Shimadzu, UV-1800 was used for determination of the amount of amino group using ninhydrin method on the modified PCL surface. Ninhydrin will react with a free alpha-amino group, NH_2-C- which is contained in all amino acids, peptides, or proteins, producing Ruhemann's purple colored complex of ninhydrin absorbs the visible light at the wavelength of 538 nm.

Attenuated Total Reflectance-Fourier Transform Infrared Spectrometer (ATR-FTIR)

All spectra are collected at resolution of 4 cm^{-1} and 128 scans using Nicolet Magna 750 FT-IR spectrometer equipped with a liquid-nitrogen-cooled mercury-cadmium-telluride (MCT) detector. A single attenuated total reflection accessory with 45° germanium (Ge) IRE (spectra Tech, USA) and a varible angle reflection accessory (Seagull^{TM}, Harrick Scientific, USA) with a hemispherial Ge IRE are employed for all ATR spectral acquisitions. Chemical functional groups that were present on the surfaces of both the neat and the surface-modified fibrous scaffolds were analyzed by ATR-FTIR spectrometer.

X-ray Photoelectron Spectrometer (XPS)

XPS was used to estimate the elemental composition and chemical state of the elements on the surface. The analysis of the samples was carried out using a Thermo Fisher Scientific Thetaprobe XPS. Monochromatic Al K_α X-ray was employed for analysis of one spot on each sample with photoelectron take-off angle of 50° (with respect to surface plane). The analysis area was approximately 400 μm, while the maximum analysis depth lay in the range of ~4 to 8 nm. A special designed electron flood gun with a few eV Ar^+ ion was used for the charge compensation. Electron beam and ion beam were focused and steered towards the analysis position. Further correction was made based on adventitious C 1s at 285.0 eV using the manufacturer's standard software. Survey spectra were acquired for surface composition analysis with Scofield sensitivity factors.

Scanning Electron Microscope

The morphology of cells on the materials was examined by using a JEOL JSM 5200 scanning electron microscope (SEM). Each sample was coated with a thin layer of gold using JEOL JFC 1100E ion sputtering device prior to SEM observation.

Cell Culture Studies

Osteoblast (MC3T3-E1) cell lines are used. MC3T3-E1 cells are cultured in α-MEM medium supplemented with 10 % FBS, 1 % L-glutamine and 1 % antibiotic and antimycotic

formulation (containing penicillin G sodium, streptomycin sulfate, and amphotericin B**)**. The medium was replaced every 2 days and the cultured cells were maintained at 37 °C in a humidified atmosphere containing 5% CO_2.

Cytotoxicity Evaluation

Direct Cytotoxicity

This test was used to evaluate the potential for use of protein directly to the cell. 4×10^4 MC3T3-E1 cells/well were cultured in 24-well plate to allow cell attachment on the plate. After incubation under 5 % CO_2 at 37 °C at least 4 hours, the cells were starved with a 2 % culture media (2 % MEM; containing MEM, 2 % FBS, 1 % L-glutamine, 1 % lactabumin, and 1 % antibiotic and antimycotic formulation.) for 24 hours. After starvation, the culture medium was removed and replaced with the as-prepared extraction media (2 % culture media with appropriate amount of proteins ; gelatin type-A , gelatin type-B, bovine serum albumin, and crude bone protein) and later incubated for 1, 2, and 3 days. The number of living cells was finally quantified with MTT assay.

Indirect Cytotoxicity

The indirect cytotoxicity evaluation was conducted on modified and unmodified PCL scaffolds in adaptation from the ISO10993-5 standard test method . The samples are pre-washed with 70 % ethanol in water for 30 minutes, washed twice with PBS solution and deionized water and immerged in a 2% MEM culture medium (2 % MEM; containing MEM, 2 % FBS, 1 % L-glutamine, 1 % lactabumin, and 1 % antibiotic and antimycotic formulation.) under 5 % CO_2 at 37 °C in 24-well plate for 24 hours to prepare the extraction media. 4×10^4 MC3T3-E1 cells/well were separately cultured in other 24-well plate to allow cell attachment on the plate at least 4 hours. The cells were further starved with a 2 % MEM and replaced in 2 hours for 3 times. After incubation under 5 % CO_2 at 37 °C, the culture medium was removed and replaced with the as-prepared extraction media and later incubated for another 1, 2 and 3 days. The number of living cells was finally quantified with MTT assay.

Cell Adhesion and Proliferation

Both modified and unmodified PCL scaffolds (diameter 1.4 cm) are sterilized by soaking in 70 % ethanol in water for 30 minutes, washed twice with PBS solution and deionized water and immerged in a 10 % MEM culture medium under 5 % CO_2 at 37 °C in 24-well plate for 24 hours. After removing of culture media, approximately 4×10^4 MC3T3-E1 cells and 0.5 mL culture medium were pipetted into each well containing as-prepared scaffolds as well as into the bottom of tissue culture polystyrene plates (TCPS) as a control and then incubated under 5 % CO_2 at 37 °C. Cell adhesion was studied on 2, 4, 6 hours culture period

while cell proliferation was investigated on 1, 2 and 3 days culture period. The number of living cells was finally quantified with MTT assay.

MTT Assay

The MTT assay is based on the reduction of the yellow tetrazolium salt to purple formazan crystals by dehydrogenase enzymes secreted from the mitochondria of metabolically active cells. The amount of the purple formazan crystal formed is proportional to the number of viable cells. After desirable culture period, the culture medium was removed to discard the unattached cell and incubated at 37 °C for 30 minutes with 300 µl/well of MTT solution at 0.5 mg/ml culture medium without phenol red. After incubation, MTT solution was removed. A buffer solution containing dimethylsulfoxide (DMSO : 900 µl/well) and glycine buffer (pH = 10 : 125 µl/well) was added into the wells to dissolve the formazan crystals. After 10 minutes of rotary agitation, the solutions were then transferred into a cuvette and placed in a spectrophotometer (Thermospectronic Genesis10 UV-visible spectrophotometer) to measure the number of viable cells at absorbance 540 nm .

Morphological Observation of Cultured Cells

After removal of the culture medium, the cell-cultured scaffold samples were rinsed with PBS twice and the cells were then fixed with 3% glutaraldehyde solution (diluted from 50 % glutaraldehyde solution with PBS), at 500 µl/well. After 30 minutes, they were rinsed again with PBS. After cell fixation, the samples were dehydrated in an ethanol solution of varying concentration (i.e. 30, 50, 70, 90, and 100 %, respectively) for about 2 minutes at each concentration. The samples were then dried in 100 % hexamethyldisilazane (HMDS) for 5 minutes and later let dry in air after removal of HMDS. After completely dried, the samples were mounted on an SEM stub, coated with gold, and observed by a JEOL JSM 5200 scanning electron microscope (SEM).

Production of Alkaline Phosphatase of Cultured Cells

ALP is considered as a relatively early marker of osteoblast differentiation. Cells were cultured on scaffold samples for 3, and 7 days to observe the production of alkaline phosphatase (ALP). The samples were rinsed with PBS after removal of culture medium. Alkaline lysis buffer (10 mM Tris-HCl, 2 mM $MgCl_2$, 0.1 % Triton-X 100, pH 10) (100 µl/well) was added and the samples were scrapped and then frozen at -20°C for at least 30 minutes prior to the next step. An aqueous solution of 2 mg/ml *p*-nitrophenyl phosphate mixed with 0.1 M amino propanol (10 µl/well) in 2 mM $MgCl_2$ (100

μl/well) having a pH of 10.5 was prepared and added into the samples. The samples were incubated at 37 °C for 15 minutes. The reaction was stopped by adding 0.9 ml/well of 50 mM NaOH and the extracted solution was transferred to a cuvette and placed in the UV-visible spectrophotometer, from which the absorbance at 410 nm was measured. The amount of ALP was then calculated against a standard curve. In order to calculate for the ALP activity, the amount of ALP had to be normalized by the amount of total protein synthesized. In the protein assay, the samples were treated in the same manner as the ALP assay up to the point was the samples were frozen. After freezing, bicinchoninic acid (BCA; Pierce Biotechnology, USA) solution was added into the samples. The samples were incubated at 37 °C for 15 minutes. The absorbance of the medium solution was then measured at 562 nm by the UV-vis spectrophotometer and the amount of the total protein was calculated against a standard curve.

Mineralization

Mineralization refers to cell-mediated deposition of extracellular calcium and phosphorus salts where anionic matrix molecules take up the Ca^{2+}, phosphate ions and serve as nucleation and growth sites leading to calcification. Mineralization was quantified by Alizarin Red-S which is a dye that binds selectively calcium salts and is widely used for mineral staining (the staining product i.e., an Alizarin Red S-calcium chelating product). MC3T3-E1 cells (4×10^4 cells/well in 24-well plate) were cultured on scaffold samples for 16 days to observe the production of mineralization. The isolated cells were plated in 24-well plate and cultured in the cultured medium. The cultured cells were changed after a 24 hours attachment period with culture medium in the presence of 5 mM *β*-glycerophosphate and 50 μg/ml ascorbic acid. The media was replaced every 2 days thereafter. After 16, 21 and 30 days, respectively, the cells were washed twice with PBS , fixed with cold methanol for 10 minutes, and stained with 1 % Alizarin red solution (prepared in distillated water and adjusted the pH about 4.1 to 4.3 using 10 % ammonium hydroxide) for 5 minutes. After removing the alizarin red-S solution, the cells were rinsed with deionized water and dried at room temperature. The images of each culture were captured and the strain was extracted with 10 % cetylpyridinium chloride in 10 mM sodium phosphate for 1 hour and the absorbance of collected dye was read at wavelength 570 nm in spectrophotometer (A Thermo Spectronic Genesis10 UV-visible spectrophotometer). In comparison, tissue culture plate without cell was treated with the procedure as previously described.

Statistical analysis

Values are expressed as the mean ± SD. Experiments are performed at least five times and results of representative experiments are presented except where otherwise indicated. Statistical analysis was performed using One-Way Analysis of Variance (ANOVA) with the Least Square Difference (LSD) test multiple comparisons posttest using SPSS version 17 software. $p < 0.05$ or $p < 0.01$ is considered statistically significant.

2. RESULTS AND DISCUSSION

4.1 Preparation of Poly(ε-caprolactone) Electrospun Fibrous Scaffold

Poly(ε-caprolactone) (PCL; M_n = 80,000 g/mol) electrospun fibrous scaffold was prepared via electrospinning process under fixed conditions as mentioned in the previous chapter. Translucent electrospun PCL fibrous scaffolds with a thickness of (130 ± 5) μm were obtained. Morphological appearance and size of the individual fibers of the scaffolds were examined by JEOL JSM 5200 scanning electron microscopy (SEM) as shown in Figure 4.1(a). At least 100 readings of the fiber diameters from various SEM images were statistically analyzed using SemAphore 4.0 software, from which the arithmetic mean value of the individual fibers within the PCL fibrous scaffolds was determined to be (0.93 ± 0.30) μm. After surface modification of PCL electrospun fibrous scaffold via aminolysis with various 1,6-hexamethylenediamine (HMD) concentration treatments, the morphology of the surface-modified scaffolds was also observed [Figure 4.1 (b,c and d)].

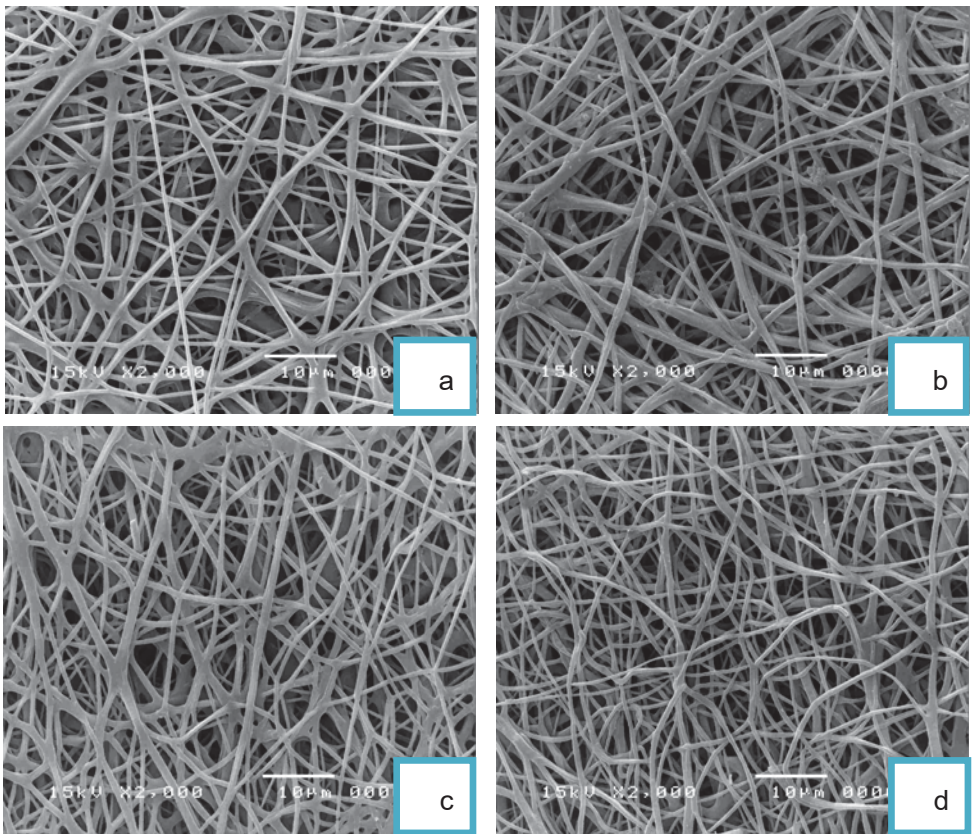


Figure 4.1 Selected SEM image of electrospun PCL fibrous scaffolds (a), aminolyzed PCL fibrous scaffolds which treated with (magnification = 2000x; scale bar = 10 μm) 1,6-hexamethylenediamine at concentration of 0.04 g/ml (b), 0.20 g/ml (c) and 0.40 g/ml (d)

4.2 Characterization of Fibrous Scaffolds

4.2.1 Density, Porosity, and Pore Volume

The density, porosity and pore volume of the unmodified PCL scaffolds and modified PCL scaffolds are shown in Table 4.1. The porosity and pore volume of these scaffolds were in the range of (96 to 97) % and (22 to 29) cm^3/g, respectively. Moreover, the density, porosity percentage and pore volume of all type of the surface-modified scaffolds were not significantly different from the unmodified PCL scaffolds.

Material	density ($x10^{-2}g/cm^3$)	porosity (%)	pore volume (cm^3/g)
PCL pure	4.69±0.44	95.91±0.38	20.62±2.07
aminolyzed PCL	4.25±0.97	96.29±0.85	23.63±5.28
activated PCL	4.14±0.57	96.39±0.50	23.64±3.07
gelatin A immobilized PCL	3.75±0.59	96.72±0.51	26.33±4.52
gelatin B immobilized PCL	3.59±0.88	96.86±0.77	28.15±6.17
BSA immobilized PCL	3.85±0.74	96.64±0.65	25.88±4.97
CBP immobilized PCL	4.58±0.93	96.00±0.81	21.64±4.35

4.2.2 Water Retention Capability

Figure 4.2 demonstrates the water retention capability of these unmodified and modified PCL scaffolds via aminolysis process with different 1,6-hexamethylenediamine (HMD) concentration at 37 °C within 48 hours. In the figure shows the water retention rate increased with increasing HMD concentration treatment.

4.2.3 Degradation Study of PCL Fibrous Scaffolds

In degradation study, the disc shape of the PCL fibrous scaffolds with diameter ~ (100 to 150) μm had been immersed in the 0.1 M phosphate buffer saline (PBS), pH 7.4 at 37 °C within 48 hours. Figure 4.3 shows the degradation rate of the PCL scaffolds at different HMD concentration treatments. The weight loss increased with time and rapidly increased in

the early 2 hours and steady stable after 18 hours. Furthermore, the weight loss values increased with increasing HMD concentration treatment.

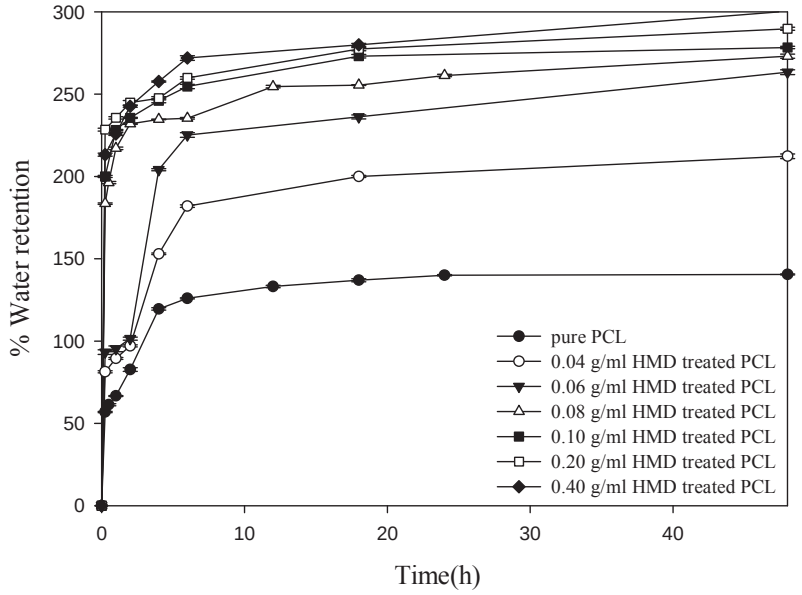


Figure 4.2 Water retention capability of these unmodified and modified PCL scaffolds via aminolysis process with different 1,6-hexamethylenediamine(HMD) concentration at 37 °C within 48 hours.

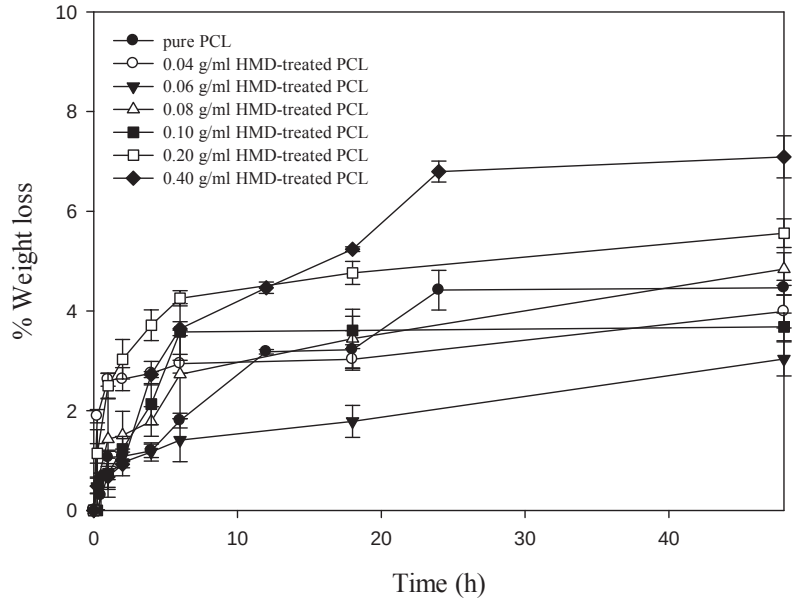


Figure 4.3 The degradation rate of the PCL scaffolds at different HMD concentration treatments.

4.3 Surface Characterization

4.3.1 Quantification of Amino Groups

Amino groups can be covalently introduced onto the surface of the electrospun PCL fibrous scaffolds by reaction with 1,6-hexamethylenediamine (HMD), One amino group (NH_2) of HMD reacts with an ester group (—COO—) of PCL to form the amide linkage (—CONH—), while another amino group which is unreacted and free can be used as active sites through which biomolecules (i.e;proteins) can be bonded to the surface using *N, N′*-disuccinimidyl carbonate (DSC) as a coupling agent. However, two-step procedure was carried out to avoid aggregation,. The attached amino groups had been first activated with DSC which *N*-hydroxysuccinimide was lost from the reaction and the as-formed succinimidyl esters were later reacted with respective biomolecules, *N*-hydroxysuccinimide again being cleaved from the reaction. The chemical pathway for the immobilization of biomolecule on the surface of electrospun PCL fibrous scaffolds is summerized in the Figure 4.4.

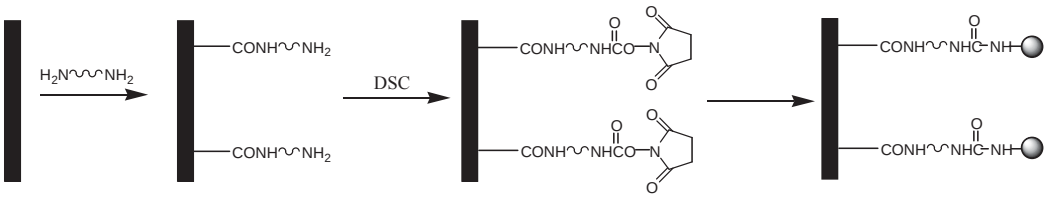


Figure 4.4 The chemical pathway for the immobilization of proteins.

The existence of free amino groups (NH_2) on PCL surface is essential for protein bonding in this modification method. It is important to confirm the existence of amino groups before protein is further introduced. Therefore, ninhydrin is used to confirm and quantify the –NH_2 density on the aminolyzed PCL surface. The NH_2 density on electrospun PCL fibrous scaffold surfaces is relative to the concentration of 1,6-hexamethylenediamine, aminolyzing time, temperature, and so on. Figure 4.5 shows that NH_2 density increased with increasing 1,6-hexamethylenediamine concentration. However, when the concentration of 1,6-hexamethylenediamine is greater than 0.20 g/ml, the structural morphology of the electrospun PCL fiber scaffolds became worse (as shown in Figure 4.1 d). To maintain structural morphology of the electrospun PCL fiber scaffolds for practical applications, PCL electrospun

fibrous scaffolds were aminolyzed in a 0.20 g/ml 1,6-hexamethylenediamine/isopropanol solution at evaluated temperature for 2 hours. According to the calibration curve obtained with 1,4-dioxane–isopropanol (1:1, v/v) solution containing 1,6-hexamethylenediamine of known concentration, the NH_2 density on PCL electrospun fibrous scaffolds aminolyzed under these conditions was 1.37 x 10^{-7} mol/cm^2.

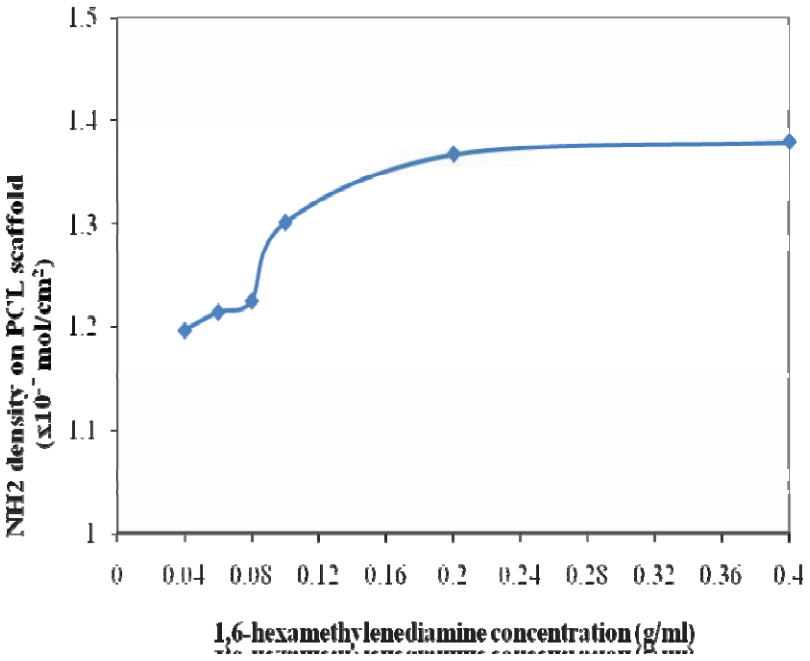


Figure 4.5 NH_2 density on PCL electrospun fibrous scaffolds as a function of concentration of 1,6-hexamethylenediamine/isopropanol solution. The PCL scaffold was aminolyzed for 2 hours.

4.3.2 Surface Wettability

To further evaluate the effect of aminolysis, surface wettability of the modified PCL fibrous scaffolds was measured. Therefore,water contact angle measurement was used to evaluate the surface wettability of the surface modified PCL fibrous scaffolds. Table 4.2 shows the water contact angle measured by the sessile drop method decreased gradually from 123.8˚ to 118.0˚ after the scaffolds were aminolyzed with 0.04 g/mL of HMD/IPA solution for 2 hours and slightly decreased with increasing HMD concentration. That is, the introduction of the amino groups on the surface of the PCL fibrous scaffolds improved the hydrophilicity of the surface. Figure 4.6 and 4.7 show that the surface became more hydrophilic after aminolysis and protein immobilization. After the aminolyzed PCL fibrous scaffolds have been activated

with DSC, their surface became more hydrophobic than the neat PCL scaffold and water contact angle also decreased after the proteins were bonded. The water drop appearance on the surface of neat PCL, gelatin type-A immobilized PCL, BSA immobilized PCL and CBP immobilized PCL are shown in Figure 4.7. CBP immobilized PCL scaffold has largest decrease of contact angle as compared with the neat PCL scaffold (control). This means that immobilization of gelatin crude bone protein can most improve the hydrophilicity of the surface.

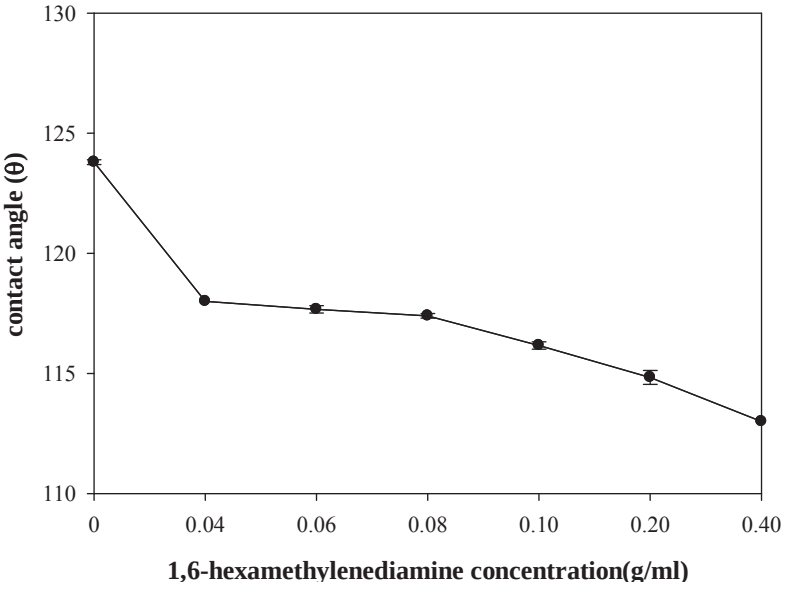


Figure 4.6 Water contact angles of the control and aminolyzed PCL scaffolds at different HMD concentration treatments measured by the sessile drop method.

Table 4.1 The water contact angle of the control and all modified PCL fibrous scaffolds measured by the sessile drop method

Material	Contact angle(θ)
Neat PCL (control)	123.7 ± 0.1
Aminolyzed PCL[a]	115.3 ± 0.2
Activated PCL[b]	118.7 ± 0.3
Gelatin type-A immobilized PCL[c1]	95.5 ± 1.1
Gelatin type-Bimmobilized PCL[c2]	94.4 ± 2.1
BSA immobilized PCL[c3]	97.5 ± 2.0
CBP immobilized PCL[c4]	48.5 ± 1.8

[a]The PCL electrospun fibrous scaffolds was immersed in 0.20 g/ml 1,6-hexamethylenediamine solution at 30 °C for 2 hours.

[b]The aminolyzed PCL scaffolds were immersed in 0.1 M DSC solution in the presence of TEA for 1 hour.

[c1,c2,c3,c4] The activated PCL scaffolds were immersed in 3.0 mg/mL gelatin type-A, gelatin type-B, BSA, and CBP solutions, respectively, for 24 h followed by the rinsing process.

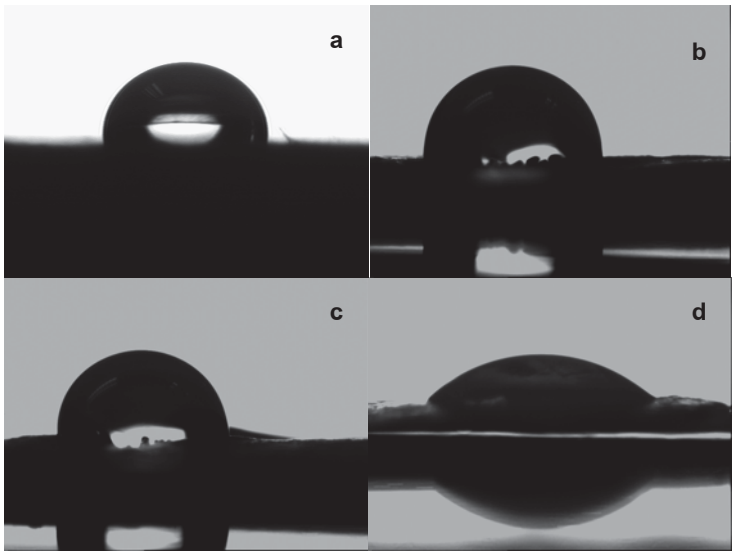


Figure 4.7 Water dropped on the surface of neat PCL fibrous scaffold (a), and PCL fibrous scaffold immobilized with 3.0 mg/ml gelatin type-A (b), 3.0 mg/ml bovine serum albumin (c) and 3.0 mg/ml crude bone protein (d).

4.3.3 Chemical Analysis of Surface

ATR-FTIR spectra of PCL and modified PCL fibrous scaffolds are shown in Figure 4.8 and 4.9 There was a major absorption peak assigned to the ester carbonyl of neat PCL appeared at 1755 cm^{-1}.

The low broad signals from N–H stretching of NH_2 at ~ (3300 to 3500) cm^{-1} or carbonyl stretching of amide group at 1650 cm^{-1} were observed on those surface modified PCL. After biomolecule immobilization, C=O stretching peak occurs at 1650 cm^{-1} (amide I) and N–H bending peak at 1550 cm^{-1} (amide II) and 1350 cm^{-1} (amide III) evidently appeared in the spectra of all biomolecule-immobilized PCL scaffolds. Moreover, the higher broad peak in the range of 3000 to 3600 cm^{-1} corresponding to N–H stretching of NH_2 in gelatin type-A, gelatin type-B, BSA and CBP was observed indicating that gelatin type-A, gelatin type-B,

BSA and CBP have been successfully immobilized on the amino-containing PCL scaffolds. However, the signal of FTIR spectrum were low, resulting from the extremely low concentration of NH_2 present within the sampling depth of ATR-FTIR (1 to 2 μm).

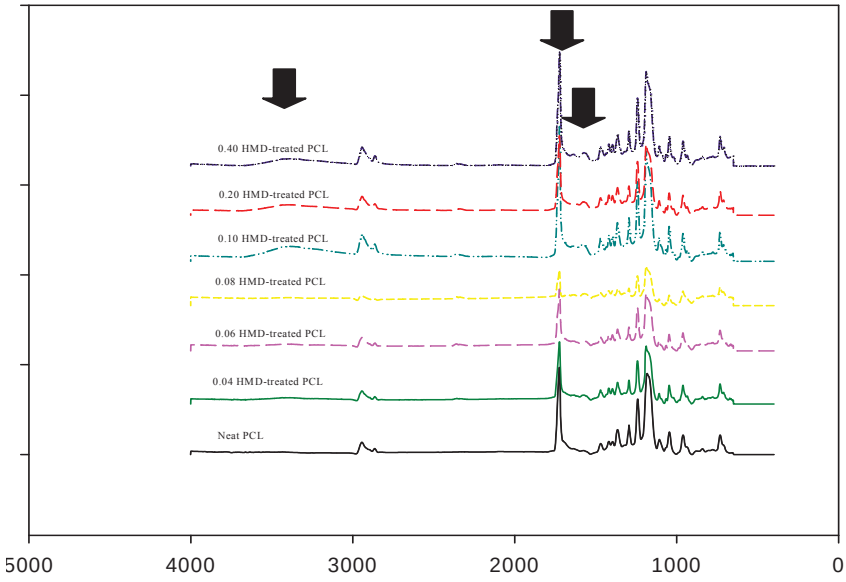


Figure 4.8 ATR-FTIR spectra of neat and aminolyzed PCL fibrous scaffolds with different HMD concentration treatments.

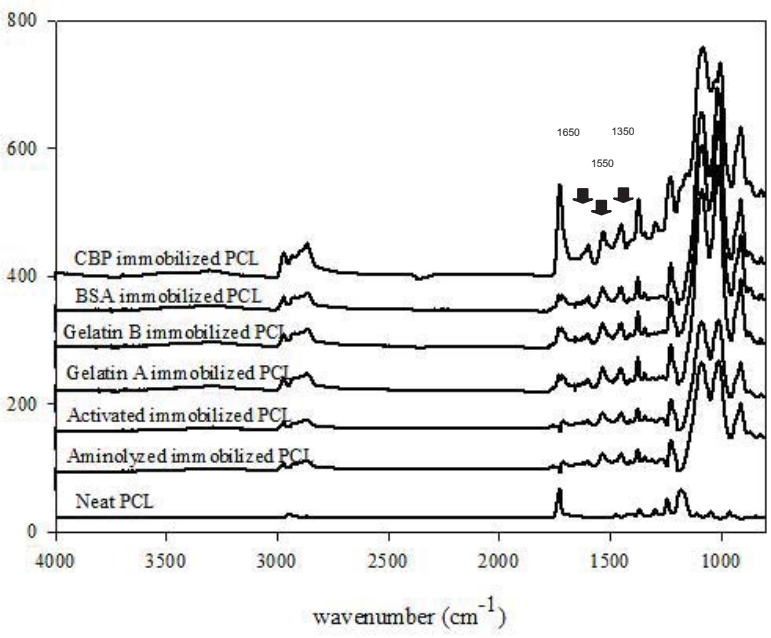


Figure 4.9 ATR-FTIR spectra of neat and modified PCL fibrous scaffolds**.**

4.3.4 Elemental Composition of the Surface

The surface of modified PCL fibrous scaffolds were further determined the elemental composition by using X-ray Photoelectron Spectrometer (XPS). To study the effect of the aminolysis condition on the surface, N_{1s}/C_{1s} ratios as a function of HMD concentration treatment were evaluated. Table 4.4 shows that the more diamine concentration treated, the more N_{1s}/C_{1s} ratio observed due to the increasing in NH_2 groups. After aminolysis, the N_{1s}/C_{1s} ratio was increased from 0 to 0.0168 because NH_2 groups were introduced on the PCL surface. Figure 4.10 demonstrated that N_{1s} peak appeared after immobilization with proteins (gelatin type-A , gelatin type-B , bovine serum albumin, and crude bone protein) due to the large amount of nitrogen atom in proteins structure was introduced.

Table 4.2 N_{1s}/C_{1s} ratios as a function of 1,6-hexanediamine concentration

1,6-hexamethylenediamine concentration (g/ml)	N_{1s}/C_{1s} ratio
0.04	0.0063
0.06	0.0079
0.08	0.0163
0.10	0.0169
0.20	0.0170
0.40	0.0170

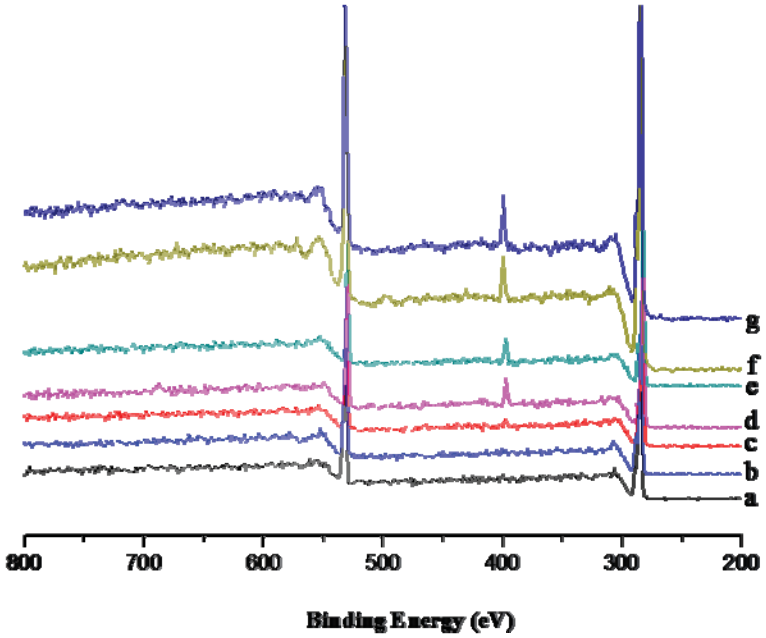


Figure 4.10 The survey XPS spectra of (a) neat PCL, (b) aminolyzed PCL with 0.20 g/ml HMD treatment, (c) activated PCL, (d) PCL immobilized with 3 mg/ml gelatin type-A solution, (e) 3 mg/ml gelatin type-B solution, (f) 3 mg/ml bovine serum albumin solution, and (g) 3 mg/ml crude bone protein solution.

4.4 Biological Characterizations

4.4.1 Cytotoxicity

4.4.1.1 Direct Cytotoxicity

Direct cytotoxicity test is a method to evaluate the toxic effect of proteins directly to cells. The effect was investigated with mouse calvaria-derived pre-osteoblastic cells (MC3T3-E1), based on the initial 40,000 cells/well seeded. MC3T3-E1 were cultured in 24-well culture plate to allow cell growth. The test was conducted by adding gelatin type-A, gelatin type-B, BSA protein and crude bone protein extracts in 2% serum-containing MEM diluted with 7-day extraction medium in seeded cells as mentioned above and cultured for 1, 2, and 3 d. Figure 4.11 shows that the viability of MC3T3-E1, cultured with 2% serum-containing MEM extraction media adding with all types of proteins for 1, 2 and 3 days, was increased with increasing the culturing time in the respective media. The viability of cells

(relative with control TCP) of all material is more than 80 %. All of the obtained results clearly suggested that all types of proteins, released no substances at levels that were harmful to cells.

4.4.1.2 Indirect Cytotoxicity

The potential use of these fibrous scaffolds as bone scaffolds was first evaluated by an indirect cytotoxicity test with mouse calvaria-derived pre-osteoblastic cells (MC3T3-E1), based on the initial 40,000 cells/well seeded. The test was carried out on TCP (control), the neat PCL, aminolyzed PCL, activated PCL, gelatin type-A, gelatin type-B, BSA and CBP immobilized PCL fibrous scaffolds. MC3T3-E1 were cultured in a 24-well culture plate in 2 % serum-containing MEM extraction medium from all type of fibrous scaffolds for 1, 2, and 3 days. Figure 4.12 shows that the viability of MC3T3-E1, cultured with 2 % serum-containing MEM diluted with 1-day extraction media prepared by all types of modified scaffolds, was increased with increasing the culturing time in the respective media and the viability of cells on all types of material measured by MTT assay was more than 80 %. All of the obtained results clearly suggested that all types of the PCL fibrous scaffolds, released no substances at levels that were harmful to cells.

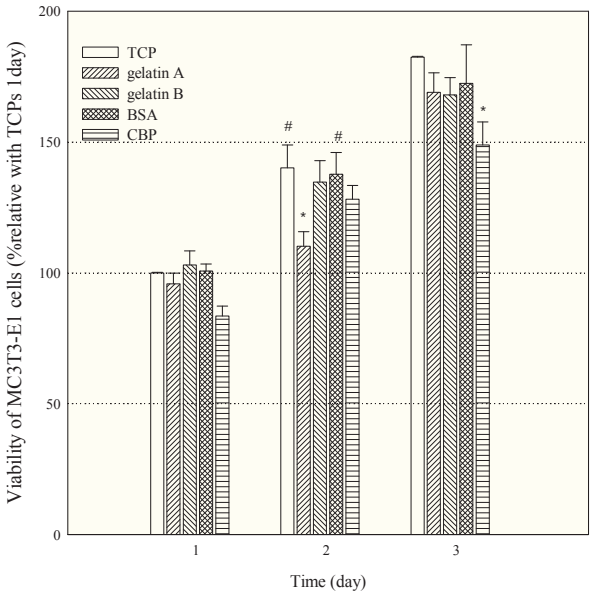


Figure 4.11 The viability of MC3T3-E1, cultured with 2% serum-containing MEM extraction media adding with all types of proteins for 1, 2 and 3 days. Statistical significance: $*p < 0.05$ compared with control and $^{\#}p < 0.05$ compared to the neat PCL fibrous scaffolds at any given time point.

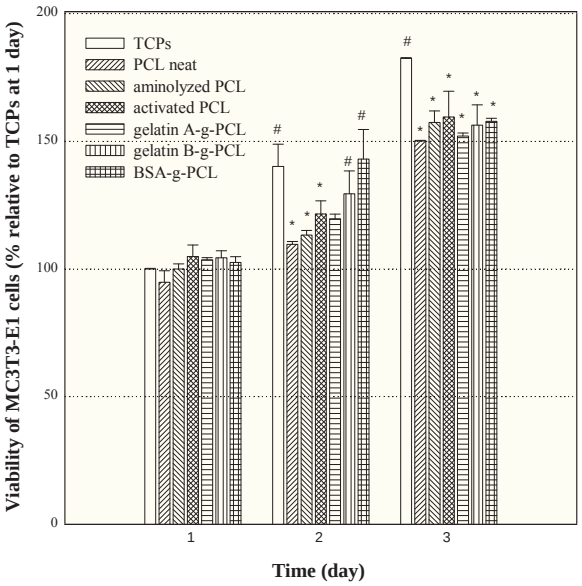


Figure 4.12 The viability of MC3T3-E1, cultured with 2% serum-containing MEM extraction media from all type of PCL fibrous scaffolds for 1, 2, and 3 days relative to TCPS at 1 day Statistical significance: $^{*}p < 0.05$ compared with control and $^{\#}p < 0.05$ compared to the neat PCL fibrous scaffolds at any given time point.

4.4.2 Cell Attachment and Proliferation

The potential for use of the neat and the modified PCL fibrous scaffolds was further evaluated by determination their ability to support both the adhesion and the proliferation of MC3T3-E1. The viability of the cells that had been cultured on the surface of TCPS for 2 h was taken as the basis to arrive at the relative viability shown in a Figure. Figure 4.13 shows the attachment of MC3T3-E1 on the surfaces of TCPS, neat PCL, aminolyzed PCL, activated PCL, and protein-immobilized PCL at 2, 4, and 6 h after cell seeding in terms of viability. On TCPS, the number of the attached cells increased rapidly from ~100% at 2 h after cell seeding to ~257% at 6 h after cell seeding, based on the initial number of cells seeded (40,000 cells/well). While, the number of cells attached on these fibrous scaffolds was lower in comparison with that on TCPS at any given time point. There was the most viability of cells on crude bone protein-immobilized PCL fibrous scaffold among various types of the modified fibrous scaffolds. This obtained result suggested that the cells prefer to adhere on CBP-immobilized PCL fibrous scaffold rather than other modified scaffolds. However, The lesser viability of cells in the attachment period on various types of the fibrous scaffolds in comparison with that on TCPS could be due to the lesser number of cells that were able to

attach on the rough surface of the fibrous scaffolds in comparison with the smoother and hydrophilic surface of TCPS.

Figure 4.14 shows the proliferation of MC3T3-E1 on the surfaces of TCPS, neat PCL, aminolyzed PCL, activated PCL and protein-immobilized PCL on day 1, 2, and 3 after cell culture in terms of viability (%relative to TCPS at day1). On TCPS, the number of cells increased from ~100% at 1 day after cell culture to ~133 % at 3 days after cell culture, based on the initial 40,000 cells/well seeded. In comparison with that on TCPS, the viability of the cells cultured on various types of PCL fibrous scaffolds were significantly higher at any given time point. The viability of cells proliferated on these fibrous scaffolds, at day 3, was higher than TCPS of about (3 to 4) fold for neat PCL, aminolyzed PCL, and activated PCL and about 8 fold for all type of protein-immobilized PCL. The improvement was achieved with the protein-immobilized PCL fibrous scaffolds on day 3 after cell culture. The greater number of cells in the proliferation period on all types of fibrous scaffolds could be because of high surface area to volume and high porosity of the electrospun fibrous scaffolds through which the cells were able to penetrate into the scaffolds. Among the various modified PCL fibrous scaffolds, the BSA-immobilized PCL fibrous scaffolds provided the most significant improvement in the ability to support the proliferation of the cells which could be due to the protein-containing and more hydrophilic surface of the substrate.

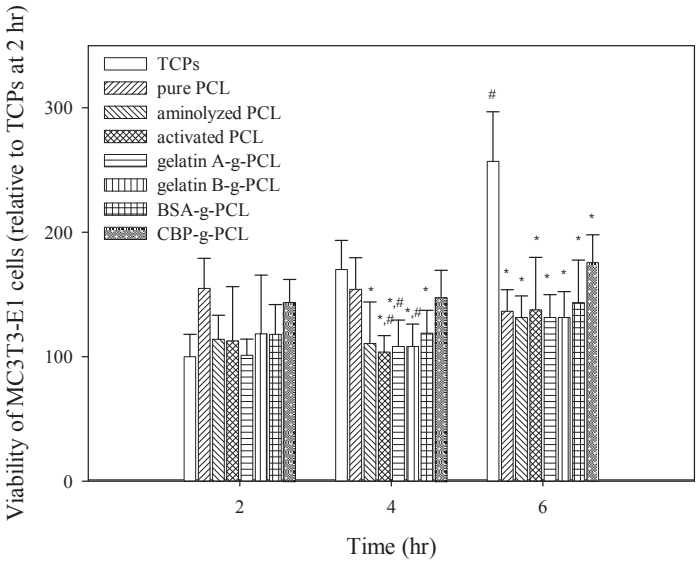


Figure 4.13 Attachment of MC3T3-E1 that had been seeded or cultured on the surfaces of TCPS and the neat and the modified PCL fibrous scaffolds for 2, 4, and 6 h. Statistical

significance: $*p < 0.05$ compared with control and $^{\#}p < 0.05$ compared to the neat PCL fibrous scaffolds at any given time point.

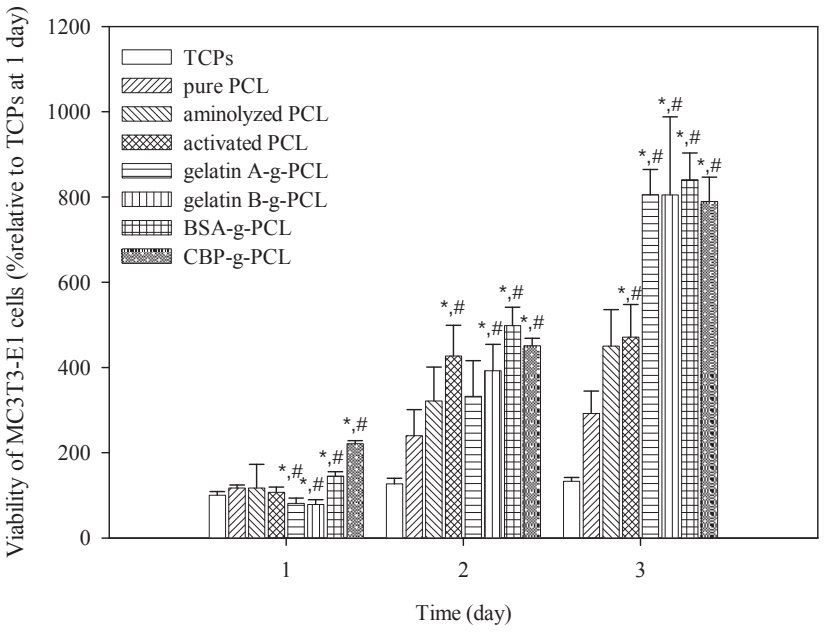


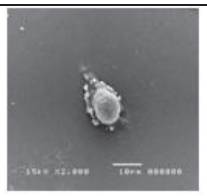
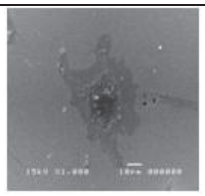
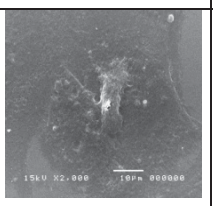
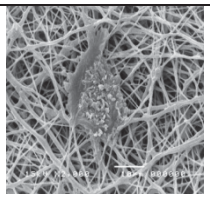
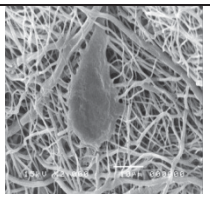
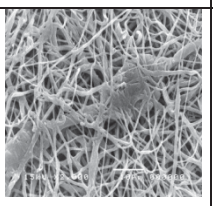
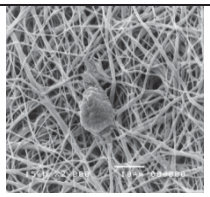
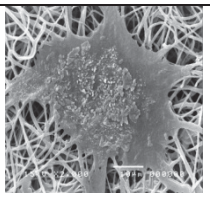
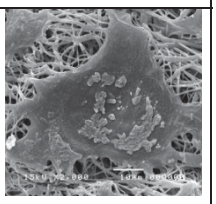
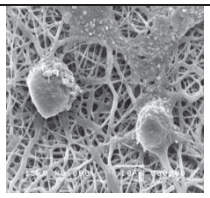
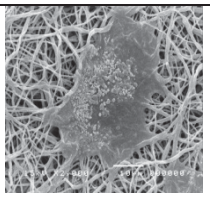
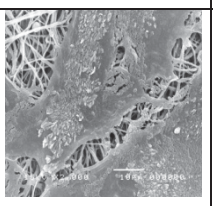
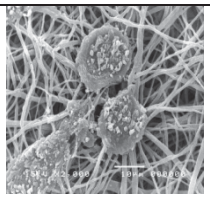
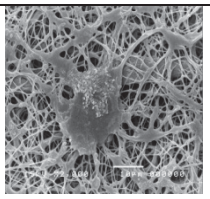
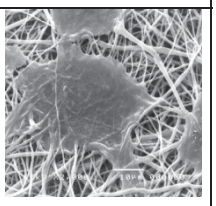
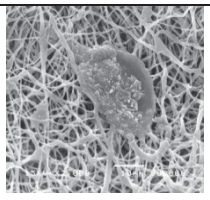
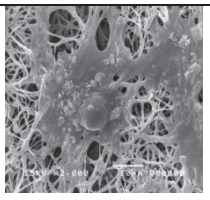
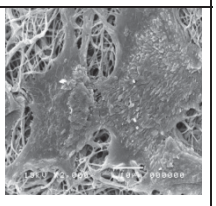
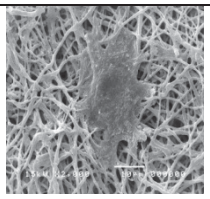
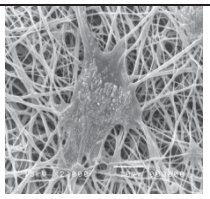
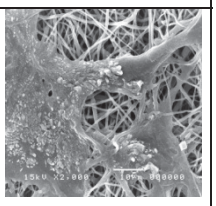
Figure 4.14 Proliferation of MC3T3-E1 that had been seeded or cultured on the surfaces of TCPS and the neat and the modified PCL fibrous scaffolds for 1, 2, and 3 days. Statistical significance: $*p < 0.05$ compared with control and $^{\#}p < 0.05$ compared to the neat PCL fibrous scaffolds at any given time point.

4.4.3 Cell Morphology

Table 4.6 and 4.7 show selected SEM image (magnification = 2000X; scale bar = 10 μm) of MC3T3-E1 that were cultured on the surfaces of neat PCL, activated PCL and gelatin type-A, gelatin type-B, bovine serum albumin, and crude bone-immobilized PCL at different time points. These images provided snap shots in time that revealed the morphology of the cells and interaction between the cells and the tested surfaces. At 2 hours after cell seeding, based on the initial 40,000 cells/well seeded, the morphology of cells on almost all types of the modified PCL scaffolds became round. Exceptionally, the morphology of cells on BSA-immobilized and CBP-immobilized started to extend their cytoplasm and became ellipse. At 4 h after cell seeding, the majority of the cells on all types of modified PCL scaffolds extended their cytoplasm, an evidence of the ability of the cells to attach on the modified surface. At 6 h after cell seeding, expansion of the cytoplasm of the majority of the cells was evident. The majority of MC3T3-E1 that had been seeded on the surfaces of unmodified PCL

fibrous scaffolds for 4 h was remained round, but a closer examination around the edge of the cells revealed an evidence of filopodia. The majority of the cells were evidently expanded after 6 h of cell seeding. On the other hand, the majority of the cells seeded on the surfaces of various types of modified PCL fibrous scaffolds showed an evidence of the extension of their cytoplasm on the fibrous surface even at 4 h after cell seeding. These results suggested that the cells prefer the fibrous surfaces of modified PCL over that of the unmodified. At 1,2, and 3 days after cell seeding, the majority of the cells seeded on the surfaces of all types of modified PCL fibrous scaffolds expanded over the area of the scaffolds which was the most expansion on the surface of BSA-immobilized and CBP-immobilized PCL fibrous scaffolds. From the attachment, proliferation and cell morphology results, we can suggest that the cell prefer to grow and expand on BSA-immobilized and CBP-immobilized PCL fibrous scaffolds over other materials.

Table 4.3 Selected SEM images of cultured specimens, i.e., glass (i.e., control), neat PCL, aminolyzed PCL, activated PCL, and protein-immobilized PCL fibrous scaffolds at various time points after MC3T3-E1 were seeded on their surfaces (magnification = 2,000X; scale bar = 10 μm)

Material	2 h	4 h	6 h
Glass (control)			
Neat PCL			
Aminolyzed PCL			
Activated PCL			
Gelatin A immobilized PCL			
Gelatin B immobilized PCL			
BSA immobilized PCL			

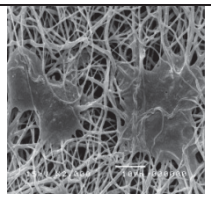
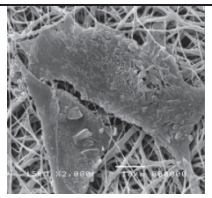
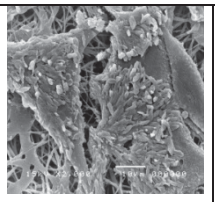
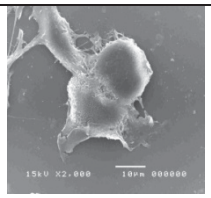
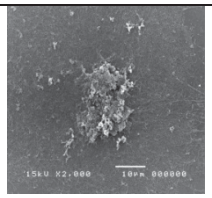
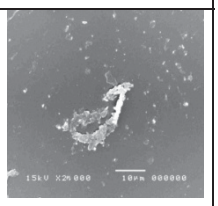
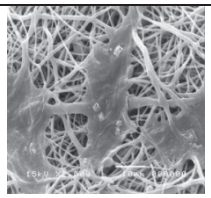
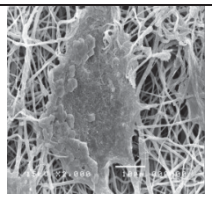
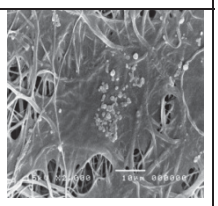
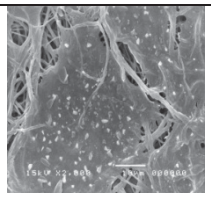
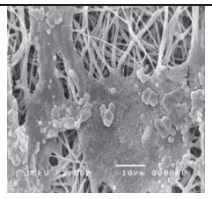
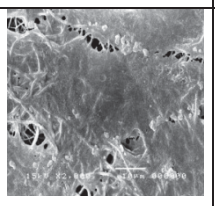
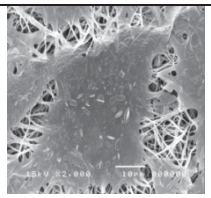
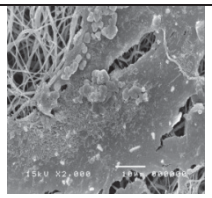
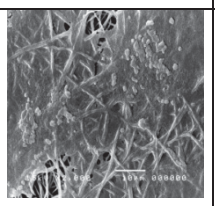
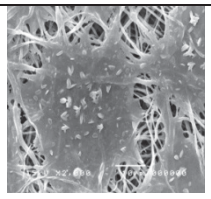
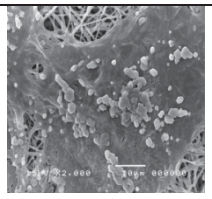
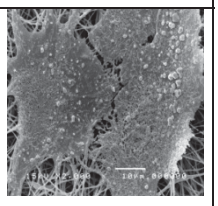
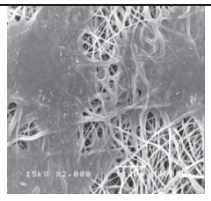
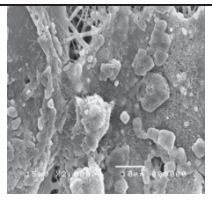
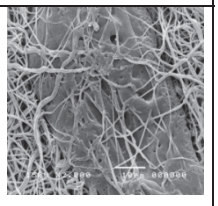
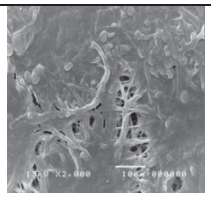
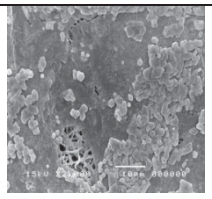
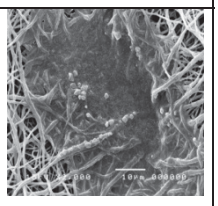
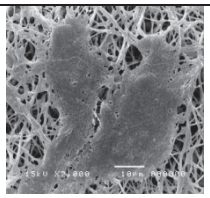
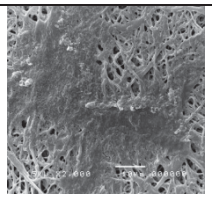
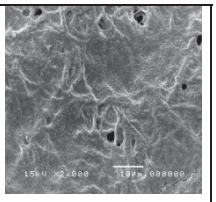
CBP immobilized PCL			

Table 4.4 Selected SEM images of cultured specimens, i.e., glass (i.e., control), neat PCL, aminolyzed PCL, activated PCL, and protein-immobilized PCL fibrous scaffolds at various time points after MC3T3-E1 were seeded on their surfaces (magnification = 2,000X; scale bar = 10 μm)

Material	1 day	2 day	3 day
	2000x	2000x	2000x
Glass(control)			
Neat PCL			
Aminolyzed PCL			
Activated PCL			
Gelatin A immobilized PCL			
Gelatin B immobilized PCL			
BSA immobilized PCL			

CBP immobilized PCL			

4.4.4 Alkaline Phosphatase Activity (ALP)

The ability for these PCL fibrous scaffolds to support differentiation, in addition to attachment and proliferation, of cultured cells is another important purpose suggesting potential for use of the scaffold. Alkaline phosphatase is used as an osteoblastic differentiation marker, as it is produced only by cells showing mineralized ECM. The ALP activity of MC3T3-E1 on TCPS (i.e. controls), neat PCL, aminolyzed PCL, activated PCL, and protein-immobilized PCL were evaluated at 3 and 7 days in culture. Figure 4.15 apparently shows the amount of ALP synthesized by the cells that were cultured on TCPS and all of the fibrous scaffolds increased with the initial increase in time in culture. In comparison with other substrates, BSA immobilized PCL fibrous scaffolds exhibited the highest ALP activity of MC3T3-E1 which is close to that of the activated PCL and TCPS at day 7 of cell culturing time. From the obtained results, it was suggested that BSA-immobilized PCL fibrous scaffold was the best among the fibrous scaffolds that promoted both proliferation and differentiation of MC3T3-E1. However, additional long term experiments in order to clarify the effect of scaffolds on the differentiation of osteoblasts are currently determined.

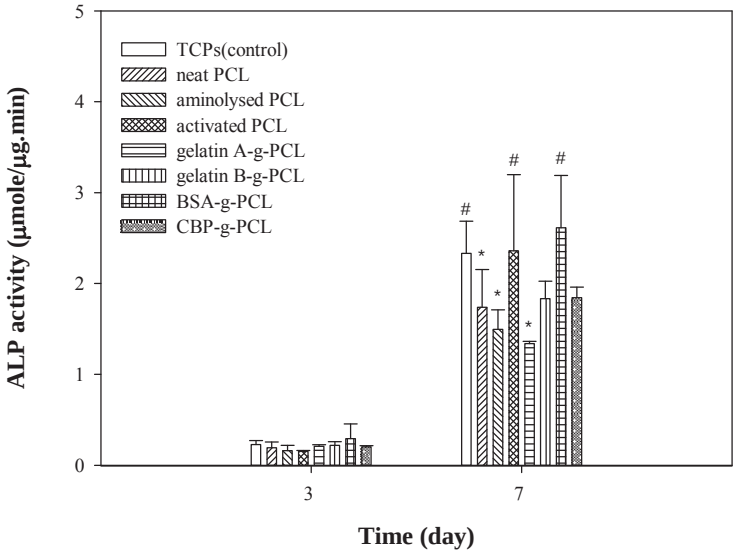


Figure 4.15 Alkaline phosphatase activity (ALP) of MC3T3-E1 that were cultured on the surfaces of TCPS and the neat and the modified PCL fibrous scaffolds for 3 and 7 d. Statistical significance: $*p < 0.05$ compared with control and $^{\#}p < 0.05$ compared to the neat PCL fibrous scaffolds at any given time point

4.4.5 Mineralization

Mineralization was quantified by Alizarin Red-S which is a dye that binds selectively calcium salts. The strain was extracted with 10 % cetylpyridinium chloride in 10 mM sodium phosphate for 1 hour and the absorbance of collected dye was read at wavelength 570 nm in spectrophotometer (A Thermo Spectronic Genesis10 UV-visible spectrophotometer). The absorbance is relative to the quantity of deposited minerals on the materials as shown in Figure 4.16. The images of scaffolds seeded with MC3T3-E1 for 21 days and stained with Alizarin Red-S illustrated in Figure 4.17 confirmed that the above data where high intensity of stained minerals were observed on all type of immobilized PCL scaffolds. and. The CBP-immobilized PCL scaffolds showed the highest mineral deposition compared with control, neat PCL, and other modified materials. This result can be used to support that the crude bone protein immobilization is an attractive method to be used for fabrication of further developed fibrous scaffolds for bone tissue engineering.

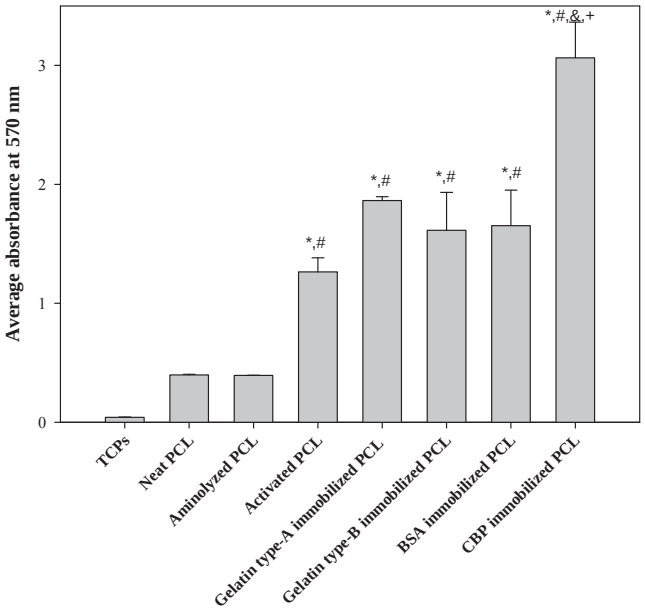


Figure 4.16 Quantification of mineral deposition in MC3T3-E1 at 21 d by the method of Alizarin Red-S staining measured the absorbance by UV-vis spectrometer at 570 nm. Statistical significance: $^{*}p < 0.01$ compared with control, $^{\#}p < 0.01$ compared to the neat PCL, $^{\&}p < 0.01$ compared with gelatin type-A immobilized PCL, and $^{+}p < 0.01$ compared with gelatin type-B immobilized PCL fibrous scaffolds at any given time point.

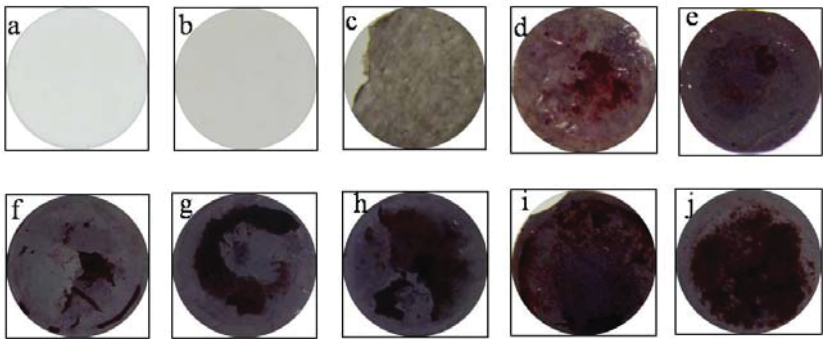


Figure 4.17 Image of Alizarin Red-S staining for the mineralization in MC3T3-E1 cells for 21 d: TCPS without (a) and with (b) cells , neat PCL without (c) and with (d) cells, aminolyzed (e) and activated PCL (f),and gelatin type-A (g), gelatin type-B (h), bovine serum albumin (i) and crude bone protein (j) immobilized PCL fibrous scaffold

3. Conclusions

Polycaprolactone fibrous scaffolds were prepared by electrospinning process from a neat 12 % w/v PCL solution in 50:50 v/v DCM/DMF. The PCL electrospun fibrous scaffolds with a thickness of (130 ± 5) μm were obtained. The scaffold was subsequently immersed in various concentrations of 1,6-hexamethylene diamine (HMD) / isopropanol (IPA) solution (0.04, 0.06, 0.08, 0.10, 0.20, and 0.40 g/ml) for 2 hours at 30 °C. To determine the optimum concentration of HMD used in the step of aminolysis, ninhydrin method, degradation experiment, water retention experiment and SEM observation were used. The results show that the optimum condition for aminolysis are 0.20 g/ml HMD treatment for 2 hours at 30 °C. Density, porosity, and pore volume were evaluated to characterize the electrospun scaffolds. The NH_2 density on the aminolyzed PCL surface was confirmed and quantified using ninhydrin method. The NH_2 density increased with increasing 1,6-hexamethylenediamine concentration. However, when the concentration of 1,6-hexamethylenediamine is greater than 0.20 g/ml, the structural morphology of the electrospun PCL fiber scaffolds became worse. In the other word, water contact angle slightly decreased with increasing HMD concentration. This means that aminolysis can improve the hydrophilicity of the surface. Macromolecules i.e. gelatin type-A, gelatin type-B, bovine serum albumin, and crude bone protein were further immobilized using *N*,*N*'-disuccinimidyl carbonate (DSC) as a coupling agent. Various techniques; Attenuated Total Reflectance-Fourier Transform Infrared Spectrometer (ATR-FTIR), X-ray Photospectroscopy (XPS), Scaning Electron Microscopy (SEM), and water contact angle measurement were used to monitor the scaffold surfaces after each modification step. In XPS experiment, The N_{1s}/C_{1s} ratio was increased after immobilization with proteins (gelatin type-A, gelatin type-B, bovine serum albumin and crude bone protein) due to the large amount of nitrogen atom in protein structure was introduced. The potential use of the surface-modified PCL scaffolds as bone scaffolds was evaluated with a murine pre-osteoblastic cell line (MC3T3-E1). The cytotoxicity test showed all types of proteins and PCL fibrous scaffolds released no substances at levels that were harmful to cells. The number of cells attached on these fibrous scaffolds was lower in comparison with that on TCPS at any given time point. There was the most viability of cells on crude bone protein-immobilized PCL fibrous scaffold among various types of the modified fibrous scaffolds. MC3T3-E1 proliferation was improved remarkably on the modified surface, with the cells growing on the bovine serum albumin-immobilized PCL fibrous scaffolds showing the greatest proliferation after cell culture as well as the highest ALP activity. In long term experiments, the image of scaffolds seeded with MC3T3-E1 for 21 days and stained with Alizarin Red-S and quantification of deposited minerals measured by UV-vis spectrometer confirmed that high intensity of stained minerals were observed on all type of immobilized PCL scaffolds. The CBP-immobilized PCL scaffold showed the

highest mineral deposition compared with control, neat PCL, and other modified materials. This result supported that the crude bone protein immobilization was able to induce the cell differentiation to bone the most. All the obtained results suggested that bovine serum albumin and crude bone protein immobilization are an attractive method to fabricate of further developed fibrous scaffolds for bone tissue engineering.

4. DEVELOPMENT OF POROUS HYDROXYAPATITE PARTICLES AS CARRIERS OF PROTEINS FOR BONE TISSUE ENGINEERING

Experimental section

4.1 Materials

- Dicalcium phosphate dihydrate (DCPD; Fluka, Germany)
- Calcium carbonate ($CaCO_3$; Carlo Erba, Italy)
- Tris-base (Tris[hydroxymethyl]amino methane) (Sigma-Aldrich, USA)
- Nitric acid (ACS reagent 69%; J.T.Baker, USA)
- Ovalbumin (OVA; Sigma-Aldrich, USA)
- Gelatin type B (Sigma-Aldrich, USA)
- Bovine serum albumin (BSA; Sigma-Aldrich, USA)
- Sodium phosphate monobasic (NaH_2PO_4) and sodium phosphate dibasic (Na_2HPO_4; Ajex Finechem, Australia)

4.2 Preparation of Protein-Loaded Hydroxyapatite

Calcium hydrogen phosphate dihydrate ($CaHPO_4.H_2O$, DCPD) and calcium carbonate ($CaCO_3$) were used as precursors of Ca and P to prepare protein-loaded hydroxyapatite. The molar ratios of Ca to P were fixed at 1.67 which mixed with nitric acid 1 mol/l at 75 ºC for 1 h under stirring. Then, pour distilled water at room temperature following protein. Ovalbumin (Sigma-Aldrich A-5253), Gelatin type B, Bovine serum albumin (BSA, Aldrich A-3912) and Crude bone protein from pork bone were selected as candidate proteins in this study. The proteins aqueous solution were prepared by dissolving proteins powder or pellet into distilled water for each synthesis. Regulated pH at a constant value, tris(hydroxymethyl) aminomethane. The aggregates were rinsed with the distilled water until pH=7 (DI water was boiled and decarbonated before use) and further centrifuged at 4500 rpm for 10 mins, freezed at -45 ºC and lyophilized at -50 ºC. The samples were kept in dessicator until used.

4.3 Crude Bone Protein preparation

CBP was extracted from the pork bone. In particular, bone was initially washed and cleaned thoroughly in tap water and then sectioned into small pieces with a high speed motor machine. Pieces of bones were further crushed into powder in liquid nitrogen. Then, the as-prepared powder was immersed in 0.6 N HCl at 4 °C. After three days, the bony solution was centrifuged and the supernatant was collected, dialyzed for 48 h and lyophilized. The dry CBP was kept in desiccators until use (Hariraksapitak, *et al*., 2009).

4.4 Characterization

4.4.1 Thermogravimetric Analysis (TGA)

The relative amount of the proteins associated with the HAp was determined using thermogravimetric analysis, TG-DTA (Perkin Elmer) instrument under N_2 flow of 5 ml/min. The heating process was conducted from 30-950 °C at a rate of 10 °C/min.

4.4.2 Fourier-transformed infrared spectrophotometer (FT-IR)

A Thermo Nicolet Nexus® 670 Fourier-transformed infrared spectrophotometer (FT-IR) was used to investigate chemical functionalities of hydroxyapatite powder by the KBr disk method. Hydroxyapatite powders were randomly selected from each group of samples and detected for the FT-IR spectra with a resolution of 4 cm^{-1} in the range of 4000-400 cm^{-1} and were averaged from 32 scans.

4.3 Autosorb-1

The BET method uses gas with a known adsorption area per 1 g to measure the surface area of samples based on gas quantites adsorbed to the sample surface. Fifty mg of the sample was preheated at 200 ºC for 10 min to remove water and gas completely. Surface areas of HAp particles were analyzed by nitrogen adsorption in a Autosorb-1.

4.4 Scanning Electron Microscope (SEM)

For the morphological study, hydroxyapatite were mounted on brass stubs, coated with gold using a JEOL JFC-1100 sputtering device, and observed for their microscopic morphology using JEOL JSM-5200 scanning electron microscopy (SEM). For the morphology of the surface, pore size, distribution and also the interconnectivity.

4.5 Transmission Electron Microscope (TEM)

The microstructural and morphological features of HAp powders were analysed in JEM-2100 operating voltage of 200 kV. Sample for TEM were prepared by air-drying a drop of a sonicated ethanol suspension of particles onto a carbon-coated copper grid and air-dried.

4.6 Energy Dispersive Spectrophotometer (EDS)

The Ca/P ratio of the hydroxyapatite was studied by the X-ray microanalysis, using the method of Energy dispersive X-ray spectroscopy (EDS). EDS is an analytical technique used for the elemental compositions of the HAp.

4.7 X-ray Diffraction (XRD)

The phase compositions, crystal shape and size of HAp powders were characterized by X-ray diffraction (XRD) with copper target. Data were collected over the scanning range (2θ) from 5 º to 60 º at a scan speed 2 º /min.

The average crystallite size of the prepared hydroxyapatite samples was determined using the scherrer equation.

$$D = K \cdot \lambda / \beta \cdot \cos\theta$$

In which D is the average crystallite size (Å), K denotes the shape factor (K=0.9), λ is the X-ray wavelength (for CuKα λ=1.5418 Å), β represents the peak at half width (in rad), and θ is the Bragg angle of the peak (002 reflection of hydroxyapatite at 2θ=26 º).

4.8 UV-Visible Spectrophotometer

Determination of protein by UV/Vis spectrophotometry at 215 nm for Gelatin type B, 280 nm for OVA and BSA and 275 nm for CBP.

4.9 Zeta potential (ZP)

Zeta potentials (or electrophoretic mobility) of the hydroxyapatite were determined using Zeta-Meter 3.0+ (Zeta-Meter, Inc., USA). Briefly, the suspension of 100 mg hydroxyapatite in 20 ml of deionized water was filled in an electrophoresis cell. Two electrodes were inserted into the cell and connected to the Zeat-Meter 3.0+ unit. Once the electrodes were energized, microspheres were aroused to move toward one electrode. Particles were observed under a microscope for its movement along a specific distance which was indicated by a built in grid. The zeta potential value was detected at a right time point when the microsphere moved to the end. Measurement was repeated 10 times for each preparative condition and the average values were calculated.

4.10 Particle size distribution

The Malvern Particle size of hydroxyapatite was measured by Mastersizer 2000 a solution of the particles was sonicated in an ultra-sonic bath for 7 min immediately before measurement to ensure separation of particles. A sample of this mixture was injected into the sample cell of the Malvern Mastersizer. The obscuration was between 10 and 30 %, as required by the instrument. The Mastersizer calculates automatically the particle size and distribution from small angle light scattering using Mie theory and Fraunhofer diffraction theory. The measurements were taken with the stirrer in the Mastersizer to ensure even distribution of particles and prevent sedimentation in the sample cell. Shear forces were not a

problem in this case as the goal was to measure the primary particle size. A least 10 measurements were recorded and the average value recorded.

4.11 In vitro protein-HAp release test

Proteins-loaded Hydroxyapatite (20 mg) were dispersed in 10 ml 0.1M phosphate buffer saline (PBS) solution at pH 7.4. All samples were incubated in a shaking water bath (70 rpm) at 37 ºC. The releasing medium was withdrawn 1 ml and an equal amount of fresh medium was added to maintain a constant volume of the medium. The amount of protein in the sample solution was determined by UV-visible spectroscopy. Absorbance peaks at 280 nm to determine the ovalbumin and BSA concentration, 215 nm to determine the gelatin type B, and 275 nm to determine the crude bone protein. Concentration through the use of a pre-determined standard concentration—intensity calibration curve. An average value was calculated at each time point. The protein content of the encapsulated particles can be described by two quantities in terms of Encapsulating efficiency of protein-loaded hydroxyapatite (EE) and Loading capacity of hydroxyapatite particle (LC), which were determined according to the following equation (Freiberg and Zhu, 2004).

$$\text{Encapsulating efficiency (\%)} = \frac{\text{total mg proteins-encapsulated}}{\text{initial mg proteins-loaded}} \times 100$$

$$\text{Loading capacity (\%)} = \frac{\text{total mg proteins-encapsulated}}{\text{total mg particles}} \times 100$$

4.4 Results and Discussion

4.4.1 Thermogravimetric Analysis (TGA)

The samples were analyzed by TGA using a Perkin Elmer (TG-DTA) instrument under N_2 flow of 5 ml/min. The heating process was conducted from 30-950 °C at a rate of 10°C/min. To investigate amount of proteins-loaded hydroxyapatite.

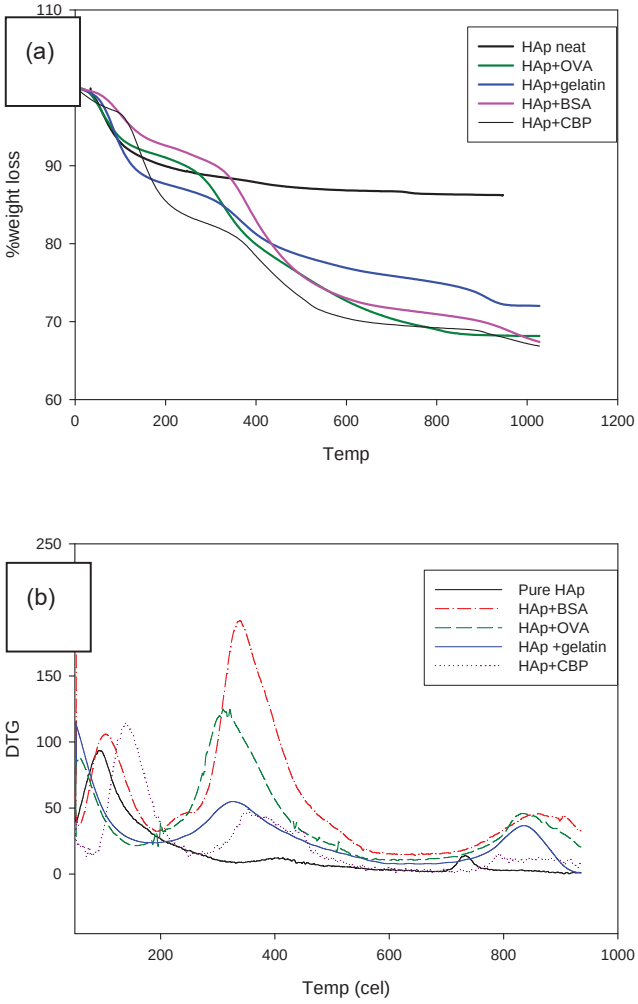


Figure 4.1 TGA-DTG curves (a) TGA, (b) DTG of proteins-loaded hydroxyapatite**.**

The features of TGA and DTA profiles of proteins-loaded hydroxyapatite were presented in Figure 4.1. The weight loss could be differentiated into three regions in the investigated temperature range such as (i) 25-210 ºC, (ii) 210-570 ºC, and (iii) 750-950 ºC. In the first region of 25-210 ºC, the weight loss for all precursors could be attributed to the removal of physically absorbed water. The second region of 210-570 ºC is a major weight loss, probably due to the combustion of proteins residuals (organic matter) and with the maximum rate at 350 ºC, and decomposition of calcium hydroxide and carbonate to water and carbon dioxide. The third region of 750-950 ºC, the weight loss can be assigned to the decomposition of carbonate compounds.

The TGA curves of the samples (Figure 4.1) show differences in the amount of protein weight loss. Weight loss of ovalbumin was 16.8 %, Gelatin type B was 10.22 %, BSA was 20.61 % and CBP from pork bone was 22 %.

4.4.2 UV-Visible Spectrophotometer

Take water after finish synthesis reaction measured by UV-Visible to determine the remaining protein after reaction. OVA and BSA were measured the wavelength with 280 nm, Gelatin type B with 215 nm and CBP from pork bone with 275 nm.

To investigate amount of proteins-loaded hydroxyapatite. Remainning OVA in the DI water is 6.12 %, Gelatin type B is 14.30 %, and BSA is 2.38 %. So, OVA, Gelatin type B, and BSA are entrapped in hydroxyapatite 20.26 %, 12.08 %, and 24% respectively. It is possible that protein may be lost during the washing HAp with DI water about 5-6 times to become neutral.

4.4.3 X-ray Diffraction

In the X-ray diffraction analysis, all synthesized precipitates showed a HAp-like pattern (Figure 4.2). The crystallinity of each precipitate was evaluated from the data of the inverse of half value breadth of the (002) peak of HAp (Figure 4.2). The crystallinity of HAp depends on its synthesized temperature in such a way that HAp synthesized at low temperature has low crystallinity. The solubility of HAp also depended on its synthesized temperature and HAp synthesized at low temperature showed high solubility (Matsumoto, T. *et al*., 2004).

For HAp powders, the crystallite size in a direction perpendicular to the crystallographic plane is always estimated according to Scherrer's formula as followed:

$$d = (0.9\lambda) / FWHM*Cos\theta$$

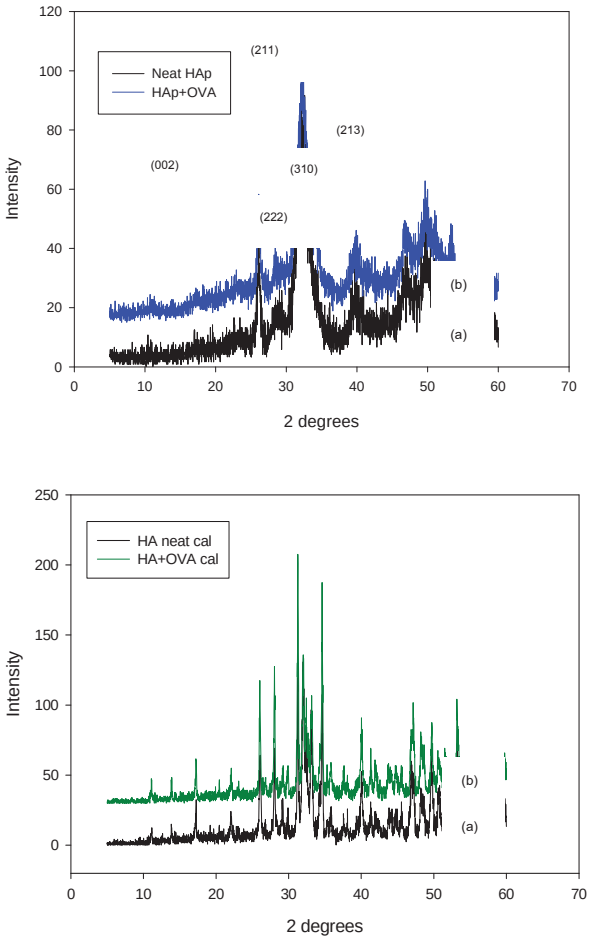


Figure 4.2 XRD pattern of HAp powders : (a) Neat HAp; (b) OVA-loaded HAp.

where d is the crystallite size (nm); λ=0.15406 nm for Cu Kα radiation of X-ray beam; FWHM the full width at half maximum for the diffraction peak (rad); and θ is the Bragg angle of the (002) diffraction angle (º). Two major characteristic diffraction peaks could be obtained for all the powdered samples: one closed at 2θ of ~26 º and the other broad one at ~32 º. According to PDF no.01-1008, The uncalcined HAp is shown the broad patterns around at (002) and (211). It indicates that the crystallites were very tiny in nature. The (002) peak (2θ~26 º) from XRD patterns was chosen for calculating the crystallite size as shown in Table 4.1 since it contains the least overlap of the broadened peaks. It could be found that the crystallite size depends on the size of the particle that observed from SEM. Crystallite size of calcined HAp powders was larger than uncalcined powder. Figure 4.2 indicated

that uncalcined HAp powders were amorphous and did not form CaP crystals, because HAp crystallization is mediated by protein and shown in Figure 4.3.

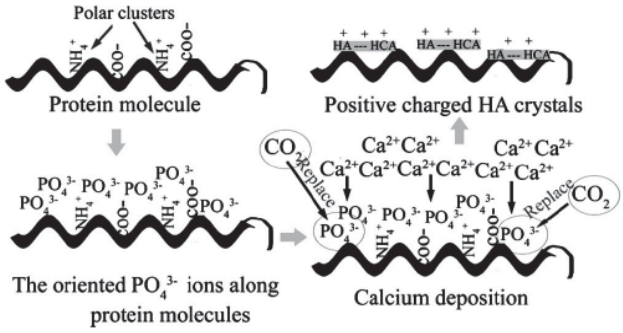


Figure 4.3 Schematic illustration of the protein-medicated crystallization of HAp crystals with positive charges (Zhao, H. *et al*., 2008).

Table 4.1 The different crystallite size of (a) calcined HAp at 800 ºC; (b) uncalcined HAp powder

(a)

Crystal plane (002)	2θ	FWHM	Crystallite size (nm)
Neat HAp calcine	26.07	0.22	40.01
OVA-HAp calcine	26.05	0.15	58.16
Gealtin-HAp calcine	26.00	0.23	38.37
BSA-HAp calcine	25.82	0.23	37.03

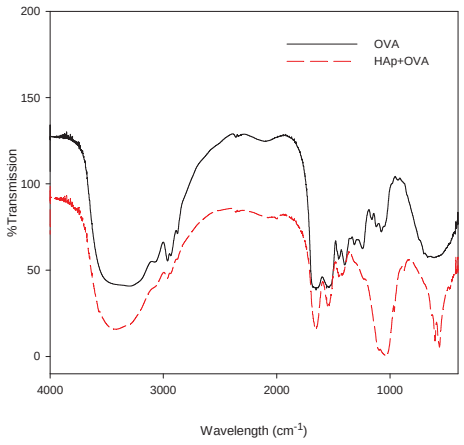
(b)

Crystal plane (002)	2θ	FWHM	Crystallite size (nm)
Neat HAp uncalcine	26.11	0.44	20.45
OVA-HAp uncalcine	26.12	0.51	17.69
Gelatin-HAp uncalcine	25.80	0.51	19.37
BSA-HAp uncalcine	25.91	0.51	16.88

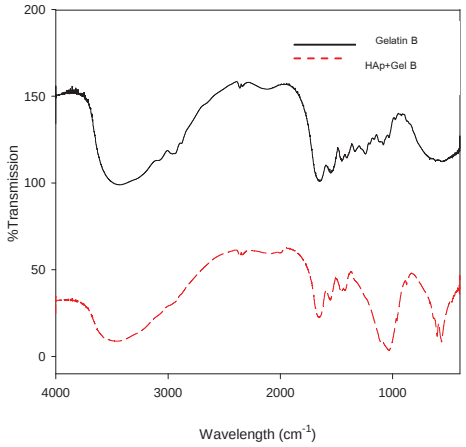
4.4.4 Fourier-Transformed Infrared Spectrophotometer

Adsorption of protein on HAp particles was detected by FTIR analysis (Figure 4.4). The spectra show the characteristic peaks of absorbed water, hydroxyl, phosphate and carbonate species. The broad peak around 3250 cm^{-1} to 3500 cm^{-1} corresponds to the adsorbed water. The spectrum clearly indicates a peak at 1640 cm^{-1} which is attributed to the presence of water associated with HAp. The

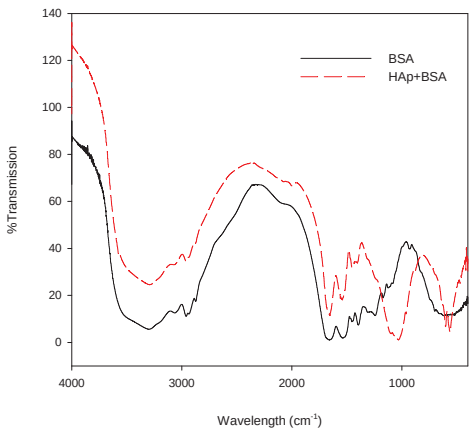
absorption bands at 1460 cm^{-1} and 875 cm^{-1} suggest the presence of CO_3^{2-}. The absorption bands at 1040, 1093, 962 and 571 cm^{-1} detected in the spectra are attributed to the PO_4^{3-} ion. The absorption bands at 1210 cm^{-1} together with one at 1130 cm^{-1} and clear absorption band at 879 cm^{-1} are attributed to the HPO_4^{2-}. The spectrum of protein exhibited an appearent absorption band at 1654 cm^{-1} assigned to amide I, C=O stretching mode. The absorption band at 1540 cm^{-1} assigned to amide II, N-H bending mode and 1384 cm^{-1} assigned to amide III, C-N stretching mode and N-H bending mode.



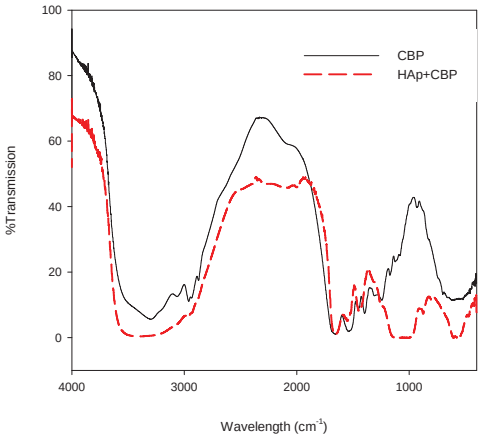
(a)



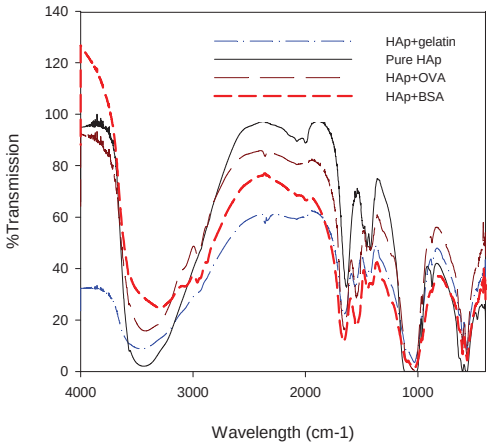
(b)



(c)



(d)



(e)

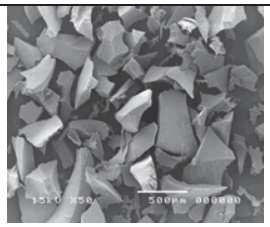
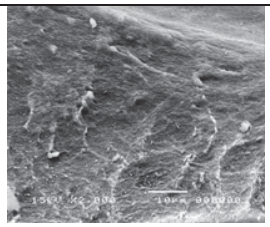
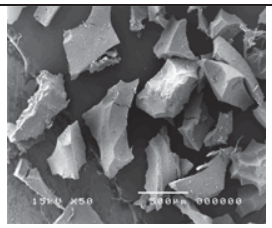
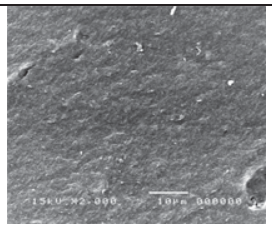
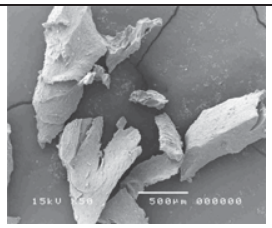
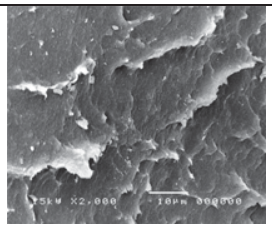
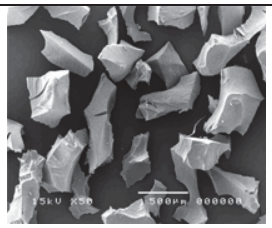
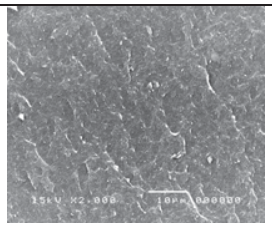
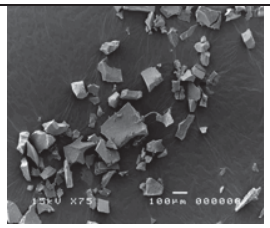
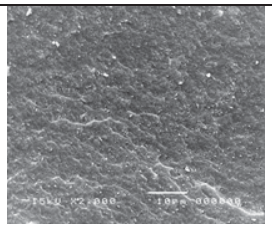
Figure 4.4 The FTIR spectra of HAp powders of : (a) OVA-loaded HAp; (b) Gelatin-loaded HAp; (c) BSA-loaded HAp; (d) CBP-loaded HAp; (e) including protein/HAp.

The possible mechanisms can be adapted to explain the interaction between the HAp and proteins molecules. The mechanism can be operated through the electrostatic interaction between the positive Ca^{2+} and COO^{-} (protein): this has been also reported by Liu who suggested that there is an intermediate complex between COO- and HAp. This complex can be formed via the electrostatic interaction between the negative COO^{-} on protein molecules and positive Ca^{2+} on the C-sites of HAp surface. Kazuhiko K. indicated that the C-sites were located on the crystal planes that are perpendicular to a-axis and b-axis of apatite crystal.

4.4.5 Scanning Electron Microscope (SEM)

To investigate the morphology of HAp powder by using SEM (JEOL, model JEM-5200). It is found that HAps have an arbitrary shape. Some gelatin grafting on the surface of HAp shown in Table 4.2.

Table 4.2 SEM of proteins-loaded HAp powder

	X200	X2000
Neat HAp		
HAp+OVA		
HAp+gelatin		
	X200	X2000
HAp+BSA		
HAp+CBP		

4.4.6 Transmission Electron Microscope (TEM)

Figure 4.5 shows the TEM photographs of HAp powders obtained neat HAp and proteins-loaded HAp. The HAp powders contain agglomerated particles consisting of rod-like shaped particle. Neat HAp powders are the short-rod crystal than proteins-loaded HAp. It is found that there are not much differences in morphology and size from the photographs of proteins-load HAp samples.

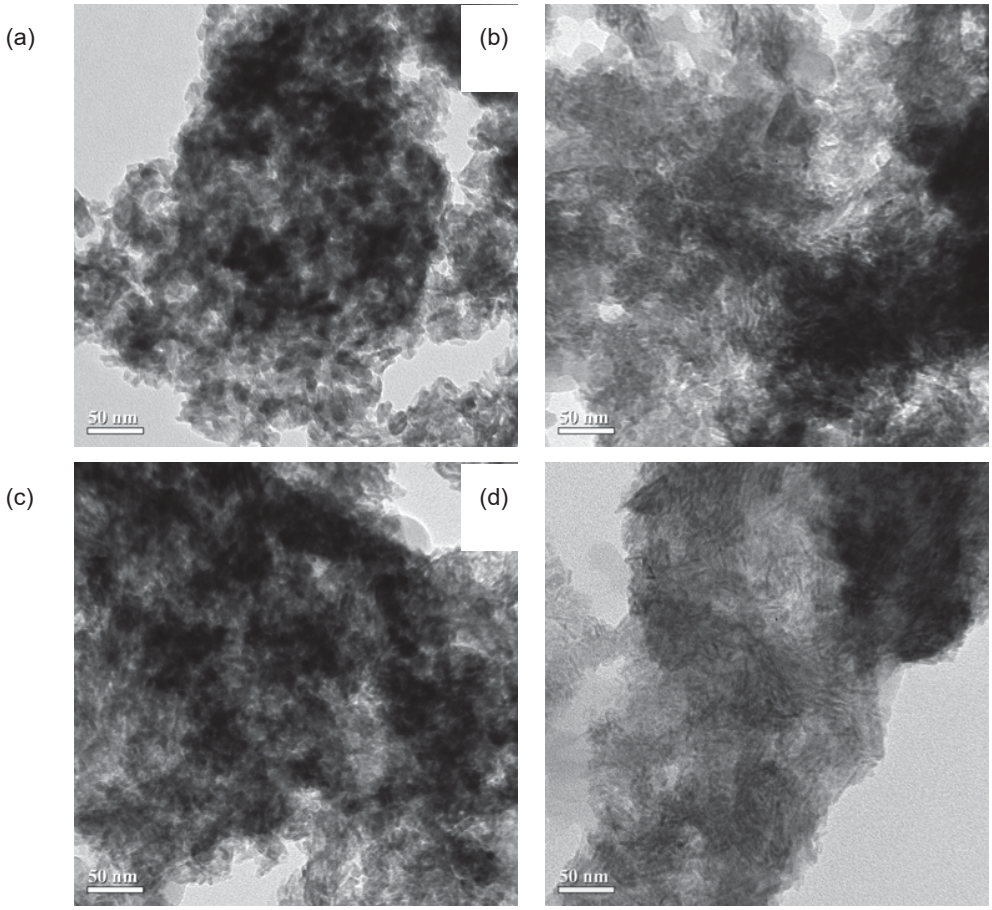


Figure 4.5 TEM micrographs of proteins-loaded HAp powder : (a) Neat HAp; (b) OVA-loaded HAp; (c) Gelatin-loaded HAp; (d) BSA-loaded HAp.

4.4.7 Zeta Potential (ZP).

Twenty mililiter of the suspension was placed in an electrophoresis cup, and the movable images of the particles were recorded by the electrophoresis apparatus. The value would also be beneficial in the study of protein-loaded HAp and releasing through HAp particles. The zeta potentials were measured by appling the electric field in the dispersion and particles in the dispersion will be migrated to electrode of opposite charge. Protein-loaded HAps were dispersed in the DI water pH about 6-7 if protein can releases from HAp, it will be showed negative charge, so zeta potential is the positive. The zeta potentials of all the samples are negative, indicating that the particles themselves have superfluous positive electrical charges. It was indicated that protein entrapped in the HAp particle

The electrical conductivities values were so close as ~ -18, -16, and -20 mV for neat HAp, OVA-loaded HAp, and Gelatin B loaded HAp particle, respectively. Zeta potential is an indicator of charge

density (Brown *et al.*, 1998). Particle size of Gelatin B-loaded HAp is the largest, so it has the highest charge density.

4.4.8 Energy Dispersive Spectrophotometer

The EDS spectrum from HAp particles (Figure 4.6) shows the characteristic peaks of calcium (Ca), phosphorus (P), and oxygen (O). EDS is composed mainly of HAp and exhibits a molar Ca/P ratio of 1.67.

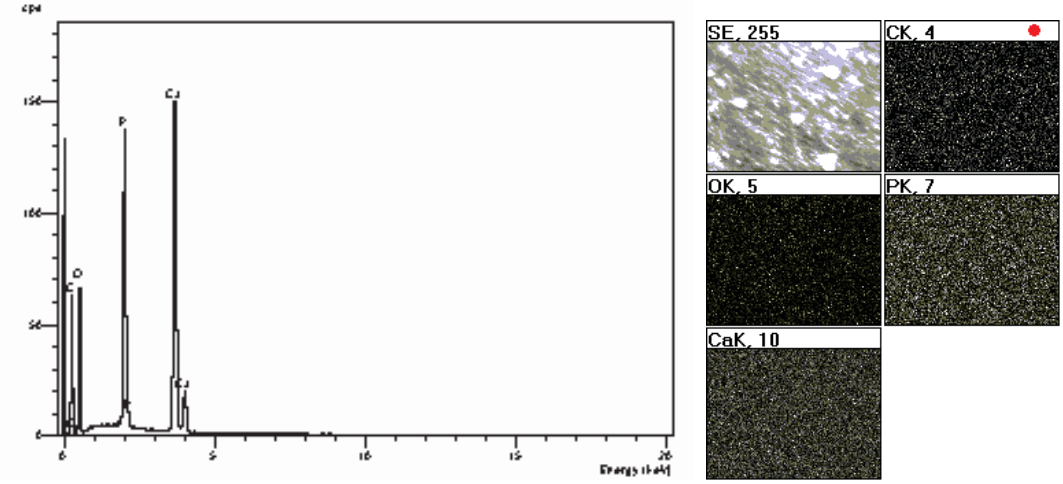


Figure 4.6 EDS spectrum of the biomimetic apatite layer deposited.

4.4.9 The Brunauer—Emmett—Teller (BET)

Surface areas and pore size of the powders were analyzed by nitrogen adsorption in Autosorb-1. The BET surface areas of the calcined samples at 800 ºC are summarized in Table 4.3. We found that they are a few differences in surface area and pore size of neat and proteins-loaded HAp. Pore size of proteins-loaded HAp are a few larger than neat HAp due to the existence of pores after the removal of organic materials (proteins) so, surface area of proteins-loaded HAp are a few lower than neat HAp.

Table 4.3 BET surface area and pore size of the calcined samples at 800 ºC

	Surface area (m^2/g)	Pore size (nm)
Neat HAp	22.64	8.75
OVA-loaded HAp	19.65	9.35
Gelatin-loaded HAp	20.06	11.42
BSA-loaded HAp	20.99	12.14

4.4.10 Particle size distribution of Hydroxyapatite

We were ground and sieved through a mesh size of 400 micron of protein-loaded HAp particles. About twenty miligrams of HAp were dispersed in water. The size distributions of HAp were measured by light scattering using particle sizer (Malvern, UK). The average particle size distributions of neat HAp and proteins-loaded HAp were about 316 μm.

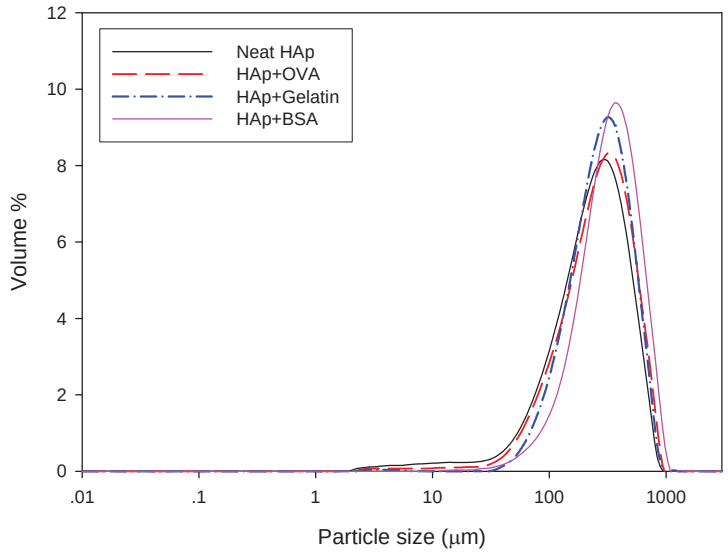


Figure 4.7 Average particle size distribution of Hydroxyapatite.

4.4.11 Controlled Release of Proteins from HAp particles

The protein content of the encapsulated particles can be described by two quantities in terms of encapsulating efficiency of protein-loaded hydroxyapatite (EE) and loading capacity of hydroxyapatite particle (LC). For encapsulating efficiency of protein-loaded hydroxyapatite (EE), the proteins release from hydroxyapatite in phosphate buffer saline solution pH 7.4 was shown in Figure 4.8. The release profile of OVA, BSA and CBP were shown long-term proteins release at least 3 week. The maximum accumulative releases were about 50 % - 60 %. For the release profile of gelatin type B, it was shown the bursting release. The accumulative release was about 12 %. For loading capacity of proteins-loaded hydroxyapatite (LC), the proteins release from hydroxyapatite in phosphate buffer saline pH 7.4 was shown in Figure 4.9. The LC of OVA, BSA, and CBP from HAp particles were shown maximum accumulative releases were about 8-12 %. For the LC of Gelatin type B from HAp particle was shown maximum accumulative releases was about 1 %. Encapsulation of proteins into hydroxyapatite particles in this study was on the basis of polyion complexation. It was expected that a degree of molecular interaction was able to take place between proteins and hydroxyapatite particles of opposite charges (Young *et al.*, 2005); as a consequence, a higher yield of the ionic complexes should result in higher encapsulation efficiency and loading capacity (Tabata and Ikada, 1998; Hoffman, 2002; Young *et al.*, 2005).

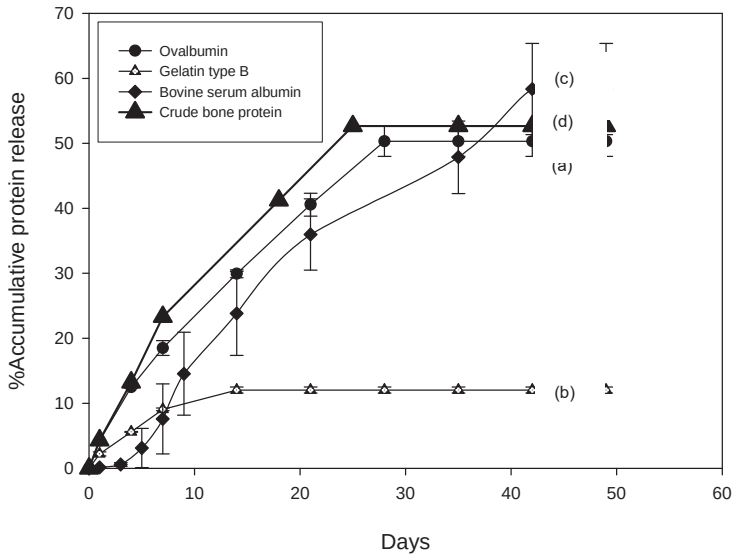


Figure 4.8 Encapsulating efficiency of protein-loaded hydroxyapatite (EE) : (a) Ovalbumin (OVA); (b) Gelatin type B; (c) Bovine serum albumin (BSA) and (d) Crude bone protein (CBP) release from HAp in phosphate buffer saline solution.

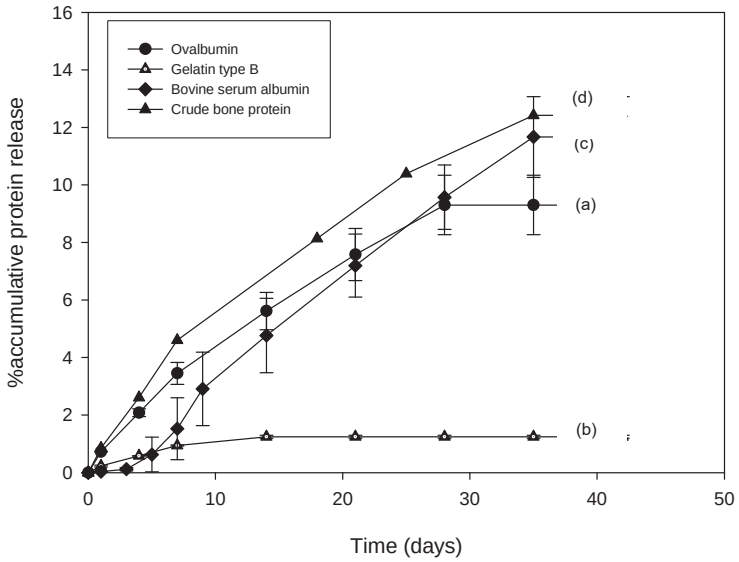


Figure 4.9 Loading capacity of protein-loaded HAp (LC) : (a) Ovalbumin (OVA); (b) Gelatin type B; (c) Bovine serum albumin (BSA) and (d) Crude bone protein (CBP) release from HAp in phosphate buffer saline solution.

4.5 Conclusion

The porous hydroxyapatite particle as a controlled release carrier of proteins were successfully synthesized by co-precipitation technique. The precursors were obtained DCPD and $CaCO_3$. Incorporation of proteins was accomplished during the co-precipitation of the two reactants. Characteristics of the HAp particles were determined by XRD, EDS, FT-IR, TGA, ZP, SEM, TEM, and Autosorb-1. Proteins-loaded HAps were dissolution tested in prolonged PBS solution. Proteins release could be regulated using HAp particles resulting in prolonged release of proteins except gelatin type B. Mechanism of proteins-loaded HAp release was believed to be the combination of diffusion or degradation of the carrier. Many factors play roles and synergistically control on the release of proteins from the hydroxyapatite which were electrostatic interaction between protein and hydroxyapatite.

5. DEVELOPMENT OF POROUS HYDROXYAPATITE PARTICLES AS CARRIERS OF PROTEINS IN A POLYCAPROLACTONE SCAFFOLD FOR BONE TISSUE ENGINEERING

Experimental

5.3.1 Materials

- Polycaprolactone (PCL;80,000 g mol^{-1}; Sigma-Aldrich, USA)
- Sodium chloride (Ajax Finechem, Australia)
- Chloroform (Labscan; Asia, Thailand)
- Modified Eagle's medium (MEM; Thermo Scientific, USA)
- Fetal bovine serum (FBS;Sorali, Campo Grande Brazil)
- 1% L-glutamine (Invitrogen Corp., USA)
- 1% Lactabumin (Invitrogen Corp., USA)
- 1% antibiotic (Invitrogen Corp., USA)
- Bicinchoninic acid (BCA; Thermo Scientific, USA)

5.3.2 Preparation of Polycaprolactone (PCL)-Hydroxyapatite (HAp) Scaffold

A solvent casting and salt particulate leaching was used to prepare the scaffold. Firstly, PCL granules were put into a glass bottle with chloroform to make up a PCL solution in the concentration of 14 percentages of polymer weight by volume of the solution (w/v), then the solution was stirred at room temperature for 2 h. Secondly, protein-loaded HAp were added into the glass bottle and they were stirred together. Thirthly, NaCl salt particles with size of 400 μm (PCL/NaCl = 1/30) (w/w) were added into the glass bottle and they were mixed together. And finally, the mixture was packed into the petri-dish with the dimension of 10x10 cm. The mold was then left in the hood for 24 h and immersed in the distill water 1 day for taking the mold out. The materials that come out were immersed in DI water for 2 days, during with time the water was changed approximately every 8 h under the room temperature for the leaching out the salt particles. Then the materials were air-dried for 24 h and freeze-dried overnight to obtain porous scaffolds (Prasansuklap *et al*., 2008).

5.4 Characterization of porous Scaffolds

5.4.1 Porosity, Pore Volume and Pore Size

The density of the scaffolds ($\rho_{scaffold}$) is determined by using a Sartorius YDK01, Germany density measurement kit (Buoyancy method) which can be calculated using the following equation.

$$\rho_{scaffold} = \frac{W_a \times \rho_{fl}}{W_a \times W_{fl}}$$

Where W_a is the weight of the scaffold in air, W_{fl} is the weight of the scaffold in water and $\rho_{scaffold}$ is the density of the water (at 25ºC, $\rho_{ft} \approx 1$ g/cm^3).

The porosity and pore volume of the scaffolds were calculated using the following equation (Hou, Qingpu *et al*., 2003)

$$\text{Porosity (\%)} = \left(1 - \frac{\rho_{scaffold}}{\rho_{polymer}}\right) \times 100$$

$$\text{Pore volume} = \frac{1}{\rho_{scaffold}} - \frac{1}{\rho_{polymer}}$$

where $\rho_{scaffold}$ is the apparent density of the porous scaffolds and $\rho_{polymer}$ is the density of the non-porous polymer, compression moulded in the same manner.

Pore size of the scaffold was measured on the SEM micrograph with the UTHSCSA Image Tool version 3.0 software. The average values were calculated from the total 25 pores and accept as the mean pore sizes.

5.4.2 Water Absorption Capability

The dry scaffold scaffolds were weighted and then were immersed in 5 ml of phosphate buffer silane solution (PBS pH 7.4) solution at room temperature for 3 days. Scaffolds were removed from the solution and carefully placed on the glass for 5 seconds to remove the excessive water and weight immediately. The water absorption was calculated using the following equation.

$$\text{Water absorption (\%)} = \frac{(M_{wet} - M_{dry}) \times 100}{M_{dry}}$$

Where M_{dry} and M_{wet} are the weight of the scaffold before and after immersion in water respectively. Five measurements were performed for the calculation of an average water absorption value.

5.4.3 Morphology of Porous Scaffolds

The morphology of the pores size of the porous scaffold were observed by a JEOL JSM-5200 scanning electron microscopy (SEM). The scaffolds were cut with razor blade at the middle of the scaffolds and mounted on stubs. Cross sections of the scaffolds were coated with thin film of gold using JEOL JFC-1100E sputtering devices for 120 second.

5.4.4 *In Vitro* Release of Proteins from Scaffold

The proteins/HAp-PCL were immersed in 1 ml of the minimum essential medium (MEM; Hyclone, Thermoscientific, USA) in 24 well plate. All samples were incubated in a shaking water bath (70 rpm) at 37ºC. The amount of proteins releasing from scaffold to the supernatant was measured by BCA protein assay at various times. After the releasing medium (sample solution) was withdrawn 20 µl to mixed with BCA solution, an equal amount of fresh medium was added to maintain a constant volume of the medium. The amount of protein in the sample solution was determined by UV-visible spectroscopy at 562 nm. The MEM used in this study contained plenty of much high molarity inorganic salts comparing with those in PBS such as NaCl 117.24 M, KCl 5.33 M, $CaCl_2$ 1.8 M, NaH_2PO_4-H_2O 1.01 M (Invitrogen, 2009).

5.5 Cell culture

Mouse calvaria-derived, pre-osteoblastic cells (MC3T3-E1) were cultured as monolayers in minimum essential medium with Earle's Balanced Salts (MEM; Hyclone, Thermoscientific, USA), supplemented with 10% FBS, 1% L-glutamine and 1% antibiotic and antimycotic formulation (containing penicillin G sodium, streptomycin sulfate, and amphopericin B (Invitrogen Corp, USA). Cells were cultivated in 5% CO_2 at 37 ºC in a humidified atmosphere.

5.5.1 Indirect Cytotoxic Study.

An indirect cytotoxic test was conducted on the proteins-loaded hydroxyapatite and PCL-HAp scaffold by use MC3T3-E1. First, extraction medias were prepared by immersing powder of each protein-loaded hydroxyapatite and circular shape of each PCL-HAp scaffold specimens about (15 mm in diameter) in wells of a 24-well culture plate in a 2% MEM (containing MEM, 2% FBS, 1% L-glutamine, 1% antibiotic and antimycotic formulation) for 24 h. Each of these extraction media was used to evaluate the cytotoxicity of the HAp powder and scaffold. MC3T3-E1 was separately cultured in wells of a 24-well culture plate in serum-containing MEM for 16 h to allow cell attachment on the plate. The cells were then starved with 2% MEM for 24 h, after which time the medium was replaced with an extraction medium.

After 24, 48, and 72 h of cell culturing in the extraction medium, a 3-(4,5-dimethylthiazol-2-yl)-2,5-diphenyl-tetrazolium bromide (MTT) assay was carried out to quantify the amount of via cells.

The MTT assay is based on the reduction of the yellow tetrazolium salt to purple formazan crystals by dehydrogenase enzymes secreted from the mitochondria of metabolically active cells. The amount of purple formazan crystals formed is proportional to the number of viable cells. First, each of culture medium was aspirated and replaced with 400 µl per well of MTT solution at 0.5 mg/ml for a 24-well culture plate. Secondly, the plate was incubated for 30 mins at 37ºC. The solution was then aspired and 900 µl per well of dimethylsulfoxide (DMSO) containing 125 µl per well of glycine buffer (pH=10) is added to dissolve the formazan crystals. Finally, after 10 min of rotary agitation, the absorbance of the DMSO solution at 570 nm was measured using a Thermospectronic Genesis 10 UV-Visible spectrophotometer.

5.5.2 Cell Attachment and Cell Proliferation Study

Mouse calvaria-derived, pre-osteoblastic cells (MC3T3-E1) were allowed to attach on the porous scaffold specimens and empty wells for 2, 4, and 6 h. For the proliferation study, the cells were allowed to attach on the porous scaffold specimens and empty wells for 1, 3, and 5 d. At each time point, a number of the attached and proliferated cells were quantified by MTT assay. Each specimen was rinsed with phosphate buffered saline to remove unattached cells prior to the MTT assay. The morphology of the cells during the attachment and proliferation periods was observed by SEM. At each time point, the culture medium was removed and then the cell-cultured scaffold specimens were rinsed with PBS twice, the cells were then fixed with 3% glutaraldehyde solution, which was dilute from 50% glutaraldehyde solution with PBS 500 µl/well. After 30 min, they were rinsed again with PBS. After cell fixation, the specimens were dehydrated in an ethanol solution of varying concentration (30%, 50%, 70% and 90%, respectively). The specimens were the dried in air. After completely dried, the specimens were mounted on an SEM blass stubs, coated with gold and observed by SEM.

5.5.3 Alkali Phosphate Analysis (ALP)

Mouse calvaria-derived, pre-osteoblastic cells (MC3T3-E1) were cultured on porous scaffolds for 5 and 7 d and in different proteins for 5 and 7 d to observe ALP activity. Each porous specimen was rinsed with PBS after removal of the culture medium. Alkaline lysis buffer (10 mM tris-HCl, 2mM $MgCl_2$, 0.1% Triton-X100), pH 10) (1000 µl/well) was added, and the specimen was scrapped and then frozen at -20ºC for at least 30 min prior to the next step. An aqueous solution of 2 mg ml^{-1} p-nitrophenyl phosphate (PNPP; Zymed Laboratories) mixed with 0.1 M aminopropanol (10µl/well) in 2 mM $MgCl_2$ (100µl/well) having a pH of 10.5 was prepared and added into the specimen. It was then incubated at 37ºC for 2 min. The reaction was stopped by the addition of 0.9 ml/well of 50 mM NaOH, and the extracted solution was transferred to cuvette and placed in the UV-Vis spectrophotometer, from which the absorbance

at 410 nm was measured. The amount of ALP was then calculated against a BSA standard curve. To determine the ALP activity, the amount of ALP had to be normalized by the amount of total proteins synthesized. In the protein assay, each specimen was treated in the same manner as in the ALP assay up to the point where it was frozen. After freezing, a bicinchoninic acid (BCA; Thermoscientific, USA) solution was into the specimen. It was subsequently incubated at 37ºC for 5 min. The absorbance of the medium solution was then measured at 562 nm by the UV-Vis spectrophotometer, and the amount of the total proteins was calculated against a BSA standard curve.

5.5.4 Mineralization Analysis

Calcium deposition was quantified by Alizarin Red S staining. MC3T3-E1 were cultured on the porous scaffolds in 24-well plate for 21 days. The cultures in 24-well plate were rinsed with PBS after that the cells were fixed with cold methanol for 10 min and washed with deionized water prior to immersion for 3 min in 370 µl of 1% Alizarin Red S solution dissolved in 1:100 (v/v) ammonium hydroxide/water mixture for 3 min (pH=3.3). Each stained specimen was washed several times with DI water and air-dried at room temperature. Calcium forms an Alizarin Red S-calcium complex in a chelating process. The stained specimen was photographed and eluted dye with 10% cetylpyridinium chloride for 20 min. The Alizarin Red concentration was determined by measuring the absorbance at 562 nm.

5.6 Results and discussion

5.6.1 Microstructure observation

Figure 5.1 demonstrated the SEM images microstructure of the as-prepared scaffolds when being viewed on the surface and cross sections. For PCL and HAp/PCL scaffold with NaCl : PCL, 30:1 weight ratio. The SEM images of (a) and (c) showed many square units occurring from the shape of NaCl porogens used in the fabricating process. They showed clearly square units due to neat PCL scaffold whereas (b) and (d) exhibited the lost square because HAps embedded in the PCL scaffold.

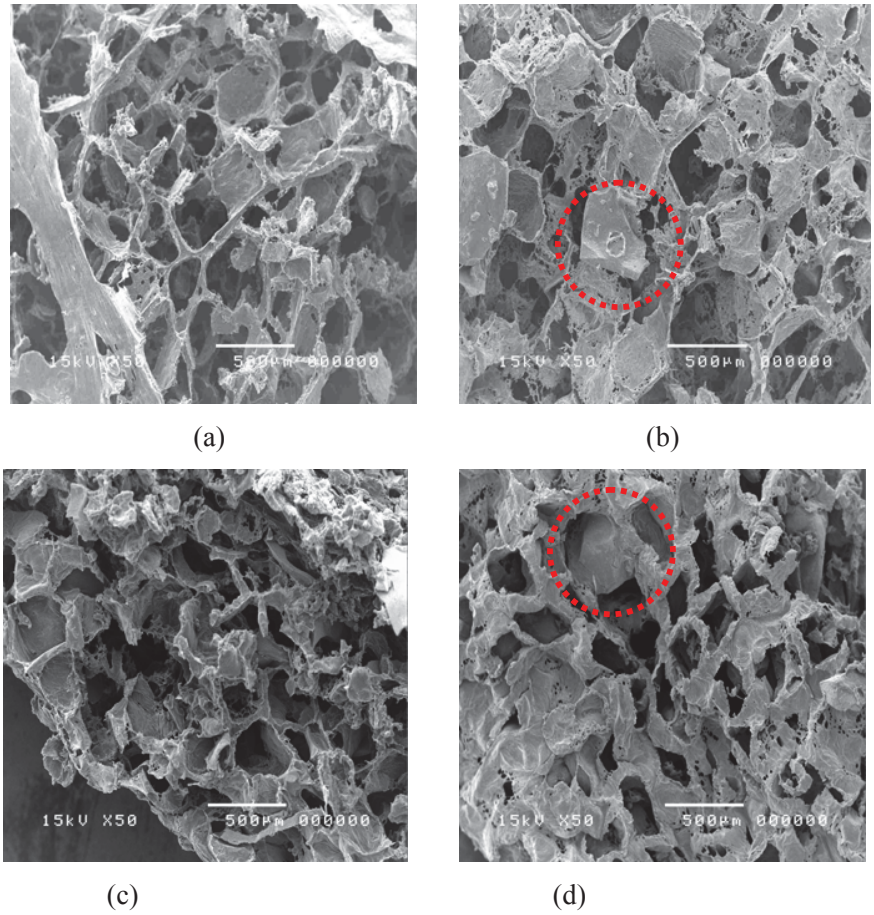


Figure 5.1 SEM images illustrate microstructure of the scaffolds on the surface: (a) PCL, (b) HAp-PCL and on the cross-sections : (c) PCL, (d) HAp-PCL.

5.6.2 Density, Porosity, Pore volume and Pore size

The density, porosity, pore volume and pore size of the scaffold was shown in Table 5.1.

Table 5.1 Density, porosity, pore volume and pore size of PCL scaffold

Scaffolds	Density (g/cm^3)	Porosity (%)	Pore volume (cm^3/g)	Pore size (µm)
PCL	0.1139	90.05	7.91	347.07 ± 42.19

5.6.3 Water absorption capability and *in vitro* degradability

Figure 5.2 illustrates the water absorption capabilities of the PCL scaffolds in 0.1 M PBS at room temperature within 3 days (72 h). The water absorption rate was rapidly increased in the early 24 hours and maintained stable.

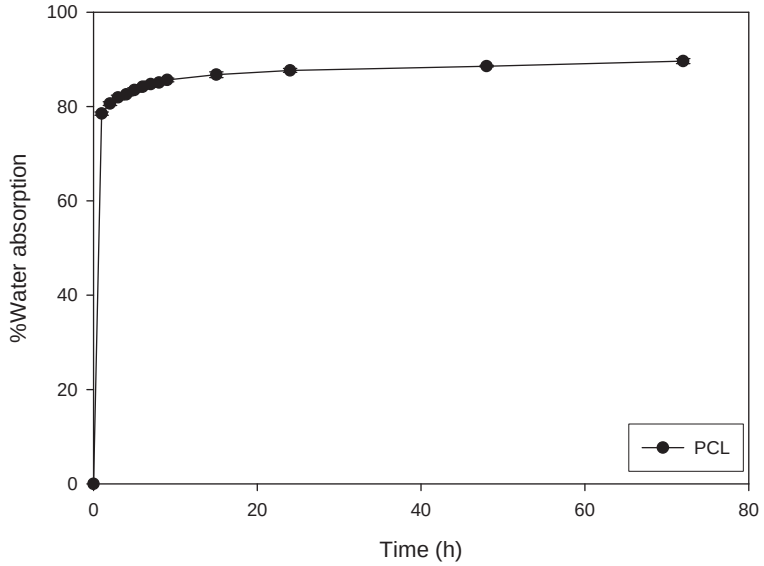


Figure 5.2 Water absorption capability of the PCL scaffolds in 0.1 M PBS at room temperature within 3 days.

5.6.4 *In vitro* OVA, Gelatin type B, BSA, and CBP Release

The release of proteins from HAp-PCL scaffolds were investigated by immersing HAp-PCL scaffolds into *in vitro* culturing environment, 10% MEM (containing MEM, 10% FBS, 1% L-glutamine, 1% antibiotic). All samples were incubated in a shaking water bath (70 rpm) at 37ºC for 21 days. The result shows gelatin and CBP started to before day 7 whereas OVA and BSA release after day 7. The amount of released proteins gradually increased time dependently. This result correspond to the work done by proteins releasing from HAp particles, however, protein release from scaffold spends a longer time due to different media. It is different in ionic strength, in MEM shows higher ionic strength. High ionic strength should promote aggregation of protein and retard release.

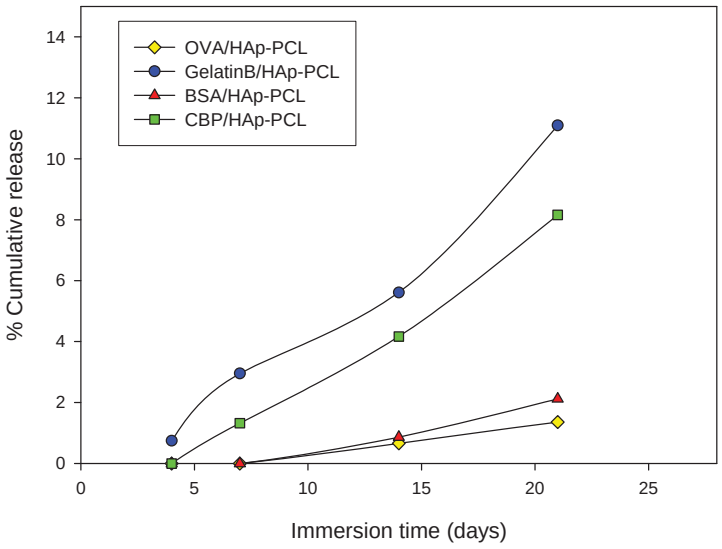


Figure 5.3 Release profile from protein-loaded HAp-PCL scaffold in MEM.

5.7 Cell Culture

5.7.1 Cytotoxicity

Indirect cytotoxicity in this studied can be classified into 3 process are indirect cytotoxicity for protein, HAp, and HAp-PCL scaffold. Firstly, an direct cytotoxicity test of proteins were performed in 4 types which are Ovalbumin (OVA), Gelatin type B, Bovine serum albumin (BSA), and Crude bone protein. MC3T3-E1, pre-osteoblast cell lines, in culture of 40,000 cell/well seeded with 10 µg/ml concentration in 2% MEM for 24, 48, and 72 h. The results are shown in Figure 5.4 with %viability of MC3T3-E1 relative to tissue culture polystyrene (TCPS) in all types of proteins show that increasing with cuturing time. The %viability of MC3T3-E1 is more than 80%, so all types of proteins were no toxicity to cells. Secondly and Thirdly are indirect cytotoxicity test of proteins-loaded HAp and HAp-PCL scaffold. MC3T3-E1 were cultured in 2% MEM extraction media from proteins-loaded HAp (Figure 5.5) and HAp-PCL scaffold (Figure 5.6) for 24, 48, and 72 h. The %viability of MC3T3-E1 in extraction media of each time are more than 80%, so proteins-loaded HAp and HAp-PCL scaffold were no toxicity to cell.

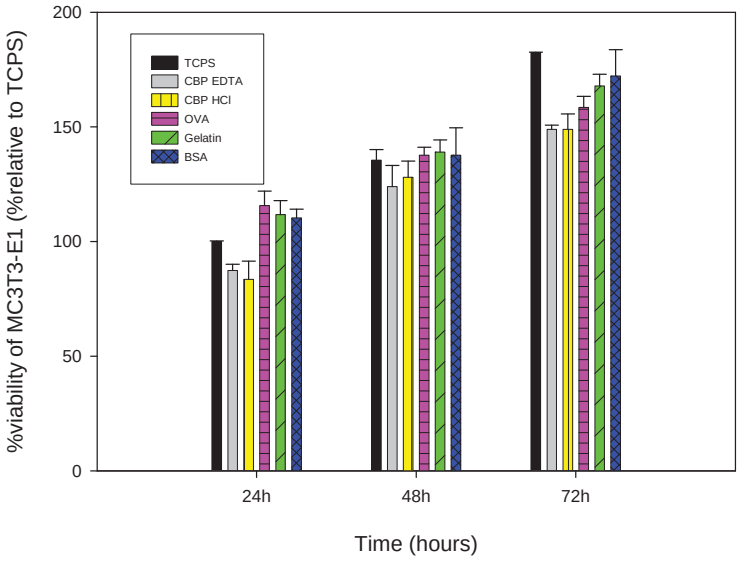


Figure 5.4 Direct cytotoxicity evaluation of proteins based on the viability of MC3T3-E1.

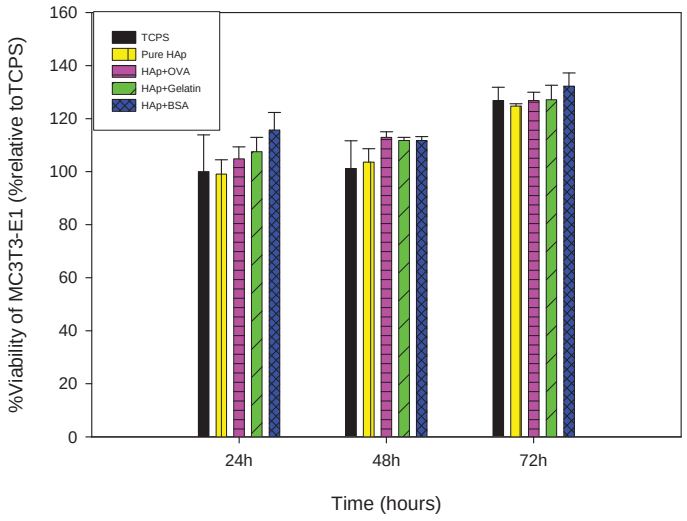


Figure 5.5 Indirect cytotoxicity evaluation of protein-loaded HAp based on the viability of MC3T3-E1.

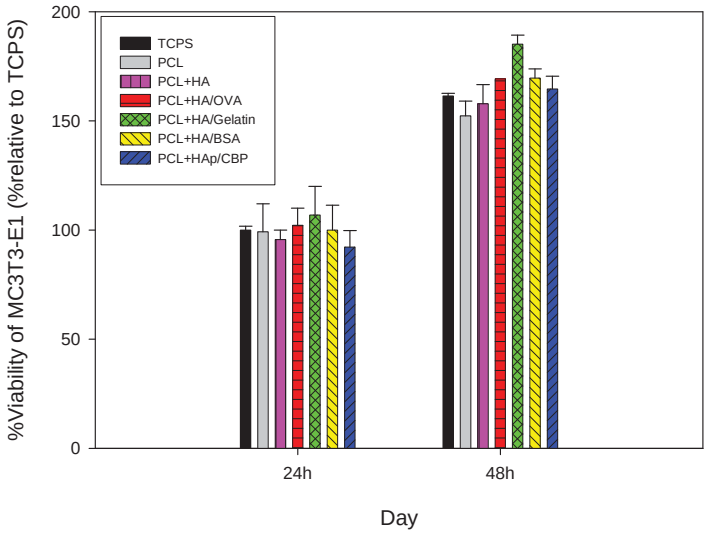


Figure 5.6 Indirect cytotoxicity evaluation of HAp-PCL scaffold based on the viability of MC3T3-E1.

5.7.2 Cell Attachment and Proliferation

Attachment of mouse calvaria-derived, pre-osteoblastic cells (MC3T3-E1) on scaffolding substrate could be quantified by the UV absorbance from MTT assay. Figure 5.7 shows attachment of MC3T3-E1 on the surface of TCPS, PCL, HAp-PCL, OVA/HAp-PCL, Gelatin type B/HAp-PCL, BSA/HAp-PCL, CBP/HAp-PCL at 2, 4, and 6 h after cell seeding. The number of cell attachment on all of the surfaces increase with culturing time. The number of cell attachment on TCPS was the greatest than all of HAp-PCL and proteins-loaded HAp scaffolds at any given time point, in culture of 40,000 cell/well. On TCPS, the number of cell attachment rapidly increased from 100% at 2 h after cell seeding to ~200% at 4 h after cell seeding. Whereas the number of cell attachment on PCL, HAp-PCL and proteins-loaded HAp were lower than TCPS could be because MC3T3-E1 like to attach the smoother surface of TCPS than rough surface of PCL, HAp-PCL and proteins-loaded HAp-PCL scaffold. However, Table 5.2 shows that almost of the formazan crystal still adhere within the scaffolds after using DMSO as eluting agent.

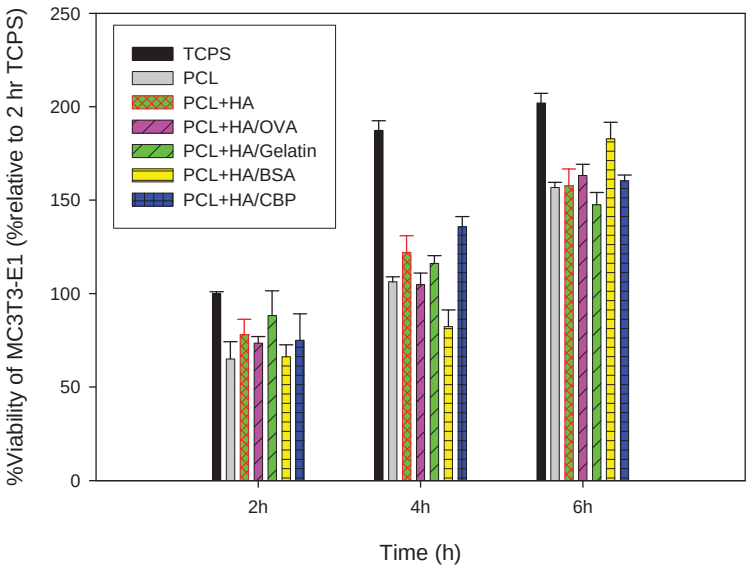


Figure 5.7 Attachment of MC3T3-E1 on control TCPS, PCL, HAp/OVA-PCL, HAp/gelatin B-PCL, and HAp/BSA-PCL

Table 5.2 Formazan crystal within TCPS, PCL, HAp-PCL scaffold were eluted with DMSO after cell seeding 6 h. (a) Eluted formazan from TCPS. (b), (c) Formazan still adhere in scaffold. (f), (g) Eluted formazan from scaffold. (d), (e) scaffold without cells inside. (h), (i) Eluted scaffolds without cells

 (a)	 (b)	 (c)	 (d)	 (e)
	 (f)	 (g)	 (h)	 (i)

Proliferation of mouse calvaria-derived, pre-osteoblastic cells (MC3T3-E1) on scaffolding substrate could be quantified by the UV absorbance from MTT assay. Figure 5.8 shows proliferation of MC3T3-E1 on the surface of TCPS, PCL, HAp-PCL, OVA/HAp-PCL, Gelatin type B/HAp-PCL, BSA/HAp-PCL, CBP/HAp-PCL at 1, 2, and 3 d after cell seeding in culture of 40,000 cell/well. The number of cell prolieration on all of the surfaces at any given time point were constant. The number of cell proliferation on TCPS was greater than all of PCL, HAp-PCL, and proteins-loaded HAp-PCL scaffolds at any given time point. On PCL, HAp-PCL and proteins-loaded HAp-PCL scaffold, the number of cell proliferation was only 60%. Whereas the number of cell attachment on HAp-PCL and proteins-loaded HAp were lower than TCPS could be because MC3T3-E1 like to proliferate the smoother surface of TCPS than rough surface of PCL, HAp-PCL and proteins-loaded HAp-PCL scaffold. The difference between the number of cell proliferation to PCL, HAp-PCL, and protein-loaded HAp-PCL scaffold are not clear because of no effect of proteins release from HAp. However, Table 5.3 shows that almost of the formazan crystal still adhere within the scaffolds after using DMSO as eluting agent.

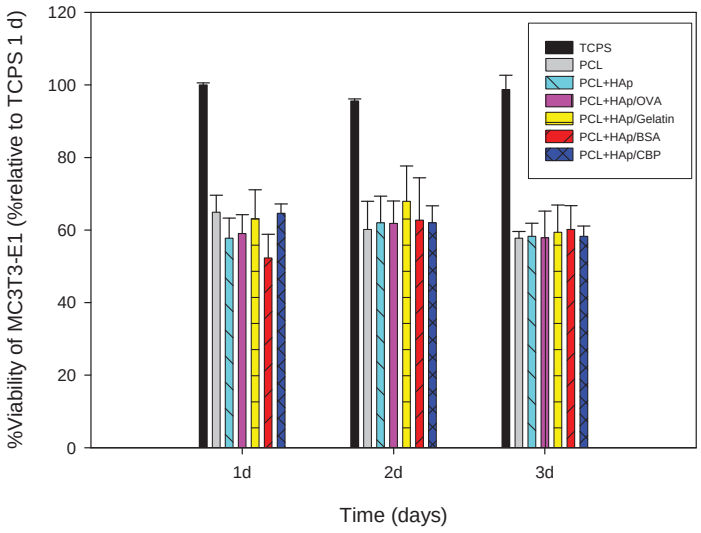


Figure 5.8 Proliferation of MC3T3-E1 that had been seeded or cultured on the surfaces of TCPS, PCL, HAp-PCL and proteins-loaded HAp-PCL scaffolds at 2 and 3 d.

Table 5.3 Formazan crystals within scaffolds after using eluting dye (DMSO) after cell seeding 1 d. (a) Eluted formazan with DMSO from TCPS. (b), (c) Formazan crystal still adhere in scaffolds. (f), (g) eluted formazan crystal with DMSO from scaffolds. (d), (e) scaffold without cells inside. (h), (i) eluted DMSO from scaffolds without cells.

 (a)	 (b)	 (c)	 (d)	 (e)
	 (f)	 (g)	 (h)	 (i)

5.7.3 Cell Morphological

Table 5.4 shows selected the attachment SEM images of MCT3T-E1 (magnification = 2000X; scale bar = 10 μm) at 2, 4, and 6 h. Based on the initial 40,000 cells/well of cells seeded, the majority of the cells on the glass surface and porous scaffolds were still in the round shape at 2 h and started to extend their cytoplasm at 4 h. After cell seeding, expansion of the cytoplasm of the majority of the cells was evident at 6 h. Table 5.5 shows that the selected proliferation SEM images of MC3T3-E1 (magnification = 2000X; scale bar = 10 μm) were cultured on the surfaces of glass, PCL, HAp-PCL, and proteins-loaded HAp scaffolds. The use of glass as the control instead of TCPS was due to the ease of taking the samples to SEM observation. These images provided snap shots in time that revealed the morphology of the cells and interaction between the cells and the tested surfaces. The expansion of the cells was evident with depend on the increasing time at 1, 2, and 3 days. All proteins within the HAp show the same results due to at that time the proteins were no affect to the cells.

Table 5.4 Selected SEM images of MC3T3-E1 after seeding on TCPS, PCL, OVA/HAp-PCL, Gelatin type B/HAp-PCL, BSA/HAp-PCL, and CBP/HAp-PCL scaffolds at 2, 4, and 6 h (magnification = 2,000X; scale bar = 10 μm)

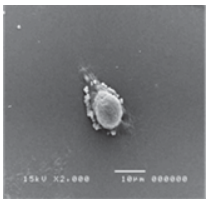
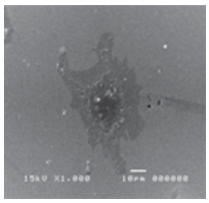
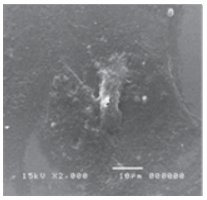
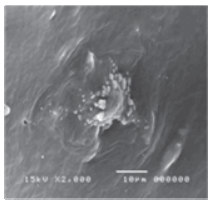
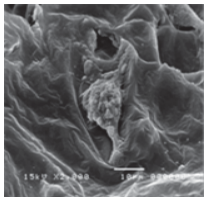
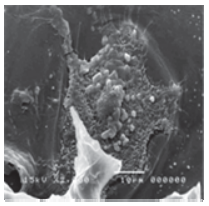
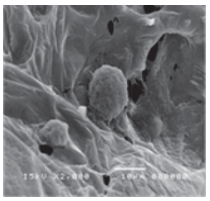
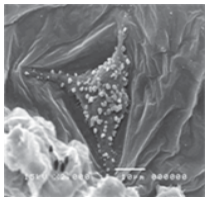
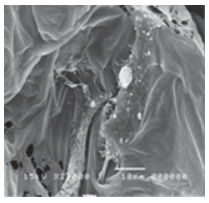
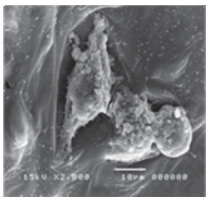
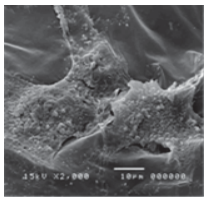
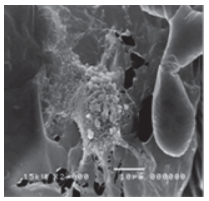
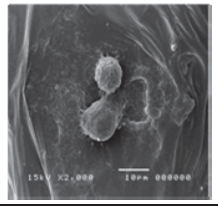
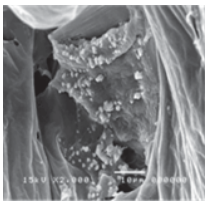
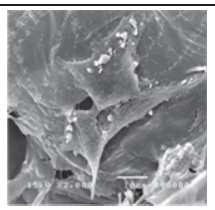
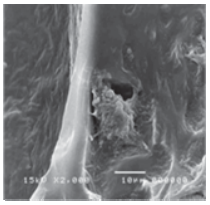
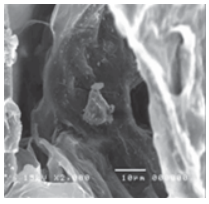
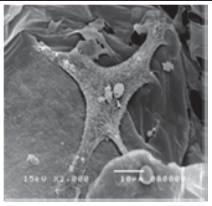
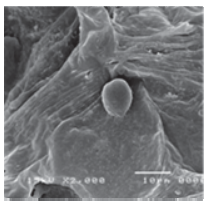
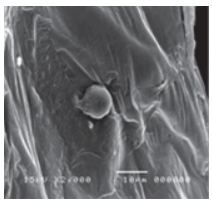
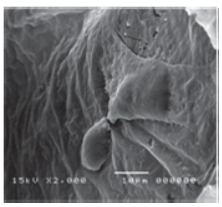
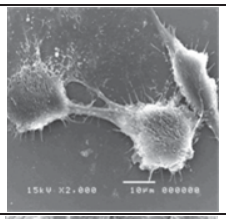
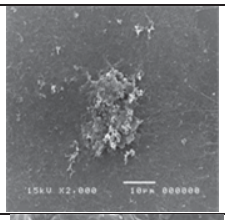
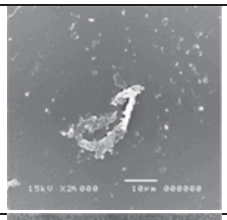
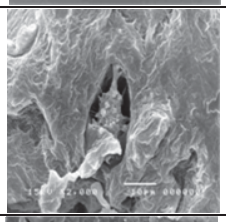
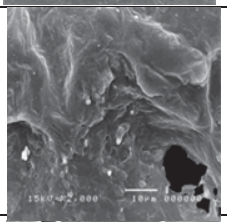
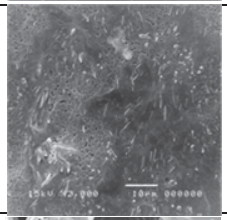
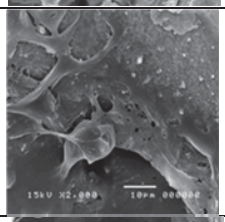
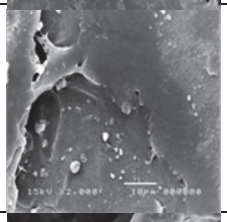
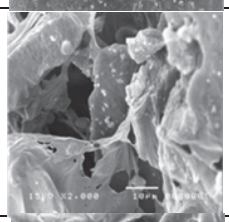
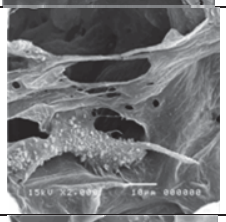
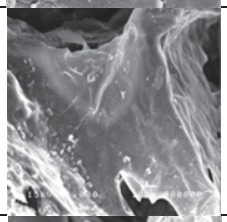
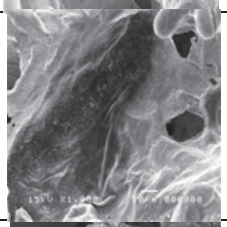
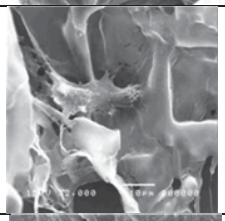
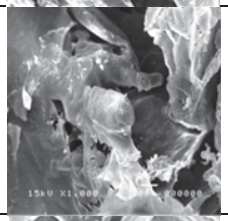
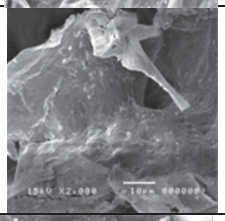
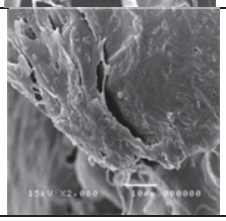
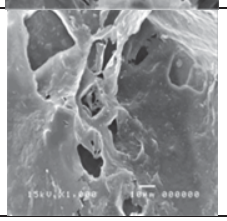
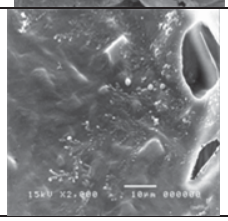
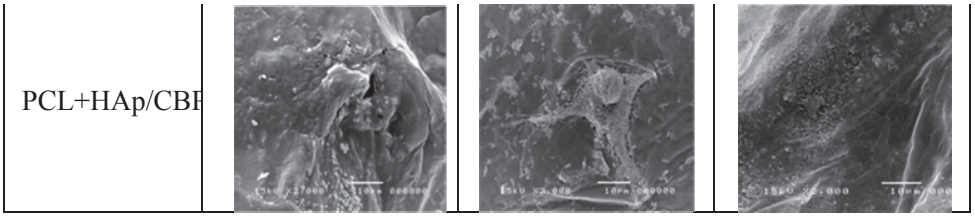
	2 h	4 h	6 h
Glass			
PCL			
PCL + HAp			
PCL+HAp/OVA			
PCL+HAp/Gel B			
PCL+HAp/BSA			
PCL+HAp/CBP			

Table 5.5 Selected SEM images of MC3T3-E1 after seeding on TCPS, PCL, HAp-PCL, OVA/HAp-PCL, Gelatin type B/HAp-PCL, and BSA/HAp-PCL scaffolds at 1, 2, and 3 days

X 2000	1 d	2 d	3 d
Glass			
PCL			
PCL + HAp			
PCL+HAp/OVA			
PCL+HAp/Gel B			
PCL+HAp/BSA			



5.7.4 Alkaline phosphatase (ALP) activity

Alkaline phosphatase is an indicator of osteoblast phenotype activity. It was determined after culturing the cells seeded onto the scaffold. The ALP activity of MC3T3-E1 on TCPS, PCL, HAp-PCL, OVA/HAp-PCL, Gelatin type B/HAp-PCL, BSA/HAp-PCL and CBP/HAp-PCL were monitored at 3 and 7 days in culture. In Figure 5.9 at 3 days shows the maximum level of ALP activity and at 7 days, ALP activity was decreased. In actually, ALP activity of PCL, HAp-PCL, OVA/HAp-PCL, Gelatin type B/HAp-PCL, BSA/HAp-PCL and CBP/HAp-PCL scaffold should be the same result of cell proliferation due to at that time the proteins were no effect to the cell, however, they were slightly fluctuated because PCL, HAp-PCL, OVA/HAp-PCL, Gelatin type B/HAp-PCL, BSA/HAp-PCL and CBP/HAp-PCL scaffolds were porous materials, so the cells could go through their scaffolds and could not extract the cells completely. In Figure 5.9, The ALP activity of MC3T3-E1 in OVA, Gelatin type B, BSA, and CBP with 100 µg/ml concentrations in 2%MEM was monitored at 5 and 7 days in culture. At 5 days shows the maximum level of ALP activity and at 7 days, ALP activity was decreased due to cellular process switching to mineralization. This result correspond to the work done by ALP activity of MC3T3-E1 on substrates.

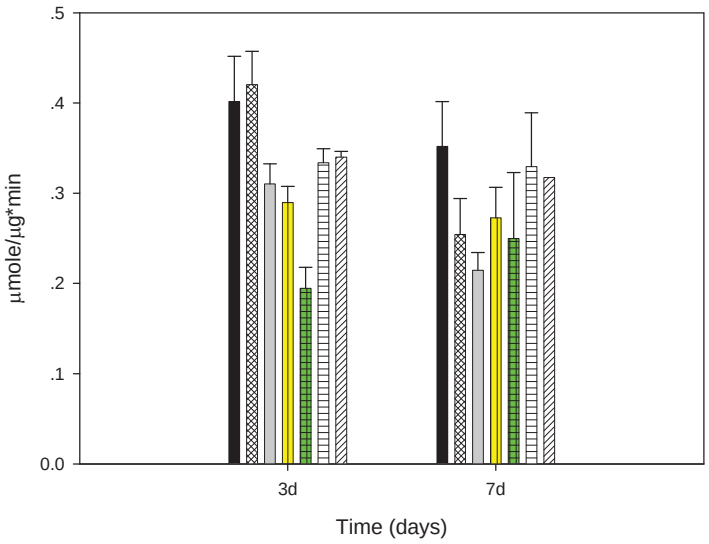


Figure 5.9 ALP activity of MC3T3-E1 cultured on TCP, PCL, HAp-PCL, OVA/HAp-PCL, Gelatin B/HAp-PCL, BSA/HAp-PCL and CBP/HAp-PCL porous scaffolds after 3 and 7days in culture.

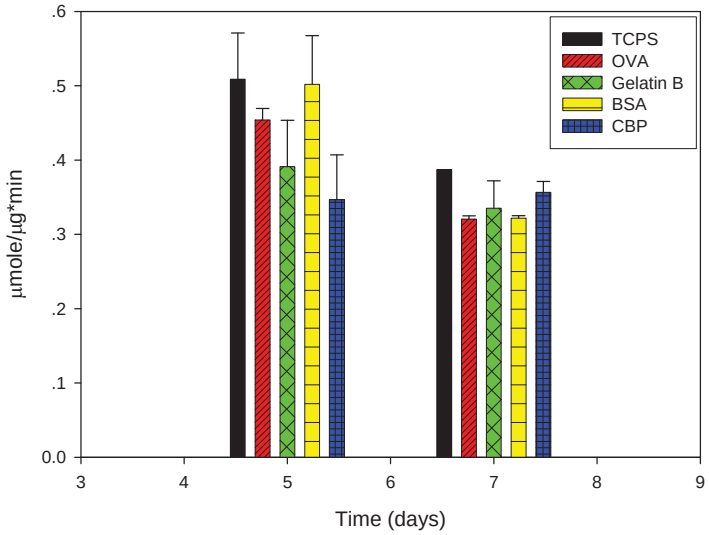
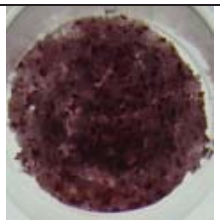
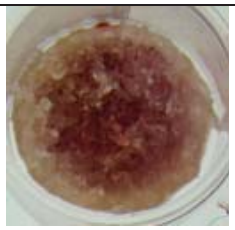
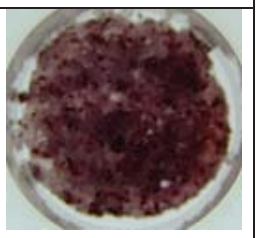
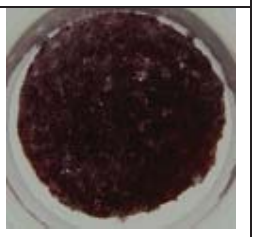


Figure 5.10 ALP activity of MC3T3-E1 cultured with 100 µg/ml in 2%MEM, OVA, Gelatin type B, BSA and CBP after 5 and 7 days in culture.

5.7.5 Mineralization

Mineralization refers to the process where an organic substrance is converted to an inorganic substrance. Alizalin Red S staining was used to characterize the bone formation of MC3T3-E1. Table 5.6, and Figure 5.11 show photographic images of Alizarin Red S staining of cells cultured on the different surfaces on 21 days. In the presence of calcium, the staining product such as an Alizarin red S-calcium chelating product appeared red. The results showed that PCL, HAp-PCL, and proteins-loaded-HAp scaffold were significantly higher than that on TCPS. Calcium content from MC3T3-E1 culture on CBP/HAp-PCL scaffold was the most positive staining.

Table 5.6 Alizarin Red S staining for mineralization assessment of MC3T3-E1 on 21 days after being cultured on the surfaces of neat PCL, HAp-PCL, HAp/OVA-PCL, HAp/Gelatin-PCL, HAp/BSA-PCL, and HAp/CBP-PCL

Substrate	21 d.		21 d.
TCPS		HAp/OVA-PCL	
Neat PCL		HAp/GelB-PCL	
Control		HAp/BSA-PCL	
HAp-PCL		HAp/CBP-PCL	

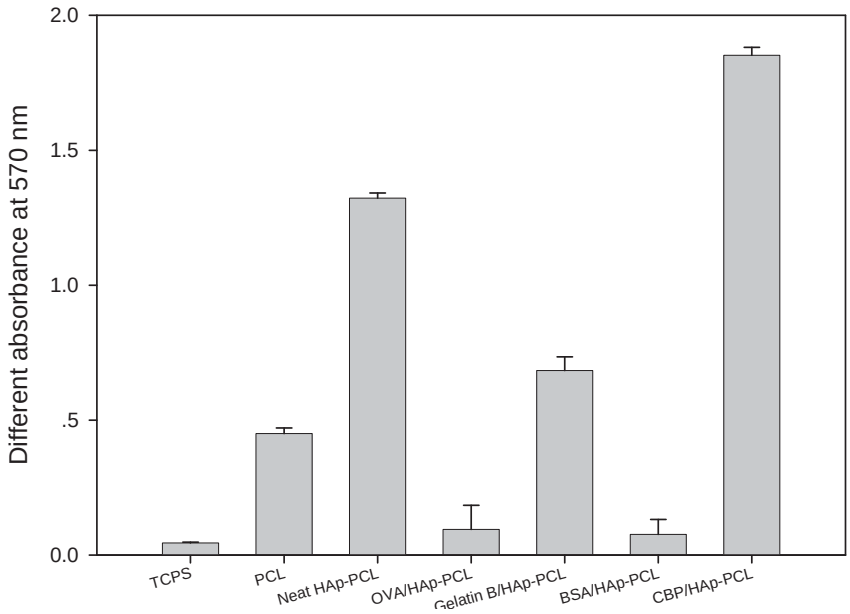


Figure 5.11 Different absorbance of alizalin red S from MC3T3-E1 on TCPS, PCL, HAp-PCL, proteins-loaded HAp-PCL at 21 days.

5.7 Conclusions

The amount of HAp in the PCL scaffold was 40% (w/w, based on the amount of PCL). The direct and indirect cytotoxicity evaluation of the proteins, HAp and protein-loaded HAp-PCL scaffold with MC3T3-E1 indicated that non-toxic. Potential for using of proteins-loaded HAp-PCL scaffolds was assessed in terms of cell attachment, cell proliferation, and ALP activity were no effect of proteins release from HAp. Alkaline phosphatate (ALP) activity at 7 days showed decreasing of the ALP activity due to cellular process switching to mineralization. According to mineralization or calcium deposition of cell for 21 days, the CBP/HAp-PCL scaffold was better than HAp/PCL, PCL, Gelatin/HAp-PCL, OVA/HAp-PCL, BSA/HAp-PCL, TCPS respectively.

6. SURFACE MODIFICATION OF POLY(LACTIC ACID) FIBERS VIA AMINOLYSIS AND COLLAGEN IMMOBILIZATION FOR BONE TISSUE ENGINEERING

Experimental Section

1. Materials. Materials used in the fabrication of the fibrous scaffolds were poly(lactic acid) (PLA; M_n = 80,000 g mol^{-1}; Aldrich, USA), dichloromethane (DCM; Carlo Erba, Italy), and *N*,*N*' dimethylformamide [DMF; Lab-Scan (Asia), Thailand]. Materials used in the surface modification of the PLA fibrous scaffolds were type-I collagen (from calf skin; Sigma, USA), 1,6-hexamethylene-diamine (HMD; Aldrich, USA), and *N*,*N*′-disuccinimidylcarbonate (DSC; Aldrich, USA). All other chemicals were of analytical reagent grade and used without further purification.

2. Preparation and characterization of e-spun PLA fibrous scaffolds. Electro-spun fiber mats of poly(lactic acid) were prepared by e-spinning from 10% w/v PLA solution in 7:3 v/v dichloromethane/ *N*,*N*'-dimethylformamide (DCM/DMF). The as-prepared PLA solutions were continuously stirred until clear solutions were obtained. The solution was fed into a glass syringe fitted with a blunt 20-gauge stainless steel hypodermic needle (OD = 0.91 mm), which used as the nozzle. An aluminum sheet wrapped around a home-made rotating cylinder (width and diameter ≈15 cm; rotational speed ≈ 50 rpm) was used as the collector. The distance from the tip of the needle to the surface of the Al sheet (measured at right angle to the surface) defining the collection distance was fixed at 18 cm. A Gamma High-Voltage Research Inc. (Ormond Beach, Florida), DC power supply was used to generate a high dc potential which was fixed at 20 kV. The emitting electrode of positive polarity was connected to the needle, while the grounding one was to the collector. E-spinning of the as-prepared PLA solution was done continuously for 12 h. The obtained translucent electro-spun PLA fibrous scaffolds were dried in *vacuo* at room temperature prior to further modification. The thickness of the obtained PLA fiber mats was ~136 ± 5 μm. Morphological appearance and size of the individual fibers of the scaffolds were examined by JEOL JSM 5410LV scanning electron microscopy (SEM) (see Supporting Information). At least 100 readings of the fiber diameters from various SEM images were statistically analyzed using SemAphore 4.0 software, from which the arithmetic mean value of the individual fibers within the PLA fiber mats was determined to be 0.63 ± 0.1 μm.

3. Surface modification of PLA fibrous scaffolds. The PLA fibrous membranes were first immersed in an ethanolic aqueous solution (1:1 v/v) for 2 to 3 h to cleanse the fiber surface and then washed with a large amount of deionized water. The scaffolds were subjected to aminolysis through an immersion in a 1,6-hexamethylene-diamine/isopropanol (HMD/IPA) solution of varying concentration (i.e., 0.02, 0.04, 0.06, 0.08, and 0.1 gml^{-1}) and varying reaction time (i.e., 2, 5, 8, 15, 20, 30 min) at 50°c. The aminolyzed PLA fibrous scaffolds were then rinsed with deionized water for 24 h at room temperature to

remove unreacted HMD and dried *in vacuo* at room temperature to reach a constant weight. Immobilization of type-I collagen on the surface of the PLA fibrous scaffolds was carried out by first activating the aminolyzed PLA fibrous scaffolds in 0.1 M *N,N′*-disuccinimidyl carbonate/dimethylsulfoxide (DSC/DMSO) solution in the presence of 0.1 M triethylamine (TEA) for 3 h at room temperature, followed by rinsing the fiber mats with a large quantity of deionized water. The activated PLA fibrous scaffolds were then immersed in 0.5 or 3 $mg \cdot ml^{-1}$ of collagen/phosphate buffer saline (PBS) solution at ambient temperature for 24 h. The collagen-immobilized PLA fibrous scaffolds were rinsed by soaking in a large quantity of deionized water for 24 h and finally dried *in vacuo* at room temperature. The chemical pathway for the immobilization of type-I collagen on the surface of e-spun PLA fibrous scaffolds is summarized in the Figure 1.

4. Characterization of neat and modified PLA fibrous scaffolds.

***Quantification of free amino groups on the surface*.** UV-Vis spectroscopy was used for determination the amount of amino (NH_2) groups on the surface of the aminolyzed and the collagen-immobilized PLA fibrous scaffolds using ninhydrin method. First, the fibrous scaffolds were immersed in 1 M ninhydrin/ethanol solution for 1 min in a glass tube, followed by heating at 80°C for 15 min to accelerate the reaction between ninhydrin and the NH_2 groups that might be present on the surface of the scaffolds. As an evidence for the actual presence of the NH_2 groups, the surface of the scaffolds would turn blue. After complete evaporation of absorbed ethanol, 1,4-dioxane was added in the tube to dissolve the scaffolds. IPA was then added to stabilize the blue compound. Absorbance of the obtained compound in the UV-visible range was measured in a spectrophotometer (UV-2550, Shimadzu, Kyoto, Japan) at 538 nm against a predetermined calibration curve that was obtained from HMD solutions in 1,4-dioxane/IPA (1:1 v/v) (see Supporting Information).

***Surface Wettability*.** Water contact angles of the neat and modified PLA fibrous scaffolds were measured at room temperature and, using sessile drop method on a telescopic goniometer (KRUSS Gmbh, DSA10-Mk2 T1C, Germany) equipped with a Gilmont syringe and a 24-gauge flat-tipped needle. The measurements were carried out in pentuplicate on different areas of each sample and the resulting values were averaged.

Elemental composition of the surface. X-ray Photoelectron Spectrometer (XPS; AMICUS, KRATOS, Japan), also known as Electron Spectroscopy for Chemical Analysis (ESCA), was used to investigate the elemental composition and chemical state of the elements on the surface. The XPS N_{1s}/C_{1s} peak-area rations was used as a marker for the analysis of the relative amount of free amino groups and collagen immobilized on the surface.

5. Biological characterization of neat and modified PLA fibrous scaffolds.

Cell culture and cell seeding. Mouse fibroblasts (L929) and mouse calvaria-derived, pre-osteoblastic cells (MC3T3-E1) were used as reference cell lines. L929 were cultured as monolayer in Dulbecco's modified Eagle's medium (DMEM; Sigma-Aldrich, USA), supplemented with 10% fetal bovine serum (FBS; BIOCHROM AG), 1% L-glutamine (Invitrogen Corp.), and a 1% antibiotic and antimycotic formulation [containing penicillin G sodium, streptomycin sulfate, and amphotericin B (Invitrogen Corp., USA)]. MC3T3-E1 were cultured in Minimum Essential Medium (with Earle's Balanced Salts) (MEM; Hyclone, USA), supplemented by 10% fetal bovine serum (FBS; BIOCHROM AG, Germany), 1% L-glutamine (Invitrogen Corp., USA) and 1% antibiotic and antimycotic formulation [containing penicillin G sodium, streptomycin sulfate, and amphotericin B (Invitrogen Corp., USA)]. The medium was replaced every 2 days and the cultures were maintained at 37°C in a humidified atmosphere containing 5% CO_2.

Each scaffold was cut into circular discs (about 15 mm in diameter) and the disc specimens were placed in wells of a 24-well tissue-culture polystyrene plate (TCPS; Biokom Systems, Poland), and were later sterilized in 70% ethanol for 30 min. The specimens were then washed with autoclaved de-ionized water, PBS and subsequently immersed in MEM overnight. To ensure a complete contact between the specimens and the wells, the specimens were pressed with a metal ring (about 12 mm in diameter). MC3T3-E1 from the culture was trypsinized [0.25% trypsin containing 1 mM EDTA (Invitrogen Crop., USA)] and counted by a hemacytometer (Hausser Scientific, USA). MC3T3-E1 were seeded at a density of about 60,000 cells/well for attachment study and 30,000 cells/well for proliferation study, on the scaffold specimens and empty wells of TCPS that were used as control. For indirect cytotoxicity, alkaline phosphatase activity, mineralization evaluations, MC3T3-E1 were seeded at a density of about 40,000 cells/well on the scaffold specimens and empty wells of TCPS. The culture was maintained in an incubator at 37°C in a humidified atmosphere containing 5% CO_2.

Cytotoxicity evaluation. Two types of cells were used: 1) mouse calvaria-derived, pre-osteoblastic cells (MC3T3-E1) and 2) mouse fibroblasts (L929). Indirect cytotoxicity test was conducted on TCPS, neat PLA, aminolyzed PLA, activated PLA, collagen-immobilized PLA, and polycaprolactone/hydroxyapatite (PCL/HA) which used as positive control. First, extraction media were prepared by immersing samples (about 15 mm in diameter) in a serum-free medium (SFM; containing DMEM, 1% L-glutamine, 1 % lactabumin, and 1% antibiotic and antimycotic formulation for L929 and containing MEM, 1% L-glutamine, 1 % lactabumin, and 1% antibiotic and antimycotic formulation for MC3T3-E1) for 1, 3, and 7 days. Each of these extraction media was used to evaluate the cytotoxicity of the scaffolds. L929 or MC3T3-E1 were separately cultured in wells of a 24-well culture plate in 10%serum-containing DMEM and MEM, respectively, for 16 h to allow cell attachment on the plate. Then, the cells were starved with SFM for 24 h, after which time the medium was replaced with an extraction medium. After 24 h of cell culturing in the extraction medium, 3-(4,5-dimethylthiazol-2-yl)-

2,5-diphenyl-tetrazolium bromide (MTT) assay was carried out to quantify the amount of viable cells (see Supporting Information). The experiments were carried out in triplicate.

Another experiment was conducted to confirm the cytocompatibility of the materials on MC3T3-E1. Extraction media were prepared by immersing samples (about 15 mm in diameter) in a serum-free medium (SFM; MEM, 1% L-glutamine, 1 % lactabumin, and 1% antibiotic and antimycotic formulation for MC3T3-E1) for 7 d. The sample was treated in the same manner as the previous experiment up to the point was the cells were starved. After that the SFM was replaced with 2%serum-containing MEM diluted with as-prepared 7-day extraction medium for 1, 2, and 3 d to allow cell growth on the plate. After which time the viability of cell was again quantified by MTT assay in triplicate.

Cell attachment and cell proliferation. Cell behavior such as adhesion and proliferation represent the initial phase of cell–scaffold communication that subsequently effect differentiation and mineralization. For attachment study, MC3T3-E1 was allowed to attach to TCPS, aminolyzed PLA, activated PLA, collagen-immobilized PLA for 2, 4 and 16 h, respectively. At each specified seeding time, the number of the attached cells was quantified by MTT assay. Each sample was rinsed with PBS to remove unattached cells prior to MTT assay. Morphological appearance of the cells during attachment period was observed by SEM. For proliferation study, the viability of cells on the specimens was determined after 1, 2, and 3 day of cell culturing by MTT assay. The experiments were carried out in triplicate.

Morphological observation of cultured cells. After removal of the culture medium, the cell-cultured scaffold specimens were rinsed with PBS twice and the cells were then fixed with 3% glutaraldehyde solution, which was diluted from 50% glutaraldehyde solution (Sigma, USA) with PBS, at 500 µl/well. After 30 min, they were rinsed again with PBS. After cell fixation, the specimens were dehydrated in an ethanol solution of varying concentration (i.e. 30, 50, 70, 90, and 100%, respectively) for about 2 min at each concentration. The specimens were then dried in 100% hexamethyldisilazane (HMDS; Sigma, USA) for 5 min and later let dry in air after removal of HMDS. After completely dried, the specimens were mounted on an SEM stub, coated with gold, and observed by a JEOL JSM-5200 scanning electron microscope (SEM).

Production of Alkaline Phosphatase of Cultured Cells. ALP activity of MC3T3-E1 was measured using Alkaline Phosphate Yellow Liquid. In this reaction, ALP catalyzes the hydrolysis of colorless organic phosphate ester substrate, *p*-nitrophenyl phosphate (pNPP) to a yellow product, p-nitrophenol, and phosphate. MC3T3-E1 was cultured on scaffold specimens for 3, 5, and 7 day to observe the production of alkaline phosphatase (ALP). The specimens were rinsed with PBS 2 times after removal of culture medium. Alkaline lysis buffer (10 mM Tris-HCl, 2 mM $MgCl_2$, 0.1% Triton-X100, pH 10) (100 µl/well) was added and the samples were scrapped and then frozen at -20°C for at least 30 min prior to the next step. An aqueous solution of 2 mg/ml *p*-nitrophenyl phosphate (pNPP; Zymed Laboratories, USA) mixed with 0.1 M

amino propanol (10 µl/well) in 2 mM $MgCl_2$ (100 µl/well) having a pH of 10.5 was prepared and added into the specimens (110 µl/well). The specimens were incubated at 37°C for 15 min. The reaction was stopped by adding 900 µl /well of 50 mM NaOH and the extracted solution was transferred to a cuvette and placed in the UV-visible spectrophotometer, from which the absorbance at 410 nm was measured. The amount of ALP was then calculated against a standard curve. In order to calculate for the ALP activity, the amount of ALP had to be normalized by the amount of total protein synthesized. In the protein assay, the samples were treated in the same manner as the ALP assay up to the point was the specimens were frozen. After freezing, bicinchoninic acid (BCA; Pierce Biotechnology, USA) solution was added into the specimens. The specimens were incubated at 37°C for 15 min. The absorbance of the medium solution was then measured at 562 nm by the UV-visible spectrophotometer and the amount of the total protein was calculated against a standard curve.

Mineralization analysis. Alizarin Red-S is a dye that binds selectively calcium salts and is widely used for mineral staining (the staining product i.e., an Alizarin Red S-calcium chelating product). The isolated osteoblastic cells were plated in 24-well plates at 40,000 cells/well and cultured in the culture medium. After 24 h, the cultures were treated with culture medium, with the supplement of 50 µg/ml ascorbic acid (Sigma, USA), 5 mM β-glycerophosphate (Sigma, USA), and 0.2 µg/ml dexamethasone (Sigma, USA), the medium was replaced every 2 days. After 16 days treatment, cells were washed with PBS and fixed with ice-cold absolute methanol for 10 min. Fixed cells were stained with 1% Alizarin Red in deionized water (Sigma, USA) (pH 4.2) for 2-3 min. After removing alizarin red-S solution, the cells were rinsed with deionized water and dried at room temperature. The images of each culture were captured and the stain was extracted with the use of 10% cetylpyridinium chloride (Sigma, USA) in 10 mM sodium phosphate for 1 h and absorbance of the collected dye was read at 570 nm in spectrophotometer (Thermo Spectronics Genesis10 UV-visible spectrophotometer).

6. Statistical analysis. Values expressed as the mean ± standard deviation. Statistical analysis of different data groups was performed using One-Way Analysis of Variance (ANOVA) with the least-significant difference (LSD) test using SPSS software version 11.5. The values of p lower 0.05 were considered statistically significant.

Results and Discussion

By reaction with diamine, 1,6-hexanediamine (HMD), amino groups can be covalently introduced onto the surface of the electro-spun PLA fibrous membranes to obtain the aminolyzed PLA fibrous membranes. One amino group (NH_2) of HMD reacts with an ester group (—COO—) of PLA to form the amide linkage (—CONH—), while another amino group is unreacted and free for the further reaction.

These free NH_2 groups can be used as active sites through which proteins like collagen can be bonded to the surface using *N*,*N*′-disuccinimidyl carbonate (DSC) as a coupling agent. However, to avoid aggregation, two-step procedure was employed. The attached amino groups had been first activated with DSC with *N*-hydroxysuccinimide being lost from the reaction and the as-formed succinimidyl esters were later reacted with respective collagen, with *N*-hydroxysuccinimide again being cleaved from the reaction.

1. Characterization of neat and modified PLA fibrous scaffolds.

Quantification of free amino groups on the surface. The existence of free amino groups (NH_2) on PLA surface is a prerequisite for protein bonding in this modification method. It is important to confirm the existence of amino groups before protein is further introduced. Herein, ninhydrin is used as an indicator to confirm and quantify the $–NH_2$ moiety on the aminolyzed PLA surface. The NH_2 density on e-spun PLA fibrous scaffold surface was influenced by the concentration of HMD, aminolyzing time, temperature, and so on. Because the glass transition temperature (T_g) of the present PLA is ~60-70°C, the aminolyzing temperature should be lower than this value to maintain the shape of the material. Hence, 50°C was chosen to perform the following reactions. Table 1 shows that NH_2 density increased with increasing HMD concentration. However, when the concentration of HMD is equal to or greater than 0.1 g/ml, the mechanical integrity of the e-spun PLA fiber mats was affected. Table 2 shows that the surface-bound NH_2 increased with increasing aminolyzing time to reach a maximum value at about 15 min, and then decreased slightly. The decrease at the longer reaction time may be caused by a further reaction of the free amino group on the terminal chain with other ester groups, or by the degradation of the superficial layer[27]. Both of these situations will reduce the density of the surface amino groups and thus intensity of purple colored complex. To maintain enough mechanical integrity for practical applications, PLA e-spun fiber mats were aminolyzed in a 0.04 g/ml HMD/IPA solution at 50°C for 15 min. According to the calibration curve obtained with 1,4-dioxane/isopropanol (1:1, v/v) solution containing HMD of known concentration, the NH_2 density on PLA e-spun fiber mat aminolyzed under these conditions was $(3.7 \pm 0.02) \times 10^{-7}$ mol/cm^2 (see Table 3). It also shows that after immobilization with 0.5 mg/ml and 3.0 mg/ml type-I collagen, the average areal density of the amino groups on the surface of the PLA fibrous scaffolds were $(4.52 \pm 0.08) \times 10^{-9}$ and $(3.21 \pm 0.2) \times 10^{-8}$, respectively.

Surface Wettability. To further evaluate the effect of aminolysis and collagen immobilization, surface wettability of the modified PLA fibrous scaffolds with respect to that of the neat PLA fibrous scaffolds was measured. Table 4 shows the surface wettability of neat PLA, aminolyzed PLA, activated PLA, collagen-immobilized PLA (without coupling agent; collagen = 0.5 mg/ml), collagen-immobilized PLA (collagen = 0.5 mg/ml), and collagen-immobilized PLA (collagen = 3 mg/ml) fibrous scaffolds. The water contact angle measured by the sessile drop method decreased slightly from 106.8˚ to 99.5˚ after the scaffold was aminolyzed with 0.04 g/ml of HMD/IPA solution for 15 min. That is, the introduction of the

amino groups on the surface of the PLA fibrous scaffolds improved the hydrophilicity of the surface. After the aminolyzed PLA fibrous scaffolds has activated with DSC, their surface became more hydrophobic as evidenced by the water contact angle of 112.5˚. Water contact angle decreased substantially after the collagen was bonded. Figure 2 shows that the surface became much more hydrophilic after collagen immobilization. Water contact angle was 79.4˚ for collagen 0.5 mg/ml immersion and was 73.0˚ for collagen 3 mg/ml immersion. These results show that the more collagen concentration used, the more collagen can be bonded to the PLA surface. It has been known that physisorption processes are virtually always involved in a coating procedure. In our case, we had tried physical coating of collagen on unactivated PLA fibrous scaffolds. Water contact angle measurements showed that water contact angle of physisorbed collagen-coated PLA surfaces was slightly lower than the aminolyzed PLA surface. On the other hand, for collagen-covalently bonded surface, they exhibited much lower water contact angle. That means activation step is an important step in protein grafting process.

Elemental composition of the surface. The surface alteration after the PLA fibrous scaffolds were modified was studied by X-ray Photoelectron Spectrometer (XPS). To study the effect of the aminolysis condition on the surface alteration, N_{1s}/C_{1s} ratios as a function of HMD concentration and aminolyzing time were evaluated. Table 5 shows that the more diamine concentration used, the more N_{1s}/C_{1s} ratio observed which could be due to increasing in introduced NH_2 group concentration. Table 6 shows that the N_{1s}/C_{1s} ratio increased with increasing aminolyzing time to reach a maximum value at about 15 min, and then decreased slightly, which, in addition to the results on ninhydrin analysis method. Figure 3 shows that N_{1s} peaks obviously appeared after immobilization of collagen, which confirmed protein grafting. Table 7 shows N_{1s}/C_{1s} ratio of the neat and the modified PLA fibrous scaffolds. After aminolysis of PLA fibrous scaffold, the N_{1s}/C_{1s} ratio was increased from 0 to 0.0290 because of NH_2 groups introduced on the surface. The N_{1s}/C_{1s} ratio was further increased to 0.0381 by reaction with DSC. It shows that the nitrogen concentration increased when succinimidyl esters was formed. Finally, it was obviously increasing in N_{1s}/C_{1s} ratio after collagen immobilization due to the large amount of nitrogen atom in collagen structure was additionally introduced.

2. Biological evaluation of neat and modified PLA fibrous scaffolds.

Indirect cytotoxicity evaluation. The biocompatibity of these PLA e-spun fiber mats as bone scaffolds was assessed by an indirect cytotoxicity evaluation with mouse fibroblastic cells (L929) and mouse calvaria-derived pre-osteoblastic cells (MC3T3-E1), based on the initial 40,000 cells/well of cells seeded. Indirect cytotoxicity test was conducted on neat, aminolyzed, activated, collagen-immobilized PLA fibrous scaffolds. In this experiment, the PCL/HA that was prepared from particulate leaching technique, was chosen to be the positive control. Even though we were interested in using the obtained modified fiber mats as potential bone scaffolds, it was mandatory to test the materials with L929 just to comply with the

ISO10993-5 standard test method. Figure 4a shows %viability obtained from MTT assay of L929 which were cultured with the 1, 3, 7 day- extraction media in comparison with those cultured with SFM (i.e. control). The viability of the cells that had been cultured with SFM at any given time point was taken as the basis to arrive at the relative viability shown in the figure. Evidently, the viability of L929 for all types of modified PLA fibrous scaffolds exhibited slightly lower, in comparison with that of the control (100%). While the neat PLA fiber and PCL/HA scaffold which used as positive control exhibited comparable viability. In a similar manner was found for MC3T3-E1 (see Figure 4b). However, the viability of cells that were cultured with 7-day extraction media prepared from modified scaffolds were significantly lower, in comparison with that were cultured with 7-day extraction media prepared from the neat PLA scaffold and PCL/HA. Thus, we had to set other experiment to confirm the cytocompatibility of the modified PLA fibrous scaffolds.

MC3T3-E1 was cultured in wells of a 24-well culture plate in 2%serum-containing MEM diluted with 7-day extraction medium for 1, 2, and 3 d to allow cell growth on the plate. Figure 5 shows that the viability of MC3T3-E1, cultured with 2%serum-containing MEM diluted with 7-day extraction media prepared by all types of modified scaffolds, were increased with increasing the culturing time in the respective media. All of the obtained results clearly suggested that all types of the PLA fibrous scaffolds, released no substances at levels that were harmful to both types of cells.

Cell attachment and cell proliferation. The potential for use of the neat and the modified PLA fibrous scaffolds was further evaluated by observing their ability to support both the adhesion and the proliferation of MC3T3-E1. The viability of the cells that had been cultured on the surface of TCPS for 2 h was taken as the basis to arrive at the relative viability shown in a figure. Figure 6 shows the attachment of MC3T3-E1 on the surfaces of TCPS, neat PLA, aminolyzed PLA, activated PLA and collagen-immobilized PLA at 2, 4, and 16 h after cell seeding in terms of viability. On TCPS, the number of the attached cells increased from ~100% at 2 h after cell seeding to ~111% at 16 h after cell seeding, based on the initial number of cells seeded (60,000 cells/well). With regards to MC3T3-E1, the surfaces of all of the PLA fibrous scaffolds were inferior in supporting the attachment of the cells to that of TCPS. Specifically, the number of cells attached on these fibrous scaffolds was only ~50% in comparison with that on TCPS at any given time point. There was not significantly different in the viability among all types of the fibrous scaffolds. Figure 7 shows the proliferation of MC3T3-E1 on the surfaces of TCPS, neat PLA, aminolyzed PLA, activated PLA and collagen-immobilized PLA on day 1, 2, and 3 after cell culture in terms of viability (%relative to TCPS at day1). On TCPS, the number of cells increased from ~100% on day1 after cell culture to ~187% (i.e., an increase of about 2 fold from the initial number of cells seeded) on day 3 after cell culture, based on the initial 30,000 cells/well of cells seeded. In comparison with that on TCPS, the viability of the cells cultured on the modified PLA fibrous scaffolds were significantly higher at any given

time point. The viability of cells proliferated on these fibrous scaffolds, at day 3, was higher than TCPS of about 2 fold for neat PLA, aminolyzed PLA, and activated PLA and about 3.5 fold for collagen-immobilized PLA. Marked improvement was achieved with the collagen-immobilized PLA fibrous scaffolds on day 3 after cell culture.

The lesser viability of cells in the attachment period on various types of the fibrous scaffolds in comparison with that on TCPS could be due to the lesser number of cells that were able to attach on the rougher and more hydrophobic surface of the fibrous scaffolds in comparison with the smoother and hydrophilic surface of TCPS. On the contrary, the greater number of cells in the proliferation period on all types of PLA fibrous scaffolds could be because of high surface area to mass or volume and high porosity of the e-spun fiber mats though which the cells were able to penetrate into the scaffolds. Among the various modified PLA fibrous scaffolds, the collagen-immobilized PLA fibrous scaffolds provided the most significant improvement in the ability to support the proliferation of the cells which could be due to the protein-containing and hydrophilic surface of the substrate.

Cell Morphology. Table 8 shows selected SEM image (magnification = 2000X; scale bar = 10 μm) of MC3T3-E1 that were cultured on the surface of glass, neat PLA, aminolyzed PLA, activated PLA and collagen-immobilized PLA at two different time points, while the SEM images at magnification = 500X are available as Supporting Information. The use of glass as the control instead of TCPS was due to the ease of taking the samples to SEM observation. These images provided snap shots in time that revealed the morphology of the cells and interaction between the cells and the tested surfaces. At 4 h after cell seeding, based on the initial 60,000 cells/well of cells seeded, the majority of the cells on the glass surface started to extend their cytoplasm, an evidence of the ability of the cells to attach on the surface. At 16 h after cell seeding, expansion of the cytoplasm of the majority of the cells was evident. While the majority of MC3T3-E1 that had been seeded on the surfaces of unmodified PLA fibrous scaffolds for 4 h was remained round, but a closer examination around the edge of the cells revealed an evidence of filopodia (i.e., slender cytoplasmic projections extending from the leading edge of the migrating cells that help the cells during their migration over the surface of a scaffolds). The majority of the cells were evidently expanded after 16 h of cell seeding. On the other hand, the majority of the cells seeded on the surfaces of various types of modified PLA fibrous scaffolds showed an evidence of the extension of their cytoplasm on the fibrous surface even at 4 h after cell seeding, with collagen-immobilized PLA surface did so to a greater extent. These results suggested that the cells prefer the fibrous surfaces of modified PLA over that of the unmodified. Specifically, the cells were seemed to prefer the collagen-containing than others.

Alkaline Phosphatase (ALP) Activity. The ability for these PLA fibrous scaffolds to support differentiation, in addition to attachment and proliferation, of cultured cells is another important aspect suggesting actual applicability of the scaffold. Alkaline phosphatase is a membrane bound enzyme and its

activity is used as an osteoblastic differentiation marker, as it is produced only by cells showing mineralized ECM. The ALP activity of MC3T3-E1 on TCPS (i.e. controls), neat PLA, aminolyzed PLA, activated PLA, and collagen-immobilized PLA were monitored at 3, 5 and 7 days in culture (see Figure 8). Apparently, the amount of ALP synthesized by the cells that were cultured on TCPS and all of the fibrous scaffolds increased with the initial increase in time in culture between day 3 and 5, reached a maximum level on day 5, and decreased with a further increase in culture after day 3. In comparison with other substrates, TCPS exhibited the highest ALP activity of MC3T3-E1. According to Figure 8, activated PLA and collagen-immobilized PLA fibrous scaffolds showed the highest ALP activity among the various fibrous scaffolds investigated at day 3 of cell culturing time. And at day 5 and day 7 collagen-immobilized PLA fibrous scaffolds exhibited the highest ALP activity.

The decrease in the ALP activity, after day 5 for the cells grown on both TCPS and PLA fibrous scaffolds, with a further increase in the culturing time can be due to cellular process switching onto further step (i.e. mineralization).[31,32] Since ALP is not an exclusive protein synthesized by osteoblasts as it is also found in tissues of such organs as kidneys, small intestines, and placenta, the presence of ALP of MC3T3-E1 that were cultured on these substrates could not be used as the sole marker to confirm the osteoblastic phenotype of the cells.[33] From the obtained results, it was suggested that collagen-immobilized PLA fibrous scaffold was the best among the PLA fibrous scaffolds that promoted both proliferation and differentiation of MC3T3-E1.

Mineralization. Mineralization refers to cell-mediated deposition of extracellular calcium and phosphorus salts where anionic matrix molecules take up the Ca^{2+}, phosphate ions and serve as nucleation and growth sites leading to calcification. Mineralization was quantified by Alizarin Red-S studies (see Figure 9), showing degree of mineralization as indicated by extracted stain absorbance obtained on day 16 of cell culture was in the order of collagen-immobilized PLA > aminolyzed PLA > neat PLA > activated PLA > TCPS > glass. The collagen-immobilized PLA scaffold showed 16% higher mineralization than neat PLA scaffold with significant level of $p < 0.05$ confirming the effectiveness of collagen immobilization of PLA e-spun fibers in mineral formation by MC3T3-E1. The photographic images (see Figure 10) of scaffolds stained with Alizarin Red-S for 16 days supported the above data where high intensity of staining minerals was observed on various type of PLA fibrous scaffolds displaying an overall enhancing effect in mineralization of MC3T3-E1 cells and proving collagen immobilization as an indispensable method for the fabrication of superior fibrous scaffolds for bone tissue engineering.

Conclusion

In the present study, type-I collagen was used to modify PLA in the form of electro-spun fibrous membranes for the purpose of improving cytocompatibility. The XPS confirmed that collagen was immobilized on the surface of PLA fiber mats by the reaction of aminolyzed PLA and type-I collagen employing DSC as a coupling agent. The existence of NH_2 groups on aminolyzed PLA surfaces has been characterized by ninhydrin analysis method, which revealed that the NH_2 density was influenced by the HMD concentration and aminolyzing time. The data of contact angle against water revealed that it had improved the surface hydrophilicity by the aminolysis and the further immobilization of collagen. The cultured MC3T3-E1 *in vitro* proved that the cell proliferation, alkaline phosphatase (ALP) activity and mineralization of modified PLA e-spun fibers were improved compared with the neat PLA fiber. Among the various modified PLA scaffolds, collagen-immobilized PLA showed the greatest ability to support cell proliferation, alkaline ALP activity, and mineralization. Therefore, collagen-immobilized PLA fibrous scaffold is promising material to accelerate bone regeneration.

7. Use of 2-hydroxypropyl-β-cyclodextrin as adjuvant for enhancing encapsulation and release characteristics of asiaticoside within and from cellulose acetate films

Experimental details

Materials

Cellulose acetate (CA; white powder; Mw ≈30,000 Da; acetyl content = 39.7 wt.%; degree of acetyl substitution≈2.4) and 2-hydroxypropyl-β-cyclodextrin (HPβCD; Mw ≈1,380 Da; average number of substituent per glucopyranose unit≈0.6) were purchased from Sigma–Aldrich (Switzerland). Asiaticoside (AC; 90%purity) was purchased from Shanghai Angoal Chemical Co., Ltd.(China). N,N-Dimethylacetamide (DMAc, Lab-Scan Asia, Thailand),glacial acetic acid (Carlo Erba, Italy), anhydrous disodium hydrogen orthophosphate, sodium dihydrogen orthophosphate, and sodium chloride (Ajax Chemicals, Australia) were used as-received. All chemicals were of analytical reagent grades and used without further purification.

Stoichiometry of AC/HPˇCD complex in solution state

Phase solubility studies

Phase solubility of AC in HPβCD was studied in distilled water. Briefly, excess amounts of AC were put into aqueous HPβCD solutions(1 mL). The amount of HPβCD in the solutions was varied between 0 and 30mM. The sample solutions were then stirred at room temperature (25ฑ1 ◦C) for 24 h. It should be noted that the stirring time of 24 h was enough for the solubilization of AC in HPβCD to reach equilibrium. After reaching the equilibrium, unsolubilized AC in the sample solutions was filtered out through a filter membrane (0.45μmin pore diameter). The filtrates were later quantified for the amounts of the solubilized AC by reversed-phase high performance liquid chromatography (HPLC; see later). The association constant (Ka) was then calculated from the following equation (Higuchi & Connors, 1965):

$$K_a = \frac{m}{s_0(1-m)}, \quad (1)$$

where m is the slope of the plot between the solubility of AC in distilled water as a function of the HPβCD concentration and s0 is the solubility of AC in distilled water in the absence of HPβCD. In addition, the complexation efficiency (CE) and the AC:HPβCD molar ratio ([AC]:[CD]) were calculated as follows (Loftsson, Hreindóttir, & Másson, 2007):

$$CE = s_0 K_{1:1} = \frac{[AC]/[CD]}{[CD]} = \frac{m}{1-m}, \quad (2)$$

$$\frac{[AC]}{[CD]} = \frac{1}{1+(1/CE)}, \quad (3)$$

where $K_{1:1}$ is the association constant for the AC:HP_CDmolar ratio of 1:1.

The phase solubility of AC in HP_CD was also studied in a 90:10 (v/v) mixture of 80 vol.% acetic acid and DMAc. To ensure the formation of the AC/HPβCD complex in the solvent mixture, the preparation procedure was similar to what had been described above, with an exception to the fact that the mixture of acetic acid and DMAc was used instead of the distilled water.

1H-NMR studies

A Varian UNITYINOVA 1H-nuclear magnetic resonance spectrometer(1H-NMR), operating at 400MHz and 25 ◦C, was used to determine the stoichiometric ratio of the AC/HPβCD complex.

Based on the Job's continuous variation method (Job, 1928), the 1H-NMR spectra were recorded from a mixture of AC (10mM) and HPβCD (10mM) in 10% (v/v) DMSO-d6/D2O mixture at various volumetric ratios between these two solutions at the final concentrations of AC of 1–10mM, prior to being stirred for 24 h.

Preparation of AC/HPβCD complex in solid state

The AC/HPβCD complex was prepared according to the method previously described by Higuchi and Connors (1965), with slight modification. Briefly, a weighed amount of HP_CD was first dissolved in distilled water. A weighed amount of AC was then added to the solution and stirred at room temperature (25±1 ◦C) for 24 h. The stoichiometric AC:HPβCD molar ratio, as obtained from the studies in Section 2.2, was utilized throughout the rest of the studies. The solution/suspension was filtered through a nylon filter (average pore size = 0.45μm) prior to being frozen at −40±2 ◦C for 24 h. After that, the obtained mass was lyophilized (Labconco FreeZone 6-Liter Benchtop Freeze Dry System). A physical blend of AC and HPβCD at the same molar ratio was also prepared for comparison.

Characterization of solid AC/HPβCD complex

1. X-ray powder diffractometry

X-ray powder diffractograms of the AC/HP_CD complex and the corresponding physical mixture were obtained on a Bruker Model D8 Advance, equipped with a Cu Kλ radiation source, over a scattering (2º) range of 5 and 60◦ at room temperature (25 ±1 ◦C). The scan rate, the operating voltage, and the filament current were set at 0.2◦ min−1, 40 kV, and 30 mA, respectively.

2. Two dimensional 1H-NMR studies

To obtain the 2D 1H-NMR spectrum of the AC/HPβCD complex, the freeze-dried product was dissolved in D2O at room temperature (25±1 ◦C) and investigated under the following conditions: acquisition time of 0.205 s, sweep width of 5006.3 Hz, pulse width of 6.3_s, time domain of 2048, Fourier number of 2048 and temperatureof 298 K.

Preparation of AC- and AC/HPβCD complex-loaded CA films

CA films containing either AC or AC/HPβCD complex were prepared by solvent casting technique. AC or a AC/HPβCD complex that had been prepared at different mixing molar ratios of HPβCD to AC (i.e., 0.5, 1.0, or 2.0) was incorporated at a concentration of 10%, based on the dry weight of CA powder, in a 90:10 (v/v) mixture of 80 vol.% acetic acid and DMAc. The concentration of CA in the final solutions was 4% w/v. The as-prepared solutions were stirred at room temperature (25±1 ◦C) for 24 h. Prior to the addition of CA powder, each of the sample solutions was characterized for the particle size of the self-assembling aggregates by a Malvern Zetasizer ZS nanosizer [based on the dynamic light scattering (DLS) principle]. CA powder was then added to the sample solution and subsequently stirred at room temperature (25±1 ◦C) for 3 h until CA was completely dissolved. The solutions were subsequently poured onto glass Petri dishes and dried under a reduced pressure. The films were dried until of a constant weight and stored in a desiccator in vacuo for at least 24 h, prior to further use. The thicknesses of the as-cast films were 80±10_m.

Characterization of AC- and AC/HPβCD complex-loaded CA films

Morphologies of AC- and AC/HPβCD complex-loaded CA films were studied by a JEOL JSM-6400 scanning electron microscope(SEM). All of the specimens were vacuum-coated with a thin layer of gold using a JEOL JFC-1100E sputtering device. The average diameters of the self-assembling aggregates and the pores that were formed after the films had been immersed in a phosphate buffer saline solution (PBS; see later for its preparation) containing 10% (v/v) methanol (hereafter, P/B/M medium) for 24 h were determined by measuring the diameters of the micro-aggregates and the micro-pores at 100 different points on the SEM images of 7500 magnification with SemAphore 4.0 software. For each sample, the diameters were presented as the average±standard deviation.

Water retention and weight loss behavior of the AC- and the AC/HPβCD complex-loaded CA films were investigated after their immersion in the P/B/M medium at 37 ◦C for 24 h. The water retention and the weight loss behavior were calculated as follows:

$$\text{Water retention}\,(\%) = \frac{M - M_d}{M_d} \times 100, \qquad (4)$$

and

$$\text{Weight loss}\,(\%) = \frac{M_i - M_d}{M_d} \times 100, \qquad (5)$$

where M and Md are wet and dry weights of the film specimens after immersion in the buffer solution, respectively, and Mi is the initial, dry weight of the specimens. All measurements were carried out in triplicate.

Release of AC from AC- and AC/HPβCD complex-loaded CA films

1. Preparation of releasing medium

To prepare 1 L of the PBS solution, 6.177 g of anhydrous disodium hydrogen orthophosphate and 1.1014 g of sodium dihydrogen orthophosphate were dissolved under mechanical stirring in distilled water at room temperature (25±1 ◦C) until the flakes were completely dissolved. Later, 8.7 g of sodium chloride was added into 20mL of the solution. The volumewas adjusted to the required volume with distilled water. The pH of the final solution was 7.4.

2. Actual AC content
The actual amounts ofACin the AC- and the AC/HPβCD complex loaded CA films were quantified by dissolving the samples (circulardisc: about 1.5cm in diameter) in 4mL of 2:1 (v/v) acetone/DMAc. After that, 0.5mL of the solutions were pipetted and diluted into 8mL of the P/B/M medium. Finally, the AC contents in the diluted sample solutions were determined by HPLC (see later) and then back-calculated from the obtained data against a calibration curve for AC.
3. AC release assay
The release characteristics ofACfrom the AC- and the AC/HPβCD complex-loaded CA films were determined by the total immersion method. Each of the specimens (circular disc of about 1.5cm in diameter) was immersed in 25mL of the P/B/M medium at the physiological temperature of 37 ◦C. At each time point, ranging between 0 and 24 h(1440 min), 1mL of themedium was withdrawn (i.e., sample solution) and an equalamountof the fresh mediumwas refilled. The amounts of AC in the sample solutions were quantified by HPLC (see later) and then back-calculated from the obtained data against the calibration curve for AC.

Determination of AC content
The amount of AC in a given sample solution was determined by HPLC (Shimadzu LC-10 AD). The sample solution was filtered through a nylon filter (average pore size = 0.45_m) and then separated in an Inertsil ODS-3 C18 column (particle size = 5_m; column dimension = 4.6mm̃250mm) with an Inertsil ODS-3 guard column (particle size = 5_m; column dimension = 4.0mm̃10mm) at a flow rate of 1mLmin−1. A UV–Visible detector was set a (_max) 204 nm. The mobile phase for the AC separation consisted of acetonitrile, methanol, and distilled water at 26:24:50 (v/v/v) and the retention time was 7.7 min. The calibration curve for AC was obtained over a concentration range of 0.005–0.200mgmL−1.

Statistical analysis
One-way ANOVA was used to analyze the means of different data sets. The significance for all of the tests was accepted at a 0.05 confidence level.

Results and discussion

Stoichiometry of AC/HPβCD complex in solution state
The solubility of AC in the absence or the presence of HPβCD was studied in two types of medium (i.e., distilled water or 90:10 (v/v) of 80% acetic acid and DMAc) and the results are graphically shown in Fig. 2. In the absence of HPβCD, the solubility of AC in any type of the studied medium (i.e., s0) was low (i.e., 0.7mM in distilled water and 48.7mM in 90:10 (v/v) of 80% acetic acid and DMAc). Marked increase in the amounts of solubleACin either mediumwas evident in the presence of HPβCD. At the greatest amount of HPβCD investigated (i.e., 30 mM), the amounts of soluble AC increased to 15.3 and 60.0mM in distilled water and 90:10 (v/v) of 80% acetic acid and DMAc, respectively. Obviously, the amounts of soluble AC in both types of medium exhibited linear relationships with the HPβCD content in the solutions. The association constants, Ka, characterizing the solubility of AC in distilled water and 90:10 (v/v) of 80% acetic acid and DMAc, can be calculated from the slopes of the plots such as those shown inFig. 2. The slopes of the least-squared lines drawn through both sets of data were less than one, with the values being 0.505 and0.380, respectively. According to the definition set forth by Higuchi and Connors (1965), these could be categorized as AL type and a 1:1 complex between AC and HPβCD could be assumed. Based on the values of the slopes obtained, the Ka values (or the K1:1 values, for this particular case) can be calculated, based in Eq. (1), to be 11,726.5 and 12.5M−1, respectively. According to Eq. (2), the complexation coefficient values, CE, were determined to be 1.020 and 0.613, respectively, while, according to Eq. (3), the AC:HPβCD molar ratios were 1:2 and 1:3, respectively. This means that, despite the stoichiometric 1:1 molar ratio between AC and HPβCD in the as-formed complex, only 1 in every 2 or 3 molecules of HPβCD underwent the complexation with AC.

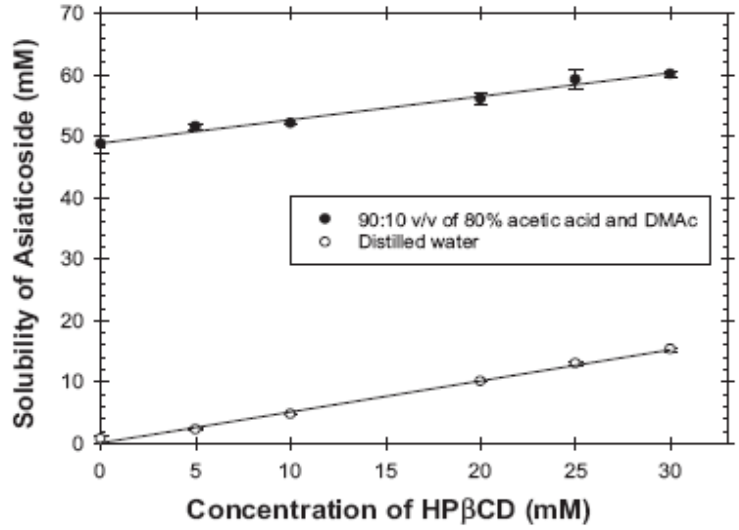


Fig. 2. Phase solubility diagrams of AC in the absence or the presence of 2-hydroxypropyl-β-cyclodextrin (HPβCD) in distilled water and 90:10 (v/v) of 80% acetic acid and DMAc at room temperature.

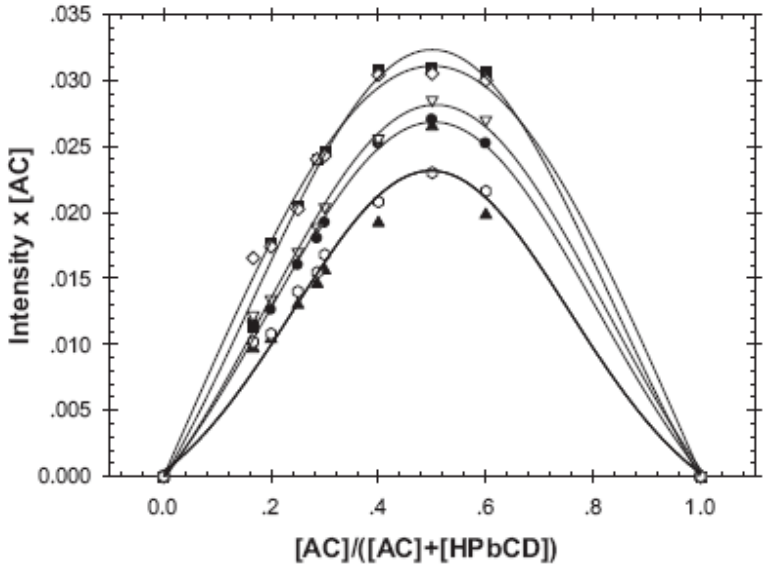


Fig. 3. Job's continuous variation plots of the chemical shifts of the protons, i.e., (▽) H-12, (◊) H-18, (▲) CH_3-26, (●) CH_3-29, (■) Glc-1, and (○) Rha-5, of AC, in the presence of different HPβCD concentrations in the 90:10 (v/v) mixture of D_2O and DMSO-d_6.

One dimensional 1H-NMR spectroscopy is useful for studying the inclusion complex of HPβCD with various organic compounds. The variation in the chemical shift of the protons of organic compounds (_ı= ıc −ı0, where ıc and ı0 are the chemical shifts of a specific chemical species in the complex and the free forms, respectively), due to the screening environment by magnetic nuclei within the HPβCD cavity, was recorded. In particular, changes in the chemical shifts of protons of the guest molecule(s) within the

CD cavity can be used to quantify the stoichiometry of the complex, simply by plotting them as a function of the mole fraction of the guest molecule(s) or the CD molecule [i.e., Job's continuous variation plots (Job, 1928)]. The mole fraction at the maximum peak(s) is taken as the stoichiometric ratio of the complex. According to Fig. 3, the chemical shifts of CH3-26, CH3-29, H-12, H-18, Rha-5, and Glc-1 protons in the AC/HPβCD mixtures, in 90:10 (v/v) mixture of D2O and DMSO-d6, exhibited the maximum peaks at [AC]/([AC] + [HPβCD]) = 0.5, corresponding to the AC:HPβCD molar ratio of 1:1. In addition, Table 1 shows the chemical shift signals of protons of AC and HP_CD, both in the free and the complex states, inD2Oat equi-molar ratio between AC and HPβCD, along with their differences.

Characterization of AC/HPβCD complex in solid state

X-ray powder diffractometry

The freeze-dried product from the equi-molar mixture of AC and HPβCD was white powder. X-ray powder diffractometry was then used to confirm the formation of the AC/HPβCD complex. Fig. 4 shows the X-ray diffractograms of AC, HPβCD, the AC/HPβCD complex, and the physical mixture of AC and HPβCD. Sharp diffraction peaks were evident for the as-received AC, indicating its crys talline nature. On the other hand, only diffused, scattering peaks were observed for the as-received HPβCD, with the scattering center being observed at the scattering angle, 2_, of about 18◦. This indicates the amorphous nature of HPβCD. As for the AC/HPβCD complex, only the scattering peaks similar to those of HPβCD were obtained, indicating the amorphous nature of the material. When AC was physically mixed with HPβCD, however, both the sharp diffraction peaks of AC and the diffused, scattering peaks of HPβCD were evident. These results confirmed the inclusion of AC within the cavity of HPβCD.

Two dimensional 1H-NMR

To investigate the spatial arrangement of AC within the HPβCD cavity, Nuclear Overhauser Effect Spectroscopy (NOESY) was applied on the stoichiometric AC/HP_CD complex (1:1 molar ratio) that had been dissolved in D2O and the result is shown in Fig. 5a.Cross-peaks were observed between the CH3-29 and CH3-27 protons of AC and the H-3 inner-cavity proton of HP_CD (located at the wide side of the cavity) and between the CH3-26 and H-6 protons of AC and the H-5 inner-cavity proton of HP_CD (located at the narrow side of the cavity). This indicates that the cyclohexene ring moiety of AC is captivated within the cavity of HP_CD, as depicted in Fig. 5b, hence confirming the stoichiometric 1:1 molar ratio between AC and HP_CD in the solid complex. Notwithstanding, the specific interactions between H-12, H-18, Glc-1, Rha-5, and Rha-Me protons of AC and the H-2, H-4, and H-6 outer-cavity protons of HP_CD are believed to be the probable cause for the self-aggregation of adjacent AC/HP_CD entities.

Characterization of AC- and AC/HPˇCD complex-loaded CA films

Physical appearance

Prior to the addition of CA powder into the AC/HP_CD solutions, the diametric dimensions of the self-assembling aggregates of the AC/HP_CD complex that had been prepared at different HP_CD to AC molar ratios of 0.5, 1, and 2 were determined by the nanosizer to be 2.38฿1.39, 3.34฿0.66, and 3.84 ฿0.53_m, respectively (see Supplementary data). Evidently, the size of the aggregates was an increasing function of the HP_CD proportion in the solution. CDs are known to form into self-assembling aggregates, which is facilitated by their ability to form inter-molecular hydrogen bonding (Coleman & Nicolis, 1992; Gonzцlez-Gaitano et al., 2002; Suzuki, Tsutsui, & Ohmori, 1994). In addition, Mele et al. (1998) reported that _-carotene in its complexation with _ and _-CDs in water existed as large aggregates, as revealed by both light scatteringand 1H NMR techniques. Factors that influence the formation of self-assembling aggregates are, for examples, concentration and molecular weight of CDs, pH, and temperature, while high pH, high temperature, and the addition of an electrolyte have been used as

means to prevent the aggregation (Bonini et al., 2006; Das, Mallick, Sarkar, & Chattopadhyay, 2008; He, Fu, Shen, & Gao, 2008).

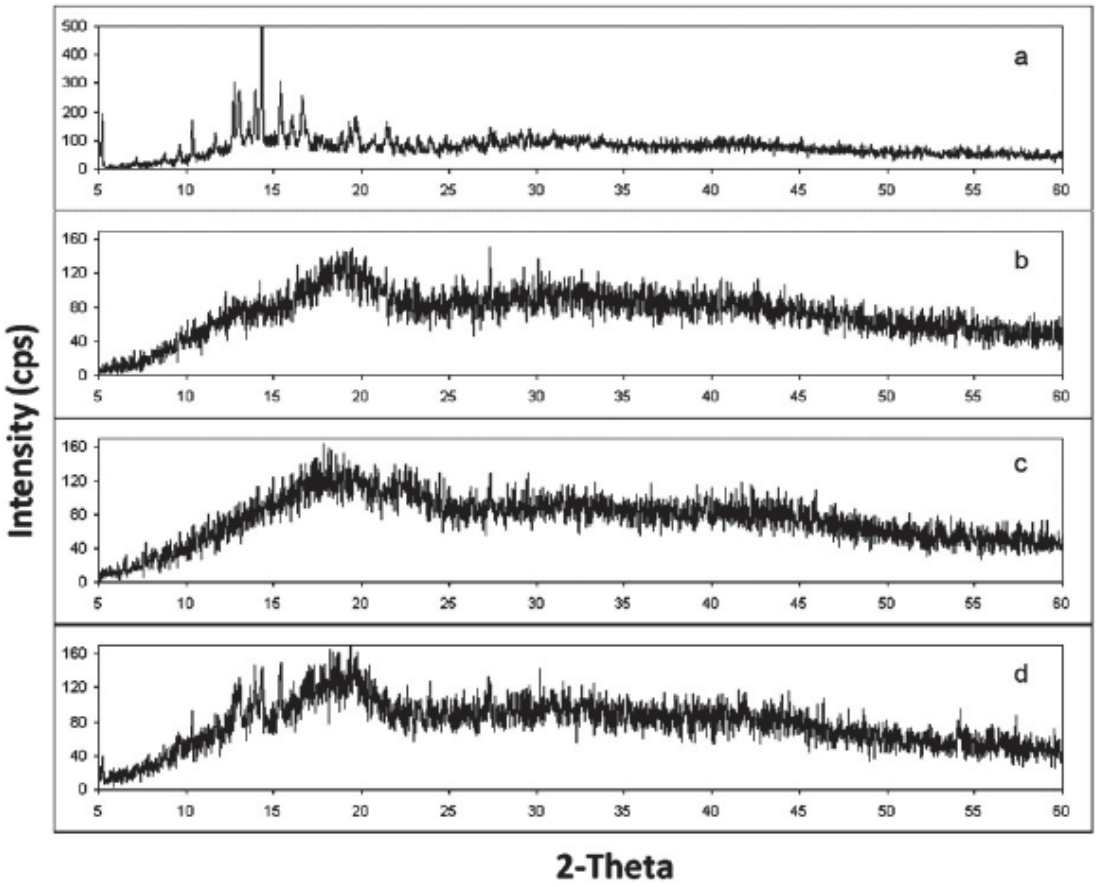


Fig. 4. X-ray diffractograms of (a) AC, (b) HPβCD, (c) AC/HPβCD complex, and (d) physical mixture of AC and HPβCD.

Table 1
Chemical shift signals of protons (in ppm) of AC and HPβCD in the free (δ_0) and the complexed (δ_c) states in D_2O at the equi-molar ratio between AC and HPβCD of the inclusion complex, along with their differences.

Proton	δ_0	δ_c	$\Delta\delta\,(\delta_c - \delta_0)$
AC			
H-12	5.162	5.216	0.054
H-18	2.033	2.087	0.054
CH_3-24	0.644	0.667	0.023
CH_3-26	0.777	0.831	0.054
CH_3-27	1.132	1.134	0.002
CH_3-29	0.844	0.869	0.025
Glc-1	4.385	4.323	−0.062
Rha-CH_3	1.301	1.321	0.002
Rha-5	3.942	3.988	0.046
HPβCD			
H-1	5.090	5.086	−0.004
H-2	3.542	3.546	0.004
H-3	3.817	3.896	0.079
H-4	3.525	3.526	0.001
H-5	3.600	3.620	0.020
H-6	3.682	3.760	0.078

SEM was used to investigate the morphologies of the obtained AC- and AC/HP_CD complex-loaded CA films. Representative images are illustrated in Table 2. Apparently, the surface of the AC-loaded CA film was rough, with no evidence of any specific pattern on it. This should be due to the complete dissolution of AC in the 90:10 (v/v) mixture of 80 vol.% acetic acid and DMAc, prior to the addition of the CA powder, resulting in rather homogeneous distribution of AC throughout the mass of the resulting CA film. On the other hand, specific pattern in the form of spherical aggregates was observed on all of the AC/HP_CD complex-loaded CA films. Specifically, an increase in the HP_CD to AC molar ratio resulted in a monotonous decrease in the sharpness of the boundary of these aggregates. It is believed that these entities were the self-assembling aggregates of the AC/HP_CD complex that had been formed in the AC/HP_CD solutions. The diameters of the aggregates that had been formed at the AC:HP_CD molar ratios of 1:0.5 and 1:1 were 0.73฿0.13 and 0.84฿0.12_m, respectively. However, those of the ones that had been formed at the AC:HP_CD molar ratio of 1:2 could not be precisely measured. Clearly, the dimensions of these self-assembling aggregates of the AC/HP_CD complex were much smaller than those determined by the nanosizer. Such discrepancy could be based on a couple of reasons: (i) the dry or the solvated state of the materials during the measurements by the SEM or the nanosizer, respectively, and (ii) the dependence of diametric projection of the spherical aggregates of the AC/HP_CD complex across the thickness of the AC/HP_CD complex-loaded CA films.

Water retention and weight loss behavior

The CA films containing either AC or the AC/HP_CD complex were further characterized to investigate water retention and weight loss behavior in the P/B/M medium at 37 ◦C. After the specified immersion time of 24 h had been reached, the weights of the film specimens were recorded and these were calculated to obtain the property values, as reported in Fig. 6. Among the various CA films investigated, the AC-loaded CA films (shown in the figure as the samples with the HP_CD to AC molar ratio of 0) exhibited the lowest water retention (i.e., at about 12%). Such values for the CA films containing either AC or CACE at 40 wt.%, after immersion in the P/B/M medium at 37 ◦C for 24 h, were reported to be about 39

and 52%, respectively (Suwantong et al., 2008). Compared with the value obtained in the present work, the greater water retention values as reported in the work of Suwantong et al. (2008) could be due to a couple of reasons: (i) the difference in the solvent type used in the fabrication of the films that could affect the physico-chemical properties of the resulting films (Li, Ren, Fane, Li, & Wong, 2006; Romero, Leite, & Goncalves, 2009; Valente, Polishchuk, Burrows, & Lobo, 2005) and (ii) the difference in the as-loaded amounts of the drug within the films that could affect the porosity of the films after the drug molecules had been released into the medium (Suwantong, Opanasopit, Ruktanonchai, & Supaphol, 2007). On the other hand, the water retention of the AC/HP_CD complex-loadedCA films was much greater than those of the AC-loaded CA films, with the average value increasing from about 38% at the HP_CD to AC molar ratio of 0.5 to about 68% at the HP_CD to AC molar ratio of 2.0. The AC-loaded CA films also exhibited the lowest weight loss after immersion in the medium (at about 3%). Slightly greater values at about4or7%were reported bySuwantonget al. (2008) for the CA films that contained either AC or CACE at 40 wt.%, respectively.The reasons for the discrepancy in the property values as reportedin the presentworkand those in theworkof Suwantong et al. (2008)are similar to those given in the previous paragraph. On the contrary,the loss in the weight of the AC/HP_CD complex-loaded CA films was much greater than those of the AC-loaded CA films, withthe average value increasing from about 19% at the HP_CD to ACmolar ratio of 0.5 to about 30% at the HP_CD to AC molar ratio of2.0. The loss in the weight of a drug-loaded material in a mediumdepends on a number of factors, e.g., the solubility of the drug, thesolubility of the carrier material, the diffusion of the drug from thecarrier material, and so forth. Due to the low aqueous solubility of both AC and CA in water, the presence of methanol in the medium and of HP_CD in the AC/HP_CD complex-loaded CA films were the obvious reasons for the improvement in the aqueous solubility of both the drug and the matrix materials.

Release of AC from AC- and AC/HP˘CD complex-loaded CA films

The effect of HP_CD on the release characteristics of AC from the CA films at different AC:HP_CD molar ratios was evaluated by the total immersion method in the P/B/M medium. They were reported as the percentages of the ratios of the cumulative amounts of AC released to the amounts of the drug actually loaded within the filmsor to the actual weights of the films, as shown in Fig. 7. The actualamounts of AC within the AC- and the AC/HP_CD complex-loaded CAfilms were a priori determined to be 70.7, 80.3, 69.2, and 83.0% on average (based on the as-loaded amounts of AC within the casting solutions), for the CA films that had been prepared at the AC:HP_CDmolar ratios of 1:0, 1:0.5, 1:1, and 1:2, respectively. For the AC-loaded CA films (the content of AC initially loaded in the casting solution was 10 wt.%, denoted in Fig. 7 as the samples with the AC:HP_CD molar ratio of 1:0), none of the as-loaded AC, at any given immersion time point, was able to release intothe medium. Suwantong et al. (2008) reported that the maximal amounts of AC released from the CA films that had been prepared from the casting solution containing 40 wt.% of the drug were about 11% on average (based on the AC amounts initially loaded within the films). The discrepancy between the amounts of AC released from the CA films in the present work and those reported in the work of Suwantong et al. (2008) should be influenced by the fact that the amounts of AC initially loaded within the films, as reported in the two studies, were different (i.e., 10 versus 40 wt.%), hence the difference in the driving force for diffusion. The different types of the solvent used in the fabrication of the films [i.e., 90:10 (v/v) mixture of 80 vol.% acetic acid and DMAc as in the present work versus 2:1 (v/v) acetone/DMAc as in the work of Suwantong et al. (2008)], which could render different densities to the obtained films, may also contribute to the discrepancy in the results obtained in the two studies.

In comparison with the AC-loaded CA films, the presence of HP_CD in the AC/HP_CD complex-loaded CA films was clearly responsible for the significantly greater amounts ofACreleased into the medium. Furthermore, the cumulative amounts of AC released from the films, at any given immersion time point, increased with an increase in the HP_CD content. Specifically, about 25% of the AC actually loaded within the AC/HP_CD complex-loaded CA films, a priori prepared at the AC:HP_CD molar ratios of 1:0.5, 1:1, and 1:2, was able to release into the medium within about 1200, 60, and

30 min, respectively. The maximal amounts of AC released from these materials, after having been immersed in the medium for 1440 min, were about 30, 78, and 98% of the amounts of AC actually contained within the CA films, respectively. These values corresponded to about 2.2, 3.9, and 5.8% of the released amounts of AC, when calculated based on the actual weights of the film specimens.
As mentioned, as the HP_CD content in the films increased, significantly more amounts of AC could be released into the medium. The complexation of a poorly water-soluble drug with a native cyclodextrin (CD) as well as its derivatives improves tremendously the aqueous solubility and the dissolution rate of the drug within an aqueous medium. This phenomenon is especially important for a highly hydrophilic derivative of CD, such as HPβCD. Pose-Vilarnovo et al. (2001) reported that the aqueous solubility of sulfamethizole (i.e., a sulfonamide antibiotic drug) was improved significantly upon forming into an inclusion complex with βCD or HPβCD. The difference as observed in the cumulative amounts of AC released from the AC/HPβCD complex-loaded CA films that had been prepared at various AC:HPβCD molar ratios could be explained based on a couple of reasons. Firstly, the ability of AC to form an inclusion complex with HPβCD disfavored the crystallization of the herb, as evidenced from the X-ray results (see Fig. 4). This allows greater opportunity for the solvent molecules to interact with those of the drug. Secondly, the presence of HPβCDincreased the hydrophilicity of the films, as evidenced by the increase in the water retention of the films with an increase in the HPβCD content (see Fig. 6). Lastly, due to the highly hydrophilic nature of HPβCD, the dissolution of the unassociated HPβCD as well as the AC/HPβCD inclusion complex into the releasing medium could occur easily, which helped facilitate the solubilization of the drug within the medium. This is evidenced by the observed increases in both the weight loss of the films in and the cumulative amounts of AC released from the films into the medium with an increase in the HPβCD content (see Figs. 6 and 7, respectively).

The latter case was accented by the observation of microholes on the AC/HPβCD complex-loaded CA films after having been immersed in the releasing medium (see Table 2). The diametric dimensions of these holes, as measured directly from the SEM images shown in Table 2, were 0.87±0.14, 1.17±0.28, and 1.20±0.19_m for the films that had been prepared at the AC:HPβCD molar ratios of 1:0.5, 1:1, and 1:2, respectively. These dimensions were essentially similar to the spherical aggregates that had been observed on the films prior to the immersion (see Table 2 and related texts in Section 3.3.1).

Conclusions

Asiaticoside (AC), from the medicinal plant Centella asiatica L., readily forms a complex with 2-hydroxypropyl-_-cyclodextrin(HPβCD) at a 1:1 molar ratio both in distilled water and 90:10 (v/v) mixture of 80 vol.% acetic acid and N,N-dimethylacetamide (DMAc).The average diametric dimension of the self-assembling aggregates of the AC/HPβCD complex, in the solvated state, increased from about 2.4_mat the HPβCD to AC molar ratio of 0.5 to about 3.8_m at theHP_CDto AC molar ratio of 2. In the solid state, the AC/HPβCDcomplex that had been prepared at the stoichiometric molar ratioof 1:1 did not show the crystalline nature of the as-received AC. Two-dimensional NMR revealed that the cyclohexene ring moiety of AC is captivated well within the HPβCD cavity. The solvent-castcellulose acetate (CA) films that had been prepared in the presenceof amixture of AC/HPβCDof varying molar ratios (i.e., 1:0.5, 1:1, and 1:2) showed evidence of spherical aggregates on their surfaces. Thedimensions of these aggregates were lower than those of the selfassembling aggregates of the AC/HPβD complex in the solvated state. While AC could not be released from the AC-loaded CA film into the phosphate buffer saline solution (PBS) containing 10% (v/v)methanol (i.e., P/B/M medium), its cumulative amounts that had been released from the AC/HPβCD complex-loaded CA films were much greater, with values increasing with an increase in theHP βCD content. At 24 h of immersion in the medium at 37 ◦C, the maximal amounts of AC released from these materials were about 2.2,3.9, and 5.8% (based on the actual weights of the film specimens), respectively.

8. Effect of Degree of Acetylation on in VitroBiocompatibility of Electrospun Cellulose Acetate-Based Fibrous Matrices

EXPERIMENTAL DETAILS

Materials

Cellulose acetate (CA; white powder; M_w= 30,000 Da; degree of acetyl substitution H 2.4; acetyl content = 39.7%) was purchasedfrom Sigma-Aldrich (USA). Sodium hydroxide(NaOH) was purchased from AjaxFinechem (Australia) and hydrochloric acid(HCl) was from J.T. Baker (USA). Acetone(Carlo Erba, Italy), *N, N*-dimethylacetamide[DMAc, Labscan (Asia), Thailand], andethanol [Labscan (Asia), Thailand] wereused as-received.

Preparation of Electrospun CA FiberMats

The electrospinning of CA was carried out based on the method described in apublished work by some of us and another colleague [26]. Briefly, a weighed amount of CA powder was dissolved in 2:1 v/v acetone/DMAc to obtain a CA solution at a fixed concentration of 17% w/v. Electrospinning of the solution was carried out using a Gamma High Voltage Research ES30P high voltage dc power supply as the power source, a flat-tipped 20-gauge stainless steel needle (OD = 0.91 mm) as the nozzle, and an aluminum foil wrapped around a home-made rotating metal drum (OD = 9 cm) as the fiber collection device. The electric field was 17.5 kV/15 cm, the rotational speed of the rotating drum was 60 ± 5 rpm, and the feed rate of the solutions was 1 mL h^{-1}. For 9 h of continuous electrospinning, the thicknesses of the CA fiber mats were 20-30 ⌈m.

Thermal Treatment and Alkaline Treatment

The CA fiber mats were peeled off from the aluminum foil, sandwiched between two polytetrafluoroethylene (PTFE) sheets, and put in a hot-air oven at 208°C for 1 h [25]. They were then immersed in 0.1 N NaOH solution in 4:1 v/v water/ethanol mixture at room temperature (25 ± 1°C) for varying time intervals, ranging from 10 min to 24 h. The alkaline-treated CA fiber mats were then rinsed in deionized (DI) water and kept in a desiccator prior to further uses.

Characterization

Physical characteristics

Morphological appearance of the neat, the heat-treated, and the alkaline-treated CA fiber mats was observed by a JEOL JSM-5200 scanning electron microscope (SEM). They were sputtered with a thin layer of gold using a JEOL JFC-1100E ion sputtering device prior to SEM observation.

Chemical functionalities and degree of deacetylation

Chemical functionalities of the neat and the alkaline-treated CA fiber mats were investigated by a Nicolet Nexus 670 Fouriertransform infrared spectroscope (4 cm^{-1} resolution with 4 scans over the wavenumber range of 400-4000 cm^{-1}). The degree of deacetylation (*%DD*) of the alkaline-treated CA fiber mats was evaluated by a titration method. Specifically, weighed samples of the CA fiber mats (2.8 cm in diameter) were immersed in 0.1 N of NaOH solution in 4:1 v/v water/ethanol mixture at the ratio of 1:1 w/v. After 10 min to 24 h of immersion, 5 mL of the NaOH solution was pipettedout and then titrated with 0.1 N HCl aqueous solution, with phenolphthalein being used to indicate the basicity-to-acidity crossover. The amount of the hydroxyl ions participatedin the deacetylation reaction of CA could then be calculated from the amount of the titrant, which was used to calculate the *%DD*, i.e.

$$\%DD = \frac{m_i - m_f}{m_i} \times 100, \quad (1)$$

where m_i and m_f are the moles of the acetyl groups in the CA fiber mats before and

Wide-angle X-ray diffraction studies

The crystalline nature of the neat, the heat-treated, and the alkaline-treated CA fiber mats was examined by a JEOL JDX 3530 wide-angle X-ray diffractometer (30 kV and 40 mA over the 2Theta range of 5 to 50°).

Physico-chemical characteristics

The water retention and the loss in the mass upon submersion in water of the neat and the alkaline-treated CA fiber mats were measured after their submersion in distilled water at 37°C for 24 h. If M_i denotes the initial mass of each fiber mat sample in its dry state and M and M_d are its masses after submersion in distilled water in its wet and dry states, respectively, the property values can be calculated as follows:

$$\text{Water retention (\%)} = \frac{M - M_d}{M_d} \times 100 , \quad (2)$$

$$\text{Mass loss (\%)} = \frac{M_i - M_d}{M_i} \times 100 . \quad (3)$$

Biological Evaluation

The potential for use of the neat and the alkaline-treated CA fiber mats as wound dressing materials was assessed by the indirect cytotoxicity evaluation and the direct cultures of mammalian cellsonto their surfaces. Two types of cells were used: 1) human foreskin fibroblasts(HFF) and 2) immortalized non-tumorigenic human keratinocytes (HaCaT). The experiments were done in adaptation from previously-published protocols [12]. Briefly, either type of cells was first cultured in Dulbecco's modified Eagle's medium (DMEM; Sigma-Aldrich, USA), supplemented with fetal bovine serum (FBS; Biochrom, UK), L-glutamine (Invitrogen, USA), penicillin (Gibco→, Invitrogen, USA) and streptomycin (Gibco→, Invitrogen, USA). When the cells reached 80% confluence, theywere trypsinized and counted by ahemacytometer, prior to further uses.The indirect cytotoxicity of the fibrousmaterials was assessed based on the method that was adapted from the ISO10993-5standard test method. Briefly, the specimens(~14 mm in diameter), pre-washed with 70% ethanol for 30 min, were washed with autoclaved phosphate buffer saline (PBS)solution twice and once with the culture medium. Either type of cells was seeded in wells of a 24-well tissue-culture polystyrene plate (TCPS; Corning, USA) at $2 \cdot 10^4$ cells/ well. After 24 h of attachment, the culture medium was replaced with serum-free medium (SFM; DMEM containing penicillinand streptomycin, but without FBS). Each of the specimens was then place into each well and both the cells and the specimen were incubated further for 1, 3, and 5 d.

The extraction ratio was fixed at 10 mg mL^{-1}. After each specified time interval was reached, the medium in each well was removed. The viability of the cells was then quantified by 3-(4,5-dimethylthiazol-2-yl)-2,5-diphenyltetrazolium bromide (MTT) assay. The viabilities of the cells that had been cultured with fresh SFM were used as control.

For the direct cell culture studies, the well-washed specimens were placed in wells of 24-well TCPS. A stainless steel metal ring (12 mm in diameter) had been placed on top of each fiber mat specimen and 500 mL of the culture medium had been pipette into each well, prior to the cell culturing. Subsequently, $2 \cdot 10^4$ cells/well of either type of cells were seeded onto each specimenand allowed to attach and proliferate for 1, 3,and 5 d. After rinsing the specimens withPBS twice to remove unattached cells, the viabilities of the cells were quantified by the MTT assay and the viabilities of the cells that had been cultured on TCPS were used as control. Lastly, the morphology of the cultured cells was investigated. The cellcultured specimens were harvested and washed with PBS twice. After the cells had been fixed with 3% glutaraldehyde aqueous solution and washed with 0.2 M PBS aqueous solution, the specimens were dehydrated through a series of grade ethanol solutions and pure ethanol for 2 minand finally dried in air. Finally, they werobserved by SEM.

Statistical Analysis

All the quantitative values were expressed as means ± standard deviation values. Statistical comparisons were performed using one-way ANOVA with SPSS 13.0 for Windows software (SPSS, USA). *P* values < 0.05 were considered statistically significant ($n = 3$).

RESULTS AND DISCUSSION

Morphology

The as-prepared 17% w/v CA solution in 2:1 v/v acetone/DMAc was electrospun under the electric field of 17.5 kV/15 cm for a fixed collection time of about 9 h [26]. A selected SEM image of the obtained fiber mats is shown in Figure 1a. The diameters of these individual fiber segments were determined to be 265 ± 39 nm (n ε 50). Due to the fluffiness of the obtained fibrous matrices, further treatment in an alkaline aqueous solution would become a problem, as the materials could easily lose their physical integrity. Ma et al. [25] suggested that this shortcoming could be solved by thermally-treating the fiber mats at 208°C for 1 h. Figure 1b shows the morphology of the representative heat-treated fiber mat, which is obviously similar to that of the untreated precursor. The thermal treatment not only imparted the ease of handling to the fibrous matrices, but also helped maintain their physical integrity after having been submerged in 0.1 N NaOH solution in 4:1 v/v water/ethanol mixture at 25 ± 1°C for periods of up to 24 h. Figure 1c-e shows the morphology of the fiber mats after they had been submerged in the alkaline solution for 10 min, 30 min and 24 h, respectively. Apparently, the fibrous character of the alkaline-treated fiber mats was still intact, with no evidence of the individual fibers being destroyed. On the other hand, Son et al. [24] reported that, after being submerged in a potassium hydroxide (KOH) solution in ethanol for 30 min, obvious destruction of the CA fiber mats was evident.

Chemical Functionalities and *%DD*

The deacetylation reaction of the alkaline-treated CA fiber mats was followed qualitatively by FT-IR and quantitatively by titration. Figure 2 illustrates representative FT-IR spectra of a neat CA fiber mat and some of the CA fiber mats that had beensubmerged in the alkaline solution for 10 min, 30 min, and 24 h. For the neat CA fiber mat, a strong absorption peak centering at 1750 cm^{-1}, corresponding to the carbonyl groups (C=O) of the acetyl esters of CA, was evident. After 10 min of the alkaline treatment, the intensity of this peak decreased appreciably. Further increasing the alkaline treatment time resulted in a monotonous decrease in the intensity of the peak. The peak disappeared completely after submerging the mat in the NaOH solution for 24 h, thereby confirming the successful formation of RC fiber mats. In a similar manner, the presence of the peak centering at 1232 cm^{-1}, corresponding to the C-O stretching of the ester/ether groups of CA, decreased in its intensity upon submersion in the alkaline solution and even disappeared completely after 24 h of submersion in the alkaline solution. At 24 h of submersion in the NaOH solution, the presence of the peak centering at 1068 cm^{-1}, corresponding to the C-O stretching of the alcohol groups of cellulose, was clearly visible. Strikingly, the peak associated with the O-H stretching, centering at 3480 cm^{-1}, became more intense and broader for the alkaline-treated CA fiber mats, especially for the ones that had been submerged in the alkaline solution for 24 h.

The *%DD* values of all of the alkalinetreated CA fiber mats were determined by titration and the results are shown in Figure 3. It should be noted that the degree of acetyl substitution and the acetyl content of the as-received CA were 2.4 and 39.7%. The titration procedure was to quantify, in percentage, the amount of the acetyl groups that had been abstracted by the treatment with the NaOH solution. According to the obtained result, the *%DD* increased sharply from about 40% after 10 min of submersion in the alkaline solution to about 79% after 60 min of submersion. Further increase in the submersion time interval only resulted in a slight increase in the *%DD* to finally reach plateau values of about 88-90% after the CA fiber mats had been submerged in the alkaline solution for 7 to 24 h.

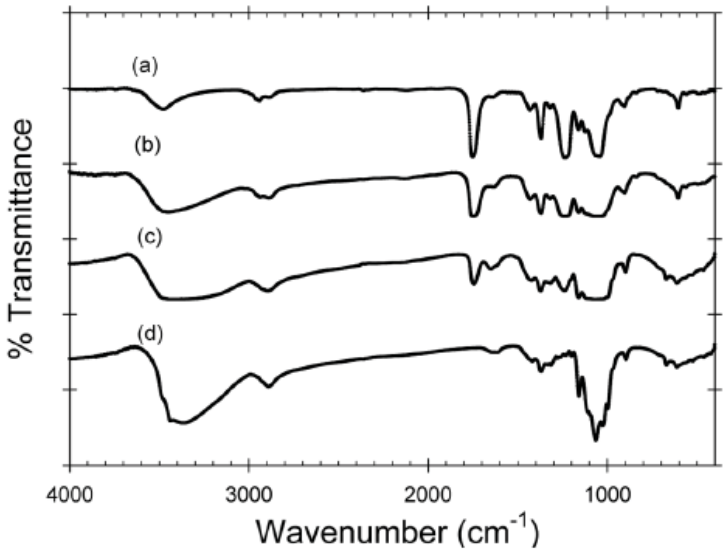


Figure 2. Representative FT-IR spectra of (a) a neat electrospun CA fiber mat and some of the thermally-treated fiber mats that had been submerged in 0.1 N NaOH solution in 4:1 v/v water/ethanol mixture at 25 ± 1°C for a period of (b) 10 min, (c) 30 min, and (d) 24 h.

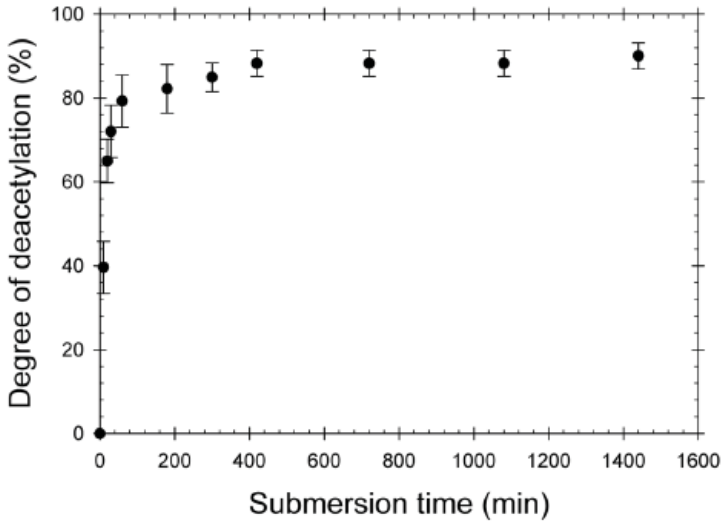


Figure 3. Degrees of deacetylation (*%DD*) of thermally-treated electrospun CA fiber mats that had been submerged in the NaOH solution as a function of submersion time (n = 5).

X-ray Diffraction

Figure 4 shows the X-ray diffraction patterns of the neat, the heat-treated, and some of the alkaline-treated CA fiber mats. For the neat CA fiber mat, two peaks at the 2Theta values of about 10.0 and 17.4° were observed. These peaks correspond respectively to the crystalline domains of CA and cellulose (ca. the acetyl content of the as-received CA was 39.7%). The intensity of these peaks increased appreciably after the thermal treatment, most likely a result of the increase in the mobility of the CA chains during the thermal treatment, hence the increase in the crystallinity of the crystalline domains. Kamide and Saito [27] reported a relationship between the glass transition temperatures (T_g, °C) and the degrees of acetyl substitution (z, □ [0,3]) of CA, which was given as $T_g = 249.9 - 20.3z$. For z = 2.4, T_g of the as-received CA should be about 201°C. At the treatment temperature of 208°C, CA molecules should, therefore, have enough mobility to form more stablecrystallites, hence the observed increase in the intensity of the crystalline peaks. The increase in the crystallinity of the thermally-treated CA would increase its stiffness and, at the same time, reduce the subservience to penetration by chemicals, hence an improvement of its physical integrity.

As for the alkaline-treated CA fiber mats, while the intensity of the low-angle peak decreased and shifted towards a higher2Theta value with an increase in the treatment time interval, that of the high-angle peak increased and also shifted towards a higher 2Theta value. As the intensity of the high-angle peak increased with an increase in the alkaline treatment time, it becomes obvious that the decrease in the acetyl content along the CA chains was responsible for the observed increase in the crystallinity of the alkaline-treated CA fiber mats as well as the rearrangement of the crystalline packing into that of cellulose. The reappearance of the-OH groups, hence the occurrence of the hydrogen bonding, should be responsible for the observed increase in the crystallinity of the alkalinet reated CA fiber mats.

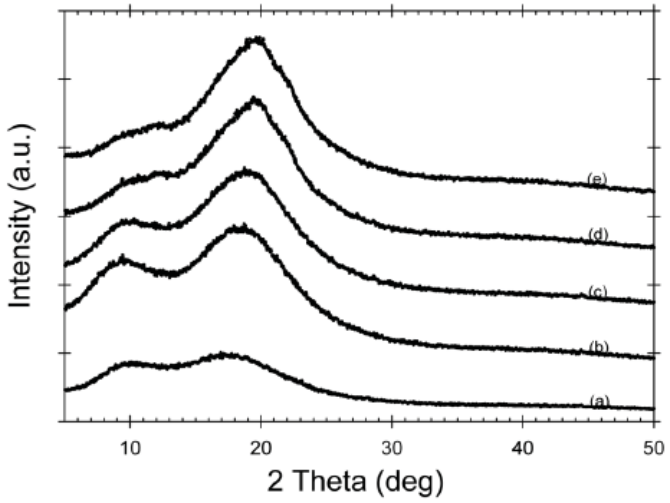


Figure 4. X-ray diffraction patterns of electrospun CA fiber mats (a) before and (b) after thermal treatment at 208°C for 1 h and those of the thermally-treated fiber mats that had been submerged in the NaOH solution for (c) 10 min, (d) 30 min, and (e) 24 h.

Physico-chemical Characteristics

The neat CA fiber mats and the CA fiber mats that had been treated with the alkalinesolution for 10 min, 30 min, and 24 h were studied further. Based on Figure 3, the acetyl contents of these fibrous materials were estimated to be about 40, 24, 11, and 4%, respectively. These materials were tested for the water retention and the loss in the mass upon submersion in water for 24 h and the results are summarized in Table 1. The water retention decreased after the CA fiber mats underwent the alkaline treatment and the variation in the submersion time did not have a strong influence on the property values. It should be noted that the retention of water in an ultrafine fibrous material originates from the absorption of water within the mass of the material and from the retention of water between inter-fibrous pores due to the capillary action. While the latter should increase when the CA fiber mats had been treated with the NaOH solution (i.e., due to the increase in the hydrophillicity), the fact that the water retention values of the alkaline-treated CA fiber mats were lower than that of the neat materials should be a result of the decrease in the absorbed amount of water within the mass of the matrix material. This, in turn, resulted from the fact that the CA fiber mats had to be thermally treated prior to being treated with the NaOH solution. The thermal treatment caused the crystallinity of the matrix material to increase, hence less amount of water to be absorbed. On the other hand, after the alkaline treatment, the loss in the mass of the fiber mats increased very slightly. It is well-known that cellulose undergoes alkaline degradation, the degradation occurs from the reducing ends of the molecule and produces watersoluble *D*-glucoisosaccharinic acid as a byproduct [28].

Table 1. Water retention and the loss in the mass of thermally-treated electrospun CA fiber mats before and after submersion in the NaOH solution for 10 min, 30 min, and 24 h ($n = 5$).

Sample	Water retention (%)	Mass loss (%)
Neat	420 ± 19	0.6 ± 0.5
10 min of alkaline treatment	335 ± 13	1.0 ± 0.7
30 min of alkaline treatment	326 ± 25	1.1 ± 0.7
24 h of alkaline treatment	336 ± 16	1.4 ± 0.6

* These fiber mat samples had been submerged in distilled water at 37°C for 24 h.

Indirect Cytotoxicity Evaluation

The indirect cytotoxicity of the neat CA fiber mats and the CA fiber mats that had been treated with the alkaline solution for 10 min, 30 min, and 24 h were evaluated against HFF and HaCaT. Here, it is assumed that the viability of the culturedcells was proportional to the MTT absorbance. Figure 5 shows the viabilities of the cells that had been cultured in SFM both in the absence and in the presence of the fiber mat specimens for 1, 3, or 5 d were reported relatively to that of the cells that had been cultured in the absence of the specimens for 1 d. Evidently, the viabilities of both types of cells that had been cultured on the surface of TCPS, without or with the presence of the fiber mat specimens, increased monotonically with an increase in the cell culturing time. In fact, the viabilities of the cells, at any given cell culturing time point, were statistically the same, without or with the presence of the fiber mat specimens. The results indicate clearly that the proliferative ability of the cultured cells was unaffected, despite the presence of the fiber mat specimens in the culture medium of up to 5 d. In other words, these fibrous materials released no substances in the levels that would be harmful or pose any adverse effect to the growth in the number of the cells.

. Cell Culture Studies

As previously mentioned, the acetyl contents of the neat CA fiber mats and the CA fiber mats that had been treated with the alkaline solution for 10 min, 30 min, and 24 h were about 40, 24, 11, and 4%, respectively. These fibrous materials were tested further for *in vitro* biocompatibility with HFF and HaCaT. The cells were directly seeded and cultured on these fibrous matrices for 1, 3, and 5 d and those seeded and cultured on bare wells of TCPS were used as positive control. Again, theviability of the seeded and the cultured cell was proportional to the MTT absorbance. Evidently, both types of cells adhered and proliferated well on the surface of TCPS. On day 1 of cell seeding, the viabilities ofboth types of cells that had been seeded on all of the fibrous matrices were not significantly different from those on TCPS,except for those of HaCaT that had been seeded on the neat CA fiber mats showing significantly lower values. On days 3 and 5, the viabilities of both types of cells that had been cultured on all of the fibrous matrices were inferior to those on TCPS.

For HFF, the variation in the acetyl contents of the CA-based fibrous matrices did not pose strong effect on the viabilities of the cells cultured on them on day 1. Such an effect was seen when the cells had been grown for longer periods of time (i.e., 3 and 5 d). On day 3, only the neat CA fiber mats could support the growth of the cells particularly better than the alkaline-treated counterparts. On day 5, the viabilities of the cells grown on the CA fiber mats that had been treated with the alkaline solution for 30 min increased, while those on the neat CA counterparts decreased, causing the 30 min-alkaline treated CA fiber mats to be the better support for the growth of the cells. For HaCaT, the variation in the acetyl contents of the CA-based fibrous matrices did not affect the viabilities of the cells grown on them on days 1 and 3, despite the slight increase in the viabilities of the cells on day 3, when compared with those on day 1. On day 5, the viabilities of the cells grown on the neat CA fiber mats and the CA fiber mats that had been treated with the alkaline solution for 24 h, which showed equivalent values, increased slightly from day 3, those of the cells grown on the CA fiber mats that had been treated with the alkaline solution for 10 and 30 min decreased slightly.

The morphologies of both HFF and HaCaT that had been seeded and culturedon the surfaces of the CA-based fibrous matrices are shown in Table 2. On day 1, both types of cells extended their cytoplasm over the surfaces of the fibrous matrices particularly well and even appeared in their normal cell shapes (i.e., spindle-like morphology for HFF and cobblestone morphology for HaCaT). On day 3, HFF on the neat CA fiber mat still appeared expanded over the surface, but the extent of the cellular expansion was much decreased, when compared with the cells on day 1. HFF on the surfaces of the alkalinetreated CA fiber mats, on the other hand, were completely round. The change of the cell shape from spindle-like into round morphology, as the cell culturing time increased, suggested that the CA-based fibrous matrices are not supportive of the growth of human fibroblasts. This is in line with the observation reported by Sanchavanakit et al. [29] on bacterial cellulose fibrous membranes. Unlike HFF, HaCaT, on day 3 in their culture on the surfaces of all of the fibrous matrices, still retained their cobblestone morphology. However, the cells appeared to be more aggregated, especially those that had been cultured on the surfaces of the CA fiber mat that had been treated with the alkaline solution for 10 and 30 min. Despite the aggregation of the cells, the numbers of HaCaT on the surfaces of the CA fiber mat and the CA fiber mat that had been treated with the alkaline solution for 24 h increased from those on day 1. As reported by Sanchavanakit et al. [29], bacterial cellulose fibrous membranes showed good support for adhesion and proliferation of human keratinocytes.

CONCLUSIONS

FT-IR, titration, and X-ray diffraction confirmed partial removal of acetyl groups from the thermally-treated (208°C for 1 h) electrospun CA fiber mats upon submersion in 0.1 N NaOH solution in 4:1 v/v water/ethanol mixture at 25 ± 1°C. For the CA fiber mats that had been treated with the alkaline solution for 10 min, 30 min, and 24 h, the acetyl contents were about 24, 11, and 4%, respectively (cf. the acetyl content of about 40% for the asreceived CA). The indirect cytotoxicity evaluation of the CA and the RC fibrous matrices against human fibroblasts (HFF) and human keratinocytes (HaCaT)

indicated that these materials did not release any substance in the level that would be toxic or suppress the growth of both types of cells. Further evaluation with the direct culture of the cells on the materials revealed that these materials could only support the short term culture of both types of cells (i.e., 1 d) and only the neat CA fiber mats and the CA fiber mats that had been treated with the NaOH solution for 24 h showed marginally good support for the proliferation of the human keratinocytes. These results suggested the potential for use of the fibrous matrices as temporary dressings of skin wounds and this should be evaluated further *in vivo*.

9. PREPARATION CHARACTERIZATION AND STUDY OF CRUDE BONE PROTEIN DELIVERY FORM GELATIN MICROSPHERES AND GELATIN MICROSPHERES INTEGRATED HYALURONAN GELATIN BLENDED SCAFFOLD FOR BONE TISSUE REGERNATION

EXPERIMENTAL SECTION

1. Materials

Gelatin from porcine skin (type A, Bloom no.170-180) was purchased form Fluka (Switzerland). Gelatin form bovine skin (type B, Bloom no.175-225) was purchased from Sigma Aldrich (USA). Hyaluronan (MW 1.35×10^6) was purchased from Coach Industries Inc (Japan). Albumin from bovine serum, tetramethylrhodamine conjugate (MW 66,000 Da) was purchased from Molecular Probes Inc (USA). Rhodamine protein label kit was purchased form Pierce (USA). Saturated Glutaraldehyde aqueous solution (5.6 M) was purchased from Fluka (Switzerland). 1-ethy-3-(3-dimethylaminopropyl)carbodiimide (EDC) was purchased form Fluka (Switzerland). Acetone (AR grade) was purchased from Lab-Scan (Thailand). All other chemical agents were of analytical grade and used without further purification.

2. Gelatin microspheres preparation

Gelatin microspheres were prepared by a thermal gelation technique with modification. In detail, 10 ml of 15% w/v gelatin (type A or B) aqueous solution was prepared at 40°C. In addition to the physiologic pH which is 5.2 or 4.95 for the gelatin type A or B respectively, pH of the gelatin solution was adjusted to 7.4 and 10.0 by the addition of 1N HCl or 1M NaOH with an aim to study the effects of pH and type of gelatin on behaviors of the as-prepared microspheres. Then, the solution was added dropwise into 200 ml of Soya oil preheated at 40°C under continuously stirring at 1,000 rpm with a homogenizer to form water-in-oil emulsion. After 10 min, temperature of the emulsion was reduced to be 4°C with an ice bath while stirring was continued for an additional 30 min to allow for physically thermal gelation of the gelatin. Afterward, 200 ml of pre-cooled (4°C) acetone was added and stirred for the next 60 min in order to dehydrate and flocculate the coaceravate droplets. The microspheres were collected by filtration through a

sintered glass filter (1 μm pores size) under vacuum, washed three times with 100 ml of cool (4°C) acetone to remove residual oil, and dried in air at room temperature over 24 h.

To crosslink the gelatin microspheres, 250 mg of the dry microspheres was suspended in 10 ml of acetone-water (2:1, v/v) containing 1% (w/v,~100mM) Glutaraldehyde solution and stirred at 4°C, 500 rpm for 1 h. The crosslinked microspheres were collected through a sintered glass filter and washed with precooled (4°C) acetone. Then, the crosslinked microspheres were suspended in 20 ml of 10 mM aqueous glycine solution containing Tween 80 (0.1 wt%), shaken at 37 °C, 50 rpm for 1 h to block the residual aldehyde groups of the unreacted glutaraldehyde. The crosslinked microspheres were then washed twice with 60 ml of the cool deionized water (4°C), with cool acetone, filtered, and eventually air-dried at room temperature for over 24 h.

3. Crude Bone Protein preparation

CBP was extracted from the bovine jaws bone. In particular, bone was initially washed and cleaned thoroughly in tap water and then sectioned into small pieces with a diamond disc driven by a rotor. Pieces of bones were further crushed into powder in liquid Nitrogen. Then, the as-prepared powder was immersed in 0.6 N HCl at 4°C and shaken continuously on an orbital shaker. After three days, the bony solution was centrifuged and the supernatant was collected, dialyzed for 48 h and lyophilized. The dry CBP was kept in desiccators until use.

4. Fluorescent labeling of Crude Bone Protein

Crude Bone Protein (CBP) was fluorescent-labeled with the 5-(and 6)-carboxytetramethylrhodamine, succinimidyl ester (NHS-Rhodamine). Briefly, 10 mg/ml of CBP solution was prepared with 50mM borate buffer, pH 8.5 and transferred to a reaction tube. Then, 10 mg/ml of NHS-Rhodamine in DMSO was added. The reaction solution was gently mixed well and incubated in the dark at room temperature for 1 hour. To remove the non-reacted NHS-Rhodamine, the reaction solution was filtered through a D-salt dextran desalting column using 10 mM phosphate buffered saline (PBS) with 0.15 M NaCl as a filtrating medium. The effluent solution was collected in 500-μl fraction. All fractions were subsequently detected by measuring the absorbance with spectrophotometer at 280 nm to identify the fraction containing NHS-Rhodamine-labeled CBP (hereafter, CBP-Rhod). The concentration of the CBP-Rhod existing in the selected fraction was further determined using spectrofluorometer (Cary Eclipse™) at 541 and 572 nm for the excitation and emission wavelength respectively, based on a BSA-Rhod (Molecular Probes™) standard curve over the concentration range 1-50 μg/ml (r^2=0.996). The CBP-Rhod fraction was stored at 4°C and protected from light until ready to use.

5. CBP-Rhod loading into gelatin microspheres

Crosslinked gelatin microspheres were loaded with CBP-Rhod by diffusion method. In particular, the aforementioned CBP-Rhod fraction was diluted with 10 mM PBS, 0.15 M NaCl, pH 7.2 to achieve the concentration ~700 μg/ml. Gelatin microspheres were immersed in the diluted CBP-Rhod solution to attain the loading dose of 4 μg CBP-Rhod per mg dried microspheres. The resulting mixture was vortexed for 1 h and incubated at 4°C for 24 h to let the CBP-Rhod infuse. The impregnated microspheres were frozen at -40°C for 24 h, lyophilized, and kept in the dark at 4°C until use.

6. Fabrication of porous composite hyaluronan-gelatin scaffolds

Porous composite hyaluronan (HA)-gelatin scaffolds were fabricated by the solvent casting and freeze-drying technique. Briefly, 2% (w/w) aqueous solution of a HA and gelatin mixture (1:1, w/w) was prepared at 50°C and left to cool down to room temperature. Then, in order to facilitate the blending of HA and gelatin, ionic strength of the mixture was adjusted by adding the equal amount of NaCl to HA (1:1, mole/equ) and being mixed up for 30 min. The resulting mixture became clearer and more translucent. To crosslink the polymers, calculated amount of EDC (1x to HA, mole/equ) was added and reacted under 200 rpm stirring at room temperature for 2 h. Afterward, the neat or the CBP-Rhod labeled microspheres were suspended in HA-gelatin mixture at 1% (w/w) concentration, which equals to 50% (w/w) of the polymer weight. The suspension was continuously stirred until the microspheres were well dispersed in the mixture and the then was cast in polypropylene discs at a constant weight, freezed at -40°C and lyophilized at -50°C. The samples were kept in desiccators until use.

7. Characterization

7.1. Size and morphology of gelatin microspheres and microspheres integrated HA-Gelatin scaffold

Gelatin microspheres were initially inspected under the computer connected Polarizing Optical Microscope (DMRXP, Leica) at 20x magnification. The images were recorded and further used to measure the diameters of the microspheres with the UTHSCSA Image Tool version 3.0 software. One hundred microspheres were measured for each preparative condition and the average values of their sizes were calculated. The data were also used to determine size distribution of the microspheres both before and after crosslinking with 100mM Glutaraldehyde. For the morphological study, gelatin microspheres and the as-prepared scaffolds were mounted on brass stubs, coated with gold using a JEOL JFC-1100 sputtering device, and observed for their microscopic morphology using JEOL JSM-5200 scanning electron microscopy (SEM).

7.2. Swelling ability of gelatin microsphere

Swelling ability was determined by the alteration of microspheres' size after water uptake. 20 mg of the dry crosslinked microspheres were incubated in 10 ml of 10 mM PBS with 0.15 M NaCl at 37°C for 24 h. Then, sizes of the swelling microspheres were examined with the same procedure as previously described in 2.7.1. One hundred microspheres of each preparative condition were measured and the average diameters were calculated. The swelling ability was calculated according to the following equation:

$$\text{Swelling} = Ø_{swell} / Ø_{dry}$$

where $Ø_{swell}$ and $Ø_{dry}$ are the averaged diameter of the microspheres before and after incubation, respectively.

7.3. Zeta potential determination

Zeta potentials (or electrophoretic mobility) of the gelatin microspheres were determined using Zeta-Meter 3.0+ (Zeta-Meter, Inc., USA). Briefly, the suspension of 25 mg gelatin microspheres in 10 ml of deionized water was filled in an electrophoresis cell. Two electrodes were inserted into the cell and connected to the Zeat-Meter 3.0+ unit. Once the electrodes were energized, microspheres were aroused to move toward one electrode. A microsphere was observed under a microscope for its movement along a specific distance which was indicated by a built in grid. The zeta potential value was detected at a right time point when the microsphere moved to the end. Measurement was repeated 10 times for each preparative condition and the average values were calculated.

7.4. Actual loading of CBP-Rhod in gelatin microspheres

5 mg of Rhodamine-labeled gelatin microspheres were suspended in 1 ml of 10 mM PBS with 0.15 M NaCl in a 1.5 ml microcentrifuge tube. The tube was then placed in cool water and sonicated with the Sonicator (Vibracell™, Sonic, USA) at 20% amplitude. After 1 h, the suspension was centrifuged at 5,000 rpm for 5 min and the supernatant was collected. The actual amount of the CBP-Rhod in supernatant was determined using spectrofluorometer (Cary Eclipse™) by the same procedure done in the step of NHS-Rhodamine labeling (2.4). The experiment was carried out in triplicate and the results were presented in terms of Encapsulating efficiency of CBP-Rhod (EE) and Loading capacity of gelatin microspheres (LC), which were determined according to the following equation [31]:

$$\text{Encapsulating efficiency (\%)} = (\text{total } \mu\text{g CBP-Rhod encapsulated} / \text{initial } \mu\text{g CBP-Rhod loaded}) \times 100$$

$$\text{Loading capacity (\%)} = (\text{total mg CBP-Rhod encapsulated} / \text{total mg microspheres}) \times 100$$

7.5. In vitro CBP-Rhod release

In vitro release of CBP-Rhod from gelatin microspheres and the microspheres integrated HA-gelatin scaffold were investigated in buffer solution by a standard sampling-separation method. In the release assay, 5 mg of the CBP-loaded microspheres and one piece of the microspheres integrated HA-gelatin scaffold (circular shape with 10 mm in diameter and 2 mm in height), which contained 2.5 mg of gelatin microspheres, were separately immersed in 1 mL of 10 mM PBS with 0.15 M NaCl, and incubated in a shaking water bath (70 rpm) at 37°C. At a given time point, 500 µl of the buffer solution (hereafter, the sample solution) was withdrawn and an equal amount of fresh medium was added in order to maintain a constant volume of the medium. The sample solution was centrifuged at 5000 rpm for 5 min at room temperature and the amount of CBP-Rhod in the sample solution was determined by spectrofluorometry at 541 and 572 nm for the excitation and emission respectively, as previously described. An average value was calculated at each time point. The experiment was done in triplicate.

7.6. Statistical analysis

Data were analyzed using the SPSS software version 14.0 for window. Initially, the normal distribution was assessed by the Shapiro-Wilk test. The normal distribution data, representing the homogeneity of the variances, shown by the Levene's test, were then investigated by the one-way analysis of variance (ANOVA) with the Tukey HSD post hoc multiple comparisons. Otherwise, the Dunnett T3 would be applied if the data did not exhibit the homogeneity of the variances. For the data of which the normal distribution was absent but the variance was homogeneous, the Kruskal-Wallis H was applied. To compare the means between 2 data groups, the students' unpaired t-test was used. The significant level was indicated at $p < 0.05$ in any case.

RESULTS AND DISCUSSION

1. Morphology of gelatin microspheres and microspheres integrated HA-Gelatin scaffold

The selected SEM images of the uncrosslinked gelatin microspheres are shown in Fig.1. As observed, the microspheres prepared at any given condition presented entirely spherical geometry with a smooth surface, on which the macroscopic pores were not detected. Aggregation of the various sizes microspheres into many small clusters was shown in all cases. In our opinion, such aggregation was caused by the direct contact between the adjacent particles once the solvent was expelled during microspheres preparation. The electrical charge on the surface of particles might be diminished in dry environment so that the electrostatic repulsive force was also weakened; as a consequence, repulsion among particles was unlikely illustrated.

Fig. 2 show the selected SEM images of internal architecture of the composite HA-gelatin scaffold. A well-defined porous structure and the inter-pore connectivity were observed throughout the bulk. The incorporated gelatin microspheres were extensively embedded into the wall of scaffold without deterioration of their geometry. Nevertheless, exceptional for the quite small particles, almost microspheres were not thoroughly submerged in thin walls of scaffold. This manifestation may be responsible for controlled release of the absorbed protein since the releasing medium could transport through the exposed microspheres differently from the one covered with walls of scaffold.

2. Effect of gelatin type and pH on size of the gelatin microspheres

Upon the preparation of gelatin microspheres by thermal gelation technique, the average size of particles depends on several manufacturing parameters, for instance, the type and dimension of stirrer, diameter of the vessel or container, volume ratio between aqueous and oil phases and their respective viscosities, stirring speed, and the surface tension between the two immiscible phases governed by type of the selected oil phase [32]. In this study, all parameters were identically controlled in order to investigate the effect of gelatin type and pH on the microspheres size, and it was found that sizes of the as-prepared microspheres varied from ~4 to ~40 μm in which over 85% of the microspheres range between ~8 to ~25 μm (Fig. 3). For all given conditions, the size distributions presented a similar pattern of which the curves of normal distribution were observed.

The average sizes of the as-prepared gelatin microspheres at various conditions are presented in Fig. 4. Diameters of the uncrosslinked samples range between ~10 and ~20 μm for gelatin A microspheres, and between ~11 and ~ 23 μm for gelatin B microspheres. Average sizes of the microspheres were apparently in the same dimensional range for any preparative condition. However, when the data were statistically analyzed with the Univariate analysis of variance; test of between-subjects effects, sizes of the as-prepared microspheres were significantly different through the influence of the interaction between type of gelatin and pH. Effect of gelatin type or pH on microspheres size, therefore, can not be individually analyzed. The data were thus reorganized into six discrete groups and analyzed further with one-way ANOVA. The results presented that sizes of both gelatin A and B microspheres prepared at pH 7.4 and 10.0 are statistically the same, in contrast to the microspheres prepared at their physiologic pH at which gelatin A microspheres were significantly smaller than those of gelatin B. The effect of interaction between gelatin type and pH are thus limited at a certain condition, probably only at the physiologic pH.

Considering the crosslinked samples, only gelatin A microspheres prepared at its physiologic pH (5.2) presented a significant reduction in particle size comparing with the others which were ~11 and ~15 μm respectively. The difference in particle sizes might be due to the difference in crosslinking intensity of gelatin A from the others which was particularly favored at its physiologic pH, resulting in a denser

network and smaller particle sizes [19]. Such observation was also detected in the size of swelling microspheres. Since the CBP was anticipated to be incorporated into gelatin microspheres by diffusion method, swelling ability of the microspheres was required to facilitate absorption of the CBP solution. The as-prepared microspheres illustrated ability to absorb and retain water as the hydrated swelling characteristic was remarkably observed in every study group (Fig. 5). With the crosslinking condition done in this study, the as-prepared microspheres could swell in water significantly at ~1.3 to 1.6 folds over their sizes in the dry state (Table 1). However, the difference of their swelling ability was not noticeably observed at any particular preparative condition.

The type of gelatin used and pH, thus, did not have a clear effect on the resulting size of the microspheres behaving in the uncrosslinked, crosslinked or swelling condition. The result of this study partially corresponded to that of Vandervoort and Ludwig in 2004 [19] which found that type of gelatin did not influence the resulting size of nanoparticle prepared by desolvation method where as the pH did.

3. Zeta potentials

The zeta potentials value of the microspheres was measured at all given conditions with an aim to study the influence driven from gelatin type and pH. The value would also be beneficial in the study of CBP loading and releasing through gelatin microspheres.

The zeta potentials of the microspheres at all given conditions were investigated with an aim to study the influence of gelatin type and pH on zeta potentials of the resulting microspheres. The impact of zeta potentials on CBP loading and releasing was also investigated

Zeta potentials values of the as-prepared microspheres are shown in Fig. 6.. Evidently, both gelatin A and B microspheres presented different zeta potentials values at different pH. In addition, those samples prepared with the same type of gelatin but at different pH also presented different zeta potentials values. Only the pH 10.0 at which statistic analysis was carried out due to the zeta potential values were so close as ~-54 and ~-58 mV for gelatin A and B microspheres, respectively in order to ensure the significance of difference. The analysis revealed their statistically different, therefore, both type of gelatin and pH do have significant influences on the zeta potential value of the microspheres obtained.

Since zeta potential is an indicator of charge density [21], the pH-induced disparity of zeta potential value can be explained with the isoelectric point (IEP), which factually is the pH at which net molecular charge and thus zeta potential is equal to zero. The IEP of gelatin A and B are ~9 and ~5, respectively [19,22], bringing about a different electrical charge of both gelatin types in function of the pH. The electrical charges of gelatin A and B are both positive at their physiologic pH since the pH was under IEP. At pH 7.4, gelatin A has a net positive charge by the under-IEP pH, while gelatin B is charged

negatively by the over-IEP pH. And eventually at pH 10.0 which is over the IEP, they both present negative charge.

Concerning gelatin microspheres, the IEP of type A and B gelatin microspheres located somewhere in between pH 7.4-10.0 and pH 4.95-7.4, respectively (see Fig. 6). The IEP of the obtained microspheres corresponded to the theoretical IEP of gelatin precursor at any given pH. Therefore, the procedure of microspheres preparation used in this study, the thermal gelation in water-in-oil emulsion technique, does not affect the microspheres zeta potentials.

4. Loading of CBP in gelatin microspheres

Encapsulation of CBP into gelatin microspheres in this study was on the basis of polyion complexation. It was expected that a degree of molecular interaction was able to take place between bone proteins and gelatin microspheres of opposite charges [22]; as a consequence, a higher yield of the ionic complexes should result in higher encapsulation efficiency and loading capacity [1,22,23].

In order to overcome either the inactivity of bone protein from those procedures of microspheres preparation or the low loading yield of bone protein which was available in limited quantity, this study designed to incorporate CBP into the preformed empty gelatin microspheres by rehydrating the freeze-dried gelatin microspheres with a solution of the CBP-Rhod at 4°C for 24 h. Such condition should be favorable for the complete absorption [23]. The amount of CBP-Rhod that had been loaded in gelatin microspheres was reported as either the encapsulating efficiency (EE) or the loading capacity (LC) as shown in Table 2.

As observed, the EE of CBP-Rhod ranges highly between ~70 to ~ 90 % for both gelatin types. Comparatively, pH was deemed to influence on the EE with an opposing manner between gelatin A and B microspheres. The EE in groups of gelatin A microspheres was found to be significantly highest at pH 10.0 in which the electrostatic charge was negative; whereas such statistically indifferent highest EE was also found in groups of gelatin B microspheres but at the physiologic pH in which the charge was positive (see also Fig. 6). Basing on the polyion complexation, this observation suggests the existence of both positively and negatively charged protein molecules in the crude bone extracts.

In addition, the encapsulation of CBP was not only influenced by the pH but also the gelatin type. The EE at pH 10.0 was found to be significantly different between gelatin A and B microspheres while the EE at pH 7.4 were insignificantly different. A disparity of zeta potential value due to pH change was not the only answer of the case as shown by the Univariate analysis of variance; test of between-subjects effects (data not shown) that the interaction between gelatin type and pH affect significantly to the EE and LC. As a consequence, both factors could not be separately considered.

Concerning the LC, the result ranges between ~ 280 to ~370 μg of the CBP-Rhod per 100 mg of microspheres. Reliance of the LC on type of gelatin and pH at any given condition was found to be identical

with the EE. Therefore, the encapsulation of the CBP into microspheres evidently depends on both type of the gelatin and pH.

5. In vitro CBP-Rhod release

5.1. CBP-Rhod release form gelatin microspheres

The CBP-Rhod release form gelatin microspheres and the composite scaffolds were presented in term of CBP-Rhod cumulative releasing percentage from which the actual quantity of CBP-Rhod loaded in gelatin microspheres was calculated, as shown in Fig. 7.

The profiles of CBP-Rhod release form gelatin microspheres are apparently different from the composite scaffolds. Though the release profiles are similar at any given condition of either gelatin microspheres or the composite scaffolds, the amounts of CBP-Rhod release are remarkably different. In particular, the extremely high and low release is observed at the pH 10.0 of gelatin B and A microspheres respectively, where as those of the other conditions are quite the same. However, all profiles astoundingly illustrate the initial burst release of CBP-Rhod within the first hour which was about 73-96 %.

In order to study the CBP release kinetics, the semi-empirical equation based on a power-law expression was introduced as follows [33,34]

$$M_t/M_\infty = kt^n$$

where M_t/M_∞ is the fractional release of the CBP-Rhod, k is a constant concerning the structure and geometry of the releasing device and n is the releasing exponent indicating the mechanism of drug release. By using the least square method, the k and n can be detected from a profile in the plot of log M_t/M_∞ as a function of log t (min), as presented in Fig. 8 and Table 3.

From the log M_t/M_∞ - log t plot, The CBP-Rhod release profiles showed biphasic modulation characterized by an initial relatively rapid release period within the first 30 minutes followed by a slower release phase. The phase separation is indicated by the difference of the n value calculated as the slope of a straight line fitted to the profile with a satisfactory high correlation coefficient (see table xxx). The n values of all samples are close to zero particularly in phase 2 which is the slower release phase, leading the factor "t^n" of the semi-empirical equation close to 1 at any time point. Comparatively, the results are much different form what have been theoretically identified as the n values of the monodispersed sphere are 0.43 and 0.85 for Fickian diffusion and the Case-II transport respectively, or 0.30 and 0.45 respectively for the mixture of multiple sizes microspheres [34,35]. The CBP-Rhod releases from gelatin microspheres, therefore, are constant and hardly depend on the time observed. The fast release implies that the anticipated polyion complexation between the CBP-Rhod and gelatin microspheres did not completely occur. This may be due to the molecule of Rhodamine which from the covalent amide bond to primary amine on the protein restricts the ionic interaction between the molecules of protein and gelatin.

5.2. CBP-Rhod release form composite scaffolds.

Comparing to the gelatin microspheres, the releases of CBP-Rhod from the composite scaffolds are slower and a period of sustained release is illustrated at any preparative condition. The amount of CBP-Rhod release within the first hour was approximately 36-50%. Interestingly, the extremely high and low release is also observed at scaffolds incorporated with pH 10.0 gelatin B and A microspheres respectively.

From the log Mt/M∞ - log t plot, The CBP-Rhod release profiles showed three phases of release according to the calculated n values (see Fig. 8 and Table 3). Phase 1 correlated to an initial burst release of CBP-Rhod from the scaffolds within the first 30 min. The n values in this phase range from 0.37 to 0.62 which correlate to the theoretical value as mention earlier. Phase 2 corresponded to the sustained release of CBP-Rhod starting from 1 hour to 7 days. The n values of this slow release phase are much lesser than those in phase 1, but are in the same range as the n values of the initial burst CBP-Rhod release form gelatin microspheres. Phase 3, eventually, represented the CBP-Rhod release with an increasing rate from phase 2 but not faster than phase 1.

Considering the mechanism of CBP-Rhod release from the composite scaffolds, the initial burst release may be the combination of diffusion and dissolution release since the n values are in between 0.30 and 0.45[34,35] (except for gelatin B pH 7.4). Such observation is not found in case of CBP-Rhod release from gelatin microspheres. It is believed that CBP-Rhod might partially release into the HA-Gelatin blended solution in which the CBP-Rhod encapsulated gelatin microspheres were dispersed during the process of composite scaffolds fabrication. As a consequence, the releasing CBP-Rhod was also integrated in the mass of HA-Gelatin scaffolds. The initial burst release, therefore, may be the release from the scaffold matrix instead of the incorporated gelatin microspheres.

The mechanism of the sustained release in phase 2 may be the same as that of the initial burst release form gelatin microspheres, but occurs at a slower rate due to their comparable n values and lesser constant (k) values in most samples of the former case. This observation suggests that the sustained release concerns the release of CBP-Rhod from the incorporated gelatin microspheres exposing into porosities within scaffolds.

During phase 3 release, the degradation of HA-Gelatin scaffold might occur, as being observed during sampling, and induce the exposure of the underneath scaffold matrix including the gelatin microspheres which were previously submerged. The rate of CBP-Rhod release is thus higher, but the mechanism can not be truly described regarding the theoretical n values because the mostly n values of phase 3 are lesser than the lower range of the theoretical n values. However, it is believed that phase 3 release is influenced by degradation and diffusive processes.

In this study, the difference in size between the gelatin microspheres was probably not large enough to result in a significantly different CBP-Rhod release rate [33,36]. However, the ongoing mechanism of the CBP controlled release can be the organization of a diffusion-erosion process contributed by the capability of water uptake into the gelatin microspheres and the ability of protein transportation through the scaffold. Microspheres formulation mainly controls the induction time necessary to achieve protein release while the composition of polymeric scaffold controls the release rate [37]. Therefore, a temporal and spatial control of signaling molecules may be obtained by the combination of the appropriated microspheres and scaffold formulations.

CONCLUSION

Type of gelatin and the preparative pH are the two factors that should be considerably controlled in the design of bone protein delivery scaffold which contains gelatin microspheres as an incorporated delivery device. Interaction between those two factors influences significantly on size of the as-prepared microspheres, surface charge or the zeta potential, swelling ability and encapsulation capability of the CBP. This effect, however, is not observed in the drug release studies. The ionic interaction between molecules of bone protein and gelatin in the microspheres was not large enough to provide sustained release of the CBP. Incorporation of the CBP loaded gelatin microspheres into HA-Gelatin blended scaffold create a complex environment and the synergistic functions between gelatin microspheres and scaffold in which controlled release was evidently presented.

10. Development of polycaprolactone porous scaffold by combined solvent casting, particulate leaching and polymer leaching techniques for bone tissue engineering

Experimental Section

Materials. Polycaprolactone (PCL; 80,000 $gmol^{-1}$) were purchased from Sigma-Aldrich, USA. Polyethylene glycol (PEG; MW = 200, 600, and 1,000 $gmol^{-1}$) was purchased from Merck,Germany. Chloroform (Labscan; Asia, Thailand) was used as solvent for these polyesters. Sodium chloride (Ajax Finechem, Australia) was used as porogen. All other chemicals were of analytical reagent grade and used without further purification.

Preparation of PCL scaffolds. A solvent casting, polymer leaching and salt particulate leaching was used to prepare the scaffold. Briefly, the polymer solution was prepared by mixing the PCL pellet, PEG and chloroform in the concentration of 28% w/v, then the solution was stirred at room temperature for 2-3 hr, after that NaCl salt particles with size of 400-500 μm (polymer/NaCl = 1/30 w/w) were added. The mixture was then packed into Petri dishes and the cylindrical mold with the dimension of 1.2 mm in diameter and 0.8 mm in thickness. The molds were then placed in the hood overnight for solvent evaporation. After the time, the materials were immersed in deionized(DI) water for 48 hr with repeated change of DI water every 8 hr for leaching out the PEG and salt particles. Scaffolds were air-dried for 24 hr and vacuum-dried overnight. The salt-PEG leached PCL scaffolds have highly interconnectivity pores network. Prior to casting, each of the PCL and PCL-PEG blend solutions was characterized for its viscosity by using a Brookfield DV-III programmable viscometer. The measurement was carried out at room temperature (that is, 25±1 ℃).

Characterization of PCL scaffolds.

Microstructure observation. The morphology of the pores, their size, distribution and the interconnectivity between these pores of the porous scaffolds were observed by JEOL JSM-5200 scanning electron microscopy (SEM), Olympus SZH10 stereomicroscope, and Carl Zeiss Mirax desk visual slide microscope. One cylindrical scaffold was randomly selected from each group, cut with razor blade at the middle of the scaffold and mounted onto SEM stub. Cross sections of the scaffolds were coated with thin film of gold using JEOL JFC-1100E sputtering devices for 5 min prior to observation under SEM

Porosity, pore volume, and pore size. Porosity and pore volume of the scaffolds were measured gravimetrically according to the following equations:

$$Porosity\,(\%) = \left(1 - \frac{\rho_{scaffold}}{\rho_{polymer}}\right) x\ 100$$

$$Pore\ volume = \left(\frac{1}{\rho_{scaffold}} - \frac{1}{\rho_{polymer}}\right) x\ 100$$

where $\rho_{polymer}$ is the density of the polymer from which the scaffolds were fabricated and $\rho_{scaffold}$ is the apparent density of the scaffolds which was measured by a Sartorius YDK01 density measurement kit. Here, ρ_{PCL} was taken the value of 1.145 g cm^{-1}. Five specimens were measured for both the porosity and the pore volume and an average value for each property was calculated. On the other hand, pore size of the scaffolds was directly measured from SEM images, using a SemAfore Digital slow scan image recording

system version 5.0 software. At least 30 pores for each of the cross- and the longitudinal sections (i.e., at least 60 pores in total) were measured and the average values for all of the scaffolds investigated were calculated.

Water absorption capability. The scaffold specimens, cut from the moldings that had been cast in the Petri dishes (circular shape with 15 mm in diameter and 3 mm in height), were first dried, weighed, and individually immersed in 10 mL of 10 mM phosphate buffer saline solution (PBS; pH 7.4) at room temperature. At a given time point, the specimens were taken out, carefully placed on the glass for 5 sec to remove the excessive water and weighed immediately. The amount of water retained in the specimens was determined according to the following equation:

$$Water\ absorption\,(\%) = \frac{(Ww - Wd)}{Ww}\ x\ 100$$

where W_d and W_w are the weight of the specimens before and after submersion in the medium, respectively. The experiment was carried out in pentuplicate and the measurements were carried out at different time intervals within a period of 14 d.

Water permeability. To obtain information about pore interconnection, flow resistance was evaluated by sealing the scaffolds between two rubber rings at the bottom of a measuring tube ending and filled with 10 cm of water. To keep the water level as even as possible during flow, the tube was communicating with a large diameter reservoir. Before each test, samples were preconditioned in water for 24 h. Flow resistance of scaffolds was then evaluated as the time needed for 10 ml of water to flow through the scaffold.

Compressive modulus. Compressive Modulus of the scaffolds were determined with a universal testing machine (Lloyd LRX, UK) using 500 N loaded cell in the dry state at room temperature, the both before and after degraded scaffolds at the different time interval were vertically compressed at the crosshead speed of 3 mm/min. The load was applied until the scaffolds were compressed to approximately 70% of their original thickness. The initial compressive modulus was determined as the slope of the linear portion of the stress strain curve at a compressive strain of 20%.

Biological characterization of PCL scaffolds.

Cell culture and cell seeding. Mouse fibroblasts (L929) and mouse calvaria-derived, pre-osteoblastic cells (MC3T3-E1) were used as reference cell lines. L929 were cultured as monolayer in Dulbecco's modified Eagle's medium (DMEM; Sigma-Aldrich, USA), supplemented with 10% fetal bovine serum (FBS; BIOCHROM AG), 1% L-glutamine (Invitrogen Corp.), and a 1% antibiotic and antimycotic formulation [containing penicillin G sodium, streptomycin sulfate, and amphotericin B (Invitrogen Corp.,

USA)]. MC3T3-E1 were cultured in Minimum Essential Medium (with Earle's Balanced Salts) (MEM; Hyclone, USA), supplemented by 10% fetal bovine serum (FBS; BIOCHROM AG, Germany), 1% L-glutamine (Invitrogen Corp., USA) and 1% antibiotic and antimycotic formulation [containing penicillin G sodium, streptomycin sulfate, and amphotericin B (Invitrogen Corp., USA)]. The medium was replaced every 2 days and the cultures were maintained at 37°C in a humidified atmosphere containing 5% CO_2.

Each scaffold was cut into circular discs (about 15 mm in diameter) and the disc specimens were placed in wells of a 24-well tissue-culture polystyrene plate (TCPS; Biokom Systems, Poland), and were later sterilized in 70% ethanol for 30 min. The specimens were then washed with autoclaved de-ionized water, PBS and subsequently immersed in MEM overnight. To ensure a complete contact between the specimens and the wells, the specimens were pressed with a metal ring (about 12 mm in diameter). MC3T3-E1 from the culture was trypsinized [0.25% trypsin containing 1 mM EDTA (Invitrogen Crop., USA)] and counted by a hemacytometer (Hausser Scientific, USA). MC3T3-E1 were seeded at a density of about 60,000 cells/well for attachment study and 30,000 cells/well for proliferation study, on the scaffold specimens and empty wells of TCPS that were used as control. For indirect cytotoxicity, alkaline phosphatase activity, mineralization evaluations, MC3T3-E1 were seeded at a density of about 40,000 cells/well on the scaffold specimens and empty wells of TCPS. The culture was maintained in an incubator at 37°C in a humidified atmosphere containing 5% CO_2.

Cytotoxicity evaluation. Two types of cells were used: 1) mouse calvaria-derived, pre-osteoblastic cells (MC3T3-E1) and 2) mouse fibroblasts (L929). Indirect cytotoxicity test was conducted on TCPS, salt leached PCL, salt-PEG 200 leached PCL, salt-PEG 600 leached PCL, and salt-PEG 1000 leached PCL. First, extraction media were prepared by immersing samples (about 15 mm in diameter) in a serum-free medium (SFM; containing DMEM, 1% L-glutamine, 1 % lactabumin, and 1% antibiotic and antimycotic formulation for L929 and containing MEM, 1% L-glutamine, 1 % lactabumin, and 1% antibiotic and antimycotic formulation for MC3T3-E1) for 1, 3, and 7 days. Each of these extraction media was used to evaluate the cytotoxicity of the scaffolds. L929 or MC3T3-E1 were separately cultured in wells of a 24-well culture plate in 10%serum-containing DMEM and MEM, respectively, for 16 h to allow cell attachment on the plate. Then, the cells were starved with SFM for 24 h, after which time the medium was replaced with an extraction medium. After 24 h of cell culturing in the extraction medium, 3-(4,5-dimethylthiazol-2-yl)-2,5-diphenyl-tetrazolium bromide (MTT) assay was carried out to quantify the amount of viable cells. The experiments were carried out in triplicate.

MTT Assay. The MTT assay is based on the reduction of the yellow tetrazolium salt to purple formazan crystals by dehydrogenase enzymes secreted from the mitochondria of metabolically active cells. The amount of purple formazan crystals formed is proportional to the number of viable cells. First, each culture medium was aspirated and replaced with 400 mL/well of MTT solution at 0.5 mg mL

for a 24-well culture plate. Secondly, the plate was incubated for 30 minutes at 37 °C. The solution was then aspirated and 1 mL/well of dimethylsulfoxide (DMSO) containing 125 mL/well of glycine buffer (pH 10) was added to dissolve the formazan crystals. Finally, after 5 min of rotary agitation, the absorbance of the DMSO solution at 540 nm was measured using a Thermospectronic Genesis10 UV/Visible spectrophotometer.

Cell attachment and proliferation. Cell behavior such as adhesion and proliferation represent the initial phase of cell–scaffold communication that subsequently effect differentiation and mineralization. For attachment study, MC3T3-E1 was allowed to attach to TCPS, salt leached PCL, salt-PEG 200 leached PCL, salt-PEG 600 leached PCL, and salt-PEG 1000 leached PCL for 2, 4 and 6 h, respectively. Each sample was rinsed with PBS to remove unattached cells prior to morphological observation. Morphological appearance of the cells during attachment period was observed by SEM. For proliferation study, the viability of cells on the specimens was determined after 1, 2, and 3 day of cell culturing by DNA Quantification assay. The experiments were carried out in triplicate.

DNA Quantification Assay. The amount of DNA signifying the number of proliferated cells that had been cultured on each of the scaffolds for 1, 2, and 3 day was quantified by a DNA Quantification Kit (SigmaAldrich, USA). Briefly, the cultured cells were thoroughly washed twice with 400 μL of PBS. The cells were then lysed with 400 μL of a cell lysis buffer. The obtained suspension was centrifuged for 10 min to precipitate the cell debris. The supernatant was pipetted out at 20 μL, which was later mixed with 2mL of 0.1 μg/mL Bisbenzimide H 33258 solution in 10X Fluorescent Assay Buffer. The fluorescent emission intensity of the obtained solution was then measured at 460 nm, after it had been excited at 360 nm, using the microplate reader.

Morphological observation of cultured cells. After removal of the culture medium, the cell-cultured scaffold specimens were rinsed with PBS twice and the cells were then fixed with 3% glutaraldehyde solution, which was diluted from 50% glutaraldehyde solution (Sigma, USA) with PBS, at 500 μl/well. After 30 min, they were rinsed again with PBS. After cell fixation, the specimens were dehydrated in an ethanol solution of varying concentration (i.e. 30, 50, 70, 90, and 100%, respectively) for about 2 min at each concentration. The specimens were then dried in 100% hexamethyldisilazane (HMDS; Sigma, USA) for 5 min and later let dry in air after removal of HMDS. After completely dried, the specimens were mounted on an SEM stub, coated with gold, and observed by a JEOL JSM-5200 scanning electron microscope (SEM).

Production of Alkaline Phosphatase of Cultured Cells. ALP activity of MC3T3-E1 was measured using Alkaline Phosphate Yellow Liquid. In this reaction, ALP catalyzes the hydrolysis of colorless organic phosphate ester substrate, *p*-nitrophenyl phosphate (pNPP) to a yellow product, p-nitrophenol, and phosphate. MC3T3-E1 was cultured on scaffold specimens for 3, 5, and 7 day to observe the production of

alkaline phosphatase (ALP). The specimens were rinsed with PBS 2 times after removal of culture medium. Alkaline lysis buffer (10 mM Tris-HCl, 2 mM $MgCl_2$, 0.1% Triton-X100, pH 10) (100 µl/well) was added and the samples were scrapped and then frozen at -20°C for at least 30 min prior to the next step. An aqueous solution of 2 mg/ml *p*-nitrophenyl phosphate (pNPP; Zymed Laboratories, USA) mixed with 0.1 M amino propanol (10 µl/well) in 2 mM $MgCl_2$ (100 µl/well) having a pH of 10.5 was prepared and added into the specimens (110 µl/well). The specimens were incubated at 37°C for 15 min. The reaction was stopped by adding 900 µl /well of 50 mM NaOH and the extracted solution was transferred to a cuvette and placed in the UV-visible spectrophotometer, from which the absorbance at 410 nm was measured. The amount of ALP was then calculated against a standard curve. In order to calculate for the ALP activity, the amount of ALP had to be normalized by the amount of total protein synthesized. In the protein assay, the samples were treated in the same manner as the ALP assay up to the point was the specimens were frozen. After freezing, bicinchoninic acid (BCA; Pierce Biotechnology, USA) solution was added into the specimens. The specimens were incubated at 37°C for 15 min. The absorbance of the medium solution was then measured at 562 nm by the UV-visible spectrophotometer and the amount of the total protein was calculated against a standard curve.

Mineralization analysis. Alizarin Red-S is a dye that binds selectively calcium salts and is widely used for mineral staining (the staining product i.e., an Alizarin Red S-calcium chelating product). The isolated osteoblastic cells were plated in 24-well plates at 40,000 cells/well and cultured in the culture medium. After 24 h, the cultures were treated with culture medium, with the supplement of 50 µg/ml ascorbic acid (Sigma, USA), 5 mM β-glycerophosphate (Sigma, USA), and 0.2 µg/ml dexamethasone (Sigma, USA), the medium was replaced every 2 days. After 14 days treatment, cells were washed with PBS and fixed with ice-cold absolute methanol for 10 min. Fixed cells were stained with 1% Alizarin Red in deionized water (Sigma, USA) (pH 4.2) for 2-3 min. After removing alizarin red-S solution, the cells were rinsed with deionized water and dried at room temperature. The images of each culture were captured and the stain was extracted with the use of 10% cetylpyridinium chloride (Sigma, USA) in 10 mM sodium phosphate for 1 h and absorbance of the collected dye was read at 570 nm in spectrophotometer (Thermo Spectronics Genesis10 UV-visible spectrophotometer).

Statistical analysis. Values expressed as the mean ± standard deviation. Statistical analysis of different data groups was performed using One-Way Analysis of Variance (ANOVA) with the least-significant difference (LSD) test using SPSS software version 11.5. The values of *p* lower 0.05 were considered statistically significant.

Results

Preparetion of PCL scaffolds.

Table 1 show the viscosity of PCL solution and PEG-PCL blend solution in chloroform. The PCL solution was 1064 ± 15 cP on average while the PEG-PCL blend solution were in the range of 989 – 1106 cP on average.

Characterization of PCL scaffolds.

Microstructure Observation.

Figure 1 shows the stereomicroscope images of porous scaffolds formed by PCL, different types of PEG and NaCl salts in chloroform following NaCl and PEG leaching out in deionized water. Figure 2 and 3 show the visual slide microscope images of porous PCL scaffolds.

Fig. 4 and 5 show the SEM micrographs of microporous scaffolds formed by PCL/PEG blends by various types of PEG (PEG, MW = 200, 600, and 1,000) following by leaching in aqueous medium. The highly interconnected pores were formed in scaffolds after PEG was leached out, and corresponded to the transpaprent spots shown in stereomicroscope and visual slide microscope images. The size of pores in scaffolds prepared from PEG leached out were larger than that from no PEG leached out and more interconnected channels were distributed throughout the former ones. Well defined and interconnected pores, detected by optical microscope and SEM analysis of PCL scaffolds, resulted from the use of both salt and PEG. An irregular geometry of pores was obtained for NaCl leached and NaCl-PEG leached scaffolds. The pore dimensions of the obtained scaffolds ranges between 378 and 435 μm on average ($n \geq 30$).

Porosity, Pore volume and Pore size.

As shown on table 2. , the porosity of scaffold showed the reverse trend with the density value. The porosity values of salt leached PCL scaffolds was 91.6% while the porosity values of the salt-PEG leached PCL scaffold were in the range of 91.2-92.6% on average (n=5).The density of scaffolds were in the range of 0.096-0.101.

Specially, the porosity increased from ∽ 91.6% for salt leached scaffold to ∽ 91.8% for salt-PEG 600 leached scaffold and 92.6% for salt-PEG 1000 leached scaffold, and pore volume increased from 9.6 cm^3g^{-1} for salt leached scaffold to 9.9 cm^3g^{-1} and 10.9 cm^3g^{-1} for salt-PEG 600 leached and salt-PEG1000 leached PCL scaffold . The pore volume increased with an increased the porosity.

Water absorption capability.

Figure 6 illustrates the water absorption capabilities of the salt leached, salt-PEG 200 leached, salt-PEG 600 leached and salt-PEG 1000 leached PCL scaffolds in 0.1 M PBS at room temperature within 7 days. All salt-PEG leached PCL scaffolds showed a similar profile of the water absorption, the water absorption rate increased rapidly in the early 30 minute and maintained stable in 24 hr. While salt leached PCL scaffold showed a different profile of the water absorption, the water absorption rate slightly increased

in the early 24 hr and maintained stable. Moreover, the water absorption capabilities of the PCL scaffolds were compared at 24 hr; it found that the salt leached PCL scaffold exhibited the lowest level of water absorption compared to the others.

Water permeability

Figure 7 show the flow resistance for the salt leached, salt-PEG 200 leached, salt-PEG 600 leached and salt-PEG 1000 leached PCL scaffolds. The flow resistance of salt leached PCL scaffold was in the range of 14.2-21.6 sec/10 ml (distance ∽ 15-50 cm). The flow resistance of salt-PEG 200 leached PCL scaffold was in the range of 11.1-15 sec/10 ml (distance ∽ 15-50 cm). The flow resistance of salt-PEG 600 leached PCL scaffold was in the range of 11.7-13.5 sec/10 ml (distance ∽ 15-50 cm). The flow resistance of salt-PEG 1000 leached PCL scaffold was in the range of 10.2-13.2 sec/10 ml (distance ∽ 15-50 cm).

Compressive modulus.

The increase in the porosity of the scaffolds resulted in an decrease in compressive properties. The compressive modulus decreased from ∽ 88 kPa for the salt leached scaffold to 28, 42, and 49 for salt-PEG 200 leached, salt-PEG 600 leached, and salt-PEG 1000 leached PCL scaffold, respectively.

The compressive modulus of the scaffolds was found to decrease as follow:

Salt leached > salt-PEG 1000 leached > salt-PEG 600 leached > salt-PEG 200 leached PCL scaffold.

Biological evaluation of neat and modified PLA fibrous scaffolds.

Indirect cytotoxicity evaluation.

Both mouse calvaria-derived preosteoblastic cells(MC3T3-E1) and mouse fibroblasts cells (L929) were used in the assessment. However we were interested in using the obtained scaffolds as potential bone scaffolds, it was mandatory to test the materials with L929 just to comply with the ISO10993-5 standard test method. For both types of cells, about 40,000 cells/well were seeded in empty wells of TCPS. Indirect cytotoxicity test was conducted on salt leached, salt-PEG 200 leached, salt-PEG 600 leached, and salt-PEG 1000 leached PCL scaffolds. Figure 8 a) and 8 b) show the viability of the cells obtained from MTT assay after the cells had been cultured with the 1, 3, 7 day- extraction media from scaffolds as compared with the fresh SFM(control TCPS). The viability of the cells was reported as the percentage with respect to that of the control. Evidently, the viability ratio of cells that had been cultured with all of extraction media (and with control TCPS) is greater than 80%. This results can be indicated that all types of PCL scaffolds released no substances at levels that were harmful to cells.

Cell attachment and cell proliferation.

The biocompatility of PCL scaffolds was evaluated in the terms of their ability to promote the proliferation of the cells that had been allowed to attach on their surfaces. Figure 9 shows the proliferation of MC3T3-E1 on the surface of TCPS and the PCL scaffolds on day 1-3 after cell culturing in terms of the

viability of cells. The viability of cells on a scaffold could be quantified by Fluorescent emission intensity from the DNA Quantification test.

On day 1, the viability of cells on the salt-PEG leached scaffold was equivalent to that on TCPS while the viability of cell on the salt-PEG 200 leached, salt-PEG 600 leached, salt leached PCL scaffold was slightly lower than that on TCPS. On day 2, the viability of cell on the salt-PEG 1000 leached was equivalent to that on salt leached PCL scaffold. In comparison with TCPS the salt-PEG 200 leached scaffold was significantly lower. The proliferation of cells on salt-PEG 600 leached and salt-PEG 1000 leached PCL scaffold was significantly greater than that on TCPS and salt leached PCL scaffold on day 3.

Cell Morphology.

Table 2 and 3 show selected SEM images (magnification = 3500X; scale bar = 5 μm) of MC3T3-E1 that were either seeded or cultured on the surfaces of glass, salt leached, salt-PEG 200 leached, salt-PEG 600 leached, salt-PEG 1000 leached PCL scaffolds at different time points.

According to these images, cell morphology and interaction between cells and the scaffolds can be visualized. At 2 h after cells seeding, the majority of cells on the glass surface was stilled rounded. At 4 h after cells seeding, the majority of cells on the glass surface started to extend their cytoplasm. At 6 h after cells seeding, the majority of cells showed evidence of the extension of their cytoplasm on the surface. For the cells that were seeded on the surface of various types of scaffolds, at 2 h after cells seeding, the majority of cells on surface was rounded. At 4 h after cells seeding, the majority of cells was remained round, but a closer examination around the edge of the cells revealed an evidence of filopodia. At 6 h after cells seeding, the majority of cells on the scaffolds were evidently expanded.

At 1, 2, and 3 days after cells seeding, the majority of the cells seeded on the surfaces of all types of scaffolds expanded over the area of the scaffolds which were the most expansion on the surface of salt-PEG 600 leached and salt-PEG 1000 leached PCL scaffolds.

Alkaline Phosphatase (ALP) Activity.

Among the various biological functions of osteoblasts, secretion of alkaline phosphatase (ALP) is an important indicator determining the activity of the cells on a scaffold. The ALP activity of MC3T3-E1 that were cultured on PCL scaffolds, in comparison with that of TCPS, for 3, 5, and 7 days. The ALP activity of MC3T3-E1 on TCPS (i.e. controls), salt leached, salt-PEG 200 leached, salt-PEG 600 leached, salt-PEG 1000 leached PCL scaffolds were monitored at 3, 5 and 7 days in culture (see Figure 10). For all of PCL scaffolds investigated, the ALP activity on day 3 was lower than TCPS, while the ALP activity on day 5 was quite similar to TCPS. On day 7, the highest ALP activity of MC3T3-E1 was observed on the salt-PEG 1000 leached scaffold compared to TCPS, while the ALP activity of MC3T3-E1 on salt leached scaffold was lowest and lower than on TCPS.

Mineralization.

Alizarin Red S staining was used to quantify the mineral deposition of MC3T3-E1 that were cultured on the surfaces of TCPS, salt leached, salt-PEG 200 leached, salt-PEG 600 leached, and salt-PEG 1000 leached PCL scaffolds for 14 days.

Figure11. shows photographic images of the stained specimens. The appearance of red on the stained product shows the presence of calcium. The quantitative analysis of the results shown in Figure 12. was carried out by elution of calcium deposition with cetylpyridinium chloride and spectrophotometically read at 570 nm. The results revealed that the mineral deposition of cells cultured in the (salt-PEG 600 leached and) salt-PEG 1000 leached PCL scaffold were significantly greater than that of the cells cultured on the salt leached PCL scaffolds and TCPS.

Discussion

The polarities of PCL and PEG were quite different, when mixing of both, PEG phase spontaneously and spherically dispersed in PCL phase in order to diminish the surface energy on the PCL-PEG interface.[16] Resulting that after the spherical PEG were leaching out, the interconnected pores network were formed in the salt-PEG leached PCL scaffolds.

A stereomicroscope, visual slide microscope and SEM were used to observe the pores, pores distribution and the interconnected pores network of the scaffolds. The effect of PEG leached out scaffolds is illustrated in Figure 1-5. Figure 1 is the stereomicroscope images of the PCL scaffolds. Highly porous PCL scaffold were obtained for all salt and salt-PEG leached PCL scaffolds. Figure 2 and 3 show the inner morphology of the scaffolds; the salt-PEG leached PCL scaffold show the highly porous with high interconnected network.

The PCL-PEG 1000 blend solution has the highest viscosity compared to PCL-PEG 200 and PCL-PEG 600 blend solution. On the other hand, base on Kamide's theory about particle growth during membrane formation,[15] since the molecular size of PEG MW = 200 and 600 g/mol would move with a larger diffusion velocity and higher collision frequency than PEG MW = 1000 g/mol would. This resulted in creating more uniform pore and interconnected pores by leaching PEG MW = 1000 g/mol out rather than leaching out PEG MW = 200 and 600 g/mol. Salt-PEG 600 leached and salt-PEG 1000 leached PCL scaffolds have better pores and interconnected pore distribution than salt-PEG 200 leached PCL scaffold. The distribution of pores in scaffolds prepared from PEG MW. 1000 g/mol was greatest and more interconnected networks were distributed throughout the scaffolds.

The salt-PEG leached PCL scaffolds show highly interconnectivity pores network in the scaffolds, which is not in case of the salt leached PCL scaffold. The pores of the salt-PEG leached scaffolds are interconnected and the inner surface of pores looks quite coarse. The developed interconnected pore network is likely to facilitate transporting nutrients and wastes for a facile cell growth and blood vessel

invasion. The interconnected pores network and coarse surface are beneficial for all coherence and quick propagating of cell.

The interconnectivity and dimensions of the pores of the scaffolds affect not only the transport of nutrients into and wastes out of the cells through the pore structure of the scaffolds, but also other properties of the scaffolds. The porosity increased with increased the interconnectivity. According to the results in table 2, the greatest porosity, pore volume, and pore size values and the highest interconnectivity observed for salt-PEG 1000 leached PCL scaffolds are the obvious reasons for their greatest water absorption capability. The water absorption capability is an important property of a functional scaffold, as it allows the absorption and retention of wound exudates. In addition, the passage of exudates through the pore structure provides a possibility for certain proteins which is one steps required for bone regeneration to be absorbed on the scaffold surface.[19-21]

At any distance, the flow resistance was significantly higher for salt leached PCL scaffold compared to salt-PEG 200 leached, salt-PEG 600 leached, and salt-PEG 1000 leached PCL scaffolds. Standard deviation of flow resistance was higher for salt-PEG 200 leached and salt-PEG 600 leached PCL scaffolds, to indicate a more irregular structure with non uniform distribution of interconnections between pores compared to salt-PEG 1000 leached PCL scaffold. The higher percentage of closed cells account for the higher flow resistance observed for the salt leached PCL scaffold.

The higher porosity (92.6% as opposed to 91.6%) of the scaffolds decreased compressive modulus from 88 to 49 kPa. The porosity is an important parameter of scaffolds, playing a significant role for cell proliferation and growth. The higher porosities can provide cells spacious surrounding for their propagation, but if porosities are too high,[22] it is very dificult for the scaffolds to maintain enough mechanical rigidity.[23] Although increased porosity facilitate bone ingrowth, the result is a reduction in meachanical properties, since this compromises the structural integrity of the scaffold, since this compromises the structural integrity of the scaffold.[24]

The biocompatibity of these PCL scaffolds as bone scaffolds was assessed by an indirect cytotoxicity evaluation with mouse fibroblastic cells (L929) and mouse calvaria-derived pre-osteoblastic cells (MC3T3-E1), based on the initial 40,000 cells/well of cells seeded. Even though we were interested in using the obtained scaffolds as potential bone scaffolds, it was mandatory to test the materials with L929 just to comply with the ISO10993-5 standard test method. The viability ratio of cells that had been cultured with all of extraction media (and with control TCPS) is greater than 80%. All of the obtained results clearly suggested that all types of the PLA fibrous scaffolds, released no substances at levels that were harmful to both types of cells. Similar to our results, Jie et al.[25] showed that the cytotoxicity of poly(D,L-lactide)/nano-hydroxyapatite composites was 79.6-82.6% and the cytotoxicity of these scaffolds was in grade I according to ISO10993-1, that means these kind of materials have very good cytocompatibility.

In comparison with TCPS, the viability of cell on the salt-PEG 200 leached, salt-PEG 600 leached, salt leached PCL scaffold was slightly lower on day 1 and the proliferation of cells on salt-PEG 600 leached and salt-PEG 1000 leached PCL scaffold was significantly greater on day 3. The lesser viability of cells in the attachment period on various types of the scaffolds in comparison with that on TCPS In contrast, the greater number of cells in the proliferation period on PCL scaffolds could be because of high porosity and high interconnectivity network of the PCL scaffolds though which the cells were able to penetrate into the scaffolds. As a result, higher porosity did not affect cell attachment, but resulted in increased cell proliferation, due to pore space increased with porosity and facilitated transport of oxygen and nutrients.[24,26]

ALP activity was measured to compare the effects of the scaffolds on osteoblastic differentiation by culturing MC3T3-E1 cells for 3, 5, and 7 days on PCL scaffolds. As shown in Figure 10, the ALP activities of the MC3T3-E1 cells cultured on the salt-PEG 1000 leached PCL scaffold was significantly higher than that on TCPS on day 7. When the culture was maintained up to 14 days, significantly greater amount of calcium deposition was observed in the salt-PEG 1000 leached PCL scaffolds compared to the TCPS and salt leached PCL scaffolds, as determined by the alizarin red-S staining and the quantification of calcium deposition. Base on all results, the good in biocompatibility of the salt-PEG 1000 leached PCL scaffolds could be result from the high porosity and high interconnectivity network of PCL scaffolds that can permit cell intrusion, and permeation.

Conclusion

Three-dimensional PCL scaffolds with highly porous, and highly interconnectivity network can be prepared by our modified solvent casting, particulate leaching, and polymer leaching techniques using sodium chloride and polyethylene glycol(PEG) as a porogen. Scanning electron microscopic (SEM) and optical microscope images confirm that the scaffolds fabricated using this method have highly interconnected network, equal distribution, and uniform size of 400-500 μm pores. The greatest porosity, pore volume, and pore size values and the highest interconnectivity observed for salt-PEG 1000 leached PCL scaffolds are the obvious reasons for their greatest water absorption capability. The potential of use these scaffolds in bone tissue engineering application was evaluated in vitro with mouse calvaria-derived, pre-osteoblastic cells (MC3T3-E1). Indirect cytotoxicity evaluation revealed that scaffolds fabricated using this method released no substances at levels that were harmful to cells. Scanning electron microscopy observation showed the majority of the cells seeded on the surfaces of scaffolds at 3 days expanded over the area of the scaffolds which was the most expansion on the surface of scaffolds fabricated using this method. For mineralization, cells cultured on surfaces of PCL scaffolds fabricated using this method showed the highest mineral deposition. All of obtained results can be implied their potential for utilization as bone-scaffolding materials.

11. Preparation and Properties of a-Chitin-Whisker-Reinforced Hyaluronan–Gelatin Nanocomposite Scaffolds

Materials

Chitin powder (crab shells, a form, weight-average molecular weight = 4 x 10^5 g/mol) was purchased from Fluka (St. Gallen, Switzerland). Gel (porcine skin, type A, 170–180 bloom) was purchased form Fluka. HA (weight-average molecular weight = 1.4 x 10^6 g/mol) was purchased from Coach Industries (Osaka, Japan). 1-Ethyl-3-(3-dimethylaminopropyl)carbodiimide (EDC) was purchased form Fluka. HCl [37% (w/w), analytical-reagent grade] was purchased from Labscan Asia (Bangkok, Thailand). All other chemicals were analytical-reagent grade and were used without further purification.

Preparation of the CWs CWs were prepared by the acid hydrolysis of chitin powder with 3N HCl at 120 °C for 6 h under vigorous stirring and refluxing. The ratio of HCl to chitin powder was 30 mL/g. After acid hydrolysis, the obtained CW suspensions were diluted with distilled water and were then centrifuged at 10000 rpm for 5 min and decanted in triplicate. The suspensions were then transferred to dialysis bags and dialyzed in running water for 2 h and later in distilled water for 2 days. The dispersion of CWs was completed by a 5-min ultrasonification treatment for every 40 mL aliquot. The solid fraction of the as-prepared CW suspensions was gravimetrically determined to be 1.43 wt % on average. The CW suspensions were stored at 4 °C before further use.

Preparation of the neat HA–Gel scaffolds and the CW-reinforced HA–Gel scaffolds

An equal mass of HA and Gel powder was first mixed and dissolved in deionized (DI) water at 50 °C to obtain a blend solution of the polymers (i.e., HA–Gel) at a fixed concentration of 2 wt %. The blend solution was left to cool to room temperature before various amounts of the as-prepared CW suspensions were added to the solution. The six different mass ratios between the CWs and HA–Gel were 0, 2, 5, 10, 20, and 30% (w/w). The mixtures were continuously stirred until they were fully homogenized. To crosslink HA–Gel, 1 mmol of EDC was added, and the mixtures were further stirred for 2 h at room temperature.

Volumes of the mixtures were poured into polypropylene dishes to obtain molding specimens of two different shapes and dimensions (i.e., cylindrical and disc shapes), frozen at 40°C for 24 h, and lyophilized at 50°C for another 24 h. The obtained cylindrical scaffolds were about 10 mm in diameter and 2 mm in height, whereas the disc-shaped scaffolds were about 1 mm in thickness; these were later cut into a desired shape and size for the mechanical property assessment. The as-prepared scaffold specimens were kept in a desiccator before further use.

Characterization Microstructure observation and pore size determination

One cylindrical scaffold was randomly selected fromeach group of the scaffolds. It was cut into pieces along both the longitudinal and the transverse directions. The cut pieces were mounted on copper stubs, coated with gold with a JEOL JFC-1100 sputtering device (Tokyo, Japan) and observed for their microscopic structure with a JEOL JSM-5200 scanning electron microscope. To determine the dimensions of the pores, 50 pores for each of the cross sections and the longitudinal sections (i.e., 100 pores in total) were directly measured from the scanning electron microscopy (SEM) images with The University of Texas Health Science Center at San Antonio (UTHSCSA) Image Tool version 3.0 software. The average values for all of the specimens investigated were calculated and reported.

Mechanical properties For the tensile mechanical integrity, specimens (50 x 5 x 1mm^3) were cut from the disc-shaped scaffolds. The mechanical integrity of the specimens, measured in their dry state, in terms of the tensile strength, Young's modulus, and elongation at break was assessed with a Lloyd LRX-Plus universal testing machine (West Sussex, UK) with a 10-N load cell at room temperature (26 ± 2°C). The gauge length was 30 mm, and the crosshead speed was 10 mm/min. The measurements were carried out in pentuplicate for each group of the scaffolds.

Water-retention capacity

Cylindrical scaffolds, in their dry state, were weighed and then individually immersed in DI water at room temperature. At a given time point, the specimens were taken out, blotted on a glass plate, which was set at

about 45°from a horizontal baseline for 5 s to remove excessive water, and immediately weighed. The amount of water retained in the specimens was determined according to the following equation:

$$Water\ absorption\,(\%) = \frac{(Ww - Wd)}{Ww}\ x\ 100$$

where W_d and W_w are the weight of the specimens before and after submersion in the medium, respectively. The experiment was carried out in pentuplicate and the measurements were carried out at different time intervals within a period of 24 h

In vitro degradation

The in vitro degradation study of the scaffolds was carried under three conditions. In the first, cylindrical scaffolds were individually immersed in a 10 mM phosphate buffer saline (PBS) solution (pH 7.4) at room temperature without shaking for 24 h. Under the other two conditions, they were individually immersed in either PBS or bacterial collagenase at a concentration of 373 ng/mL at 37°C undershaking(70rpm) for 24 h. After the specified time, the specimens were removed from the media, frozen at 40°C for 24 h, and lyophilized at 50 °C for another 24 h. The degradability of the specimens was then quantified according to the following equation:

$$\text{Degradability}(\%) = W_t/W_i \times 100;$$

where Wi is the initial dry weight of the specimens and W t is the dry weight of the specimens after each respective in vitro degradation assay. The measurements for each group of the scaffolds were carried out in triplicate.

Infrared (IR) spectroscopy and thermal analyses

A Thermo Nicolet Nexus 670 Fourier transform infrared (FTIR) spectrophotometer (Madison, WI) was used to investigate the chemical functionalities of the as-prepared scaffolds by the KBr disk method. One

cylindrical scaffold was randomly selected from each group of scaffolds and subsequently subjected to FTIR scanning over 32 scans at a resolution of 4 cm^{-1}. The thermal stability of the selected cylindrical scaffold specimens was assessed in terms of their degradation temperature with a PerkinElmer TGA-7 thermogravimetric analyzer (Waltham, MA) over a temperature range of 30–600 °C at a heating rate of 10 °C/min under a nitrogen atmosphere. The weights of the specimens ranged between 3 and 5 mg. A PerkinElmer DSC-7 differential scanning calorimeter (Waltham, MA) was used to determine the glass transition temperature (T g) of the scaffold specimens over a temperature range of 25–80°C at a heating rate of 10 °C/min. The specimens, weighing around 5–6 mg, were subjected to a preheating run to erase their thermal history before the test.

Biological evaluation Cell culture

Human osteosarcoma cells (SaOS-2) were cultured as a monolayer in a-minimum essential medium (a-MEM; Sigma–Aldrich, St. Louis, MO), supplemented by 10% fetal bovine serum (Biochrom, Cambridge, UK), 1% Lglutamine (Invitrogen, Carlsbad, CA), and a 1% antibiotic and antimycotic formulation containing penicillin G sodium, streptomycin sulfate, and amphotericin B (Invitrogen). The cells were maintained at 37°C in a 95% humidified atmosphere containing 5% CO2 and passaged once every 3–4 days.

Cytotoxicity evaluation

Only the cylindrical scaffolds containing 0 and 30%CWs were used in these studies. The cytotoxicity of the scaffolds was evaluated by the indirect method with SaOS-2 as the reference cells. First, the extraction media were prepared by immersion of the scaffold specimens in 500 µL of serum-free medium (SFM; containing MEM, 1% L-glutamine, 1% lactabumin, and a 1% antibiotic and antimycotic formulation) for 24 h. Each of these extraction media was later used in the indirect cytotoxicity evaluation. SaOS-2 were cultured in wells of a 24-well culture plate at 4 $x10^4$ cells/well in serum-containing MEM for 16 h to allow attachment of the cells to the plate. The cells were then starved with SFM for 24 h, after which time, the

medium was replaced with an extraction medium. After 24 h of cell culturing in the extraction medium, a 3-(4,5-dimethylthiazol-2-yl)2,5-diphenyl tetrazolium bromide (MTT) assay (see details in the Supporting Information) was carried out to determine the viability of the cells. The experiment was carried out in quadruplicate.

Cell attachment and cell proliferation

A primary evaluation for cell attachment was carried out by a direct morphological observation of SaOS-2 cells that had been seeded on the surface of the scaffold specimens. Only the cylindrical scaffolds containing 30% CWs were used in the study. Specifically, the cylindrical scaffold specimens were put in wells of a 24-well culture plate and sterilized with 1 mL of 70% ethanol for 30 min. They were then washed with sterilized DI water twice and later immersed in a-MEM overnight. SaOS-2 cells were then seeded on the surfaces of the specimens at 4 x 10^4cells/specimen in a minimum volume of the culture medium and were allowed to attach on the surfaces for 3 h before the addition of 1.5 mL/well of the culture medium. The cells were cultivated at 37 °C in a humidified atmosphere containing 5% CO2

for 1 and 7 days, after which time, the morphology of the cultured cells was observed by SEM. After the removal of the culture medium, the cell-cultured scaffold specimens were rinsed with PBS twice, and the cells were fixed with a 3% glutaraldehyde solution, which was diluted from a 50% glutaraldehyde solution (Electron Microscopy Science, Hatfield, PA) with PBS for 30 min. The specimens were then dehydrated in graded ethanolic solutions (i.e., 30, 50, 70, and 90%) and in pure ethanol for about 2 min each. They were further dried in 100% hexamethyldisilazane (Sigma-Aldrich) for 5 min, dried in air after the removal of hexamethyldisilazane, mounted on SEM stubs, coated with gold, and finally, observed by SEM. The examinations were performed on three randomly selected scaffold specimens.

To quantify the viability of the attached and the proliferated cells, SaOS-2 cells had first been seeded or cultured on each of the four randomly selected specimens from each group of the scaffolds for 1, 24, 48, and 72 h before they were evaluated by the MTT assay at each time point. Only the cylindrical scaffolds were used in this study.

Statistical analysis

Data were analyzed with SPSS software version 14.0 for Windows (SPSS, Chicago, IL). Initially, the normal distribution was assessed by the Shapiro–Wilk test. The normal distribution data, representing the homogeneity of the variances, shown by the Levene's test, were then investigated by a one-way analysis of variance (ANOVA) with the Tukey HSD post hoc multiple comparisons. Otherwise, the Dunnett T3 was applied if the data did not exhibit the homogeneity of the variances. For the data of which the normal distribution was absent but the variance was homogeneous, the Kruskal–Wallis H was applied. To compare the means between two data groups, the Student unpaired t test was used. The significant level was indicated at $p < 0.05$ in any case.

RESULTS AND DISCUSSION

Characterization of the CWs

The dialyzed CWs exhibited colloidal behavior in water. Protonation of the amino groups of chitin under acidic conditions induced positive charges (NH_3^+) on the surface of the CWs, which generated electrostatic repulsion among the nanocrystallites.30 However, protonation of amino groups was not complete on all of the CW particles; hence, the hydrogen bonding associated with the free amino groups on the CWs caused them to aggregate. The representative TEM image of the as-prepared CWs, which were prepared from a dilute suspension, is illustrated in Figure 1. It was evident that the CWs were present as individual and partially aggregated entities. The aggregation of the CWs was facilitated by the increase in the pH of the suspension during dialysis, hence, the deprotonation of some of the protonated amino groups that occurred during the acid hydrolysis to prepare the CWs. According to the TEM results, the as-prepared CWs were present as slender rods with sharp points on both ends. The lengths (L's) and widths (d's) of these rods were 255 6 56 and 31 6 6 nm, respectively, with an L/d ratio of about 8. The histograms illustrating the distribution of the lengths and the widths of the as-prepared CWs, as shown in the Supporting Information, indicated that over 50% of the CWs exhibited lengths and the widths in the range 203–277 and 27–35 nm, respectively. These dimensions compared well with the reported values for CWs obtained from crab shells (L ≈ 50–300 nm and d ≈ 6–8 nm,30 L ≈ 100– 600 nm and d ≈ 4–40 nm,35 and L ≈ 100–650 nm and d ≈ 10–80 nm36).

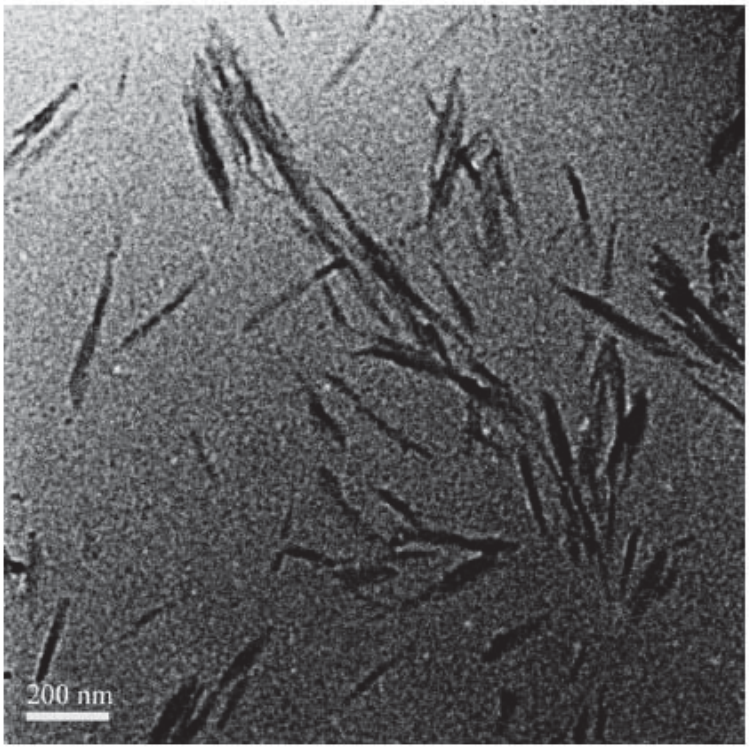


Figure 1 Representative TEM image of CWs prepared from a diluted suspension of acid-hydrolyzed chitin powder from crab shells.

Characterization of the CW-reinforced
HA–Gel scaffolds
Physical characteristics
Representative photographic images of the as-prepared cylindrical scaffolds are shown in the Supporting Information. These scaffolds were extremely light in weight because of their highly porous nature. The color of these scaffolds ranged from the pure white of the neat HA–Gel scaffolds to the light brown of the 30% (w/w) CW-reinforced HA–Gel scaffolds. The brown color resulted from the presence of the CWs dispersing within the mass of the scaffolds. Representative SEM images illustrating the microstructure of the as-prepared scaffolds viewed on the surface perpendicular to the transverse direction (i.e., the surface of the transverse sections) are shown in Figure 2, whereas those illustrating the microstructure of the scaffolds viewed on the surface perpendicular to the longitudinal direction (i.e., the surface of the longitudinal sections) are shown in the Supporting Information. All of the scaffolds exhibited a well-defined porous structure, and regardless of the surface under consideration, the interpore connectivity was discernible throughout the bulk of the scaffolds. For a given group of the scaffolds, no significant difference in terms of the morphology of the pore structure was observed between the two sections. This was in exception to the one that contained 30% CWs, which showed a disruption in its microstructure when viewed on the surface of the longitudinal sections. The dimensions of the pores observed in these SEM images were determined and analyzed and are reported in Table I. The size of the pores for all of the scaffolds in both the transverse and the longitudinal sections ranged between 92 and 230 lm, with the average value ranging between 139 and 166 lm. An increase in the content of the CWs

did not have a significant effect on the pore dimensions. A comparison of the pore dimensions that were observed in the two sections for each group of the scaffolds was evaluatedstatistically, and there was no difference, except for those observed for the neat HA–Gel sample group.With an average pore size smaller than 200 lm, the transportation of nutrients and oxygen and the ingrowth of new blood vessels into the inner pores ofthe scaffolds were somewhat restricted. The lack of ample oxygen supply leads to a medical condition known as hypoxia, which is suitable for the regenerationof cartilage but certainly not bone.37,38 To obtain scaffolds with larger pore dimensions, the cooling rate associated with the freezing of the HA–Gel solutionor the HA–Gel/CWs suspensions before the subsequent sublimation of the ice crystals needs tobe decreased further because it is a known fact that a fast cooling rate induces the formation of tiny ice crystals, hence, the small pore dimensions.39,40

TABLE I
Dimensions of the Pores of the Neat HA–Gel Scaffolds and the CW-Reinforced HA–Gel Scaffolds Observed on the Surfaces of Both Transverse and Longitudinal Sections

	Pore size (μm)			
	Transverse sections		Longitudinal sections	
Specimen	Range (Minimum – Maximum)	Average (Mean ± Standard deviation)	Range (Minimum – Maximum)	Average (Mean ± Standard deviation)
0% CW	92.3–208.8	140.9 ± 21.8^{a}	112.8–231.4	165.8 ± 27.7^{a}
2% CW	114.4–182.0	139.4 ± 16.0^{b}	108.4–182.1	145.4 ± 15.3^{b}
5% CW	104.1–224.5	153.2 ± 23.9^{c}	110.6–171.1	142.7 ± 13.8^{c}
10% CW	118.0–202.3	158.9 ± 19.1^{d}	104.3–205.4	162.8 ± 23.6^{d}
20% CW	113.5–200.5	151.4 ± 19.3^{e}	105.8–181.0	143.9 ± 17.2^{e}
30% CW	108.5–184.4	155.4 ± 15.7^{f}	97.2–231.3	149.0 ± 25.1^{f}

Superscript letters indicate comparisons only between sections of a given group of specimens at $p < 0.05$ (one-way ANOVA with Tukey HSD, $n = 50$).

Mechanical properties

Mechanical properties, expressed in terms of the modulus of elasticity, elongation at break, and tensile strength, of the as-prepared scaffolds were evaluated, and the results are summarized in Table II. Statistical analysis indicated that inclusion of theCWs in amounts of 2–30% in the HA–Gel scaffolds resulted in a significant increase in the modulus of elasticity from that of the neat scaffolds. Nevertheless, the property values among the various groups of the CW-reinforced HA–Gel scaffolds were not statistically different, except for the one containing20% CWs, which showed significantly lower values. For the elongation at break, the neat HA–Gel scaffolds exhibited significantly greater values over all of the reinforced samples, which statistically showed equivalent values among themselves. With regard to the tensile strength, it was obvious that the HA–Gel scaffolds that contained 2% CWs exhibited the property values that were significantly greater than those of the other groups of samples, which, among themselves,showed equivalent values. The result agreed well with the report of Sriupayo et al.,34 who found that the greatest tensile strength of CW-reinforced chitosan films was observed at a CW content of 2.96% and an increase in the CW content resulted in a reduction in the property values. To put it into perspective, the modulus of elasticity and the tensile strength values of the scaffolds containing 2% CWs were much lower than those of bone, which are 16.4 GPa and 117.4 MPa, respectively, on average.4

TABLE II
Mechanical Properties of the Neat HA–Gel Scaffolds and the CW-Reinforced HA–Gel Scaffolds

Specimen	Modulus of elasticity (MPa)	Elongation at break (%)	Tensile strength (MPa)
0% CW	0.99 ± 0.10^{a}	53.48 ± 10.69^{a}	0.52 ± 0.06^{a}
2% CW	14.10 ± 2.23^{b}	28.35 ± 6.16^{b}	1.03 ± 0.09^{b}
5% CW	19.96 ± 3.64^{b}	06.36 ± 1.42^{c}	$0.53 \pm 0.15^{a,c}$
10% CW	12.46 ± 2.00^{b}	$11.63 \pm 4.15^{c,d}$	$0.48 \pm 0.19^{a,c}$
20% CW	07.10 ± 0.93^{c}	$16.07 \pm 0.96^{b,d}$	0.47 ± 0.06^{a}
30% CW	11.96 ± 0.47^{b}	$16.03 \pm 3.40^{b,d}$	0.72 ± 0.08^{c}

Superscript letters indicate comparisons between groups of specimens for a single property at $p < 0.05$ (one-way ANOVA with Dunnett T3, $n = 5$).

Water absorption and in vitro degradability

The ability of the neat and CW-reinforced HA–Gel scaffolds to absorb water at room temperature within 24 h is graphically shown in Figure 3. All groups of the scaffolds demonstrated comparable water absorption within the first 60 min, which accounted for more than about 95% of their total wet weights. The values were as high as that of a superabsorbent.42 The results were similar to those reported by Park et al.43 on collagen–HA sponges. Such a great tendency to absorb a great amount of water is characteristic of a hydrogel material, such as HA and Gel, which are very hydrophilic in nature. 9 With the absorbed water, the interior of a scaffold becomes a hydrated environment, which facilitates the process of tissue regeneration by protecting cells and their products, such as secreted ECM. Furthermore, the hydrated environment facilitates the transportation of nutrients into and wastes out of the cells.24 According to Figure 3, all groups of the scaffolds exhibited similar water absorption values and equivalent profiles; that is, the property values decreased gradually with increasing submersion time. The absorption of water in a given group of the scaffolds reached a maximum only after having been submerged in DI water for 15 min, and the inclusion of the CWs within the scaffolds did not strongly influence the water absorption. This was due to the inherent hydrophilicity of all of the compositions, the interconnectivity of the pore structures, and the similarity in the pore dimensions of all of the scaffolds, which facilitated the capillary action and, hence, the rapid adsorption of water.42 The observed decrease in the amounts of water absorbed as the immersion time increased might have been due to the fact that the scaffolds began to disintegrate or partially dissolve, which diminished their capacity to imbibe both free and bound water.24,43

Despite the many benefits of the high water absorption of a scaffold, certain drawbacks should also be considered, such as weakening and acceleration due the to degradation of the scaffold.24 The degradation of a scaffold occurs mainly by either a physical or chemical pathway. The physical pathway involves dissolution and hydrolysis, whereas the chemical pathway involves enzymatic cleavage in the presence of a suitable enzyme.9 Here, we investigated the dissolution and hydrolytic degradation of the scaffolds in PBS over a submersion period of 24 h under both static conditions at room temperature and dynamic conditions, that is, by means of a shaking water bath at 70 rpm and 37_C. The enzymatic

degradation of the scaffolds was also investigated in 373 ng/mL of bacterial collagenase, which represented a model concentration of tissue collagenase in the synovial fluid of the patients with osteoarthritis.44,45 The investigation was carried out in the shaking water bath at 70 rpm and 37_C for 24 h. The results of thesstudies are graphically shown in Figure 4. Figure 4 shows the remaining weights of the scaffolds after submersion in PBS or collagenase (COL) solution for 24 h. Upon submersion in PBS under the static conditions at room temperature, the remaining weights of the scaffolds were about 58–76% of their original dry weights, with no significant difference among all groups of the scaffolds. Under the dynamic conditions, on the other hand, the remaining weights, for a given group of the scaffolds, were significantly lower than those observed under the static conditions. The enhancement in the weight loss was obviously due to the added energy from the agitation, which increased the kinetic energy of the system. In addition, the thermal degradation of the HA molecules could occur to a certain extent at 37_C.18 These could have been factors contributing to the observed values of the remaining weights of the scaffolds at 33–60% of the original dry weights of the scaffolds. The incorporation of CWs in the amounts of 20–30% in the HA–Gel scaffolds enhanced the resistance to degradation under the dynamic conditions compared with the neat scaffolds. Although a trend was observed for the relationship between the remaining weights of the scaffolds and the CW content, statistical analysis among the scaffolds that contained 5–30% CWs did not show a significant difference in their property values. In the collagenase medium, the degradation of the scaffolds was noticeably enhanced as the remaining weights, for a given group of the scaffolds, were the lowest. Regardless of the CW content, the values were in the range 11–52% of the original dry weights of the scaffolds. In addition to the agitation and the hypothetical thermal degradation of HA, the scission of Gel peptide bonds at glycine subunits by the enzyme was the main contributing factor.43 The presence of the CWs at levels of 5% or more significantly enhanced the stability to degradation of the scaffolds in the presence of the enzyme. Such an enhancement could have been due to the interaction between the CWs and the HA–Gel matrix molecules, which reduced the enzyme accessibility.46

IR spectroscopy analysis

Figure 5 illustrates FTIR spectra of the neat and CW reinforced HA–Gel scaffolds over the wave-number range 3500–500 cm_1. Those of the constituting materials are also shown for comparison. The absorption peaks at 1656, 1547, 1450, and 1237 cm_1, characteristic of amide bonds (COANH), were observed in the spectrum of Gel,43,47,48 whereas those at 1412 and 1076 cm_1, corresponding to carboxylate salts (symmetric stretching) and ester bonds, respectively, were observed in the spectrum of HA, of which repeating units comprised glucuronic acid and acetylglucosamine. The spectrum of the CWs should have been similar to that of HA because both of them were polysaccharides. Being crystalline entities, however, the CWs presented sharper and more intense signals at certain positions, 49 particularly at 1076 (ester bonds), 1378 (carboxylate salts), and 3267 and 3446 cm_1 (hydroxyl groups).48 Additionally, the CWs exhibited characteristic amide I peaks at 1621 and 1656 cm_1 and the amide II peak at 1556 cm_1.35,47 The peak at 1621 cm_1 was only specific to CWs, whereas that at 1656 cm_1, representing the stretching of hydrogen bonds between carbonyl groups and the neighboring amine groups of intrachains, could also be found for the amide bonds of a protein.49 For the neat HA–Gel scaffolds, the peaks at 1650, 1550, 1412, and 1076 cm_1 were discernible. Crosslinking with EDC generated both the amide and the ester linkages in the structure of the blends.50 The amide bonds were formed between the carboxyl groups of Gel and/or of the glucuronic acid in HA and the amino groups of Gel. The ester bonds, on the other hand, were formed between the carboxyl groups and the hydroxyl groups of Gel and/or of HA.51,52 For the scaffolds that contained CWs, the presence of the CWs were confirmed by the presence of characteristic peaks at 1378 and 1076 cm_1 and the absorption shoulder at 3267 cm_1, and the intensities of these peaks and the shoulder were found to increase with an increase in the content of the CWs.

Thermal characteristics

Figure 6 shows thermogravimetric analysis thermograms of the as-prepared scaffolds. All samples

exhibited similar profiles of weight change. Table III summarizes the values of the temperatures at which the losses in the weight of the scaffolds reached 5, 25, and 50% (on the basis of their original weights). Apparently, at temperatures lower than 200_C, the loss in the weight of all of the scaffolds, except for the ones containing 5% CWs, was less than 5%, with no particular relationship with the CW content. At temperatures around 210–230_C, the loss in the weight increased abruptly to reach maximum values at temperatures around 245–250_C, as indicated by the positions of the peaks of the corresponding derivative curves (not shown). As the temperatures increased to around 260–360_C, the loss in the weight of the different groups of the scaffolds became most noticeably different and inversely related to the CW content within the scaffolds. Careful consideration of the results revealed that the temperatures required for the scaffolds that contained 10–30% CWs to reach 25 and 50% of the weight loss were significantly greater than those of the neat scaffolds and the ones containing 2 and 5% CWs. This demonstrated that reinforcing the scaffolds with 10–30% CWs enhanced the thermal stability of the resulting scaffolds. Notwithstanding, such enhancement was only reflected in a limited temperature range, that is, 260–360_C, as the residual weights of all of the scaffolds at 550_C were comparable.

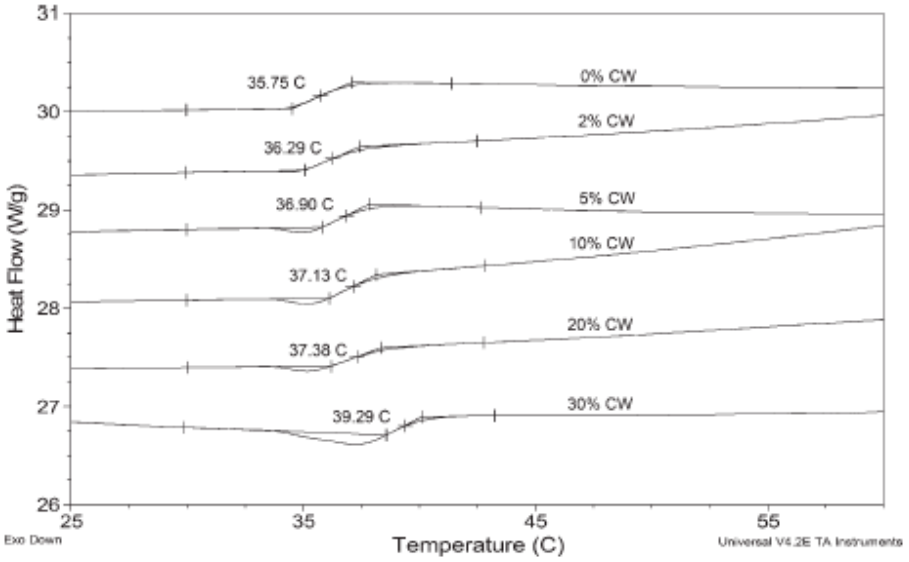


Figure 7 Differential scanning calorimetry thermograms (10°C/min in a nitrogen atmosphere) of the neat HA–Gel scaffolds and the CW-reinforced HA–Gel scaffolds. Their T_g's are illustrated.

Figure 7 shows the differential scanning calorimetry thermograms of the as-prepared scaffolds. The range of the temperature was chosen such that it revealed the glass transitions of the materials. Apparently,the neat HA–Gel scaffolds exhibited the Tg at about 35.8_C. With the addition and increasing amount of the CWs, Tg was found to increase from that of the neat materials to 36.3_C at 2% CWs and finally to 39.3_C at 30% CWs. With the Tg values of the HA–Gel scaffolds that contained 5–30% CWs in the range 36.9–39.3_C, the enhancement in the resistance to biodegradation of the corresponding scaffolds by collagenase, as previously shown, could have been, at least partly, due to the observed increase in the Tg values from that of the neat materials. The increased Tg values that were close to or greater than the physiological temperature of 37_C should have resulted in less mobility of the matrix molecules and, thus, the lower tendency for conformational change. However, because the Tg values of these scaffolds were measured in their dry state, the actual values in the physiological environment (i.e., wet conditions) should be much less because of the plasticizing effect from absorbed water molecules.

Nevertheless, the marked increase in the Tg values for the scaffolds that contained 5–30% CWs coincided with the observed improvement in the resistance to enzymatic degradation of these scaffolds.

Cytotoxicity and in vitro response of bone cells

We first investigated the cytotoxicity of the as-prepared scaffolds. The assessment was carried out on the basis of the indirect cytotoxicity assay, in which the extraction media from the neat and the 30% CWreinforced HA–Gel scaffolds were used to incubate SaOS-2 osteosarcoma cells for 24 h. The viability of the cells, determined spectrophotometrically at 570 nm, was compared with that of the cells that had been incubated with SFM for the same period of time. The results are shown in Table IV. Evidently, the viability of the cells that were cultured with either the extraction media from the neat scaffolds or the SFM was statistically the same, a result indicating that the neat HA–Gel scaffolds were biocompatible with the bone cells. Nevertheless, the viability of the cells decreased significantly when they were cultured with the extraction media form the scaffolds that contained 30% CWs. This result suggests that the presence of the CWs (at 30%) had an adverse effect on cell viability. Further evaluation by the direct culturing of the cells onto the scaffolds was then carried out to confirm whether they were toxic to the cells.

Figure 8 shows representative SEM images in various magnifications of SaOS-2 cells that were cultured on the surfaces of the 30% CW-reinforced HA–Gel scaffolds for 1 or 7 days. On day 1, the cells attached well to the surfaces of the scaffolds. The majority of the cells exhibited evidence of cytoplasmic process in the form of filopodia over the surfaces [see Fig. 8(b,c), as indicated by arrows]. The observation of cytoplasmic expansion indicated a good initial response of the cells to the as-prepared scaffolds, which influenced the subsequent cellular processes of proliferation and differentiation.53 On day 7, the morphology of the cells changed from the rather well-defined round shape observed on day 1 to fully expanded and even fused to the underlying surfaces of the scaffolds [see Fig. 8(d–f), as indicated by arrows]. Such an observation confirmed the preference of the cells to the surfaces, as they adhered and spread well over the surfaces. Despite the fact that the indirect cytotoxicity evaluation of the studied scaffolds produced a poor result, the observation of the bone cells that appeared to attach and expanded well over their surfaces indicated the applicability of the scaffolds for bone cell culture.

To investigate the effect of CW content on the proliferation of bone cells, the viability of SaOS-2 cells that were cultured on the neat and CW-reinforced HA–Gel scaffolds for 1, 24, 48, and 72 h was evaluated by the MTT assay. The results are graphically shown in Figure 9. At 1 h after cell seeding, the viability of the adherent cells on the surfaces of the scaffolds was either as good as or better than that on the tissue culture plate. At 24 h after cell culturing, only the cells that had been cultured on the surfaces of the 10% CW-reinforced HA–Gel scaffolds showed viability greater than the other groups of the scaffolds and the tissue culture plate. At 48 and 72 h after cell culturing, the viability of the cells on the tissue culture plate was significantly greater than that of those cultured on the surfaces of the scaffolds. Among the various groups of the scaffolds, the ones containing 10% CWs, again, exhibited the greatest viability of the cultured bone cells. It has been suggested that the presence of HA is not always positive in regulating the functions of cells.54 Liu et al.27 reported that HA–Gel–chitosan ternary blend films with a weight content of HA of 0.31% significantly promoted the attachment, migration, and proliferation of fibroblasts better than those with weight contents of HA of 1.56 and 3.11%. On the basis of these negative reports, the composition of HA within the scaffolds could be reduced to establish a much better positive environment for cell culture. Notwithstanding, among the various groups of the scaffolds, the ones that contained 10% CWs showed the most promising results for the attachment and proliferation of the bone cells.

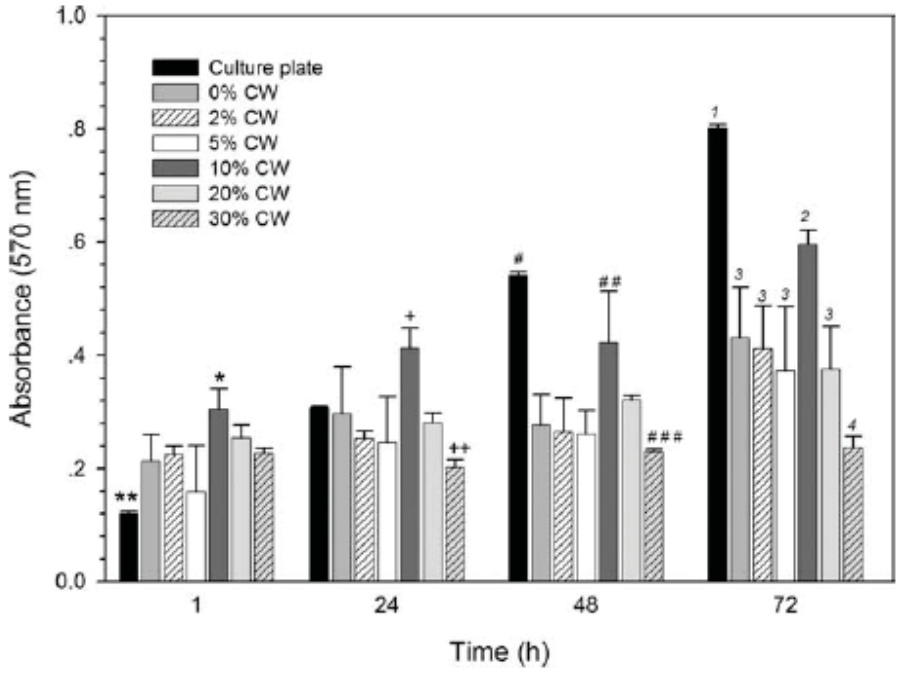


Figure 9 Viability of SaOS-2 cultured on the surfaces of the neat HA–Gel scaffolds and the CW-reinforced HA–Gel scaffolds. $^{*,+,\#,1}p < 0.05$ (one-way ANOVA with Tukey HSD, $n = 4$).

CONCLUSIONS

CW-reinforced HA–Gel nanocomposite scaffolds were successfully fabricated by the freeze-drying method. The variation in the amount of the incorporated CWs did not have an obvious effect on the morphology of the internal structure of the scaffolds. Nevertheless, the characteristics of the as-prepared scaffolds could be regulated through the variation in the amount of the incorporated CWs so that the optimal balance among their physicochemical, mechanical, and biological properties could be achieved. A high proportion of incorporated CWs was found to enhance the thermal stability and the resistance to biodegradation, whereas a rather lo proportion of the CWs increased the tensile strength and enhanced the biocompatibility in terms of the attachment and proliferation of the cultured human osteosarcoma cells of the resulting scaffolds. Although the scaffolds that contained 10% CWs showed great promise as substrates for bone cell culture, their actual utilization could be limited to a low-stressbearing area, such as the socket of a dental root.

12. Preparation and Characterization of Caffeic Acid-Grafted Electrospun Poly(L-Lactic Acid) Fiber Mats for Biomedical Applications

EXPERIMENTAL SECTION

Materials. PLLA (Mn = 80 000 g mol−1), CA, HMD, EDC, and NHS were purchased from Sigma-Aldrich (USA). DCM (Carlo Erba, Italy), DMF [Lab-Scan (Asia), Thailand], and ethanol [Lab-Scan (Asia), Thailand] were of analytical reagent grade and used withoutfurther purification.

Preparation of Electrospun PLLA Fiber Mats. Electrospinning of PLLA was carried out based on a previously published method.14 Briefly, 10% w/v PLLA solution in 7:3 v/v DCM/DMF was fed into a glass syringe fitted with a blunt 20-gauge stainless steel hypodermic needle (OD = 0.91 mm), used as the nozzle. An aluminum sheet wrapped around a homemade rotating cylinder (width and diameter ≈ 15 cm; rotational speed ≈ 50 rpm) was used as the collector. The solution was charged with a Gamma High Voltage Research DES30PN/ M692 at a fixed electric field of 20 kV/18 cm. After the solution had been electrospun continuously for 18 h, the thicknesses of the obtained fiber mats were measured to be 120 ± 15 μm. Surface Modification of Electrospun PLLA Fiber Mats. Aminolysis of the PLLA fiber mats was carried out based on a previously published method,22 with slight modification. Specifically, the fiber mats had been washed in an ethanolic aqueous solution (1:1 v/v) for 2 to 3 h, prior to being washed with a large quantity of deionized (DI) water. The aminolysis was then carried out by immersing the fiber mats in a HMD/isopropanol (IPA) solution of varying concentrations (i.e., 0.02, 0.04, 0.06, and 0.08 g mL−1) for varying periods of the reaction time (i.e., 5, 10, 15, 20, and 30 min) at 50 °C. The aminolyzed PLLA fiber mats (hereafter, a-ePLLA) had been rinsed in DI water for 24 h at room temperature to remove unreacted HMD, prior to being dried in vacuo at room temperature until of a constant mass. Activation of CA was done based on a previously published method,23 with slight modification. Specifically, 250 mg of CA, a priori dissolved in 10 mL of ethanolic aqueous solution (1:1 v/v), was reacted with 169 mg of EDC and later with 102 mg of NHS. The mixture was stirred in an ice−water bath for 1 h to finally obtain a solution of the activated CA. The aminolyzed PLLA fiber mats were subsequently immersed into the activated CA solution and stirred in the ice−water bath for 30 min. After 24 h of the reaction time at room temperature, the CA-grafted PLLA fiber mats (CA-gePLLA) were washed thoroughly with ethanol several times and finally dried in vacuo at room temperature.

Materials Characterization.

The free amino (NH2) groups on the surfaces of the neat and the modified PLLA fiber mats were quantified by ninhydrin or 2,2-dihydroxyindane-1,3-dione assay.22 The fiber mat samples were first immersed in 1 M ninhydrin/ethanol solution for 1 min, transferred into a glass tube, and then heated at 80 °C for 15 min to accelerate the reaction between ninhydrin and the NH2 groups that might be present on the surfaces of the fiber mat samples. If there were enough NH2 groups on the surfaces, they would turn blue. Upon complete evaporation of the adsorbed ethanol, 1,4-dioxane was added to dissolve the fiber mat samples. IPA was subsequently added to stabilize the blue compound. The absorbance of the obtained solutions were read at 538 nm using a Shimadzu UV-2550 ultraviolet−visible (UV−vis) spectrophotometer and the concentrations of the NH2 groups in the sample solutions were calculated from a standard calibration curve of HMD solutions in 1,4-dioxane/IPA (1:1 v/v) (see Figure I in the Supporting Information). Surface elemental chemistry of the neat and the modified PLLA fiber mats was analyzed by a Thermo Fisher Scientific Thetaprobe Xray photoelectron spectroscope (XPS).24 Monochromatic Al Kα X-ray was employed for the analysis of one spot on each sample with a photoelectron emission angle of 50° (with respect to the surface

normal). The analytical area was approximately 400 μm × 400 μm, and the maximal analytical depth was in the range of ∼4−8 nm. A few eV Ar+ ions, generated by an electron flood gun, were used for charge compensation. Electron and ion beams were focused and steered toward the analytical area. Further correction was made based on adventitious C 1s at 285 eV, using the manufacturer's standard software. Survey spectra were acquired for surface composition analysis with sensitivity factors from Scofield library. The amounts of the immobilized CA on the surfaces of the CA-gePLLA specimens were also investigated. Specimens (circular disk; ∼2.8 cm in diameter; cut from randomly selected areas of three different fiber mats) were individually dissolved in 10 mL of 7:3 v/v DCM/DMF solution. The absorbance of the sample solutions was spectrophotometrically read at 243 nm and the concentrations of the immobilized CA were calculated from a standard calibration curve of CA solutions in 7:3 v/v DCM/DMF (see Figure II in the Supporting Information).

Static water contact angles of the neat and the modified PLLA fiber mats were measured at room temperature using a Krüss DSA 100 drop shape analyzer,25 equipped with a Gilmont syringe and a 24-gauge flat tipped needle. Five droplets of distilled water (10 μL) were placed randomly at different positions on each sample. The projected images of the droplets, after they had been settled on the surfaces until of no noticeable change in their shapes, were analyzed for the contact angles.

Morphological appearance and size of the individual fibers of the neat and the modified PLLA fiber mats were examined by a JEOL JSM 5410LV scanning electron microscope (SEM). At least 100 readings of the fiber diameters from various SEM images were analyzed using SemAphore 4.0 software. Mechanical properties in terms of stress at maximum load, strain at maximum load, Young's modulus, and elongation at break of the neat and the modified PLLA fiber mats were tested on a Lloyd LRX universal testing machine (gauge length = mm and crosshead speed = 100 mm min−1). The specimens were cut into a rectangular shape (10 mm ×100 mm). The measurements were carried out on ten different specimens.

Biological Evaluation. Murine dermal fibroblasts (L929) and human dermal fibroblasts (HDFa) were used as reference cells. L929 and HDFa were cultured as monolayer in Dulbecco's modified Eagle's medium (DMEM; Sigma-Aldrich, USA), supplemented with 10% fetal bovine serum (FBS; Biochrom, UK), 1% L-glutamine (Invitrogen, USA), and a 1% antibiotic and antimycotic formulation [containing penicillin G sodium, streptomycin sulfate, and amphotericin B Invitrogen, USA)]. The medium was replaced on every other day and the cultures were maintained at 37 °C in a humidified atmosphere containing 5% CO2.

In the indirect cytotoxicity evaluation, the fiber mat specimens were assessed using a procedure adapted from the ISO10993−5 standard test method. First, extraction media were prepared by immersing the fiber mat specimens (∼15 mm in diameter) in a serum-free medium (SFM; containing DMEM, 1% L-glutamine, 1% lactabumin, and 1% antibiotic and antimycotic formulation) for 1, 2, or 3 d in an incubator

at the extraction ratio of 20 mg/mL. L929 or HDFa (∼40 000 cells/ well) were separately cultured in wells of a 24-well tissue-culture polystyrene plate (TCPS; Biokom, Poland) in 10% serum-containing DMEM for 16 h to allow cell attachment onto the well surface. After starving the cells with SFM for 24 h, the medium was replaced with 0.5 mL of an extraction medium and the cells were reincubated for another 24 h. The viability of the cells cultured with each of the extraction media and the fresh SFM that had been preincubated for an equivalent time interval (i.e., control) was determined with 3-(4,5-dimethylthiazol-2-yl)-2,5-diphenyl-tetrazolium bromide (MTT) assay. The MTT assay is based on the reduction of the yellow tetrazolium salt to purple formazan crystals by dehydrogenase enzymes secreted from the mitochondria of metabolically active cells. The amount of formazan crystals is supposedly proportional to the number of viable cells. First, each specimen was incubated at 37 °C with 300 μL/well of MTT solution at 0.5 mg mL−1, without phenol red. After 30 min of incubation, the MTT solution was removed. A buffer solution containing dimethylsulfoxide (DMSO; 900 μL/well) and glycine buffer (pH 10; 125 μL/well) was added into the wells to dissolve the formazan crystals. After 10 min of agitation, the solutions were measured for their absorbance at 540 nm, using a Thermospectronic Genesis10 UV−visible spectrophotometer.

In the cell attachment and the cell proliferation studies, only HDFa were used. Specimens (∼15 mm in diameter) were placed in wells of a 24-well TCPS and subsequently sterilized in 70% ethanol for 1 h. The specimens, after having been washed successively with autoclaved deionized water and phosphate saline solution (PBS), were immersed in DMEM overnight. A stainless steel ring (∼12 mm in diameter) was placed on top of each specimen to ensure its complete contact to the bottom of the well. HDFa (∼40,000 cells/well) were seeded on the fiber mat specimens and empty wells of TCPS (i.e., control) and incubated at 37 °C in a humidified atmosphere containing 5% CO2. In the attachment study, the cells had been allowed to attach onto the substrates for 2, 4, or 18 h, prior to being quantified for their viability by the MTT assay. Prior to the measurement, each cell-plated specimen had to be rinsed with PBS to remove unattached cells. In the proliferation study, the cells had been allowed to attach onto the substrates for 16 h, prior to being quantified for their viability by the MTT assay on days 1, 2, and 3 after cell culturing. The morphology of the cells at some time points was observed by SEM. After removal of the culture medium, each cell-cultured specimen was rinsed twice with PBS and the cells were fixed with 3% glutaraldehyde solution [diluted from 50% glutaraldehyde solution (Sigma-Aldrich, USA) with PBS] at 500 μL/well. After 30 min, the specimen was rinsed again with PBS and underwent dehydration with

ethanolic aqueous solutions of varying concentrations (i.e., 30, 50, 70, and 90 vol %) and pure ethanol for ~2 min each. It was then dried in hexamethyldisilazane (HMDS; Sigma-Aldrich, USA) for 5 min and finally in air. The specimens were then observed by a JEOL JSM-5200 scanning electron microscope (SEM). The morphology of the cells that had been seeded or cultured on glass substrates (12 mm in diameter; Menzel, Germany) was used as positive control.

Protein Adsorption. Specimens (~15 mm in diameter) were placed in wells of a 24-well TCPS. A stainless steel ring (~12 mm in diameter) was placed on top of each specimen to ensure its complete contact to the bottom of the well. A solution of type I collagen in PBS (0.1 mg·mL−1 for 0.5 mL) was then added to each well. After 2, 4, 24, 48, and 72 h of immersion, each specimen was thoroughly rinse with DI water to remove excess collagen. The amount of adsorbed collagen on each specimen was carried out by first immersing the specimen in 2 mL of 1% w/v sodium dodecyl sulfate (SDS) aqueous solution for 30 min. The concentration of the dissolved collagen was then quantified by BCA protein assay kit (Thermo Fisher Scientific, USA). Specifically, 25 μL of each of the dissolved collagen sample solutions had been pipetted into a 96-well TCPS, before the BCA working solution of 200 μL was added. The plate was sealed and incubated at 60 °C for 30 min. The absorbance measurements were taken at 562 nm at room temperature. The collagen concentration was calculated from a standard calibration curve (see Figure III in the Supporting Information).

Antioxidant Activity. The antioxidative activity of CA after it had been grafted onto the surfaces of the PLLA fiber mats was assessed by the DPPH assay. The procedure was carried out based on a previously published method,14,26 with slight modification. Specifically, each specimen (~2.8 cm in diameter) was dissolved in 10 mL of 7:3 v/v DCM/DMF solution. The sample solution was then diluted with 10 mL methanol. After that, 3 mL of an ethanolic solution of DPPH (100 μM) was added into 1 mL of the sample solution. The mixture had been incubated at room temperature in darkness for 30 min, prior to being spectrophotometrically read at 517 nm. The neat fiber mat specimens were used as internal control and the amount of the immobilized CA participated in scavenging activity of the DPPH radical species could be quantified against a standard curve of CA (see Figure IV in the Supporting Information). The antioxidant activity (% AA) was then expressed as the percentage of the absorbance value of the DPPH radical species that was decreased in comparison with that of the control condition (i.e., the testing solution without the addition of the dissolved specimens), according to the following equation

$$\%AA = \frac{(A_{\text{control}} - A_{\text{sample}})}{A_{\text{control}}} \times 100 \quad (1)$$

where Acontrol and Asample represent the absorbance values of the blank and the sample solutions, respectively.

Statistical Analysis. All values were presented as the means ± standard deviations. Statistical analysis between two data sets was performed using One-Way Analysis of Variance (ANOVA) and Scheffe's post hoc test in SPSS (SPSS, USA). The values of p lower than 0.05 were considered statistically significant.

RESULTS AND DISCUSSION

The purpose of chemical immobilization of CA onto the surfaces of the individual electrospun PLLA fibers is 2-fold. The first is to increase the hydrophilicity of the surfaces, as the hydroxyl moieties of CA are more hydrophilic than the ester linkages indigenous to PLLA. Second, it is aimed at impartingthe antioxidant activity to the modified PLLA fibrous matrices,as this activity is deemed important for an active wound dressing. According to the reaction schemes shown in Figures 1 and 2, the grafting of CA onto the surfaces of the individual electrospun PLLA fibers can be done in two sequential steps. In the first step, amino groups were covalently introduced onto the surfaces of the individual electrospun PLLA fibers through the reaction with HMD to obtain the aminolyzed PLLA fiber mats (a-ePLLA). Here, an amino moiety (−NH2) of HMD would react with an ester linkage (−COO−) of PLLA to from the amide linkage (−CONH−), whereas the other amino moiety would be left available for further reaction. In the second step, the CA-grafted PLLA fiber mats (CA-g-ePLLA) were obtained through the reaction between CA, the carboxylic acid moiety (−COOH) of which had been activated sequentially with EDC and NHS, and the other amino moiety of HMD, which had been introduced on the surfaces of the aePLLA in the first step.

Characterization of Neat and Modified PLLA Fibrous Matrices. Quantification of Free Amino Groups.

Quantification of the amino moieties that had been introduced on the surface of the a-ePLLA was evaluated with the ninhydrin assay. A number of factors would influence the amounts of the amino groups that would be introduced on the surface of the a-ePLLA. Some of these are the initial concentration of HMD, the reaction time, and the reaction temperature. Here, only the effects of the HMD concentration (see Table 1) and the reaction time (see Table 2) were studied.

Table 1. Surface Density of $-NH_2$ Groups on the a-ePLLA as a Function of HMD Concentration at a Fixed Reaction Time of 10 Min[a]

HMD concentration (g mL^{-1})	surface density of $-NH_2$ ($\times 10^{-7}$ mol cm^{-2})
0.02	0.82 ± 0.06
0.04	1.20 ± 0.03
0.06	1.65 ± 0.05
0.08	1.96 ± 0.04

[a]The reaction temperature was fixed at 50 °C.

Table 2. Surface Density of $-NH_2$ Groups on the a-ePLLA as a Function of Reaction Time at a Fixed HMD Concentration of 0.04 g mL^{-1}[a]

reaction time (min)	surface density of $-NH_2$ ($\times 10^{-7}$ mol cm^{-2})
5	0.76 ± 0.04
10	1.20 ± 0.03
15	1.77 ± 0.07
20	1.82 ± 0.06
30	3.10 ± 0.04

[a]The reaction temperature was fixed at 50 °C.

Within the investigated ranges of the HMD concentrations and the reaction times, the density of the amino groups was an increasing function of both independent parameters. Nevertheless, treating the neat

PLLA fibrous membranes at a high HMD concentration and/or a long reaction time would jeopardize both the physical and the mechanical integrity of the modified fibrous membranes. As the aminolytic condition becomes harsher (i.e., a result of the increased HMD concentration, increased reaction time, etc.), increasing numbers of ester linkages would be cleaved and the carboxylic acid chain ends would react with HMD, resulting in greater numbers of shorter PLLA chains and this occurs from the surface in. Here, the optimized aminolytic condition that resulted in the a-ePLLA that did not disintegrate while undergoing further reaction and/or evaluation is 0.04 g mL−1 of HMD/IPA solution at 50 °C for 10 min. At this condition, the surface density of the introduced amino groups was 0.120 ± 0.003 μmol cm−2.

Elemental Composition of Surfaces and Quantification of Immobilized CA.
XPS was used to examine the chemical composition at the surfaces of the neat and the modified PLLA fibrous matrices. Quantitative analysis of the obtained results is shown in Table 3.

Table 3. Percentages of Area under the Peaks of High-Resolution C 1s, O 1s, and N 1s XPS Spectra, Including the Ratios of the Percentages of the Area under the Peaks O 1s/C 1s, N 1S/C 1s, and N 1s/O 1s, of the Neat and the Modified PLLA Fibrous Matrices

sample	C 1s	O 1s	N 1s	O 1s/C 1s	N 1s/C 1s	N 1s/O 1s
ePLLA	61.1	38.9	0	0.6367	0	0
a-ePLLA	64.4	34.8	0.8	0.5404	0.0125	0.0230
CA-g-ePLLA	60.6	39.0	0.4	0.6436	0.0066	0.0103

As expected, no nitrogen-based moieties were observed on the surfaces of the neat PLLA fibrous membranes (i.e., the ePLLA). This was evidenced by the nonexistence of the N 1s spectra. In addition, the ratio between the surface oxygen atoms and the surface carbon atoms (i.e., O 1s/C 1s) was about 0.64. For the a-ePLLA, this ratio decreased to about 0.54 and, at the same time, surface nitrogen atoms could then be detected. This is because aminolysis introduced both the carbon and the nitrogen atoms on the fiber surfaces. For the CA-g-ePLLA, the O 1s/C 1s ratio increased again to about 0.64. This is because the grafting of CA introduced both the carbon and the oxygen atoms on the fiber surfaces. This resulted in the simultaneous decrease in the number of surface nitrogen atoms, as evidenced by the decrease in the N 1s/C 1s and the N 1s/O 1s ratios from those of the a-ePLLA. The surface density of the immobilized CA on the CA-gePLLA was quantified spectrophotometrically to be 6.2 ± 0.2 μg cm−2 or 0.034 ± 0.003 μmol cm−2 (based on the projection area of the specimens and note that Mw of CA = 180.16 g·mol−1) (n = 5). This implies that about 28% of the amino groups on the surface of the a-ePLLA participated in the immobilization reaction with CA. When calculated based on the actual weights of the specimens, the amount of the immobilized CA on the CA-g-ePLLA was 1.13 ± 0.03 μg mg−1 or 0.0063 ± 0.0006 μmol mg−1. To see whether the as-grafted CA could be released from the CA-g-ePLLA or not, a separate

experiment was carried out. Here, the CA-g-ePLLA specimens (∼2.8 mm in diameter) were immersed in

PBS at 37 °C for periods of 1, 3, and 7 days. After each time point, a sample solution was withdrawn and spectrophotometrically read at 243 nm. The obtained results confirmed nonexistence of CA in the sample solutions. This clearly implies that there was no physical adsorption of CA on the surfaces of a-ePLLA and that the cleavage of the amide linkages could not occur in PBS.

Wettability and Morphology.
Static contact angles of water droplets on the surfaces of the neat and the modified PLLA fibrous membranes were used to assess the hydrophilicity of these surfaces. Such values for the neat PLLA

fibrous matrices were 104.8° ± 0.3°. The surfaces became much more hydrophilic after the aminolytic treatment in 0.04 g mL−1 of HMD/IPA solution at 50 °C for 10 min (i.e., the water contact angles = 83.3° ± 0.4°). The hydrophilicity of the surfaces increased even more after CA having been grafted onto the surfaces of the a-ePLLA (i.e., the water contact angles = 55.5° ± 0.5°). The wettability of a surface depends not only on the chemical modification of the surface, but on the typographical nature of it as well. For an electrospun fibrous membrane, the wettability of its surface depends on the topography, the size, the arrangement,25 and the surface chemistry of the individual, underlying fibers.22 To ascertain that the increase in the hydrophilicity of the modified PLLA fibrous membranes over that of the neat ones was not due to any change in their surface topography, the morphology of the neat and the modified PLLA fibrous membranes was investigated (see Figure 3). Evidently, there is no obvious discrepancy in the morphology of the modified fibers from that of the neat ones, as the surface of all of these individual fibers was smooth. Nonetheless, the diameters of the modified fibers (i.e., ∼850 and ∼920 nm on average after the aminolysis and the grafting of CA, respectively) were generally greater than those of the neat ones (i.e., ∼620 nm on average). The increase in the electrospun fiber diameters after a surface modification was also reported on electrospun poly(D,L-lactic acid) (PDLLA) fibers that had been grafted with chitosan.27 Recently, It has been demonstrated that an increase in the size of the individual fibers increased the hydrophobicity of the electrospun fibrous membranes.25 Thus, the increase in the hydrophilicity of the modified PLLA fibrous membranes over that of the neat materials was certainly not due to the change in the size of these individual fibers.

Mechanical Integrity.

The mechanical properties of the ePLLA and the CA-g-ePLLA were investigated. The stress at maximum load and the Young's modulus of the ePLLA were 3.6 ± 0.2 and 351 ± 5 MPa, respectively, whereas the strain at maximum load and the strain at break of the materials were 75.6 ± 4.6 and 87.7 ± 4.6%, respectively. On the other hand, the stress at maximum load and the Young's modulus of the CA-g-ePLLA were 0.89 ± 0.29 and 154 ± 14 MPa, respectively, whereas the strain at maximum load and the strain at break of the materials were 2.2 ± 0.2 and 5.8 ± 0.5%, respectively. Upon ePLLA surfaces, both the stiffness and the extensibility of the CA-g-ePLLA decreased significantly.

Biological Evaluation of Neat and Modified PLLA Fibrous Matrices.

Indirect Cytotoxicity Evaluation.

The potential for use of the neat and the modified PLLA fibrous membranes in biomedical applications was first assessed by the indirect cytotoxicity evaluation assay, using L929 and HDFa as reference cells. In the assessment, the extraction media were prepared by immersing each fiber mat sample in SFM for different periods of up to 3 days. The viability of the cells that had been cultured with each of these media, in comparison with that of the cells that had been cultured with the fresh SFM that had been preincubated for similar periods of time, for 1 day isshown in Figure 4. The viability of the cells that had been cultured with the fresh SFM that had been preincubated for 1 d was used as the basis to obtain the relative viabilities shown in the figure. For both cell types, the viability of the cells that had been cultured with the fresh SFM was found to decrease with an increase in the preincubation period, which may be due to the increase in the dissolved CO2 level upon the prolonged incubation. Notwithstanding, the viabilities

of either cell type were greater than ~80% on average. For L929 that had been cultured with the extraction media from both the neat and the modified PLLA fibrous matrices, the viabilities of the cells showed increasing trends, with the values ranging from ~92 to ~109% on average. For HDFa on the other hand, decreasing trends were observed, with the values ranging from ~82 to ~95% on average. Because the viabilities were greater than ~80%, the obtained results indicated nontoxicity of all of the fibrous matrices, as none of the materials released substances in the levels that were detrimental to the cells.

Cell attachment and Cell Proliferation.

All of the fibrous matrices were evaluated further for their potential for use as wound dressing materials. For this, HDFa were directly seeded or cultured on their surfaces in order to assess the ability of the materials in supporting the attachment and the proliferation of the cells. The viabilities of the cells that had been grown on the surfaces of TCPS at 2 h after cell seeding (for the attachment assay) and on day 1 after cell culturing (for the proliferation assay) were used as the bases to obtain the relative viabilities shown in Figure 5.

For the attachment assay, the viability of the attached cells on the surface of TCPS at 4 h was lower than that at 2 h, whereas that of the attached cells at 16 h was greater. At any given time point, the viabilities of the attached cells on all of the fibrous matrices were lower than that on the control surface. At 2 and 4 h after cell seeding, the ability to support the attachment of the cells for a given type of the fibrous matrices was not of statistical difference. At 16 h, however, the viabilities of the cells attached on all types of the fibrous matrices increased tremendously to approach that of the cells that could adhere onto the control surface. Noticeably, the CA-g-ePLLA were better than the a-ePLLA in supporting the attachment of HDFa at any given time point. On day 1 after cell culturing, the viabilities of the cells on all of the fibrous matrices were still inferior to that of the cells on TCPS. Interestingly, the profiling of viabilities was similar to that observed at 16 h after cell seeding. This result could be interpreted that at least 24 h was

required for HDFa to completely adhere to these surfaces.Significant increase in the proliferation of the cultured cells on all types of the fibrous matrices was observed on days 2 and 3 after cell culturing. Though not statistically significant, the ability of the CA-g-ePLLA in supporting the proliferation of HDFa was better than that of the a-ePLLA, which in turn was better than that of the ePLLA. The inferiority of all of the fibrous matrices to TCPS in supporting the attachment of HDFa could be due to the lesser numbers of cells that were able to attach on the rougher and more hydrophobic surfaces of the fibrous matrices in comparison with the smoother and more hydrophilic surface of TCPS. Surfaces of different degrees of hydrophilicity (orhydrophobicity) would influence different types and amounts of proteins to adsorb. Even though a rough surface of the fibrous matrices possesses a greater specific surface area than asmoother surface of TCPS, the types and amounts of the proteins that are adsorbed on the smooth and hydrophilic surface of TCPS may mediate the adherence of the cells much better than do those adsorbed on the rough and hydrophobic surface of the fibrous matrices. The flat surface of TCPS also ensures that the adsorbed proteins are readily accessible to the cells. Unlike the flat surface of TCPS, only a limited part of the adsorbed proteins on the rough surface is accessible to the cells. Furthermore, the kinetics of the protein adsorption on the surfaces of different characters (i.e., different surface topographies, different effective surface areas, different surface wetting phenomena, etc.) play important roles in regulating the different time intervals for which the proteins require to adsorb in the amounts that are effective for mediating cellular behavior. Here, it is logical to hypothesize that a much longer time is needed for a much greater amount of proteins required to adsorb on the surfaces of the fibers to have a mediating effect to the cultured cells. Hence, on days 2 and 3, we see much greater increase in the proliferation of the cells grown on all types of the fibrous matrices and such an increase should be a result of the greater surface areas of the fibrous substrates. Among the three types of the fibrous matrices, the CA-g-ePLLA were the best in supporting the attachment and the proliferation of HDFa (i.e., based on the average values of the viabilities shown in Figure 5). Because the surface of the CA-g-ePLLA was more hydrophilic than those of the ePLLA and the a-ePLLA, the greater adsorption of proteins on their surface should be the main reason.

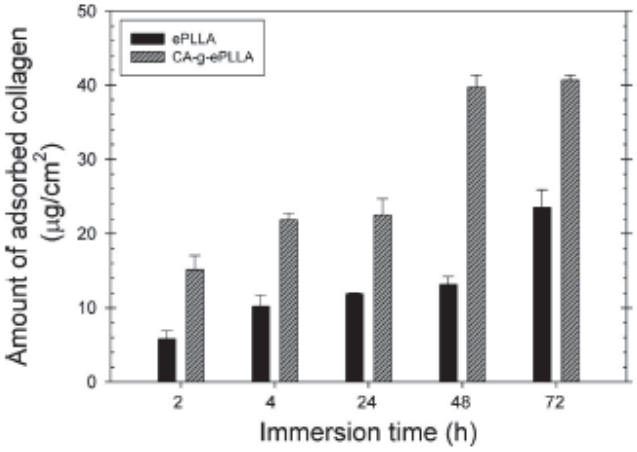
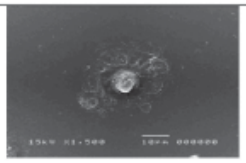
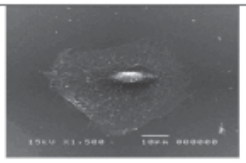
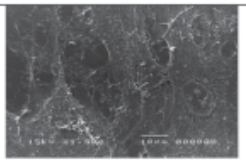
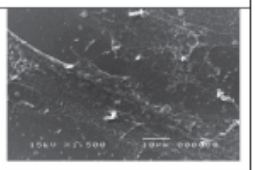
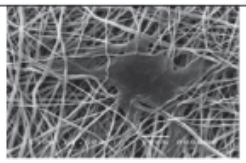
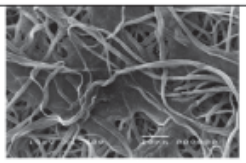
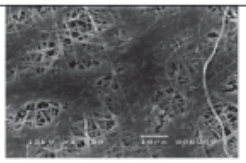
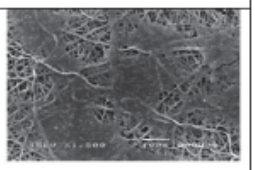
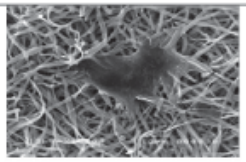
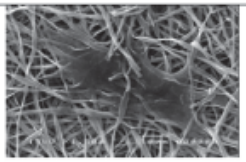
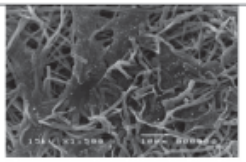
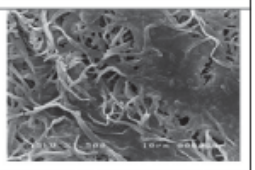
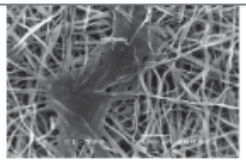
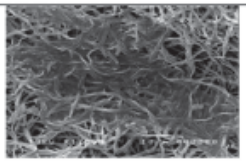
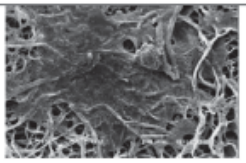
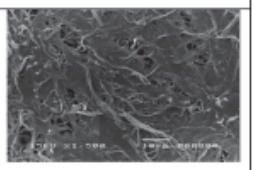


Figure 6. Areal amounts of type I collagen adsorbed on the surfaces of ePLLA and CA-g-ePLLA (i.e., the adsorbed amounts divided by the projection area of the specimens) at various immersion time points. All data sets at any given time point were significantly different ($*p < 0.05$).

Here, a separate experiment was carried out to quantify the amounts of a model protein that were able to adsorb onto the surfaces of the ePLLA and the CA-g-ePLLA. Type I collagen was used as the model protein. The amounts of the adsorbed proteins were reported at various immersion time points and the results are shown in Figure 6. Obviously, increasing the immersion time in the protein solution caused the amount of the absorbed protein to increase, except for the CA-g-ePLLA at 48 and 72

h that showed equivalent values (suggesting that the maximal adsorption was already reached at these time points). Regardless of the time points investigated, the adsorption of CA-g-ePLLA should be responsible for the greater amounts of type I collagen adsorbed on their surfaces.

Table 4. Representative SEM Images (magnification = 1500×; scale bar = 10 μm) of Cultured HDFa on Glass, ePLLA, a-ePLLA, and CA-g-ePLLA at Four Different Time Points after Cell Seeding or Cell Culturing

Material	Cell seeding/culturing time point			
	2 h	4 h	1 d	3 d
Glass (control)				
ePLLA				
a-ePLLA				
CA-g-ePLLA				

Cell Morphology.

The morphology of HDFa that had been seeded or cultured on the surfaces of the neat and the modified PLLA fibrous membranes was also investigated. Here, glass was used as the control substrate instead of TCPS because of the ease of taking the specimens for SEM observation. Representative SEM images are shown in Table 4. At 2 h after cell seeding, the majority of the cells on the glass surface was still round, while, at 4 h, the evidence of cytoplasmic process was already observed. The full cytoplasmic expansion of the cells on the glass substrate was realized after they had been cultured on the surface for 1 and 3 d. At 4 h after cell seeding, the majority of the cells on the surfaces of the ePLLA and the aePLLA was rather round, whereas that on the surface of the CA-g-ePLLA was more expanded. The full cytoplasmic expansion of the cells grown on these fibrous substrates was observed at 4 h after cel seeding, particularly for that of the cells grown on the CA-g-ePLLA. On day 1 after cell culturing, HDFa, in their fully expanded form, covered about 80% or more on the surfaces of all of the fibrous substrates. On day 3, the cell-covered areas were evidently increased, especially for that observed on the CA-g-ePLLA. The obtained results clearly confirmed the preference of HDFa toward the CA-g-ePLLA surface.

Antioxidant Activity of CA-g-ePLLA.

The antioxidant activity of the CA-g-ePLLA was determined by the DPPH assay. DPPH• is a stable free radical, exhibiting a characteristic UV absorption at 517 nm, and has been extensively used toevaluate the antioxidant activity of a variety of substances. 14,28−30 CA, which can act as a donor of an H-atom or electron in a similar manner to gallic acid, can transform DPPH• into its reduced form DPPH•-H.31 The antioxidant activity of CA, as the grafted species on the surface of the PLLA fibers, was determined to be

88.4 ± 1.3% (n = 5). The result confirmed that CA still retains its free radical scavenging ability, even though its mobility was limited because of its chemical immobilization onto the surface of the PLLA fibers. Interestingly, the amount of the as-grafted CA on the surfaces of the individual fibers of the CA-g-ePLLA that participated the scavenging activity of the DPPH radical species was determined to be 2.73 ± 0.10 μg·cm−2 (based on the projection area of the specimens) or 0.49 ± 0.17 μg mg−1 (based on the actual weights of the specimens) or about 44% (based on the amount of the immobilized CA).

CONCLUSION

Electrospun PLLA fiber mats, with the average fiber diameter about 620 nm, were prepared from 10% w/v PLLA solution 7:3 v/v DCM/DMF. The surfaces of the individual PLLA fibers were successfully modified by CA via a two-step grafting procedure and the reactions were confirmed by the ninhydrin assay and XPS. Amino groups were introduced first on the fiber surface and the optimal condition was 0.04 g mL−1 of HMD/ IPA solution at 50 °C for 10 min, resulting in the surface density of the introduced amino groups of (1.20 ± 0.03) 10−7 mol cm−2. After this step, the wettability of the fiber mat surface improved significantly, as the water contact anglesreduced from those of the neat PLLA fiber mats (i.e., 104.8° 0.3°) to 83.3° ± 0.4°. The wettability of the fiber mat surface improved even further after the chemical immobilization of CA (with the water contact angles being 55.5° ± 0.5°). Such the

chemical modifications caused the fiber diameters to increase to ∼850 and ∼920 nm on average after the

aminolysis and the grafting of CA, respectively. In the indirect cytotoxicity assay, none of the fibrous materials released substances in the levels that were detrimental to the cells. In the direct cell culturing assay, all of the fibrous matrices showed very good support for the proliferation of HDFa on days 2 and 3 after cell culturing, with the CA-modified fibrous substrates being the best. Lastly, the antioxidant activity of the grafted CA moieties on the PLLA fibers was determined to be 88.4 ± 1.3%.

13. **Effect of the Surface Topography of Electrospun Poly(ε-caprolactone)/ Poly(3-hydroxybuterate-co-3-hydroxyvalerate) Fibrous Substrates on Cultured Bone Cell Behavior**

Experimental part

1. Preparation of Fibrous Substrates.

Blend solutions of 50/50 w/w PCL/PHBV of varying concentrations ranging from 4 to 14 wt % were prepared in 80/20 v/v chloroform/DMF at roomtemperature (25 (1 C). PCL solution at 12 wt %was prepared in 50/50 v/v DCM/DMF at room temperature, and PHBV solution at 14 wt % was prepared in chloroform at 50 °C.

The electrospinning of these solutions was carried out using a typical method. Briefly, each of the solutions was contained in a glass syringe, the open end of which was connected to a gauge-20 stainless steel needle (o.d. = 0.91 mm), used as the nozzle. An aluminum (Al) sheet wrapped around a rotating

drum (width and o.d. of the drum ~15 cm; rotational speed ~50rpm)wasemployedasa collector. The distance fromthe tip of the needle to the outer surface of the Al sheet was set at 10 cm. A Gamma High-Voltage Research D-ES30PN/M692 power supply was used to generate a high dc potential (i.e., 21 kV for the blend and PCL solutions and 12 kV for the PHBV solution). The emitting electrode (+) of the power supply was attached to the needle, and the grounding electrode was attached to the collector. A Kd Scientific syringe pump was used to maintain the feed rate of the solution at ~1mL/ h. The solutions were electrospun consecutively for ~10 h.

2.Characterization.

The viscosities of the polymer solutions were measured by a Brookfield DVIII Ultra rheometer at room temperature and 20 rpm rotational speed of the spindle (n = 5).

The surface topographies and sizes of the individual fibers as well as those of the beads (in the case of the beaded fibers) of the obtained fibrous substrates were analyzed by a JEOL JSM-5410LV scanning electron microscope (SEM). For each sample, the sizes of the individual fibers (and beads, where

applicable) were measured from various positions of at least five different SEM images by SemAphore 4.0 software (n g50). Additionally, the thicknesses of the fibrous substrates were measured by a Mitutoyo digital micrometer (n = 5).

The chemical integrity of the obtained fibers was identified by a Nicolet NEXUS407 Fourier transform infrared spectrometer in attenuated total reflection mode (ATR-FTIR), at a resolution of 4 cm over a wavenumber range of 4000 to 400 cm^{-1}.

Static water contact angles of the obtained fibrous substrates were measured with a Kr€uss DSA 100 drop shape analysis system. Ten droplets of distilled water (10 μL) were placed randomly at different positions on each sample. The projected images of the droplets, after they had been allowed to stay on the substrates until no further change in their shapes was observed, were analyzed for the contact angles, and the data were averaged.

The mechanical integrity, in terms of the tensile strength and Young's modulus, of the obtained fibrous substrates (rectangular shape, 10 mm 100 mm) was assessed using a Lloyd LRX universal testing machine (gauge length = 50 mm and crosshead speed = 20 mm/min)(n =5).

The true densities of the obtained fibrous substrates (ρ scaffold) were measured on ∼1 g samples using a

Quantachrome Ultrapycnometer-1000 gas pycnometer (n = 5). On the basis of the obtained data, the porosities and pore volumes of the matrices can be calculated from the followingexpressions, respectively:

(1 - (ρscaffold /ρpolymer)) x 100 and (1/ ρscaffold - 1/ρpolymer), where ρscaffold represents the bulk

density of the polymeric constituent(s). Here, ρPCL, ρPHBV ,and ρPCL/PHBV(50/50 w/w), were taken as 1.145, 1.250, and 1.198 $g.cm^{-3}$ respectively.

Cell Culturing. Mouse-calvaria-derived preosteoblastic cells (MC3T3E1; ATCC CRL-2593) were cultured in minimum essential medium with Earle's Balanced Salts (MEM; HyClone, USA), supplemented by 10% fetal bovine serum (FBS; Biochrom, U.K.), 1% L-glutamine (Invitrogen, USA), and a 1% antibiotic and antimycotic formulation (containing penicillin G sodium, streptomycin sulfate, and amphotericin B; Invitrogen, USA). The medium was replaced every other day, and the cultures were maintained at 37 °C in a humidified atmosphere containing 5% CO_2

. Fibrous substrate specimens (circular discs, ~15 mm in diameter) were placed in wells of a 24-well tissue-culture polystyrene plate (TCPS; Corning, USA) and subsequently sterilized in 70% ethanol for 90 min. The specimens were then washed with autoclaved deionized water and then immersed in MEM overnight. A metal ring (~12 mm in diameter) was placed on top of each specimen to ensure good contact of the specimen with the bottom of each well.

MC3T3-E1 fromthe cultures were trypsinized (0.25% trypsin containing 1 mMethylenediaminetetraacetic acid (EDTA); Invitrogen, USA), counted by a Hausser Scientific hemacytometer, and seeded at ~40 000 cells cm^{-2} on each of the specimens and the empty wells of a TCPS (i.e., positive control). In the attachment and the proliferation studies, cells were cultured in the same media as mentioned above. For other studies, cells were cultured in MEM supplemented by 2% FBS, 1% L-glutamine, and 1% antibiotic and antimycotic during the first 3 days, after which they were cultured in the same medium but with the addition of an osteogenic supplement (i.e., 5 mM glycerol-2-phosphate disodium salt hydrate (β-glycerophosphate; Sigma-Aldrich, USA) and 50 μg . L-ascorbic acid (Sigma-Aldrich, USA)).

Cell Attachment and Cell Proliferation. The cells were allowed to attach to the fibrous substrate specimens and empty wells of a TCPS for 2, 4, and 6 h in the attachment study (n = 4). At each time point, the number of attached cells was quantified by a 3-(4,5-dimethylthiazol-2-yl)2,5-diphenyl-tetrazolium bromide (MTT; Sigma-Aldrich, USA) assay. Additionally, the cells were first allowed to attach to the specimens and empty wells of a TCPS for 16 h and then were measured at 24 h. The number of proliferated cells was also determined by MTT assay on days 1, 2, and 3 after cell culturing (n = 4). The appearance of the cells during the attachment and proliferation periods was characterized by SEM (discussed later).

Quantification of Viable Cells (MTT Assay). MTT assay is a cell quantification method that measures the activity of mitochondria in their ability to reduce a tetrazolium-based compound, MTT, to a purplish formazan product. The amount of purplish formazan product is proportional to the number of viable cells. Each cell-cultured specimen was incubated at 37 C for 30 min with MTTsolution, and the formazan product was then dissolved in a mixture of dimethylsulfoxide (DMSO; Carlo Erba, Italy; 900 μL/well) and glycine buffer (pH 10; 125 μL/well). The absorbance of the supernatant was evaluated with a Thermospectronic Genesis10 UV visible spectrophotometer at 570 nm. The observed UV absorbance values were converted to the number of cells using predetermined standard calibration curves.

Morphological Observation of Cultured Cells. Each cellcultured specimen, after the removal of the culture medium, was rinsed with PBS twice, and the cells were then fixed with 3% glutaraldehyde solution (Electron Microscopy Science, USA) at 500 μL/well for 30 min. The specimen was rinsed again with PBS and dehydrated in ethanolic aqueous solutions of varying concentrations (i.e., 30, 50, 70, and 90

vol %) and in pure ethanol for ~2mineach.Itwasdriedin 100% haxamethyldisilazane (HMDS; Sigma-

Aldrich, USA) for 5 min and subsequently in air. The specimens were then observed by SEM, and the

morphology of the cells that had been cultured on glass substrates (12 mm in diameter; Menzel, Germany) was used as a positive control.

Alkaline Phosphatase (ALP) Analysis. MC3T3-E1 were cultured on the fibrous substrate specimens and the empty wells of a TCPS for 3 and 7 days to determine the ALP activity (n = 4). Each specimen, after the removal of the culture medium, was rinsed with PBS. Alkaline lysis buffer (10 mM Tris-HCl, 2 mM MgCl, 0.1% Triton-X 100, pH 10) (100 μL/well) was added, and the specimen was scrapped, sonicated,

and then frozen at 20 Cfor~30 min. Anqueous solution of 2 mg / mL . p-nitrophenyl phosphate (PNPP;

Invitrogen, USA) mixed with 0.1 M aminopropanol (10 μL/well) in 2mMMgCl(100 μM/well) was added to the specimen, which washen incubated at 37 C for 30 min. An aqueous solution of NaOH(50 nM at 0.9 mL/well) was added, and the extracted solution was measured spectrophotometrically at 410 nm. The amount of ALP was calculated against a predetermined standard curve and then normalized by the total protein content. For the protein assay, each specimen was treated in the same manner as in the ALP assay up to the point where it was frozen. A bicinchoninic acid (BCA; Pierce Biotechnology, USA) solution was then added to the specimen and incubated at 37 C for 30 min. The absorbance of the medium solution was finally measured spectrophotometrically at 562 nm, and the amount of total proteins was calculated against a predetermined standard curve.

Mineralization Analysis. Calcium deposition was investigated by Alizarin Red-S (Sigma-Aldrich, USA) staining. MC3T3-E1 had been cultured on the fibrous substrate specimens and empty wells of a TCPS for 14 days (n = 4), after which the cells were fixed with cold methanol for 10 min, washed with deionized water, and immersed in 1% Alizarin Red-S solution in a mixture of 0.4 mL ammonium hydroxide/40 mL water for 3 min. Each stained specimen was washed several times with deionized water and air dried at room temperature. The stained specimen was photographed, and the redness, signifying the amount of

calcium deposition, was quantified by destaining with 10% cetylpyridinium chloride monohydrate (Sigma-Aldrich, USA) in 10 mM sodium phosphate at room temperature for 15 min and spectrophotometically read at 570 nm.

Statistical Analysis. All values were presented as means (standard deviations. The significance between two data sets was determined by one-way ANOVA analysis using the t test for all analyses, except for the attachment, proliferation, and ALP activity analytical studies. Scheffe's test was applied to the three studies. The statistical significance was accepted at a 0.05 confidence level.

RESULTS AND DISCUSSION

Characterization of Polymer Solutions and Fibrous Substrates.

As previously mentioned, the shear viscosity poses a strong influence on the morphology of the individual electrospun fibers.10 Prior to electrospinning, the PCL/PHBV solutions were measured for the shear viscosities (Table 1). As the total concentration of the blend solutions increased from 4 to 14 wt %, the shear viscosity increased from ~290 to ~580 mPa 3 s. Electrospinning of these solutions was carried out under an electric field of 21 kV/10 cm. (See Figure 1 for the representative SEM images of the obtained products.) At 4 wt %, a combination of discrete beads (~16 μm on average) and smooth fibers (~0.4 μm on average) was obtained. At 6 and 8 wt %, a combination of beaded and smooth fibers was evident. At these concentrations, the sizes of the beads were in the range of 2.6_3.4 μmon average and those of the fibers were in the range of 0.5_0.6 μm on average. The densities of the beads that were observed on the electrospun products from 4 to 8 wt % PCL/ PHBV solutions were 1420, 3480, and 3020 beads 3mm_2, on average. Between 10 and 14 wt %, only smooth fibers were generated. The size of these fibers increased from ~0.8 μm on average at 10 wt% to~1.8 μmon average at 14 wt %. It should be mentioned at this point that the blend composition of 50/50 w/w between PCL and PHBV was chosen on the basis of preliminary results, which showed that the fibers that had been obtained from other blend

compositions were very nonuniform (results not shown). This may arise from the immiscibility of the two polymers (later discussion). From these SEM images, the individual fibers in all of the fibrous substrates were randomly aligned, and they appeared to conglutinate to one another at touching points. Although the random alignment related directly to the slow rotational speed of the collection device used during fiber collection, the partial conglutination was due to the rather short collection distance and hence incomplete evaporation of the solvent from the jet segments during their flights to the collector.10 Electrospinning of the neat PCL and PHBV solutions was also carried out for comparison (Figure 1). The obtained fibers shared essentially the same features as those obtained from the 10_14 wt % PCL/PHBV solutions. The

sizes of these fibers were∼1.0 and∼2.2 μm on average, respectively. Upon consecutive spinning for ∼10

h, the thicknesses of the blend fibrous substrates ranged between ∼90 and ∼110 μm on average whereas

those of the PCL and the PHBV counterparts were ∼120 and ∼90 μm on average, respectively. The actual

sizes of the fibers and beads, where applicable, are also summarized in Table 1. The chemical integrity of the PCL/PHBV fibers was investigated by ATR-FTIR (Figure 2).

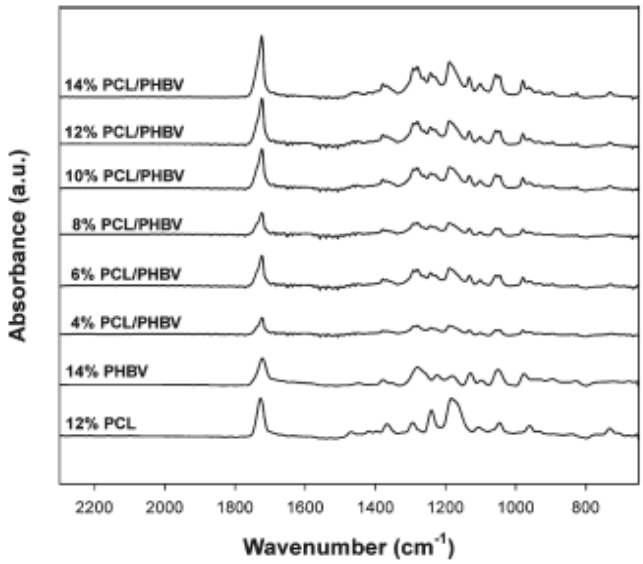


Figure 2. ATR-FTIR spectra of the obtained electrospun fibrous substrates.

Those of the neat PCL and PHBV counterparts are also shown for comparison. The absorption peak, centered at around 1724 cm_1 and belonging to the stretching vibrations associated with the crystalline conformations of the carbonyl ester (CdO),26 was evident in all of the IR spectra. For the blend fibers, the way in which this peak increased in its intensity with an increase in the total

concentration of the solutions is indicative of the increase in the total crystallinity. Referring to Figure 2, because all of the characteristic peaks of the neat polymers can be observed in the IR spectra of the blend fibers, the existence of both PCL and PHBV components within the blend fibers was confirmed. Furthermore, because no peak shifts or new absorption peaks were observed for the blend fibers, it is expected that specific interactions between PCL and PHBV molecules were inexistent. Qiu et al.27 showed that solvent-cast PCL/PHBV blend films exhibited distinctive and unchanged glass-transition and melting temperatures of either component, which is indicative of an immiscible polymer blend.

The physico-chemistry, in terms of static water contact angles, of all of the fibrous substrates was investigated (Table 1). When the size of the plated water droplet is much greater than that of the underlying fibers of a fibrous substrate, both the size and the topography of the underlying individual fibers play important roles in controlling the contact angle of the water droplet.28,29 For the beaded fibers, as the size of the beads decreased
(corresponding to the increase in the solution concentration), the water contact angle was found to increase, hence leading to a decrease in the wettability.28 As the beads disappeared completely (i.e., smooth fibers), a sudden decrease in the water contact angles and hence a sudden increase in the wettability was observed.28 For the smooth fibers, an increase in the sizes of the fibers was responsible for the observed increase in the water
contact angles and hence the decrease in the wettability.29

Here, as the total concentration of the PCL/PHBV solutions increased from 4 to 8 wt %, the average water

contact angle of the obtained beaded fibers decreased from ~121 to ~106_. A sharp drop in the average

water contact angle was observed when only the smooth fibers were the main products at 10 wt %, but as the concentration of the blend solutions increased from 10 to 14 wt %,the average water contact angle of

the obtained smooth fibersincreased again from ~85 to ~99_. Evidently, the wettability of the fibrous

substrate that had been obtained from the 10 wt %
blend solution was the greatest. On the basis of the SEM images of the PCL/PHBV fibrous substrates in Figure 1, it can be postulated that the smoother the surface of the fibrous substrates, the greater the wettability. For comparison, the average water contact angles of the PCL and PHBV fibrous substrates

were ~103 and ~115_, respectively.

The mechanical integrity in terms of the tensile strength, Young's modulus, and elongation at break of the fibrous substrates is also investigated (Table 1). For the blend fibrous substrates, the tensile strength and

the elongation at break values were found to increase (i.e., from ~0.98 to ~1.95 MPa on average for the

tensile strength and from ~1.4 to ~4.9% on average for the elongation at break), whereas that of the

Young's modulus was found to decrease (i.e., from ~162 to ~103 MPa on average), with an increase in the total concentration of the PCL/PHBV solutions from 4 to 14 wt %. Interestingly, the neat PCL fibrous substrates exhibited the greatest values of the tensile strength and elongation at the break (i.e.,~2.41 MPa

and~5.7% on average, respectively,) and at the same time they had the

lowest value of the Young's modulus (i.e., ~82.4 MPa on average). The property values of the neat

PHBV fibrous substrates, on the other hand, were relatively moderate (Table 1). The true densities, porosities, and pore volumes of the obtained fibrous substrates were investigated (Table 2).

Table 2. True Densities, Porosities, and Pore Volumes of the Obtained Electrospun Fibrous Substrates

sample	true density, $\rho_{scaffold}$ ($\times 10^{-2}$ g·cm^{-3})	porosity (%)	pore volume (cm^3·g^{-1})
4% PCL/PHBV	2.30 ± 0.26	98.1 ± 0.5	42.6 ± 3.2
6% PCL/PHBV	2.61 ± 0.15	97.8 ± 0.3	33.2 ± 2.5
8% PCL/PHBV	2.86 ± 0.54	97.6 ± 0.7	34.1 ± 3.0
10% PCL/PHBV	3.19 ± 0.23	97.3 ± 0.4	30.5 ± 1.7
12% PCL/PHBV	3.57 ± 0.39	97.0 ± 0.7	27.2 ± 1.7
14% PCL/PHBV	3.93 ± 0.38	96.7 ± 0.6	24.6 ± 2.4
12% PCL	4.69 ± 0.11	95.9 ± 0.4	20.6 ± 2.1
14% PHBV	2.13 ± 0.17	98.3 ± 0.2	46.1 ± 2.6

For the blend fibrous substrates, the true density was found to increase (i.e., from ~2.3 _ 10_2 to ~3.9 _ 10_2 g 3 cm_3 on average), and those of the porosity and the pore volume were found to decrease (i.e.,

from ~98.1 to ~96.7% on average for the porosity and from ~42.6 to ~24.6 cm3 3 g_1 on average for

the pore volume), with an increase in the total concentration of the PCL/PHBV solutions from 4 to 14 wt %. The results imply that as the total concentration of the blend solutions increased the packing of the underlying fibers also increased. Among all of the fibrous substrates investigated, those made of PCL exhibited the lowest porosity and those made of PHBV were the greatest (Table 2).

Cell Attachment and Cell Proliferation.

Quantitative analysis for the adherence of MC3T3-E1 after having been seeded on the surfaces of TCPS and all types of fibrous substrates for 2, 4, and 6 h is shown in Figure 3. For any given type of substrate, the number of cells increased with an increase in the cell seeding time. At 2 h, the numbers of cells on the surfaces of almost all types of fibrous substrates, except for those of the substrates from 4 wt % PCL/PHBV and 14 wt % PHBV solutions that exhibited significantly lower values, were equivalent to that on TCPS. At 4 h, the numbers of cells on the surfaces of the fibrous substrates from 4, 10, and 12 wt % PCL/PHBV and 12 wt % PCL solutions were equivalent to that on TCPS. At 6 h, only the numbers of cells on the surfaces of the fibrous substrates from 10 and 12 wt % PCL/PHBV solutions were equivalent to that on TCPS. Among the various types of fibrous substrates, those from 10 and 12 wt % PCL/PHBV and 12 wt % PCL solutions, regardless of the cell seeding time, appeared to support the attachment of the investigated bone cells slightly better than did the others.

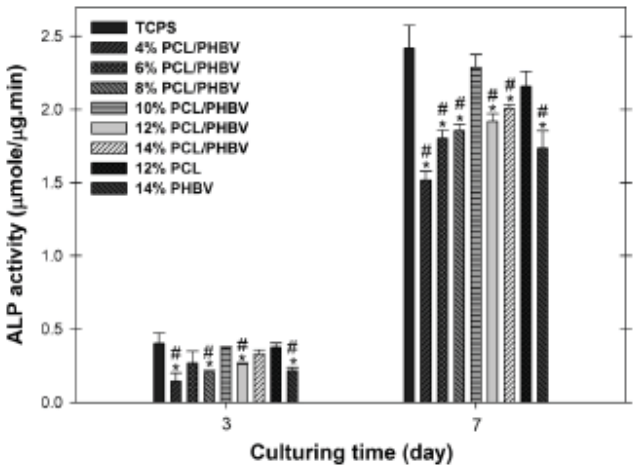


Figure 6. ALP activity of MC3T3-E1 that was cultured on the surfaces of TCPS and various types of fibrous substrates at various given time points after cell culturing. *Significance at $p < 0.05$ with respect to TCPS. #Significance at $p < 0.05$ with respect to the fibrous substrate from 12 wt % PCL solution.

A quantitative analysis of the proliferation of MC3T3-E1 after having been cultured on the surfaces of TCPS and all types of fibrous substrates for 1_3 days is shown in Figure 4. For any given type of substrate, the number of cells increased with an increase in the cell culturing time. On day 1, the numbers of cells on the surfaces of fibrous substrates from 6 to 12 wt % PCL/ PHBV were equivalent to that on TCPS. On days 2 and 3, the numbers of cells on the surfaces of fibrous substrates from 6, 10, and 14 wt % PCL/PHBV and 12 wt % PCL solutions were equivalent to that on TCPS. Nevertheless, the average number of cells proliferated on the surface of the fibrous substrate from 10 wt % PCL/PHBV solution was greater than those on the surfaces of the other types of fibrous substrates. Particularly on day

3, the average number of cells on the surface of the fibrous substrate from 10 wt % PCL/PHBV solution was significantly greater than that of the fibrous substrate from 12 wt % PCL and slightly greater than that on TCPS.

Though not totally relevant, Kumbar et al.30 demonstrated that the biological response of human skin fibroblasts (hSF) that had been cultured on the surfaces of poly(lactic acid-co-glycolic acid) (PLAGA) fibrous substrates was, in many respects, fibersize- dependent. Specifically, the PLAGA fibrous substrates with the diameters of the underlying fibers ranging from 250 to 1200 nm showed significantly greater support for the proliferation and the expression of collagen III of the cultured hSF than the matrices with lower or larger fiber diameters. However, no particular trends were observed for the production of collagen I and elastin with the variation in fiber diameter.30 Khang et al.31 prepared poly(L-lactide-co-glycolide) (PLGA) films with chemogradient wettability by a corona treatment and found that fibroblasts adhered, spread, and grew particularly better onto positions with moderate

hydrophilicity (i.e., a water contact angle of ~55_). On the basis of these studies,30,31 both the size

of the underlying fibers and hence the wettability of a fibrous substrate should play important roles in mediating the cell behavior. Here, the mouse bone cells appeared to attach and proliferatewell on the surface of the fibrous substrate from 10 wt% PCL/PHBV solution, which exhibited the lowest water

contact angle of ~85_ on average.

Because the adsorption of proteins is influenced by the hydrophilicity/hydrophobicity of a surface, a surface with a certain water contact angle would favor the adsorption of certain proteins, which may or may not act as cellular mediators.Additionally, it is hypothesized that both the size and the topography of the underlying fibers of a fibrous substrate may directly influence the organization of organelles within the attached cells. Different organizations of the organelles may result in different chemosignaling pathways that directly influence the cell behavior. Although the effect of different surface topographies on the wettability, adsorption of proteins, and responses of the cultured bone cells should be a subject of thorough investigation, the effect of different organizations of organelles, in response to different surface topographies, on certain behaviors of the cultured bone cells can be rationalized from an existing published report.32 In an attempt to investigate the effect of fiber alignment on the responses of MG63 human osteosarcoma cells that had been cultured on the surfaces of randomly aligned and well-aligned poly(L-lactic acid) (PLLA) fibrous substrates, Wang et al.32 found that the cells on the well aligned fibrous substrate elongated their cytoplasms along the fiber axis but appeared to attach, proliferate, and differentiate better on the randomly aligned fibrous substrate. This exemplifies the importance of the surface topography of a scaffold in cellular behavior.

Selected SEM images illustrating the morphologies of MC3T3-E1 that had been cultured on the surfaces of glass and all types of fibrous substrates for various time intervals are shown in Figure 5. At 2 h after cell seeding, most of the cells on almost all types of the fibrous substrates were still round, except for those on the surfaces of the fibrous substrates from 6 wt%PCL/PHBV, 10 wt % PCL/PHBV, and 12 wt % PCL solutions that showed a slight expansion of their cytoplasms. At this time point, the cells on the control glass substrate were also still round, but a cytoplasmic process in the form of filopodia was clearly visible. At 4 and 6 h after cell seeding, the cells on all types of substrates became more expanded. Interestingly, the cells on the fibrous substrate from 14 wt % PHBV solution were very small, and because of the large size of the individual fibers, the cells appeared to elongate their cytoplasms along the fiber axis. On days 1 and 2 after cell culturing, the cells, in their expanded morphology, proliferated well

to cover~30 to~40% of the surfaces on almost all types of fibrous substrates.On day 3, full expansion of the cells on all types of substrates was seen. Strikingly, most of the cells expansion was observed for the cells on the fibrous substrate from 10 wt % PCL/PHBV solution, which proliferated to cover ~70% of the surface. Noticeably, the cells on the fibrous substrate from 14 wt % PHBV solution grew in size but still exhibited the elongation of their cytoplasms along the fiber axis. On the basis of the results shown in Figure 5, the fibrous substrate from 10 wt % PCL/PHBV solution was clearly the best among the investigated fibrous substrates for supporting the growth of MC3T3-E1.

Alkaline Phosphatase (ALP) Activity.
The expression of ALP from MC3T3-E1 that had been cultured on TCPS and all types of fibrous substrates for 3 and 7 days is shown in Figure 6.On day 3, the ALP activities of the cells that had been grown on the surfaces of TCPS and the fibrous substrates from 6, 10, and 14 wt % PCL/ PHBV and 12 wt % PCL solutions were statistically the same, which appeared to be greater than that of cells on the rest of the fibrous substrates. On day 7, increases in the ALP activity from that observed on day 3 of the cells that had been grown on all types of substrates were evident. Strikingly, only the cells that had been grown on the surfaces of the fibrous substrates from10 wt % PCL/PHBV and 12 wt % PCL solutions exhibited ALP activity at levels that are statistically equivalent to those that had been grown on TCPS, whereas the cells that had been grown on the surfaces of all other types of fibrous substrates had much lower values. Because ALP is usually secreted from normal bone cells during the early matrix formation and maturation period and is triggered by cellular contacts (when the cells reach confluence) and/or by the expression of ample amounts of early matrix proteins (e.g., type I collagen, fibronectin, and/or TGF-β1),4,33 it is logical to note that the fibrous substrates from 10 wt % PCL/PHBV and 12 wt % PCL solutions were both able to up-regulate the ALP production of MC3T3-E1much better than the rest of the fibrous substrates. Between the two types of the fibrous substrates, the one from 10 wt % PCL/PHBV solution was able to support the ALP production of the cells slightly better than the one from the 12 wt%PCL solution (on the basis of the average values of the obtained results).

Mineralization.
The ability to promote bone formation is the most important characteristic of a bone scaffold. Here, photographic images of Alizarin Red S staining of MC3T3-E1 that had been cultured on TCPS and all types of fibrous substrates for 14 days, along with their quantitative analyses, are shown in Figure 7. Because of the presence of calcium ions in the mineralized tissues, the staining product with Alizarin Red S appeared red. According to the obtained results, the cells that had been cultured on all types of the fibrous substrates stained positively for calcium deposition along with those that had been cultured on the fibrous substrate from 10 wt % PCL/PHBV solution exhibiting the greatest intensity, followed by those that had been cultured on the fibrous substrate from 12 wt % PCL solution. Interestingly, despite the high attachment, high proliferation, and high expression of ALP for the cells that had been grown on TCPS, mineralization of the cells on this control surface on day 14 was the lowest. All of the obtained results emphasize the importance of a thorough investigation for the efficacy of a bone scaffold because themineralization of the bone cells does not rely solely on the ability of the scaffold to promoting the attachment, the proliferation, and/ or the secretion of ALP of the cells. The obtained results also imply that both the topography (i.e., patterning and/or roughness) and the physicochemical characteristic (i.e., hydrophilicity/ hydrophobicity) of the surface of a scaffold are important factors in determining the

efficacy of the scaffolds. To this end, it should also be emphasized that before a scaffold that has been evaluated as positive for promoting infiltration, attachment, proliferation, and differentiation of the target cells in vitro can be used in vivo, it should also be tested for inflammatory reactions because it has recently been demonstrated that the in vitro inflammatory response of a scaffold by macrophages is also surface-topography-dependent.34

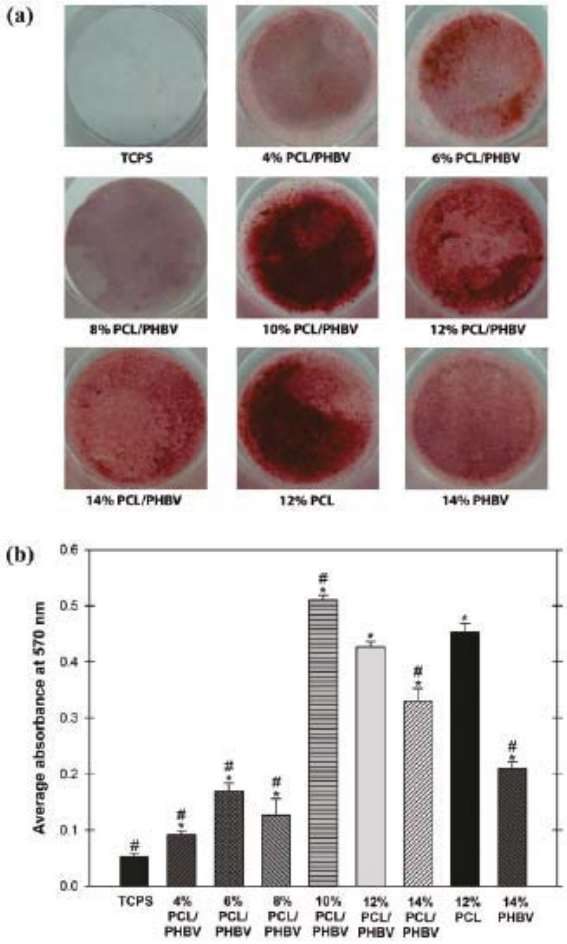


Figure 7. Alizarin Red S staining for the mineralization of MC3T3-E1 on day 14 after being cultured on the surfaces of TCPS and various types of fibrous substrates: (a) photographic images of the stained specimens and (b) the corresponding quantitative analyses. *Significance at $p < 0.05$ with respect to TCPS. #Significance at $p < 0.05$ with respect to the fibrous substrate from 12 wt % PCL solution.

,

CONCLUDING REMARKS

The fibrous substrates with different morphologies of the individual fibers were prepared from solutions of 50/50 w/w PCL/PHBV in 80/20 v/v chloroform/DMF by electrospinning. As the concentration of the solutions increased from4 to 14 wt %, the topography of the individual fibers changed from discrete beads/smooth fibers to beaded fibers/smooth fibers and finally to smooth fibers, and the size of the

individual fibers increased from ~0.4 to ~1.8 μm on average. Among the various fibrous substrates, the

one prepared from10 wt % PCL/PHBV solution exhibited the lowest static water contact angles of ~85_ on average. Likely because of the smoothness of the obtained fibrous substrate and the lowest water contact angles of its surface, the fibrous substrate from 10 wt % PCL/PHBV solution, with an average fiber diameter of ~0.8 μm, was the best at promoting the attachment, proliferation, and differentiation of the cultured mouse bone cells (MC3T3-E1). This type of fibrous matrix could be used as scaffolding substrates for calvarial defects.

14. Comparison of isolation techniques for bone marrow derived canine mesenchymal stem cells (MSCs) and the effects of MSCs loaded onto polycarpolactone hydroxyapatite scaffold on non-union bone healing

Materials and methods

All chemicals used in this study were purchased from Sigma Aldrich, St. Louis, USA, unless otherwise specified.

1 Collection and isolation of canine bone marrow derived mesenchymal stem cells

This study was approved by the Committee for the Ethical Care of Animals of the Chulalongkorn University. Seven mature dogs, mixed breeds, weighed between 10 to 15 kg were enrolled in this study. All dogs were physically examined and remained health entirely the experiment. Routine blood analysis was performed preoperatively. Acepromazine 0.02 mg/kg and morphine 0.5 mg/kg were administered intramuscularly, and the anesthesia was induced with propofol (Fresenius Kabi, Austria GmbH, Graz, Austria) and maintained with isoflurane in 100% oxygen. Cefazolin (25 mg/kg) was administered intravenously as prophylactic antibiotic. Epidural anesthesia using 0.5% bupivacaine (1 mg/kg) combined with morphine (0.1 mg/kg) was additionally performed to relief pain sensation caused by bone marrow aspiration procedure. Fifteen milliliters of bone marrow were harvested from the iliac crest of each dog with a heparinized syringe.

The bone marrow aspirate (15 ml) was equally divided into 3 aliquots, and each aliquot of 5 ml bone marrow was then submitted to one of the following isolation techniques: 1) direct plating, 2) red blood cell lysis treatment and 3) gradient density.

1.1 Direct plating

Direct plating was performed by adding bone marrow aspirate directly into a 10 cm Petri-dish (BD-Falcon™, Franklin Lake, NJ, USA) containing with 7 ml of MSC culture medium. After 24 of culture, the attached cells were washed with Dulbecco's phosphate buffered saline without calcium and magnesium (DPBS, Invitrogen, Carlsbad, CA, USA) for 2-3 times, and the fresh MSC medium was then added.

1.2 Red blood cell lysis treatment

Red blood cell lysis buffer (8.3 g/L ammonium chloride in 0.01 M Tris-HCl buffer, pH 7.5 $\pm$ 0.2) was used to eliminate the contaminated red blood cells (RBC) in the bone marrow aspirate. The RBC lysis buffer was mixed at a ratio of 1: 1 with bone marrow aspirate and then incubated at room temperature (approximately 25-26^{o}C) for 5 min. The mixture was then centrifuged at 1000 rpm for 5 min. After the supernatant was discarded, the pellet was resuspended with MSC medium, and the isolated cells were cultured in MSC culture medium. The non-attached cells were washed out in the following day.

1.3 Gradient density

Bone marrow aspirate (5 ml) was gently layered onto a histopaque® 1077 (density 1.077 $\pm$0.001) in a 15 ml conical tube (BD-Falcon™, Franklin Lake, NJ, USA). The centrifugation was performed at 26^{o}C and 400g for 30 min, and the interface containing mononuclear cells was then collected. The presumptive MSCs were washed with MSC culture medium for two times prior to culture.

2.2 Culture of bone marrow derived mesenchymal stem cells

Following MSC isolation (day 0) as previously described, the isolated cells were allowed to attach to the culture plate for 24 h prior to washing with DPBS. These cultured cells were assigned as primary cells at passage 0 (P_0). MSC culture medium was composed of a low-glucose Dulbecco's modified Eagle's medium (low glucose DMEM) supplemented with 10% (v/v) fetal bovine serum (FBS,

Invitrogen), 2 mM L-glutamine (Invitrogen, Carlsbad, USA), 100 unit/ml penicillin G, 100 µg/ml streptomycin, 40µg/ml gentamicin and 5 µg/ml amphotericin B.

Subculture of MSCs was performed after treating the cells with 0.05% (w/v) trypsin-EDTA (Invitrogen). The disaggregated cells were then centrifuged and split into new Petri-dish at a ratio of 1:3. Putative MSCs at passages 3 (P_3) were used for flow cytometric analysis in order to examine the expression of cell-surface antigens and also for *in vitro* differentiation. In all cases, the culture condition was performed at 37^{o}C in a humidified condition of 5 % CO_2 in air.

3 Assessing the characteristics of canine mesenchymal stem cells

3.1 Flow cytometry

The examination of MSCs was performed as essentially described by Tharasanit et al. (2011). Canine MSCs at the 3rd passages from a total of 5 dogs (Dog no. 1, 4, 6, 7 and 8) were immunologically examined for surface markers. These makers included the positive (CD 44, CD 90) and negative (CD 34) makers. The MSCs were first dissociated from the Petri dishes with Trypsin- EDTA and then centrifuged. A total of 200,000 to 300,000 cells were used for immunolabeling. Rat monoclonal anti-canine CD 90 (AbD serotec, Kidlington, UK) with rabbit anti-rat FITC secondary antibodies and monoclonal anti-canine CD44 antibody conjugated with allophycocyanin (APC) (R&D system, Minneapolis, USA) were used as MSC positive markers. A rat monoclonal anti-canine CD 34 antibody conjugated with fluorescein isothiocyanate (FITC) was used as the negative MSC marker. Fluorescently-labeled MSCs were washed and fixed with 1% (w/v) paraformaldehyde in PBS and stored at 4°C in the dark until analysis. Non-staining MSCs and MSCs labeled with only the secondary antibody were used as controls. At least 20,000 MSCs were analyzed by flow cytometry.

3.2 *In vitro* bone differentiation of MSCs

Canine bone marrow derived MSCs at passage 3 from four dogs were simultaneously induced to osteogenic lineage (each dog represented one replicate). Osteogenic differentiation was performed as essentially described by Bosch et al. (2006) with minor modifications. The MSCs were first cultured to

reach approximately 80% confluence, the osteogenic medium containing MSC medium supplemented with 0.1 μM dexamethasone, 50 μM ascorbic acid, 10 mM β-glycerophosphate (Merck, Darmstadt, Germany) was then added into the culture dish. The *in vitro* bone differentiation was performed for 21 days. Von Kossa staining was used to detect deposition of calcium phosphate indicating *de novo* bone formation.

3.3 Scaffold preparation and MSC transplantation

PCL/HA composite scaffolds were prepared as previously described [28]. The scaffold were cut into 10x5x25 millimeters and sterilized with 100% (v/v) absolute ethanol for 1 h. The scaffolds were washed thoroughly with sterilized distilled water and then DPBS to remove the ethanol.

Anesthesia and surgical procedures were performed as similar as previously described. Brachial plexus block using 0.5% bupivacaine (1.3 mg/kg) was additionally performed prior bilateral ulnar osteotomy to reduce pain. A total of 3 dogs were induced bilateral ulnar non-union (n=6) by cutting the mid-shaft of the ulnar bone (2.5 cm) using an oscillating saw. The osteotomized sites were implanted with the PCL/HA composite scaffold to improve bone stability. After the operation, all forelimbs were applied with modified Robert Jone bandages reinforced with thermoplastic splint (Vet-lite, Bangkok, Thailand). All dogs also received 5 mg/kg enrofloxacin (Bayer, Bangkok, Thailand) and 4 mg/kg carprofen (Pfizer, Bangkok, Thailand) orally for 7 days after implantation. All dogs demonstrated for bone non-union during 12 weeks after scaffold implantation. For transplantation, autologous MSCs were subcultured to passage 4 as previously described. After trypsinization, approximately $10x10^6$ cells/ml were loaded into a syringe containing with minimum volume (0.5 ml) of DMEM supplemented with 1% (v/v) FBS. Three MSC transplanted sites (proximal, middle and distal parts of the PCL/HA scaffold implant) were injected via a 23 G indwelling intravenous catheter with MSCs under a fluoroscope (Philips healthcare, Eindhoven, the Netherlands).

4 Examination of bone formation

4.1 Radiography

The lateral radiographs were taken immediately at 2, 4, 6, 8, 10 and 12 weeks post-operation in all dogs. Bone healing was evaluated using radiographic scoring system previously described [29] as shown in

table 1. Bone union was justified grading from 0 to 3 at the proximal and distal of implanted material. In addition, the new bone formation was scored 0 to 4.

4.2 Angiography

Fluoroscopic angiography was performed in two experimental dogs at 12 weeks before MSC injection (dog no. 1, 2) and 16 weeks after MSC injection (dog no.1) in order to observe blood vessels at an implantation site. Anesthesia and surgical procedures were performed as previously described. The 23 G intravenous catheter connected with an extension tube was inserted into the axillary vein and the radiographic contrast medium (iohexol, Omnipaque®, G E healthcare, Buckinghamshire, UK) was slowly administrated in order to observe the presence of the blood vessel at the MSC transplanted site using fluoroscopy.

4.3 Histological examination of MSCs loaded scaffold

The biopsy was performed both before (n=2) and after MSC transplantation (n=2) at 12 and 20 weeks post-transplantation. The biopsy samples were fixed with 10% (v/v) buffered formalin, and the fixed samples were embedded in paraffin and processed following guideline for a routine histological procedure. The sections were stained with hematoxylin & eosin (H&E) and examined for neovascularization and bone formation under a light microscope. Occasionally, Masson's trichrome staining was additionally performed to detect the presence of collagen fibers.

3. Statistical analysis

Values are present as means ± standard deviation (SD). Efficacy for different MSC isolation techniques on the number of isolated MSCs, viability and expression of MSC markers were compared by one-way analysis of variance (ANOVA) and post-hoc analysis with the least significant difference (LSD). Angiographs and histological findings were descriptively analyzed. The differences in radiographic scores at 2, 4, 6 and 8 weeks post MSC transplantation were evaluated using Kruskal-Wallis one way analysis and Mann-Whitney U test. In all cases, statistical analysis was performed using SPSS statistical program (version 17.0). P values <0.05 were considered statistically significant.

Results

Following MSC isolation, putative MSCs were attached onto Petri-dish. These MSCs irrespective the MSC isolation techniques demonstrated a typical MSC morphology (figure 1 A-C). There were several cell types including thin spindle shaped, typical fibroblast-like, and mantle cells. On day 7 after MSC isolation, the total number of MSCs obtained from a 5-ml of bone marrow aspirate was ranged from 0.35×10^6 to 2.8×10^6, 0.04×10^6 to $1.43\times$, 0.03×10^6 to 0.75×10^6 for gradient density, RBC lysis treatment and direct plating, respectively (Table 2). The gradient density techniques significantly increased the numbers of isolated MSCs when compared with direct plating technique ($P<0.05$), while cell yields obtained from this gradient density was efficiently comparable to RBC lysis treatment ($P>0.05$).

Cell-surface antigen profiles of canine MSCs was ascertained after immunolabeling with canine-specific/cross-reacted monoclonal antibodies and examined with a flow cytometer. Ranges and averages of percentage of cells positive for CD 44, CD 90 and CD34 are shown in table 2. Canine MSCs at passage 3 highly expressed CD 44 (95.66-99.89) and rarely expressed CD 34 in all cases (table 2). Furthermore, the cultured MSCs demonstrated to have capability to differentiate into osteogenic lineage as they positively stained with Von Kossa following osteogenic induction (figure 2).

Following MSC transplantation into non-union sites, all three dogs could walk properly within 24 hours after surgery. Neither radiological changes at scaffold-ulna interface nor callus formation was presented at the implant sites of PCL/HA alone (figure 3A) and PCL/HA combined with MSCs (figure 3B) at 2, 4, 6, 8 and 12 weeks post-operatively. The density of the implant grafts was comparable to soft tissue density. The radiographic scores was 0 in all cases.

Fluoroscopic angiography indicated the presence of blood vessels within the PCL/HA scaffolds at 12 weeks after implantation (figure 4A). These blood vessels descriptively appeared to increase when examined at 16 weeks after MSC injection (figure 4B). This result was in an accordance with histology of the host-PCL/HA transplanted sites that neovascularization was observed in PCL/HA both with and without MSC injection. However, no such osteoid formation was observed in the histological sections. The transplanted PCL/HA scaffolds was filled with loose and unorganized connective tissue (figure 5A) but the

thickness of the fibrous tissues and the number of small blood vessels were likely to increase at 20 weeks after MSCs injection (figure 5B). The fibrous tissue was mainly comprised of the spindle cells with extensive collagen deposition which was confirmed by Masson's trichrome staining (Figure 5B). Interestingly, we also found a number of multinucleated gaint cells and lymphocytes within the scaffolds indicating the inflammatory response.

Discussion

In the present study, we demonstrated that bone marrow derived canine MSCs could be enriched by treating the bone marrow aspirate prior to culture, and these harvested cells were highly expressed MSC markers (CD 44 and CD 90) and had a potential to differentiate into osteogenic lineage in vitro. However, the de novo bone formation following transplantation of the MSCs into PCL/HA scaffold was compromised.

Bone marrow was considered as a primary source of MSCs but only 0.001 to 0.01% of bone marrow mononuclear cells in rodents and felines were identified as MSCs [13, 14]. In addition, no consensus makers have been defined as conclusive markers for canine MSCs and thus the ability of cells that can adhere onto plastic Petri-dish is often used.[30] In the current study, we first examined the different techniques to enrich MSCs from bone marrow aspirate and found that gradient density significantly increased the numbers of isolated MSC on day 7 of culture when compared with direct plating technique ($P<0.05$, table 2). It had become clear that the presence of RBC in the culture dish negatively affected on the number of harvested MSCs probably because the RBC may compromise the MSCs to settle and adhere to the Petri-dish.[31] In addition, excessive RBC lysis during culture may cause the release of free hemoglobin that can induce cellular stress and apoptosis [32, 33]. Although the efficacy of the gradient density was similar to that of RBC lysis treatment ($P>0.05$), the RBC lysis buffer treatment is preferable for clinical use since it requires less time-consuming and inexpensive. This technique may also be beneficial for initial growth of the isolated MSCs due to the platelet derived growth factor secreted from the remaining platelets following RBC lysis. [30] In addition to the effect of isolation techniques on MSC derivation, the numbers of MSCs

isolated were considerably variable among donors, irrespective the isolation techniques used. This result was in an agreement to the facts that the number of bone marrow MSCs significantly decreases with increased age and poor health status [34-37], while the cells obtained from young donors grew more rapidly.[38] However, there was no effect of isolation techniques on the expression of MSC makers (CD 40 and CD 90) and also in vitro differentiation, suggesting that MSC properties could be maintained using the current culture system. However, study on the effect of long term culture of these MSCs on MSC proliferation activity and also differentiation capability remains elusive. This aspect is important given that the large numbers of cells would be required for cell/tissue engineering. [6]

To date, several attempts have been made on transplantation of MSC into long-bone defects. [3, 13, 39, 40] However, the de novo bone formation following transplant has been unsuccessful [13] especially in dog that has a slower bone turnover rate compared with mouse. [41] Furthermore, the injured bone site often becomes ischemic due to the excessive vascular destruction [42] A combination of osteopotential cell and biolodegradable scaffold is one of the most successful strategies in bone tissue engineering. Our previous data suggested that PLC/HA composite scaffold demonstrated as a promising approach for promoting new bone formation when transplanted to calvarial defect in mouse. [43] In order to minimize the risk of ischemic lesion, we therefore first transplanted the PCL/HA scaffold to the large bone lesion allowing the neovascularization within the scaffold before MSC transplantation. After 12 week of PCL/HA scaffold transplant, no bone formation was found but the fluoroscopy indicated the neovascularization within the scaffold (figure 4A). However, no osteogenic differentiation was observed following MSC transplant into the vascularized scaffolds. From this result, it has become clear that implanted site of scaffold and species employed plays an important role for bone regeneration (i.e. cortical versus cancellous bone) [44]. Furthermore, a large size and slow degradable PCL-HA scaffolds may also create an unfavorable environment for bone formation [45-47]. In this study, several multinucleated giant cells in the PLC/HA scaffold indicated chronic reactions due to the foreign body response. Similar tissue reaction was previously reported.[48-50]. Although the scaffolds used in this study were contaminated with copper (probably from hydroxyapatite ceramic) as we further we analyzed the scaffold using energy dispersive x-ray (SEM/EDX)

analysis (unpublished data), the failure for osteogenesis of transplanted MSCs in the scaffold was probably not caused by the cell cytotoxicity of the contaminated copper. There was a good evidence of fibrovascular tissue infiltration with an extent matrix deposition throughout the entire PCL/HA scaffold, and injection of MSCs into the scaffold seemed to increase the thickening size of the fibroblastic mass and vascularization (figure 5B). In fact, several factors are critical for bone tissue engineering, the main hallmark remains to be the sufficient osteogenic factors to stimulate de novo bone differentiation of the transplanted MSCs [2]. Several growth factors and pathways have been demonstrated to be necessary for bone development. [51] For example, bone morphologic protein-2 (BMP-2) increased osteocalcin release from MSCs promoting and healing response and induced chondrogenic and osteogenic differentiation of human bone marrow MSCs [52-54] and also promoted the new bone formation in femoral defects in rats [40] and increased the local population of cells and the connective tissue progenitors in a canine femur defect model with the combination of MSCs. [55]

In conclusion, this study revealed that MSCs can be derived from bone marrow. These MSCs could further enrich by treating bone marrow aspirate with gradient density and red blood cell lysis treatment. Although these MSCs highly expressed the MSC markers and also retained the differentiation potentials, the bone differentiation following implantation was compromised. Further novel strategy in particular the combination of tissue engineering and osteogenic substances that can create a proper environment for de novo bone formation remain to be studied.

Table 1 Radiographic scoring system for evaluation of bone healing.[39]

	Score	Description
Bone formation	0	No new bone; graft approximates density of soft tissue
		Minimal new bone composed mostly of noncontiguous
	1	Areas of minimal density
	2	New bone present as mostly contiguous areas of normal

		Density and fills approximately 50% of the defect
		New bone present as mostly contiguous areas of normal
	3	Density and fills approximately 51-95% of the defect
	4	New bone a solid contiguous mass that fills > 95% of the defect
Bone union	0	No contact between new bone and noninvolved adjacent normal bone
	1	Partial bridge (< 50%) from new bone to adjacent normal bone
	2	Partial bridge (> 50%) from new bone to adjacent normal bone
	3	Complete bridge from new bone to adjacent normal bone

Table 2 Mean ± SD (range) of total number of MSCS on day 7 and the proportion of MSCs (passage 3) positive to cell surface markers. The MSCs were isolated from bone marrow using three different techniques.

	Total cell number ($x10^6$)	Cell surface markers		
		CD 44	CD 90	CD 34
Whole aspiration	0.26 ± 0.28^{a}	98.74+1.73	95.84+3.05	0.018+0.03
	(0.03-0.75)	(95.66-99.59)	(91.93-99.15)	(0-0.01)
RBC lysis treatment	$0.94 \pm 0.55^{a,b}$	99.28+0.82	93.48+10.76	0.014+0.03
	(0.04-1.43)	(99.18-99.89)	(74.3-99.21)	(0-0.06)
Gradient	1.08 ± 0.92^{b}	99.2+0.96	93.62+6.65	0.012+0.027
	(0.35-2.8)	(99.02-99.89)	(82.53-98.88)	(0-0.06)

Figure 1 Morphology of canine MSCs derived from bone marrow using direct plating (A), RBC lysis treatment (B) and gradient density (C).

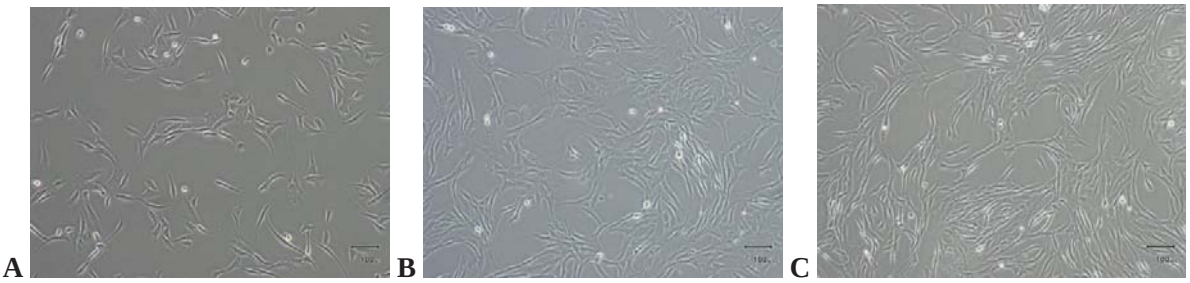


Figure 2 An example of canine bone marrow MSCs that were induced to differentiate into osteogenic lineage as they were positive to Von Kossa staining

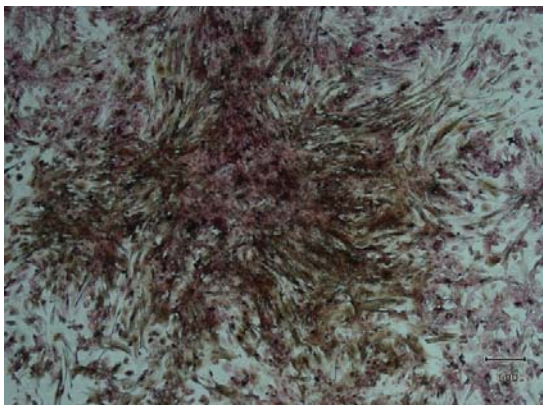
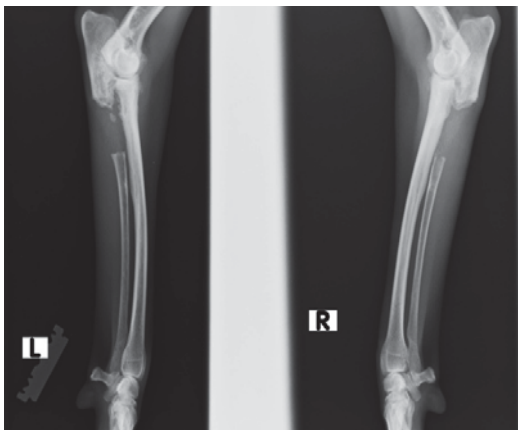


Figure 3 Radiographs demonstrating canine ulnar segment defect with PCL/HA alone (A) or PCL/HA combined with MSCs at 12 weeks (B) postoperatively. Note that no *de novo* bone formation was observed.

A 

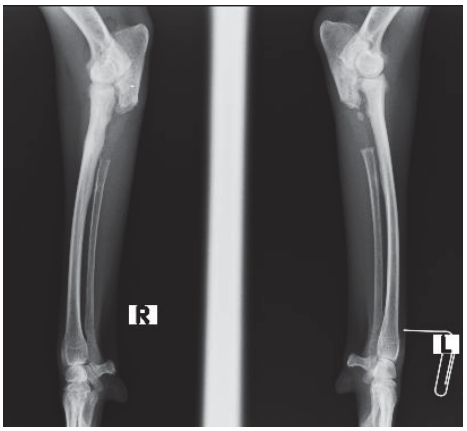
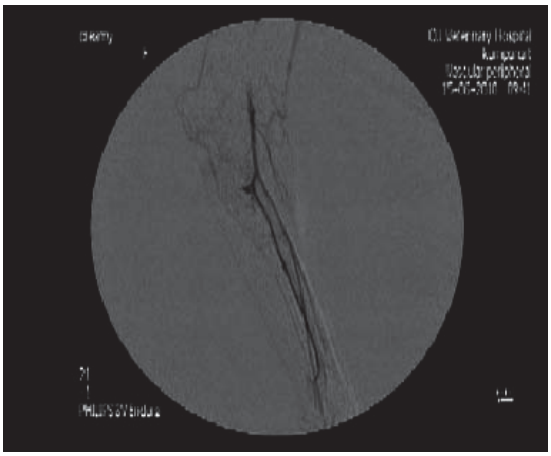
B 

Figure 4 Fluoroscopic angiography at 12 weeks (A) after PCL/HA scaffold implant and at 16 weeks after MSC injection (B). The increased blood vessels were observed at the implantation site after BMSC injection.

A 

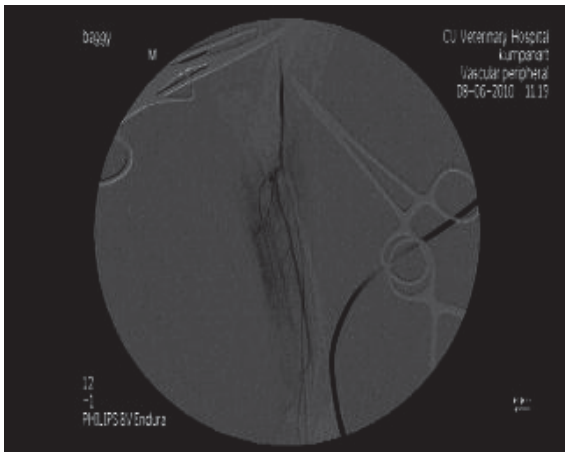
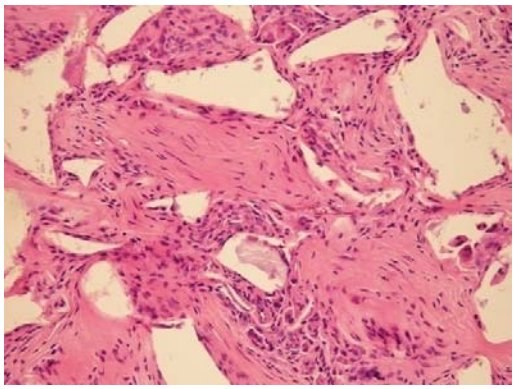
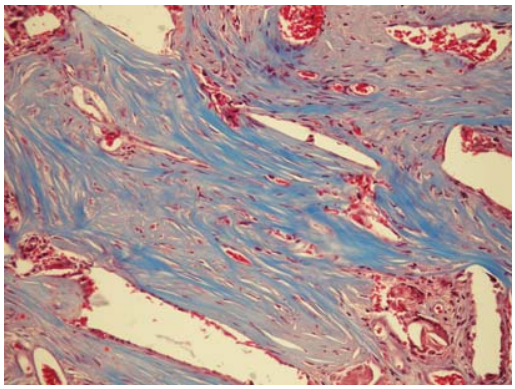
B 

Figure 5 Histology of PCL/HA implanted site at 12 weeks after surgery (A) and at 20 weeks after MSC injection (B) indicates the newly formation of capillaries and arterioles. Masson's trichrome staining (B) indicates that the thickening of fibrous tissue mainly constructed by an extensive collagen fibers.

A  B 

15. The effects of mesenchymal stem cells combined with polycapolactone/hydroxyapatite composite scaffold on the healing of ulnar defect in dogs

Materials and Methods

All chemicals used in this study were purchased from Sigma Aldrich, St. Louis, USA, unless otherwise specified.

1 Scaffolds

PCL/HA composites scaffolds used in this study were prepared as previously described (Wutticharoenmongkol et al., 2006). Scaffolds were prepared from Polycaprolactone (PCL;

Aldrich, USA; *M*w = 80,000 g·mol^{-1}) incorporated with 40% w/w HA powder by solvent casting and particular leaching technique. Sucrose with diameter around 400–500 μm was used as the porogen to create the interconnected network. The scaffold porosity was in the range of 85-87%. PCL/HA composite scaffolds were cut into 5 x 5 x 5 mm and 10 x 5 x 25 mm for *in vitro* and *in vivo* studies, respectively. The scaffolds were sterilized with 100% (v/v) absolute ethanol for 1 hour and washed thoroughly with steriled distilled water and DPBS to remove residual ethanol. The scaffolds were preconditioned in culture medium for 2 hours prior to seeding procedure.

2 Animals

All protocols used in this study were approved by the Committee for the Ethical Care of Animals of the Chulalongkorn University. Seven mongrel dogs were enrolled in this study with various sexes (male=2, female=5), body weights were ranging from 12 to 16 kg. In each dog, a 2.5 cm bilateral ulnar ostectomy was performed to create critical sized defects. One dog had to undergo the second operation in order to get the total of 15 defect sites. Complete blood counts and blood chemical profiles were also examined prior surgery. Acepromazine maleate (0.02 mg/kg) (Vetranquil^{TM}, Ceva Sante animal, Libourne, France) combined with morphine sulphate (0.5 mg/kg) (Food and drug administration, Bangkok, Thailand) were used as the premedication drugs which administered intramuscularly. General anesthesia was induced with 4-6 mg/kg propofol (Fresenius Kabi Austria GmbH, Graz, Austria) intravenously and then maintained with an inhalation anesthesia using isoflurane in 100% oxygen via the rebreathing anesthetic circuit. Cefazolin (250 mg/ml) 25 mg/kg was administered intravenously as the prophylactic antibiotic. Additionally, brachial plexus nerve block using 0.5% bupivacaine (1 mg/kg) was performed to minimize pain sensation (Skarda and Tranquilli, 2007) that may occur during ulnar ostectomy.

3 MSCs isolation and culture expansion

The bone marrow contents (5-10 ml) from 4 dogs were collected using a 18 G needle connecting to a 5 ml heparinized syringe. To remove an excessive RBC, 5 ml of red blood cell lysing buffer (8.3 g/L ammonium chloride in 0.01 M Tris-HCl buffer pH 7.5 $\pm$ 0.2; Sigma-Aldrich, USA) was added into 5 ml aspirated bone marrow in a 15 ml sterile plastic tube (BD Falcon^{TM}, Becton Dickinson, Thailand). The solution was gently mixed followed by centrifugation at 1000 rpm for 5 minutes at 26 ˚C. The supernatant was discarded and the pellet was resuspended with 1 ml of MSC culture medium containing low-glucose Dulbecco's modified Eagle's medium (low glucose DMEM; Sigma, USA.) supplemented with 10% (v/v) fetal bovine serum (FBS) (Invitrogen, Carlsbad, USA), 2 mM L-glutamine, 100 unit/ml penicillin G, 100 µg/ml streptomycin and 5 µg/ml amphotericin B. Cells were plated in 100 mm tissue culture dish (BD Falcon^{TM}, Thailand) in 6 ml of culture medium. The initial seeding density was approximately between 50-60% confluences. The culture plate was gently mixed before incubated at 37^{o}C in a humidified condition of 5% CO_2.

4 Characterization of canine mesenchymal stem cells

4.1 Flow cytometry

The examination of MSCs was performed as essentially described by Tharasanit et al. (2011). Canine MSCs at the 3rd passages from a total of 4 dogs were immunologically examined for surface markers. These makers included the positive (CD 44, CD 90) and negative (CD 34) makers. The MSCs were first dissociated from the Petri dishes with Trypsin- EDTA and then centrifuged. A total of 200,000 to 300,000 cells were used for immunolabeling. Rat monoclonal anti-canine CD 90 (AbD serotec, Kidlington, UK) with rabbit anti-rat FITC secondary antibodies and monoclonal anti-canine CD44 antibody conjugated with allophycocyanin (APC) (R&D system, Minneapolis, USA) were used as MSC positive markers. A rat monoclonal anti-canine CD

34 antibody conjugated with fluorescein isothiocyanate (FITC) was used as the negative MSC marker. Fluorescently-labeled MSCs were washed and fixed with 1% (w/v) paraformaldehyde in PBS and stored at 4°C in the dark until analysis. Non-staining MSCs and MSCs labeled with only the secondary antibody were used as controls. At least 20,000 MSCs were analyzed by flow cytometry.

4.2 *In vitro* bone differentiation of MSCs

Canine bone marrow derived MSCs at passage 3 from four dogs were simultaneously induced to osteogenic lineage (each dog represented one replicate). Osteogenic differentiation was performed as essentially described by Bosch et al. (2006) with minor modifications. The MSCs were first cultured to reach approximately 80% confluence, the osteogenic medium containing MSC medium supplemented with 0.1 μM dexamethasone, 50 μM ascorbic acid, 10 mM β-glycerophosphate (Merck, Darmstadt, Germany) was then added into the culture dish. The *in vitro* bone differentiation was performed for 21 days. Von Kossa staining was used to detect deposition of calcium phosphate indicating *de novo* bone formation.

5 *In vitro* assay for MSC and scaffold interaction

For *in vitro* study of biocompatibility of MSC and the scaffold, PCL/HA scaffolds were seeded with canine MSCs at a density of 100,000 cells/scaffold. The loaded scaffolds were incubated at 37˚C in a humidified condition of 5% CO_2 in air After 45 min of incubation, a 5-ml of culture medium was added to cover the entire scaffold.

5.1 Scanning electron microscopy

Scanning electron microscope (SEM) was performed to illustrate MSC morphology and the ability to attach on the PCL/HA scaffold on day 1, 3 and 5 after seeding. Briefly, the loaded

PCL/HA scaffolds were washed twice with PBS (pH 7.2) and fixed with ice-cold 3% glutaraldehyde for 30 min. Then, the scaffolds were dehydrated with serial ethanol dilutions (30%, 50%, 70%, 90% and 100% (v/v) ethanol, respectively) for 2 min at each concentration. Finally, the scaffolds were soaked with Hexamethyldisilazane (HMDS) for 5 min and allow to air dried overnight at room temperature, so that HMDS was evaporated from the scaffolds before coating with gold. The SEM was performed using a JSM-5410LV scanning electron microscope (JEOL, Japan).

5.2 MSC viability and proliferative capacity

After 1 day of seeding, MSC-loaded scaffolds were cut into thin sections for evaluation of canine MSC viability. The viability assay was performed by dual fluorescent staining method using calcein AM and ethidium homodimer. A bright green fluorescence from calcein AM demonstrated the presence of active esterase enzyme activity while cell plasma membrane disrupted cells (dead cells) exhibited red fluorescent color. For MSC proliferation evaluation, PCL/HA scaffolds were seeded with canine at a density of 50,000 cells per scaffold. The proliferative capacity was qualitatively analyzed based on the serial fluorescent images of canine MSCs staining with 4', 6-diamidino-2-phenylindole dihydrochloride (DAPI; Roche, Germany) in conjunction with a quantitative analysis of the total protein content by the bicinchoninic acid (BCA) protein assay kit (Pierce Biotechnology, USA). For DAPI fluorescence staining, the loaded PCL/HA scaffolds were fixed at day 1, 2 and 4 of incubation with 3.7% formaldehyde. MSC loaded-PCL/HA scaffold were then stained with DAPI (1:1000) for 10 min and observed under Zeiss Axio Observer fluorescence microscope (Carl Zeiss, Germany) at a wavelength of 380 nm. The total protein quantification of MSC-loaded PCL/HA construct was determined on day 1, 3 and 5 after seeding. The BCA assay is a colorimetric detection and quantification of total protein in the

cell/scaffold construct by measuring the purple water-soluble product resulting from the chelation of BCA and Cu^{+1}. Briefly, the working solution was prepared by mixing Reagent A and reagent B in the ratio of 50:1. Then the loaded PCL/HA scaffolds were washed twice with PBS to eliminate the contaminated protein from the culture medium and chopped with a shaped scissors into small pieces before adding 200 µl of 2% sodium dodecly sulfate in a 1 ml of microcentrifuge tube. Mixed thoroughly by vortexing for 1 min and centrifuged at 5000 rpm for 1 min. A 50 µm of the supernatant was transferred into new 1 ml of microcentrifuge tube then added 1 ml of working solution, mixed thoroughly by vortexing, and incubated at 37ºC for 30 min. Finally, 80 µl of the final solution was pipetted into a 24-well plate and measured the absorbance at 562 nm wavelength using an absorbance microplate reader (ELx800^{TM}; Biotek, Vermont). All data were collected and analyzed by microplate data collection and analysis Software (Gen5^{TM}; Biotek, Vermont) with the reference to bovine serum albumin.

Osteogenic differentiation of MSC within PCL/HA scaffold

The ability of canine MSCs to differentiate into an osteoblastic lineage on PCL/HA scaffold was investigated by seeding MSCs at a density of 50,000 cells onto the PCL/HA scaffold size 5 x 5 x 5 mm. The MSC loaded PCL/HA scaffold treated with the bone induction medium on day 3 of culture, and differentiation was confirmed by using Alizarin Red staining on day 14 of induction.

6 Effect of PCL/HA and MSCs on bone healing of critical- size ulnar defects

To perform bilateral ulnar ostectomy, dogs were anaesthetized as mentioned above. A 10 cm incision was made through the skin and subcutaneous tissue over the caudolateral aspect of the ulna. The bilateral 2.5 cm ulnar ostectomy was performed using an oscillating saw. No internal fixation was used in this study due to the canine model is mechanically stability without further fixation as the radius is the major load-bearing structure in the canine forelimb. In this study, defects on the left ulnae were implanted with the corticocancellous autografts to serve as a control group (n=7) while defects on the

right ulnae were randomly implanted with PCL/HA composite scaffold alone (n=4) or PCL/HA combined with canine MSCs (n=4). After the operation, all forelimbs were applied with modified Robert Jone bandages reinforced with thermoplastic splints (Vet-lite, BEC, Thailand) for 2 weeks. The dogs were received 5 mg/kg enrofloxacin (Baytril; Bayer, USA) and 4 mg/kg carprofen (Rimadly; Pfizer, USA) orally twice a day for 7 days after implantation.

6.1 Examination of bone healing by Radiographic examination

The craniocaudal (CrCd) radiographs were taken immediately after operation and at 2, 4, 6, 8 weeks postoperatively. Bone healing was evaluated and scored by 3 radiologists in a blinded fashion using the radiographic scoring system described by Jones et al. (2008) (Table 4)

6.2 histological analysis of PCL/HA scaffold implant

At the 8 weeks after implantation, biopsy was performed to verify the formation of bone following transplantation. The sites of biopsy included the middle portion of the implant and the host bone-implant interface. The sample was fixed in 10% (v/v) formalin and processed as a routine histological procedure as described elsewhere. The samples were sectioned and stained with hematoxylin and eosin (H&E).

Table 1 Radiographic scoring system for bone healing evaluation (Jones et al., 2008)

Description	**Radiographic score**
No change from immediate postoperative appearance	0
A slight increase in radiodensity distinguishable from the graft	1
Recognizable increase in radiodensity, bridging of one cortex with new bone	2

formation to the graft	
Bridging of at least one cortex with material of nonuniform radiodensity, early incorporation of the graft suggested by obscurity of graft borders	3
Defect bridged on both medial and lateral sides with bone of uniform radiodensity, cut ends of the cortex still visible, graft and new bone not easy to differentiate	4
Same as grade 3, with at least one of four cortices obscured by new bone	5
Defect bridged by uniform new bone, cut ends of cortex no longer distinguishable, graft no longer visible	6

Statistical analysis

For total protein concentrations, Leven test was used to assess the homogeneity of variance among the groups and all data was analyzed using analysis of Variance (ANOVA) to determine the difference in protein concentrations between day 1, 3 and 5 after seeding. Significance was defined when a p value was less than 0.05.

For radiographic scores which were nonparametric data, Kruskal-Wallis one-way analysis of variance was used to determine the difference in healing efficacy of the implants at 2, 4, 6 and 8 weeks postoperatively. Significance was defined as a p value less than or equal to 0.05.

Result

At 24 hours after plating, adherent cells demonstrated heterogeneous morphology including a fibroblastic-like cell, polygonal cell and round cell. Non-adherent cells were removed by changing the culture medium and cells were distributed more homogeneous population of

spindle-shaped cells was mainly observed (Fig. 2). The total number of adherent cells on day 7 of culture was $1.327x10^6$ cells and the percentages viability was 98.64.

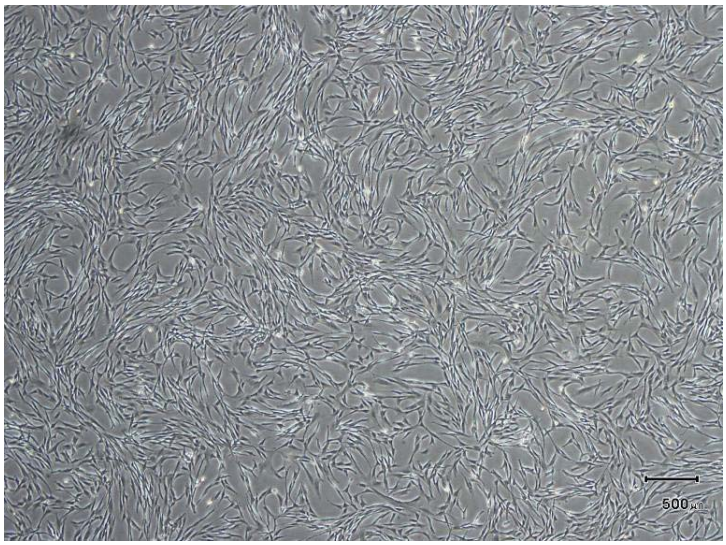


Figure 1 Canine bone marrow derived mesenchymal stem cells at passage 1 on day 3 of culture (100 X magnification, 500 μm scale bar)

The percentage of cells positive for each CD was demonstrated in table 5. The percentage of CD 44 expressed by canine MSCs at passage 3 was more than 97% while the percentage of CD 90-positive cells was more than 93%. In addition, less than 1% of MSC population expressed CD 34.

Canine MSCs at passage 3 were subjected to demonstrate the mesenchymal differentiation capacity with the specific condition according to the cell type. Histochemical special staining was performed in order to verify each differentiation on day 21 after induction. Von Kossa, Oil Red O and Alcian blue staining were used to confirm osteoblastic, adipogenic and chondrogenic differentiation, respectively. Under an osteogenic condition (Figure 4), the former spindle-shaped

cells gradually transformed into polygonal, cuboidal, osteoblast-like cells extending their long processes connecting to each other to form a cellular network and started to synthesize the extracellular matrix that was positive to Von Kossa (Figure 5A) and Alizarin Red (Figure 5B). For adipogenic differentiation, thin fibroblastic cells became oval to round-shaped cells with large cytoplasm containing lipid vacuoles stained positively with Oil Red O (Figure 6). Finally, chondrogenic differentiation was achieved by culturing canine MSCs in a pellet cultural system combining with a special chondrogenic induction medium. MSCs were slowly aggregated and developed into a small round nodule within the first week of induction. The nodule was positively stained with Alcian blue indicated the presence of glycosaminoglycans at 3 weeks of induction.

Table 2 The percentage of canine MSCs positive for CD 44, CD 90 and CD 34 determined by flow cytometry at passage 3

		Markers		
Dog	**Passage**	**CD34**	**CD44**	**CD90**
Dog 1	3	0	99.82	99.21
Dog 2	3	0	99.89	98.02
Dog 3	3	0	99.95	93.52
Dog 4	3	0.06	97.91	96.92

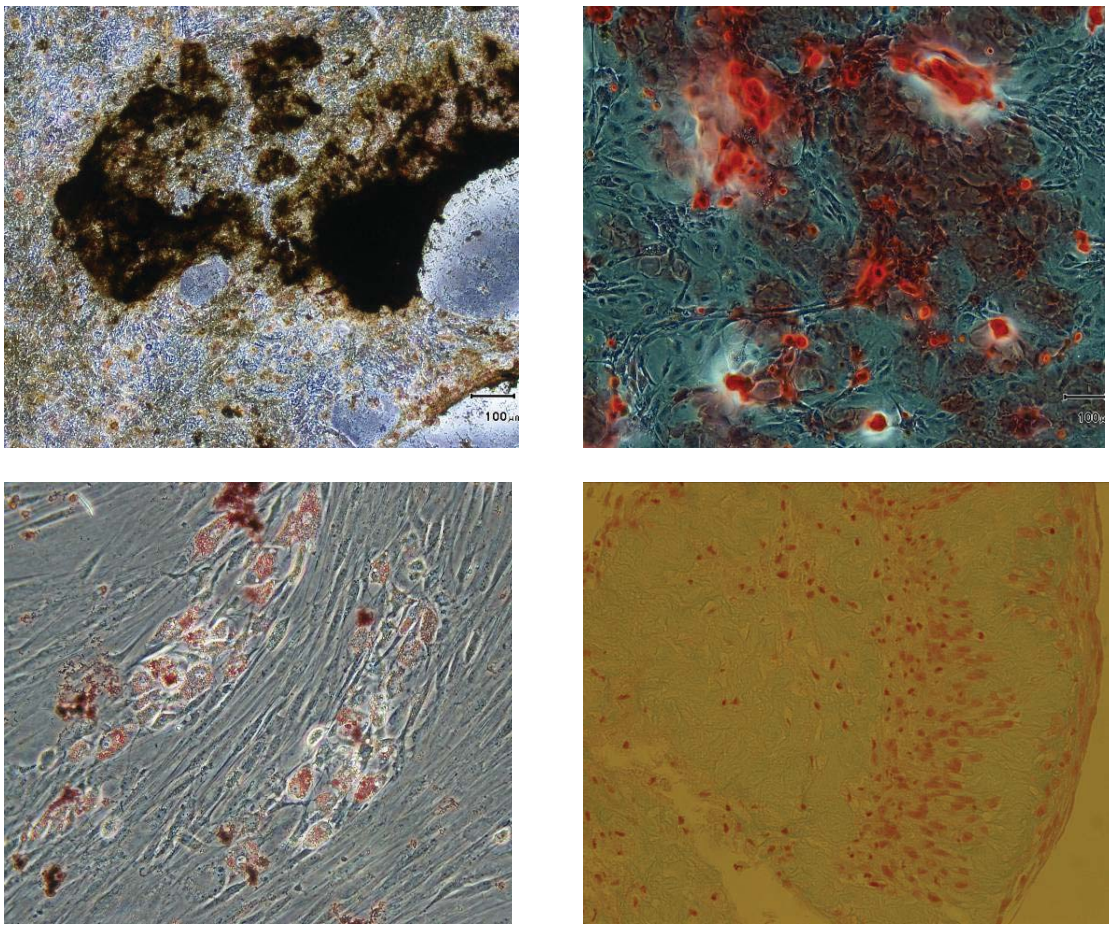


Figure 2 Von Kossa Alizarin Red and Oil Red O staining were used to validate the differentiation capacity of canine MSC into the osteogenic lineage

In vitro studies of canine MSCs behavior on PCL/HA composite scaffold was evaluated in terms of MSC attachment, morphology, the ability to growth and proliferation within the scaffold. The combination of calcein AM and ethidium homodimer fluorescence staining was used to assess MSC viability. A green fluorescence from calcein AM represented the viable MSCs while a red fluorescence indicated the non-viable cells (Figure 8). On day 1 after seeding, a mixed population of viable and non-viable canine MSCs was observed. The majority of the cells exhibited green calcein fluorescence with a small number of cells was labeled with red fluorescence. In addition, MSCs were found throughout the sample represented a good cell distribution within the scaffold.

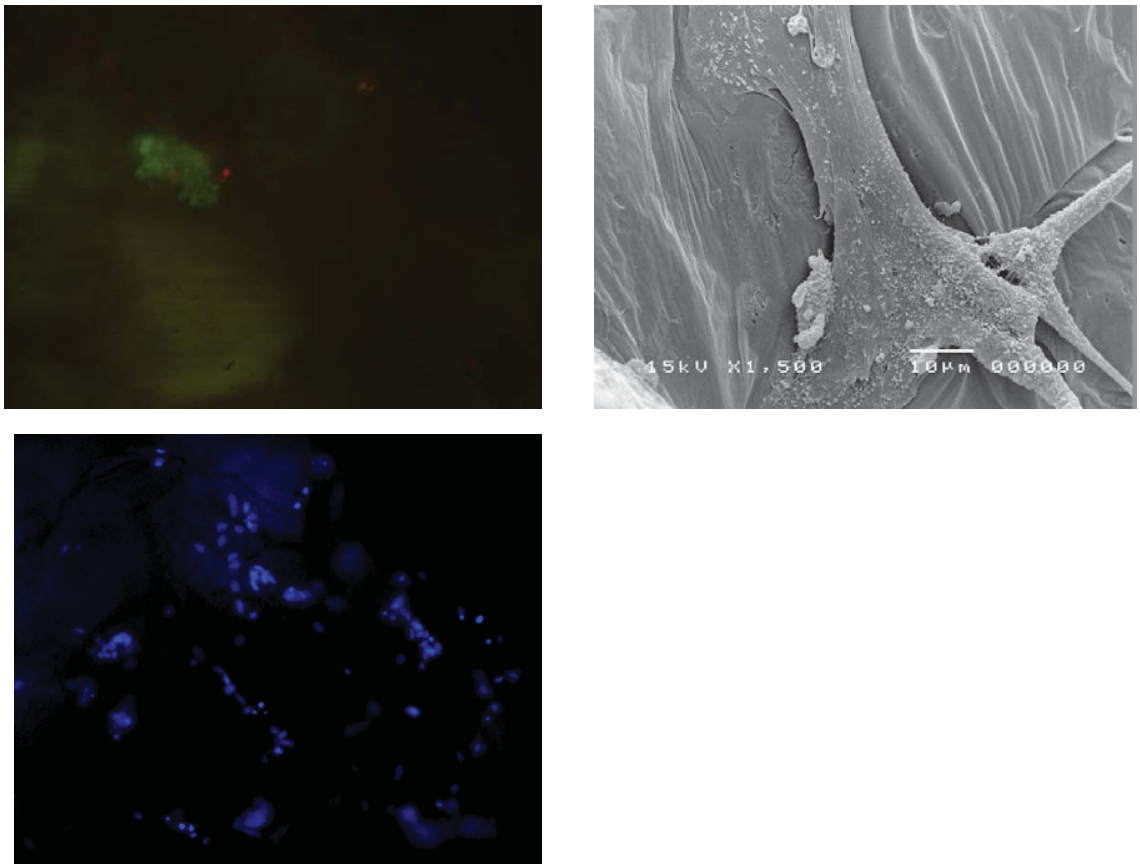


Figure 3 Photomicrographs indicating viability of MSCs within the scaffold. A: viability of canine MSCs 12 hours after seeding and B: SEM image of canine MSCs attached and expanded the cellular process onto the scaffold (3 days after MSC seeding), c: fluorescent analysis of canine MSC proliferation using DAPI nuclear staining

Canine MSC attachment and morphology was observed by SEM on day 1, 3 and 5 after seeding. On day 1 after seeding, MSCs appeared as flat cells spreading onto the surface of scaffold with finger-like projection of cell membrane (filopodia) adhered to the scaffold (Fig 9A). MSCs became

more spread and elongated with an enlargement of adhesive areas between cells and scaffold on day 3 of seeding. In addition, on day 3, more cells were observed and appeared to form small cell clusters with an intercellular connection (Fig 9B).

The proliferation of canine MSCs within PCL/HA scaffold was determined by qualitative comparison of serial DAPI fluorescent images on day1 (Figure 10A and B), 2 (Figure 10C and D) and 4 (Figure 10 E and F) after seeding. An increase MSC population was observed by an increase in DAPI-stained nuclei density over time. The quantitative analysis of the protein content was conducted to evaluate MSC growth and proliferation within PCL/HA scaffold using the BCA protein assay. The amount of protein (µg/ml) in each samples were calculated from the absorbance of the sample solution measured at a wavelength of 562 nm with reference to the standard protein (Table 6). The total protein concentration of MSC-loaded PCL/HA scaffold on day 1, 3 and 5 was 523±15.27, 626.67±71.12 and 861.67±127.16 µg/ml, respectively. A significant differences were found between protein content of PCL/HA alone and MSC-loaded PCL/HA scaffold at all time points. A significant increase in total protein concentration of MSC-loaded PCL/HA scaffold were observed between day 1 and day 5 and day 3 and day 5 ($p<0.05$). However, no significant difference was found between day 1 and 3 (Figure 11). Notably, the color of the sample solution was changed from green to purple in the proportion to the protein concentration in the scaffold (Figure 12).

To confirm an osteogenic differentiation potential of canine MSCs after seeding on PCL/HA scaffold, Alizarin Red staining was performed on day 14 of induction. Positive Alizarin Red staining was observed in both PCL/HA scaffolds alone and MSC-loaded PCL/HA scaffolds. After washed the samples several time with PBS, only PCL/HA scaffolds that combined with

canine MSCs were still remained positive to Alizarin Red suggested the presence of calcium deposition within scaffolds.

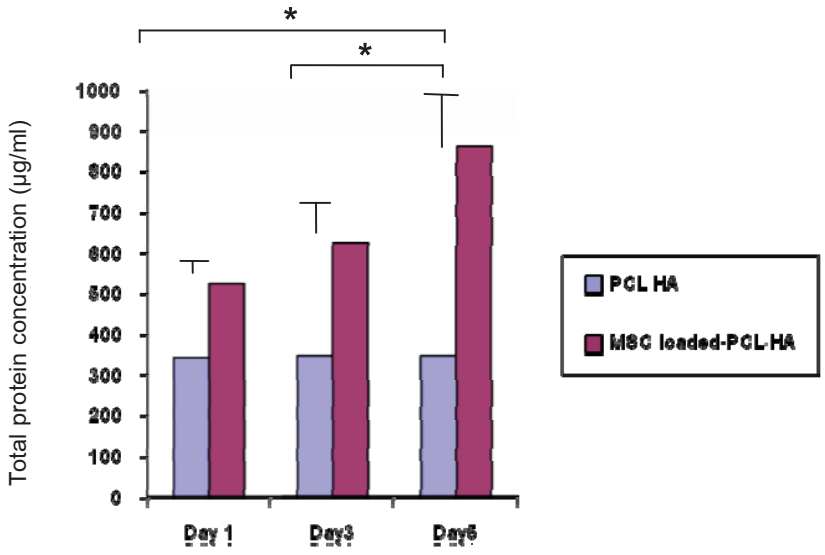


Figure 4 Quantitative measurement of total protein concentrations of PCL/HA and MSC loaded-PCL/HA scaffolds on day 1, 3 and 5 of culture. *Significant increase in protein concentration was observed ($p<0.05$)**.**

The craniocaudal radiographs of the defects were taken immediately and at 2, 4, 6 and 8 week postoperatively (Fig. 13A, B, C and D) illustrated the progressive bone healing of the ulnar defect that treated with corticocancellous bone graft (group 1). Slightly new bone formation was visible during the first 4 weeks postoperatively. At 6week, the bone bridge formation between graft and host bone was evident at the distal part of the defect. By 8 weeks postoperatively, the bone bridging was clearly observed on both side of cortices. An increase in radiodensity of the graft-host bone interfaces with time demonstrated a progressive healing of the defect. Neither new bone nor callus formation was observed in the defect site treated with PCL/HA alone (group 2)

(Figure 14A, B, C and D) and MSC-loaded PCL/HA (group 3) (Figure 15A, B, C and D) at any time point. A slightly increase in radiodensity was observed within the implant site in both groups. There were statistically significant differences ($p<0.05$) in radiographic score between group 1, 2 and 3 at 6 weeks and between group 1 and 2 and group 1 and 3 at 8 weeks postoperatively. No significant differences in radiographic score were detected between treatment groups at 2 and 4 weeks postoperatively ($p>0.05$)



Figure 5 Radiographs of canine ulnar segmental defects treated with the autogenous cancellous bone graft (A-D) and PCL/HA scaffold implant (E-H) at (A, E) 2 weeks; (B, F) 4 weeks; (C, G) 6 weeks and (D, H) 8 weeks postoperatively

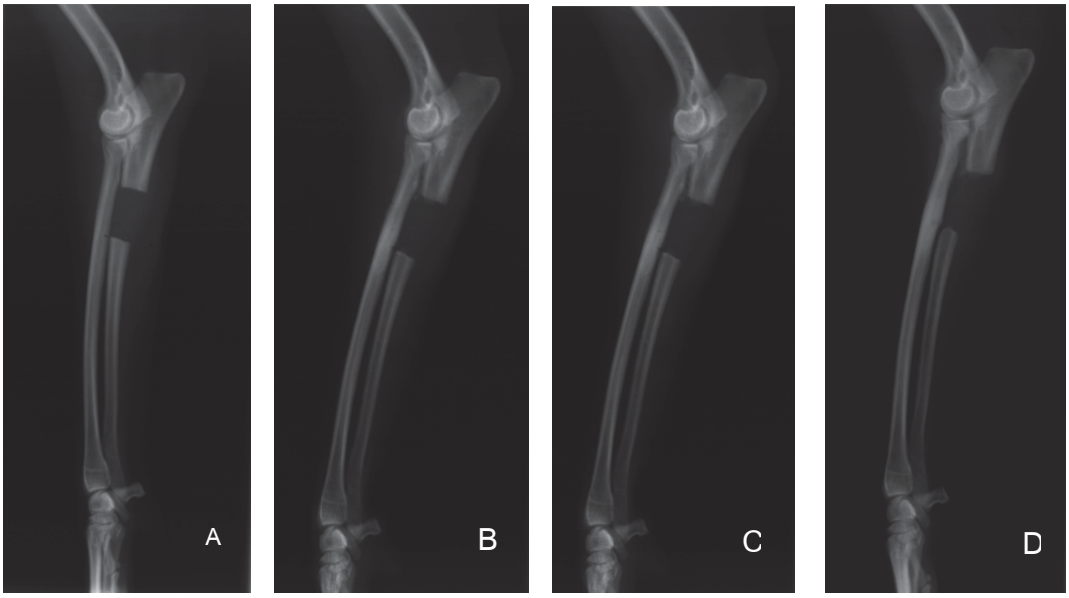


Figure 6 Radiographs of canine ulnar segmental defects treated with MSC-loaded PCL/HA scaffold at (A) 2 weeks; (B) 4 weeks; (C) 6 weeks and (D) 8 weeks postoperatively

Histopathology of the defect implanted with autogenous cancellous bone graft (group 1) showed a good incorporation between the graft and host bone (Figure 16A) with the osteoid formation and new bone formation along the graft-host bone junction. The longitudinal section of

the graft revealed the re-establishment of vascular supply within the marrow cavity (Figure 16B). In group 2, the incorporation of the PCL/HA scaffold and host bone was mainly achieved by fibrocartilaginous tissue with minimal osteoid formation (Figure 17A). The defect site was filled with loose and unorganized connective tissue with new vascular ingrowth. There were still some remnants of the scaffold which sloughed off during the histological preparation (Figure 17B). Finally, in group 3, more fibrovascular tissue was observed in the defect, which implanted with MSC-loaded PCL/HA scaffold compared with PCL/HA group (Figure 18). The fibrous tissue is mainly comprised of spindle-shaped cells with extensive collagen deposition confirmed by Masson's Trichrome staining (Figure 19). It is notable that numerous of multinucleated giant cells were found adjacent to remnants of the scaffold indicating a chronic inflammation with foreign body giant cell response to the scaffold.

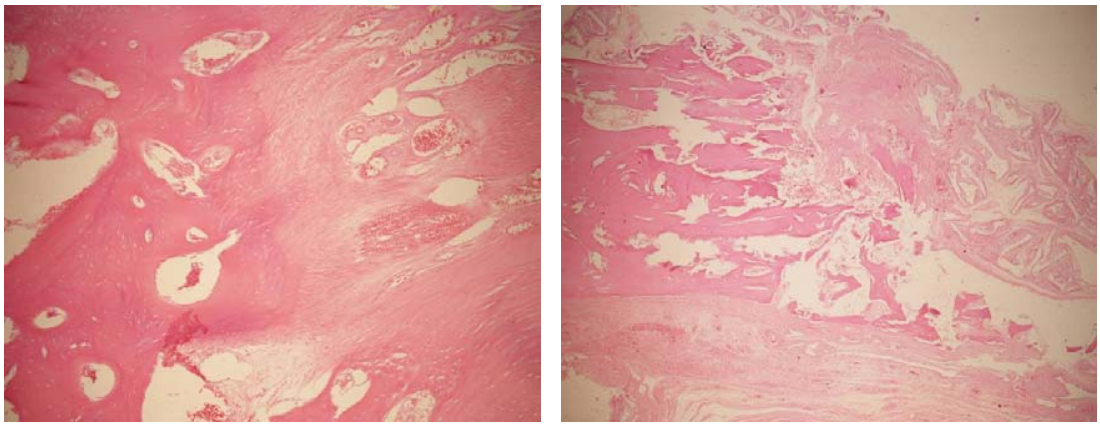


Figure 7 Histological sections of an ulnar defect implanted with cancellous bone graft (A) and with PCL/HA scaffold (B) at 8 week postoperatively. The junction between host bone (HB) and the graft (CB) and scaffold (PCL/HA)

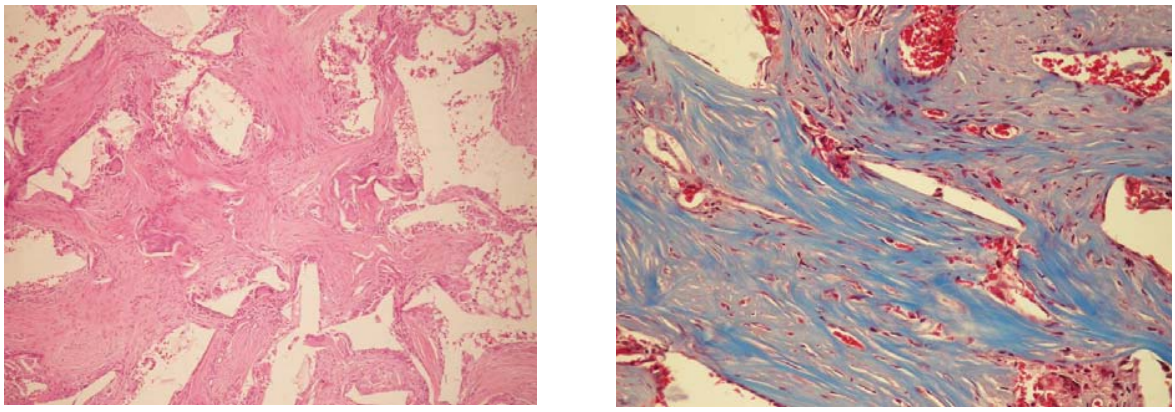


Figure 8 Histological sections of an ulnar defect implanted with MSC-loaded PCL/HA scaffold at 8 week postoperatively. A: H&E staining and Masson's trichrome staining (B)

Discussion

Implantation of biological bone substitutes is one of the promising bone tissue engineering strategies for treatment of extensive bone defects. Mesenchymal stem cell in combination with polymer/ceramic composite scaffold has been widely investigated as an alternative to autogenous cancellous bone graft. In this study, we successfully isolated canine MSCs from bone marrow and identified these cells according to the multipotent human MSCs characterization which recently proposed by International Society for Cellular Therapy (Dominici et al., 2006). Then, we investigated the interaction between canine MSCs and PCL/HA composite scaffold in terms of cell viability, proliferative capacity and ability to differentiate into osteoblast. Finally, we evaluated the

efficacy of canine MSCs combined with PCL/HA composite scaffold in comparison with PCL/HA alone and autogenous on the healing of ulnar critical sized defects in dog.

MSCs reside in various adult tissues such as bone marrow, adipose tissue, skin, periosteum and placenta (Tuan et al., 2002). These cells are responsible for regulating tissue homeostasis, repair and regeneration. Although MSCs originated from various tissue sources possess similar phenotypic expression, significant difference in cell proliferation and multilineage differentiation potentials are observed. In this study, bone marrow was chosen as a source of MSCs because it is easy to assess and can be aspirated in large volume. Moreover, MSCs derived from bone marrow and synovium are superior to periosteum-, adipogenic- and skeletal muscle- derived MSCs with regard to self renewal, expansion and differentiation potential (Sakaguchi et al., 2005). Canine MSCs were harvested from the bone marrow samples aspirated from the dorsal iliac crest of 4 dogs. Red blood cell lysing buffer was added to enrich the initial MSC population by eliminating the contaminated red blood cells before culture. Canine MSCs used in the present study were isolated by their ability to adhere to the polystyrene plastic plate and subsequently subcultured when cells reached 80-90% confluence. Owing to the absence of MSC specific antigen marker, at least three minimum criteria were required to characterize MSCs are as follows: the ability to adhere to plastic surface, the expression of cell surface antigen and the capacity to differentiate along the mesenchymal lineage (Dominici et al., 2006). The isolated cells exhibited classical spindle shaped morphology and expressed high levels of MSC markers inculding CD 44 and CD 90. The flow cytometric analysis of cell surface protein revealed more than 94% of the isolated cells were positive for both CD 44 and CD 90 which corresponding with previous study (Kern et al., 2006; Jung et al., 2008). No expression of CD34 was observed which indicated no contamination of hematopoietic stem cells was found in the culture. And finally, these isolated

cells were capable of differentiation into a mesenchymal lineage when cultured in a proper condition.

Due to the major concern in the survival and proliferative capacity of cells within the large scaffold constructs, an *in vitro* study of canine MSCs behavior was performed on 3D PCL/HA scaffolds. Dual fluorescence viability assay using calcein AM and ethidium homodimer was performed to determine the MSC viability within PCL/HA scaffold. This assay allows the simultaneous visualization of viable and dead cells within the scaffold (Decherchi et al., 1997). Calcein AM is a hydrophobic compound which can diffuse through intact cell membrane of viable cells and subsequently hydrolyze intracellular esterase result in calcein, a green fluorescence, retained in the cytoplasm. In contrast to calcein AM, ethidium homodimer can penetrate only damaged cell membranes and bind to DNA of the dead cells result in emission of red fluorescence. From dual viability assay, an intense green fluorescence was mainly observed through the entire scaffold indicated the majority of canine MSCs remained viable on day 1 after seeding. A small number of dead cells were found in the outer part of the scaffold and became more prominent in the middle of the scaffold. This may be due to the diffuse limitation of oxygen and nutrient caused by the scaffold thickness. Moreover, all MSC loaded-scaffolds were cultured under a static condition may even hinder the fluid transportation result in an accumulation of waste products within the scaffold. To overcome these problems, dynamic culture conditions such as a spinner flask, orbital shaker or perfusion system has been used since the approach can improve cell viability, uniform distribution and subsequently increase in extracellular matrix deposition (Yeatts and Fisher, 2011). Nerurkar et al. (2011) suggested that the dynamic culture condition using orbital shaker enhanced MSC infiltration and collagen deposition on electrospun PCL nanofibrous scaffold. Additionally, transient shaking culture significantly improved MSC distribution, provided

favorable condition for chondrogenic differentiation and increased glycosaminoglycans accumulation within the scaffold. The results from SEM images showed that canine MCSs adhered favorably to PCL/HA scaffold. Cells exhibited flat morphology with filopodia projected from cell body and attached to the scaffold surface. Filopodia are protrusion of cell membrane which play an important role in the formation of adhesive connection between cell and the extracellular matrix (Yang et al., 2010). The attached cells became more elongated in shaped with an enlargement of focal adhesion suggested growth and maturation of canine MSCs in PCL/HA scaffold over time. MSC proliferative capacity on 3D PCL/HA scaffold was evidenced by comparison of serial DAPI fluorescence images. DAPI is a DNA-specific dye which has been commonly used for DNA detection and visualization. This dye binds specifically to A-T base pair in DNA sequence results in formation of the DAPI-DNA complex which exhibits a blue fluorescence emission under a fluorescence microscope. An increase in DAPI stained nuclei was observed over time reflected the proliferative capacity of the loaded MSCs. Notably, the background interference was observed during the fluorescent microscopical analysis of the loaded scaffold in both dual viability assay and DAPI fluorescent staining. It is thought that the autofluorescence emission of the polymers caused by an aromatic and aliphatic ester bond when excited with green or blue wavelength. Moreover, the fluorescent interference is even more exaggerated due to the light scattering caused by the thickness of the polymer and its porous nature. To avoid these interferences, a thin section of the sample can diminish light scattering and minimize over all autofluorescence from polymer or using other fluorescent probe that can be excited and emits in the different wavelength. Jaafar et al. (2011) applied the use of Sudan Black B (SB) as an autofluorescence quencher for 4 types of polymer, including polyglycerol sebacate, polyurethane, polylactice-co-caprolactone, and polylactic acid-co-glycolic acid. SB is a

lysochrome diazo dye which has been commonly used as a neutral triglyceride and lipid staining. Reduction of an overall background interference was based on two mechanisms, the light absorption capacity of SB and the ability to modify the surface of the polymers. No interaction between SB and fluorescently labeled cells was observed.

Despite the promising result from the visual DAPI fluorescence image analysis, the uncertainty of the outcome may occur due to the subjective evaluation of these images. Therefore, the BCA protein assay was performed in order to quantify proliferative capacity of canine MSCs after seeded onto the scaffold (Sachana and Hargreaves, 2007). The assay is based on the ability of the peptide bonds in protein to reduce Cu^{+2} into Cu^{+1} and the chelation of Cu^{+1} with BCA result in purple-colored products that can be measured with spectrophotometer. The total protein concentration are calculated from the optical density of each the samples at a wavelength of 562 nm with respect to the standard curve. Significant increases in the protein concentration were observed between day 1 and day 5 and day 3 and day 5 ($p<0.05$). An increase in the absorbance of the loaded PCL/HA is correlated with the greater amount of the protein concentration in the sample indicated the growth and proliferative capacity of canine MSCs resided in the scaffold. As expected, there was no significant difference in protein concentration was found between day 1 and day 3. These may result from the physical adaptation of cells to the change in environment. Moreover, the newly seeded cells may also require time to adjust and adhere onto the new surface condition and subsequently reformation of the intercellular connection which necessary for optimal cell proliferation. And finally, the present *in vitro* study demonstrated the ability of canine MSCs to differentiate into an osteogenic lineage after seeded onto 3D PCL/HA scaffold as evidenced by Alizarin staining on day 14 of induction.

As the combination of osteopotential cell and biolodegradable scaffold is one of the most successful strategies in bone tissue engineering and the use of PLC/HA composite scaffold fabricated by solvent casting and particular leaching techniques has been demonstrated as a promising approach for promoting new bone formation (Chuenjitkuntaworn et al., 2010). This study was performed as a further investigation using canine model in order to evaluate the efficacy of PCL/HA and MSC-loaded PCL/HA on the healing of ulnar critical size defects. Key (1934) has defined the ulnar critical sized defect as a segmental defect that larger than 1 to 1.5 times of the diameter of the shaft of the bone. All dogs were able to stand and ambulate on day 1 and 2 after surgery, respectively. Defects in PCL/HA group were healed with fibrous connective tissue consisted of long spindle-shaped fibroblastic cells and collagen fiber as an extracellular matrix. The presence of capillaries within the graft sites suggested that PCL/HA scaffolds can support the ingrowth of vascular tissue. Similar results were obtained in the group that treated with MSC-loaded PCL/HA scaffold, however, Mason's trichrome staining suggested that more collagen deposition was found when compared to PCL/HA group. Although there was a good evidence of fibrovascular tissue infiltration with an extent matrix deposition throughout the entire PCL/HA scaffold, no osteogenic differentiation was observed. In contrast to the promising result in a calvarial defect of mouse (Chuenjitkuntaworn et al., 2010) neither new bone nor callus formation was observed in defects treated with PCL/HA alone or MSC-loaded PCL/HA scaffold. Several possible reasons could explain for this inconsistency. It is believed that larger animal possesses bone regenerative capacity to a lesser extent than small animal. Moreover, the physiological differences between dog and mouse with regard to the slower bone turnover rate lower basal metabolic rate and longer lifespan in dog may contribute to different bone healing result (Cook et. al., 1994). The variation in size, location and the mechanical environment of the defects may

impact on the biological response to the scaffold. PCL/HA scaffolds used in the present study were not only larger in size but also thicker in dimension than the previous study. This may cause a massive release of the degradation product, caproic acid, from the scaffold and subsequently creating an unfavorable environment for bone regeneration (Böstmann et al. 1990; Bergsma et al., 1995; Prokop et al., 2004). And finally, the major consideration was given to the different types of bone defect (flat bone versus long bone), the loading condition of the bone (non-loading calvarial versus loading ulnar bone). A calvarial defect is considered as a non-weight-bearing model which experiences lesser mechanical interference than a long bone model. Therefore, a calvarial bone defect may provide more favorable environment for new bone regeneration than an ulnar bone defect in a biomechanical aspects.

Canine ulna defect model has been extensively used as a study model to evaluate the efficacy of biomaterials in bone tissue engineering application because no fixation is required as the radius is the major load-bearing bone of the forearm and the interosseous ligament between the radius and the ulna was remained intact. Moreover, the ulnar ostectomy procedure can be done on both sides simultaneously, thus reducing the number of animal used in the study (Salkeld et al., 2001; Paskalev et al., 2006; Jones et al., 2008). Several successful results have been reported using a canine ulnar model without fixation (Heiple et al., 1963; Nillson et. al., 1986; Cook et al., 1994; Salkeld et al., 2001; Paskalev et al., 2006; Jones et al., 2008). However, there might be some mechanical interference between defect sites causing an unfavorable condition for mesenchymal stem cells to differentiate into osteoblastic cells. To overcome this problem, intramedullary pins or plates and screws may use to stabilize canine ulnar defect in order to optimize the new bone formation.

Last but not least, histological analysis demonstrated the presence of numerous multinucleated giant cells within defect sites that implanted with PCL/HA and MSC-loaded PCL/HA scaffold. These giant cells appeared adjacent to remnants of the scaffold which reflected chronic inflammation with foreign body response. For this reason, scaffold samples were sent to identify the contamination using scanning electron microscope with energy dispersive x-ray (SEM/EDX) analysis. The result of the SEM/EDX analysis showed that the scaffolds were contaminated with copper (Cu) from hydroxyapatite ceramic. Thus, chronic inflammation with foreign body giant cell response from copper contamination may result in an impaired new bone formation at defect site. Similar tissue reaction was reported by Linder and Lundskog (1975), Völker et al. (1997), Tindel et al. (2001) and Saitoh et al. (2010). Saitoh and his group investigated an in vivo tissue response to three different metal particles including copper, nickel and titanium by subcutaneous implantation in mouse. One week after implantation, subcutaneous tissue was excised for evaluation of tissue reaction using histological and transmission electron microscopic analysis. The result of this study showed that copper particles caused the highest degree of inflammation. Similar result was observed in the study of Linder and Lundskog that compared the reaction of bone to copper, stainless steel, titanium and vitallium.

Conclusions

The present study was conducted in order to investigate the *in vitro* interaction between canine MSCs and PCL/HA composite scaffolds by seeding cells onto the scaffold and observed for cell behaviors with respect to cell viability, cell attachment and morphology, the proliferative capacity and the ability to differentiate into osteogenic lineage. The *in vitro* study demonstrated a good biocompatibility between canine MSCs and PCL/HA scaffolds. From dual fluorescence

viability assay showed that the majority of seeded cells emitted green fluorescence indicating most of cells remained viable on day 1 after seeding. Similarly the result from SEM analysis revealed that canine MSCs adhered favorably onto PCL/HA scaffold. Cells already attached on the scaffold with flat morphology and filopodia projection within day 1 of seeding. More cell numbers were observed with formation of cell cluster in some area of scaffold suggested that canine MSCs were able to growth and maturation after seeding. To confirm the proliferative capacity of the seeded cell, serial DAPI florescent image analysis combined with BCA protein assay were performed. A progressive increase in DAPI-stained cells was observed under a fluorescent microscope on day 1, 2 and 4 after seeding which collated to an increase in total protein concentration on day 1 (523.33±15.27), day 3 (626.67±71.12) and day 5 (861.67±127.16) after seeding. Moreover, a significant increase ($p<0.05$) in protein concentration was observed between day 1 and 5 and day 3 and 5 of seeding. And finally, the ability of canine MSCs to differentiate into osteoblats were confirmed by Alizarin Red staining on day 14 of osteogenic induction. The present *in vitro* study concluded that there was a good interaction between canine MSCs and PCL/HA scaffold.

Despite a promising result from an *in vitro* study, neither bone nor callus formation was observed in canine ulnar defects that implanted with PCL/HA and PCL/HA scaffolds. Defects in these two groups were healed with fibrovascular tissue which infiltrated through the pore of the scaffold. Surprisingly, numerous of multinucleated giant cells were found indicating chronic inflammation with foreign body giant cell response due to the presence of remnants of PCL/HA scaffold.

4. ท่านได้พบอุปสรรคในการดำเนินงานหรือไม่ ถ้าพบกรุณาระบุว่ามีอะไรบ้าง และแก้ไขอย่างไรบ้าง

ไม่พบอุปสรรคในการดำเนินงาน

5. ข้อคิดเห็นและข้อเสนออื่น ๆต่อสกว.

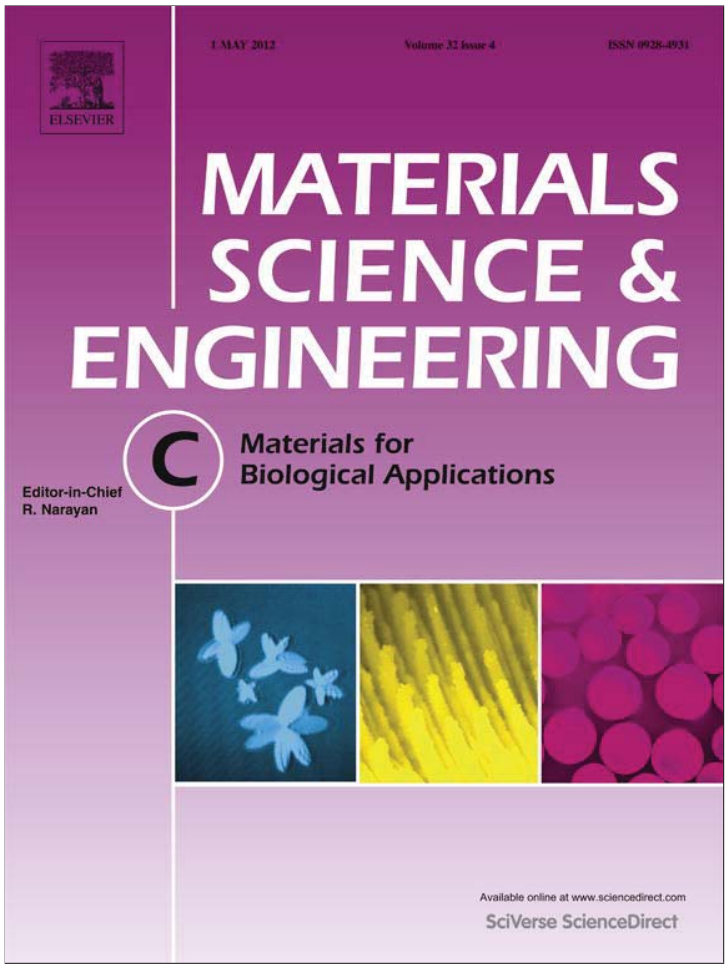
ลงนาม.....

(ศาสตราจารย์พิชญ์ ศุภผล)

(หัวหน้าโครงการวิจัยรับทุน)

วันที่.....

Provided for non-commercial research and education use.
Not for reproduction, distribution or commercial use.



This article appeared in a journal published by Elsevier. The attached copy is furnished to the author for internal non-commercial research and education use, including for instruction at the authors institution and sharing with colleagues.

Other uses, including reproduction and distribution, or selling or licensing copies, or posting to personal, institutional or third party websites are prohibited.

In most cases authors are permitted to post their version of the article (e.g. in Word or Tex form) to their personal website or institutional repository. Authors requiring further information regarding Elsevier's archiving and manuscript policies are encouraged to visit:

http://www.elsevier.com/copyright

Author's personal copy

Materials Science and Engineering C 32 (2012) 758–762

Contents lists available at SciVerse ScienceDirect

Materials Science and Engineering C

journal homepage: www.elsevier.com/locate/msec

Hydroxyapatite/ovalbumin composite particles as model protein carriers for bone tissue engineering: I. Synthesis and characterization

Prae-ravee K-hasuwan [a,b], Neeranut Kuanchertchoo [c,*], Nuanchawee Wetprasit [d], Pitt Supaphol [a,b,**]

[a] The Petroleum and Petrochemical College, Chulalongkorn University, Bangkok 10330, Thailand
[b] Center of Excellence on Petrochemical and Materials Technology, Chulalongkorn University, Bangkok 10330, Thailand
[c] Department of Materials Technology, Faculty of Science, Ramkhamhaeng University, Bangkok 10240, Thailand
[d] Department of Biotechnology, Faculty of Science, Ramkhamhaeng University, Bangkok 10240, Thailand

ARTICLE INFO

Article history:
Received 6 April 2011
Received in revised form 20 November 2011
Accepted 19 January 2012
Available online 28 January 2012

Keywords:
Hydroxyapatite
Ovalbumin
Composite particles

ABSTRACT

Hydroxyapatite (HAp) nanoparticles were synthesized from the co-precipitation reaction between calcium oxide from discarded egg shells and phosphoric acid in the absence and the presence of ovalbumin (OVA). 2-Amino-2-hydroxymethyl-propane-1,3-diol (tris-base) was used to control the pH during the co-precipitation (i.e., 7–9). The formation of HAp was confirmed by X-ray diffraction analysis, while both the Fourier-transform infrared spectroscopy and the thermogravimetric analysis confirmed the existence of OVA within the HAp–OVA particles. The crystallite sizes of the individual crystalline entities within the HAp and the HAp–OVA particles were approximated from the (002) reflection peaks by means of the Scherrer's equation. The average particle sizes of the HAp and the HAp–OVA particles were measured by particle size analysis. Transmission electron microscopy revealed that these particles were aggregates of rod-like HAp nanocrystals, whereas scanning electron microscopy revealed that these particles ultimately formed into larger aggregates. Lastly, the decrease in the pH during the precipitation process and the presence of OVA were responsible for the observed increase in the values of pore size, BET specific surface area, and pore volume of the resulting HAp particles.

© 2012 Elsevier B.V. All rights reserved.

1. Introduction

Hydroxyapatite (HAp, $Ca_{10}(PO_4)_6(OH)_2$), the major inorganic composition of hard bone tissues, is usually fabricated or imparted into prosthetic devices for bone implantation/replacement. This is because of its biocompatibility and osteoconductivity [1–3]. Recently, porous HAp particles with pore sizes of 2–50 nm (mesoporous) or <2 nm (microporous) were deemed highly suitable for biomedical applications, especially for bone tissue engineering [4,5]. Mesoporous HAp particles having high surface areas and large pore volumes can be excellent carriers for delivery of functional biomolecules [6]. Such HAp particles can be prepared by many means, e.g., hydrothermal [3], emulsion [7], sol–gel [1,8], and precipitation [9,10]. They can also be synthesized from many types of chemical templates, such as cationic surfactants, e.g., cetyltrimethylammonium bromide (CTAB) [6,10,11]; non-ionic surfactants, e.g., a triblock copolymer of pluronic F127 (EO99PO65EO99) [12]; and anionic surfactants, e.g., mono-*n*-dodecyl phosphate [13]. The chemical templating technique may pose some disadvantages, however. These are, for example, the deterioration of the mesopores [6] and the wide variation of the pore sizes [10] after calcination. Biosurfactants can also be used to prepare mesoporous apatitic materials, because of their non-toxicity, low production cost, and the possibility of imparting relatively large pore sizes (>5 nm) [14]. Among the various biosurfactants, ovalbumin is of high interest, because of its availability at low price and capability of forming into cross-linking structures that are highly hydrated and porous-like [14,15].

The present contribution reports an environmentally friendly strategy towards the synthesis of protein-incorporated hydroxyapatite (HAp) particles, using egg shells and egg ovalbumin (OVA) as raw materials. In addition to the use of OVA to enlarge the mesoporous structure of the obtained HAp particles, it was also used as the model, incorporating protein.

2. Experimental procedures

2.1. Materials and material synthesis

The chemical reagents, e.g., nitric acid (HNO_3, A.R. grade), phosphoric acid (H_3PO_4, A.R. grade), 2-amino-2-hydroxymethyl-propane-1,3-

* Correspondence to: N. Kuanchertchoo, Department of Materials Technology, Ramkhamhaeng University, Hua Mark, Bangkapi, Bangkok 10240, Thailand. Tel.: +66 2 310 8408; fax: +66 2 310 8696.
** Correspondence to: P. Supaphol, The Petroleum and Petrochemical College, Chulalongkorn University, Soi Chula 12, Phyathai Road, Pathumwan, Bangkok 10330, Thailand. Tel.: +66 2 218 4131; fax: +66 2 215 4459.
E-mail addresses: neeranutk@gmail.com (N. Kuanchertchoo), pitt.s@chula.ac.th (P. Supaphol).

0928-4931/$ – see front matter © 2012 Elsevier B.V. All rights reserved.
doi:10.1016/j.msec.2012.01.020

Author's personal copy

diol (tris-base, A.R. grade), and chicken egg white ovalbumin (OVA, grade II), were purchased from Sigma-Aldrich (USA). These were used without further purification. In the synthesis process, calcium oxide (CaO) was first synthesized from discarded egg shells [16]. Briefly, the egg shells were cleaned with distilled water at 80 °C and dried *in vacuo*. They were then calcined at 1000 °C in a Lindberg LBF799C oven, in two heating stages (i. 25 to 700 °C for 2 h to eliminate organic substances and ii. 700 to 1000 °C for another 2 h to eliminate CO_2 to finally obtain CaO powder). Then, 2.5 g of the CaO powder was dissolved in 25 mL of 1 M HNO_3 under gentle stirring at 70 °C for 3 h. Subsequently, 3.0 g of conc. H_3PO_4 (85 wt.-%) was added dropwise into the solution to adjust the Ca/P ratio to 1.67. The pH of the mixed solution was maintained at 2.0 and the whole system was continuously stirred at room temperature. Precisely 2.0 g of OVA was then added into 500 mL of the obtained solution under vigorous stirring for 1 h. Precipitation was achieved after 200 mL of 1, 1.5, or 2 M tris-base had been added into the solution to impart the buffering effect to the solution at the pH of 7, 8, or 9, respectively. The mixture was vigorously stirred. The precipitates were filtered, washed several times with deionized water, and lyophilized for 48 h. The procedure was repeated to obtain the precipitates that did not contain OVA for comparative purposes.

2.2. Characterization

A Rigaku D/MAX 2000 X-ray diffractometer (XRD) was used to investigate the crystalline nature of the obtained powdery precipitates, using Cu Kα (1.54 Å) radiation over the 2θ range of 5–60° with 0.02° scanning step. The crystalline phase of the powder was identified with JCPDS standard (9-432). A Nicolet NEXUS 670 Fourier-transform infrared spectroscope (FT-IR), operating at a resolution of 4 cm^{-1} over a wavenumber range of 4000 to 400 cm^{-1}, was used to examine the chemical functionalities of the powdery products. A Perkin-Elmer TGA-7 thermogravimetric analyzer (TGA) was used to investigate the thermal degradation behavior of the powder at a heating rate of 10 °C·min^{-1} in air. Some of the powdery products, after having been subjected to the thermal treatment in TGA, were reanalyzed by XRD. Microscopic morphology of the powder was observed by a JEOL JEM-2100 transmission electron microscope (TEM), operating at 200 kV. Surface morphology of the obtained products was investigated by a JEOL JSM-5410LV scanning electron microscope (SEM). Particle size distribution (PSD) of the powder was collected by a Mastersizer 2000 Malvern particle size analyzer (PSA). The powder was dispersed ultrasonically in water during the measurement. The pore characteristics and the Bruaauer–Emmett–Teller (BET) specific surface area of the obtained powdery products were determined based on the physisorption of N_2 at a temperature of 77 K using a Quantachrome AS-1 autosorb-1 instrument. Lastly, the ζ potentials of the powdery products were measured by electrophoresis, using a Zeta-meter 3.0+ analytical system. Briefly, a suspension of 100 mg of the HAp or the HAp/OVA particles in 20 mL of deionized water was filled in an electrophoresis cell. Once energized, the powder was aroused to move towards one of the electrodes. The unit automatically converted the electrophoretic mobility of the particles into the ζ values using the Smoluchowski equation.

3. Results and discussion

Because of the similarity of the results obtained for the HAp particles that had been obtained at pHs 7, 8, and 9, only those of the particles that had been obtained at pH 9 were extensively reported and discussed. As shown in Fig. 1, all of the crystalline peaks as observed in the XRD patterns of the precipitated powdery products that had been obtained, both in the absence and the presence of OVA, at pH 9 could be assigned to those of HAp [i.e., the hexagonal P63/m space group with the lattice constants of $a = b = 0.9418$ nm and $c = 0.6884$ nm (cf. JCPDS No. 09-0432)]. The average crystallite

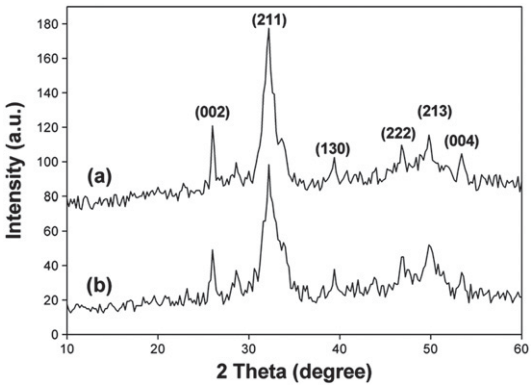


Fig. 1. XRD patterns of (a) pure HAp and (b) HAp–OVA particles that had been obtained at pH 9.

sizes, as estimated from the width of the (002) reflection peaks using the Scherrer's equation [17], were around 17.3–20.9 nm and 16.8–19.8 nm for the HAp and the HAp–OVA particles, respectively (see Table 1). In particular, the average value of the crystallite size decreased with an increase in the pH used during the precipitation process. As the pH increased, more tris-base molecules, in their free form, would be available to nucleate the HAp crystalline entities (cf. the pK_a of tris-base = 8.06), hence the observed decrease in the crystallite size. At the same pH, the presence of OVA resulted in a slight reduction in the average value of the size of the obtained HAp crystals. The presence of OVA could retard the influx of Ca^{2+} and PO_4^{3-} into the growth face, as OVA would adsorb readily onto the HAp crystallites during the crystal growth.

The FT-IR spectra of the HAp and the HAp–OVA particles that had been obtained at pH 9 as well as that of the as-received OVA in its dry state are shown in Fig. 2. For the HAp particles, the adsorption bands centering at 3569 and 1630 cm^{-1} could be assigned to the OH stretching and the OH vibration of the apatitic group [18]. The bands centering at 1035, 601, and 563 cm^{-1} should correspond to PO_4^{3-} ions in the HAp structure. However, the band centering at 1384 cm^{-1} was thought to belong to the carbonate functionality, which might be a result of the contamination from the reaction with CO_2 in the atmosphere [11]. As for the as-received OVA, the characteristic absorption peaks at 3299, 1652, 1539, and 1457 cm^{-1} could be ascribed to the N–H stretching, the carbonyl, the C–N, and the C–H stretching vibrations, respectively [19]. For the HAp–OVA particles, the presence of the absorption bands centering at 1654 and 1539 cm^{-1} confirmed the presence of OVA within the obtained HAp particles.

The HAp and the HAp–OVA particles that had been obtained at pH 9 were evaluated thermogravimetrically and the results are shown in Fig. 3a. For the HAp particles, three main stages in the loss of their mass were observed. The first stage, over the temperature range of

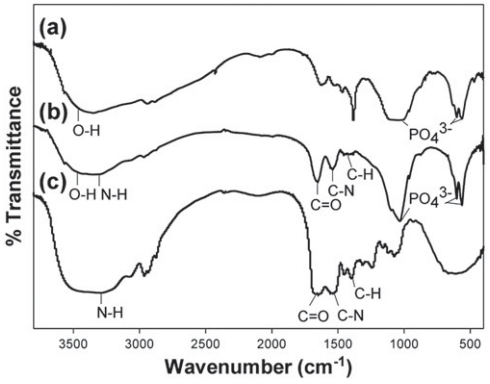


Fig. 2. FT-IR spectra of (a) pure HAp and (b) HAp–OVA particles that had been obtained at pH 9 as well as that of (c) as-received OVA in its dry state.

Author's personal copy

Table 1
Textural parameters of pure HAp and HAp–OVA particles that had been obtained at different pH conditions.

Type of HAp	Crystallite size (nm) ($n=3$)	Average size of primary particles (nm) ($n=3$)	Pore diameter (nm) ($n=2$)	BET Specific surface area ($m^2\ g^{-1}$) ($n=2$)	Pore volume ($cm^3 \cdot g^{-1}$) ($n=2$)	ζ potential (mV) ($n=10$)
HAp (pH 7)	20.9 ± 0.06	59.3 ± 0.25	8.9 ± 0.2	17.2 ± 0.7	0.079 ± 0.006	−31.6 ± 2.4
HAp (pH 8)	19.2 ± 0.08	57.7 ± 0.43	8.3 ± 0.1	16.1 ± 0.5	0.053 ± 0.003	−32.7 ± 1.6
HAp (pH 9)	17.3 ± 0.11	56.5 ± 0.28	8.1 ± 0.2	15.6 ± 0.3	0.029 ± 0.004	−36.9 ± 2.5
HAp–OVA (pH 7)	19.8 ± 0.09	50.4 ± 0.27	15.5 ± 0.4	21.3 ± 0.3	0.089 ± 0.002	−19.7 ± 1.3
HAp–OVA (pH 8)	18.4 ± 0.05	49.1 ± 0.41	14.4 ± 0.2	19.5 ± 0.4	0.058 ± 0.002	−20.2 ± 0.7
HAp–OVA (pH 9)	16.8 ± 0.06	46.2 ± 0.36	14.1 ± 0.3	16.6 ± 0.7	0.036 ± 0.003	−23.2 ± 1.1

60–160 °C, should correspond to the loss of adsorbed water. The second stage, with the onset temperature at about 240 °C, should relate to the loss of tris-base from the HAp structure. The last stage at the onset temperature of about 740 °C was thought to relate to the loss of the remaining organic residues within the HAp structure. As for the HAp–OVA particles, all of the three stages were evident. However, the presence of an additional step at the onset temperature of about 330 °C should correspond to the loss of the incorporated OVA. After the TGA analysis, these HAp and the HAp–OVA particles were reanalyzed by XRD (Fig. 3b). Apparently, the crystalline peaks associated with HAp became much sharper (cf. Fig. 1), indicating further crystallization of HAp during the thermal treatment. Additionally, crystalline peaks that belong to other calcium-based chemical species such as CaO and carbonate apatite became much more evident (cf. Fig. 1). This suggests that parts of the imperfectly-formed HAp entities may undergo thermal decomposition or solid state chemical reaction at high temperatures. Notwithstanding, both the FT-IR and the TGA results confirmed the presence of OVA within the structure of the obtained HAp–OVA particles.

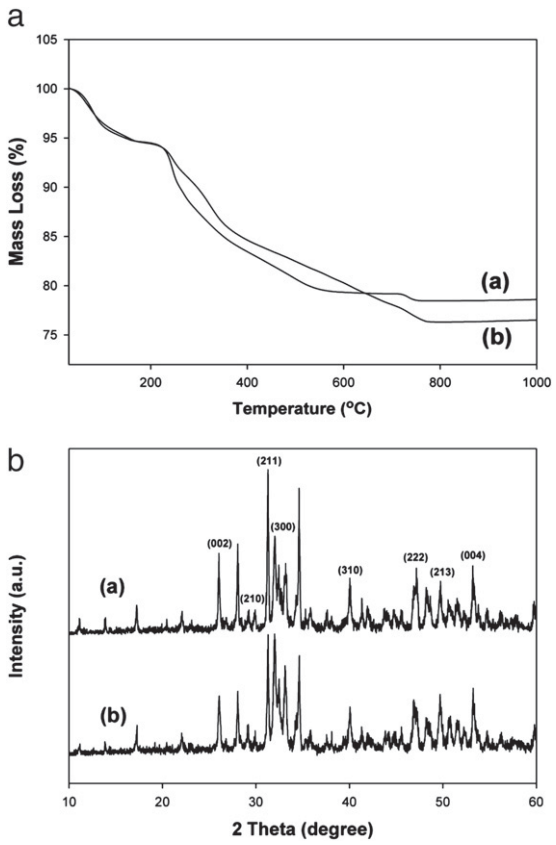


Fig. 3. (a) TGA curves of (a) pure HAp and (b) HAp–OVA particles that had been obtained at pH 9 and (b) XRD patterns of these particles after having been subjected to the TGA analysis.

The particle size distribution (PSD) curves of the HAp and the HAp–OVA particles that had been obtained at pH 9 are shown in Fig. 4. Based on the PSD results, the HAp and the HAp–OVA primary particles had the average sizes of around 56–59 nm and 46–50 nm, respectively. The average sizes of the HAp and the HAp–OVA primary particles that had been obtained at all pH levels investigated were measured and summarized in Table 1. Apparently, the presence of OVA resulted in significant reduction in the sizes of the obtained HAp primary particles. On the contrary, the average value of the primary particle size decreased slightly with an increase in the pH used during the precipitation process. Both of these should be a result of the increase in the number of nucleation sites, i.e., owing to the presence of OVA in the former and the more availability of the free tris-base molecules in the latter [20]. As for the effect of tris-base, the greater the amount of tris-base used, the greater the number of nuclei, hence the observed reduction in the sizes of the HAp primary particles.

The nano-crystalline structure of the HAp and the HAp–OVA particles that had been obtained at pH 9 was investigated by TEM (see Fig. 5). The rod-like morphology of the obtained HAp crystals, both in the absence and in the presence of OVA, was evident. The TEM results were consistent with the results obtained from the particle size analyzer (i.e., the PSD results), which revealed that the primary particles were in the nanometer range and the presence of OVA led to the reduction in the size of the primary particles. Despite the nano-crystalline nature of the individual primary particles, representative SEM images of the precipitated HAp and HAp–OVA powder that had been obtained at pH 9 (see Fig. 6) revealed the existence of large agglomerates and the extent of the agglomeration was accented by the presence of OVA. In addition, the HAp particles obtained at higher pH values existed as larger aggregates, owing possibly to the increase in the overall crystallization rate (viz. due to the increase in the nucleation rate, earlier mentioned) [21]. Notwithstanding, the existence of such agglomerates could easily be a result of lyophilization during the drying of the powdery products.

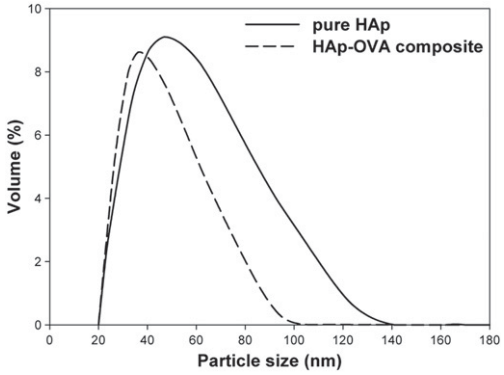


Fig. 4. PSD curves of pure HAp and HAp–OVA particles that had been obtained at pH 9.

Author's personal copy

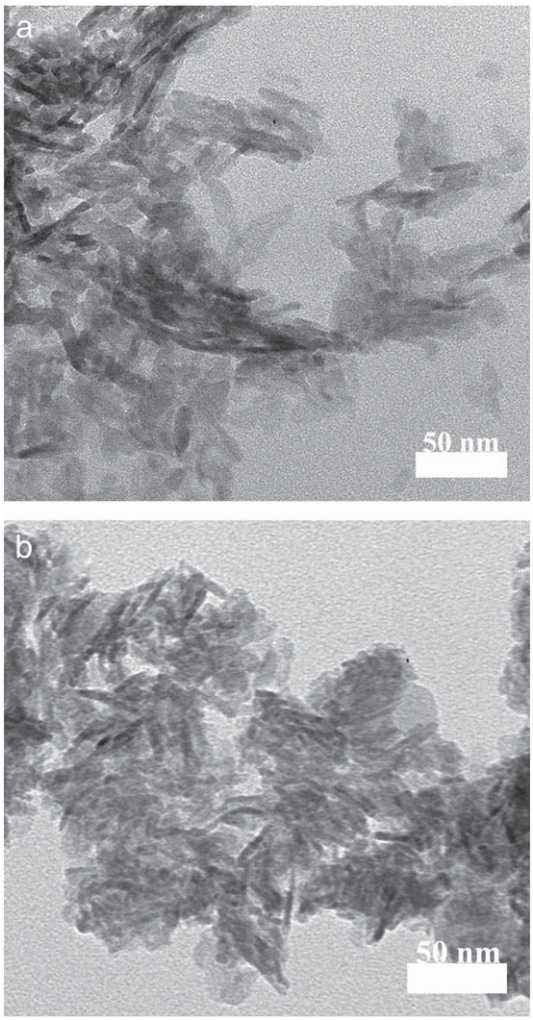


Fig. 5. TEM micrographs of (a) pure HAp and (b) HAp–OVA particles that had been obtained at pH 9.

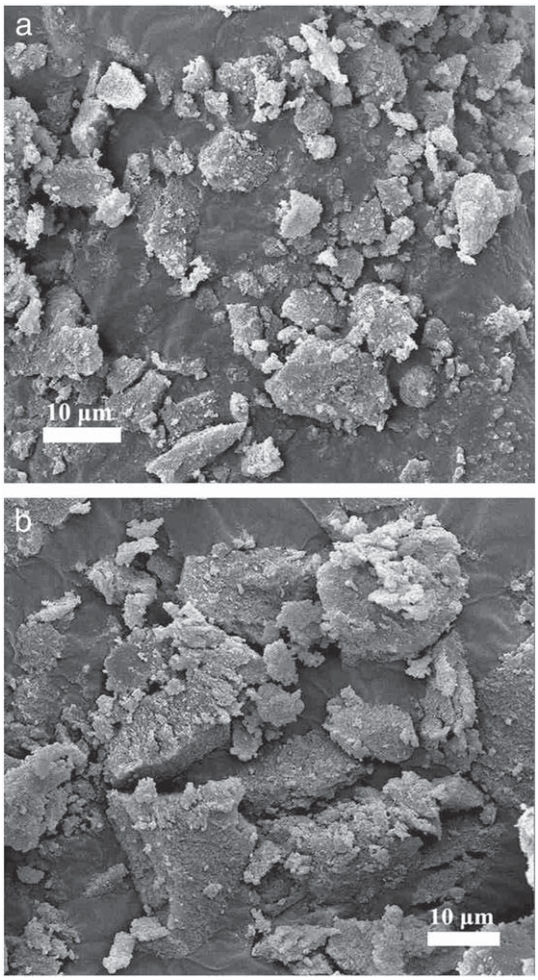


Fig. 6. SEM images of (a) pure HAp and (b) HAp–OVA particles that had been obtained at pH 9.

The N_2 adsorption–desorption isotherms and the pore size distribution as calculated from the adsorption branch of the isotherms based on the Bopp–Jancsó–Heinzinger (BJH) model for the HAp and the HAp–OVA particles that had been synthesized at pH 9 are shown in Fig. 7 and in the inset of the figure, respectively. The isotherms can be categorized as type IV, which can be further categorized into H1-hysteresis loops of mesoporous materials [22]. The average pore sizes of the HAp and the HAp–OVA particles were determined to be about 8.1 nm and 14.1 nm, respectively. The isotherms and the pore size distribution of these two cases were slightly different. For the HAp–OVA particles, the isotherm exhibited a slightly steeper slope with a greater pore volume and the pore size distribution was narrower, owing to the more uniform pore sizes. This indicates that the aggregation of OVA within the HAp structure affected slightly the basic pore structure of the obtained mesoporous HAp particles. The pore diameter and the BET specific average surface area for each of the obtained products are summarized in Table 1. In the absence of OVA within the HAp structure, the pore sizes were 8.1–8.9 nm. Larger pore sizes were observed for the OVA-incorporated HAp particles (i.e., 14.1–15.5 nm). These correspond to the BET specific average surface area values of 15.6–17.2 and 16.6–21.3 $m^2 \cdot g^{-1}$, respectively, and the pore volume values of 0.029–0.079 and 0.036–0.089 $cm^3 \cdot g^{-1}$, respectively. These pores were thought to be generated upon the sublimation of the ice crystals formed during the lyophilization step [23,24]. The presence of OVA resulted in hypothetical increases in the values of all of the pore parameters of the resulting HAp particles, while the increase in the pH during the precipitation process led to opposing trends. Furthermore, since the characteristic FT-IR bands associated with both HAp and OVA components were not shifted, it is expected that the mesopores may be present as the voids located at the grain boundaries of the aggregates of the rod-like HAp particles.

The ζ potentials of the HAp and the HAp–OVA particles were finally measured based on the electrophoretic mobilities of these particles in deionized water. The average values for the HAp particles were in the range of −31.6 to −36.9 mV, while those for the HAp–OVA particles were in the range of −19.7 to −23.2 mV. Evidently, an increase in the pH during the precipitation process caused the ζ potentials of the HAp and the HAp–OVA particles to become more negative. It was reported that the ζ potentials of commercial HAp particles depended strongly on the pH of the suspending medium [25], in which the values varied from −5 to −37 mV as the pH increased from 5.0 to 8.0. Over the pH levels of 7.0–8.0 however, the ζ potentials varied within a small range of −35 to −37 mV. Such a value for commercial HAp particles in phosphate buffer solution (pH = 7.4) was determined to be −36 mV [26]. Clearly, the values of the ζ potentials for the HAp particles, as obtained here, agreed particularly well with those reported in the literature. Upon the addition of OVA, which is an acidic protein (cf. isoelectric point = 4.7 [26]) during the precipitation process to obtain the HAp–OVA particles, the ζ potentials decreased by about 12 mV on average. This reduction is a clear indication of the adsorption of

Author's personal copy

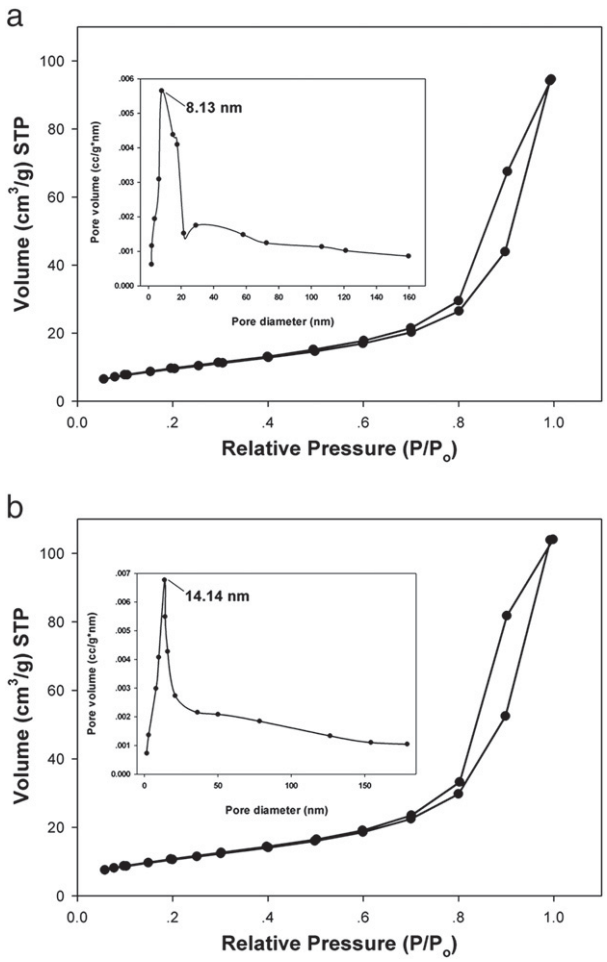


Fig. 7. Adsorption–desorption isotherms of N_2 within the pore structures of (a) pure HAp and (b) HAp–OVA particles that had been obtained at pH 9. The size distribution of the pores as determined based on the Bopp–Jancsó–Heinzinger (BJH) model is shown as the inset.

the protein on the surface of the HAp crystallites. Marginal reduction in the values of the ζ potentials of the HAp particles was observed when their surfaces were covered with acidic and neutral proteins, while more significant reduction was observed when their surface was covered with basic proteins [25,26].

4. Conclusions

An economical and simple synthetic route for HAp–OVA particles from discarded egg shells and OVA, as the model incorporating protein, by co-precipitation method was proposed. Both XRD and FT-IR results confirmed the formation of HAp, while PSD and TEM results indicated the formation of discrete HAp nanocrystals, which were rod-like in nature. Both the crystallite sizes (as calculated from breadth of the (002) reflection peak) and the sizes of the individual nanocrystalline particles decreased in the presence of OVA. Electrophoretic analysis indicated that OVA adsorbed readily on the surfaces of the HAp nano-crystallites and this was responsible for their agglomeration into larger particles, as revealed by SEM analysis. The knowledge obtained from the preparation of these HAp–OVA materials could be used as a promising archetype for synthesizing composite particles of HAp and another functional protein for biomedical applications or bone tissue engineering purposes in particular.

Acknowledgements

The authors acknowledge the partial support received from 1) The Thailand Research Fund (TRF, grant no.: DBG5280015), 2) The Institute for the Promotion of Teaching Science and Technology (IPST, for the doctoral scholarship of PK), 3) The Petroleum and Petrochemical College (PPC), Chulalongkorn University, and 4) Center of Excellence on Petrochemical and Materials Technology, Chulalongkorn University.

References

[1] T.A. Kuriakose, S.N. Kalkura, M. Palanichamy, D. Arivuoli, K. Dierks, G. Bocelli, C. Betzel, J. Cryst. Growth 263 (2004) 517–523.
[2] M.S. Djošic, V.B. Miškovic-Stankovic, S. Minlojic, Z.M. Kacarevic, N. Bibic, J. Stojanovic, Mater. Chem. Phys. 111 (2008) 137–142.
[3] K. Ioku, M. Kamitakahara, Phosphorus Res. Bull. 23 (2009) 25–30.
[4] P.M.S.L. Shanthi, R.V. Mangalaraja, A.P. Uthirakumar, S. Velmathi, T. Balasubramanian, M. Ashok, J. Colloid Interface Sci. 350 (2010) 39–43.
[5] E.M. Fischer, P. Layrolle, C.A. Van Blitterswijk, J.D. De Bruijn, Tissue Eng. 6 (2003) 1179–1188.
[6] Y.B. Li, W. Tjandra, K.C. Tam, Mater. Res. Bull. 43 (2008) 2318–2326.
[7] S. Bose, S.K. Saha, Chem. Mater. 15 (2003) 4464–4469.
[8] S. Bose, S.K. Saha, J. Am. Ceram. Soc. 86 (2003) 1055–1057.
[9] B. Viswanath, N. Ravishankar, Biomaterials 29 (2008) 4855–4863.
[10] H. Wang, L. Zhai, Y. Li, T. Shi, Mater. Res. Bull. 43 (2008) 1607–1614.
[11] Y.J. Wang, J.D. Chen, K. Wei, S.H. Zhang, X.D. Wang, Mater. Lett. 60 (2006) 3227–3231.
[12] Y.F. Zhau, J. Ma, Microporous Mesoporous Mater. 87 (2005) 110–117.
[13] Y. Wu, S. Bose, Langmuir 21 (2005) 3232–3234.
[14] H.S. Zhao, W. He, Y.J. Wang, Y.Z. Yue, X.G. Guo, Z.M. Li, S.P. Yan, W.J. Zhou, X.D. Zhang, Mater. Chem. Phys. 111 (2008) 265–270.
[15] H.S. Zhao, W. He, Y.J. Wang, X.D. Zhang, Z.M. Li, S.P. Yan, W.J. Zhou, G.C. Wang, Mater. Lett. 62 (2008) 3603–3605.
[16] E.M. Rivera, M. Araiza, W. Brostow, V.M. Castaño, J.R. Díaz-Estrada, R. Hernández, J.R. Rodríguez, Mater. Lett. 41 (1999) 128–134.
[17] A.L. Patterson, Phys. Rev. 56 (1939) 978–982.
[18] Y. Suwa, H. Banno, M. Mizuno, H. Saito, J. Ceram. Soc. Jpn. 101 (1993) 642–647.
[19] H.S. Zhao, W. He, Y.J. Wang, X.Z. Zhang, Z.M. Li, S.P. Yan, W.J. Zhou, J. Chem. Eng. Data 53 (2008) 2735–2738.
[20] M.C. Chang, C.C. Ko, W.H. Douglas, Biomaterials 24 (2003) 2853–2862.
[21] W.P. Inskeep, J.C. Silvertooth, Geochim. Cosmochim. Acta 52 (1998) 1883–1893.
[22] S.J. Gregg, K.S.W. Sing, Adsorption, Surface area and Porosity, Academic Press, London, 1982, pp. 233–238.
[23] Y. Zhang, K.H. Zuo, Y.P. Zeng, Ceram. Int. 35 (2009) 2151–2154.
[24] S. Yunoki, T. Ikoma, A. Monkawa, M. Kikuchi, S. Sotome, K. Shinomiya, J. Tanaka, Mater. Lett. 60 (2006) 999–1002.
[25] M. Matsumoto, T. Miyake, H. Noshi, M. Kambara, K. Konishi, Colloids Surf. 40 (1989) 77–84.
[26] K. Kawasaki, M. Kambara, H. Matsumura, W. Norde, Colloids Surf. B Biointerfaces 32 (2003) 321–334.

Comparative Study of Protein Carriers Based on Hydroxyapatite Particles for Bone Tissue Engineering

Prae-ravee K-hasuwan[a,b], Neeranut Kuanchertchoo[c], Prasit Pravasant[d], Pitt Supaphol[a,b,*]

[a] The Petroleum and Petrochemical College, Chulalongkorn University, Bangkok, 10330, Thailand

[b] The Center for Petroleum, Petrochemicals and Advanced Materials, Chulalongkorn University, Bangkok 10330, Thailand

[c] Department of Materials Technology, Faculty of Science, Ramkhamhaeng University, Bangkok, 10240, Thailand

[d] Department of Anatomy, Faculty of Dentistry, Chulalongkorn University, Bangkok, 10330, Thailand

ABSTRACT

Different starting materials (natural and chemical substances) were employed for synthesizing hydroxyapatite (HAp) particles as a protein carrier. Egg albumin (OVA), the main constituent of egg white with high functionality including modifying HAp properties, was used as a model protein. HAp particles were prepared via a co-precipitation method with various amounts of OVA (1g, 2g, and 3g/500 ml distilled water) and pH conditions (pH 7 and pH 9); also, the chemical properties of the obtained HAp particles were investigated. The incorporated and released amounts of OVA from the HAp particles were examined. Both incorporated and released OVA contents slightly increase with increasing the initial amount of OVA, but significantly increase with lowering pH value. Besides, a larger number was observed in the obtained carriers synthesized from the chemical starting material compared to the natural one. The release profiles demonstrated a slowly releasing behavior within 21 days,

followed by a plateau release without the initial bursting, suggesting that the OVA release was clearly prolonged by the incorporation. This release characteristic could be promising for bone tissue engineering applications.

Keywords: Protein carriers; Hydroxyapatite; Egg albumin; Bone tissue engineering

* Corresponding author. Postal Address: The Petroleum and Petrochemical College Chulalongkorn University, Soi Chula 12, Phyathai Road, Pathumwan, Bangkok 10330, Thailand. Tel.: +66-2-218-4131; fax: +66-2-215-4459.

E-mail address: pitt.s@chula.ac.th (P. Supaphol)

1. Introduction

To be bone substitutes as orthopedic or dental prostheses, artificial materials with the chemical and morphological similarity to the natural bone are required [1,2]. A large number of biomaterials have been widely investigated as the synthetic bone substitutes [3]. Owing to its mineral phase resemblance to human bone, Hydroxyapatite (HAp), one of calcium phosphate (CaP) based ceramic materials, has been applied in various medical applications such as dental implants, drug delivery systems, and so forth. More importantly, this bioactive ceramic is the best for inducing osteogenesis and new bone formation in soft tissues [4,5].

Considering the several utilizations of HAp in clinical fields, many preparation methods of HAp particles, including electrochemical synthesis [6], reflux procedure [7], capillary microfluidic technique [8], hydrothermal treatment [9], microemulsion route [10], precipitation [11,12], and sol-gel approach [13] have been reported. Besides, numerous biosurfactants have also been presented to be efficient templates for particle size, shape, and morphology. For instance, yeast cells, sucrose, and even proteins were employed as template materials to improve the surface area and the formation of the HAp particles [13-15]. Among them, the proteins have been documented to have better biocompatibility and more sufficient hemostatic properties [16]. Thus, extensive studies in combining of proteins on apatite forms have been indicated to analyze the release characteristics for enhancing osteoinduction [17]. Egg albumin (OVA), a stable and inexpensive protein readily extracted from egg white, can lead to either controlled HAp growths or modified HAp properties. With its functional groups, this phosphoglycoprotein has strong negative dipoles to chelate the free Ca^{2+} cations in calcium phosphate solution [18]. Hence, it is of interest to incorporate OVA during HAp formation to generate protein carriers for the release applications.

Herein, we performed two kinds of starting materials with various OVA contents and pH values through a simple co-precipitation method for OVA-incorporated HAp (HAp-OVA) synthesis. Firstly, we purpose egg shells (CaO) as a calcium source and H_3PO_4 as a phosphorous source. Secondly, Calcium carbonate ($CaCO_3$) and Calcium hydrogen phosphate dihydrate ($CaHPO_4.2H_2O$) were used as calcium and phosphorous sources, respectively. The comparative studies of these two cases OVA carriers were evaluated. Also, the incorporation capacities and release kinetics of OVA were examined.

2. Experimental procedure

2.1. Materials

All chemical reagents including Calcium hydrogen phosphate dihydrate ($CaHPO_4.2H_2O$, A.R. grade, Fluka), Calcium carbonate ($CaCO_3$, A.R. grade, Carlo Erba), Nitric acid (HNO_3, A.R. grade, Labscan), Phosphoric acid (H_3PO_4, A.R. grade, Labscan), Tris (hydroxymethyl)-aminomethane (tris-base, A.R. grade, Sigma), and Egg albumin (OVA, grade II, Sigma) were used without further purification. CaO from egg shells was prepared following the previous report of Rivera *et al.* [19].

2.2. Synthesis of hydroxyapatite

HAp was prepared by co-precipitation method. In the typical procedure, 2.00 g of $CaHPO_4.2H_2O$ (as a phosphorous source) and 0.79 g of $CaCO_3$ (as a calcium source) were dissolved in 1 M HNO_3 25 ml under gentle stirring at 70 ˚C for 2 h and the pH of the solution was kept to 2. OVA, subsequently, was added in the amount of 0, 1, 2, and 3 g/ 500 ml of the

mixed solution at room temperature. 200 ml of 1 M and 2 M tris-base solution were then poured into the mixture generating the precipitation at pH 7 and pH 9, respectively. The precursor solution was stirred vigorously to yield a homogeneous product. The product was then filtered off and washed several times with deionized water. After centrifugation, the resulting material was freeze-dried for 48 h to obtain the fine powder products. The similar process with the use of 1.25 g of CaO and 1.50 g of H_3PO_4 as calcium and phosphorous sources respectively was performed for comparison. With many synthetic conditions above, the sample names were specified as shown in Table 1.

2.3. Release kinetics of OVA from HAp particles

About 20 mg of HAp-OVA particles were immersed in 10 ml phosphate buffer solution at pH 7.4, in which matches the normal body and blood system of a human being. The controlled release systems were shaken in the water bath with a stirring rate of 70 rpm at 37 ˚C. The amount of released OVA in the supernatant was measured at various times by UV-VIS spectrophotometer (UV-1800) at the wavelength of 280 nm through the use of a pre-determined standard calibration curve. Furthermore, the gravimetric analysis was used to confirm the amounts of OVA loss again after 21 days.

2.4. Characterization

The crystallographic phases of the HAp-OVA particles were analyzed by X-ray diffractometer (WDXRD, D/MAX 2000 series Rigaku) with an incident X-ray wavelength of 1.54 Å (Cu Kα line) at the scanning rate of 0.02° per minute over a range of 2θ from 5° to 60° with JCPDS database (9-432). Fourier transform infrared (FT-IR) spectrograph carried

out on a Nicolet Nexus spectrometer (NEXUS 670, Nicolet) was performed using the KBr pellet technique, working in the wavelength from 4000 to 400 cm^{-1}. The structural morphology images were recorded on a transmission electron microscope (TEM, JEM-2100, JEOL) with an acceleration voltage of 200 kV. Energy dispersive X-ray (EDX) element analysis of the samples was also investigated with scanning electron microscope (SEM, JSM-5410LV, JEOL) operated at 15 kV. The average pore diameters of the obtained particles were taken on autosorb-1 instrument (AS-1, Quantachrome) using physisorption of nitrogen at temperature of 77 K. Thermogravimetric analysis (TGA, TGA7, Perkin Elmer) was carried out on the dried samples (5 mg) to examine the relative amount of OVA associated with HAp particles with a heating rate of 10 ˚C /min under a flowing air atmosphere.

2.5. Statistical Analysis

All quantitative examinations were collected in triplicate and the results were presented as means and standard deviations. Significance between the mean values was determined by ANOVA one-way analysis using Tukey's test for variances at a 95% confidence level.

3. Results and discussion

3.1. Material characterization

The formation of HAp particles was ascertained by X-ray diffraction (XRD) analysis. The XRD patterns of the HAp-OVA particles with particular peaks ascribed to the lattice constant of HAp according to the JCPDS database (9-432) were given in the comparative

chart of Fig. 1. From these results, the presence of the OVA during the synthesis does not have an influence on the structural development of HAp. Besides, no difference in HAp-OVA characteristic diffraction peaks was perceived for all synthetic cases given above. These XRD data also show poorly-crystallized traces of the powders due to water sublimation in the freeze-drying process [20], resulting in estimated crystallite sizes. Calculations of the crystallite size using the Scherrer equation were performed for the (002) reflection peak corresponding to $2\theta = 26^{\circ}$ because of well resolved characteristics [21]. The mean sizes of crystallites are within the range of 16-20 nm.

Fig. 2 exhibits the FT-IR spectra of the HAp-OVA particles. The IR spectra of pure OVA and HAp are also shown for comparison. The OVA spectrum displayed the typical bands at 3299 cm^{-1}, 1652 cm^{-1}, 1539 cm^{-1}, and 1457 cm^{-1} represented to the nitrogen-hydrogen stretch (N-H), the carbonyl vibration (C=O), the carbon-nitrogen vibration (C-N), and the stretching vibration of carbon-hydrogen (C-H), respectively [15]. The spectrum of pure HA demonstrates the adsorption bands at 3569 cm^{-1} assigned to OH stretching, 1630 cm^{-1} assigned to OH vibration of the apatitic group, 1035 cm^{-1} assigned to PO_4^{3-} stretching vibration, as well as 601 cm^{-1} and 563 cm^{-1} assigned to PO_4^{3-} deformation vibration [22,23]. The bands at 1654 cm^{-1} and 1539 cm^{-1} of HAp-OVA spectra, therefore, ascertained that OVA was incorporated in HAp particles.

EDX analysis was performed to give further confirmation of a molar Ca/P ratio of the samples. The EDX characteristic peaks indicated the existence of calcium (Ca), phosphorous (P), and oxygen (O) with proportional counts (Fig. 3). The molar Ca/P ratio of all samples revealed that the obtained samples synthesized by using the chemical starting material have the Ca/P ratio of 1.67-1.68 very close to the ideal one of 1.67 for HAp in human bone, while the Ca/P ratio measured for the obtained samples synthesized from the natural starting

material are within the range 1.62-1.65. On the other hand, there were not statistically significant differences for the Ca/P ratio of both starting materials ($p > 0.05$).

The HAp-OVA particles were also examined by transmission electron microscopy (TEM). The TEM micrographs of the samples synthesized from both natural and chemical substances at pH 7 and pH 9 with 1 g OVA show little difference in morphology (Fig. 4). In all obtained specimens, the primary particles have a rod-like shape with dimensions of 3-10 nm in diameter and 15-30 nm in length. However, it was noticed that the sizes of primary particle slightly increase with a higher OVA content and a lower pH condition.

3.2. Incorporation of OVA into HAp particles

The physi-sorption of nitrogen was performed to collect the average pore diameters of the pure HAp and HAp-OVA particles (see Table 2). The average pore sizes of HAp particles with the presence of OVA are larger than those of the absence ones, suggesting the incorporation of OVA within HAp particles by bond formation. The mechanism was that the carbonyl group and the phosphorous group of OVA have negative dipoles which could chelate the free Ca^{2+} ions; subsequently, the PO_4^{3-} ions may bond with OVA-associated calcium to generate HAp-OVA aggregates [18]. OVA, furthermore, could be adsorbed on the HAp surfaces by the crystal surface area available for growth [24]. When considering HAp-OVA particles, their average pore diameters at lower pH are bigger than those at higher pH. At the same pH, the chemical starting material shows the higher values of the average pore diameter compared with the natural one. The average pore diameters, nevertheless, are quite similar in cases of varying initial OVA contents. Therefore, it could be assumed that difference in these initial amounts of added OVA has a little influence on the average pore size.

For thermal behavior, TGA profiles of the obtained HAp and HAp-OVA powders prepared in several conditions are presented in Fig. 5. The mass loss could be differentiated into four regions in the investigated temperature range of (1) 60-200˚C, (2) 200-400 ˚C, (3) 400-780 ˚C, and (4) 780-1200 ˚C. The mass loss below 200 ˚C was attributed to the loss of adsorbed water. From 200-400 ˚C, an obvious mass loss was detected due to the loss of tris-base (endothermic peak around 240˚C), OVA (endothermic peak around 330˚C), and other absorbed species. The mass loss between 400 and 780˚C corresponded to the decomposition of remained organic residues was rather small for all particulate HAp samples. Above 780 ˚C, a very small transition was mainly attributed to the weight loss of carbonate. The amounts of incorporated OVA within HAp particles based on the total amount of 5 mg of the dried samples shown in Table 2 could be determined from these TGA results by subtracting pure HAp content. For all obtained specimens, the mass loss slightly increased when increasing the initial amounts of OVA, which meant that the amounts of incorporated OVA did not significantly increase with the increase of the initial OVA contents ($p > 0.05$). However, a larger quantity of incorporated OVA was noticed in the HAp particles synthesized from the chemical starting material compared to those prepared from the natural one. The starting-material type, therefore, caused honestly significant differences in the incorporated OVA content ($p < 0.05$). A lower pH in the synthesis procedure resulted in a significantly greater amount of incorporated OVA for both starting materials ($p < 0.05$) because there is the electrostatic repulsion force between OVA and HAp, which predominates in a higher pH solution (pH 9) compared to a lower pH solution (pH 7). As a result, increasing pH solution brought about a decreased amount of incorporated OVA [25].

3.2. Controlled release of OVA

The OVA release experiments carried out in PBS (pH 7.4) to simulate the local pH of the homeostatic body fluid were performed for all particulate HAp and HAp-OVA. The OVA release profiles and its release amounts based on the incorporated OVA amounts all the obtained particles are shown in Fig. 6 and Table 2, respectively. It was found that the obtained particles prepared from both starting materials demonstrated a slow release behavior increased time dependently within 21 days; a plateau release was then followed and the burst release was not observed. The OVA release profiles, suggesting a single-stage release mechanism, were assigned to the OVA molecules incorporated into HAp particles (OVA-HAp complex) [25]. The complex was formed by the adsorption of OVA on the Ca-site of HAp by ionic interaction between carboxyl acid groups on OVA and the positively charged Ca-sites. Phosphate ions from PBS can be also adsorbed onto the Ca-sites, so the competition between acidic protein molecules and phosphate ions occurs, resulting in the desorption of OVA from the HAp particles [26,27]. The sustained release profiles of OVA, moreover, can be possibly attributed to the formation of porous structure of HAp particles. About 50-54% and 38-41% of loaded OVA was released from the HA particles synthesized by using the natural starting material after 35 days in pH 7 and 9, respectively. A more sustained OVA release was fulfilled for the HAp particles prepared from the chemical starting material. Around 57-62% and 42-44% of loaded OVA was release out after the same period for pH 7 and 9, respectively. Hence, the OVA releases from the chemical starting material were significantly greater than those from the natural one ($p < 0.05$). The higher OVA releases were also noticed in pH 7 significantly than those in pH 9 ($p < 0.05$) because of a smaller adding amount of tris-base leading to a looser and weaker bond formation. Thereby, the quantity of OVA release considerably relies on the pH condition and the type of the starting material. All of the release patterns also reveal the OVA incomplete release owing to OVA instability problems such as non-specific adsorption and aggregation [28]. The HAp particles

with the presence of higher initial OVA amount manifest a little higher OVA-release percentage, depending on the incorportaed OVA content, so the OVA release amount was not significantly dependent on the initial amount of added OVA ($p > 0.05$).

4. Conclusions

Protein carriers based on HAp were designed as potential devices for the controlled release system. HAp-OVA particles were obtained by the co-precipitation method with varying the starting material, pH value, and initial amount of OVA. The incorporated and released OVA amounts highly increased with lowering pH value to be neutral and slightly increased with increasing initial OVA content. A greater OVA incorporation and release were also observed in the HAp-OVA particles synthesized from the chemical starting material compared to those prepared from the natural one. All of the release kinetics exhibited a slow release in a sustained manner without initial OVA burst, resulting in prolonged release behavior. Consequently, it may be practicable to use these HAp particles with other protein drugs and growth factors as effective carries to achieve specific targets for bone tissue engineering applications.

Acknowledgements

The authors acknowledge the partial support received from 1) the Thailand Research Fund (TRF), 2) Development and Promotion of Science and Technology talents project (DPST), and 3) The Petroleum and Petrochemical College (PPC), Chulalongkorn University.

References

[1] I. Sopyan, M. Mel, S. Ramesh, K.A. Khalid, Porous hydroxyapatite for artificial bone applications, Sci. Technol. Adv. Mater. 8 (2007) 116-123.

[2] G. Carutenuto, G. Spagnuolo, L. Ambrosio, L. Nicolais, Mesoporous hydroxyapatite as alloplastic material for dental applications, J. Mater. Sci.: Mater. Med. 10 (10/11) (1999) 671-676.

[3] T. Kokubo, H.M. Kim, M. Kawashita, Novel bioactive materials with different mechanical properties, Biomaterials 24 (2003) 2161-2175.

[4] H.N. Wang, Y.B. Li, Y. Zuo, J.H. Li, S.S. Ma, L. Cheng, Biocompatibility and osteogenesis of biomimetic nano-hydroxyapatite/polyamide composite scaffolds for bone tissue engineering, Biomaterials 28 (2007) 3338-3348.

[5] A. Krisanapiboon, B. Buranapanitkit, K. Oungbho, Biocompatibility of hydroxyapatite composite as a local drug delivery system, J. Orthop. Surg. 14 (3) (2006) 315-318.

[6] M.S. Djosic, V.B. Miskovic-Stankovic, S. Milonjic, Z.M. Kacarevic-Popovic, N. Bibic, J. Stojanovic, Electrochemical synthesis and characterization of hydroxyapatite powders, Mater. Chem. Phys. 111 (2008) 137-142.

[7] F. Ye, H.F. Guo, H.J. Zhang, Biomimetic synthesis of oriented hydroxyapatite mediated by nonionic surfactants, Nanotechnology 19 (2008) 245605.

[8] H.C. Shum, A. Bandyopadhyay, S. Bose, D.A. Weitz, Double emulsion droplets as microreactors for synthesis of mesoporous hydroxyapatite, Chem. Mater. 21 (22) (2009) 5548-5555.

[9] Y.J. Wang, J.D. Chen, K. Wei, S.H. Zhang, X.D. Wang, Surfactant-assisted synthesis of hydroxyapatite particles, Mater. Lett. 60 (2006) 3227-3231.

[10] G.C. Koumoulidis, A.P. Katsoulidis, A.K. Ladavos, P.J. Pomonis, C.C. Trapalis, A.T. Sdoukos, T.C. Vaimakis, Preparation of hydroxyapatite via microemulsion route, J. Colloid Interface Sci. 259 (2003) 254-260.

[11] C. Santos, R.P. Franke, M.M. Almeida, M.E.V. Costa, Nanoscale characterization of hydroxyapatite particles by electron microscopy, Microsci. Microanal. 14 (2008) 67-70.

[12] B. Viswanath, N. Ravishankar, Controlled synthesis of plated-shape hydroxyapatite and implications for the morphology of the apatite phase in bone, Biomaterials 29 (2008) 4855-4863.

[13] S. Bose, S.K. Saha, Synthesis of hydroxyapatite nanopowders via sucrose-templated sol-gel method, J. Am. Ceram. Soc. 86 (6) (2003) 1055-1057.

[14] W. He, Z.M. Li, Y.J. Wang, X.F. Chen, X.D. Zhang, H.S. Zhao, S.P. Yan, W.J. Zhou, Synthesis of mesoporous structured hydroxyapatite particles using yeast cells as the template, J. Mater. Sci.: Mater. Med. 21 (1) (2010) 155-159.

[15] H.S. Zhao, W. He, Y.J. Wang, X.D. Zhang, Z.M. Li, S.P. Yan, W.J. Zhao, Biomimetic synthesis and characterization of hydroxyapatite crystal with low phase transformation temperature, J. Chem. Eng. Data 53 (2008) 2735-2738.

[16] M. Sivakumar, K.P. Rao, Preparation, characterization and in vitro release of gentamicin from coralline hydroxyapatite-gelatin composite microsphere, Biomaterials 23 (2002) 3175-3181.

[17] Y. Liu, P. Layrolle, J. de Bruijn, C.V. Blitterswijk, K. de Groot, Biomimetic coprecipitation of calcium phosphate and bovine serum albumin on titanium alloy, J. Biomed. Mater. Res. 57 (3) (2001) 327-335.

[18] H.S. Zhao, W. He, Y.J. Wang, X.D. Zhang, Z.M. Li, S.P. Yan, W.J. Zhou, G.C. Wang, Biomineralization of large hydroxyapatite particles using ovalbumin as biosurfactant, Mater. Lett. 62 (2008) 3603-3605.

[19] E.M. Rivera, M. Araiza, W. Brostow, V.M. Castano, J.R. Diaz Estra, R. Hernandez, J.R. Rodriguez, Synthesis of hydroxyapatite from egg shells, Mater. Lett. 41 (1999) 128-134.

[20] S. Jalota, S.B. Bhaduri, A.C. Tas, A new rhenanite (β-$NaCaPO_4$) and hydroxyapatite biphasic biomaterial for skeletal repair, J. Biomed. Mater. Res. Part B.: Appl. Biomater. 80 (2007) 304-316.

[21] V.M. Suru, C.H. Ng, M. Wilke, B. Tiersch, P. Fratzl, M.G. Peter, Size-controlled hydroxyapatite nanoparticles as self-organized organic-inorganic composite materials, Biomaterials 26 (2005) 5414-5426.

[22] Y. Suwa, H. Banno, M. Mizuno, H. Saito. Synthesis of compositionally regulated hydroxyapatite from $Ca(OH)_2$ and H_3PO_4, J. Ceram. Soc. Japan, Int. Edition 101 (1993) 642-647.

[23] Q.G. Xu, Y. Tanaka, J.T. Czernuszka, Encapsulation and release of a hydrophobic drug from hydroxyapatite coated liposomes, Biomaterials 28 (2007) 2687-2694.

[24] K. IJntema, W.J.M. Heuvelsland. C.A.M.C. Dirix, A.P. Sam, Hydroxyapatite microcarriers for biocontrolled release of protein drugs, Inter. J. Pharmaceutics 112 (1994) 215-224.

[25] T.Y. Liu, S.Y. Chen, D.M. Liu, S.C. Liou, On the study of BSA-loaded calcium-deficient hydroxyapatite nano-carriers for controlled drug delivery, J. Control. Release 107 (2005) 112-121.

[26] T. Kawasaki, M. Niikura, Y. Kobayashi, Fundamental study of hydroxyapatite high-performance liquid chromatography: II. Experimental analysis on the basis of the general theory of gradient chromatography, J. Chromatogr. 515 (1990) 91-123.

[27] T. Akasawa, M. Kobayashi, Surface characteristics of hydroxyapatite controlling albumin adsorption behavior, J. Mater. Sci. Lett. 15 (1996) 1319-1320.

[28] H.K. Kim, T.G. Park, Comparative study on sustained release of human growth hormone from semi-crystalline poly(L-lactic acid) and amorphous poly(D,L-lactic-co-glycolic acid) microsphere: morphological effect on protein release, J. Control. Release 98 (2004) 115-125.

Table 1

Experimental conditions of HAp and HAp-OVA particles

Starting materials	Initial amounts of OVA (g)	pH conditions	Sample names
$CaCO_3$	-	7	0D-7
+	1	7	1D-7
$CaHPO_4.2H_2O$	2	7	2D-7
	3	7	3D-7
	-	9	0D-9
	1	9	1D-9
	2	9	2D-9
	3	9	3D-9
CaO (Egg shells)	-	7	0E-7
+	1	7	1E-7
H_3PO_4	2	7	2E-7
	3	7	3E-7
	-	9	0E-9
	1	9	1E-9
	2	9	2E-9
	3	9	3E-9

Table 2

Physico-chemical characteristics of HAp and HAp-OVA particles

Samples	Average pore diameter (nm)	Incorporated OVA amounts		Released OVA amounts	
		(%)*	(mg)*	(%)#	(mg)#
0D-7	9.43 ± 0.02	-	-	-	-
1D-7	16.4 ± 0.15	8.01 ± 0.92	0.40 ± 0.08	57.5 ± 3.71	0.92 ± 0.04
2D-7	16.8 ± 0.11	9.32 ± 0.37	0.47 ± 0.03	60.0 ± 4.10	1.12 ± 0.07
3D-7	16.9 ± 0.07	9.94 ± 0.96	0.49 ± 0.08	62.0 ± 3.82	1.23 ± 0.06
0D-9	8.69 ± 0.14	-	-	-	-
1D-9	13.7 ± 0.18	7.54 ± 0.83	0.38 ± 0.07	42.1 ± 2.73	0.63 ± 0.04
2D-9	14.2 ± 0.06	7.99 ± 0.68	0.40 ± 0.06	43.7 ± 2.90	0.70 ± 0.05
3D-9	14.8 ± 0.03	8.21 ± 0.74	0.41 ± 0.07	44.0 ± 1.95	0.72 ± 0.03
0E-7	8.91 ± 0.19	-	-	-	-
1E-7	15.0 ± 0.14	6.17 ± 0.45	0.31 ± 0.04	50.1 ± 3.06	0.62 ± 0.05
2E-7	15.3 ± 0.27	7.61 ± 0.33	0.38 ± 0.03	52.6 ± 2.81	0.80 ± 0.04
3E-7	15.6 ± 0.29	8.89 ± 0.87	0.44 ± 0.07	54.2 ± 3.66	0.96 ± 0.06
0E-9	8.18 ± 0.03	-	-	-	-
1E-9	13.5 ± 0.22	5.24 ± 0.72	0.26 ± 0.06	38.8 ± 1.13	0.41 ± 0.02
2E-9	13.9 ± 0.26	6.01 ± 0.79	0.30 ± 0.08	40.3 ± 2.09	0.48 ± 0.03
3E-9	14.3 ± 0.15	6.93 ± 0.44	0.35 ± 0.04	40.8 ± 1.84	0.56 ± 0.03

***** based on around 5 mg of total weight of the particle analyzed from TGA

based on the incorporated OVA amounts into 20 mg of total weight of the particle

Captions of Figures

Fig. 1. XRD patterns of HAp-OVA particles prepared under various conditions: (a) 1D-7, (b) 1D-9, (c) 1E-7, (d) 1E-9.

Fig. 2. FT-IR spectra of pure HAp: (a) 0D-7, HAp-OVA particles synthesized under different starting materials and pH conditions: (b) 1D-7, (c) 1D-9, (d) 1E-7, (e) 1E-9, and as-received OVA in its dry state (f).

Fig. 3. EDX analysis of HAp-OVA particles: (a) 1D-7, (b) 1D-9, (c) 1E-7, (d) 1D-9.

Fig. 4. TEM micrographs of HAp-OVA particles synthesized under different conditions: (a) 1E-7, (b) 1E-9, (c) 1D-7, (d) 1D-9.

Fig. 5. TGA profiles of the obtained HAp and HAp-OVA particles synthesized at various conditions.

Fig. 6. OVA release profiles of the obtained HAp and HAp-OVA particles synthesized under different conditions.

Polycaprolactone Fibrous Membranes Modified with Gelatin, Bovine Serum Albumin or Crude Bone Protein Extract and Their Potential for Use as Bone Scaffolds.

Sutthilak Chaichamnarn,[1] Prasit Pavasant,[2] and Pitt Supaphol [1,*]

[1] The Petroleum and Petrochemical College and The Center for Petroleum, Petrochemicals and Advanced Materials (C-PPAM), Chulalongkorn University, Bangkok 10330, Thailand

[2] Department of Anatomy, Faculty of Dentistry, Chulalongkorn University, Bangkok 10330, THAILAND

1. ABSTRACT

Immobilization of biomolecules; i.e. gelatin type-A, gelatin type-B, bovine serum albumin (BSA) and crude bone protein (CBP), making polycaprolactone (PCL) fibrous scaffolds that have been fabricated by electrospinning more suitable for bone tissue engineering. PCL scaffolds were first covalently introduced with amino groups on their surfaces through the aminolysis reaction using 1,6-hexamethylenediamine (HMD) and later immobilized with the above mentioned biomolecules using disuccinimidyl carbonate (DSC) as the coupling agent. Various techniques; ATR-FTIR, XPS, SEM, and water contact angle measurement were used to monitor the scaffold surfaces after each modification step. The potential use of the modified materials as bone scaffolds was evaluated with a murine pre-osteoblastic cell line (MC3T3-E1). MC3T3-E1 proliferation was improved remarkably on the modified surface, especially the BSA-immobilized PCL fibrous scaffolds which showed the greatest proliferation after cell culture as well as the highest ALP activity. In mineralization, the deposited minerals was highest on the CBP-immobilized PCL scaffolds. All the obtained results suggested that immobilization of BSA and CBP is an attractive method for fabricating of fibrous scaffolds for bone tissue engineering.

Keywords: Polycaprolactone / Immobilization/ Bovine serum albumin/ Crude bone proteins / X-ray Photospectroscopy / Contact angle

2. INTRODUCTION

Tissue engineering is the new approach field of science that applies the principles of engineering and the life sciences towards the development of biological substitutes that restore, maintain, or improve tissue function. In contrast to classic biomaterial approach, Tissue engineering is based on the

[*] Authors to whom correspondence should be addressed: pitt.s@chula.ac.th (P. Supaphol)

understanding of tissue formation and regeneration, and aims to regenerate new functional tissues, rather than just to implant new spare parts (Salgado *et al*., 2004). Therefore, harvested cells, signalling molecules (e.g. protein, and growth factor) and biocompatible scaffolds are the main components of tissue engineering. For the restoration of large tissue defects, scientific efforts have demonstated the utility of implanting tissue scaffolds, to which allow cell attachment, growth and proliferation. In bone tissue engineering need to develop a suitable bone scaffold with sufficient mechanical strength and porosity to allow the ingrowth of new tissue, enhancing growth and proliferation results in good integration with surrounding tissue. Accordingly, the following discussion examines novel, degradable, polymeric scaffolds developed to act as a temporary matrix for cell growth and extracellular matrix deposition, with consequent bone in-growth until the new bony tissue is totally restored or regenerated (Hutmacher D. W., 2000).

Thermoplastic aliphatic polyesters such as polylactide, polyglycolide, polycaprolactone and especially the copolymers of lactide and glycolide such as poly(lactide-co-glycolide) have generated interest for bone regeneration because of their excellent biocompatibility, biodegradability, and mechanical strength. PCL was chosen as a model polymer due to its lack of toxicity, low cost and slow degradation.(Yoshimoto *et al*., 2003) The challenge in tissue engineering is the design of scaffolds that can mimic the structure and biological functions of the natural extracellular matrix (ECM). Electrospinning has drawn a lot of attention recently as a suitable method to fabricate scaffolds, owing to its simple process, its increased surface areas, ability to mimic the extracellular matrix (Venugopal *et al*., 2008), its versatility to create fibrous scaffolds from a wide range of starting materials, and as a carrier to deliver clinically relevant proteins like growth factors.

It has been known that certain surface characteristics of polymer can influence the interactions between cells and material. The hydrophobic surface of PCL was not adequate for cell attachment and growth. Therefore, it is important to develop different physical and/or chemical methods to modify the scaffold surface for cytocompatibility improvement for cell

attachment and proliferation. It has been reported that several methods (such as plasma treatment, ozone or photoinduced grafting and surface oxidation) have been employed to introduce hydrophilic compounds onto polymeric scaffold surfaces. Moreover, biomaterials can be coated with extracellular matrix (ECM) proteins (such as collagen, fibronectin, laminin), which usually have promoted cell adhesion and proliferation (Zhu *et al*, 2002).

In this study, PCL scaffolds were prepared by electrospinning techniques followed by immobilization of gelatin, bovine serum albumin (BSA), and crude bone protein extracted from pork bone via chemical surface modification method to promote cell behavior including their adhesion, growth, differentiation. The potential use of these electrospun fibrous scaffolds was further evaluated *in vitro* with MC3T3-E1 in terms of cytotoxicity, attachment, proliferation, alkaline phosphatase activity (ALP), and mineralization of the cells that were cultured directly on the scaffolds, in comparison to those of the cells on a tissue-culture polystyrene plate (TCPS).

3. EXPERIMENTAL SECTION

a. Materials

Materials used in the Fibrous Scaffolds Preparation and Surface Modification

- Poly(ε-caprolactone) (PCL) (M_n = 80,000 g/mol; Aldrich, USA)
- Dichloromethane (DCM; Lab-Scan (Asia), Thailand)
- *N,N′*-dimethylformamide (DMF; Lab-Scan (Asia), Thailand)
- 1,6-hexamethylenediamine (HMD; Aldrich, USA)
- *N*,*N*'-disuccinimidyl carbonate (DSC; Aldrich, USA)
- Ninhydrin (Aldrich, USA)
- Bovine serum albumin (BSA; Sigma, USA)
- Gelatin from porcine skin ,type A (Sigma, USA)
- Gelatin type-B (Sigma, USA)

- Triethylamine (TEA; Sigma, USA)
- Ethanol (J. T. Beaker, USA)
- Isopropanol (IPA; Fisher Sciencific (Asia), Thailand)
- 1,4-dioxane (Fisher Sciencific (Asia), Thailand)
- Dimethylsulfoxide (DMSO; Lab-Scan (Asia), Thailand)
- Phosphate buffer saline (PBS)

Materials used for cell culture

Model Cells

Model cells in this study were mouse calvaria-derived pre-osteoblastic cells (MC3T3-E1).

Medium for MC3T3-E1 cells

Minimum Essential Medium (with Earle's Balanced Salts) (MEM; Hyclone, USA), supplemented by 10% fetal bovine serum (FBS; Sorali, Campo Grande, Brazil), 1% L-glutamine (Invitrogen Corp., USA) and 1% antibiotic and antimycotic formulation [containing penicillin G sodium, streptomycin sulfate, and amphotericin B (Invitrogen Corp., USA)] was used as culture media for MC3T3-E1.

Material for Cell Culture Study

- 3-(4,5-dimethyl-thiazol-2-yl)-2,5-diphenyltetrazolium bromide (MTT; USB Corporation., USA)
- Trypsin-EDTA (GibThai Co.,Ltd.)
- Fetal Bovine Serum (Sorali, Campo Grande, Brazil)
- DMEM without phenol red (GibThai Co.,Ltd.)
- L-Glutamine (GibThai Co.,Ltd.)
- 50% Glutaraldehyde solution (Sigma, USA)
- Hexamethyl disilazane HMDS; Sigma, USA)
- p-nitrophenylphosphate (PNPP; Zymed Laboratories, USA)
- Bicinchoninic acid protein assay (BCA; Pierce Biotechnology, USA)
- L-ascorbic acid (Sigma, USA)

- β-glycerophosphate (Sigma, USA)
- Cetylpyridinium chloride (Sigma, USA)

b. Equipment

Equipment for Electrospinning Process

- High voltage power supply from Gamma High Voltage Research Inc. (Ormond Beach, Florida), model D-ES30PN/M692 DC
- Syringe with volume size of 25 ml
- Stainless steel needle with gauge number 20 (or the inner diameter of 0.91 mm)
- The rotating drum which covered with aluminum sheet has the width and OD about 14 and 15 cm, respectively.

Equipment for Characterization of Materials

- UV-Vis spectrophotometer (UV-1800; Shimadzu, Kyoto, Japan)
- quartz tube
- Fourier-transformed infrared spectrometer (FT-IR); attenuated total reflection (ATR-FTIR; Thermo Nicolet Nexus 670; resolution of 4 cm-1 and 128 scans)
- Contact angle goniometer (KRUSS Gmbh Germany; Model: DSA10-Mk2 T1C)
- Scanning electron microscope (SEM; A JEOL JSM 5200)
- X-ray Photoelectron Spectrometer (XPS; Thermo Fisher Scientific Thetaprobe; Monochromatic Al Kα X-ray, the analysis area was approximately 400 μm , while the maximum analysis depth lay in the range of ~4 to 8 nm.)

Equipment for Study of Cell Culture

- A Thermo Spectronic Genesis10 UV-vis spectrophotometer
- Laminar flow hood

c. Experimental Procedures

Preparation of Polycaprolactone Scaffolds

Preparation and Characterization of Fibrous Scaffolds

Electrospun Polycaprolactone fibrous scaffolds were prepared by electrospinning from a neat 12 % w/v PCL solution in 50:50 v/v DCM/DMF. The as-prepared PCL solution was contained in a glass syringe, the open end of which was connected to a blunt gauge-20 stainless steel hypodermic needle (o.d.0.91 mm) used as the nozzle. An Al sheet wrapped around a rotating cylinder (width and o.d. of the cylinder: 15 cm; rotational speed: 50 rpm) was used as the collector. The distance from the tip of the needle to the surface of the Al sheet defining the collection distance was fixed at 10 cm. A gamma high-voltage research D-ES30PN/M692 power supply was used to generate a high dc potential (i.e., 21 kV). The spinning time was carried out continuously for 10 hours.

Morphological appearance and size of the individual fibers of the scaffolds were examined by a JEOL JSM-5200 scanning electron microscope (SEM). Fibrous scaffolds were dried in vacuum at 30 °C overnight to remove solvent. Each sample was plated in the stub and coated with a thin layer of gold by using a JEOL JFC-1100E ion sputtering device prior to SEM observation. The average diameters of as-spun fibers were determined by measuring the diameters. At least 100 readings of the fiber diameters from at least five SEM images are statistically analyzed using SemAphore 4.0 software, from which the arithmetic mean values of the individual fibers in the PCL fibrous scaffolds were determined to be 0.93 and 1.26 μm, respectively.

Preparation of Crude Bone Protein.

Crude bone protein (CBP) was extracted from the pork bone. In particular, bone was initially washed and cleaned thoroughly in tap water and then sectioned into small pieces with a high speed motor machine. Pieces of sectioned bones were further crushed into powder in liquid nitrogen. Then, the as-prepared powder was immersed in 0.6 N HCl at 4°C and shaken continuously on an orbital shaker. After three days, the bony solution was centrifuged and the supernatant was collected, dialyzed for 48 h and lyophilized. The dry CBP was kept in desiccators until use.

Surface Modification of PCL Scaffold via Aminolysis and Immobilization of Proteins

The scaffold was cut into disc shape with diameter 1.4 cm and immersed in ethanol/water (1:1, v/v) solution for 2 to 3 hours to clean oily dirt and then washed with a large amount of deionized water. The scaffold was subsequently immersed in various concentrations of 1,6-hexamethylene diamine (HMD) /isopropanol (IPA) solution (0.04, 0.06, 0.08, 0.10, 0.20 ,and 0.40 g/ml) for 2 hours at 30 °C. The resulting aminolyzed PCL scaffold was rinsed with deionized water for 24 hours at room temperature to remove free 1,6-hexamethylenediamine and dried under vacuum at 30 °C to constant weight. To determine the optimum concentration of HMD used for aminolysis using ninhydrin method, degreadation experiment, water retention experiment and SEM observation.

Aminolyzed PCL scaffold obtained using the optimum condition was immersed in 0.1 M *N,N'*-disuccinimidyl carbonate (DSC)/dimethylsulfoxide (DMSO) solution in the presence of 0.1 M triethylamine (TEA) for 1 hour at ambient temperature followed by rinsing with large amount of deionized water. The scaffold was then directly transferred to 3 mg/ml of gelatin type-A, gelatin type-B, bovine serum albumin (BSA) or crude bone protein (CBP) in phosphate buffer saline (PBS) solution at ambient temperature for 24 hours. PCL scaffolds immobilized with proteins were rinsed by soaking in deionized water for 24 hours. The samples were dried under vacuum before surface characterization.

Characterization of Fibrous Scaffolds

Density, Porosity and Pore Volume

The density of the scaffolds ($\rho_{scaffolds}$) can be calculated using the following equation

Apparent density ($\rho_{scaffold}$, g/cm^3) = $\frac{m}{txA}$ ----------

(3.1)

where m is the mass of the scaffold (g), t is the thickness of the scaffold (cm) and A is the area of the scaffold (cm^2)

The porosity and pore volume of the scaffolds can be calculated using the following equation (Hou *et al*. 2003).

Porosity (%) = $\left(1 - \frac{\rho_{scaffold}}{\rho_{polymer}}\right) x100$ ---------

(3.2)

Pore volume = $\left(\frac{1}{\rho_{scaffold}} - \frac{1}{\rho_{polymer}}\right)$ ----------

(3.3)

where $\rho_{scaffold}$ is the apparent density of the fibrous scaffolds(g/cm^3) and $\rho_{polymer}$ is the density of the non-fibrous polymer ($\rho_{polymer}$ of PCL is 1.145 g/cm^3).

Water Retention Capacity

The dry scaffolds were weighed and then immersed in 5 mL of 0.1 M PBS solution at 37 °C within 48 hours. At the predetermined time point, scaffold were removed from the solution and carefully placed on glass for 5 seconds to remove the excessive water and weighed immediately.

The water retention was calculated by using the following equation (Kothapalli *et al*., 2005).

$$\textbf{Water Retention (\%)} = \left(\frac{M_{wet} - M_{dry}}{M_{dry}}\right) x100 \quad \text{----------} \quad (3.4)$$

where M_{dry} and M_{wet} are the weight of the scaffold before and after immersion in 0.1 M PBS solution respectively. Five measurements were performed for the calculation of an average water retention value.

Degradation Study of Fibrous Scaffolds

In degradation study, the disc shape of the fibrous scaffolds with diameter 1.4 cm had been immersed in the 0.1 M PBS pH 7.4 at 37 °C within 48 hours. The fibrous scaffolds were then dried in the vacuum to constant weight.

The rate of degradation can be calculated using the following equation.

$$\textbf{Weight loss (\%)} = \left(\frac{Mf - Mi}{Mi}\right) x100 \quad \text{----------} \quad (3.5)$$

where M_i is the initial weight of the scaffolds and M_f and is the weight of the scaffold at the given degradation time point, immersed in 0.1 M PBS solution. Five measurements were performed for the calculation of an average water degradation rate value.

Determination of the Amino Groups on PCL Surface after Aminolysis and Protein Immobilization

The ninhydrin analysis method was carried out to quantitatively determine the amount of NH_2 groups on the aminolysed PCL and biomolecule-immobilized PCL scaffolds. The scaffold was immersed in 1 M ninhydrin/ethanol solution for 15 minutes. After the adsorbed ethanol had

evaporated, 1,4-dioxane was added to dissolve the scaffold. When the scaffold surface turned blue, isopropanol (IPA) was then added to stabilize the blue compound. This mixture was transfered to quartz tube and measured the absorbance at the wavelength of 538 nm using a UV-vis spectrophotometer. A calibration curve was obtained with known concentration of 1,6-hexamethylenediamine in 1,4-dioxane/IPA (1:1, v/v) solution.

Surface Characterization

Water Contact Angle Measurements

Contact angle goniometer (KRUSS Gmbh Germany; Model: DSA10-Mk2 T1C) were used for the determination of water contact angles. The measurements were carried out by the sessile drop method in air at room temperature. The reported angle was an average of 5 measurements on different area of each sample.

UV-Vis Spectrophotometer

UV-vis spectrophotometer Model Shimadzu, UV-1800 was used for determination of the amount of amino group using ninhydrin method on the modified PCL surface. Ninhydrin will react with a free alpha-amino group, NH_2-C- which is contained in all amino acids, peptides, or proteins, producing Ruhemann's purple colored complex of ninhydrin absorbs the visible light at the wavelength of 538 nm.

Attenuated Total Reflectance-Fourier Transform Infrared Spectrometer (ATR-FTIR)

All spectra are collected at resolution of 4 cm^{-1} and 128 scans using Nicolet Magna 750 FT-IR spectrometer equipped with a liquid-nitrogen-cooled mercury-cadmium-telluride (MCT) detector. A single attenuated total reflection accessory with 45° germanium (Ge) IRE (spectra Tech, USA) and a varible angle reflection accessory (Seagull™, Harrick Scientific, USA) with a hemispherial Ge IRE are employed for all ATR spectral acquisitions. Chemical functional groups that were present on the surfaces of both the neat and the surface-modified fibrous scaffolds were analyzed by ATR-FTIR spectrometer.

X-ray Photoelectron Spectrometer (XPS)

XPS was used to estimate the elemental composition and chemical state of the elements on the surface. The analysis of the samples was carried out using a Thermo Fisher Scientific Thetaprobe XPS. Monochromatic Al K_α X-ray was employed for analysis of one spot on each sample with photoelectron take-off angle of 50° (with respect to surface plane). The analysis area was approximately 400 μm, while the maximum analysis depth lay in the range of ~4 to 8 nm. A special designed electron flood gun with a few eV Ar^+ ion was used for the charge compensation. Electron beam and ion beam were focused and steered towards the analysis position. Further correction was made based on adventitious C 1s at 285.0 eV using the manufacturer's standard software. Survey spectra were acquired for surface composition analysis with Scofield sensitivity factors.

Scanning Electron Microscope

The morphology of cells on the materials was examined by using a JEOL JSM 5200 scanning electron microscope (SEM). Each sample was coated with a thin layer of gold using JEOL JFC 1100E ion sputtering device prior to SEM observation.

Cell Culture Studies

Osteoblast (MC3T3-E1) cell lines are used. MC3T3-E1 cells are cultured in α-MEM medium supplemented with 10 % FBS, 1 % L-glutamine and 1 % antibiotic and antimycotic formulation (containing penicillin G sodium, streptomycin sulfate, and amphotericin B**)**. The medium was replaced every 2 days and the cultured cells were maintained at 37 °C in a humidified atmosphere containing 5% CO_2.

Cytotoxicity Evaluation

Direct Cytotoxicity

This test was used to evaluate the potential for use of protein directly to the cell. 4×10^4 MC3T3-E1 cells/well were cultured in 24-well plate to allow cell attachment on the plate. After incubation

under 5 % CO_2 at 37 °C at least 4 hours, the cells were starved with a 2 % culture media (2 % MEM; containing MEM, 2 % FBS, 1 % L-glutamine, 1 % lactabumin, and 1 % antibiotic and antimycotic formulation.) for 24 hours. After starvation, the culture medium was removed and replaced with the as-prepared extraction media (2 % culture media with appropriate amount of proteins ; gelatin type-A , gelatin type-B, bovine serum albumin, and crude bone protein) and later incubated for 1, 2, and 3 days. The number of living cells was finally quantified with MTT assay.

Indirect Cytotoxicity

The indirect cytotoxicity evaluation was conducted on modified and unmodified PCL scaffolds in adaptation from the ISO10993-5 standard test method . The samples are pre-washed with 70 % ethanol in water for 30 minutes, washed twice with PBS solution and deionized water and immerged in a 2% MEM culture medium (2 % MEM; containing MEM, 2 % FBS, 1 % L-glutamine, 1 % lactabumin, and 1 % antibiotic and antimycotic formulation.) under 5 % CO_2 at 37 °C in 24-well plate for 24 hours to prepare the extraction media. 4×10^4 MC3T3-E1 cells/well were separately cultured in other 24-well plate to allow cell attachment on the plate at least 4 hours. The cells were further starved with a 2 % MEM and replaced in 2 hours for 3 times. After incubation under 5 % CO_2 at 37 °C, the culture medium was removed and replaced with the as-prepared extraction media and later incubated for another 1, 2 and 3 days. The number of living cells was finally quantified with MTT assay.

Cell Adhesion and Proliferation

Both modified and unmodified PCL scaffolds (diameter 1.4 cm) are sterilized by soaking in 70 % ethanol in water for 30 minutes, washed twice with PBS solution and deionized water and immerged in a 10 % MEM culture medium under 5 % CO_2 at 37 °C in 24-well plate for 24 hours. After removing of culture media, approximately 4×10^4 MC3T3-E1 cells and 0.5 mL culture medium were pipetted into each well containing as-prepared scaffolds as well as into the bottom of tissue culture polystyrene

plates (TCPS) as a control and then incubated under 5 % CO_2 at 37 °C. Cell adhesion was studied on 2, 4, 6 hours culture period while cell proliferation was investigated on 1, 2 and 3 days culture period. The number of living cells was finally quantified with MTT assay.

MTT Assay

The MTT assay is based on the reduction of the yellow tetrazolium salt to purple formazan crystals by dehydrogenase enzymes secreted from the mitochondria of metabolically active cells. The amount of the purple formazan crystal formed is proportional to the number of viable cells. After desirable culture period, the culture medium was removed to discard the unattached cell and incubated at 37 °C for 30 minutes with 300 µl/well of MTT solution at 0.5 mg/ml culture medium without phenol red. After incubation, MTT solution was removed. A buffer solution containing dimethylsulfoxide (DMSO : 900 µl/well) and glycine buffer (pH = 10 : 125 µl/well) was added into the wells to dissolve the formazan crystals. After 10 minutes of rotary agitation, the solutions were then transferred into a cuvette and placed in a spectrophotometer (Thermospectronic Genesis10 UV-visible spectrophotometer) to measure the number of viable cells at absorbance 540 nm .

Morphological Observation of Cultured Cells

After removal of the culture medium, the cell-cultured scaffold samples were rinsed with PBS twice and the cells were then fixed with 3% glutaraldehyde solution (diluted from 50 % glutaraldehyde solution with PBS), at 500 µl/well. After 30 minutes, they were rinsed again with PBS. After cell fixation, the samples were dehydrated in an ethanol solution of varying concentration (i.e. 30, 50, 70, 90, and 100 %, respectively) for about 2 minutes at each concentration. The samples were then dried in 100 % hexamethyldisilazane (HMDS) for 5 minutes and later let dry in air after removal of HMDS. After completely dried, the samples were mounted on an SEM stub, coated with gold, and observed by a JEOL JSM 5200 scanning electron microscope (SEM).

Production of Alkaline Phosphatase of Cultured Cells

ALP is considered as a relatively early marker of osteoblast differentiation. Cells were cultured on scaffold samples for 3, and 7 days to observe the production of alkaline phosphatase (ALP). The samples were rinsed with PBS after removal of culture medium. Alkaline lysis buffer (10 mM Tris-HCl, 2 mM $MgCl_2$, 0.1 % Triton-X 100, pH 10) (100 µl/well) was added and the samples were scrapped and then frozen at -20°C for at least 30 minutes prior to the next step. An aqueous solution of 2 mg/ml *p*-nitrophenyl phosphate mixed with 0.1 M amino propanol (10 µl/well) in 2 mM $MgCl_2$ (100 µl/well) having a pH of 10.5 was prepared and added into the samples. The samples were incubated at 37 °C for 15 minutes. The reaction was stopped by adding 0.9 ml/well of 50 mM NaOH and the extracted solution was transferred to a cuvette and placed in the UV-visible spectrophotometer, from which the absorbance at 410 nm was measured. The amount of ALP was then calculated against a standard curve. In order to calculate for the ALP activity, the amount of ALP had to be normalized by the amount of total protein synthesized. In the protein assay, the samples were treated in the same manner as the ALP assay up to the point was the samples were frozen. After freezing, bicinchoninic acid (BCA; Pierce Biotechnology, USA) solution was added into the samples. The samples were incubated at 37 °C for 15 minutes. The absorbance of the medium solution was then measured at 562 nm by the UV-vis spectrophotometer and the amount of the total protein was calculated against a standard curve.

Mineralization

Mineralization refers to cell-mediated deposition of extracellular calcium and phosphorus salts where anionic matrix molecules take up the Ca^{2+}, phosphate ions and serve as nucleation and growth sites leading to calcification. Mineralization was quantified by Alizarin Red-S which is a dye that binds selectively calcium salts and is widely used for mineral staining (the staining product i.e., an Alizarin Red S-calcium chelating product). MC3T3-E1 cells (4×10^4 cells/well in 24-well plate) were cultured on

scaffold samples for 16 days to observe the production of mineralization. The isolated cells were plated in 24-well plate and cultured in the cultured medium. The cultured cells were changed after a 24 hours attachment period with culture medium in the presence of 5 mM *β*-glycerophosphate and 50 μg/ml ascorbic acid. The media was replaced every 2 days thereafter. After 16, 21 and 30 days, respectively, the cells were washed twice with PBS , fixed with cold methanol for 10 minutes, and stained with 1 % Alizarin red solution (prepared in distillated water and adjusted the pH about 4.1 to 4.3 using 10 % ammonium hydroxide) for 5 minutes. After removing the alizarin red-S solution, the cells were rinsed with deionized water and dried at room temperature. The images of each culture were captured and the strain was extracted with 10 % cetylpyridinium chloride in 10 mM sodium phosphate for 1 hour and the absorbance of collected dye was read at wavelength 570 nm in spectrophotometer (A Thermo Spectronic Genesis10 UV-visible spectrophotometer). In comparison, tissue culture plate without cell was treated with the procedure as previously described.

Statistical analysis

Values are expressed as the mean ± SD. Experiments are performed at least five times and results of representative experiments are presented except where otherwise indicated. Statistical analysis was performed using One-Way Analysis of Variance (ANOVA) with the Least Square Difference (LSD) test multiple comparisons posttest using SPSS version 17 software. $p < 0.05$ or $p < 0.01$ is considered statistically significant.

4. RESULTS AND DISCUSSION

4.1 Preparation of Poly(*ε*-caprolactone) Electrospun Fibrous Scaffold

Poly(*ε*-caprolactone) (PCL; M_n = 80,000 g/mol) electrospun fibrous scaffold was prepared via electrospinning process under fixed conditions as

mentioned in the previous chapter. Translucent electrospun PCL fibrous scaffolds with a thickness of (130 ± 5) μm were obtained. Morphological appearance and size of the individual fibers of the scaffolds were examined by JEOL JSM 5200 scanning electron microscopy (SEM) as shown in Figure 4.1(a). At least 100 readings of the fiber diameters from various SEM images were statistically analyzed using SemAphore 4.0 software, from which the arithmetic mean value of the individual fibers within the PCL fibrous scaffolds was determined to be (0.93 ± 0.30) μm. After surface modification of PCL electrospun fibrous scaffold via aminolysis with various 1,6-hexamethylenediamine (HMD) concentration treatments, the morphology of the surface-modified scaffolds was also observed [Figure 4.1 (b,c and d)].

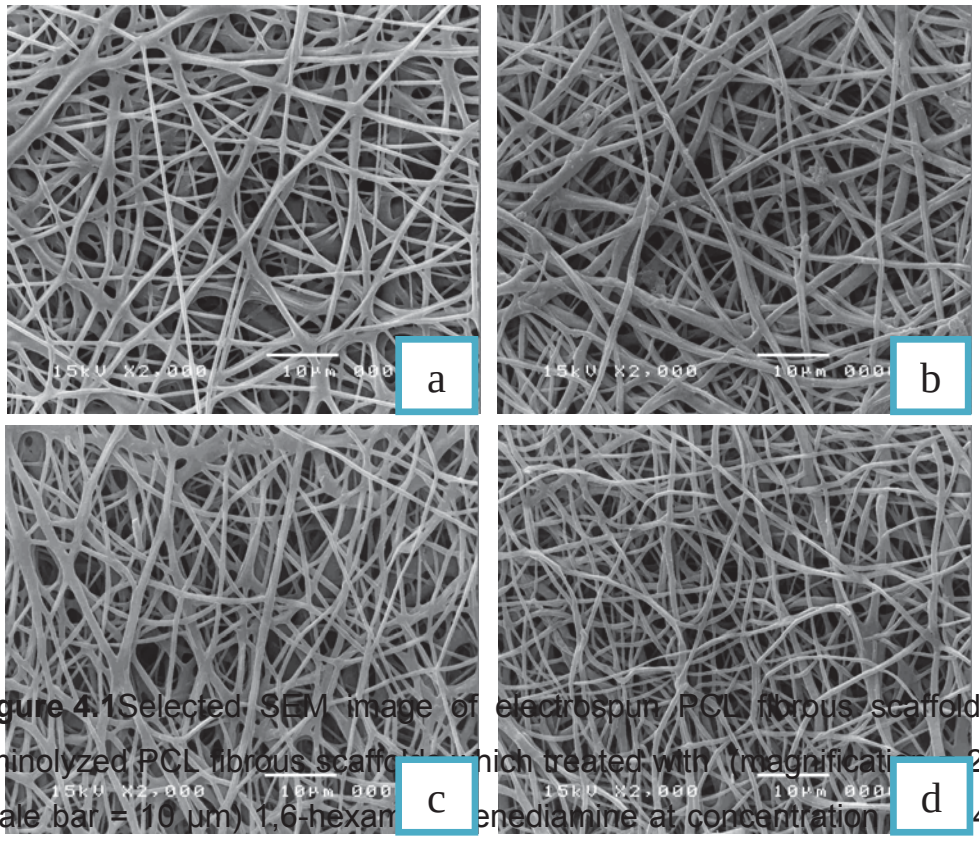


Figure 4.1 Selected SEM image of electrospun PCL fibrous scaffolds (a), aminolyzed PCL fibrous scaffolds which treated with (magnification 2000x; scale bar = 10 μm) 1,6-hexamethylenediamine at concentration 0.04 g/ml (b), 0.20 g/ml (c) and 0.40 g/ml (d)

4.2 Characterization of Fibrous Scaffolds

4.2.1 Density, Porosity, and Pore Volume

The density, porosity and pore volume of the unmodified PCL scaffolds and modified PCL scaffolds are shown in Table 4.1. The porosity and pore volume of these scaffolds were in the range of (96 to 97) % and (22 to 29) cm^3/g, respectively. Moreover, the density, porosity percentage and pore volume of all type of the surface-modified scaffolds were not significantly different from the unmodified PCL scaffolds.

Material	density ($x10^{-2} g/cm^3$)	porosity (%)	pore volume (cm^3/g)
PCL pure	4.69 ± 0.44	95.91 ± 0.38	20.62 ± 2.07
aminolyzed PCL	4.25 ± 0.97	96.29 ± 0.85	23.63 ± 5.28
activated PCL	4.14 ± 0.57	96.39 ± 0.50	23.64 ± 3.07
gelatin A immobilized PCL	3.75 ± 0.59	96.72 ± 0.51	26.33 ± 4.52
gelatin B immobilized PCL	3.59 ± 0.88	96.86 ± 0.77	28.15 ± 6.17
BSA immobilized PCL	3.85 ± 0.74	96.64 ± 0.65	25.88 ± 4.97
CBP immobilized PCL	4.58 ± 0.93	96.00 ± 0.81	21.64 ± 4.35

4.2.2 Water Retention Capability

Figure 4.2 demonstrates the water retention capability of these unmodified and modified PCL scaffolds via aminolysis process with different 1,6-hexamethylenediamine (HMD) concentration at 37 °C within 48 hours. In the figure shows the water retention rate increased with increasing HMD concentration treatment.

4.2.3 Degradation Study of PCL Fibrous Scaffolds

In degradation study, the disc shape of the PCL fibrous scaffolds with diameter ~ (100 to 150) μm had been immersed in the 0.1 M phosphate buffer saline (PBS), pH 7.4 at 37 °C within 48 hours. Figure 4.3 shows the degradation rate of the PCL scaffolds at different HMD

concentration treatments. The weight loss increased with time and rapidly increased in the early 2 hours and steady stable after 18 hours. Furthermore, the weight loss values increased with increasing HMD concentration treatment.

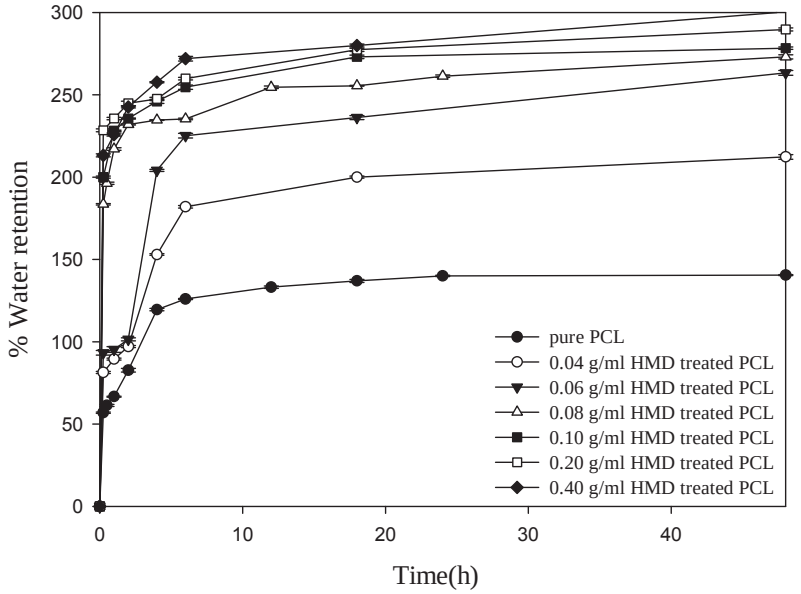


Figure 4.2 Water retention capability of these unmodified and modified PCL scaffolds via aminolysis process with different 1,6-hexamethylenediamine(HMD) concentration at 37 °C within 48 hours.

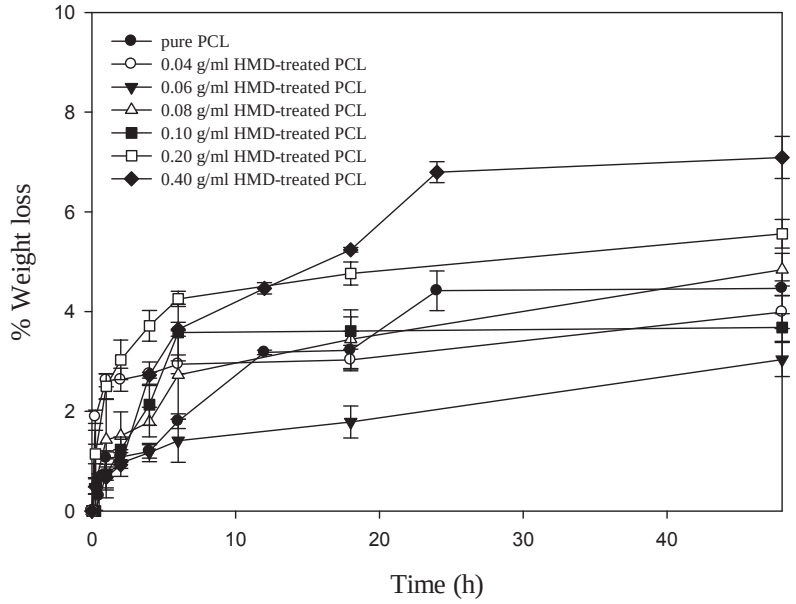


Figure 4.3 The degradation rate of the PCL scaffolds at different HMD concentration treatments.

4.3 Surface Characterization

4.3.1 Quantification of Amino Groups

Amino groups can be covalently introduced onto the surface of the electrospun PCL fibrous scaffolds by reaction with 1,6-hexamethylenediamine (HMD), One amino group (NH_2) of HMD reacts with an ester group (—COO—) of PCL to form the amide linkage (—CONH—), while another amino group which is unreacted and free can be used as active sites through which biomolecules (i.e;proteins) can be bonded to the surface using *N, N′*-disuccinimidyl carbonate (DSC) as a coupling agent. However, two-step procedure was carried out to avoid aggregation,. The attached amino groups had been first activated with DSC which *N*-hydroxysuccinimide was lost from the reaction and the as-formed succinimidyl esters were later reacted with respective biomolecules, *N*-hydroxysuccinimide again being cleaved from the reaction. The chemical pathway for the immobilization of

biomolecule on the surface of electrospun PCL fibrous scaffolds is summerized in the Figure 4.4.

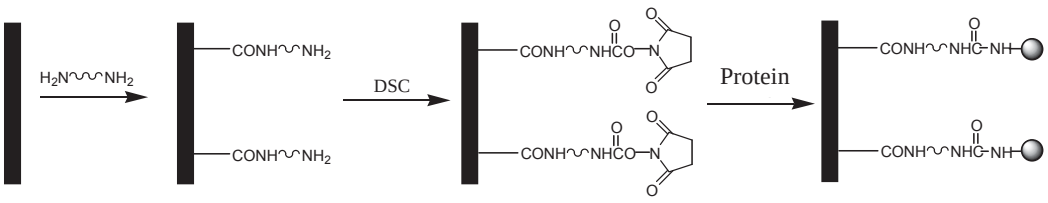


Figure 4.4 The chemical pathway for the immobilization of proteins.

The existence of free amino groups (NH_2) on PCL surface is essential for protein bonding in this modification method. It is important to confirm the existence of amino groups before protein is further introduced. Therefore, ninhydrin is used to confirm and quantify the $–NH_2$ density on the aminolyzed PCL surface. The NH_2 density on electrospun PCL fibrous scaffold surfaces is relative to the concentration of 1,6-hexamethylenediamine, aminolyzing time, temperature, and so on. Figure 4.5 shows that NH_2 density increased with increasing 1,6-hexamethylenediamine concentration. However, when the concentration of 1,6-hexamethylenediamine is greater than 0.20 g/ml, the structural morphology of the electrospun PCL fiber scaffolds became worse (as shown in Figure 4.1 d). To maintain structural morphology of the electrospun PCL fiber scaffolds for practical applications, PCL electrospun fibrous scaffolds were aminolyzed in a 0.20 g/ml 1,6-hexamethylenediamine/isopropanol solution at evaluated temperature for 2 hours. According to the calibration curve obtained with 1,4-dioxane–isopropanol (1:1, v/v) solution containing 1,6-hexamethylenediamine of known concentration, the NH_2 density on PCL electrospun fibrous scaffolds aminolyzed under these conditions was 1.37×10^{-7} mol/cm^2.

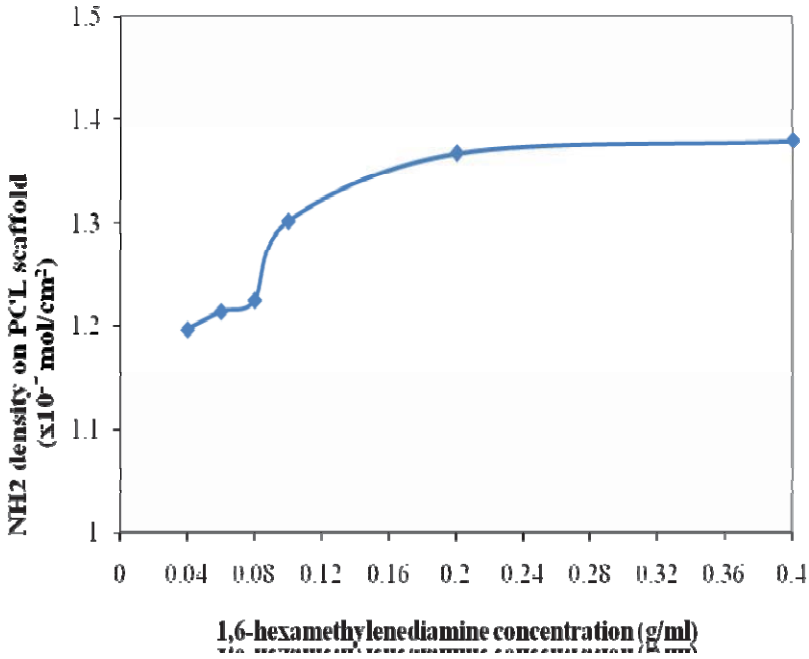


Figure 4.5 NH_2 density on PCL electrospun fibrous scaffolds as a function of concentration of 1,6-hexamethylenediamine/isopropanol solution. The PCL scaffold was aminolyzed for 2 hours.

4.3.2 Surface Wettability

To further evaluate the effect of aminolysis, surface wettability of the modified PCL fibrous scaffolds was measured. Therefore,water contact angle measurement was used to evaluate the surface wettability of the surface modified PCL fibrous scaffolds. Table 4.2 shows the water contact angle measured by the sessile drop method decreased gradually from 123.8˚ to 118.0˚ after the scaffolds were aminolyzed with 0.04 g/mL of HMD/IPA solution for 2 hours and slightly decreased with increasing HMD concentration. That is, the introduction of the amino groups on the surface of the PCL fibrous scaffolds improved the hydrophilicity of the surface. Figure 4.6 and 4.7 show that the surface became more hydrophilic after aminolysis and protein immobilization. After the aminolyzed PCL fibrous scaffolds have been activated with DSC, their surface became more hydrophobic than the neat PCL scaffold and water contact angle also decreased after the proteins

were bonded. The water drop appearance on the surface of neat PCL, gelatin type-A immobilized PCL, BSA immobilized PCL and CBP immobilized PCL are shown in Figure 4.7. CBP immobilized PCL scaffold has largest decrease of contact angle as compared with the neat PCL scaffold (control). This means that immobilization of gelatin crude bone protein can most improve the hydrophilicity of the surface.

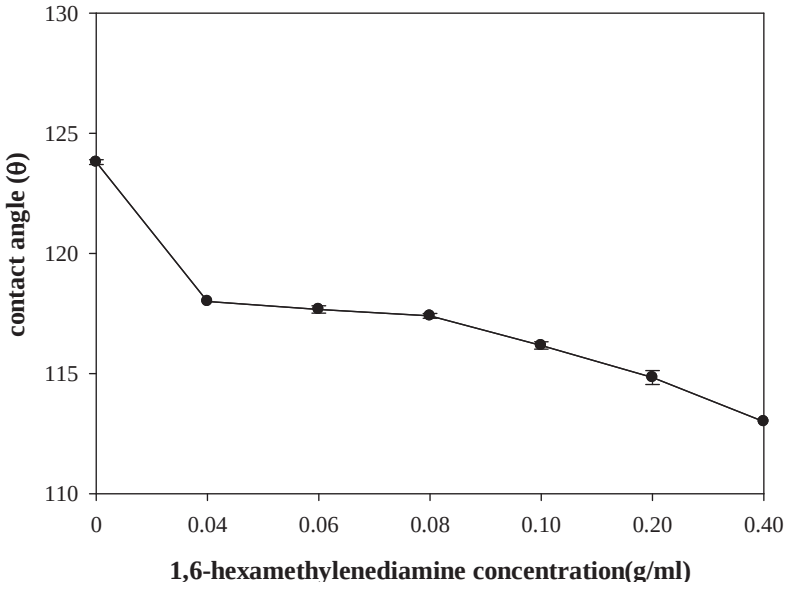


Figure 4.6 Water contact angles of the control and aminolyzed PCL scaffolds at different HMD concentration treatments measured by the sessile drop method.

Table 4.1 The water contact angle of the control and all modified PCL fibrous scaffolds measured by the sessile drop method

Material	Contact angle(θ)
Neat PCL (control)	123.7 ± 0.1
Aminolyzed PCL[a]	115.3 ± 0.2
Activated PCL[b]	118.7 ± 0.3

Gelatin type-A immobilized PCL[c1]	95.5 ± 1.1
Gelatin type-Bimmobilized PCL[c2]	94.4 ± 2.1
BSA immobilized PCL [c3]	97.5 ± 2.0
CBP immobilized PCL [c4]	48.5 ± 1.8

[a]The PCL electrospun fibrous scaffolds was immersed in 0.20 g/ml 1,6-hexamethylenediamine solution at 30 °C for 2 hours.

[b]The aminolyzed PCL scaffolds were immersed in 0.1 M DSC solution in the presence of TEA for 1 hour.

[c1,c2,c3,c4] The activated PCL scaffolds were immersed in 3.0 mg/mL gelatin type-A, gelatin type-B, BSA, and CBP solutions, respectively, for 24 h followed by the rinsing process.

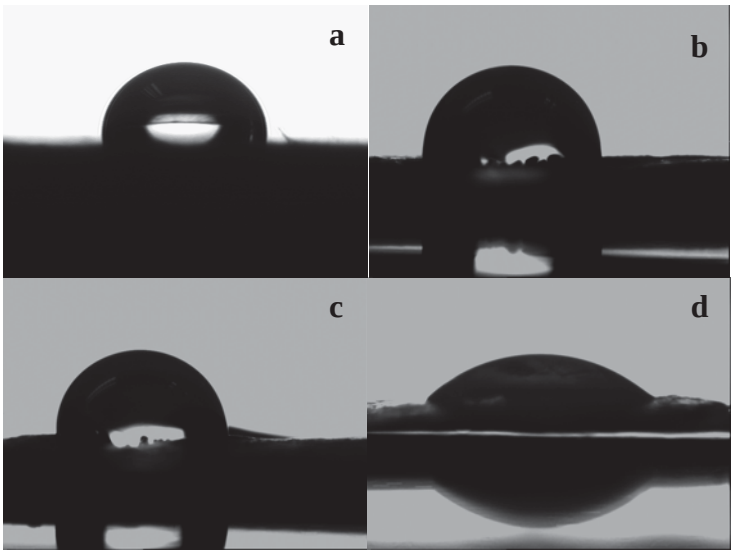


Figure 4.7 Water dropped on the surface of neat PCL fibrous scaffold (a), and PCL fibrous scaffold immobilized with 3.0 mg/ml gelatin type-A (b), 3.0 mg/ml bovine serum albumin (c) and 3.0 mg/ml crude bone protein (d).

4.3.3 Chemical Analysis of Surface

ATR-FTIR spectra of PCL and modified PCL fibrous scaffolds are shown in Figure 4.8 and 4.9 There was a major absorption peak assigned to the ester carbonyl of neat PCL appeared at 1755 cm^{-1}.

The low broad signals from N–H stretching of NH_2 at ~ (3300 to 3500) cm^{-1} or carbonyl stretching of amide group at 1650 cm^{-1} were observed on those surface modified PCL. After biomolecule immobilization, C=O stretching peak occurs at 1650 cm^{-1} (amide I) and N–H bending peak at 1550 cm^{-1} (amide II) and 1350 cm^{-1} (amide III) evidently appeared in the spectra of all biomolecule-immobilized PCL scaffolds. Moreover, the higher broad peak in the range of 3000 to 3600 cm^{-1} corresponding to N–H stretching of NH_2 in gelatin type-A, gelatin type-B, BSA and CBP was observed indicating that gelatin type-A, gelatin type-B, BSA and CBP have been successfully immobilized on the amino-containing PCL scaffolds. However, the signal of FTIR spectrum were low, resulting from the extremely low concentration of NH_2 present within the sampling depth of ATR-FTIR (1 to 2 μm).

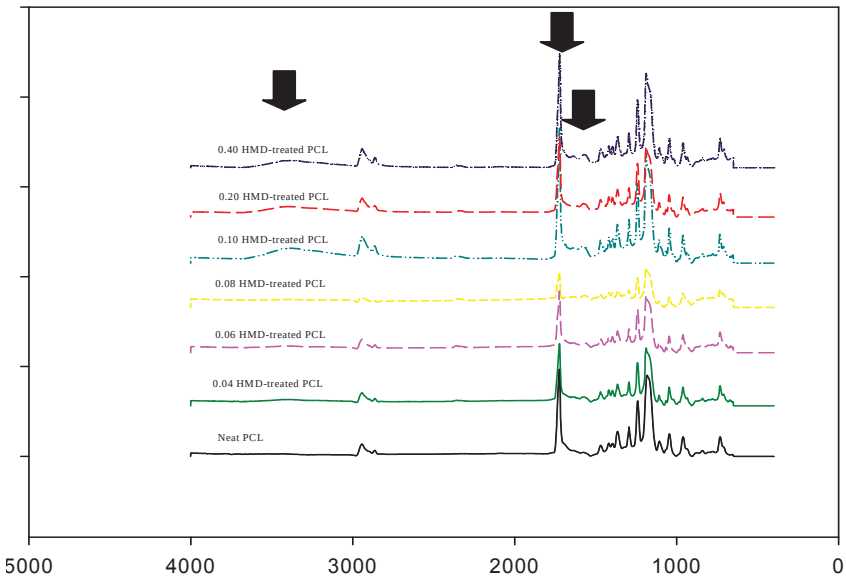


Figure 4.8ATR-FTIR spectra of neat and aminolyzed PCL fibrous scaffolds with different HMD concentration treatments.

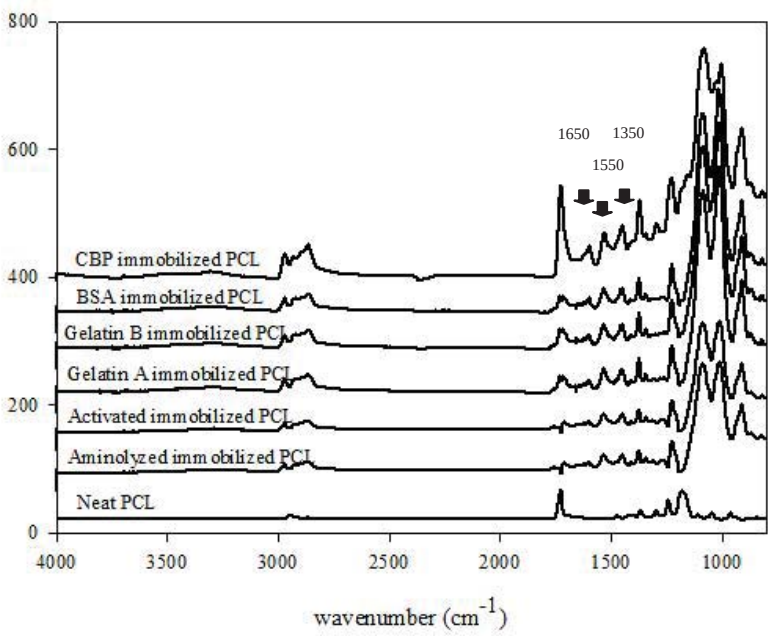


Figure 4.9ATR-FTIR spectra of neat and modified PCL fibrous scaffolds**.**

4.3.4 Elemental Composition of the Surface

The surface of modified PCL fibrous scaffolds were further determined the elemental composition by using X-ray Photoelectron Spectrometer (XPS). To study the effect of the aminolysis condition on the surface, N_{1s}/C_{1s} ratios as a function of HMD concentration treatment were evaluated. Table 4.4 shows that the more diamine concentration treated, the more N_{1s}/C_{1s} ratio observed due to the increasing in NH_2 groups. After aminolysis, the N_{1s}/C_{1s} ratio was increased from 0 to 0.0168 because NH_2 groups were introduced on the PCL surface. Figure 4.10 demonstrated that N_{1s} peak appeared after immobilization with proteins (gelatin type-A , gelatin type-B , bovine serum albumin, and crude bone protein) due to the large amount of nitrogen atom in proteins structure was introduced.

Table 4.2 N_{1s}/C_{1s} ratios as a function of 1,6-hexanediamine concentration

1,6-hexamethylenediamine concentration (g/ml)	N_{1s}/C_{1s} ratio
0.04	0.0063
0.06	0.0079
0.08	0.0163
0.10	0.0169
0.20	0.0170
0.40	0.0170

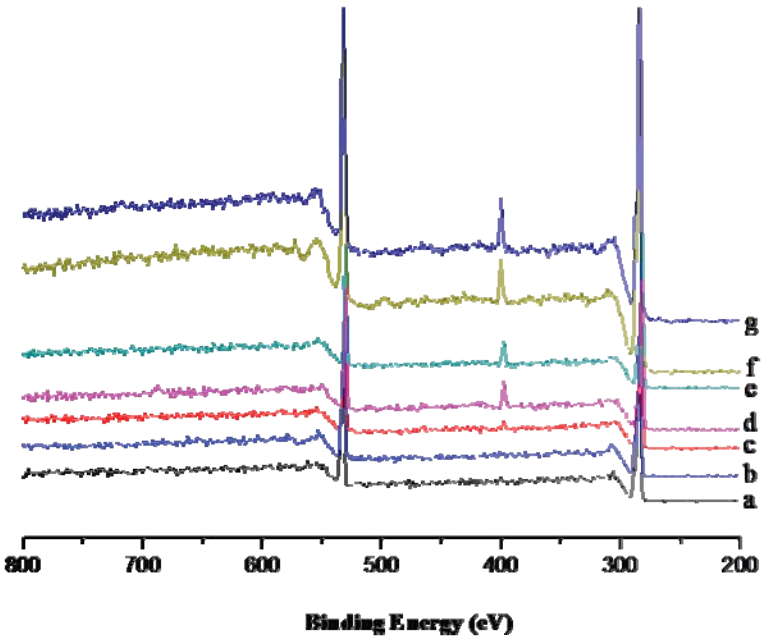


Figure 4.10 The survey XPS spectra of (a) neat PCL, (b) aminolyzed PCL with 0.20 g/ml HMD treatment, (c) activated PCL, (d) PCL immobilized with 3 mg/ml gelatin type-A solution, (e) 3 mg/ml gelatin type-B solution, (f) 3 mg/ml bovine serum albumin solution, and (g) 3 mg/ml crude bone protein solution.

4.4 Biological Characterizations

4.4.1 Cytotoxicity

4.4.1.1 Direct Cytotoxicity

Direct cytotoxicity test is a method to evaluate the toxic effect of proteins directly to cells. The effect was investigated with mouse calvaria-derived pre-osteoblastic cells (MC3T3-E1), based on the initial 40,000 cells/well seeded. MC3T3-E1 were cultured in 24-well culture plate to allow cell growth. The test was conducted by adding gelatin type-A, gelatin type-B, BSA protein and crude bone protein extracts in 2% serum-containing MEM diluted with 7-day extraction medium in seeded cells as mentioned above and cultured for 1, 2, and 3 d. Figure 4.11 shows that the viability of MC3T3-E1, cultured with 2% serum-containing MEM extraction media adding with all types of proteins for 1, 2 and 3 days, was increased with increasing the culturing time in the respective media. The viability of cells (relative with control TCP) of all material is more than 80 %. All of the obtained results clearly suggested that all types of proteins, released no substances at levels that were harmful to cells.

4.4.1.2 Indirect Cytotoxicity

The potential use of these fibrous scaffolds as bone scaffolds was first evaluated by an indirect cytotoxicity test with mouse calvaria-derived pre-osteoblastic cells (MC3T3-E1), based on the initial 40,000 cells/well seeded. The test was carried out on TCP (control), the neat PCL, aminolyzed PCL, activated PCL, gelatin type-A, gelatin type-B, BSA and CBP immobilized PCL fibrous scaffolds. MC3T3-E1 were cultured in a 24-well culture plate in 2 % serum-containing MEM extraction medium from all type of fibrous scaffolds for 1, 2, and 3 days. Figure 4.12 shows that the viability of MC3T3-E1, cultured with 2 % serum-containing MEM diluted with 1-day extraction media prepared by all types of modified scaffolds, was increased with increasing the culturing time in the respective media and the viability of cells on all types of material measured by MTT assay was more

than 80 %. All of the obtained results clearly suggested that all types of the PCL fibrous scaffolds, released no substances at levels that were harmful to cells.

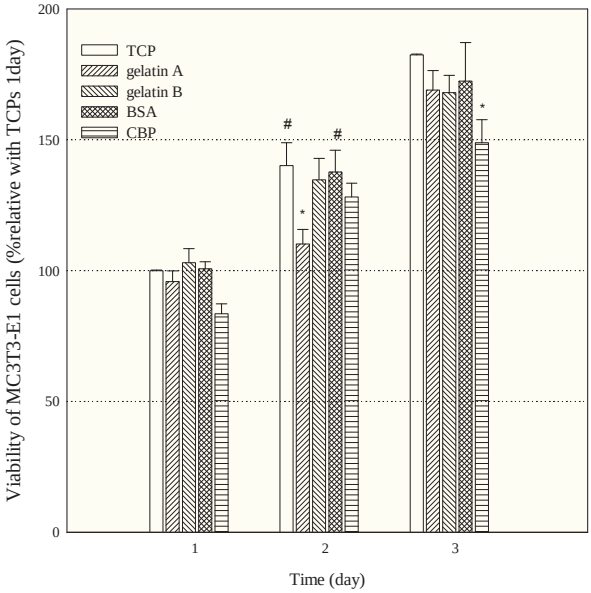


Figure 4.11 The viability of MC3T3-E1, cultured with 2% serum-containing MEM extraction media adding with all types of proteins for 1, 2 and 3 days. Statistical significance: $^{*}p < 0.05$ compared with control and $^{\#}p < 0.05$ compared to the neat PCL fibrous scaffolds at any given time point.

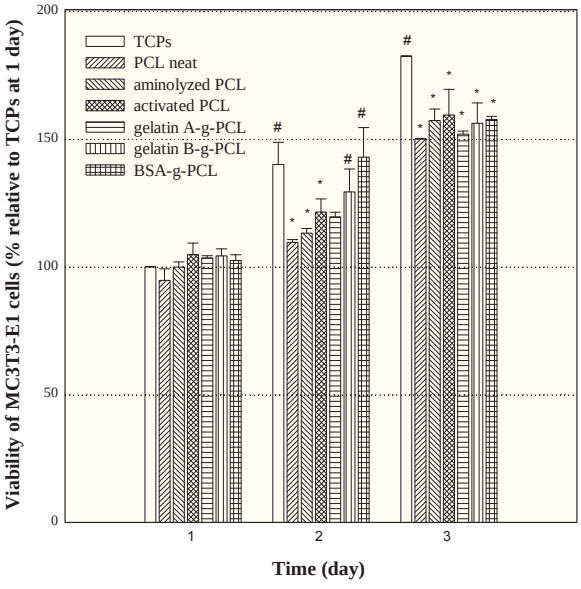


Figure 4.12 The viability of MC3T3-E1, cultured with 2% serum-containing MEM extraction media from all type of PCL fibrous scaffolds for 1, 2, and 3 days relative to TCPS at 1 day Statistical significance: $*p < 0.05$ compared with control and $^{\#}p < 0.05$ compared to the neat PCL fibrous scaffolds at any given time point.

4.4.2 Cell Attachment and Proliferation

The potential for use of the neat and the modified PCL fibrous scaffolds was further evaluated by determination their ability to support both the adhesion and the proliferation of MC3T3-E1. The viability of the cells that had been cultured on the surface of TCPS for 2 h was taken as the basis to arrive at the relative viability shown in a Figure. Figure 4.13 shows the attachment of MC3T3-E1 on the surfaces of TCPS, neat PCL, aminolyzed PCL, activated PCL, and protein-immobilized PCL at 2, 4, and 6 h after cell seeding in terms of viability. On TCPS, the number of the attached cells increased rapidly from ~100% at 2 h after cell seeding to ~257% at 6 h after cell seeding, based on the initial number of cells seeded (40,000 cells/well). While, the number of cells attached on these fibrous scaffolds was lower in comparison with that on TCPS at any given time point. There was the most viability of cells on crude bone protein-immobilized PCL fibrous scaffold among various types of the modified fibrous scaffolds. This obtained result suggested that the cells prefer to adhere on CBP-immobilized PCL fibrous scaffold rather than other modified scaffolds. However, The lesser viability of cells in the attachment period on various types of the fibrous scaffolds in comparison with that on TCPS could be due to the lesser number of cells that were able to attach on the rough surface of the fibrous scaffolds in comparison with the smoother and hydrophilic surface of TCPS.

Figure 4.14 shows the proliferation of MC3T3-E1 on the surfaces of TCPS, neat PCL, aminolyzed PCL, activated PCL and protein-immobilized PCL on day 1, 2, and 3 after cell culture in terms of viability (%relative to TCPS at day1). On TCPS, the number of cells increased from ~100% at 1 day after cell culture to ~133 % at 3 days after cell culture, based

on the initial 40,000 cells/well seeded. In comparison with that on TCPS, the viability of the cells cultured on various types of PCL fibrous scaffolds were significantly higher at any given time point. The viability of cells proliferated on these fibrous scaffolds, at day 3, was higher than TCPS of about (3 to 4) fold for neat PCL, aminolyzed PCL, and activated PCL and about 8 fold for all type of protein-immobilized PCL. The improvement was achieved with the protein-immobilized PCL fibrous scaffolds on day 3 after cell culture. The greater number of cells in the proliferation period on all types of fibrous scaffolds could be because of high surface area to volume and high porosity of the electrospun fibrous scaffolds through which the cells were able to penetrate into the scaffolds. Among the various modified PCL fibrous scaffolds, the BSA-immobilized PCL fibrous scaffolds provided the most significant improvement in the ability to support the proliferation of the cells which could be due to the protein-containing and more hydrophilic surface of the substrate.

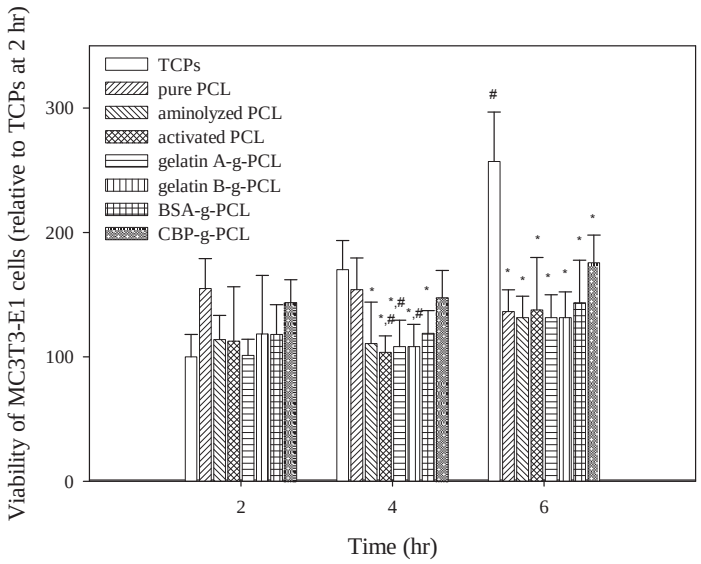


Figure 4.13 Attachment of MC3T3-E1 that had been seeded or cultured on the surfaces of TCPS and the neat and the modified PCL fibrous scaffolds for 2, 4, and 6 h. Statistical significance: $^{*}p < 0.05$ compared with control and $^{\#}p < 0.05$ compared to the neat PCL fibrous scaffolds at any given time point.

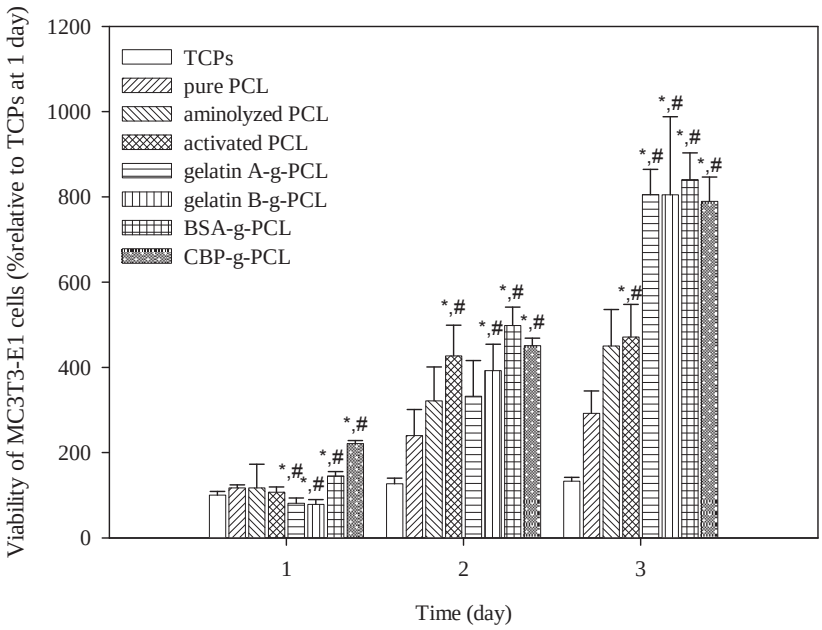


Figure 4.14 Proliferation of MC3T3-E1 that had been seeded or cultured on the surfaces of TCPS and the neat and the modified PCL fibrous scaffolds for 1, 2, and 3 days. Statistical significance: $^{*}p < 0.05$ compared with control and $^{\#}p < 0.05$ compared to the neat PCL fibrous scaffolds at any given time point.

4.4.3 Cell Morphology

Table 4.6 and 4.7 show selected SEM image (magnification = 2000X; scale bar = 10 μm) of MC3T3-E1 that were cultured on the surfaces of neat PCL, activated PCL and gelatin type-A, gelatin type-B, bovine serum albumin, and crude bone-immobilized PCL at different time points. These images provided snap shots in time that revealed the morphology of the cells and interaction between the cells and the tested surfaces. At 2 hours after cell seeding, based on the initial 40,000 cells/well seeded, the morphology of cells on almost all types of the modified PCL scaffolds became round. Exceptionally, the morphology of cells on BSA-immobilized and CBP-immobilized started to extend their cytoplasm and became ellipse. At 4 h after cell seeding, the majority of the cells on all types of modified PCL scaffolds extended their cytoplasm, an evidence of the ability of the cells to

attach on the modified surface. At 6 h after cell seeding, expansion of the cytoplasm of the majority of the cells was evident. The majority of MC3T3-E1 that had been seeded on the surfaces of unmodified PCL fibrous scaffolds for 4 h was remained round, but a closer examination around the edge of the cells revealed an evidence of filopodia. The majority of the cells were evidently expanded after 6 h of cell seeding. On the other hand, the majority of the cells seeded on the surfaces of various types of modified PCL fibrous scaffolds showed an evidence of the extension of their cytoplasm on the fibrous surface even at 4 h after cell seeding. These results suggested that the cells prefer the fibrous surfaces of modified PCL over that of the unmodified. At 1,2, and 3 days after cell seeding, the majority of the cells seeded on the surfaces of all types of modified PCL fibrous scaffolds expanded over the area of the scaffolds which was the most expansion on the surface of BSA-immobilized and CBP-immobilized PCL fibrous scaffolds. From the attachment, proliferation and cell morphology results, we can suggest that the cell prefer to grow and expand on BSA-immobilized and CBP-immobilized PCL fibrous scaffolds over other materials.

Table 4.3 Selected SEM images of cultured specimens, i.e., glass (i.e., control), neat PCL, aminolyzed PCL, activated PCL, and protein-immobilized PCL fibrous scaffolds at various time points after MC3T3-E1 were seeded on their surfaces (magnification = 2,000X; scale bar = 10 μm)

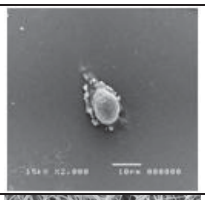
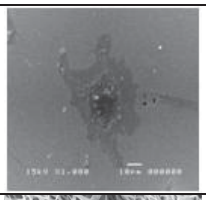
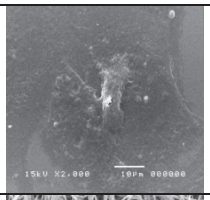
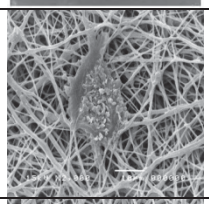
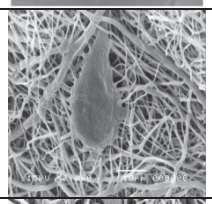
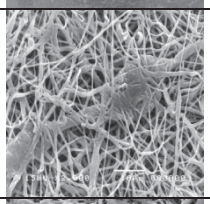
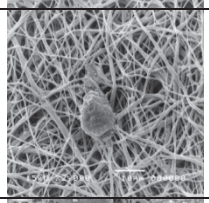
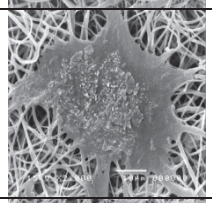
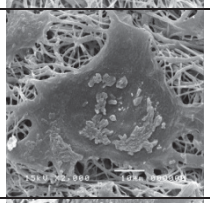
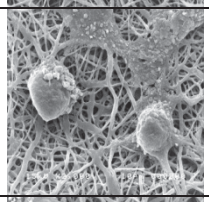
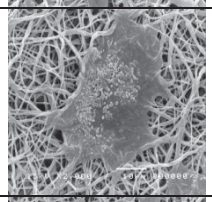
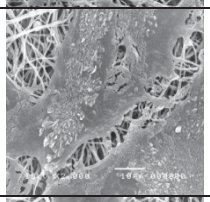
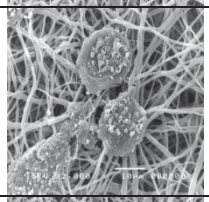
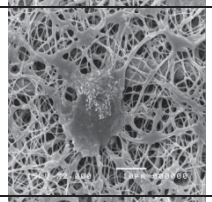
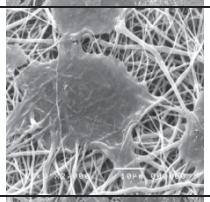
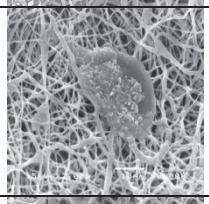
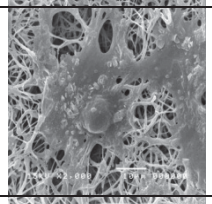
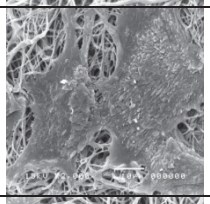
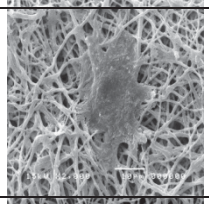
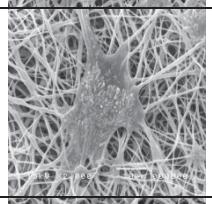
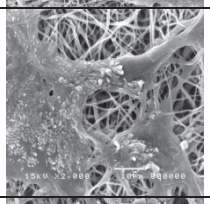
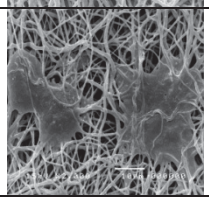
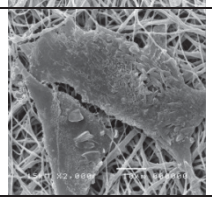
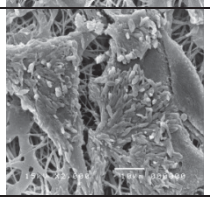
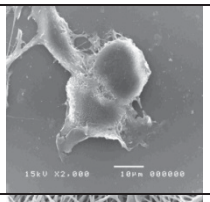
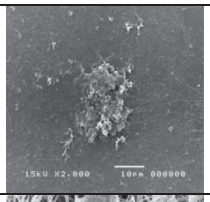
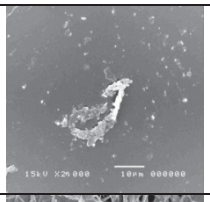
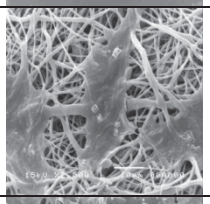
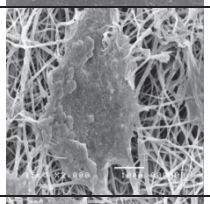
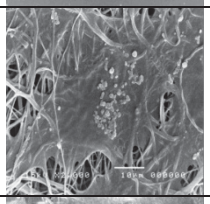
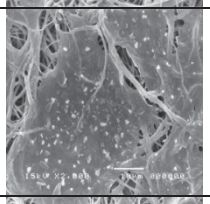
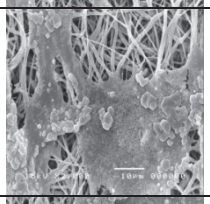
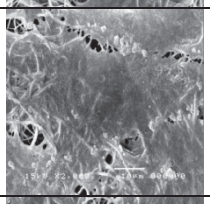
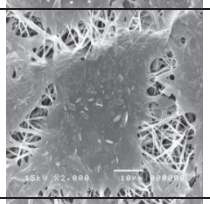
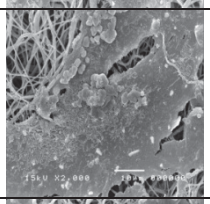
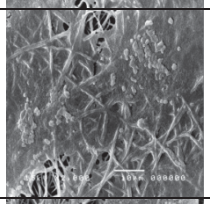
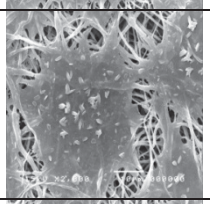
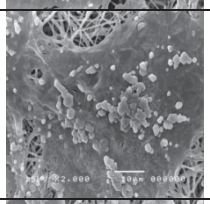
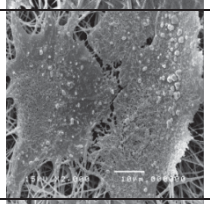
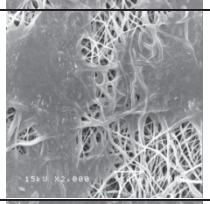
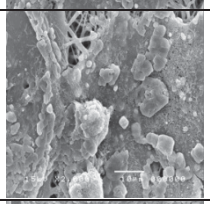
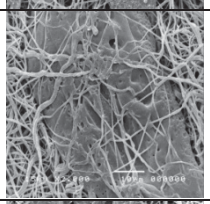
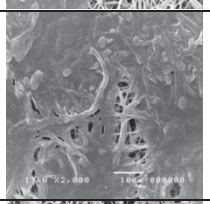
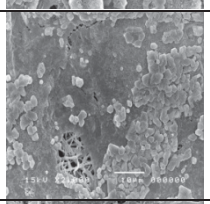
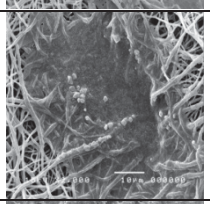
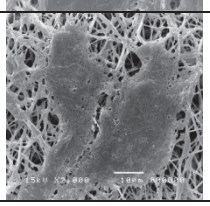
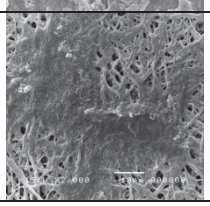
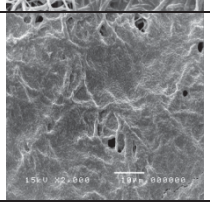
Material	2 h	4 h	6 h
Glass (control)			
Neat PCL			
Aminolyzed PCL			
Activated PCL			
Gelatin A immobilized PCL			
Gelatin B immobilized PCL			
BSA immobilized PCL			
CBP immobilized PCL			

Table 4.4 Selected SEM images of cultured specimens, i.e., glass (i.e., control), neat PCL, aminolyzed PCL, activated PCL, and protein-immobilized PCL fibrous scaffolds at various time points after MC3T3-E1 were seeded on their surfaces (magnification = 2,000X; scale bar = 10 μm)

Material	1 day	2 day	3 day
	2000x	2000x	2000x
Glass(control)			
Neat PCL			
Aminolyzed PCL			
Activated PCL			
Gelatin A immobilized PCL			
Gelatin B immobilized PCL			
BSA immobilized PCL			
CBP immobilized PCL			

4.4.4 Alkaline Phosphatase Activity (ALP)

The ability for these PCL fibrous scaffolds to support differentiation, in addition to attachment and proliferation, of cultured cells is another important purpose suggesting potential for use of the scaffold. Alkaline phosphatase is used as an osteoblastic differentiation marker, as it is produced only by cells showing mineralized ECM. The ALP activity of MC3T3-E1 on TCPS (i.e. controls), neat PCL, aminolyzed PCL, activated PCL, and protein-immobilized PCL were evaluated at 3 and 7 days in culture. Figure 4.15 apparently shows the amount of ALP synthesized by the cells that were cultured on TCPS and all of the fibrous scaffolds increased with the initial increase in time in culture. In comparison with other substrates, BSA immobilized PCL fibrous scaffolds exhibited the highest ALP activity of MC3T3-E1 which is close to that of the activated PCL and TCPS at day 7 of cell culturing time. From the obtained results, it was suggested that BSA-immobilized PCL fibrous scaffold was the best among the fibrous scaffolds that promoted both proliferation and differentiation of MC3T3-E1. However, additional long term experiments in order to clarify the effect of scaffolds on the differentiation of osteoblasts are currently determined.

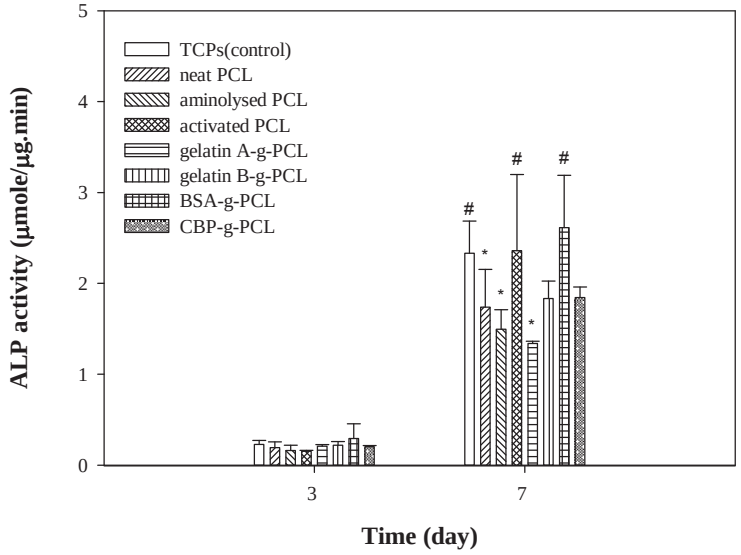


Figure 4.15 Alkaline phosphatase activity (ALP) of MC3T3-E1 that were cultured on the surfaces of TCPS and the neat and the modified PCL fibrous scaffolds for 3 and 7 d. Statistical significance: *p < 0.05 compared with control and $^{\#}p$ < 0.05 compared to the neat PCL fibrous scaffolds at any given time point

4.4.5 Mineralization

Mineralization was quantified by Alizarin Red-S which is a dye that binds selectively calcium salts. The strain was extracted with 10 % cetylpyridinium chloride in 10 mM sodium phosphate for 1 hour and the absorbance of collected dye was read at wavelength 570 nm in spectrophotometer (A Thermo Spectronic Genesis10 UV-visible spectrophotometer). The absorbance is relative to the quantity of deposited minerals on the materials as shown in Figure 4.16. The images of scaffolds seeded with MC3T3-E1 for 21 days and stained with Alizarin Red-S illustrated in Figure 4.17 confirmed that the above data where high intensity of stained minerals were observed on all type of immobilized PCL scaffolds. and. The CBP-immobilized PCL scaffolds showed the highest mineral deposition compared with control, neat PCL, and other modified materials. This result can be used to support that the crude bone protein immobilization

is an attractive method to be used for fabrication of further developed fibrous scaffolds for bone tissue engineering.

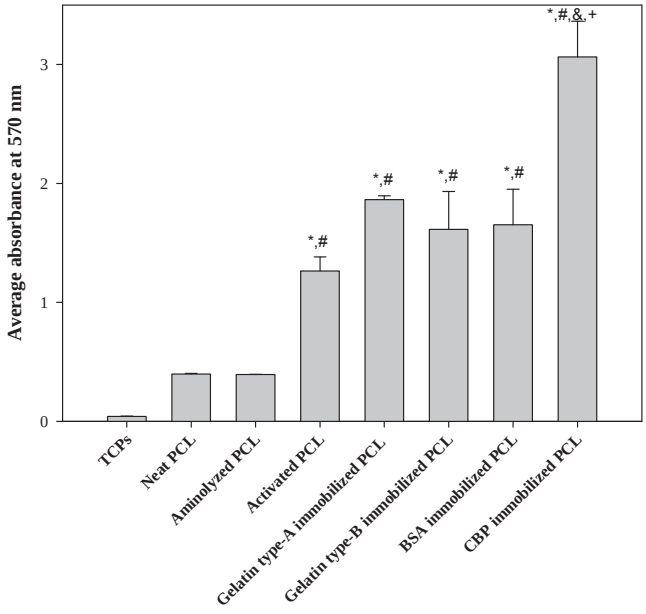


Figure 4.16 Quantification of mineral deposition in MC3T3-E1 at 21 d by the method of Alizarin Red-S staining measured the absorbance by UV-vis spectrometer at 570 nm. Statistical significance: $^{*}p < 0.01$ compared with control, $^{\#}p < 0.01$ compared to the neat PCL, $^{\&}p < 0.01$ compared with gelatin type-A immobilized PCL, and $^{+}p < 0.01$ compared with gelatin type-B immobilized PCL fibrous scaffolds at any given time point.

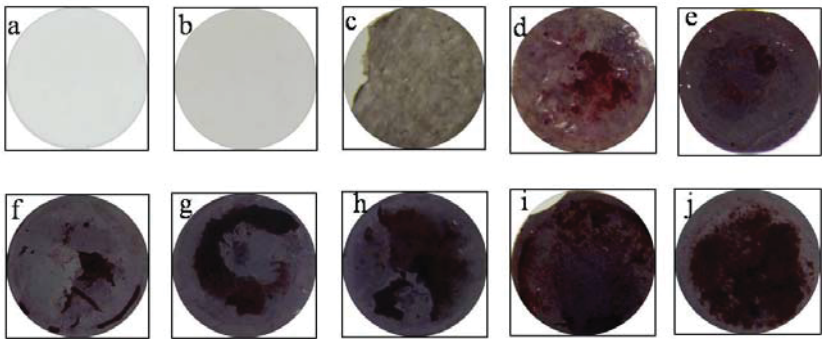


Figure 4.17 Image of Alizarin Red-S staining for the mineralization in MC3T3-E1 cells for 21 d: TCPS without (a) and with (b) cells , neat PCL without (c) and with (d) cells, aminolyzed (e) and activated PCL (f),and gelatin type-A

(g), gelatin type-B (h), bovine serum albumin (i) and crude bone protein (j) immobilized PCL fibrous scaffold

5. Conclusions

Polycaprolactone fibrous scaffolds were prepared by electrospinning process from a neat 12 % w/v PCL solution in 50:50 v/v DCM/DMF. The PCL electrospun fibrous scaffolds with a thickness of (130 ± 5) μm were obtained. The scaffold was subsequently immersed in various concentrations of 1,6-hexamethylene diamine (HMD) / isopropanol (IPA) solution (0.04, 0.06, 0.08, 0.10, 0.20, and 0.40 g/ml) for 2 hours at 30 °C. To determine the optimum concentration of HMD used in the step of aminolysis, ninhydrin method, degradation experiment, water retention experiment and SEM observation were used. The results show that the optimum condition for aminolysis are 0.20 g/ml HMD treatment for 2 hours at 30 °C. Density, porosity, and pore volume were evaluated to characterize the electrospun scaffolds. The NH_2 density on the aminolyzed PCL surface was confirmed and quantified using ninhydrin method. The NH_2 density increased with increasing 1,6-hexamethylenediamine concentration. However, when the concentration of 1,6-hexamethylenediamine is greater than 0.20 g/ml, the structural morphology of the electrospun PCL fiber scaffolds became worse. In the other word, water contact angle slightly decreased with increasing HMD concentration. This means that aminolysis can improve the hydrophilicity of the surface. Macromolecules i.e. gelatin type-A, gelatin type-B, bovine serum albumin, and crude bone protein were further immobilized using *N,N'*-disuccinimidyl carbonate (DSC) as a coupling agent. Various techniques; Attenuated Total Reflectance-Fourier Transform Infrared Spectrometer (ATR-FTIR), X-ray Photospectroscopy (XPS), Scaning Electron Microscopy (SEM), and water contact angle measurement were used to monitor the scaffold surfaces after each modification step. In XPS experiment, The N_{1s}/C_{1s} ratio was increased after immobilization with proteins (gelatin type-A, gelatin type-B, bovine serum albumin and crude bone protein) due to the large amount of nitrogen atom in protein structure was introduced. The potential use of the surface-modified PCL scaffolds as bone scaffolds was evaluated with a

murine pre-osteoblastic cell line (MC3T3-E1). The cytotoxicity test showed all types of proteins and PCL fibrous scaffolds released no substances at levels that were harmful to cells. The number of cells attached on these fibrous scaffolds was lower in comparison with that on TCPS at any given time point. There was the most viability of cells on crude bone protein-immobilized PCL fibrous scaffold among various types of the modified fibrous scaffolds. MC3T3-E1 proliferation was improved remarkably on the modified surface, with the cells growing on the bovine serum albumin-immobilized PCL fibrous scaffolds showing the greatest proliferation after cell culture as well as the highest ALP activity. In long term experiments, the image of scaffolds seeded with MC3T3-E1 for 21 days and stained with Alizarin Red-S and quantification of deposited minerals measured by UV-vis spectrometer confirmed that high intensity of stained minerals were observed on all type of immobilized PCL scaffolds. The CBP-immobilized PCL scaffold showed the highest mineral deposition compared with control, neat PCL, and other modified materials. This result supported that the crude bone protein immobilization was able to induce the cell differentiation to bone the most. All the obtained results suggested that bovine serum albumin and crude bone protein immobilization are an attractive method to fabricate of further developed fibrous scaffolds for bone tissue engineering.

6.REFERENCES

Ayhan, H. and Ayhan, F. (2002) In Vitro Evaluation of 3T3 and MDBK Cells Attachment and Proliferation on Collagen and Fibronectin Immobilized NonwovenPolylactide Matrices. Journal of Bioactive and Compatible Polymers., 17, 463-476.

Boelgen, N., Menceloglu, Y.Z., Acatay, K ., Vargel, I., and Piskin, E. (2005) In vitro

and in vivo degradation of non-woven materials made of poly(ε-caprolactone) nanofibers prepared by electrospinning under different

conditions. Journal of Biomaterials Science. Polymer Edition,16(12), 1537-1555.

Burg, K.J.L., Porter, S.,and Kellam, J.F. (2000) Biomaterial developments for bone tissue engineering. Biomaterials , 21, 2347-2359.

Calvert, J.W., Marra, K.G., Cook, L., Kumta, P.N., DiMilla, P.A., and Weiss, L.E. (2000) Characterization of osteoblast-like behavior of cultured bone marrow stromal cells on various polymer surfaces. Journal of Biomedical Materials Research, 52(2), 279-284.

Carter, D. C. and Ho, J. X. (1994) Structure of Serum Albumin. Advance in Protein Chemistry., 45, 153-203.

Cheng, Z., and Teoh, S.-H. (2004) Surface modification of ultra thin poly(ε-caprolactone) films using acrylic acid and collagen. Biomaterials, 25(11), 1991-2001.

Edlund, U., Dånmark, S., and Albertsson, A.-C. (2008) A Strategy for the Covalent Functionalization of Resorbable Polymers with Heparin and Osteoinductive

Growth Factor. Biomacromolecules, 9(3), 901-905.

Figge, J., Rossing, T. H. and Fencl, V. (1991) The Role of serum-proteins in Acid-Base Equilibria. The Journal of Laboratory and Clinical Medicine., 117, 453 - 467.

Gao, C., Guan, J., Zhu, Y., and Shen, J. (2003) Surface Immobilization of Bioactive Molecules on Polyurethane for Promotion of Cytocompatibility to Human Endothelial Cells. Macromolecular Bioscience, 3(3-4), 157-162.

Guan, J., Gao, C., Feng, L., and Shen, J. (2001) Surface modification of polyurethane for promotion of cell adhesion and growth 1: Surface photo-grafting with N,N-dimethylaminoethyl methacrylate and cytocompatibility of the modified surface. Journal of Materials Science: Materials in Medicine., 12 (5), 447-452

Habraken,W.J.E.M., Wolke, J.G.C., and Jansen, J.A. (2007) Ceramic composites

as matrices as matrices and scaffolds for drug delivery in Tissue engineering.

Adanced drug delivery review, 59, 234-248.

Hou, Q., Grijpma, D. W., Feijen, J. (2003) Porous polymeric structures for tissue engineering prepared by a coagulation, compression moulding and salt leaching technique. Biomaterials 24(11), 1937-1947.

Huang,W., Carlsen,B., Wulur,I., Rudkin,G., Ishida,K., Wu,B., Yamaguchi,D.T., Miller,T.A. (2004) BMP-2 exerts differential effects on differentiation of rabbit bone marrow stromal cells grown in two-dimensional and three-dimensional systems and is required for in vitro bone formation in a PLGA scaffold. Experimental Cell Research , 299, 325– 334

Hutmacher, D. W. (2000) Scaffolds in tissue engineering bone and cartilage. Biomaterials, 21, 2259.

Jeon,O., Songa,S.J., Kanga,S-W., Putnam,A.J., and Kim,B-S. (2007) Enhancement of ectopic bone formation by bone morphogenetic protein-2 released from a heparin-conjugated poly(L-lactic-co-glycolic acid) scaffold Biomaterials; 28: 2763–2771

Lee, S-H., and Shin, H. (2007) Matrices and scaffolds for delivery of bioactive molecules in bone and cartilage tissue engineering. Advanced drug delivery reviews ,59, 339-359.

LeGero, R.Z. (2002) Properties of osteoconductive biomaterials: calcium phosphates. Clin Orthop Relat Res, 395, 81-98.

Ma, Z., Gao, C., Yuan, J., Ji, J., Gong ,Y., and Shen,J. (2002) Surface modification of poly-L-lactide by photografting of hydrophilic polymers towards improving its hydrophilicity. Journal of Applied Polymer Science, 85 (10), 2163 – 2171

Mattanavee, W., Suwantong, O., Puthong, S., Bunaprasert, T., Hoven, V.P., and Supaphol, P. (2009) Immobilization of Biomolecules on the

Surface of Electrospun Polycaprolactone Fibrous Scaffolds for Tissue Engineering. ACS Applied Materials & Interfaces.

Meinel,L., Zoidis,E. Zapf,J. Hassa,P. Hottiger,M.O.,Auer,J.A., Schneider,R., Gander,B., Luginbuehl,V., Wolfisberger,R.B., Illi,O.E., Merkle,H.P., and Rechenberg B.von. (2003) Localized insulin-like growth factor I delivery to enhance new bone formation. Bone; 33 : 660–672

Mikos, A.G., Bao, Y., Cima, L.G., Ingber, D.E., Vacanti, J.P., Langer, R. (1993) Preparation of poly (glycolic acid) bonded fibres structures for cell attachment and transplantation. Journal of biomedical materials research, 27, 183-189.

Mikos, A.G., Sarakinos, G., Vacanti, J.P., Langer, R., and Cima, L.G. (1996) Biocompatible polymer membranes and methods of preparation of three dimensional membrane structures. United States Patent 5514378

Mikos, A.G., Thorsen, A.J., Czerwonka, L.A., Bao, Y., Langer, R.(1994) Preparation and characterisation of poly(L-lactic acid) foams. Polymer, 35, 1068-1077.

Park,K., Jung, H.J., Kim, J-J., Ahn, K-D. and Han, D.K. (2006) Acrylic Acid-Grafted Hydrophilic Electrospun Nanofibrous Poly(L-lactic acid) Scaffold. Macromolecular Research, 14 (5), 552-558

Prasansuklarb, A. (2008) Osteoblastic cell growth and enzymatic degradation of different aliphatic polyester scaffolds. Master thesis.The Petroleum and Petrochemical College, Chulalongkorn University.

Saito,N., Okada,T., Horiuchi,H., Ota,H., Takahashi,J., Murakami,N., Nawata,M., Kojima,S., Nozaki,K., and Takaoka,K. (2003) Local bone formation by injection of recombinant human bone morphogenetic protein-2 contained in polymer carriers. Bone , 32, 381–386

Salgado,A.J., Coutinho,O.P., and Reis,R.L. (2004) Bone Tissue Engineering:State of the Art and Future Trends. Macromolecular Bioscience; 4 : 743–765

Santiago, L.Y., Nowak, R.W., Rubin, J.P., and Marra, K.G. (2006) Peptide-surface modification of poly(caprolactone) with laminin-derived

sequences for adipose-derived stem cell applications. Biomaterials, 27(15), 2962-2969.

Savarino, L., Baldini, N., Greco, M., Capitani, O., Pinna, S., Valentini, S., Lombardo, B., Esposito, M.T., Pastore, L., Ambrosio, L., Battista, S., Causa, F., Zeppetelli, S., Guarino, V., and Netti, P.A. (2007) The performance of poly-ε-caprolactone scaffolds in a rabbit femur model with and without autologous stromal cells and BMP4. Biomaterials, 28(20), 3101-3109.

Shen, H., Hu, X., Yang, F., Bei, J., and Wang, S. (2009) The bioactivity of rhBMP-2 immobilized poly(lactide-co-glycolide) scaffolds. Biomaterials, 30(18), 3150-3157.

Sumner , D.R., Turner , T.M., Urban , R.M., Leven, R.M., Hawkins ,M., Nichols, E.H., McPherson, J.M., and Galante, J.O. (2001) Locally delivered rhTGF-β_2 enhances bone ingrowth and bone regeneration at local and remote sites of skeletal injury. Journal of Orthopaedic Research, 19, 85-94.

Venugopal, J.R., Low, S., Choon, A.T., Kumar, A.B., and Ramakrishna, S. (2008) Nanobioengineered Electrospun Composite Nanofibers and Osteoblasts for Bone Regeneration. Artificial Organs , 32(5), 388–397.

Wang,X., Wenk,E., Zhang,X., Meinel,L., Vunjak-Novakovic,G., and Kaplan,D.L. (2009) Growth factor gradients via microsphere delivery in biopolymer scaffolds for osteochondral tissue engineering. Journal of Controlled Release, 134, 81–90

Ward, A.G.; Courts, A. (1977) The Science and Technology of Gelatin. New York: Academic Press

Wei,G., Jin,O., Giannobile,W.V., and Ma.P.X. (2007) The enhancement of osteogenesis by nano-fibrous scaffolds incorporating rhBMP-7 nanospheres. Biomaterials, 28, 2087–2096

Wenk,E., Meinel,A.J., Wildy,S., Merkle,H.P., and Meinel,L. (2009) Microporous silk fibroin scaffolds embedding PLGA microparticles for

controlled growth factor delivery in tissue engineering. Biomaterials, 30, 2571–2581

Whang, K., Thomas, C. H., Healy, K. E. and Nuber, G. (1995) A novel method to fabricate bioabsorbable scaffolds. Polymer, 36, 837-842

Woo,B.H., Fink,B.F., Page,R., Schrier,J.A., Jo,Y.W., Jiang,G., DeLuca,M., Vasconez,H.C., and DeLuca,P.P. (2001) Enhancement of Bone Growth by Sustained Delivery of Recombinant Human Bone Morphogenetic Protein-2 in a Polymeric Matrix. Pharmaceutical Research,18(12)

Yoneda,M., Teraia,H., Imaia,Y., Okada,T., Nozaki,K.,HikaruIno, Miyamoto,S., and

Takaoka,K. (2005) Repair of an intercalated long bone defect with a Synthetic biodegradable bone-inducing implant. Biomaterials, 26, 5145–5152

Yoshimoto, H., Shin, Y.M., Terai, H., and Vacanti, J.P. (2003) A biodegradable nanofiber scaffold by electrospinning and its potential for bone tissue engineering. Biomaterials, 24(12), 2077-2082.

Zhu, Y., Chian, K.S., Chan-Park, M.B., Mhaisalkar, P.S., and Ratner, B.D. (2006) Protein bonding on biodegradable poly(l-lactide-co-caprolactone) membrane for esophageal tissue engineering. Biomaterials, 27(1), 68-78.

Zhu, Y., Cao, Liu, Y., and Shen, J. (2004) Endothelial cell functions in vitro cultured on poly(L-lactic acid) membranes modified with different methods. Journal of Biomedical Materials Research Part A, 69A(3), 436-443.

Zhu, Y., Gao, C., Liu, X., and Shen, J. (2002a) Surface Modification of Polycaprolactone Membrane via Aminolysis and Biomacromolecule Immobilization for Promoting Cytocompatibility of Human Endothelial Cells. Biomacromolecules, 3(6), 1312-1319.

Zhu, Y., Gao, C., and Shen, J. (2002 b) Surface modification of polycaprolactone with poly(methacrylic acid) and gelatin covalent

immobilization for promoting its cytocompatibility. Biomaterials, 23(24), 4889-4895.

DEVELOPMENT OF POROUS HYDROXYAPATITE PARTICLES AS CARRIERS OF PROTEINS FOR BONE TISSUE ENGINEERING

Sujittra Chaisuntharanon,[1] Prasit Pavasant,[2] and Pitt Supaphol [1,*]

[1] The Petroleum and Petrochemical College and The Center for Petroleum, Petrochemicals and Advanced Materials (C-PPAM), Chulalongkorn University, Bangkok 10330, Thailand

[2] Department of Anatomy, Faculty of Dentistry, Chulalongkorn University, Bangkok 10330, THAILAND

4.1 Abstract

Incorporation of proteins by physical absorption within porous Hydroxyapatite (HAp)-based implants has been frequently reported for orthopaedic uses whereas sequential release is hardly properly controlled. This work aims at developing HAp particles as a controlled release carrier of proteins. HAp carriers were synthesized by coprecipitation technique from dicalcium phosphate dihydrate ($CaHPO_4 \cdot 2H_2O$, DCPD) and calcium carbonate ($CaCO_3$). Incorporation of proteins was accomplished during the coprecipitation of the two reactants. Desorption behavior of proteins from HAp particles will be investigated by UV-Visible spectrophotometry.

(**Key-words**: Hydroxyapatite, protein carrier)

4.2 Introduction

Hydroxyapatite (HAp), having a chemical formula $Ca_{10}(PO_4)_6(OH)_2$ is a naturally occurring inorganic constitutent of tooth enamel, dentine, bone and other hard tissues of vertebrates. It has been widely used as bone filler, spacer, and bone graft. HAp has been well-recognized as it is an excellent affinity to biological substances such as collagen, proteins, enzymes, cells, and viruses, biocompatible, osteoconductive and bioactive material (Liu, T-Y. *et al*., 2005). With the osteoconductive properties, HAp ceramic has been

* Authors to whom correspondence should be addressed: pitt.s@chula.ac.th (P. Supaphol)

also investigated as scaffolds for cell delivery and tissue engineering. In addition, porous hydroxyapatie ceramics have a considerable potential as carriers for controlled drug release (Ijntema, K. *et al.,* 1994), protein delivery agent, catalyst, and absorbent (Li, Y. *et al*., 2008). The apatite crystal often used to carry drugs or proteins has regularly a stoichiometric composition, i.e., Ca/P=1.67 (Liu, T-Y. *et al*., 2005). The adsorption of protein onto HAp is important to accelerate tissue healing when placed in vivo (Yang, Q. *et al*., 2006) in a variety of oral or osseous biological events. HAp has also adsorptive capabilities with respect to proteins and biologically active molecules, such as osteogenic agents and growth factors. Up to now, many methods such as sol-gel, precipitation, hydrothermal, mechno-chemical, spray pyrolysis, freeze-drying and electrochemical deposition have been developed to prepared HAp powders. In these methods, wet chemical process was usually used to prepare HAp powders because it is easy to operate and need not any expensive equipments (Cao, Li-yun, *et al*., 2005).

The interaction of proteins with hydroxyapatite appeared to depend on the overall protein charge, the number of acidic and basic groups, and the specific protein structure (Ijntema, K. *et al*., 1994).

The purpose of this study is to fabricate proteins-HAp powder to control the release rate behavior of different proteins.

4.3 Experimental section

4.3.1 Materials

- Dicalcium phosphate dihydrate (DCPD; Fluka, Germany)
- Calcium carbonate ($CaCO_3$; Carlo Erba, Italy)
- Tris-base (Tris[hydroxymethyl]amino methane) (Sigma-Aldrich, USA)
- Nitric acid (ACS reagent 69%; J.T.Baker, USA)
- Ovalbumin (OVA; Sigma-Aldrich, USA)
- Gelatin type B (Sigma-Aldrich, USA)

- Bovine serum albumin (BSA; Sigma-Aldrich, USA)
- Sodium phosphate monobasic (NaH_2PO_4) and sodium phosphate dibasic (Na_2HPO_4; Ajex Finechem, Australia)

4.3.2 Preparation of Protein-Loaded Hydroxyapatite

Calcium hydrogen phosphate dihydrate ($CaHPO_4.H_2O$, DCPD) and calcium carbonate ($CaCO_3$) were used as precursors of Ca and P to prepare protein-loaded hydroxyapatite. The molar ratios of Ca to P were fixed at 1.67 which mixed with nitric acid 1 mol/l at 75 ºC for 1 h under stirring. Then, pour distilled water at room temperature following protein. Ovalbumin (Sigma-Aldrich A-5253), Gelatin type B, Bovine serum albumin (BSA, Aldrich A-3912) and Crude bone protein from pork bone were selected as candidate proteins in this study. The proteins aqueous solution were prepared by dissolving proteins powder or pellet into distilled water for each synthesis. Regulated pH at a constant value, tris(hydroxymethyl) aminomethane. The aggregates were rinsed with the distilled water until pH=7 (DI water was boiled and decarbonated before use) and further centrifuged at 4500 rpm for 10 mins, freezed at -45 ºC and lyophilized at -50 ºC. The samples were kept in dessicator until used.

4.3.3 Crude Bone Protein preparation

CBP was extracted from the pork bone. In particular, bone was initially washed and cleaned thoroughly in tap water and then sectioned into small pieces with a high speed motor machine. Pieces of bones were further crushed into powder in liquid nitrogen. Then, the as-prepared powder was immersed in 0.6 N HCl at 4 °C. After three days, the bony solution was centrifuged and the supernatant was collected, dialyzed for 48 h and lyophilized. The dry CBP was kept in desiccators until use (Hariraksapitak, *et al*., 2009).

4.3.4 Characterization

4.3.4.1 Thermogravimetric Analysis (TGA)

The relative amount of the proteins associated with the HAp was determined using thermogravimetric analysis, TG-DTA (Perkin Elmer) instrument under N_2 flow of 5 ml/min. The heating process was conducted from 30-950 °C at a rate of 10 °C/min.

4.3.4.2 Fourier-transformed infrared spectrophotometer (FT-IR)

A Thermo Nicolet Nexus® 670 Fourier-transformed infrared spectrophotometer (FT-IR) was used to investigate chemical functionalities of hydroxyapatite powder by the KBr disk method. Hydroxyapatite powders were randomly selected from each group of samples and detected for the FT-IR spectra with a resolution of 4 cm^{-1} in the range of 4000-400 cm^{-1} and were averaged from 32 scans.

4.3.4.3 Autosorb-1

The BET method uses gas with a known adsorption area per 1 g to measure the surface area of samples based on gas quantites adsorbed to the sample surface. Fifty mg of the sample was preheated at 200 ºC for 10 min to remove water and gas completely. Surface areas of HAp particles were analyzed by nitrogen adsorption in a Autosorb-1.

4.3.4.4 Scanning Electron Microscope (SEM)

For the morphological study, hydroxyapatite were mounted on brass stubs, coated with gold using a JEOL JFC-1100 sputtering device, and observed for their microscopic morphology using JEOL JSM-5200 scanning electron microscopy (SEM). For the morphology of the surface, pore size, distribution and also the interconnectivity.

4.3.4.5 Transmission Electron Microscope (TEM)

The microstructural and morphological features of HAp powders were analysed in JEM-2100 operating voltage of 200 kV. Sample for TEM were prepared by air-drying a drop of a sonicated ethanol suspension of particles onto a carbon-coated copper grid and air-dried.

4.3.4.6 Energy Dispersive Spectrophotometer (EDS)

The Ca/P ratio of the hydroxyapatite was studied by the X-ray microanalysis, using the method of Energy dispersive X-ray spectroscopy (EDS). EDS is an analytical technique used for the elemental compositions of the HAp.

4.3.4.7 X-ray Diffraction (XRD)

The phase compositions, crystal shape and size of HAp powders were characterized by X-ray diffraction (XRD) with copper target. Data were collected over the scanning range (2θ) from 5 º to 60 º at a scan speed 2 º /min.

The average crystallite size of the prepared hydroxyapatite samples was determined using the scherrer equation.

$$D = K \cdot \lambda / \beta \cdot \cos\theta$$

In which D is the average crystallite size (Å), K denotes the shape factor (K=0.9), λ is the X-ray wavelength (for CuKα λ=1.5418 Å), β represents the peak at half width (in rad), and θ is the Bragg angle of the peak (002 reflection of hydroxyapatite at 2θ=26 º).

4.3.4.8 UV-Visible Spectrophotometer

Determination of protein by UV/Vis spectrophotometry at 215 nm for Gelatin type B, 280 nm for OVA and BSA and 275 nm for CBP.

4.3.4.9 Zeta potential (ZP)

Zeta potentials (or electrophoretic mobility) of the hydroxyapatite were determined using Zeta-Meter 3.0+ (Zeta-Meter, Inc., USA). Briefly, the suspension of 100 mg hydroxyapatite in 20 ml of deionized water was filled in an electrophoresis cell. Two electrodes were inserted into the cell and connected to the Zeat-Meter 3.0+ unit. Once the electrodes were energized, microspheres were aroused to move toward one electrode. Particles were observed under a microscope for its movement along a specific distance which was indicated by a built in grid. The zeta potential value was detected at a right time point when the microsphere moved to the end. Measurement was repeated 10 times for each preparative condition and the average values were calculated.

4.3.4.10 Particle size distribution

The Malvern Particle size of hydroxyapatite was measured by Mastersizer 2000 a solution of the particles was sonicated in an ultra-sonic bath for 7 min immediately before measurement to ensure separation of particles. A sample of this mixture was injected into the sample cell of the Malvern Mastersizer. The obscuration was between 10 and 30 %, as required by the instrument. The Mastersizer calculates automatically the particle size and distribution from small angle light scattering using Mie theory and Fraunhofer diffraction theory. The measurements were taken with the stirrer in the Mastersizer to ensure even distribution of particles and prevent sedimentation in the sample cell. Shear forces were not a problem in this case as the goal was to measure the primary particle size. A least 10 measurements were recorded and the average value recorded.

4.3.4.11 In vitro protein-HAp release test

Proteins-loaded Hydroxyapatite (20 mg) were dispersed in 10 ml 0.1M phosphate buffer saline (PBS) solution at pH 7.4. All samples were incubated in a shaking water bath (70 rpm) at 37 ºC. The releasing medium was withdrawn 1 ml and an equal amount of fresh medium was added to maintain a constant volume of the medium. The amount of protein in the sample solution was determined by UV-visible spectroscopy. Absorbance peaks at 280 nm to determine the ovalbumin and BSA concentration, 215 nm to determine the gelatin type B, and 275 nm to determine the crude bone protein. Concentration through the use of a pre-determined standard concentration—intensity calibration curve. An average value was calculated at each time point. The protein content of the encapsulated particles can be described by two quantities in terms of Encapsulating efficiency of protein-loaded hydroxyapatite (EE) and Loading capacity of hydroxyapatite particle (LC), which were determined according to the following equation (Freiberg and Zhu, 2004).

$$\text{Encapsulating efficiency (\%)} = \frac{\text{total mg proteins-encapsulated}}{\text{initial mg proteins-loaded}} \times 100$$

$$\text{Loading capacity (\%)} = \frac{\text{total mg proteins-encapsulated}}{\text{total mg particles}} \times 100$$

4.4 Results and Discussion

4.4.1 Thermogravimetric Analysis (TGA)

The samples were analyzed by TGA using a Perkin Elmer (TG-DTA) instrument under N_2 flow of 5 ml/min. The heating process was conducted from 30-950 °C at a rate of 10°C/min. To investigate amount of proteins-loaded hydroxyapatite.

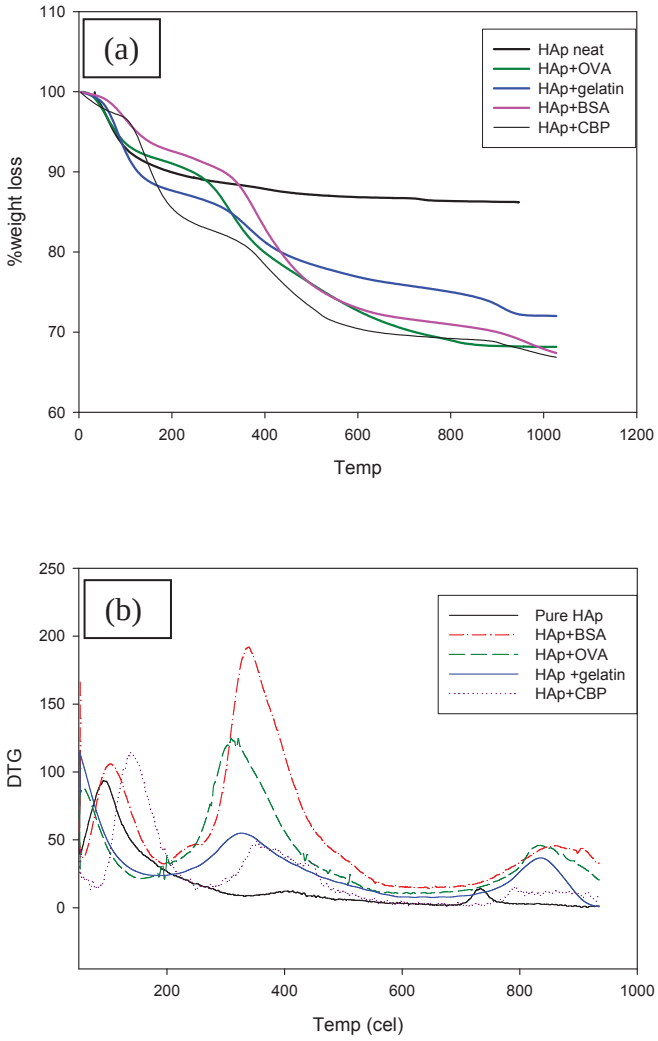


Figure 4.1 TGA-DTG curves (a) TGA, (b) DTG of proteins-loaded hydroxyapatite**.**

The features of TGA and DTA profiles of proteins-loaded hydroxyapatite were presented in Figure 4.1. The weight loss could be differentiated into three regions in the investigated temperature range such as (i) 25-210 ºC, (ii) 210-570 ºC, and (iii) 750-950 ºC. In the first region of 25-210 ºC, the weight loss for all precursors could be attributed to the removal of physically absorbed water. The second region of 210-570 ºC is a major weight loss, probably due to the combustion of proteins residuals (organic matter) and with the maximum rate at 350 ºC, and decomposition of calcium

hydroxide and carbonate to water and carbon dioxide. The third region of 750-950 ºC, the weight loss can be assigned to the decomposition of carbonate compounds.

The TGA curves of the samples (Figure 4.1) show differences in the amount of protein weight loss. Weight loss of ovalbumin was 16.8 %, Gelatin type B was 10.22 %, BSA was 20.61 % and CBP from pork bone was 22 %.

4.4.2 UV-Visible Spectrophotometer

Take water after finish synthesis reaction measured by UV-Visible to determine the remaining protein after reaction. OVA and BSA were measured the wavelength with 280 nm, Gelatin type B with 215 nm and CBP from pork bone with 275 nm.

To investigate amount of proteins-loaded hydroxyapatite. Remainning OVA in the DI water is 6.12 %, Gelatin type B is 14.30 %, and BSA is 2.38 %. So, OVA, Gelatin type B, and BSA are entrapped in hydroxyapatite 20.26 %, 12.08 %, and 24% respectively. It is possible that protein may be lost during the washing HAp with DI water about 5-6 times to become neutral.

4.4.3 X-ray Diffraction

In the X-ray diffraction analysis, all synthesized precipitates showed a HAp-like pattern (Figure 4.2). The crystallinity of each precipitate was evaluated from the data of the inverse of half value breadth of the (002) peak of HAp (Figure 4.2). The crystallinity of HAp depends on its synthesized temperature in such a way that HAp synthesized at low temperature has low crystallinity. The solubility of HAp also depended on its synthesized temperature and HAp synthesized at low temperature showed high solubility (Matsumoto, T. *et al*., 2004).

For HAp powders, the crystallite size in a direction perpendicular to the crystallographic plane is always estimated according to Scherrer's formula as followed:

$$d = (0.9\lambda) / FWHM*Cos\theta$$

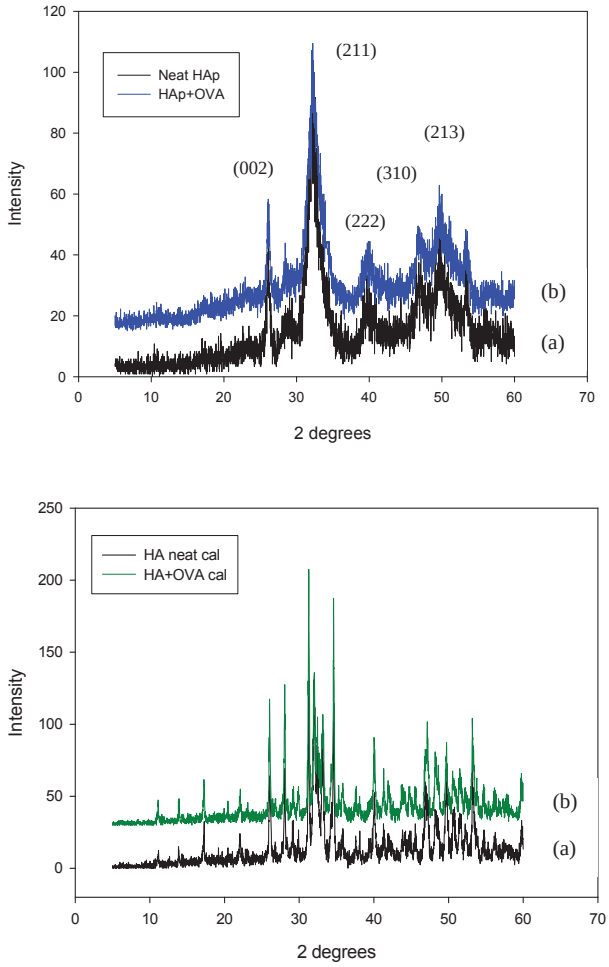


Figure 4.2 XRD pattern of HAp powders : (a) Neat HAp; (b) OVA-loaded HAp.

where d is the crystallite size (nm); λ=0.15406 nm for Cu Kα radiation of X-ray beam; FWHM the full width at half maximum for the diffraction peak (rad); and θ is the Bragg angle of the (002) diffraction angle (º). Two major characteristic diffraction peaks could be obtained for all the powdered samples: one closed at 2θ of ~26 º and the other broad one at ~32 º. According to PDF no.01-1008, The uncalcined HAp is shown the broad

patterns around at (002) and (211). It indicates that the crystallites were very tiny in nature. The (002) peak (2θ~26 º) from XRD patterns was chosen for calculating the crystallite size as shown in Table 4.1 since it contains the least overlap of the broadened peaks. It could be found that the crystallite size depends on the size of the particle that observed from SEM. Crystallite size of calcined HAp powders was larger than uncalcined powder. Figure 4.2 indicated that uncalcined HAp powders were amorphous and did not form CaP crystals, because HAp crystallization is mediated by protein and shown in Figure 4.3.

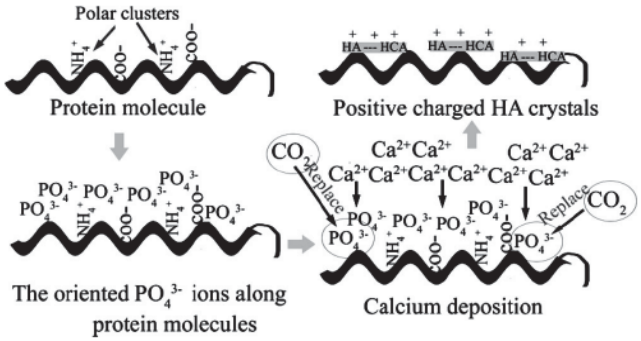


Figure 4.3 Schematic illustration of the protein-medicated crystallization of HAp crystals with positive charges (Zhao, H. *et al*., 2008).

Table 4.1 The different crystallite size of (a) calcined HAp at 800 ºC; (b) uncalcined HAp powder

(a)

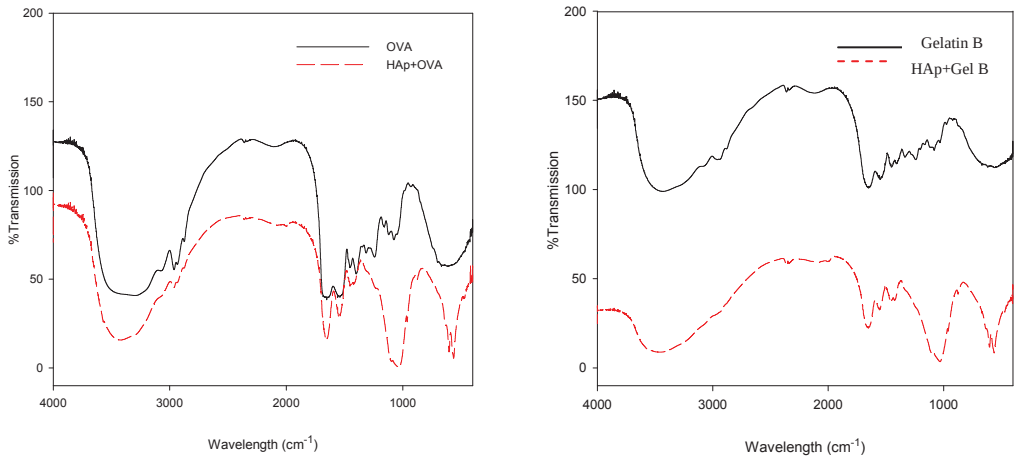
Crystal plane (002)	2θ	FWHM	Crystallite size (nm)
Neat HAp calcine	26.07	0.22	40.01
OVA-HAp calcine	26.05	0.15	58.16
Gealtin-HAp calcine	26.00	0.23	38.37
BSA-HAp calcine	25.82	0.23	37.03

(b)

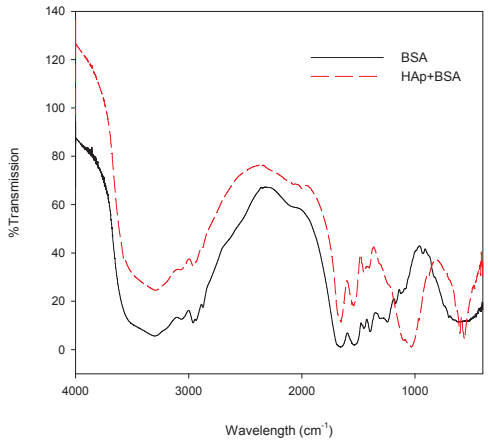
Crystal plane (002)	2θ	FWHM	Crystallite size (nm)
Neat HAp uncalcine	26.11	0.44	20.45
OVA-HAp uncalcine	26.12	0.51	17.69
Gelatin-HAp uncalcine	25.80	0.51	19.37
BSA-HAp uncalcine	25.91	0.51	16.88

4.4.4 Fourier-Transformed Infrared Spectrophotometer

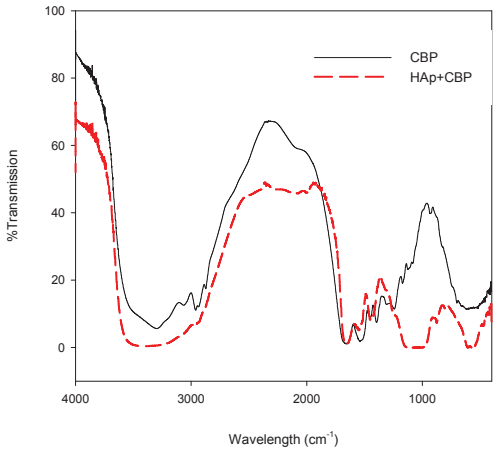
Adsorption of protein on HAp particles was detected by FTIR analysis (Figure 4.4). The spectra show the characteristic peaks of absorbed water, hydroxyl, phosphate and carbonate species. The broad peak around 3250 cm^{-1} to 3500 cm^{-1} corresponds to the adsorbed water. The spectrum clearly indicates a peak at 1640 cm^{-1} which is attributed to the presence of water associated with HAp. The absorption bands at 1460 cm^{-1} and 875 cm^{-1} suggest the presence of CO_3^{2-}. The absorption bands at 1040, 1093, 962 and 571 cm^{-1} detected in the spectra are attributed to the PO_4^{3-} ion. The absorption bands at 1210 cm^{-1} together with one at 1130 cm^{-1} and clear absorption band at 879 cm^{-1} are attributed to the HPO_4^{2-}. The spectrum of protein exhibited an appearent absorption band at 1654 cm^{-1} assigned to amide I, C=O stretching mode. The absorption band at 1540 cm^{-1} assigned to amide II, N-H bending mode and 1384 cm^{-1} assigned to amide III, C-N stretching mode and N-H bending mode.



(a)

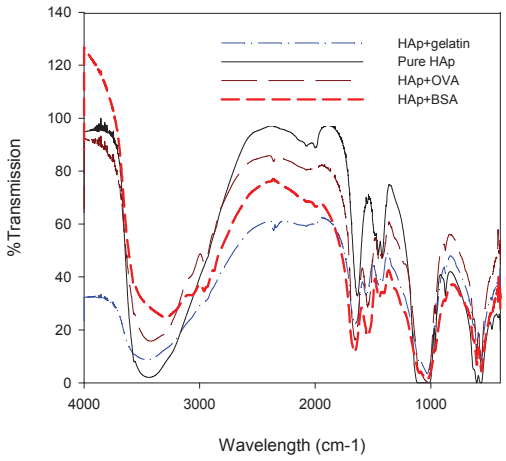


(b)



(c)

(d)



(e)

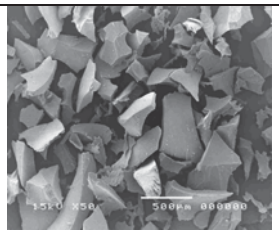
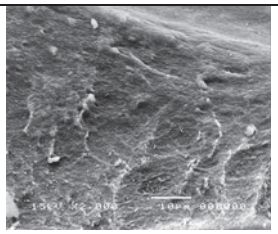
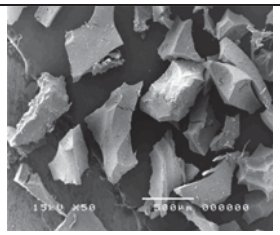
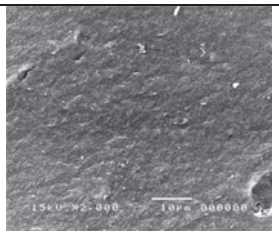
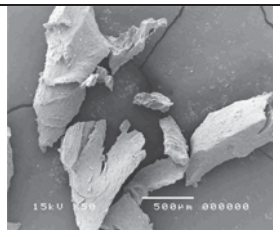
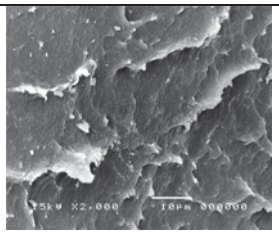
Figure 4.4 The FTIR spectra of HAp powders of : (a) OVA-loaded HAp; (b) Gelatin-loaded HAp; (c) BSA-loaded HAp; (d) CBP-loaded HAp; (e) including protein/HAp.

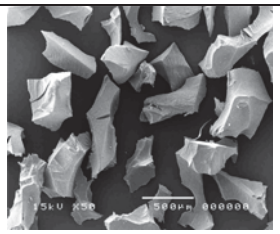
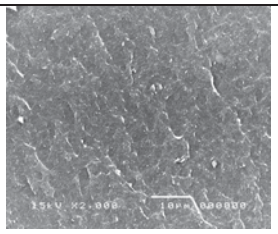
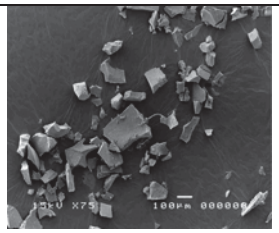
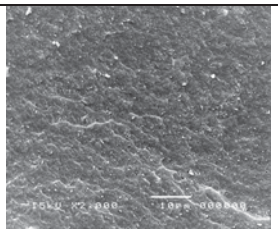
The possible mechanisms can be adapted to explain the interaction between the HAp and proteins molecules. The mechanism can be operated through the electrostatic interaction between the positive Ca^{2+} and COO^- (protein): this has been also reported by Liu who suggested that there is an intermediate complex between COO- and HAp. This complex can be formed via the electrostatic interaction between the negative COO^- on protein molecules and positive Ca^{2+} on the C-sites of HAp surface. Kazuhiko K. indicated that the C-sites were located on the crystal planes that are perpendicular to a-axis and b-axis of apatite crystal.

4.4.5 Scanning Electron Microscope (SEM)

To investigate the morphology of HAp powder by using SEM (JEOL, model JEM-5200). It is found that HAps have an arbitrary shape. Some gelatin grafting on the surface of HAp shown in Table 4.2.

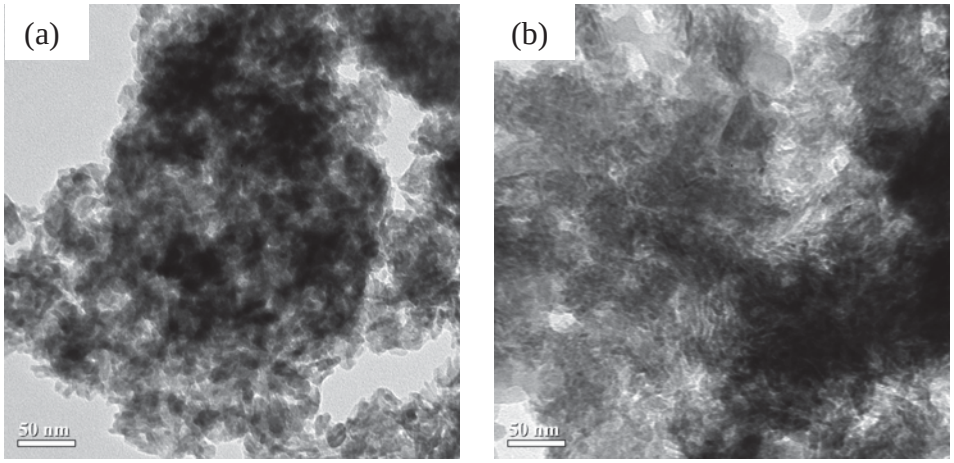
Table 4.2 SEM of proteins-loaded HAp powder

	X200	X2000
Neat HAp		
HAp+OVA		
HAp+gelatin		

	X200	X2000
HAp+BSA		
HAp+CBP		

4.4.6 Transmission Electron Microscope (TEM)

Figure 4.5 shows the TEM photographs of HAp powders obtained neat HAp and proteins-loaded HAp. The HAp powders contain agglomerated particles consisting of rod-like shaped particle. Neat HAp powders are the short-rod crystal than proteins-loaded HAp. It is found that there are not much differences in morphology and size from the photographs of proteins-load HAp samples.



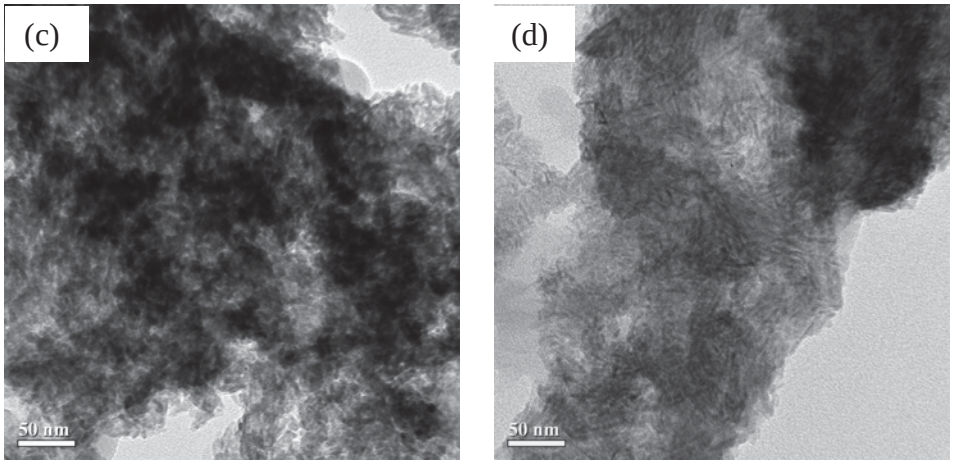


Figure 4.5 TEM micrographs of proteins-loaded HAp powder : (a) Neat HAp; (b) OVA-loaded HAp; (c) Gelatin-loaded HAp; (d) BSA-loaded HAp.

4.4.7 Zeta Potential (ZP).

Twenty mililiter of the suspension was placed in an electrophoresis cup, and the movable images of the particles were recorded by the electrophoresis apparatus. The value would also be beneficial in the study of protein-loaded HAp and releasing through HAp particles. The zeta potentials were measured by appling the electric field in the dispersion and particles in the dispersion will be migrated to electrode of opposite charge. Protein-loaded HAps were dispersed in the DI water pH about 6-7 if protein can releases from HAp, it will be showed negative charge, so zeta potential is the positive. The zeta potentials of all the samples are negative, indicating that the particles themselves have superfluous positive electrical charges. It was indicated that protein entrapped in the HAp particle

The electrical conductivities values were so close as ~ -18, -16, and -20 mV for neat HAp, OVA-loaded HAp, and Gelatin B loaded HAp particle, respectively. Zeta potential is an indicator of charge density (Brown *et al.*, 1998). Particle size of Gelatin B-loaded HAp is the largest, so it has the highest charge density.

4.4.8 Energy Dispersive Spectrophotometer

The EDS spectrum from HAp particles (Figure 4.6) shows the characteristic peaks of calcium (Ca), phosphorus (P), and oxygen (O). EDS is composed mainly of HAp and exhibits a molar Ca/P ratio of 1.67.

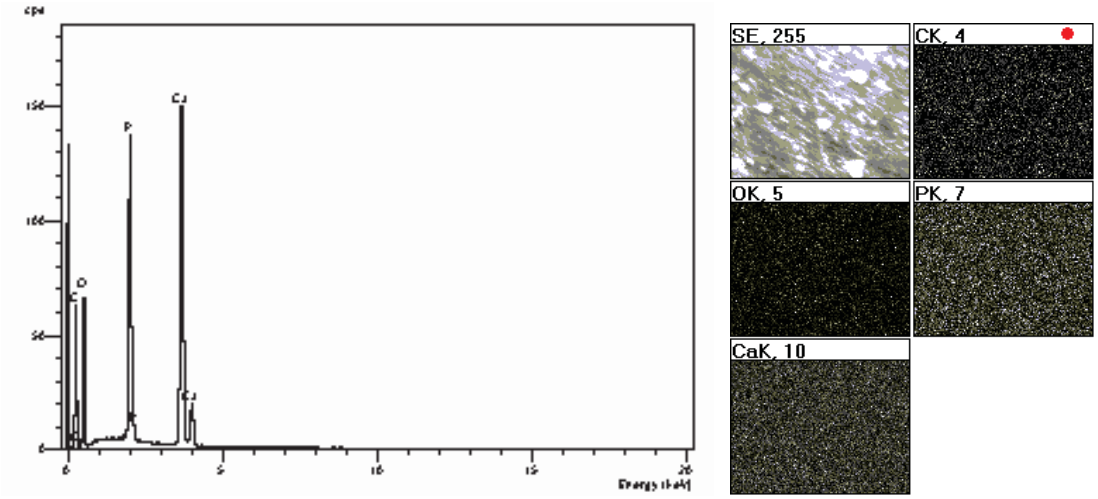


Figure 4.6 EDS spectrum of the biomimetic apatite layer deposited.

4.4.9 The Brunauer—Emmett—Teller (BET)

Surface areas and pore size of the powders were analyzed by nitrogen adsorption in Autosorb-1. The BET surface areas of the calcined samples at 800 ºC are summarized in Table 4.3. We found that they are a few differences in surface area and pore size of neat and proteins-loaded HAp. Pore size of proteins-loaded HAp are a few larger than neat HAp due to the existence of pores after the removal of organic materials (proteins) so, surface area of proteins-loaded HAp are a few lower than neat HAp.

Table 4.3 BET surface area and pore size of the calcined samples at 800 ºC

	Surface area (m^2/g)	Pore size (nm)
Neat HAp	22.64	8.75
OVA-loaded HAp	19.65	9.35
Gelatin-loaded HAp	20.06	11.42
BSA-loaded HAp	20.99	12.14

4.4.10 Particle size distribution of Hydroxyapatite

We were ground and sieved through a mesh size of 400 micron of protein-loaded HAp particles. About twenty miligrams of HAp were dispersed in water. The size distributions of HAp were measured by light scattering using particle sizer (Malvern, UK). The average particle size distributions of neat HAp and proteins-loaded HAp were about 316 μm.

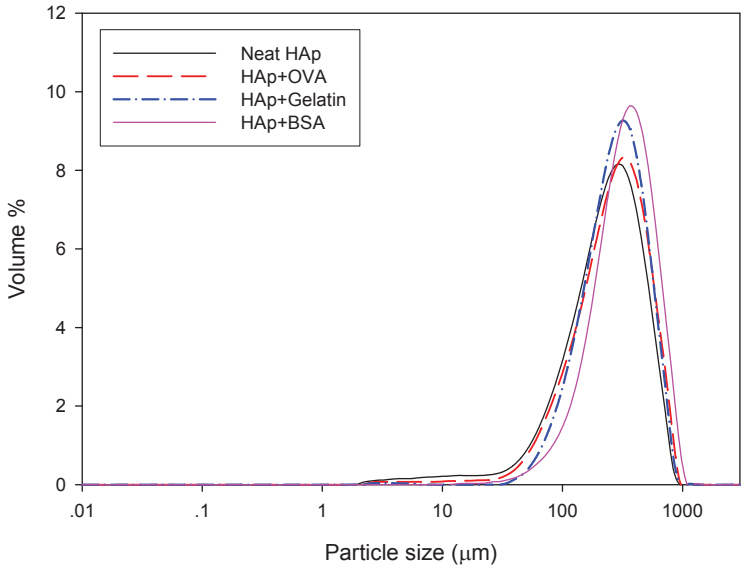


Figure 4.7 Average particle size distribution of Hydroxyapatite.

4.4.11 Controlled Release of Proteins from HAp particles

The protein content of the encapsulated particles can be described by two quantities in terms of encapsulating efficiency of protein-loaded hydroxyapatite (EE) and loading capacity of hydroxyapatite particle (LC). For encapsulating efficiency of protein-loaded hydroxyapatite (EE), the proteins release from hydroxyapatite in phosphate buffer saline solution pH 7.4 was shown in Figure 4.8. The release profile of OVA, BSA and CBP were shown long-term proteins release at least 3 week. The maximum accumulative releases were about 50 % - 60 %. For the release profile of gelatin type B, it was shown the bursting release. The accumulative release was about 12 %. For loading capacity of proteins-loaded hydroxyapatite (LC), the proteins release from hydroxyapatite in phosphate buffer saline pH 7.4 was shown in Figure 4.9. The LC of OVA, BSA, and CBP from HAp particles were shown maximum accumulative releases were about 8-12 %. For the LC of Gelatin type B from HAp particle was shown maximum accumulative releases was about 1 %. Encapsulation of proteins into hydroxyapatite particles in this study was on the basis of polyion complexation. It was expected that a degree of molecular interaction was able to take place between proteins and hydroxyapatite particles of opposite charges (Young *et al.*, 2005); as a consequence, a higher yield of the ionic complexes should result in higher encapsulation efficiency and loading capacity (Tabata and Ikada, 1998; Hoffman, 2002; Young *et al.*, 2005).

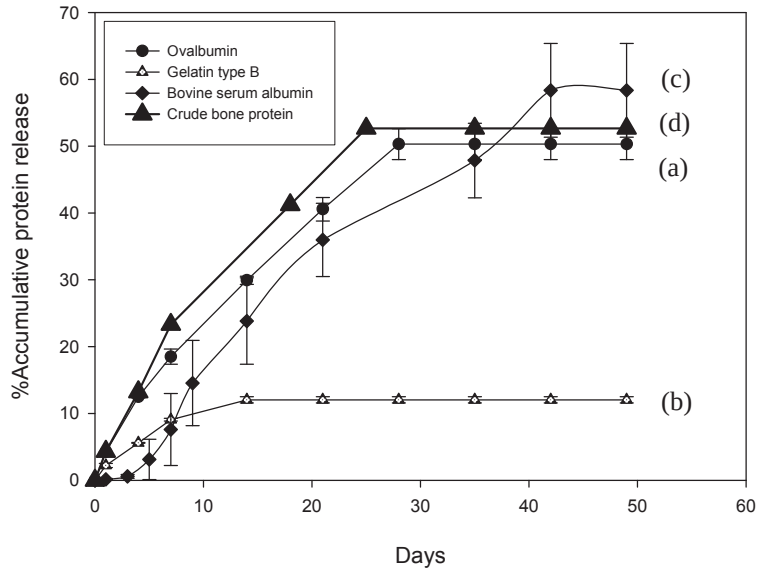


Figure 4.8 Encapsulating efficiency of protein-loaded hydroxyapatite (EE) : (a) Ovalbumin (OVA); (b) Gelatin type B; (c) Bovine serum albumin (BSA) and (d) Crude bone protein (CBP) release from HAp in phosphate buffer saline solution.

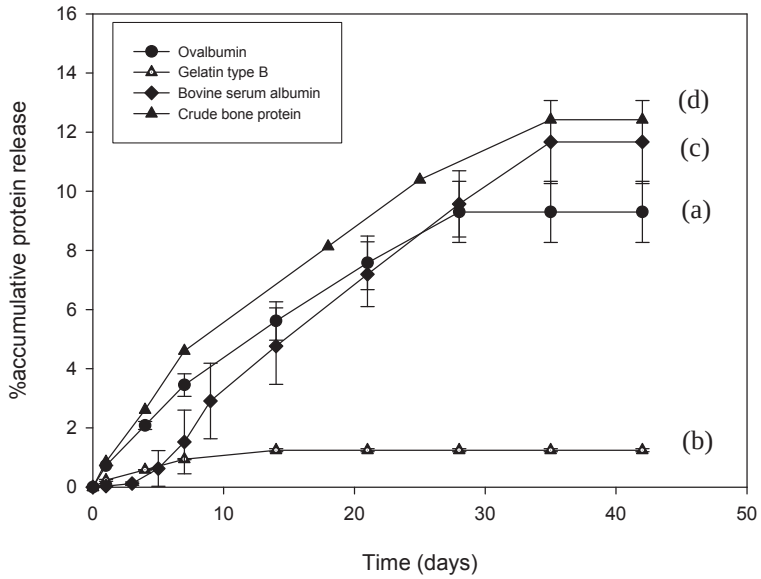


Figure 4.9 Loading capacity of protein-loaded HAp (LC) : (a) Ovalbumin (OVA); (b) Gelatin type B; (c) Bovine serum albumin (BSA) and (d) Crude bone protein (CBP) release from HAp in phosphate buffer saline solution.

4.5 Conclusion

The porous hydroxyapatite particle as a controlled release carrier of proteins were successfully synthesized by co-precipitation technique. The precursors were obtained DCPD and $CaCO_3$. Incorporation of proteins was accomplished during the co-precipitation of the two reactants. Characteristics of the HAp particles were determined by XRD, EDS, FT-IR, TGA, ZP, SEM, TEM, and Autosorb-1. Proteins-loaded HAps were dissolution tested in prolonged PBS solution. Proteins release could be regulated using HAp particles resulting in prolonged release of proteins except gelatin type B. Mechanism of proteins-loaded HAp release was believed to be the combination of diffusion or degradation of the carrier. Many factors play roles and synergistically control on the release of proteins from the hydroxyapatite which were electrostatic interaction between protein and hydroxyapatite.

4.6 Acknowledgements

The author would like to thank Prof. Pitt Supaphol, Assoc. Prof. Prasit Pavasant, Assoc. Prof. Nuanchawee wetprasit, Asst. Prof. Hathaikarn Manuspiya and Dr. Neeranut Kuanchertchoo for their sincere assistances. They have provided the very useful guidance and the great encouragement throughout this research.

The author also thanks to all of colleagues, staff and teachers in the Petroleum and Petrochemical college, Chulalongkorn University who helps greatly during studies.

The author is grateful for funding of the thesis work provided by petroleum and petrochemical college; and Center for petroleum, Petrochemicals, and Advanced Materials.

The author wishes to give thanks to all of friends in Pitt Supaphol group’s student for helps and suggestions.

Finally, the author would like to express appreciation for supporting scholarship and caring a great love of family especially mother, father, brother, and grandmother.

4.7 References

Cao, Li-Yun., Zhang, Chuan-bo., and Huang, Jian-feng (2005). Synthesis of hydroxyapatite nanoparticles in ultrasonic precipitation. Ceramics International, 31, 1041-1044.

Li, Yanbao., Tjandra, Wiliana., and Tam, Kam C (2008). Synthesis and characterization of nanoporous hydroxyapatite using cationic surfactants as templates. Materials Research Bulletin, 43, 2318–2326.

Liu, Tse-Ying., Chen, San-Yuan., Liu, Dean-Mo., and Liou, Sz-chian (2005). On the study of BSA-loaded calcium-deficient hydroxyapatite nano-carriers for controlled drug delivery. Controlled Release, 107, 112-121.

Freiberg, S., Zhu, X.X. (2004). Polymer microspheres for controlled drug release. International Journal of Pharmaceutics, 282, 1-18.

Hariraksapitak, P. (2009). Development of protein delivery scaffold with a separate drug carrier system for bone tissue regeneration. Doctor dissertation. The Petroleum and Petrochemical College, Chulalongkorn University.

Hoffman, A.S. (2002). Hydrogels for biomedical applications. Advanced Drug Delivery Reviews, 54(1), 3-12.

Matsumoto, T., Okazaki, M., Inoue, M., Yamaguchi, S., Kusunose, T., Toyonaga, T., Hamada, Y., and Takahashi (2004). Hydroxyapatite particles as a controlled release carrier of protein. Biomaterials, 25, 3807-3812.

Kandori, Kazuhiko., Shohei, Oda., Masao, Fukusumi., Yoshiaki Morisada. (2009). Synthesis of positively charged calcium hydroxyapatite nano-

crystals and their adsorption behavior of proteins. Biointerfaces, 73, 140-145.

IJntema, K., HeuveIsland, W.J.M., Dirix, C.A.M.C., and Sam, A.P (1994). Hydroxyapatite microcarriers for biocontrolled release of protein drugs. International Journal of Pharmaceutics, 112, 215-224.

Tabata, Y. and Ikada, Y. (1998) Protein release from gelatin matrices. Advanced Drug Delivery Reviews, 31(3), 287-301.

Yang, Qing., Chen, Lin., Shen, Xinyuan., and Tan Zhiqing (2006). Preparation of Polycaprolactone Tissue Engineering Scaffolds by Improved Solvent Casting/Particulate Leaching Method. Macromolecular, 45, 1171-1181.

Young, S., Wong, M., Tabata, Y., and Mikos, A.G. (2005) Gelatin as a delivery vehicle for the controlled release of bioactive molecules. Journal of Controlled Release, 109(1-3), 256-274.

Zhao, Hongshi, He, Wen., Wang, Yingjun., Zhang Xudong., Li, Zhengmao., Yan, Shunpu., Zhou, Weija. Biomimetic (2008). Synthesis and Characterization of Hydroxyapatite Crystal with Low Phase Transformation Temperature. Journal of chemical & engineering data, 53 (12), 2735-2738.

DEVELOPMENT OF POROUS HYDROXYAPATITE PARTICLES AS CARRIERS OF PROTEINS IN A POLYCAPROLACTONE SCAFFOLD FOR BONE TISSUE ENGINEERING

Sujittra Chaisuntharanon,[1] Prasit Pavasant,[2] and Pitt Supaphol [1,*]

[1] The Petroleum and Petrochemical College and The Center for Petroleum, Petrochemicals and Advanced Materials (C-PPAM), Chulalongkorn University, Bangkok 10330, Thailand

[2] Department of Anatomy, Faculty of Dentistry, Chulalongkorn University, Bangkok 10330, THAILAND

5.1 Abstract

This study aimed to develop the porous hydroxyapatite (HAp) particles as a controlled release carrier of proteins were embedded in polycaprolactone (PCL) to fabricate porous HAp-PCL scaffolds. Proteins (Ovalbumin, Gelatin type B, Bovine Serum Albumin and Crude bone protein) had been entrapped within the HAp particles. The porous HAp-PCL scaffolds were prepared by solvent casting/particulate leaching method. Desorption behavior of HAp-PCL scaffolds was investigated by UV-Visible spectrophotometry. The potential for use of HAp-PCL as bone scaffolds was assessed by mouse calvaria derived pre-osteoblastic cells, MC3T3-E1, in terms of indirect cytotoxicity, cell attachment, cell proliferation, alkaline phosphatate (ALP) activity, and mineralization.

(**Key-words**: bone scaffolds; particulate leaching; polycaprolactone; hydroxyapatite)

5.2 Introduction

Modern tissue engineering combines materials science with biotechnology and biology to repair and replace damaged. It has been shown

[*] Authors to whom correspondence should be addressed: pitt.s@chula.ac.th (P. Supaphol)

that new tissues can be engineered from living cells and three-dimensional scaffolds. The success of these approaches is largely dependent on the scaffold properties. The ideal scaffold should have the following characteristics: (1) Appropriate porosity, pore size and pore structure to ensure the nutrition of cells, cell attachment and cell proliferation within the scaffold (2) Mechanically strong enough to maintain structural integrity during culture, which is particularly important in load-bearing bone tissues. The material should be strong enough to withstand physiological stresses, and to transfer loads after implantation. (3) Adequate degradation properties in which the rate of scaffold degradation supports the maintenance of structure support for cellular proliferation and extracellular matrix (ECM). (4) Biocompatible so that the material used to manufacture the scaffold does not evoke an extreme adverse inflammatory or immune response once implanted. Instead, the material should be able to integrate with the host tissue and support cell infiltration, cell attachment for bone formation (5) Appropriate manufacturing process, the manufacturing processes should not affect the material's biocompatibility as a result of residual chemicals involved in these processes (Choong C. *et al*., 2004).

In this research, three-dimensions HAp-PCL porous scaffolds were prepared by solvent casting/particle leaching method with sodium chloride as a porogen. The inclusion of calcium phosphates (CaPs) in biodegradable polymers enhances the osteoconductive of bone scaffold. Specifically, the inclusion of CaPs in polymer scaffolds enhances its mineral deposition rate, mechanical properties, and protein adsorption, thus improving the overall potential of bone scaffold (Porter, Joshua R *et al*., 2009).

5.3 Experimental

5.3.1 Materials

- Polycaprolactone (PCL;80,000 g mol^{-1}; Sigma-Aldrich, USA)
- Sodium chloride (Ajax Finechem, Australia)

- Chloroform (Labscan; Asia, Thailand)
- Modified Eagle's medium (MEM; Thermo Scientific, USA)
- Fetal bovine serum (FBS;Sorali, Campo Grande Brazil)
- 1% L-glutamine (Invitrogen Corp., USA)
- 1% Lactabumin (Invitrogen Corp., USA)
- 1% antibiotic (Invitrogen Corp., USA)
- Bicinchoninic acid (BCA; Thermo Scientific, USA)

5.3.2 Preparation of Polycaprolactone (PCL)-Hydroxyapatite (HAp) Scaffold

A solvent casting and salt particulate leaching was used to prepare the scaffold. Firstly, PCL granules were put into a glass bottle with chloroform to make up a PCL solution in the concentration of 14 percentages of polymer weight by volume of the solution (w/v), then the solution was stirred at room temperature for 2 h. Secondly, protein-loaded HAp were added into the glass bottle and they were stirred together. Thirthly, NaCl salt particles with size of 400 μm (PCL/NaCl = 1/30) (w/w) were added into the glass bottle and they were mixed together. And finally, the mixture was packed into the petri-dish with the dimension of 10x10 cm. The mold was then left in the hood for 24 h and immersed in the distill water 1 day for taking the mold out. The materials that come out were immersed in DI water for 2 days, during with time the water was changed approximately every 8 h under the room temperature for the leaching out the salt particles. Then the materials were air-dried for 24 h and freeze-dried overnight to obtain porous scaffolds (Prasansuklap *et al*., 2008).

5.4 Characterization of porous Scaffolds

5.4.1 Porosity, Pore Volume and Pore Size

The density of the scaffolds ($\rho_{scaffold}$) is determined by using a Sartorius YDK01, Germany density measurement kit (Buoyancy method) which can be calculated using the following equation.

$$\rho_{scaffold} = \frac{W_a \times \rho_{fl}}{W_a \times W_{fl}}$$

Where W_a is the weight of the scaffold in air, W_{fl} is the weight of the scaffold in water and $\rho_{scaffold}$ is the density of the water (at 25ºC, $\rho_{ft} \approx 1$ g/cm^3).

The porosity and pore volume of the scaffolds were calculated using the following equation (Hou, Qingpu *et al*., 2003)

$$\text{Porosity (\%)} = \left(1 - \frac{\rho_{scaffold}}{\rho_{polymer}} \right) \times 100$$

$$\text{Pore volume} = \frac{1}{\rho_{scaffold}} - \frac{1}{\rho_{polymer}}$$

where $\rho_{scaffold}$ is the apparent density of the porous scaffolds and $\rho_{polymer}$ is the density of the non-porous polymer, compression moulded in the same manner.

Pore size of the scaffold was measured on the SEM micrograph with the UTHSCSA Image Tool version 3.0 software. The average values were calculated from the total 25 pores and accept as the mean pore sizes.

5.4.2 Water Absorption Capability

The dry scaffold scaffolds were weighted and then were immersed in 5 ml of phosphate buffer silane solution (PBS pH 7.4) solution at room temperature for 3 days. Scaffolds were removed from the solution and carefully placed on the glass for 5 seconds to remove the excessive water and weight immediately. The water absorption was calculated using the following equation.

$$\text{Water absorption (\%)} = \frac{(M_{wet} - M_{dry})}{M_{dry}} \times 100$$

Where M_{dry} and M_{wet} are the weight of the scaffold before and after immersion in water respectively. Five measurements were performed for the calculation of an average water absorption value.

5.4.3 Morphology of Porous Scaffolds

The morphology of the pores size of the porous scaffold were observed by a JEOL JSM-5200 scanning electron microscopy (SEM). The scaffolds were cut with razor blade at the middle of the scaffolds and mounted on stubs. Cross sections of the scaffolds were coated with thin film of gold using JEOL JFC-1100E sputtering devices for 120 second.

5.4.4 *In Vitro* Release of Proteins from Scaffold

The proteins/HAp-PCL were immersed in 1 ml of the minimum essential medium (MEM; Hyclone, Thermoscientific, USA) in 24 well plate. All samples were incubated in a shaking water bath (70 rpm) at 37ºC. The amount of proteins releasing from scaffold to the supernatant was measured by BCA protein assay at various times. After the releasing medium (sample solution) was withdrawn 20 µl to mixed with BCA solution, an equal amount of fresh medium was added to maintain a constant volume of the medium. The amount of protein in the sample solution was determined by UV-visible spectroscopy at 562 nm. The MEM used in this study contained plenty of much high molarity inorganic salts comparing with those in PBS such as NaCl 117.24 M, KCl 5.33 M, $CaCl_2$ 1.8 M, NaH_2PO_4-H_2O 1.01 M (Invitrogen, 2009).

5.5 Cell culture

Mouse calvaria-derived, pre-osteoblastic cells (MC3T3-E1) were cultured as monolayers in minimum essential medium with Earle's Balanced

Salts (MEM; Hyclone, Thermoscientific, USA), supplemented with 10% FBS, 1% L-glutamine and 1% antibiotic and antimycotic formulation (containing penicillin G sodium, streptomycin sulfate, and amphopericin B (Invitrogen Corp, USA). Cells were cultivated in 5% CO_2 at 37 ºC in a humidified atmosphere.

5.5.1 Indirect Cytotoxic Study.

An indirect cytotoxic test was conducted on the proteins-loaded hydroxyapatite and PCL-HAp scaffold by use MC3T3-E1. First, extraction medias were prepared by immersing powder of each protein-loaded hydroxyapatite and circular shape of each PCL-HAp scaffold specimens about (15 mm in diameter) in wells of a 24-well culture plate in a 2% MEM (containing MEM, 2% FBS, 1% L-glutamine, 1% antibiotic and antimycotic formulation) for 24 h. Each of these extraction media was used to evaluate the cytotoxicity of the HAp powder and scaffold. MC3T3-E1 was separately cultured in wells of a 24-well culture plate in serum-containing MEM for 16 h to allow cell attachment on the plate. The cells were then starved with 2% MEM for 24 h, after which time the medium was replaced with an extraction medium. After 24, 48, and 72 h of cell culturing in the extraction medium, a 3-(4,5-dimethylthiazol-2-yl)-2,5-diphenyl-tetrazolium bromide (MTT) assay was carried out to quantify the amount of via cells.

The MTT assay is based on the reduction of the yellow tetrazolium salt to purple formazan crystals by dehydrogenase enzymes secreted from the mitochondria of metabolically active cells. The amount of purple formazan crystals formed is proportional to the number of viable cells. First, each of culture medium was aspirated and replaced with 400 µl per well of MTT solution at 0.5 mg/ml for a 24-well culture plate. Secondly, the plate was incubated for 30 mins at 37ºC. The solution was then aspired and 900 µl per well of dimethylsulfoxide (DMSO) containing 125 µl per well of glycine buffer (pH=10) is added to dissolve the formazan crystals. Finally, after 10 min of rotary agitation, the absorbance of the DMSO solution at 570 nm was

measured using a Thermospectronic Genesis 10 UV-Visible spectrophotometer.

5.5.2 Cell Attachment and Cell Proliferation Study

Mouse calvaria-derived, pre-osteoblastic cells (MC3T3-E1) were allowed to attach on the porous scaffold specimens and empty wells for 2, 4, and 6 h. For the proliferation study, the cells were allowed to attach on the porous scaffold specimens and empty wells for 1, 3, and 5 d. At each time point, a number of the attached and proliferated cells were quantified by MTT assay. Each specimen was rinsed with phosphate buffered saline to remove unattached cells prior to the MTT assay. The morphology of the cells during the attachment and proliferation periods was observed by SEM. At each time point, the culture medium was removed and then the cell-cultured scaffold specimens were rinsed with PBS twice, the cells were then fixed with 3% glutaraldehyde solution, which was dilute from 50% glutaraldehyde solution with PBS 500 µl/well. After 30 min, they were rinsed again with PBS. After cell fixation, the specimens were dehydrated in an ethanol solution of varying concentration (30%, 50%, 70% and 90%, respectively). The specimens were the dried in air. After completely dried, the specimens were mounted on an SEM blass stubs, coated with gold and observed by SEM.

5.5.3 Alkali Phosphate Analysis (ALP)

Mouse calvaria-derived, pre-osteoblastic cells (MC3T3-E1) were cultured on porous scaffolds for 5 and 7 d and in different proteins for 5 and 7 d to observe ALP activity. Each porous specimen was rinsed with PBS after removal of the culture medium. Alkaline lysis buffer (10 mM tris-HCl, 2mM $MgCl_2$, 0.1% Triton-X100), pH 10) (1000 µl/well) was added, and the specimen was scrapped and then frozen at -20ºC for at least 30 min prior to the next step. An aqueous solution of 2 mg ml^{-1} p-nitrophenyl phosphate (PNPP; Zymed Laboratories) mixed with 0.1 M aminopropanol (10µl/well) in 2 mM $MgCl_2$ (100µl/well) having a pH of 10.5 was prepared and added into the specimen. It was then incubated at 37ºC for 2 min. The reaction was stopped by the addition of 0.9 ml/well of 50 mM NaOH, and the extracted solution was

transferred to cuvette and placed in the UV-Vis spectrophotometer, from which the absorbance at 410 nm was measured. The amount of ALP was then calculated against a BSA standard curve. To determine the ALP activity, the amount of ALP had to be normalized by the amount of total proteins synthesized. In the protein assay, each specimen was treated in the same manner as in the ALP assay up to the point where it was frozen. After freezing, a bicinchoninic acid (BCA; Thermoscientific, USA) solution was into the specimen. It was subsequently incubated at 37ºC for 5 min. The absorbance of the medium solution was then measured at 562 nm by the UV-Vis spectrophotometer, and the amount of the total proteins was calculated against a BSA standard curve.

5.5.4 Mineralization Analysis

Calcium deposition was quantified by Alizarin Red S staining. MC3T3-E1 were cultured on the porous scaffolds in 24-well plate for 21 days. The cultures in 24-well plate were rinsed with PBS after that the cells were fixed with cold methanol for 10 min and washed with deionized water prior to immersion for 3 min in 370 µl of 1% Alizarin Red S solution dissolved in 1:100 (v/v) ammonium hydroxide/water mixture for 3 min (pH=3.3). Each stained specimen was washed several times with DI water and air-dried at room temperature. Calcium forms an Alizarin Red S-calcium complex in a chelating process. The stained specimen was photographed and eluted dye with 10% cetylpyridinium chloride for 20 min. The Alizarin Red concentration was determined by measuring the absorbance at 562 nm.

5.6 Results and discussion

5.6.1 Microstructure observation

Figure 5.1 demonstrated the SEM images microstructure of the as-prepared scaffolds when being viewed on the surface and cross sections. For PCL and HAp/PCL scaffold with NaCl : PCL, 30:1 weight ratio. The SEM images of (a) and (c) showed many square units occurring from the shape of

NaCl porogens used in the fabricating process. They showed clearly square units due to neat PCL scaffold whereas (b) and (d) exhibited the lost square because HAps embedded in the PCL scaffold.

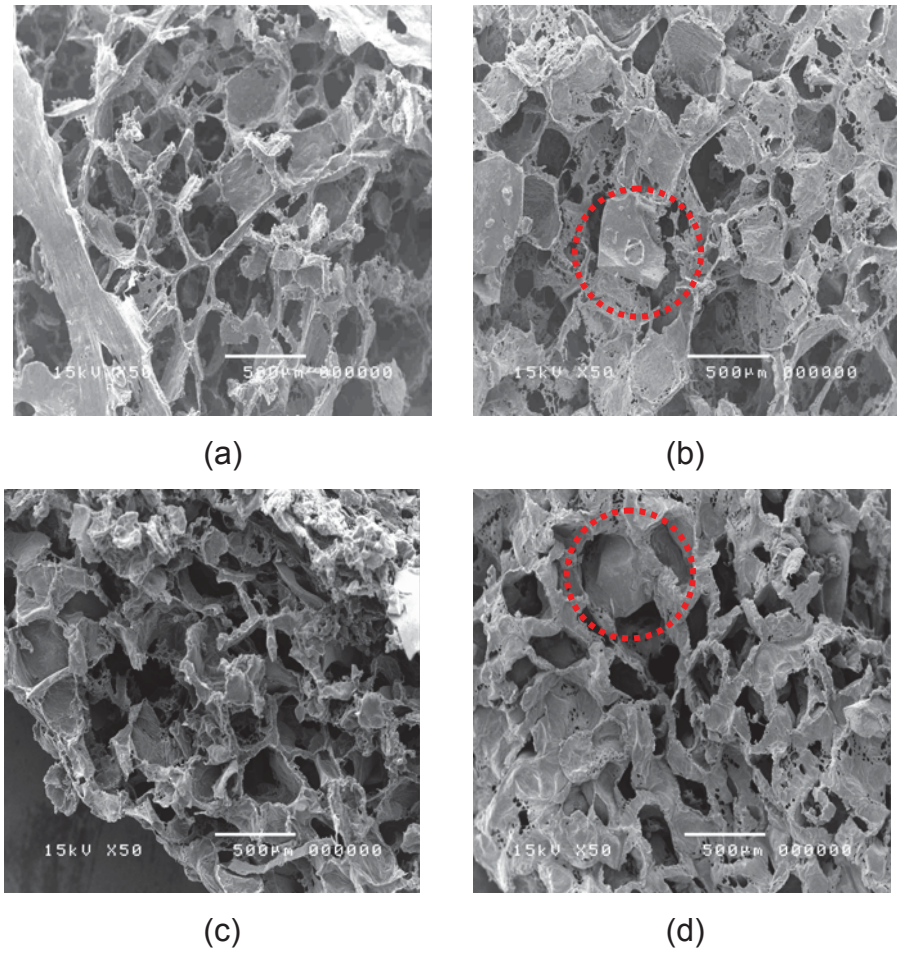


Figure 5.1 SEM images illustrate microstructure of the scaffolds on the surface: (a) PCL, (b) HAp-PCL and on the cross-sections : (c) PCL, (d) HAp-PCL.

5.6.2 Density, Porosity, Pore volume and Pore size

The density, porosity, pore volume and pore size of the scaffold was shown in Table 5.1.

Table 5.1 Density, porosity, pore volume and pore size of PCL scaffold

Scaffolds	Density (g/cm^3)	Porosity (%)	Pore volume (cm^3/g)	Pore size (μm)
PCL	0.1139	90.05	7.91	347.07 ± 42.19

5.6.3 Water absorption capability and *in vitro* degradability

Figure 5.2 illustrates the water absorption capabilities of the PCL scaffolds in 0.1 M PBS at room temperature within 3 days (72 h). The water absorption rate was rapidly increased in the early 24 hours and maintained stable.

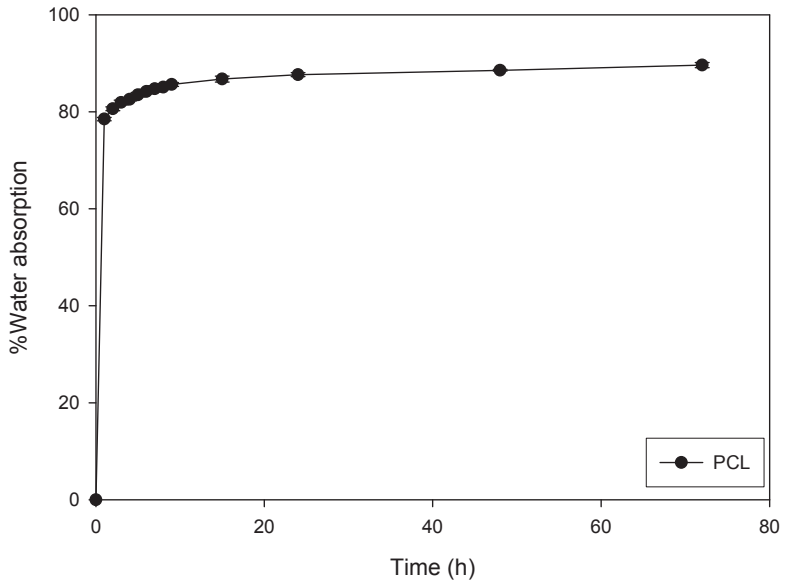


Figure 5.2 Water absorption capability of the PCL scaffolds in 0.1 M PBS at room temperature within 3 days.

5.6.4 *In vitro* OVA, Gelatin type B, BSA, and CBP Release

The release of proteins from HAp-PCL scaffolds were investigated by immersing HAp-PCL scaffolds into *in vitro* culturing environment, 10% MEM (containing MEM, 10% FBS, 1% L-glutamine, 1%

antibiotic). All samples were incubated in a shaking water bath (70 rpm) at 37ºC for 21 days. The result shows gelatin and CBP started to before day 7 whereas OVA and BSA release after day 7. The amount of released proteins gradually increased time dependently. This result correspond to the work done by proteins releasing from HAp particles, however, protein release from scaffold spends a longer time due to different media. It is different in ionic strength, in MEM shows higher ionic strength. High ionic strength should promote aggregation of protein and retard release.

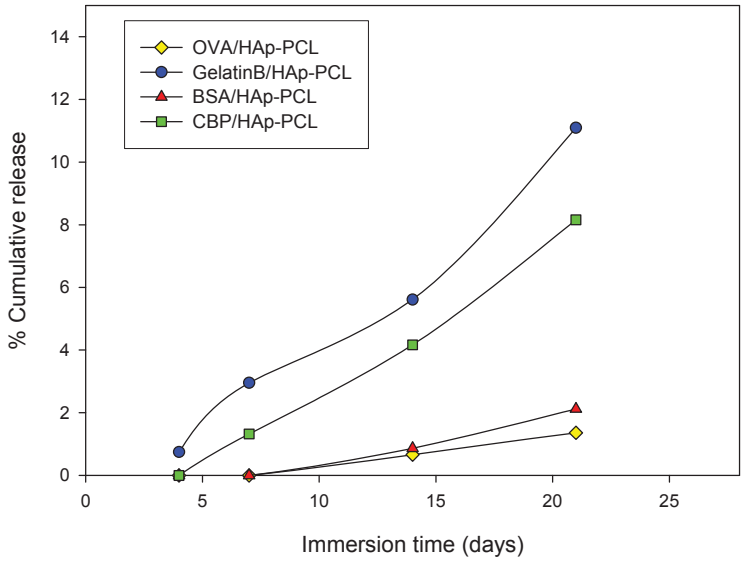


Figure 5.3 Release profile from protein-loaded HAp-PCL scaffold in MEM.

5.7 Cell Culture

5.7.1 Cytotoxicity

Indirect cytotoxicity in this studied can be classified into 3 process are indirect cytotoxicity for protein, HAp, and HAp-PCL scaffold. Firstly, an direct cytotoxicity test of proteins were performed in 4 types which are Ovalbumin (OVA), Gelatin type B, Bovine serum albumin (BSA), and

Crude bone protein. MC3T3-E1, pre-osteoblast cell lines, in culture of 40,000 cell/well seeded with 10 µg/ml concentration in 2% MEM for 24, 48, and 72 h. The results are shown in Figure 5.4 with %viability of MC3T3-E1 relative to tissue culture polystyrene (TCPS) in all types of proteins show that increasing with cuturing time. The %viability of MC3T3-E1 is more than 80%, so all types of proteins were no toxicity to cells. Secondly and Thirdly are indirect cytotoxicity test of proteins-loaded HAp and HAp-PCL scaffold. MC3T3-E1 were cultured in 2% MEM extraction media from proteins-loaded HAp (Figure 5.5) and HAp-PCL scaffold (Figure 5.6) for 24, 48, and 72 h. The %viability of MC3T3-E1 in extraction media of each time are more than 80%, so proteins-loaded HAp and HAp-PCL scaffold were no toxicity to cell.

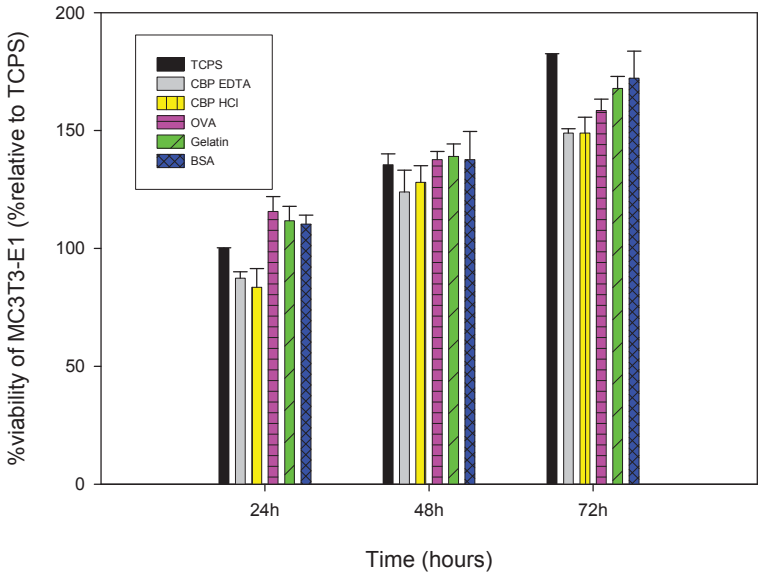


Figure 5.4 Direct cytotoxicity evaluation of proteins based on the viability of MC3T3-E1.

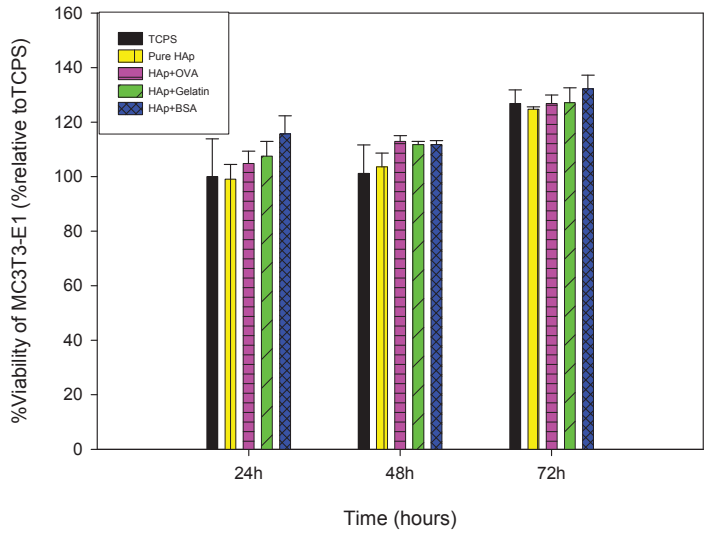


Figure 5.5 Indirect cytotoxicity evaluation of protein-loaded HAp based on the viability of MC3T3-E1.

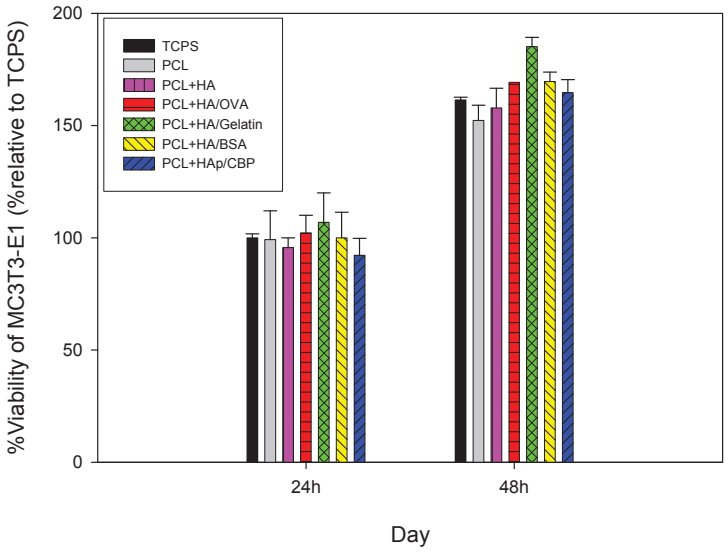


Figure 5.6 Indirect cytotoxicity evaluation of HAp-PCL scaffold based on the viability of MC3T3-E1.

5.7.2 Cell Attachment and Proliferation

Attachment of mouse calvaria-derived, pre-osteoblastic cells (MC3T3-E1) on scaffolding substrate could be quantified by the UV

absorbance from MTT assay. Figure 5.7 shows attachment of MC3T3-E1 on the surface of TCPS, PCL, HAp-PCL, OVA/HAp-PCL, Gelatin type B/HAp-PCL, BSA/HAp-PCL, CBP/HAp-PCL at 2, 4, and 6 h after cell seeding. The number of cell attachment on all of the surfaces increase with culturing time. The number of cell attachment on TCPS was the greatest than all of HAp-PCL and proteins-loaded HAp scaffolds at any given time point, in culture of 40,000 cell/well. On TCPS, the number of cell attachment rapidly increased from 100% at 2 h after cell seeding to ~200% at 4 h after cell seeding. Whereas the number of cell attachment on PCL, HAp-PCL and proteins-loaded HAp were lower than TCPS could be because MC3T3-E1 like to attach the smoother surface of TCPS than rough surface of PCL, HAp-PCL and proteins-loaded HAp-PCL scaffold. However, Table 5.2 shows that almost of the formazan crystal still adhere within the scaffolds after using DMSO as eluting agent.

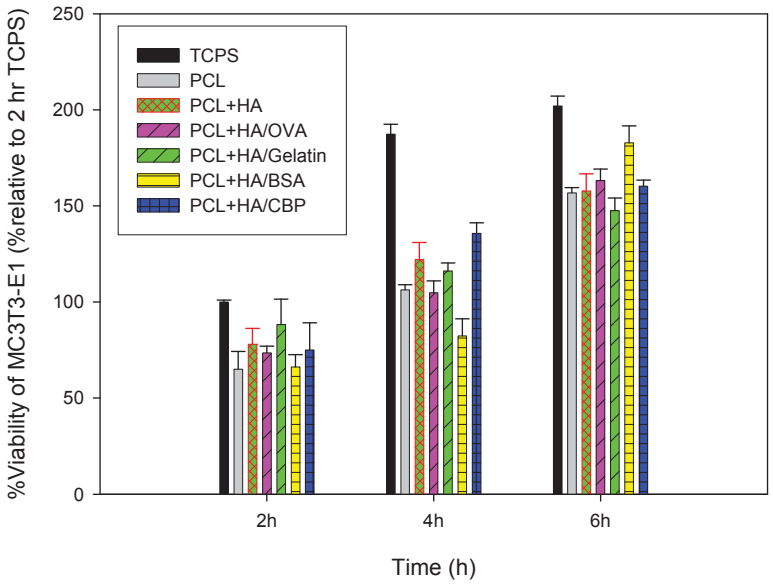


Figure 5.7 Attachment of MC3T3-E1 on control TCPS, PCL, HAp/OVA-PCL, HAp/gelatin B-PCL, and HAp/BSA-PCL

Table 5.2 Formazan crystal within TCPS, PCL, HAp-PCL scaffold were eluted with DMSO after cell seeding 6 h. (a) Eluted formazan from TCPS. (b), (c) Formazan still adhere in scaffold. (f), (g) Eluted formazan from scaffold. (d), (e) scaffold without cells inside. (h), (i) Eluted scaffolds without cells

 (a)	 (b)	 (c)	 (d)	 (e)
	 (f)	 (g)	 (h)	 (i)

Proliferation of mouse calvaria-derived, pre-osteoblastic cells (MC3T3-E1) on scaffolding substrate could be quantified by the UV absorbance from MTT assay. Figure 5.8 shows proliferation of MC3T3-E1 on the surface of TCPS, PCL, HAp-PCL, OVA/HAp-PCL, Gelatin type B/HAp-PCL, BSA/HAp-PCL, CBP/HAp-PCL at 1, 2, and 3 d after cell seeding in culture of 40,000 cell/well. The number of cell prolieration on all of the surfaces at any given time point were constant. The number of cell proliferation on TCPS was greater than all of PCL, HAp-PCL, and proteins-loaded HAp-PCL scaffolds at any given time point. On PCL, HAp-PCL and proteins-loaded HAp-PCL scaffold, the number of cell proliferation was only 60%. Whereas the number of cell attachment on HAp-PCL and proteins-loaded HAp were lower than TCPS could be because MC3T3-E1 like to proliferate the smoother surface of TCPS than rough surface of PCL, HAp-

PCL and proteins-loaded HAp-PCL scaffold. The difference between the number of cell proliferation to PCL, HAp-PCL, and protein-loaded HAp-PCL scaffold are not clear because of no effect of proteins release from HAp. However, Table 5.3 shows that almost of the formazan crystal still adhere within the scaffolds after using DMSO as eluting agent.

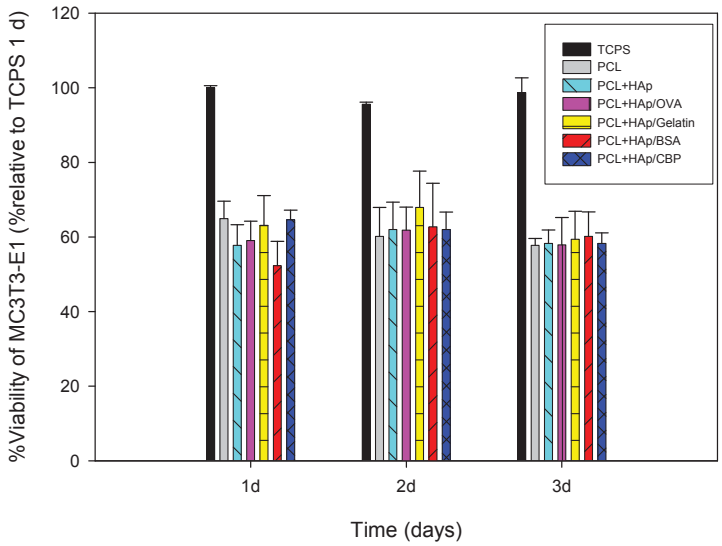


Figure 5.8 Proliferation of MC3T3-E1 that had been seeded or cultured on the surfaces of TCPS, PCL, HAp-PCL and proteins-loaded HAp-PCL scaffolds at 2 and 3 d.

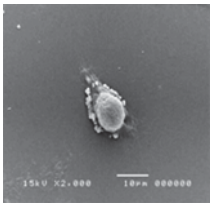
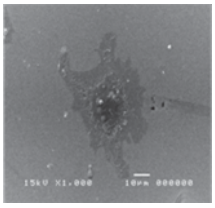
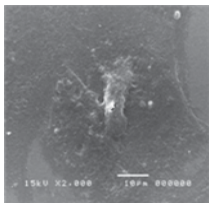
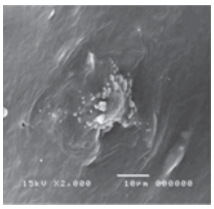
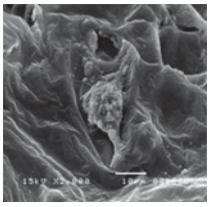
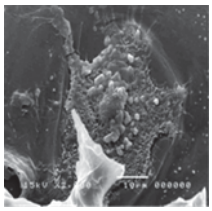
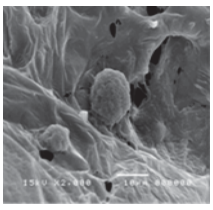
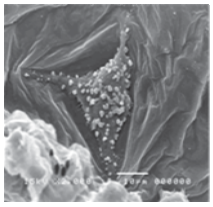
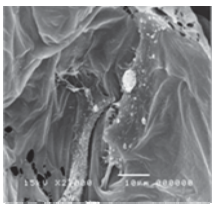
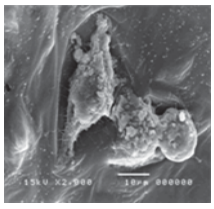
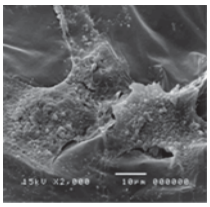
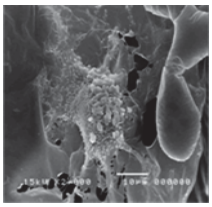
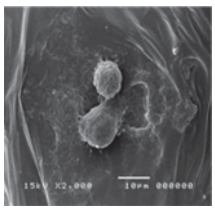
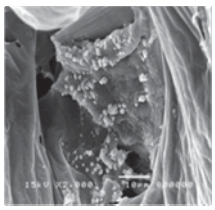
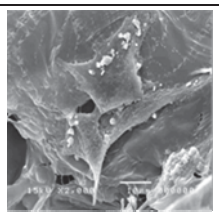
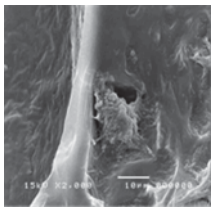
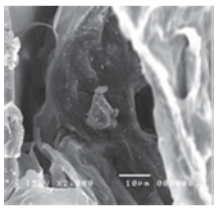
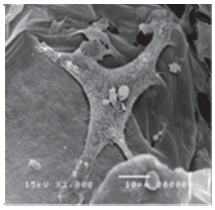
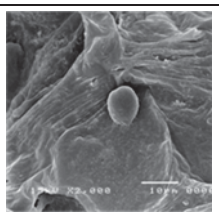
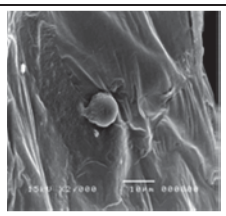
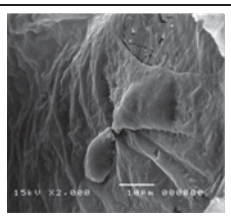
Table 5.3 Formazan crystals within scaffolds after using eluting dye (DMSO) after cell seeding 1 d. (a) Eluted formazan with DMSO from TCPS. (b), (c) Formazan crystal still adhere in scaffolds. (f), (g) eluted formazan crystal with DMSO from scaffolds. (d), (e) scaffold without cells inside. (h), (i) eluted DMSO from scaffolds without cells.

 (a)	 (b)	 (c)	 (d)	 (e)
	 (f)	 (g)	 (h)	 (i)

5.7.3 Cell Morphological

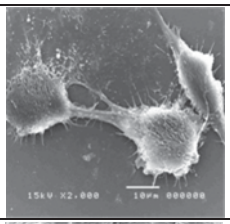
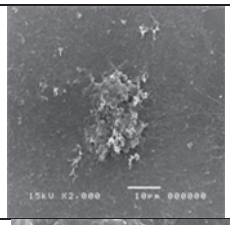
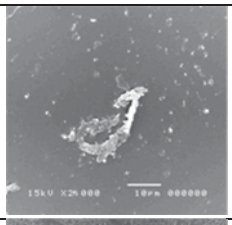
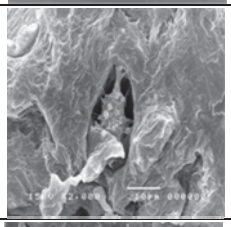
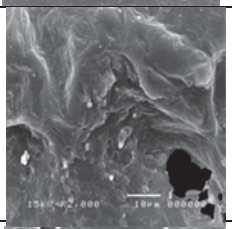
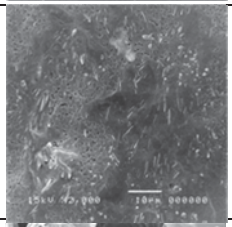
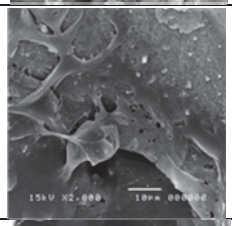
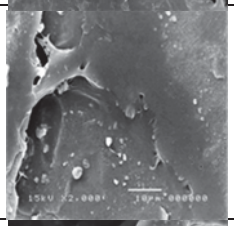
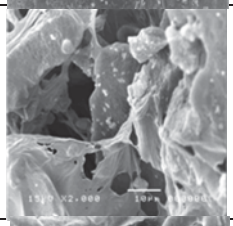
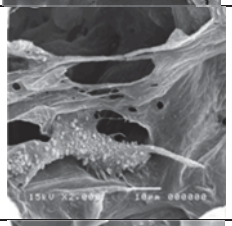
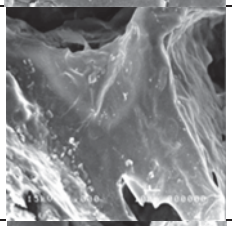
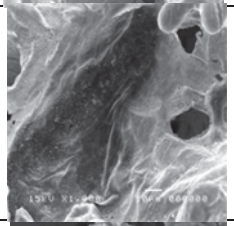
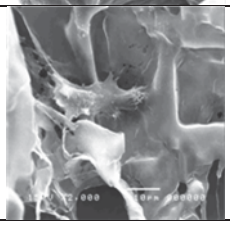
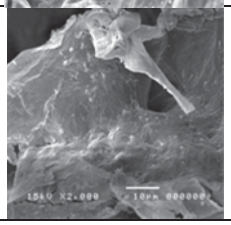
Table 5.4 shows selected the attachment SEM images of MCT3T-E1 (magnification = 2000X; scale bar = 10 μm) at 2, 4, and 6 h. Based on the initial 40,000 cells/well of cells seeded, the majority of the cells on the glass surface and porous scaffolds were still in the round shape at 2 h and started to extend their cytoplasm at 4 h. After cell seeding, expansion of the cytoplasm of the majority of the cells was evident at 6 h. Table 5.5 shows that the selected proliferation SEM images of MC3T3-E1 (magnification = 2000X; scale bar = 10 μm) were cultured on the surfaces of glass, PCL, HAp-PCL, and proteins-loaded HAp scaffolds. The use of glass as the control instead of TCPS was due to the ease of taking the samples to SEM observation. These images provided snap shots in time that revealed the morphology of the cells and interaction between the cells and the tested surfaces. The expansion of the cells was evident with depend on the increasing time at 1, 2, and 3 days. All proteins within the HAp show the same results due to at that time the proteins were no affect to the cells.

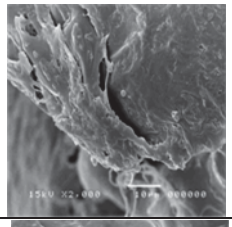
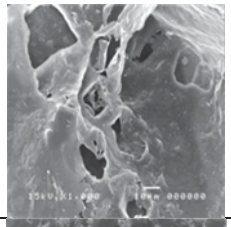
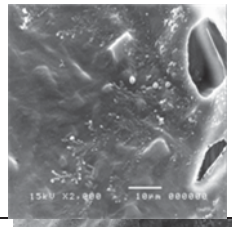
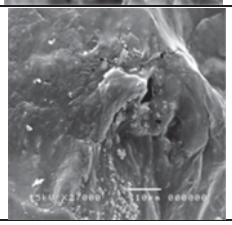
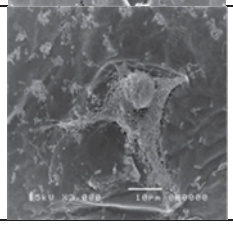
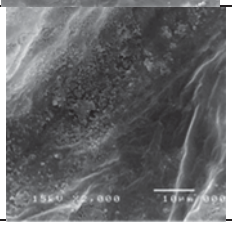
Table 5.4 Selected SEM images of MC3T3-E1 after seeding on TCPS, PCL, OVA/HAp-PCL, Gelatin type B/HAp-PCL, BSA/HAp-PCL, and CBP/HAp-PCL scaffolds at 2, 4, and 6 h (magnification = 2,000X; scale bar = 10 μm)

	2 h	4 h	6 h
Glass			
PCL			
PCL + HAp			
PCL+HAp/OVA			
PCL+HAp/Gel B			
PCL+HAp/BSA			
			

PCL+HAp/CBP			

Table 5.5 Selected SEM images of MC3T3-E1 after seeding on TCPS, PCL, HAp-PCL, OVA/HAp-PCL, Gelatin type B/HAp-PCL, and BSA/HAp-PCL scaffolds at 1, 2, and 3 days

X 2000	1 d	2 d	3 d
Glass			
PCL			
PCL + HAp			
PCL+HAp/OVA			
PCL+HAp/Gel B			

PCL+HAp/BSA			
PCL+HAp/CBP			

5.7.4 Alkaline phosphatase (ALP) activity

Alkaline phosphatase is an indicator of osteoblast phenotype activity. It was determined after culturing the cells seeded onto the scaffold. The ALP activity of MC3T3-E1 on TCPS, PCL, HAp-PCL, OVA/HAp-PCL, Gelatin type B/HAp-PCL, BSA/HAp-PCL and CBP/HAp-PCL were monitored at 3 and 7 days in culture. In Figure 5.9 at 3 days shows the maximum level of ALP activity and at 7 days, ALP activity was decreased. In actually, ALP activity of PCL, HAp-PCL, OVA/HAp-PCL, Gelatin type B/HAp-PCL, BSA/HAp-PCL and CBP/HAp-PCL scaffold should be the same result of cell proliferation due to at that time the proteins were no effect to the cell, however, they were slightly fluctuated because PCL, HAp-PCL, OVA/HAp-PCL, Gelatin type B/HAp-PCL, BSA/HAp-PCL and CBP/HAp-PCL scaffolds were porous materials, so the cells could go through their scaffolds and could not extract the cells completely. In Figure 5.9, The ALP activity of MC3T3-E1 in OVA, Gelatin type B, BSA, and CBP with 100 μg/ml concentrations in 2%MEM was monitored at 5 and 7 days in culture. At 5 days shows the maximum level of ALP activity and at 7 days, ALP activity was decreased due to cellular process switching to mineralization. This result correspond to the work done by ALP activity of MC3T3-E1 on substrates.

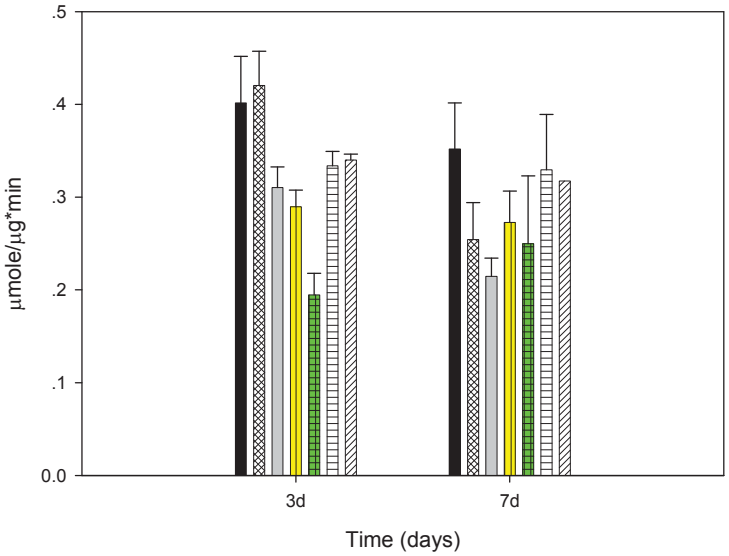


Figure 5.9 ALP activity of MC3T3-E1 cultured on TCP, PCL, HAp-PCL, OVA/HAp-PCL, Gelatin B/HAp-PCL, BSA/HAp-PCL and CBP/HAp-PCL porous scaffolds after 3 and 7days in culture.

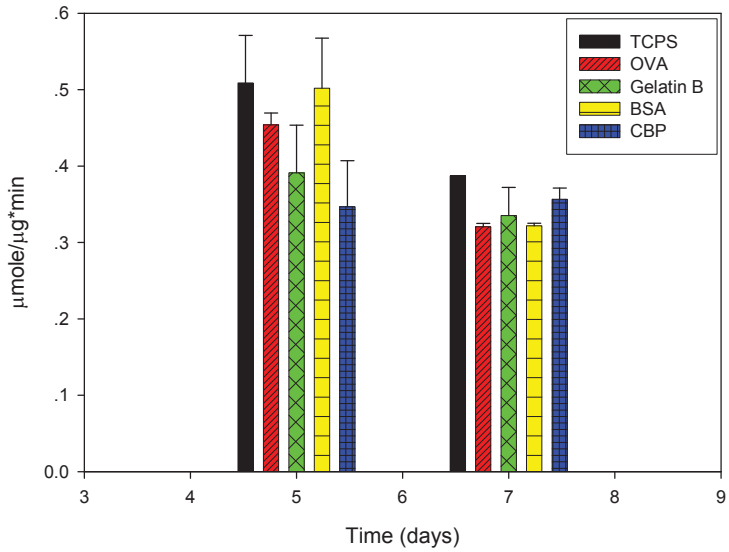
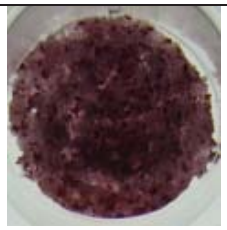
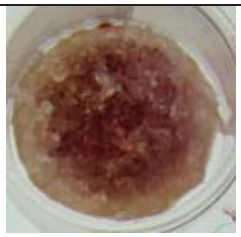


Figure 5.10 ALP activity of MC3T3-E1 cultured with 100 µg/ml in 2%MEM, OVA, Gelatin type B, BSA and CBP after 5 and 7 days in culture.

5.7.5 Mineralization

Mineralization refers to the process where an organic substrance is converted to an inorganic substrance. Alizalin Red S staining was used to characterize the bone formation of MC3T3-E1. Table 5.6, and Figure 5.11 show photographic images of Alizarin Red S staining of cells cultured on the different surfaces on 21 days. In the presence of calcium, the staining product such as an Alizarin red S-calcium chelating product appeared red. The results showed that PCL, HAp-PCL, and proteins-loaded-HAp scaffold were significantly higher than that on TCPS. Calcium content from MC3T3-E1 culture on CBP/HAp-PCL scaffold was the most positive staining.

Table 5.6 Alizarin Red S staining for mineralization assessment of MC3T3-E1 on 21 days after being cultured on the surfaces of neat PCL, HAp-PCL, HAp/OVA-PCL, HAp/Gelatin-PCL, HAp/BSA-PCL, and HAp/CBP-PCL

Substrate	21 d.		21 d.
TCPS		HAp/OVA-PCL	
Neat PCL		HAp/GelB-PCL	

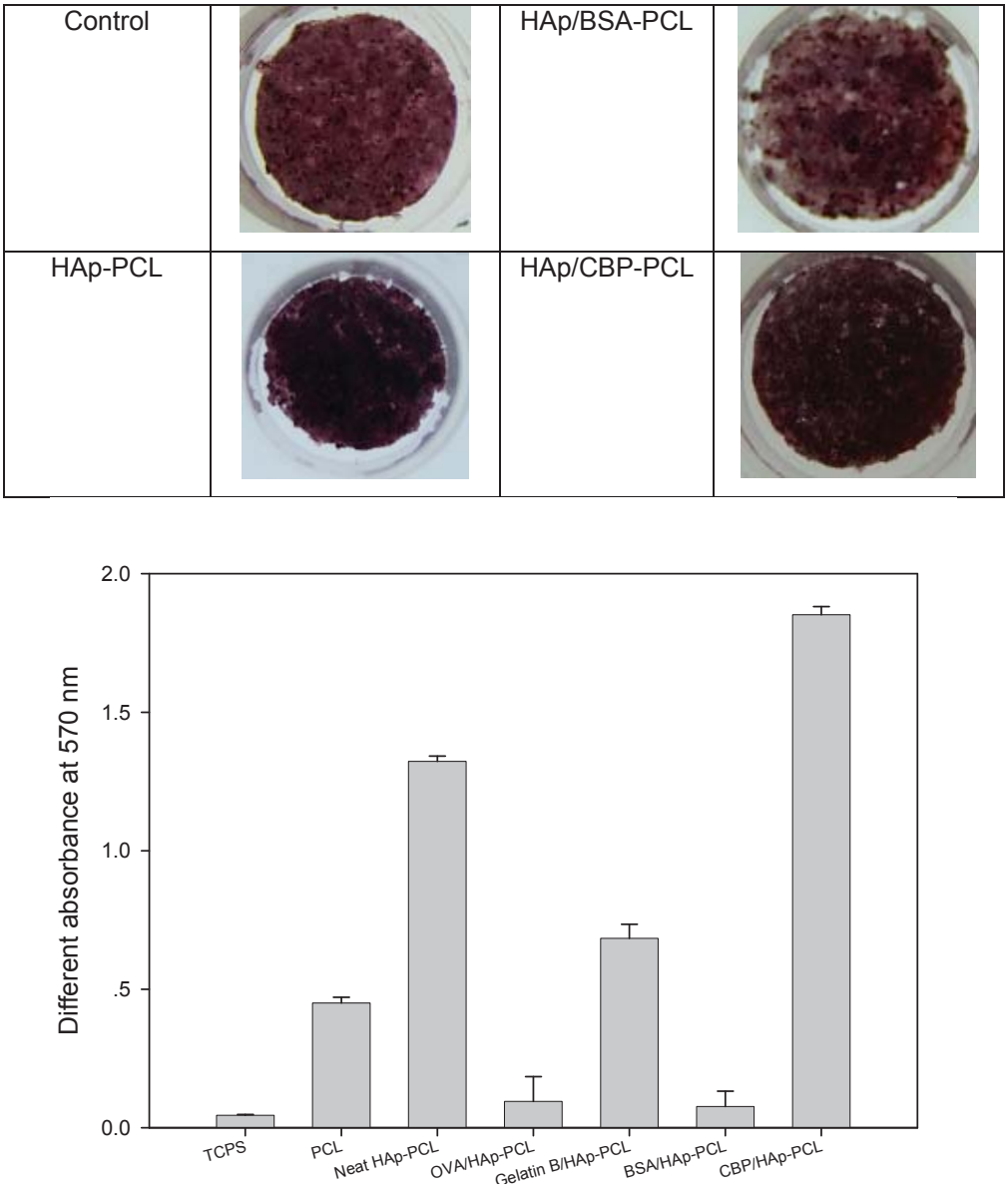


Figure 5.11 Different absorbance of alizalin red S from MC3T3-E1 on TCPS, PCL, HAp-PCL, proteins-loaded HAp-PCL at 21 days.

5.7 Conclusions

The amount of HAp in the PCL scaffold was 40% (w/w, based on the amount of PCL). The direct and indirect cytotoxicity evaluation of the proteins, HAp and protein-loaded HAp-PCL scaffold with MC3T3-E1 indicated that non-toxic. Potential for using of proteins-loaded HAp-PCL

scaffolds was assessed in terms of cell attachment, cell proliferation, and ALP activity were no effect of proteins release from HAp. Alkaline phosphatate (ALP) activity at 7 days showed decreasing of the ALP activity due to cellular process switching to mineralization. According to mineralization or calcium deposition of cell for 21 days, the CBP/HAp-PCL scaffold was better than HAp/PCL, PCL, Gelatin/HAp-PCL, OVA/HAp-PCL, BSA/HAp-PCL, TCPS respectively.

5.8 Acknowledgements

The author would like to thank Prof. Pitt Supaphol, Assoc. Prof. Prasit Pavasant, Assoc. Prof. Nuanchavee wedprasit, Asst. Prof. Hathaikarn Manuspiya and Dr. Neeranut Kuanchertchoo for their sincere assistances. They have provided the very useful guidance and the great encouragement throughout this research.

The author also thanks to all of colleagues, staff and teachers in the Petroleum and Petrochemical college, Chulalongkorn University who helps greatly during studies.

The author is grateful for funding of the thesis work provided by petroleum and petrochemical college; and Center for petroleum, Petrochemicals, and Advanced Materials.

The author wishes to give thanks to all of friends in Pitt Supaphol group's student for helps and suggestions.

Finally, the author would like to express appreciation for supporting scholarship and caring a great love of family especially mother, father, brother, and grantmother.

5.10 References

Choong, C., Triffitt, J.T., and Cui, Z.F. (2004). Polycaprolactone scaffolds for bone tissue engineering: effects of a calcium phosphate coating layer on osteogenic cells. Food and bioproducts processing, 82(C2), 117-125.

Porter, Joshua R., Henson, Andrew., and Popat, Ketul C. (2009). Biodegradable poly (ε-caprolactone) nanowires for bone tissue engineering applications. Biomaterials, 30, 780-788.

Prasansuklarb, A. (2008) Osteoblastic cell growth and enzymatic degradation of different aliphatic polyester scaffolds. Master thesis. The Petroleum and Petrochemical College, Chulalongkorn University.

Hou, Qingpu., Grijpma, Dirk W., and Feijen, Jan (2003). Porous polymeric structures for tissue engineering prepared by a coagulation, compression moulding and salt leaching technique. Biomaterials, 24, 1937-1947.

SURFACE MODIFICATION OF POLY(LACTIC ACID) FIBERS VIA AMINOLYSIS AND COLLAGEN IMMOBILIZATION FOR BONE TISSUE ENGINEERING

Palita U-prasitwong,[1] Prasit Pavasant,[2] Voravee P. Hoven,[3] and Pitt Supaphol [1,*]

[1] The Petroleum and Petrochemical College and The Center for Petroleum, Petrochemicals and Advanced Materials (C-PPAM), Chulalongkorn University, Bangkok 10330, Thailand

[2] Department of Anatomy, Faculty of Dentistry, Chulalongkorn University, Bangkok 10330, THAILAND

[3] Organic Synthesis Research Unit, Department of Chemistry, Faculty of Science, Chulalongkorn University, Bangkok 10330, Thailand

New biomaterial effective for bone regeneration consisting of electro-spun (e-spun) fiber mats of poly(lactic acid) (PLA) with type-I collagen peptide bonded covalently was developed. Surface modification techniques have been instrumental in the development of scaffolds that promote cell-surface interactions. Surface modification of PLA in the form of e-spun fibers, was achieved by introducing the amino groups (NH_2) on the scaffold surface via aminolysis with 1,6-hexamethylenediamine (HMD) as precursors. The reactive groups were subsequently used to graft extracellular matrix molecule, type-I collagen, by using *N*,*N*′-disuccinimidylcarbonate (DSC) as coupling agent. The existence of NH_2 groups was verified quantitatively by ninhydrin analysis method. XPS analysis confirmed the presence of collagen as indicated by the increase in the nitrogen/carbon ratio on the surface of the polymer. Water contact angle results showed that the hydrophilicity of the surface has improved obviously after aminolysis and collagen immobilization. The potential for use of the neat and the modified PLA fibrous scaffolds as bone scaffolds was evaluated *in vitro* with mouse calvaria-derived, pre-osteoblastic cells (MC3T3-E1). Indirect cytotoxicity evaluation revealed that both the neat and the modified PLA fibrous scaffolds released no substances at levels that were harmful to cells. The attachment on various types of PLA fibrous scaffolds was lower compared with that on TCPS. While, the proliferation, ALP activity, and mineralization were improved on the modified surface, with the cells grown on the collagen-immobilized PLA fibrous scaffolds showed the greatest.

Key-words: Electrospinning; Poly(lactic acid); Immobilization; Collagen

* Authors to whom correspondence should be addressed: pitt.s@chula.ac.th (P. Supaphol)

1. Introduction

Bone injury and bone pathologies, as well as continued bone loss associated with aging, has resulted in increased research efforts focused on understanding cell–matrix interactions required for promoting bio-mineralization. Bone tissue engineering strategies, which combine materials engineering, cellular biology, and genetic engineering, are targeted at developing living bone replacements. One promising approach is to culture cells in three-dimensional (3D) scaffolds and to develop tissues of practical size scale and predetermined shapes. The scaffolds must support and maintain the normal state of differentiation within the cellular compartment. Ideally, a functional scaffolds should mimic the structure and biological function of native extracellular matrix (ECM) proteins, which provide mechanical support and regulate cellular activities.[1] Due to the high surface area to volume or mass ratio and the vast possibilities for surface functionalities, fibers as obtained by the process known as electro-spinning (e-spinning) have recently become the most studied form of tissue engineered scaffolds.[2,3]

Biodegradable polyesters such as poly(lactide-*co*-glycotide) (PLGA), polycaprolactone (PCL), poly(lactic acid) (PLA), and poly(3-hydroxybutyrate-co-3-hydroxyvalerate) (PHBV) are paid more attentions in tissue engineering because they not only provide the necessary substance on which cells can adhere, but also guide and regulate the proliferation and activities of the supported cells.[4-7] Poly(lactic acid) (PLA) is a thermoplastic polyester synthesized from ring opening polymerization of lactides which is widely used because of its robust mechanical properties and the ability to be processed into scaffolds of different shapes. PLA has a crystallinity around 37%, the glass transition temperature, T_g around 60–70°C is followed by melting behavior between 150 and170°C.[8] The presence of ester linkages in the polymer backbone allows gradual hydrolytic degradation of the polymer with carbon dioxide and water as the degradation products which are endogenous compounds and as such are non-toxic. PLA has therefore gained the approval of US Food and Drug Administration (FDA) for a variety of human clinical applications.[9] However, their hydrophobicity leads to the inefficiency of the scaffolds in constructing a friendly interface with living cells.

Because the initial response of cells to the biomaterials mostly depends on the surface properties, surface modification of polyesters to improve their cytocompatibility is necessary. Hydrophilic and protein-containing surfaces are known to promote cellular growth, therefore, many researches have been focusing on immobilizing biomolecules, such as, gelatin,[10,11] lamanin,[12-14] chitosan,[15,16] Arg-Gly-Asp (RGD)-containing peptide,[17-19] collagen [20-23] etc., on the surface of polymeric scaffolds. Four major protein immobilization techniques are currently used. These are: (i) covalent binding, in which attachment of the active component to the substrate surface uses a chemical reaction or linkage to activated surface groups;[15,22] (ii) entrapment, which is a physical trapping of the active components into a film, a gel or coating;[9] (iii) crosslinking, which combines features of both covalent binding and entrapment in which crosslinking agents are used both to polymerize a base layer or film and to anchor the entrapped protein molecules by forming intermolecular linkages between the substrate and the protein molecules;[24] and (iv) adsorption, which applies a protein solution to a substrate or film and allows the molecule to adsorb to the substrate over a specified time

period.[25] Among all the methods, covalent binding of biomolecules by coupling-agent bridging after aminolysis is one of the most acceptable method for the convenience and applicability to scaffolds. In addition it is suitable for both plane membrane and scaffolds with irregular shape and inner structure.[26] Due to the lack of chemical functionalities, it is usually difficult for polyesters to favor polymer–protein interaction, the covalent binding. The method of aminolysis between diamine and polyester matrix introduces functional amino groups, through which proteins such as collagen, chitosan etc., can be further introduced on the surface of polymeric scaffolds. [27,28] Mattanavee *et al.* [28] revealed that among the various biomolecule-immobilized PCL fibrous scaffolds, the one that had been immobilized with type-I collagen showed the greatest ability in supporting both the attachment and the proliferation of mouse fibroblasts (L929), human epidermal keratinocytes (HEK001), and mouse calvaria-derived, pre-osteoblastic cells (MC3T3-E1). In this work, the surface hydrophobicity of e-spun PLA fiber mats was improved by aminolysis with 1,6-hexamethylenediamine (HMD) to introduce free amino groups onto a ester-containing polymer surface. Type-I collagen, which is the major collagen-based protein synthesized by osteoblasts,[29-30] was subsequently immobilized with *N,N′*-disuccinimidyl carbonate (DSC) as a coupling agent. Indirect cytotoxicity evaluation of the neat and modified PLA e-spun fiber mats based on mouse fibroblasts (L929) and pre-osteoblasts (MC3T3-E1) was investigated. The potential for use of these e-spun fiber mats as bone scaffold was further evaluated *in vitro* with MC3T3-E1 in terms of attachment, proliferation, alkaline phosphatase (ALP) activity, and mineralization of the cells that were cultured directly on the scaffolds, in comparison to those of the cells on a tissue-culture polystyrene plate (TCPS).

2. Experimental Section

2.1. Materials. Materials used in the fabrication of the fibrous scaffolds were poly(lactic acid) (PLA; M_n = 80,000 g mol^{-1}; Aldrich, USA), dichloromethane (DCM; Carlo Erba, Italy), and *N*,*N*' dimethylformamide [DMF; Lab-Scan (Asia), Thailand]. Materials used in the surface modification of the PLA fibrous scaffolds were type-I collagen (from calf skin; Sigma, USA), 1,6-hexamethylene-diamine (HMD; Aldrich, USA), and *N*,*N′*-disuccinimidylcarbonate (DSC; Aldrich, USA). All other chemicals were of analytical reagent grade and used without further purification.

2.2. Preparation and characterization of e-spun PLA fibrous scaffolds. Electro-spun fiber mats of poly(lactic acid) were prepared by e-spinning from 10% w/v PLA solution in 7:3 v/v dichloromethane/ *N*,*N*'-dimethylformamide (DCM/DMF). The as-prepared PLA solutions were continuously stirred until clear solutions were obtained. The solution was fed into a glass syringe fitted with a blunt 20-gauge stainless steel hypodermic needle (OD = 0.91 mm), which used as the nozzle. An aluminum sheet wrapped around a home-made rotating cylinder (width and diameter ≈15 cm; rotational speed ≈ 50 rpm) was used as the collector. The distance from the tip of the needle to the surface of the Al sheet (measured at right angle to the surface) defining the collection distance was fixed at 18 cm. A Gamma High-Voltage Research Inc. (Ormond Beach, Florida), DC power supply was used to generate a high dc potential which was fixed at 20 kV. The emitting electrode of positive polarity was connected to the needle, while the grounding one was to the collector. E-spinning of the

as-prepared PLA solution was done continuously for 12 h. The obtained translucent electro-spun PLA fibrous scaffolds were dried in *vacuo* at room temperature prior to further modification. The thickness of the obtained PLA fiber mats was ~136 ± 5 μm. Morphological appearance and size of the individual fibers of the scaffolds were examined by JEOL JSM 5410LV scanning electron microscopy (SEM) (see Supporting Information). At least 100 readings of the fiber diameters from various SEM images were statistically analyzed using SemAphore 4.0 software, from which the arithmetic mean value of the individual fibers within the PLA fiber mats was determined to be 0.63 ± 0.1 μm.

2.3. Surface modification of PLA fibrous scaffolds. The PLA fibrous membranes were first immersed in an ethanolic aqueous solution (1:1 v/v) for 2 to 3 h to cleanse the fiber surface and then washed with a large amount of deionized water. The scaffolds were subjected to aminolysis through an immersion in a 1,6-hexamethylene-diamine/isopropanol (HMD/IPA) solution of varying concentration (i.e., 0.02, 0.04, 0.06, 0.08, and 0.1 gml^{-1}) and varying reaction time (i.e., 2, 5, 8, 15, 20, 30 min) at 50°c. The aminolyzed PLA fibrous scaffolds were then rinsed with deionized water for 24 h at room temperature to remove unreacted HMD and dried *in vacuo* at room temperature to reach a constant weight. Immobilization of type-I collagen on the surface of the PLA fibrous scaffolds was carried out by first activating the aminolyzed PLA fibrous scaffolds in 0.1 M *N,N′*-disuccinimidyl carbonate/dimethylsulfoxide (DSC/DMSO) solution in the presence of 0.1 M triethylamine (TEA) for 3 h at room temperature, followed by rinsing the fiber mats with a large quantity of deionized water. The activated PLA fibrous scaffolds were then immersed in 0.5 or 3 $mg{\cdot}ml^{-1}$ of collagen/phosphate buffer saline (PBS) solution at ambient temperature for 24 h. The collagen-immobilized PLA fibrous scaffolds were rinsed by soaking in a large quantity of deionized water for 24 h and finally dried *in vacuo* at room temperature. The chemical pathway for the immobilization of type-I collagen on the surface of e-spun PLA fibrous scaffolds is summarized in the Figure 1.

2.4. Characterization of neat and modified PLA fibrous scaffolds.

Quantification of free amino groups on the surface. UV-Vis spectroscopy was used for determination the amount of amino (NH_2) groups on the surface of the aminolyzed and the collagen-immobilized PLA fibrous scaffolds using ninhydrin method. First, the fibrous scaffolds were immersed in 1 M ninhydrin/ethanol solution for 1 min in a glass tube, followed by heating at 80°C for 15 min to accelerate the reaction between ninhydrin and the NH_2 groups that might be present on the surface of the scaffolds. As an evidence for the actual presence of the NH_2 groups, the surface of the scaffolds would turn blue. After complete evaporation of absorbed ethanol, 1,4-dioxane was added in the tube to dissolve the scaffolds. IPA was then added to stabilize the blue compound. Absorbance of the obtained compound in the UV-visible range was measured in a spectrophotometer (UV-2550, Shimadzu, Kyoto, Japan) at 538 nm against a predetermined calibration curve that was obtained from HMD solutions in 1,4-dioxane/IPA (1:1 v/v) (see Supporting Information).

Surface Wettability. Water contact angles of the neat and modified PLA fibrous scaffolds were measured at room temperature and, using sessile drop method on a telescopic goniometer (KRUSS Gmbh, DSA10-Mk2 T1C, Germany) equipped with a Gilmont syringe and a 24-gauge flat-tipped needle. The measurements were carried out in pentuplicate on different areas of each sample and the resulting values were averaged.

Elemental composition of the surface. X-ray Photoelectron Spectrometer (XPS; AMICUS, KRATOS, Japan), also known as Electron Spectroscopy for Chemical Analysis (ESCA), was used to investigate the elemental composition and chemical state of the elements on the surface. The XPS N_{1s}/C_{1s} peak-area rations was used as a marker for the analysis of the relative amount of free amino groups and collagen immobilized on the surface.

2.5. Biological characterization of neat and modified PLA fibrous scaffolds.

Cell culture and cell seeding. Mouse fibroblasts (L929) and mouse calvaria-derived, pre-osteoblastic cells (MC3T3-E1) were used as reference cell lines. L929 were cultured as monolayer in Dulbecco's modified Eagle's medium (DMEM; Sigma-Aldrich, USA), supplemented with 10% fetal bovine serum (FBS; BIOCHROM AG), 1% L-glutamine (Invitrogen Corp.), and a 1% antibiotic and antimycotic formulation [containing penicillin G sodium, streptomycin sulfate, and amphotericin B (Invitrogen Corp., USA)]. MC3T3-E1 were cultured in Minimum Essential Medium (with Earle's Balanced Salts) (MEM; Hyclone, USA), supplemented by 10% fetal bovine serum (FBS; BIOCHROM AG, Germany), 1% L-glutamine (Invitrogen Corp., USA) and 1% antibiotic and antimycotic formulation [containing penicillin G sodium, streptomycin sulfate, and amphotericin B (Invitrogen Corp., USA)]. The medium was replaced every 2 days and the cultures were maintained at 37°C in a humidified atmosphere containing 5% CO_2.

Each scaffold was cut into circular discs (about 15 mm in diameter) and the disc specimens were placed in wells of a 24-well tissue-culture polystyrene plate (TCPS; Biokom Systems, Poland), and were later sterilized in 70% ethanol for 30 min. The specimens were then washed with autoclaved de-ionized water, PBS and subsequently immersed in MEM overnight. To ensure a complete contact between the specimens and the wells, the specimens were pressed with a metal ring (about 12 mm in diameter). MC3T3-E1 from the culture was trypsinized [0.25% trypsin containing 1 mM EDTA (Invitrogen Crop., USA)] and counted by a hemacytometer (Hausser Scientific, USA). MC3T3-E1 were seeded at a density of about 60,000 cells/well for attachment study and 30,000 cells/well for proliferation study, on the scaffold specimens and empty wells of TCPS that were used as control. For indirect cytotoxicity, alkaline phosphatase activity, mineralization evaluations, MC3T3-E1 were seeded at a density of about 40,000 cells/well on the scaffold specimens and empty wells of TCPS. The culture was maintained in an incubator at 37°C in a humidified atmosphere containing 5% CO_2.

***Cytotoxicity evaluation*.** Two types of cells were used: 1) mouse calvaria-derived, pre-osteoblastic cells (MC3T3-E1) and 2) mouse fibroblasts (L929). Indirect cytotoxicity test was conducted on TCPS, neat PLA, aminolyzed PLA, activated PLA, collagen-immobilized PLA, and polycaprolactone/hydroxyapatite (PCL/HA) which used as positive control. First, extraction media were prepared by immersing samples (about 15 mm in diameter) in a serum-free medium (SFM; containing DMEM, 1% L-glutamine, 1 % lactabumin, and 1% antibiotic and antimycotic formulation for L929 and containing MEM, 1% L-glutamine, 1 % lactabumin, and 1% antibiotic and antimycotic formulation for MC3T3-E1) for 1, 3, and 7 days. Each of these extraction media was used to evaluate the cytotoxicity of the scaffolds. L929 or MC3T3-E1 were separately cultured in wells of a 24-well culture plate in 10%serum-containing DMEM and MEM, respectively, for 16 h to allow cell attachment on the plate. Then, the cells were starved with SFM for 24 h, after which time the medium was replaced with an

extraction medium. After 24 h of cell culturing in the extraction medium, 3-(4,5-dimethylthiazol-2-yl)-2,5-diphenyl-tetrazolium bromide (MTT) assay was carried out to quantify the amount of viable cells (see Supporting Information). The experiments were carried out in triplicate.

Another experiment was conducted to confirm the cytocompatibility of the materials on MC3T3-E1. Extraction media were prepared by immersing samples (about 15 mm in diameter) in a serum-free medium (SFM; MEM, 1% L-glutamine, 1 % lactabumin, and 1% antibiotic and antimycotic formulation for MC3T3-E1) for 7 d. The sample was treated in the same manner as the previous experiment up to the point was the cells were starved. After that the SFM was replaced with 2%serum-containing MEM diluted with as-prepared 7-day extraction medium for 1, 2, and 3 d to allow cell growth on the plate. After which time the viability of cell was again quantified by MTT assay in triplicate.

Cell attachment and cell proliferation. Cell behavior such as adhesion and proliferation represent the initial phase of cell–scaffold communication that subsequently effect differentiation and mineralization. For attachment study, MC3T3-E1 was allowed to attach to TCPS, aminolyzed PLA, activated PLA, collagen-immobilized PLA for 2, 4 and 16 h, respectively. At each specified seeding time, the number of the attached cells was quantified by MTT assay. Each sample was rinsed with PBS to remove unattached cells prior to MTT assay. Morphological appearance of the cells during attachment period was observed by SEM. For proliferation study, the viability of cells on the specimens was determined after 1, 2, and 3 day of cell culturing by MTT assay. The experiments were carried out in triplicate.

***Morphological observation of cultured cells*.** After removal of the culture medium, the cell-cultured scaffold specimens were rinsed with PBS twice and the cells were then fixed with 3% glutaraldehyde solution, which was diluted from 50% glutaraldehyde solution (Sigma, USA) with PBS, at 500 µl/well. After 30 min, they were rinsed again with PBS. After cell fixation, the specimens were dehydrated in an ethanol solution of varying concentration (i.e. 30, 50, 70, 90, and 100%, respectively) for about 2 min at each concentration. The specimens were then dried in 100% hexamethyldisilazane (HMDS; Sigma, USA) for 5 min and later let dry in air after removal of HMDS. After completely dried, the specimens were mounted on an SEM stub, coated with gold, and observed by a JEOL JSM-5200 scanning electron microscope (SEM).

***Production of Alkaline Phosphatase of Cultured Cells*.** ALP activity of MC3T3-E1 was measured using Alkaline Phosphate Yellow Liquid. In this reaction, ALP catalyzes the hydrolysis of colorless organic phosphate ester substrate, *p*-nitrophenyl phosphate (pNPP) to a yellow product, p-nitrophenol, and phosphate. MC3T3-E1 was cultured on scaffold specimens for 3, 5, and 7 day to observe the production of alkaline phosphatase (ALP). The specimens were rinsed with PBS 2 times after removal of culture medium. Alkaline lysis buffer (10 mM Tris-HCl, 2 mM $MgCl_2$, 0.1% Triton-X100, pH 10) (100 µl/well) was added and the samples were scrapped and then frozen at -20°C for at least 30 min prior to the next step. An aqueous solution of 2 mg/ml *p*-nitrophenyl phosphate (pNPP; Zymed Laboratories, USA) mixed with 0.1 M amino propanol (10 µl/well) in 2 mM $MgCl_2$ (100 µl/well) having a pH of 10.5 was prepared and added into the specimens (110 µl/well). The specimens were incubated at 37°C for 15 min. The reaction was stopped by adding 900 µl /well of 50 mM NaOH and the extracted solution was transferred to a cuvette and placed in the UV-visible spectrophotometer,

from which the absorbance at 410 nm was measured. The amount of ALP was then calculated against a standard curve. In order to calculate for the ALP activity, the amount of ALP had to be normalized by the amount of total protein synthesized. In the protein assay, the samples were treated in the same manner as the ALP assay up to the point was the specimens were frozen. After freezing, bicinchoninic acid (BCA; Pierce Biotechnology, USA) solution was added into the specimens. The specimens were incubated at 37°C for 15 min. The absorbance of the medium solution was then measured at 562 nm by the UV-visible spectrophotometer and the amount of the total protein was calculated against a standard curve.

***Mineralization analysis*.** Alizarin Red-S is a dye that binds selectively calcium salts and is widely used for mineral staining (the staining product i.e., an Alizarin Red S-calcium chelating product). The isolated osteoblastic cells were plated in 24-well plates at 40,000 cells/well and cultured in the culture medium. After 24 h, the cultures were treated with culture medium, with the supplement of 50 μg/ml ascorbic acid (Sigma, USA), 5 mM β-glycerophosphate (Sigma, USA), and 0.2 μg/ml dexamethasone (Sigma, USA), the medium was replaced every 2 days. After 16 days treatment, cells were washed with PBS and fixed with ice-cold absolute methanol for 10 min. Fixed cells were stained with 1% Alizarin Red in deionized water (Sigma, USA) (pH 4.2) for 2-3 min. After removing alizarin red-S solution, the cells were rinsed with deionized water and dried at room temperature. The images of each culture were captured and the stain was extracted with the use of 10% cetylpyridinium chloride (Sigma, USA) in 10 mM sodium phosphate for 1 h and absorbance of the collected dye was read at 570 nm in spectrophotometer (Thermo Spectronics Genesis10 UV-visible spectrophotometer).

2.6. Statistical analysis. Values expressed as the mean ± standard deviation. Statistical analysis of different data groups was performed using One-Way Analysis of Variance (ANOVA) with the least-significant difference (LSD) test using SPSS software version 11.5. The values of p lower 0.05 were considered statistically significant.

3. Results and Discussion

By reaction with diamine, 1,6-hexanediamine (HMD), amino groups can be covalently introduced onto the surface of the electro-spun PLA fibrous membranes to obtain the aminolyzed PLA fibrous membranes. One amino group (NH_2) of HMD reacts with an ester group (—COO—) of PLA to form the amide linkage (—CONH—), while another amino group is unreacted and free for the further reaction. These free NH_2 groups can be used as active sites through which proteins like collagen can be bonded to the surface using *N,N′*-disuccinimidyl carbonate (DSC) as a coupling agent. However, to avoid aggregation, two-step procedure was employed. The attached amino groups had been first activated with DSC with *N*-hydroxysuccinimide being lost from the reaction and the as-formed succinimidyl esters were later reacted with respective collagen, with *N*-hydroxysuccinimide again being cleaved from the reaction.

3.1. Characterization of neat and modified PLA fibrous scaffolds.

Quantification of free amino groups on the surface. The existence of free amino groups (NH_2) on PLA surface is a prerequisite for protein bonding in this modification method. It is important to

confirm the existence of amino groups before protein is further introduced. Herein, ninhydrin is used as an indicator to confirm and quantify the $–NH_2$ moiety on the aminolyzed PLA surface. The NH_2 density on e-spun PLA fibrous scaffold surface was influenced by the concentration of HMD, aminolyzing time, temperature, and so on. Because the glass transition temperature (T_g) of the present PLA is ~60-70°C, the aminolyzing temperature should be lower than this value to maintain the shape of the material. Hence, 50°C was chosen to perform the following reactions. Table 1 shows that NH_2 density increased with increasing HMD concentration. However, when the concentration of HMD is equal to or greater than 0.1 g/ml, the mechanical integrity of the e-spun PLA fiber mats was affected. Table 2 shows that the surface-bound NH_2 increased with increasing aminolyzing time to reach a maximum value at about 15 min, and then decreased slightly. The decrease at the longer reaction time may be caused by a further reaction of the free amino group on the terminal chain with other ester groups, or by the degradation of the superficial layer[27]. Both of these situations will reduce the density of the surface amino groups and thus intensity of purple colored complex. To maintain enough mechanical integrity for practical applications, PLA e-spun fiber mats were aminolyzed in a 0.04 g/ml HMD/IPA solution at 50°C for 15 min. According to the calibration curve obtained with 1,4-dioxane/isopropanol (1:1, v/v) solution containing HMD of known concentration, the NH_2 density on PLA e-spun fiber mat aminolyzed under these conditions was $(3.7 \pm 0.02) \times 10^{-7}$ mol/cm^2 (see Table 3). It also shows that after immobilization with 0.5 mg/ml and 3.0 mg/ml type-I collagen, the average areal density of the amino groups on the surface of the PLA fibrous scaffolds were $(4.52 \pm 0.08) \times 10^{-9}$ and $(3.21 \pm 0.2) \times 10^{-8}$, respectively.

Surface Wettability. To further evaluate the effect of aminolysis and collagen immobilization, surface wettability of the modified PLA fibrous scaffolds with respect to that of the neat PLA fibrous scaffolds was measured. Table 4 shows the surface wettability of neat PLA, aminolyzed PLA, activated PLA, collagen-immobilized PLA (without coupling agent; collagen = 0.5 mg/ml), collagen-immobilized PLA (collagen = 0.5 mg/ml), and collagen-immobilized PLA (collagen = 3 mg/ml) fibrous scaffolds. The water contact angle measured by the sessile drop method decreased slightly from 106.8˚ to 99.5˚ after the scaffold was aminolyzed with 0.04 g/ml of HMD/IPA solution for 15 min. That is, the introduction of the amino groups on the surface of the PLA fibrous scaffolds improved the hydrophilicity of the surface. After the aminolyzed PLA fibrous scaffolds has activated with DSC, their surface became more hydrophobic as evidenced by the water contact angle of 112.5˚. Water contact angle decreased substantially after the collagen was bonded. Figure 2 shows that the surface became much more hydrophilic after collagen immobilization. Water contact angle was 79.4˚ for collagen 0.5 mg/ml immersion and was 73.0˚ for collagen 3 mg/ml immersion. These results show that the more collagen concentration used, the more collagen can be bonded to the PLA surface. It has been known that physisorption processes are virtually always involved in a coating procedure. In our case, we had tried physical coating of collagen on unactivated PLA fibrous scaffolds. Water contact angle measurements showed that water contact angle of physisorbed collagen-coated PLA surfaces was slightly lower than the aminolyzed PLA surface. On the other hand, for collagen-covalently bonded surface, they exhibited much lower water contact angle. That means activation step is an important step in protein grafting process.

Elemental composition of the surface. The surface alteration after the PLA fibrous scaffolds were modified was studied by X-ray Photoelectron Spectrometer (XPS). To study the effect of the aminolysis condition on the surface alteration, N_{1s}/C_{1s} ratios as a function of HMD concentration and aminolyzing time were evaluated. Table 5 shows that the more diamine concentration used, the more N_{1s}/C_{1s} ratio observed which could be due to increasing in introduced NH_2 group concentration. Table 6 shows that the N_{1s}/C_{1s} ratio increased with increasing aminolyzing time to reach a maximum value at about 15 min, and then decreased slightly, which, in addition to the results on ninhydrin analysis method. Figure 3 shows that N_{1s} peaks obviously appeared after immobilization of collagen, which confirmed protein grafting. Table 7 shows N_{1s}/C_{1s} ratio of the neat and the modified PLA fibrous scaffolds. After aminolysis of PLA fibrous scaffold, the N_{1s}/C_{1s} ratio was increased from 0 to 0.0290 because of NH_2 groups introduced on the surface. The N_{1s}/C_{1s} ratio was further increased to 0.0381 by reaction with DSC. It shows that the nitrogen concentration increased when succinimidyl esters was formed. Finally, it was obviously increasing in N_{1s}/C_{1s} ratio after collagen immobilization due to the large amount of nitrogen atom in collagen structure was additionally introduced.

3.2. Biological evaluation of neat and modified PLA fibrous scaffolds.

Indirect cytotoxicity evaluation. The biocompatibity of these PLA e-spun fiber mats as bone scaffolds was assessed by an indirect cytotoxicity evaluation with mouse fibroblastic cells (L929) and mouse calvaria-derived pre-osteoblastic cells (MC3T3-E1), based on the initial 40,000 cells/well of cells seeded. Indirect cytotoxicity test was conducted on neat, aminolyzed, activated, collagen-immobilized PLA fibrous scaffolds. In this experiment, the PCL/HA that was prepared from particulate leaching technique, was chosen to be the positive control. Even though we were interested in using the obtained modified fiber mats as potential bone scaffolds, it was mandatory to test the materials with L929 just to comply with the ISO10993-5 standard test method. Figure 4a shows %viability obtained from MTT assay of L929 which were cultured with the 1, 3, 7 day- extraction media in comparison with those cultured with SFM (i.e. control). The viability of the cells that had been cultured with SFM at any given time point was taken as the basis to arrive at the relative viability shown in the figure. Evidently, the viability of L929 for all types of modified PLA fibrous scaffolds exhibited slightly lower, in comparison with that of the control (100%). While the neat PLA fiber and PCL/HA scaffold which used as positive control exhibited comparable viability. In a similar manner was found for MC3T3-E1 (see Figure 4b). However, the viability of cells that were cultured with 7-day extraction media prepared from modified scaffolds were significantly lower, in comparison with that were cultured with 7-day extraction media prepared from the neat PLA scaffold and PCL/HA. Thus, we had to set other experiment to confirm the cytocompatibility of the modified PLA fibrous scaffolds.

MC3T3-E1 was cultured in wells of a 24-well culture plate in 2%serum-containing MEM diluted with 7-day extraction medium for 1, 2, and 3 d to allow cell growth on the plate. Figure 5 shows that the viability of MC3T3-E1, cultured with 2%serum-containing MEM diluted with 7-day extraction media prepared by all types of modified scaffolds, were increased with increasing the culturing time in the respective media. All of the obtained results clearly suggested that all types of the PLA fibrous scaffolds, released no substances at levels that were harmful to both types of cells.

***Cell attachment and cell proliferation*.** The potential for use of the neat and the modified PLA fibrous scaffolds was further evaluated by observing their ability to support both the adhesion and the proliferation of MC3T3-E1. The viability of the cells that had been cultured on the surface of TCPS for 2 h was taken as the basis to arrive at the relative viability shown in a figure. Figure 6 shows the attachment of MC3T3-E1 on the surfaces of TCPS, neat PLA, aminolyzed PLA, activated PLA and collagen-immobilized PLA at 2, 4, and 16 h after cell seeding in terms of viability. On TCPS, the number of the attached cells increased from ~100% at 2 h after cell seeding to ~111% at 16 h after cell seeding, based on the initial number of cells seeded (60,000 cells/well). With regards to MC3T3-E1, the surfaces of all of the PLA fibrous scaffolds were inferior in supporting the attachment of the cells to that of TCPS. Specifically, the number of cells attached on these fibrous scaffolds was only ~50% in comparison with that on TCPS at any given time point. There was not significantly different in the viability among all types of the fibrous scaffolds. Figure 7 shows the proliferation of MC3T3-E1 on the surfaces of TCPS, neat PLA, aminolyzed PLA, activated PLA and collagen-immobilized PLA on day 1, 2, and 3 after cell culture in terms of viability (%relative to TCPS at day1). On TCPS, the number of cells increased from ~100% on day1 after cell culture to ~187% (i.e., an increase of about 2 fold from the initial number of cells seeded) on day 3 after cell culture, based on the initial 30,000 cells/well of cells seeded. In comparison with that on TCPS, the viability of the cells cultured on the modified PLA fibrous scaffolds were significantly higher at any given time point. The viability of cells proliferated on these fibrous scaffolds, at day 3, was higher than TCPS of about 2 fold for neat PLA, aminolyzed PLA, and activated PLA and about 3.5 fold for collagen-immobilized PLA. Marked improvement was achieved with the collagen-immobilized PLA fibrous scaffolds on day 3 after cell culture.

The lesser viability of cells in the attachment period on various types of the fibrous scaffolds in comparison with that on TCPS could be due to the lesser number of cells that were able to attach on the rougher and more hydrophobic surface of the fibrous scaffolds in comparison with the smoother and hydrophilic surface of TCPS. On the contrary, the greater number of cells in the proliferation period on all types of PLA fibrous scaffolds could be because of high surface area to mass or volume and high porosity of the e-spun fiber mats though which the cells were able to penetrate into the scaffolds. Among the various modified PLA fibrous scaffolds, the collagen-immobilized PLA fibrous scaffolds provided the most significant improvement in the ability to support the proliferation of the cells which could be due to the protein-containing and hydrophilic surface of the substrate.

***Cell Morphology*.** Table 8 shows selected SEM image (magnification = 2000X; scale bar = 10 μm) of MC3T3-E1 that were cultured on the surface of glass, neat PLA, aminolyzed PLA, activated PLA and collagen-immobilized PLA at two different time points, while the SEM images at magnification = 500X are available as Supporting Information. The use of glass as the control instead of TCPS was due to the ease of taking the samples to SEM observation. These images provided snap shots in time that revealed the morphology of the cells and interaction between the cells and the tested surfaces. At 4 h after cell seeding, based on the initial 60,000 cells/well of cells seeded, the majority of the cells on the glass surface started to extend their cytoplasm, an evidence of the ability of the cells to attach on the surface. At 16 h after cell seeding, expansion of the cytoplasm of the majority of the cells was

evident. While the majority of MC3T3-E1 that had been seeded on the surfaces of unmodified PLA fibrous scaffolds for 4 h was remained round, but a closer examination around the edge of the cells revealed an evidence of filopodia (i.e., slender cytoplasmic projections extending from the leading edge of the migrating cells that help the cells during their migration over the surface of a scaffolds). The majority of the cells were evidently expanded after 16 h of cell seeding. On the other hand, the majority of the cells seeded on the surfaces of various types of modified PLA fibrous scaffolds showed an evidence of the extension of their cytoplasm on the fibrous surface even at 4 h after cell seeding, with collagen-immobilized PLA surface did so to a greater extent. These results suggested that the cells prefer the fibrous surfaces of modified PLA over that of the unmodified. Specifically, the cells were seemed to prefer the collagen-containing than others.

***Alkaline Phosphatase (ALP) Activity*.** The ability for these PLA fibrous scaffolds to support differentiation, in addition to attachment and proliferation, of cultured cells is another important aspect suggesting actual applicability of the scaffold. Alkaline phosphatase is a membrane bound enzyme and its activity is used as an osteoblastic differentiation marker, as it is produced only by cells showing mineralized ECM. The ALP activity of MC3T3-E1 on TCPS (i.e. controls), neat PLA, aminolyzed PLA, activated PLA, and collagen-immobilized PLA were monitored at 3, 5 and 7 days in culture (see Figure 8). Apparently, the amount of ALP synthesized by the cells that were cultured on TCPS and all of the fibrous scaffolds increased with the initial increase in time in culture between day 3 and 5, reached a maximum level on day 5, and decreased with a further increase in culture after day 3. In comparison with other substrates, TCPS exhibited the highest ALP activity of MC3T3-E1. According to Figure 8, activated PLA and collagen-immobilized PLA fibrous scaffolds showed the highest ALP activity among the various fibrous scaffolds investigated at day 3 of cell culturing time. And at day 5 and day 7 collagen-immobilized PLA fibrous scaffolds exhibited the highest ALP activity.

The decrease in the ALP activity, after day 5 for the cells grown on both TCPS and PLA fibrous scaffolds, with a further increase in the culturing time can be due to cellular process switching onto further step (i.e. mineralization).[31,32] Since ALP is not an exclusive protein synthesized by osteoblasts as it is also found in tissues of such organs as kidneys, small intestines, and placenta, the presence of ALP of MC3T3-E1 that were cultured on these substrates could not be used as the sole marker to confirm the osteoblastic phenotype of the cells.[33] From the obtained results, it was suggested that collagen-immobilized PLA fibrous scaffold was the best among the PLA fibrous scaffolds that promoted both proliferation and differentiation of MC3T3-E1.

***Mineralization*.** Mineralization refers to cell-mediated deposition of extracellular calcium and phosphorus salts where anionic matrix molecules take up the Ca^{2+}, phosphate ions and serve as nucleation and growth sites leading to calcification. Mineralization was quantified by Alizarin Red-S studies (see Figure 9), showing degree of mineralization as indicated by extracted stain absorbance obtained on day 16 of cell culture was in the order of collagen-immobilized PLA > aminolyzed PLA > neat PLA > activated PLA > TCPS > glass. The collagen-immobilized PLA scaffold showed 16% higher mineralization than neat PLA scaffold with significant level of $p < 0.05$ confirming the effectiveness of collagen immobilization of PLA e-spun fibers in mineral formation by MC3T3-E1. The photographic images (see Figure 10) of scaffolds stained with Alizarin Red-S for 16 days supported

the above data where high intensity of staining minerals was observed on various type of PLA fibrous scaffolds displaying an overall enhancing effect in mineralization of MC3T3-E1 cells and proving collagen immobilization as an indispensable method for the fabrication of superior fibrous scaffolds for bone tissue engineering.

4. Conclusion

In the present study, type-I collagen was used to modify PLA in the form of electro-spun fibrous membranes for the purpose of improving cytocompatibility. The XPS confirmed that collagen was immobilized on the surface of PLA fiber mats by the reaction of aminolyzed PLA and type-I collagen employing DSC as a coupling agent. The existence of NH_2 groups on aminolyzed PLA surfaces has been characterized by ninhydrin analysis method, which revealed that the NH_2 density was influenced by the HMD concentration and aminolyzing time. The data of contact angle against water revealed that it had improved the surface hydrophilicity by the aminolysis and the further immobilization of collagen. The cultured MC3T3-E1 *in vitro* proved that the cell proliferation, alkaline phosphatase (ALP) activity and mineralization of modified PLA e-spun fibers were improved compared with the neat PLA fiber. Among the various modified PLA scaffolds, collagen-immobilized PLA showed the greatest ability to support cell proliferation, alkaline ALP activity, and mineralization. Therefore, collagen-immobilized PLA fibrous scaffold is promising material to accelerate bone regeneration.

Acknowledgments. This research work was partial supported in by 1) the Petroleum and Petrochemical College (PPC), Chulalongkorn University, 2) the National Center of Excellence for Petroleum, Petrochemicals, and Advanced Materials, Thailand, and 3) Department of Anatomy, Faculty of Dentistry, Chulalongkorn University. Associate Professor Varong Pavarajarn, department of Chemical Engineering, Faculty of Engineering, Chulalongkorn University, is acknowledged for the access to the XPS research facility.

References and Notes

(1) Rho, K. S.; Jeong, L.; Lee, G.; Seo, B. M.; Park, Y. J.; Hong, S. D.; Roh, S.; Cho, J. J.; Park, W. H.; Min, B. M. *Biomaterials* **2006**, *27*, 1452-1461.

(2) Fujihara, K.; Kotakib, M.; Ramakrishna, S. *Biomaterials* **2005**, 26, 4139–4147.

(3) Suwantong, O.; Waleetorncheepsawat, S.; Sanchavanakit, N.; Pavasant, P.; Cheepsunthorn, P.; Bunaprasert, T.; Supaphol, P. *International Journal of Biological Macromolecules.* **2007**, 40, 217–223.

(4) Hsu, S.H.; Chu, W.P.; Lin, Y.S.; Chiang, Y.L. *Journal of Biotechnology* **2004**, 111, 143–154.

(5) Wutticharoenmongkol, P.; Sanchavanakit, N.; Pavasant, P.; Supaphol, P. *Macromolecular Bioscience* **2006**, 6, 70-77.

(6) Chen, F.; Lee, C.N.; Teoh S.H. *Materials Science and Engineering* **2007**, 27, 325–332.

(7) Sombatmankhong, K.; Sanchavanakit, N.; Pavasant, P.; Supaphol, P. *Polymer* **2007**, 48, 1419-1427.

(8) Gupta, B.; Revagade, N.; Hilborn, J. *Progress in Polymer Science* **2007**, 32 , 455–482.

(9) Cui, Y.L.; Qi, A.D.; Liu, W.G.; Wang, X.H.; Wang, H.; Ma, D.M.; Yao, K.D. *Biomaterial* **2003**, 24 , 3859–3868.

(10) Zhu, Y.; Gao, C.; Shen, J. *Biomaterials* **2002**, 23, 4889–4895.

(11) Zhu, Y.; Gao, C.; He, T.; Shen, J. *Tissue Engineering* **2004**, 10, 1/2.

(12) Matsuda, A.; Kobayashi, H.; Itoh, S.; Kataoka, K.; Tanaka, J. *Biomaterials* **2005**, 26, 2273–2279.

(13) Santiago, L.Y.; Nowak, R.W.; Rubin, J.P.; Marra, K.G. *Biomaterials* **2006**, 27, 2962–2969.

(14) Koh, H.S.; Yong, T.; Chan, C.K.; Ramakrishna, S. *Biomaterials* **2008**, 29, 3574–3582.

(15) Wang, X.H.; Li, D.P.; Wang, W.J.; Feng, Q.L.; Cui, F.Z.; Xub, Y.X.; Song, X.H. *International Journal of Biological Macromolecules* **2003**, 33, 95–100.

(16) Ding, Z.; Chen, J.; Gao, S.; Chang, J.; Zhang, J.; Kang, E.T. *Biomaterials* **2004**, 25, 1059–1067.

(17) Hersel, U.; Dahmen, C.; Kessler, H. *Biomaterials* **2003**, 24, 4385–4415.

(18) Hsu, S.H.; Chu, W.P.; Lin, Y.S.; Chiang, Y.L. *Journal of Biotechnology* **2004**, 111, 143–154.

(19) Sun, H.; Wirse A.; Albertsson, A.C. *Biomacromolecules* **2004**, 5, 2275-2280.

(20) Ma, Z.; Gao, C.; Ji, J.; Shen, J. *European Polymer Journal* **2002**, 38, 2279–2284.

(21) Zhu, Y.; Gao, C.; Liu, X.; Shen, J. *Biomacromolecules* **2002**, 3, 1312-1319.

(22) Yang, Y.; Porté, M.C.; Marmey, P.; Haj, A.J.E.; Amédéé, J.; Baquey, C. *Nuclear Instruments and Methods in Physics Research B* **2003**, 207, 165–174.

(23) Cheng, Z.; Teoh, S. H. *Biomaterials* **2004**, *25*, 1991-2001.

(24) Karakeçili, A.G.; Satriano, C.; Gümüşderelioğlu; Marletta, G. *Acta Biomaterialia* **2008**, 4, 989–996.

(25) Woo, K.M.; Jun, J.H.; Chen, V.J.; Seo, J.; Baek, J.H.; Ryoo, H.M.; Kim, G.S.; Somerman, M.J.; Ma, P.X. *Biomaterials* **2007**, 28, 335–343.

(26) Zhu, Y.; Gao, C.; Liu, Y.; Shen J. *Wiley InterScience* **2004** http://www.interscience. wiley.com

(27) Zhu, Y.; Chian, K.S.; Chan-Park, M.B.; Mhaisalkar, P.S.; Ratner, B.D. *Biomaterials* **2006**, 27, 68–78.

(28) Mattanavee, W.; Suwantong, O.; Puthong, S.; Bunaprasert, T.; Hoven, V.P.; Supaphol, P., Under submission.

(29) Hernández-Gil, I. F.-T.; Gracia, M. A. A.; Pingarrón, M. D. C.; Jerez, L. B. *Medicina Oral, Patología Oral y Cirugía Bucal* **2006**, *11*,47-51.

(30) Mano, J. F.; Silva, G. A.; Azevedo, H. S.; Malafaya, P. B.; Sousa, R. A.; Silva, S. S.; Boesel, L. F.; Oliveira, J. M.; Santos, T. C.; Marques, A. P.; Neves, N. M.; Reis, R. L. *Journal of the Royal Society: Interface* **2007**, *4*, 999

(31) Choi, J. Y.; Lee, B. H.; Song, K. B.; Park, R. W.; Kim, I. S.; Sohn, K. Y.; Jo, J. S.; Ryoo, H. M. *Journal of Cellular Biochemistry* **1996**, 61(4), 609-618.

(32) Yu, H.S.; Hong, S.J.; Kim, H.W. *Materials Chemistry and Physics* **2009**, 113, 873–877.

(33) Tsukamoto, Y.; Fukutani, S.; Mori, M. *Journal of Materials Science Materials in Medicine* **1992**, 3, 180-183.

CAPTION OF FIGURES

Figure 1. The chemical pathway for the immobilization of collagen.

Figure 2. Water dropped on the surface of neat PLA fibrous scaffold(a), and PLA fibrous scaffold immobilized with 3.0 mg/ml collagen.

Figure 3. The survey XPS spectra of (a) neat PLA, (b) PLA aminolyzed at a concentration of 0.04 g/ml 1,6-hexanediamine for 15 min at 50 °C, (c) activatedPLA, (d) PLA immobilized with collagen (0.5 mg/ml), and (c) PLA immobilized with collagen (3 mg/ml).

Figure 4. Indirect cytotoxic evaluation of neat PLA fibers, modified PLA fibers, and PCL/HA based on viability of mouse fibroblasts (L929) that had been cultured with the extraction media from each of these materials against the viability of the cells that had been cultured with the respective culture media for 1 day as a function of the incubation time of the extraction and the culture media of 1, 3, or 7 d. Statistical significance: $^{*}p < 0.05$ compared with control and $^{\#}p < 0.05$ compared to the neat PLA fibrous scaffolds at any given time point.

Figure 5. Indirect cytotoxic evaluation of neat PLA fibers, modified PLA fibers, and PCL/HA based on viability of pre-osteoblast (MC3T3-E1) that had been cultured with the extraction media from each of these materials against the viability of the cells that had been cultured with the respective culture media for 1 day as a function of the incubation time of the extraction and the culture media of 1, 3, or 7 d. Statistical significance: $^{*}p < 0.05$ compared with control and $^{\#}p < 0.05$ compared to the neat PLA fibrous scaffolds at any given time point.

Figure 6. Indirect cytotoxic evaluation of neat PLA fibers, modified PLA fibers, and PCL/HA based on viability of pre-osteoblast (MC3T3-E1) that had been cultured with the 7-day extraction media from each of these materials with 2% serum-containing MEM against the viability of the cells that had been cultured with the respective culture media for 1, 2, and 3 day. Statistical significance: $^{*}p < 0.05$ compared with control and $^{\#}p < 0.05$ compared to the neat PLA fibrous scaffolds at any given time point.

Figure 7. Attachment of MC3T3-E1 that had been seeded or cultured on the surfaces of TCPS, the neat and the modified PLA fibrous scaffolds for 2, 4, or 16 h. Statistical significance: $^{*}p < 0.05$ compared with control and $^{\#}p < 0.05$ compared to the neat PLA fibrous scaffolds at any given time point.

Figure 8. Proliferation of MC3T3-E1 that had been seeded or cultured on the surfaces of TCPS, the neat and the modified PLA fibrous scaffolds for 1, 2, or 3d. Statistical significance: $^{*}p < 0.05$ compared with control and $^{\#}p < 0.05$ compared to the neat PLA fibrous scaffolds at any given time point.

Figure 9. Alkaline phosphatase (ALP) activity of MC3T3-E1 that were cultured on the surfaces of TCPS, the neat and the modified PLA fibrous scaffolds for 3, 5, or 7 d.

Figure 10. Quantification of mineral deposition in MC3T3-E1 by the method of Alizarin Red-S staining. Statistical significance: $^{*}p < 0.05$ compared with control and $^{\#}p < 0.05$ compared to the neat PLA fibrous scaffolds at any given time point.

Figure 11. Images of Alizarin Red-S staining for the mineralization in MC3T3-E1 for day 16 (a) glass (b) TCPS (c) neat PLA (d) aminolyzed PLA (e) activated PLA (f) collagen-immobilized PLA fibrous scaffold.

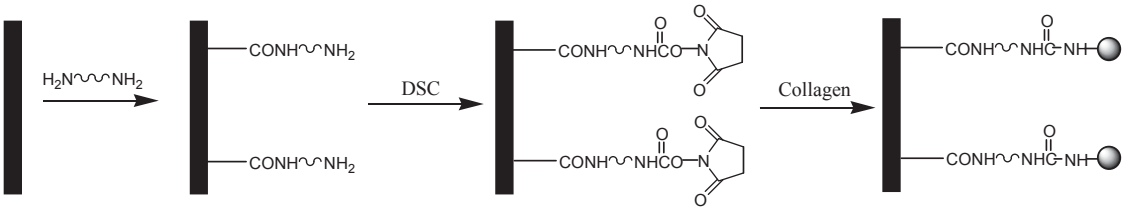


Figure 1. The chemical pathway for the immobilization of collagen.

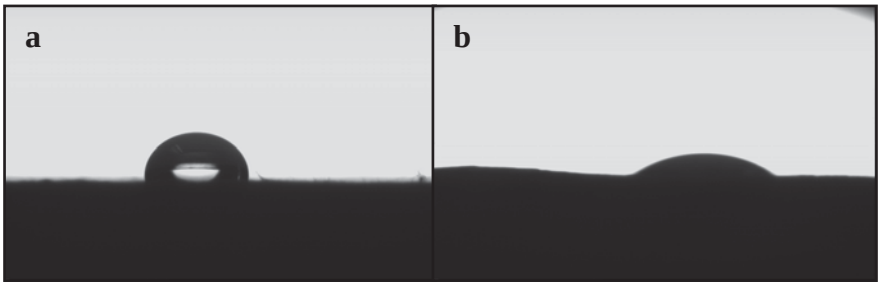


Figure 2. Water dropped on the surface of (a) neat PLA fibrous scaffold, and (b) PLA fibrous scaffold immobilized with 3.0 mg/ml collagen.

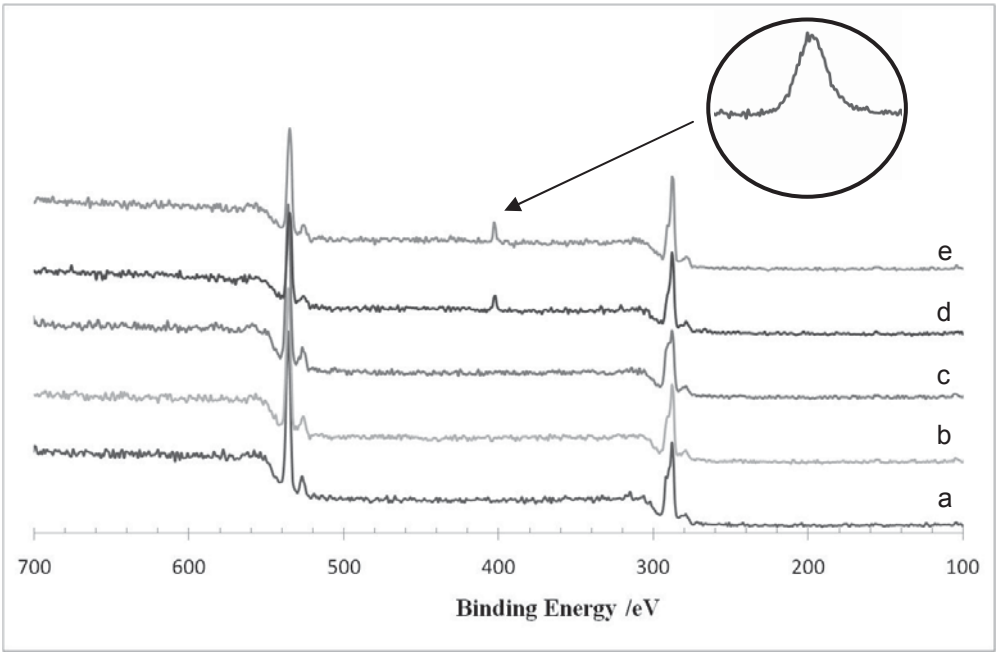


Figure 3. The survey XPS spectra of (a) neat PLA, (b) PLA aminolyzed in 0.04 g/ml HMD/IPA solution for 15 min at 50 °C, (c) activatedPLA, (d) PLA immobilized with collagen (0.5 mg/ml), and (e) PLA immobilized with collagen (3 mg/ml).

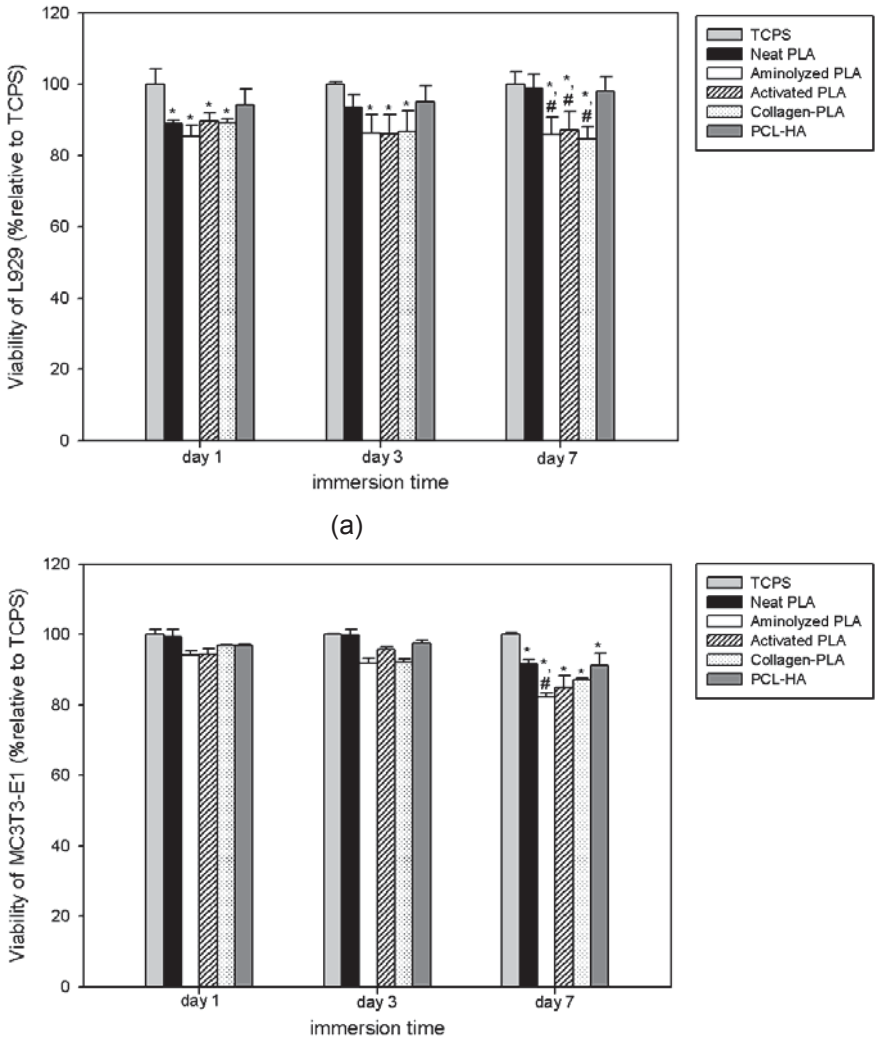


Figure 4. Indirect cytotoxic evaluation of neat PLA fibers, modified PLA fibers, and PCL/HA based on viability of (a) mouse fibroblasts (L929) and (b) pre-osteoblast (MC3T3-E1) that had been cultured with the extraction media from each of these materials against the viability of the cells that had been cultured with the respective culture media for 1 day as a function of the incubation time of the extraction and the culture media of 1, 3, or 7 d. Statistical significance: $^{*}p < 0.05$ compared with control and $^{\#}p < 0.05$ compared to the neat PLA fibrous scaffolds at any given time point.

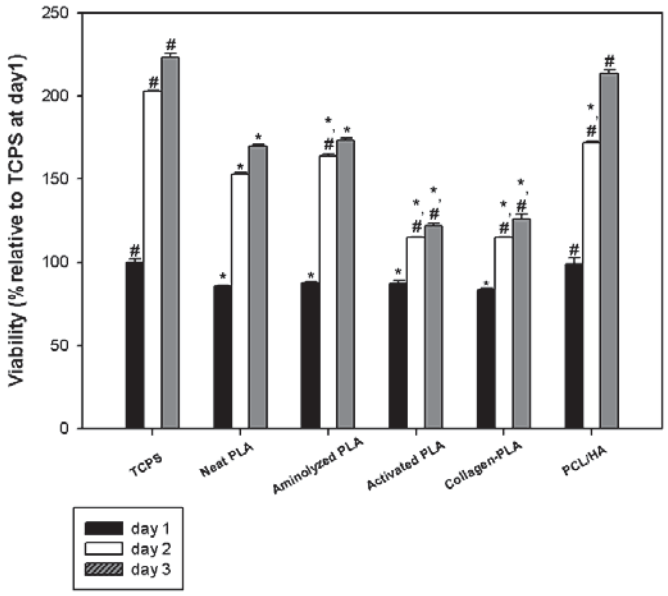


Figure 5. Indirect cytotoxic evaluation of neat PLA fibers, modified PLA fibers, and PCL/HA based on viability of pre-osteoblast (MC3T3-E1) that had been cultured with the 7-day extraction media from each of these materials with 2% serum-containing MEM against the viability of the cells that had been cultured with the respective culture media for 1, 2, and 3 day. Statistical significance: $^{*}p < 0.05$ compared with control and $^{\#}p < 0.05$ compared to the neat PLA fibrous scaffolds at any given time point.

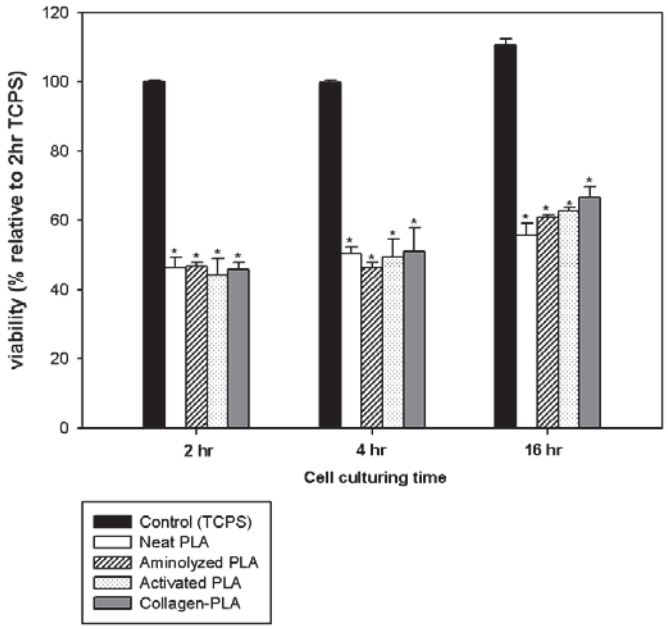


Figure 6. Attachment of MC3T3-E1 that had been seeded or cultured on the surfaces of TCPS, the neat and the modified PLA fibrous scaffolds for 2, 4, or 16 h. Statistical significance: $^{*}p < 0.05$ compared and $^{\#}p < 0.05$ compared to the neat PLA fibrous scaffolds with control at any given time point.

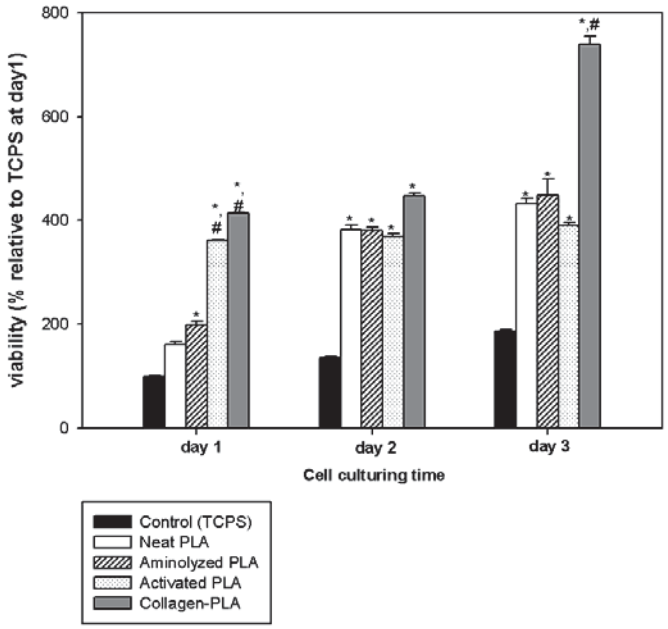


Figure 7. Proliferation of MC3T3-E1 that had been seeded or cultured on the surfaces of TCPS, the neat and the modified PLA fibrous scaffolds for 1, 2, or 3d. Statistical significance: *$p < 0.05$ compared with control and $^{\#}p < 0.05$ compared to the neat PLA fibrous scaffolds at any given time point.

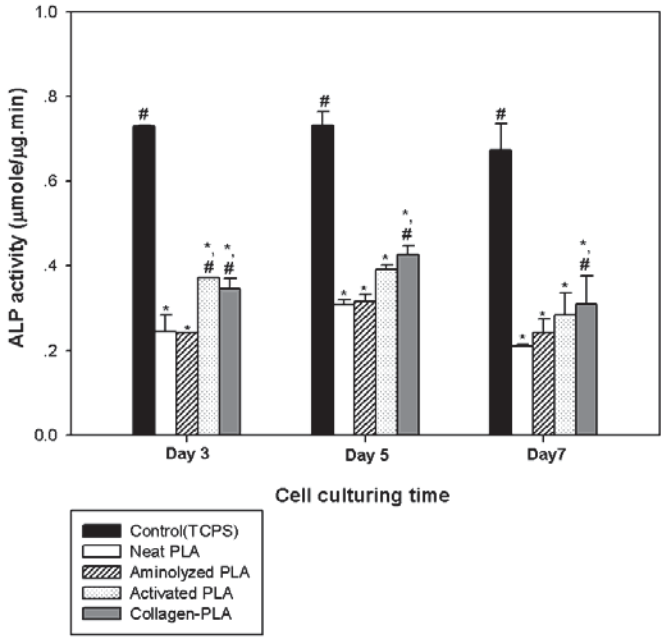


Figure 8. Alkaline phosphatase (ALP) activity of MC3T3-E1 that were cultured on the surfaces of TCPS, the neat and the modified PLA fibrous scaffolds for 3, 5, or 7 d.

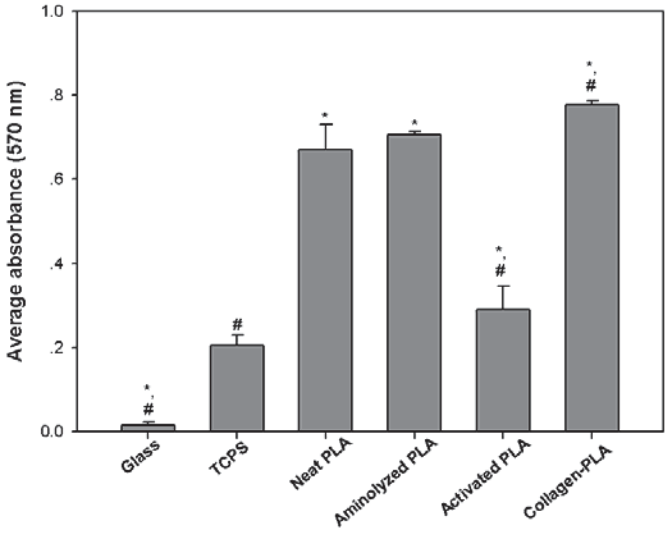


Figure 9. Quantification of mineral deposition in MC3T3-E1 by the method of Alizarin Red-S staining. Statistical significance: $^{*}p < 0.05$ compared with control and $^{\#}p < 0.05$ compared to the neat PLA fibrous scaffold at any given time point.

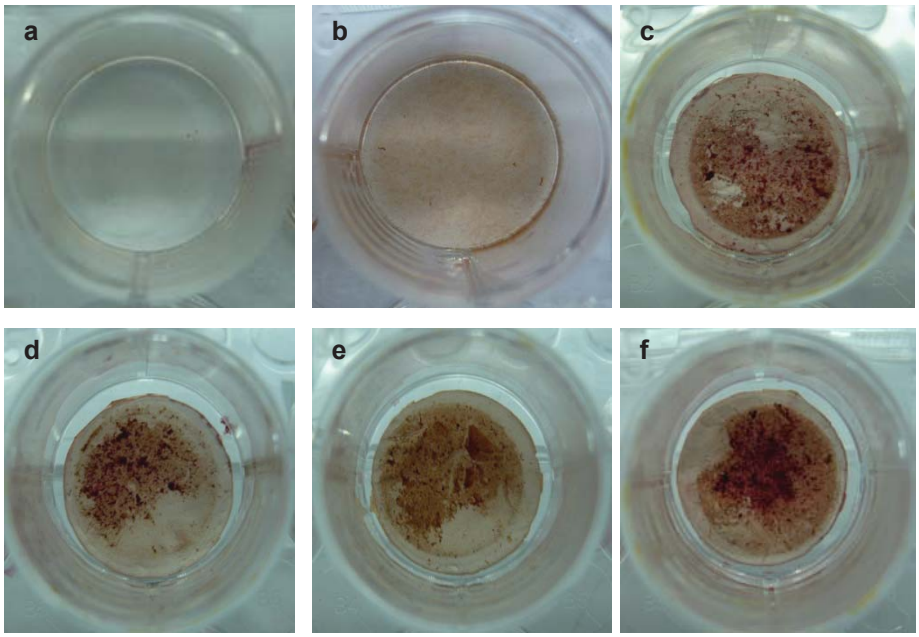


Figure 10. Images of Alizarin Red-S staining for the mineralization in MC3T3-E1 for day 16 for (a) glass (b) TCPS (c) neat PLA (d) aminolyzed PLA (e) activated PLA (f) collagen-immobilized PLA fibrous scaffold.

Table 1. NH_2 density as a function of 1,6-hexanediamine concentration

Diamine concentration (g/ml)	NH_2 conc. ($x10^{-7}$) mol/cm^2
0.02	1.91 ± 0.004
0.04	2.52 ± 0.01
0.06	3.58 ± 0.01
0.08	3.67 ± 0.01
0.10	5.10 ± 0.02

Table 2. NH_2 density as a function of aminolyzing time

Aminolyzing time (min)	NH_2 conc. ($x10^{-7}$) mol/cm^2
2	1.51 ± 0.01
4	1.57 ± 0.02
8	2.52 ± 0.01
15	3.70 ± 0.02
20	2.78 ± 0.06
30	2.60 ± 0.02

Table 3. NH_2 density on the surface of the aminolyzed and collagen-immobilized PLA fibrous scaffolds

Sample	NH_2 concentration ($mol \cdot cm^2$)
Aminolyzed PLA[a]	$3.70 \pm 0.02 \times 10^{-7}$
Collagen Immobilized PLA[b1]	$4.52 \pm 0.08 \times 10^{-9}$
Collagen Immobilized PLA[b2]	$3.21 \pm 0.20 \times 10^{-8}$

[a] The PLA e-spun fiber mat was immersed in 0.04 g/ml 1,6-hexanediamine solution at 50 °C for 15 min.
[b1,b2] The activated PLA surface was immersed in 0.5 mg/ml or 3.0 mg/ml collagen solution, respectively, for 24 h followed by the rinsing process.

Table 4. Water contact angles of the neat and modified PLA fibrous scaffolds

Samples	Water contact angle/degree (Sessile drop)
neat PLA	106.8 ± 0.20
Aminolyzed PLA[a]	99.5 ± 0.17
Activated PLA[b]	112.5 ± 0.38
Collagen Immobilized PLA (w/o coupling agent)[c]	92.1 ± 0.19
Collagen Immobilized PLA[d1]	79.4 ± 0.30
Collagen Immobilized PLA[d2]	73.0 ± 1.18

[a]The PLA e-spun fiber mat was immersed in 0.04 g/ml 1,6-hexanediamine solution at 50 °C for 15 min.
[b]The aminolyzed PLA surface was immersed in 0.1 M DSC solution for 3 h.
[c]The aminolyzed PLA surface was immersed in 0.5 mg/ml collagen solutions for 24 h followed by the rinsing process.
[d1,d2]The activated PLA surface was immersed in 0.5 mg/ml or 3.0 mg/ml collagen solution, respectively, for 24 h followed by the rinsing process.

Table 5. N_{1s}/C_{1s} ratios as a function of 1,6-hexanediamine concentration

HMD concentration (g/ml)	N_{1s}/C_{1s} ratio
0.02	0.0220
0.04	0.0237
0.06	0.0248
0.08	0.0283
0.1	0.0833

The aminolysis reaction took place at 50°c for 8 min.

Table 6. N_{1s}/C_{1s} ratios as a function of aminolyzing time

Aminolyzing time (min)	N_{1s}/C_{1s} ratio
2	0.0133
4	0.0200
8	0.0237
15	0.0290
20	0.0240
30	0.0238

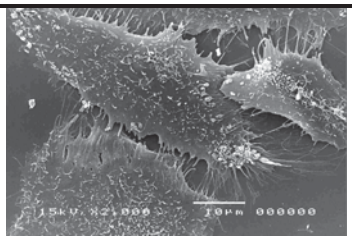
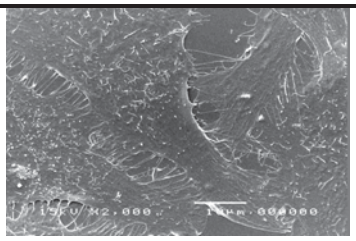
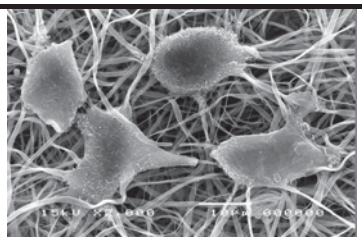
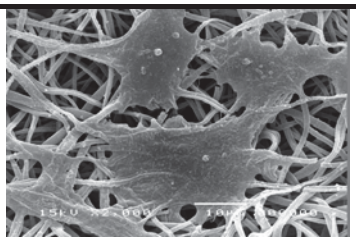
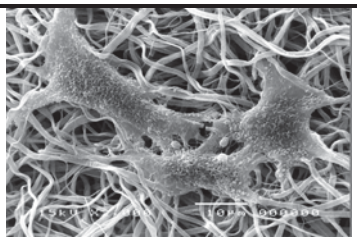
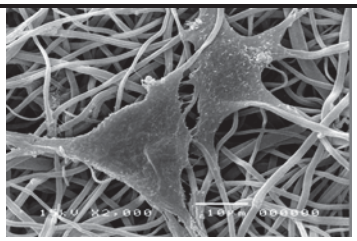
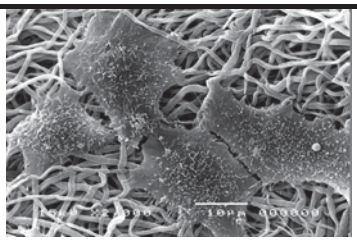
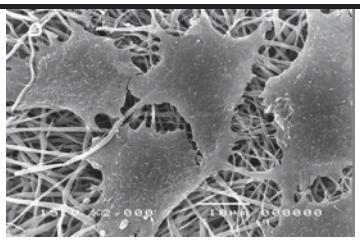
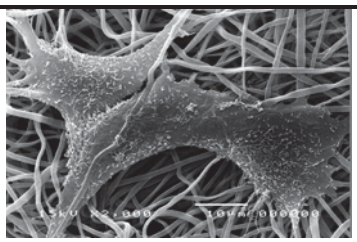
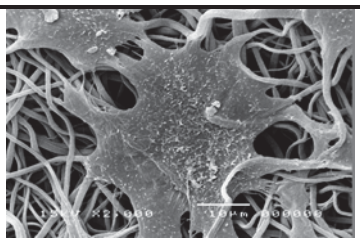
The aminolysis reaction took place at 50°c in 0.04 g/ml HMD/IPA solution.

Table 7. N_{1s}/C_{1s} ratios of the control and modified PLA fibrous scaffolds

Sample	N_{1s}/C_{1s} ratio
Neat PLA	0.0068
Aminolyzed PLA[a]	0.0290
Activated PLA[b]	0.0381
Collagen Immobilized PLA[c1]	0.2349
Collagen Immobilized PLA[c1]	0.2401

[a]The PLA e-spun fiber mat was immersed in 0.04 g/ml 1,6-hexanediamine solution at 50 °C for 15 min.
[b]The aminolyzed PLA surface was immersed in 0.1 M DSC solution for 3 h.
[c1,c2] The activated PLA surface was immersed in 0.5 mg/ml and 3.0 mg/ml collagen solutions, respectively, for 24 h followed by the rinsing process.

Table 8. Selected SEM images of cultured specimens, i.e., glass (i.e., control), neat PLA, aminolyzed PLA, activated PLA, and collagen-immobilized PLA fibrous scaffolds at two different time points after MC3T3-E1 were seeded or cultured on their surfaces (magnification = 2000X; scale bar = 10 μm).

Materials	Magnification = 2000X Scale bar = 10 μm	
	Cultured 4 h	Cultured 16 h
Glass (control)		
Neat PLA		
Aminolyzed PLA		
Activated PLA		
Collgen-PLA		

Carbohydrate Polymers 85 (2011) 251–260

Contents lists available at ScienceDirect

Carbohydrate Polymers

journal homepage: www.elsevier.com/locate/carbpol

Use of 2-hydroxypropyl-β-cyclodextrin as adjuvant for enhancing encapsulation and release characteristics of asiaticoside within and from cellulose acetate films

Jate Panichpakdee[a,b], Pitt Supaphol[a,b,*]

[a] The Petroleum and Petrochemical College, Chulalongkorn University, Phyathai Road, Pathumwan, Bangkok 10330, Thailand
[b] The Center for Petroleum, Petrochemicals and Advanced Materials, Chulalongkorn University, Phyathai Road, Pathumwan, Bangkok 10330, Thailand

ARTICLE INFO

Article history:
Received 27 August 2010
Received in revised form 13 February 2011
Accepted 14 February 2011
Available online 18 February 2011

Keywords:
Asiaticoside
Centella asiatica
2-Hydroxypropyl-β-cyclodextrin
Host–guest
Cellulose acetate
Drug release

ABSTRACT

The inclusion complex between asiaticoside (AC), an active substance from the medicinal plant *Centella asiatica* L., and 2-hydroxypropyl-β-cyclodextrin (HPβCD) was investigated. The phase solubility profiles of AC in distilled water and 90:10 (v/v) mixture of 80 vol.% acetic acid and *N*,*N*-dimethylacetamide (DMAc) both in the absence and the presence of HPβCD were classified as A_L-type and indicated a 1:1 molar ratio of the AC/HPβCD complex. The 1:1 stoichiometric molar ratio of the complex was confirmed by both the 1D and the 2D ^{1}H-nuclear magnetic resonance spectrometry. Unlike the highly crystalline nature of the native AC, the stoichiometric AC/HPβCD complex powder was amorphous in nature. The average diameters of the self-assembling aggregates of the AC/HPβCD complex, *a priori* prepared at various HPβCD to AC molar ratios of 0.5, 1, and 2, in the solution state, were about 2.4, 3.3, and 3.8 μm, respectively. The solvent-cast CA films containing these complexes showed strong evidence of the aggregates on their surfaces. The maximal cumulative released amounts of AC, a sparingly water-soluble substance, from the CA films containing a mixture of AC/HPβCD of varying molar ratios (i.e., 1:0.5, 1:1, and 1:2) in the phosphate buffer saline solution (PBS) containing 10% (v/v) methanol (i.e., P/B/M medium) were 2.2, 3.9, and 5.8% (based on the actual weights of the film specimens), respectively, which were clearly an increasing function of the HPβCD content in the films.

© 2011 Elsevier Ltd. All rights reserved.

1. Introduction

Cellulose acetate (CA) is the acetate ester of cellulose, the primary structural component of cell walls of green plants, and it is one of the most common biopolymers on earth (Anonymous, 2009). CA has been used for a wide variety of applications, including filters (Thostenson, Ren, & Chou, 2001), composite reinforcements (Bergshoef & Vancso, 1999), and topical and/or transdermal delivery of drugs (Wang et al., 2002). In the latter, Taepaiboon, Rungsardthong, and Supaphol (2000) developed electrospun CA fiber mats as carriers for the topical/transdermal delivery of all-trans retinoic acid or vitamin A acid (Retin-A) and α-tocopherol or vitamin E (Vit-E) from CA solutions in 2:1 (v/v) acetone/dimethylacetamide (DMAc) containing Retin-A or Vit-E in the amount of 0.5 or 5 wt.% (based on the weight of CA), respectively. Electrospun CA fiber mats and the corresponding solvent-cast films as carriers for the topical/transdermal delivery of four different non-steroidal anti-inflammatory drugs (NSAIDs), i.e., naproxen (NAP), indomethacin (IND), ibuprofen (IBU), and sulindac (SUL), were reported by Tungprapa, Jangchud, and Supaphol (2007), who used CA solutions in 2:1 (v/v) acetone/DMAc as the base solutions into which NAP, IND, IBU, or SUL in the amount of 20 wt.% (based on the weight of the CA) was added.

Asiaticoside (AC; see Fig. 1 for its chemical structure) is one of four major trisaccharide triterpenoid components (i.e., asiatic acid, asiaticoside, madecassic acid and madecassoside) of the extract from the medicinal plant *Centella asiatica* (L.) Urban which bears a common name in Thai as "Buabok." AC has been regarded as one of the most active compounds associated with the healing of wounds, as evidenced from the observed increase in antioxidant levels at an early stage of recovery of excision-type cutaneous wounds in rats (Shukla, Rasik, & Dhawan, 1999), the observed increase in the proliferation of human dermal fibroblasts and the expression of types I and III pro-collagen mRNA and the protein levels of the cells (Maquart, Bellon, Gillery, Wegrowski, & Borel, 1990; Shim et al., 1996), and the stimulation of extracellular matrix (ECM) accumulation in experimental wounds of rats (Maquart et al., 1999; Suguna, Sivakumar, & Chandrakasan, 1996) in response to the presence of this substance.

Recently, Suwantong, Ruktanonchai, and Supaphol (2008) reported the preparation of electrospun CA fiber mats and the corresponding solvent-cast films containing either *C. asiatica* crude

* Corresponding author at: The Petroleum and Petrochemical College, Chulalongkorn University, Phyathai Road, Pathumwan, Bangkok 10330, Thailand.
Tel.: +66 2218 4131; fax: +66 2215 4459.
E-mail address: pitt.s@chula.ac.th (P. Supaphol).

0144-8617/$ – see front matter © 2011 Elsevier Ltd. All rights reserved.
doi:10.1016/j.carbpol.2011.02.023

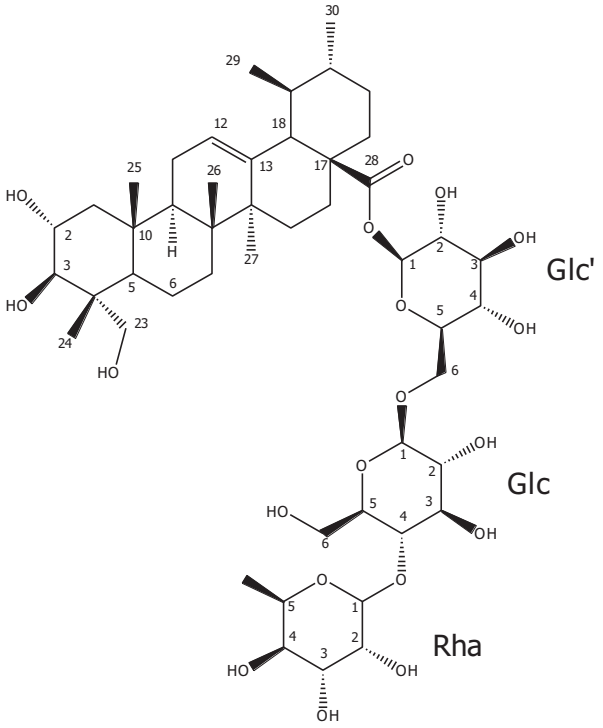


Fig. 1. Chemical structure of asiaticoside (AC).

extract (CACE) or pure AC in the amount of 40 wt.%, based on the weight of the CA powder. The release characteristics of AC from those specimens were tested by the total immersion and the transdermal diffusion through a pig skin methods in either of the acetate or the phosphate buffer solution that contained methanol (i.e., A/B/M or P/B/M medium) at the skin or the physiological temperature of 32 or 37 °C, respectively. However, the release of AC from the CA films containing either CACE or AC was too low (lower than about 2 and 3%, based on the actual weight of the specimens in the A/B/M or P/B/M medium, respectively). This was thought to be a result of the low aqueous solubility of AC (i.e., 0.67 mg mL^{-1}) as well as to the dense structure of the CA films and the inherent insolubility of CA in an aqueous medium. To increase the amount of AC that could be released from the CA matrix, the release should be less dependent on the intrinsic solubility of the active compound in the releasing medium (Sangalli et al., 2001) and/or on the microenvironment through which the drug molecules are to diffuse out (i.e., corresponding to the way in which the drug is incorporated within the matrix) should also be modified (Pose-Vilarnovo et al., 2004).

Cyclodextrins (CDs), complexing agents capable of forming host–guest interactions with a variety of compounds, are capable of interacting with many therapeutic agents, e.g., drugs, by encapsulating them, either wholly or partly, into the hydrophobic cavity of their molecules. Such inclusion complexes have been reported to exhibit several advantages, such as improving the solubility, dissolution rate and bioavailability (Freville, Dollo, Le Corre, Chevanne, & Le Verge, 1996; Loftsson & Brewster, 1996; Pose-Vilarnovo et al., 2001), decreasing toxicity (de Araujoa et al., 2008; Irie & Uekama, 1997; Rajewski & Stella, 1996), and increasing the permeation rate of the encapsulating drug molecules (Loftsson, Jarho, Másson, & Sigurjonsdóttir, 2005; Lopez, Collett, & Bentley, 2000). As a result, they are used in many applications, such as in controlled drug delivery: whether dermally, transdermally, or orally (Challa, Ahuja, Ali, & Khar, 2005). The cyclodextrin complexes have also been reported to form self-assembling entities or micelles (Loftsson, Magnúsdósdottir, Másson, & Sigurjónsdóttir, 2002; Mele, Mendichi, & Selva, 1998). Choi, Ruktanonchai, Min, Chun, and Soottitantawat (2010) prepared either self-assembling aggregates of β-CD and fish oil and studied the release characteristics of fish oil from the obtained β-CD-fish oil complexes at different ratios of the substances.

The aim of the present work was to investigate the complexation of AC within 2-hydroxypropyl-β-cyclodextrin (HPβCD) and the potential for use of the solvent-cast CA films that contained a AC/HPβCD mixture of varying molar ratios as carriers for the topical/transdermal delivery of AC. Various properties (i.e., morphology, size of self-assembling aggregates, water retention and weight loss) of both the AC- and the AC/HPβCD complex-loaded CA films and the release characteristics of AC from these materials in a phosphate buffer saline solution that contained methanol were investigated.

2. Experimental details

2.1. Materials

Cellulose acetate (CA; white powder; $M_w \approx 30{,}000$ Da; acetyl content = 39.7 wt.%; degree of acetyl substitution ≈ 2.4) and 2-hydroxypropyl-β-cyclodextrin (HPβCD; $M_w \approx 1{,}380$ Da; average number of substituent per glucopyranose unit ≈ 0.6) were purchased from Sigma–Aldrich (Switzerland). Asiaticoside (AC; 90% purity) was purchased from Shanghai Angoal Chemical Co., Ltd. (China). *N,N*-Dimethylacetamide (DMAc, Lab-Scan Asia, Thailand), glacial acetic acid (Carlo Erba, Italy), anhydrous disodium hydrogen orthophosphate, sodium dihydrogen orthophosphate, and sodium chloride (Ajax Chemicals, Australia) were used as-received. All chemicals were of analytical reagent grades and used without further purification.

2.2. Stoichiometry of AC/HPβCD complex in solution state

2.2.1. Phase solubility studies

Phase solubility of AC in HPβCD was studied in distilled water. Briefly, excess amounts of AC were put into aqueous HPβCD solutions (1 mL). The amount of HPβCD in the solutions was varied between 0 and 30 mM. The sample solutions were then stirred at room temperature (25 ± 1 °C) for 24 h. It should be noted that the stirring time of 24 h was enough for the solubilization of AC in HPβCD to reach equilibrium. After reaching the equilibrium, unsolubilized AC in the sample solutions was filtered out through a filter membrane (0.45 μm in pore diameter). The filtrates were later quantified for the amounts of the solubilized AC by reversed-phase high performance liquid chromatography (HPLC; see later). The association constant (K_a) was then calculated from the following equation (Higuchi & Connors, 1965):

$$K_a = \frac{m}{s_0(1-m)}, \tag{1}$$

where m is the slope of the plot between the solubility of AC in distilled water as a function of the HPβCD concentration and s_0 is the solubility of AC in distilled water in the absence of HPβCD.

In addition, the complexation efficiency (CE) and the AC:HPβCD molar ratio ([AC]:[CD]) were calculated as follows (Loftsson, Hreindóttir, & Másson, 2007):

$$CE = s_0 K_{1:1} = \frac{[AC]/[CD]}{[CD]} = \frac{m}{1-m}, \tag{2}$$

$$\frac{[AC]}{[CD]} = \frac{1}{1+(1/CE)}, \tag{3}$$

where $K_{1:1}$ is the association constant for the AC:HPβCD molar ratio of 1:1.

The phase solubility of AC in HPβCD was also studied in a 90:10 (v/v) mixture of 80 vol.% acetic acid and DMAc. To ensure the formation of the AC/HPβCD complex in the solvent mixture, the preparation procedure was similar to what had been described above, with an exception to the fact that the mixture of acetic acid and DMAc was used instead of the distilled water.

2.2.2. ^{1}H-NMR studies

A Varian ^{UNITY}*INOVA* ^{1}H-nuclear magnetic resonance spectrometer (^{1}H-NMR), operating at 400 MHz and 25 °C, was used to determine the stoichiometric ratio of the AC/HPβCD complex. Based on the Job's continuous variation method (Job, 1928), the ^{1}H-NMR spectra were recorded from a mixture of AC (10 mM) and HPβCD (10 mM) in 10% (v/v) DMSO-d_6/D_2O mixture at various volumetric ratios between these two solutions at the final concentrations of AC of 1–10 mM, prior to being stirred for 24 h.

2.3. Preparation of AC/HPβCD complex in solid state

The AC/HPβCD complex was prepared according to the method previously described by Higuchi and Connors (1965), with slight modification. Briefly, a weighed amount of HPβCD was first dissolved in distilled water. A weighed amount of AC was then added to the solution and stirred at room temperature (25 ± 1 °C) for 24 h. The stoichiometric AC:HPβCD molar ratio, as obtained from the studies in Section 2.2, was utilized throughout the rest of the studies. The solution/suspension was filtered through a nylon filter (average pore size = 0.45 μm) prior to being frozen at −40 ± 2 °C for 24 h. After that, the obtained mass was lyophilized (Labconco FreeZone® 6-Liter Benchtop Freeze Dry System). A physical blend of AC and HPβCD at the same molar ratio was also prepared for comparison.

2.4. Characterization of solid AC/HPβCD complex

2.4.1. X-ray powder diffractometry

X-ray powder diffractograms of the AC/HPβCD complex and the corresponding physical mixture were obtained on a Bruker Model D8 Advance, equipped with a Cu Kα radiation source, over a scattering (2θ) range of 5 and 60° at room temperature (25 ± 1 °C). The scan rate, the operating voltage, and the filament current were set at 0.2° min^{-1}, 40 kV, and 30 mA, respectively.

2.4.2. Two dimensional ^{1}H-NMR studies

To obtain the 2D ^{1}H-NMR spectrum of the AC/HPβCD complex, the freeze-dried product was dissolved in D_2O at room temperature (25 ± 1 °C) and investigated under the following conditions: acquisition time of 0.205 s, sweep width of 5006.3 Hz, pulse width of 6.3 μs, time domain of 2048, Fourier number of 2048 and temperature of 298 K.

2.5. Preparation of AC- and AC/HPβCD complex-loaded CA films

CA films containing either AC or AC/HPβCD complex were prepared by solvent casting technique. AC or a AC/HPβCD complex that had been prepared at different mixing molar ratios of HPβCD to AC (i.e., 0.5, 1.0, or 2.0) was incorporated at a concentration of 10%, based on the dry weight of CA powder, in a 90:10 (v/v) mixture of 80 vol.% acetic acid and DMAc. The concentration of CA in the final solutions was 4% w/v. The as-prepared solutions were stirred at room temperature (25 ± 1 °C) for 24 h. Prior to the addition of CA powder, each of the sample solutions was characterized for the particle size of the self-assembling aggregates by a Malvern Zetasizer ZS nanosizer [based on the dynamic light scattering (DLS) principle]. CA powder was then added to the sample solution and subsequently stirred at room temperature (25 ± 1 °C) for 3 h until CA was completely dissolved. The solutions were subsequently poured onto glass Petri dishes and dried under a reduced pressure. The films were dried until of a constant weight and stored in a desiccator *in vacuo* for at least 24 h, prior to further use. The thicknesses of the as-cast films were 80 ± 10 μm.

2.6. Characterization of AC- and AC/HPβCD complex-loaded CA films

Morphologies of AC- and AC/HPβCD complex-loaded CA films were studied by a JEOL JSM-6400 scanning electron microscope (SEM). All of the specimens were vacuum-coated with a thin layer of gold using a JEOL JFC-1100E sputtering device. The average diameters of the self-assembling aggregates and the pores that were formed after the films had been immersed in a phosphate buffer saline solution (PBS; see later for its preparation) containing 10% (v/v) methanol (hereafter, P/B/M medium) for 24 h were determined by measuring the diameters of the micro-aggregates and the micro-pores at 100 different points on the SEM images of 7500× magnification with SemAphore 4.0 software. For each sample, the diameters were presented as the average ± standard deviation.

Water retention and weight loss behavior of the AC- and the AC/HPβCD complex-loaded CA films were investigated after their immersion in the P/B/M medium at 37 °C for 24 h. The water retention and the weight loss behavior were calculated as follows:

$$\text{Water retention}\,(\%) = \frac{M - M_d}{M_d} \times 100, \tag{4}$$

and

$$\text{Weight loss}\,(\%) = \frac{M_i - M_d}{M_d} \times 100, \tag{5}$$

where M and M_d are wet and dry weights of the film specimens after immersion in the buffer solution, respectively, and M_i is the initial, dry weight of the specimens. All measurements were carried out in triplicate.

2.7. Release of AC from AC- and AC/HPβCD complex-loaded CA films

2.7.1. Preparation of releasing medium

To prepare 1 L of the PBS solution, 6.177 g of anhydrous disodium hydrogen orthophosphate and 1.1014 g of sodium dihydrogen orthophosphate were dissolved under mechanical stirring in distilled water at room temperature (25 ± 1 °C) until the flakes were completely dissolved. Later, 8.7 g of sodium chloride was added into 20 mL of the solution. The volume was adjusted to the required volume with distilled water. The pH of the final solution was 7.4.

2.7.2. Actual AC content

The actual amounts of AC in the AC- and the AC/HPβCD complex-loaded CA films were quantified by dissolving the samples (circular disc: about 1.5 cm in diameter) in 4 mL of 2:1 (v/v) acetone/DMAc. After that, 0.5 mL of the solutions were pipetted and diluted into 8 mL of the P/B/M medium. Finally, the AC contents in the diluted sample solutions were determined by HPLC (see later) and then back-calculated from the obtained data against a calibration curve for AC.

2.7.3. AC release assay

The release characteristics of AC from the AC- and the AC/HPβCD complex-loaded CA films were determined by the total immersion method. Each of the specimens (circular disc of about 1.5 cm in diameter) was immersed in 25 mL of the P/B/M medium at the physiological temperature of 37 °C. At each time point, ranging between 0 and 24 h (1440 min), 1 mL of the medium was withdrawn

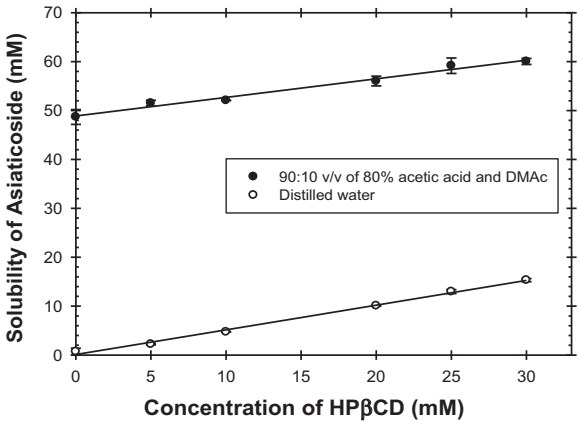


Fig. 2. Phase solubility diagrams of AC in the absence or the presence of 2-hydroxypropyl-β-cyclodextrin (HPβCD) in distilled water and 90:10 (v/v) of 80% acetic acid and DMAc at room temperature.

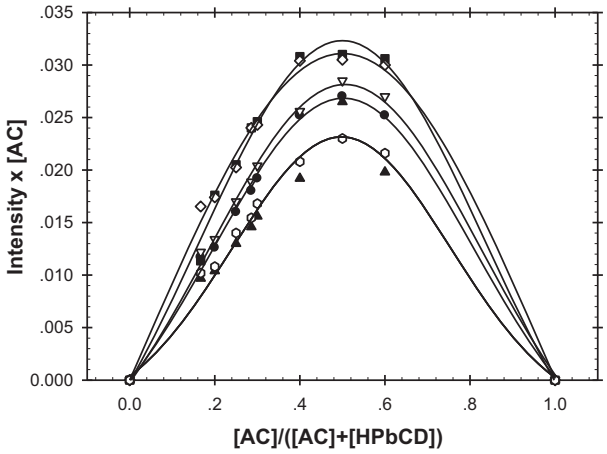


Fig. 3. Job's continuous variation plots of the chemical shifts of the protons, i.e., (▽) H-12, (◊) H-18, (▲) CH_3-26, (●) CH_3-29, (■) Glc-1, and (◯) Rha-5, of AC, in the presence of different HPβCD concentrations in the 90:10 (v/v) mixture of D_2O and DMSO-d_6.

(i.e., sample solution) and an equal amount of the fresh medium was refilled. The amounts of AC in the sample solutions were quantified by HPLC (see later) and then back-calculated from the obtained data against the calibration curve for AC.

2.8. Determination of AC content

The amount of AC in a given sample solution was determined by HPLC (Shimadzu LC-10 AD). The sample solution was filtered through a nylon filter (average pore size = 0.45 μm) and then separated in an Inertsil ODS-3 C18 column (particle size = 5 μm; column dimension = 4.6 mm × 250 mm) with an Inertsil ODS-3 guard column (particle size = 5 μm; column dimension = 4.0 mm × 10 mm) at a flow rate of 1 mL min^{-1}. A UV–Visible detector was set at (λ_{max}) 204 nm. The mobile phase for the AC separation consisted of acetonitrile, methanol, and distilled water at 26:24:50 (v/v/v) and the retention time was 7.7 min. The calibration curve for AC was obtained over a concentration range of 0.005–0.200 mg mL^{-1}.

2.9. Statistical analysis

One-way ANOVA was used to analyze the means of different data sets. The significance for all of the tests was accepted at a 0.05 confidence level.

3. Results and discussion

3.1. Stoichiometry of AC/HPβCD complex in solution state

The solubility of AC in the absence or the presence of HPβCD was studied in two types of medium (i.e., distilled water or 90:10 (v/v) of 80% acetic acid and DMAc) and the results are graphically shown in Fig. 2. In the absence of HPβCD, the solubility of AC in any type of the studied medium (i.e., s_0) was low (i.e., 0.7 mM in distilled water and 48.7 mM in 90:10 (v/v) of 80% acetic acid and DMAc). Marked increase in the amounts of soluble AC in either medium was evident in the presence of HPβCD. At the greatest amount of HPβCD investigated (i.e., 30 mM), the amounts of soluble AC increased to 15.3 and 60.0 mM in distilled water and 90:10 (v/v) of 80% acetic acid and DMAc, respectively. Obviously, the amounts of soluble AC in both types of medium exhibited linear relationships with the HPβCD content in the solutions.

The association constants, K_a, characterizing the solubility of AC in distilled water and 90:10 (v/v) of 80% acetic acid and DMAc, can be calculated from the slopes of the plots such as those shown in Fig. 2. The slopes of the least-squared lines drawn through both sets of data were less than one, with the values being 0.505 and 0.380, respectively. According to the definition set forth by Higuchi and Connors (1965), these could be categorized as A_L type and a 1:1 complex between AC and HPβCD could be assumed. Based on the values of the slopes obtained, the K_a values (or the $K_{1:1}$ values, for this particular case) can be calculated, based in Eq. (1), to be 11,726.5 and 12.5 M^{-1}, respectively. According to Eq. (2), the complexation coefficient values, CE, were determined to be 1.020 and 0.613, respectively, while, according to Eq. (3), the AC:HPβCD molar ratios were 1:2 and 1:3, respectively. This means that, despite the stoichiometric 1:1 molar ratio between AC and HPβCD in the as-formed complex, only 1 in every 2 or 3 molecules of HPβCD underwent the complexation with AC.

One dimensional ^{1}H-NMR spectroscopy is useful for studying the inclusion complex of HPβCD with various organic compounds. The variation in the chemical shift of the protons of organic compounds ($\Delta\delta = \delta_c - \delta_0$, where δ_c and δ_0 are the chemical shifts of a specific chemical species in the complex and the free forms, respectively), due to the screening environment by magnetic nuclei within the HPβCD cavity, was recorded. In particular, changes in the chemical shifts of protons of the guest molecule(s) within the CD cavity can be used to quantify the stoichiometry of the complex, simply by plotting them as a function of the mole fraction of the guest molecule(s) or the CD molecule [i.e., Job's continuous variation plots (Job, 1928)]. The mole fraction at the maximum peak(s) is taken as the stoichiometric ratio of the complex. According to Fig. 3, the chemical shifts of CH_3-26, CH_3-29, H-12, H-18, Rha-5, and Glc-1 protons in the AC/HPβCD mixtures, in 90:10 (v/v) mixture of D_2O and DMSO-d_6, exhibited the maximum peaks at [AC]/([AC] + [HPβCD]) = 0.5, corresponding to the AC:HPβCD molar ratio of 1:1. In addition, Table 1 shows the chemical shift signals of protons of AC and HPβCD, both in the free and the complex states, in D_2O at equi-molar ratio between AC and HPβCD, along with their differences.

3.2. Characterization of AC/HPβCD complex in solid state

3.2.1. X-ray powder diffractometry

The freeze-dried product from the equi-molar mixture of AC and HPβCD was white powder. X-ray powder diffractometry was then used to confirm the formation of the AC/HPβCD complex. Fig. 4 shows the X-ray diffractograms of AC, HPβCD, the AC/HPβCD complex, and the physical mixture of AC and HPβCD. Sharp diffraction peaks were evident for the as-received AC, indicating its crys-

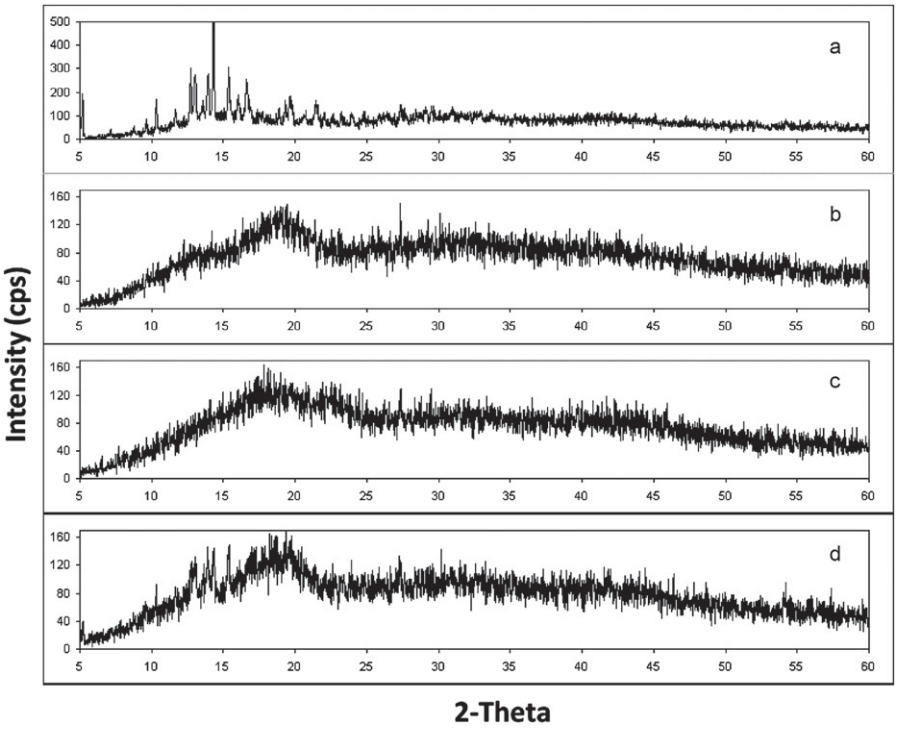


Fig. 4. X-ray diffractograms of (a) AC, (b) HPβCD, (c) AC/HPβCD complex, and (d) physical mixture of AC and HPβCD.

talline nature. On the other hand, only diffused, scattering peaks were observed for the as-received HPβCD, with the scattering center being observed at the scattering angle, 2θ, of about 18°. This indicates the amorphous nature of HPβCD. As for the AC/HPβCD complex, only the scattering peaks similar to those of HPβCD were obtained, indicating the amorphous nature of the material. When AC was physically mixed with HPβCD, however, both the sharp diffraction peaks of AC and the diffused, scattering peaks of HPβCD were evident. These results confirmed the inclusion of AC within the cavity of HPβCD.

3.2.2. Two dimensional ^{1}H-NMR

To investigate the spatial arrangement of AC within the HPβCD cavity, Nuclear Overhauser Effect Spectroscopy (NOESY) was applied on the stoichiometric AC/HPβCD complex (1:1 molar ratio) that had been dissolved in D_2O and the result is shown in Fig. 5a.

Table 1
Chemical shift signals of protons (in ppm) of AC and HPβCD in the free (δ_0) and the complexed (δ_c) states in D_2O at the equi-molar ratio between AC and HPβCD of the inclusion complex, along with their differences.

Proton	δ_0	δ_c	$\Delta\delta$ ($\delta_c - \delta_0$)
AC			
H-12	5.162	5.216	0.054
H-18	2.033	2.087	0.054
CH_3-24	0.644	0.667	0.023
CH_3-26	0.777	0.831	0.054
CH_3-27	1.132	1.134	0.002
CH_3-29	0.844	0.869	0.025
Glc-1	4.385	4.323	−0.062
Rha-CH_3	1.301	1.321	0.002
Rha-5	3.942	3.988	0.046
HPβCD			
H-1	5.090	5.086	−0.004
H-2	3.542	3.546	0.004
H-3	3.817	3.896	0.079
H-4	3.525	3.526	0.001
H-5	3.600	3.620	0.020
H-6	3.682	3.760	0.078

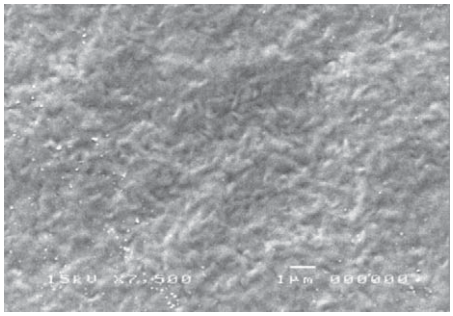
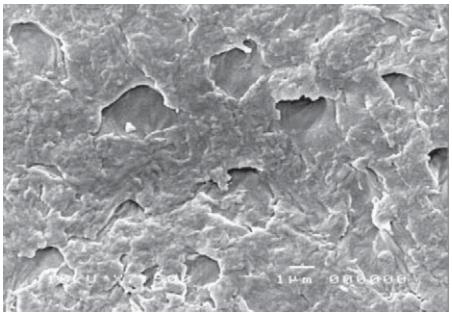
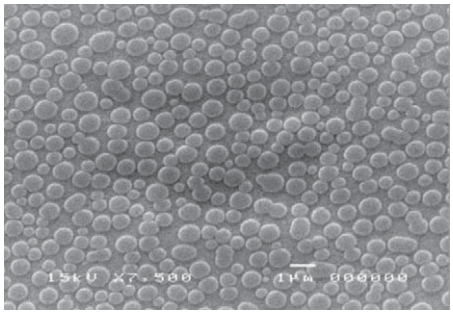
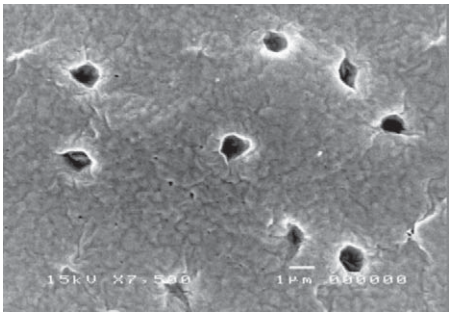
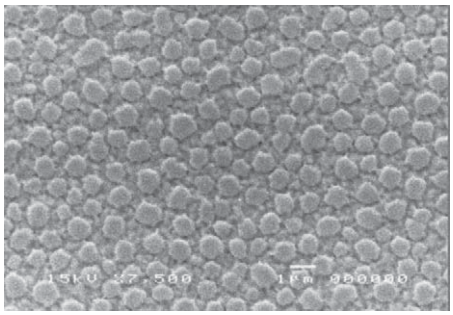
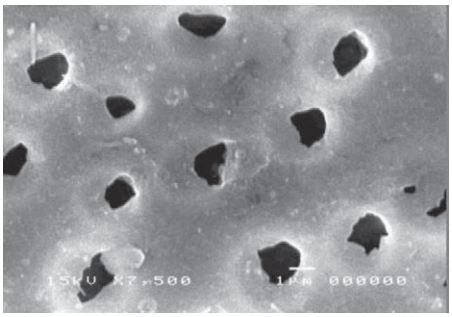
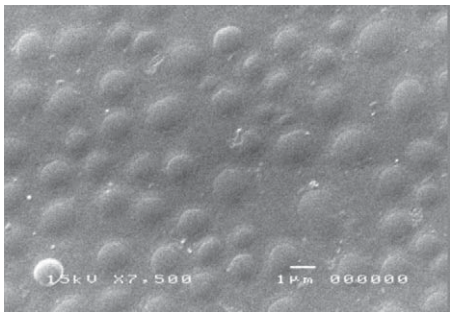
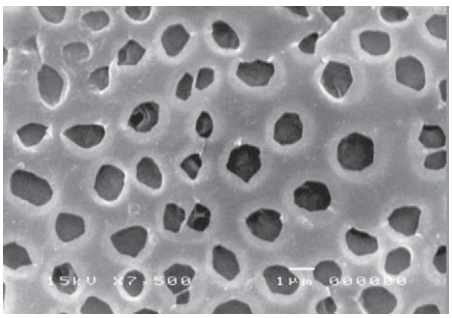
Cross-peaks were observed between the CH_3-29 and CH_3-27 protons of AC and the H-3 inner-cavity proton of HPβCD (located at the wide side of the cavity) and between the CH_3-26 and H-6 protons of AC and the H-5 inner-cavity proton of HPβCD (located at the narrow side of the cavity). This indicates that the cyclohexene ring moiety of AC is captivated within the cavity of HPβCD, as depicted in Fig. 5b, hence confirming the stoichiometric 1:1 molar ratio between AC and HPβCD in the solid complex. Notwithstanding, the specific interactions between H-12, H-18, Glc-1, Rha-5, and Rha-Me protons of AC and the H-2, H-4, and H-6 outer-cavity protons of HPβCD are believed to be the probable cause for the self-aggregation of adjacent AC/HPβCD entities.

3.3. Characterization of AC- and AC/HPβCD complex-loaded CA films

3.3.1. Physical appearance

Prior to the addition of CA powder into the AC/HPβCD solutions, the diametric dimensions of the self-assembling aggregates of the AC/HPβCD complex that had been prepared at different HPβCD to AC molar ratios of 0.5, 1, and 2 were determined by the nanosizer to be 2.38 ± 1.39, 3.34 ± 0.66, and 3.84 ± 0.53 μm, respectively (see Supplementary data). Evidently, the size of the aggregates was an increasing function of the HPβCD proportion in the solution. CDs are known to form into self-assembling aggregates, which is facilitated by their ability to form inter-molecular hydrogen bonding (Coleman & Nicolis, 1992; González-Gaitano et al., 2002; Suzuki, Tsutsui, & Ohmori, 1994). In addition, Mele et al. (1998) reported that β-carotene in its complexation with β and γ-CDs in water existed as large aggregates, as revealed by both light scattering and ^{1}H NMR techniques. Factors that influence the formation of self-assembling aggregates are, for examples, concentration and molecular weight of CDs, pH, and temperature, while high pH, high temperature, and the addition of an electrolyte have been used as means to prevent the aggregation (Bonini et al., 2006; Das, Mallick, Sarkar, & Chattopadhyay, 2008; He, Fu, Shen, & Gao, 2008).

Table 2
Representative SEM images of AC- and AC/HPβCD complex-loaded CA films both before and after their immersion in a phosphate buffer saline solution (PBS) containing 10% (v/v) methanol (i.e., P/B/M medium) for 24 h.

Type of CA film sample	Before immersion in P/B/M	After immersion in P/B/M
Containing 10 wt.% AC		
Containing 10% (w/w) AC/HPβCD at the mixing ratio of 1:0.5		
Containing 10% (w/w) AC/HPβCD at the mixing ratio of 1:1		
Containing 10% (w/w) AC/HPβCD at the mixing ratio of 1:2		

SEM was used to investigate the morphologies of the obtained AC- and AC/HPβCD complex-loaded CA films. Representative images are illustrated in Table 2. Apparently, the surface of the AC-loaded CA film was rough, with no evidence of any specific pattern on it. This should be due to the complete dissolution of AC in the 90:10 (v/v) mixture of 80 vol.% acetic acid and DMAc, prior to the addition of the CA powder, resulting in rather homogeneous distribution of AC throughout the mass of the resulting CA film. On the other hand, specific pattern in the form of spherical aggregates was observed on all of the AC/HPβCD complex-loaded CA films. Specifically, an increase in the HPβCD to AC molar ratio resulted in a monotonous decrease in the sharpness of the boundary of these aggregates. It is believed that these entities were the self-assembling aggregates of the AC/HPβCD complex that had been formed in the AC/HPβCD solutions. The diameters of the aggregates that had been formed at the AC:HPβCD molar ratios of 1:0.5 and 1:1 were 0.73 ± 0.13 and 0.84 ± 0.12 μm, respectively. However, those of the ones that had been formed at the AC:HPβCD molar ratio of 1:2 could not be precisely measured.

Clearly, the dimensions of these self-assembling aggregates of the AC/HPβCD complex were much smaller than those determined by the nanosizer. Such discrepancy could be based on a couple of reasons: (i) the dry or the solvated state of the materials during the measurements by the SEM or the nanosizer, respectively, and (ii) the dependence of diametric projection of the spherical aggregates

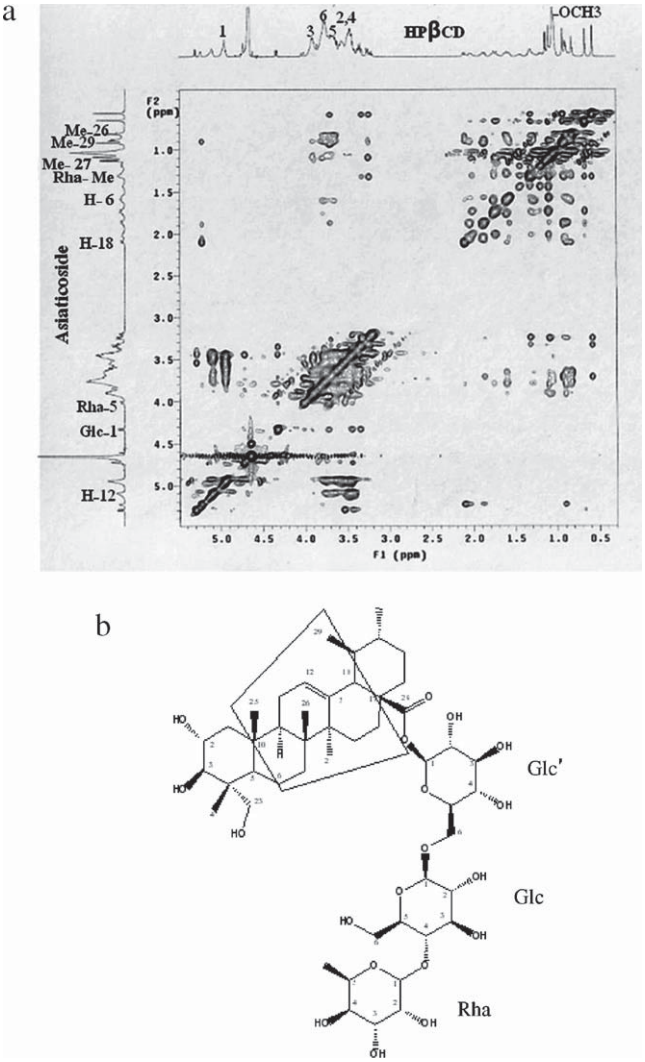


Fig. 5. (a) NOESY diagram of AC/HPβCD complex that had been dissolved in D_2O and (b) schematic arrangement of AC within the cavity of HPβCD.

of the AC/HPβCD complex across the thickness of the AC/HPβCD complex-loaded CA films.

3.3.2. Water retention and weight loss behavior

The CA films containing either AC or the AC/HPβCD complex were further characterized to investigate water retention and weight loss behavior in the P/B/M medium at 37 °C. After the specified immersion time of 24 h had been reached, the weights of the film specimens were recorded and these were calculated to obtain the property values, as reported in Fig. 6. Among the various CA films investigated, the AC-loaded CA films (shown in the figure as the samples with the HPβCD to AC molar ratio of 0) exhibited the lowest water retention (i.e., at about 12%). Such values for the CA films containing either AC or CACE at 40 wt.%, after immersion in the P/B/M medium at 37 °C for 24 h, were reported to be about 39 and 52%, respectively (Suwantong et al., 2008). Compared with the value obtained in the present work, the greater water retention values as reported in the work of Suwantong et al. (2008) could be due to a couple of reasons: (i) the difference in the solvent type used in the fabrication of the films that could affect the physico-chemical properties of the resulting films (Li, Ren, Fane, Li, & Wong, 2006; Romero, Leite, & Goncalves, 2009; Valente, Polishchuk, Burrows, & Lobo, 2005) and (ii) the difference in the as-loaded amounts of the drug within the films that could affect the porosity of the

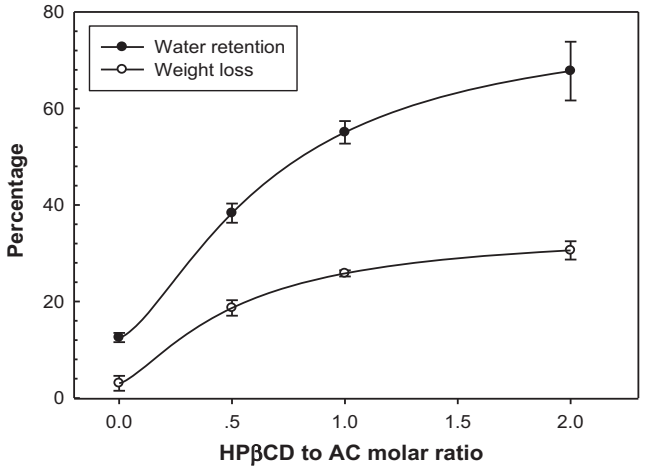


Fig. 6. Water retention and weight loss behavior of the AC/HPβCD complex-loaded CA films at different HPβCD to AC molar ratio after immersion in the P/B/M medium at the physiological temperature of 37 °C for 24 h ($n = 3$).

films after the drug molecules had been released into the medium (Suwantong, Opanasopit, Ruktanonchai, & Supaphol, 2007). On the other hand, the water retention of the AC/HPβCD complex-loaded CA films was much greater than those of the AC-loaded CA films, with the average value increasing from about 38% at the HPβCD to AC molar ratio of 0.5 to about 68% at the HPβCD to AC molar ratio of 2.0.

The AC-loaded CA films also exhibited the lowest weight loss after immersion in the medium (at about 3%). Slightly greater values at about 4 or 7% were reported by Suwantong et al. (2008) for the CA films that contained either AC or CACE at 40 wt.%, respectively. The reasons for the discrepancy in the property values as reported in the present work and those in the work of Suwantong et al. (2008) are similar to those given in the previous paragraph. On the contrary, the loss in the weight of the AC/HPβCD complex-loaded CA films was much greater than those of the AC-loaded CA films, with the average value increasing from about 19% at the HPβCD to AC molar ratio of 0.5 to about 30% at the HPβCD to AC molar ratio of 2.0. The loss in the weight of a drug-loaded material in a medium depends on a number of factors, e.g., the solubility of the drug, the solubility of the carrier material, the diffusion of the drug from the carrier material, and so forth. Due to the low aqueous solubility of both AC and CA in water, the presence of methanol in the medium and of HPβCD in the AC/HPβCD complex-loaded CA films were the obvious reasons for the improvement in the aqueous solubility of both the drug and the matrix materials.

3.4. Release of AC from AC- and AC/HPβCD complex-loaded CA films

The effect of HPβCD on the release characteristics of AC from the CA films at different AC:HPβCD molar ratios was evaluated by the total immersion method in the P/B/M medium. They were reported as the percentages of the ratios of the cumulative amounts of AC released to the amounts of the drug actually loaded within the films or to the actual weights of the films, as shown in Fig. 7. The actual amounts of AC within the AC- and the AC/HPβCD complex-loaded CA films were *a priori* determined to be 70.7, 80.3, 69.2, and 83.0% on average (based on the as-loaded amounts of AC within the casting solutions), for the CA films that had been prepared at the AC:HPβCD molar ratios of 1:0, 1:0.5, 1:1, and 1:2, respectively.

For the AC-loaded CA films (the content of AC initially loaded in the casting solution was 10 wt.%, denoted in Fig. 7 as the samples with the AC:HPβCD molar ratio of 1:0), none of the as-loaded

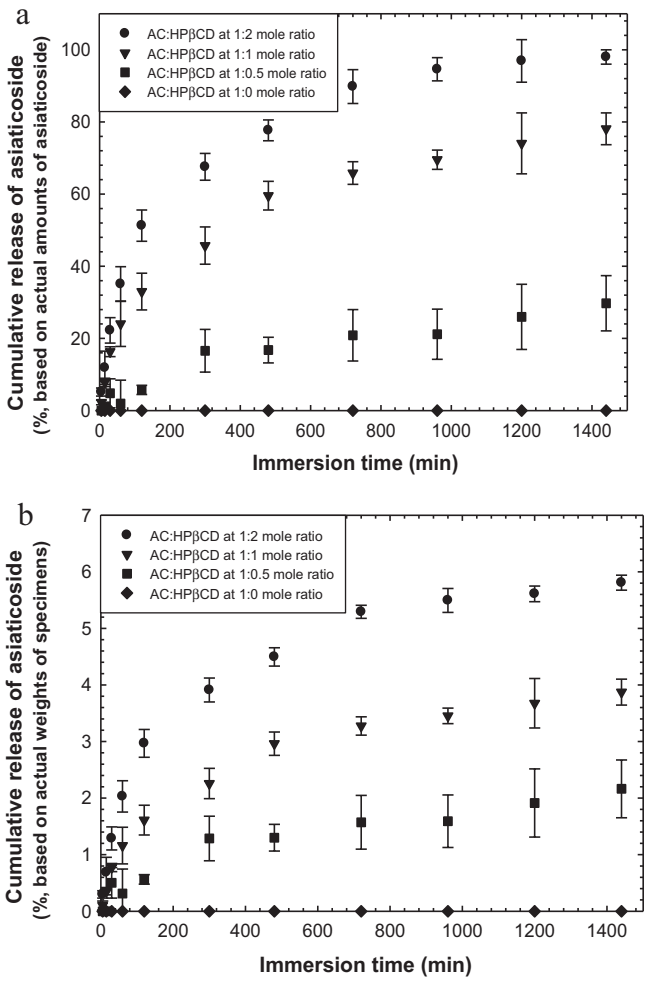


Fig. 7. Cumulative amounts of AC released from AC- and AC/HPβCD complex-loaded CA films upon immersion in the P/B/M medium at 37 °C. The results were reported as the percentages of the ratios of the amounts of the as-released AC to (a) the amounts of AC actually loaded within the films or (b) to the actual weights of the films ($n = 3$).

AC, at any given immersion time point, was able to release into the medium. Suwantong et al. (2008) reported that the maximal amounts of AC released from the CA films that had been prepared from the casting solution containing 40 wt.% of the drug were about 11% on average (based on the AC amounts initially loaded within the films). The discrepancy between the amounts of AC released from the CA films in the present work and those reported in the work of Suwantong et al. (2008) should be influenced by the fact that the amounts of AC initially loaded within the films, as reported in the two studies, were different (i.e., 10 versus 40 wt.%), hence the difference in the driving force for diffusion. The different types of the solvent used in the fabrication of the films [i.e., 90:10 (v/v) mixture of 80 vol.% acetic acid and DMAc as in the present work versus 2:1 (v/v) acetone/DMAc as in the work of Suwantong et al. (2008)], which could render different densities to the obtained films, may also contribute to the discrepancy in the results obtained in the two studies.

In comparison with the AC-loaded CA films, the presence of HPβCD in the AC/HPβCD complex-loaded CA films was clearly responsible for the significantly greater amounts of AC released into the medium. Furthermore, the cumulative amounts of AC released from the films, at any given immersion time point, increased with an increase in the HPβCD content. Specifically, about 25% of the AC actually loaded within the AC/HPβCD complex-loaded CA films, *a priori* prepared at the AC:HPβCD molar ratios of 1:0.5, 1:1, and 1:2, was able to release into the medium within about 1200, 60, and 30 min, respectively. The maximal amounts of AC released from these materials, after having been immersed in the medium for 1440 min, were about 30, 78, and 98% of the amounts of AC actually contained within the CA films, respectively. These values corresponded to about 2.2, 3.9, and 5.8% of the released amounts of AC, when calculated based on the actual weights of the film specimens.

As mentioned, as the HPβCD content in the films increased, significantly more amounts of AC could be released into the medium. The complexation of a poorly water-soluble drug with a native cyclodextrin (CD) as well as its derivatives improves tremendously the aqueous solubility and the dissolution rate of the drug within an aqueous medium. This phenomenon is especially important for a highly hydrophilic derivative of CD, such as HPβCD. Pose-Vilarnovo et al. (2001) reported that the aqueous solubility of sulfamethizole (i.e., a sulfonamide antibiotic drug) was improved significantly upon forming into an inclusion complex with βCD or HPβCD. The difference as observed in the cumulative amounts of AC released from the AC/HPβCD complex-loaded CA films that had been prepared at various AC:HPβCD molar ratios could be explained based on a couple of reasons. Firstly, the ability of AC to form an inclusion complex with HPβCD disfavored the crystallization of the herb, as evidenced from the X-ray results (see Fig. 4). This allows greater opportunity for the solvent molecules to interact with those of the drug. Secondly, the presence of HPβCD increased the hydrophilicity of the films, as evidenced by the increase in the water retention of the films with an increase in the HPβCD content (see Fig. 6). Lastly, due to the highly hydrophilic nature of HPβCD, the dissolution of the unassociated HPβCD as well as the AC/HPβCD inclusion complex into the releasing medium could occur easily, which helped facilitate the solubilization of the drug within the medium. This is evidenced by the observed increases in both the weight loss of the films in and the cumulative amounts of AC released from the films into the medium with an increase in the HPβCD content (see Figs. 6 and 7, respectively).

The latter case was accented by the observation of microholes on the AC/HPβCD complex-loaded CA films after having been immersed in the releasing medium (see Table 2). The diametric dimensions of these holes, as measured directly from the SEM images shown in Table 2, were 0.87 ± 0.14, 1.17 ± 0.28, and $1.20 \pm 0.19\,\mu m$ for the films that had been prepared at the AC:HPβCD molar ratios of 1:0.5, 1:1, and 1:2, respectively. These dimensions were essentially similar to the spherical aggregates that had been observed on the films prior to the immersion (see Table 2 and related texts in Section 3.3.1).

3.5. Release kinetics of AC from AC/HPβCD complex-loaded CA films

The release kinetics of AC from the AC/HPβCD complex-loaded CA films was analyzed by the following equation (Peppas & Khare, 1993; Philip & Peppas, 1987):

$$\frac{M_t}{M_\infty} = kt^n, \quad \text{for} \quad \frac{M_t}{M_\infty} < 0.6, \tag{6}$$

where M_t is the cumulative amount of AC released into the medium at an arbitrary time t, M_∞ is the cumulative amount of AC released into the medium at an infinite time, n is the diffusional exponent used to described the release mechanism, and k is the release rate constant of AC. For the Fickian diffusion, the parameter n is taken as 0.5 and a plot of the fractional cumulative released amounts of AC versus $t^{0.5}$ should give a straight line with a slope of k (Verreck et al., 2003). The values of k (with the values of r^2, signifying the quality of the fit, being given in parentheses) for the AC that had been released from the films, *a priori* prepared at the AC:HPβCD molar ratios of 1:0.5, 1:1, and 1:2, were determined to be $0.0010 s^{-0.5}$

(0.958), 0.0026$s^{-0.5}$ (0.951), and 0.0034$s^{-0.5}$ (0.899), respectively. Clearly, the rate of AC released from the films increased with an increase in the HPβCD content.

4. Conclusions

Asiaticoside (AC), from the medicinal plant *Centella asiatica* L., readily forms a complex with 2-hydroxypropyl-β-cyclodextrin (HPβCD) at a 1:1 molar ratio both in distilled water and 90:10 (v/v) mixture of 80 vol.% acetic acid and *N*,*N*-dimethylacetamide (DMAc). The average diametric dimension of the self-assembling aggregates of the AC/HPβCD complex, in the solvated state, increased from about 2.4 μm at the HPβCD to AC molar ratio of 0.5 to about 3.8 μm at the HPβCD to AC molar ratio of 2. In the solid state, the AC/HPβCD complex that had been prepared at the stoichiometric molar ratio of 1:1 did not show the crystalline nature of the as-received AC. Two-dimensional NMR revealed that the cyclohexene ring moiety of AC is captivated well within the HPβCD cavity. The solvent-cast cellulose acetate (CA) films that had been prepared in the presence of a mixture of AC/HPβCD of varying molar ratios (i.e., 1:0.5, 1:1, and 1:2) showed evidence of spherical aggregates on their surfaces. The dimensions of these aggregates were lower than those of the self-assembling aggregates of the AC/HPβCD complex in the solvated state. While AC could not be released from the AC-loaded CA films into the phosphate buffer saline solution (PBS) containing 10% (v/v) methanol (i.e., P/B/M medium), its cumulative amounts that had been released from the AC/HPβCD complex-loaded CA films were much greater, with values increasing with an increase in the HPβCD content. At 24 h of immersion in the medium at 37 °C, the maximal amounts of AC released from these materials were about 2.2, 3.9, and 5.8% (based on the actual weights of the film specimens), respectively.

Acknowledgements

The authors acknowledge the partial support received from (1) The Thailand Research Fund (contact grant number: DBG5280015), (2) The Petroleum and Petrochemical College (PPC), Chulalongkorn University, (3) The Development and Promotion of Science and Technology talents project (DPST).

Appendix A. Supplementary data

Supplementary data associated with this article can be found, in the online version, at doi:10.1016/j.carbpol.2011.02.023.

References

Anonymous. (2009). *Cellulose acetate*. http://en.wikipedia.org/wiki/Cellulose acetate

Bergshoef, M. M., & Vancso, G. J. (1999). Transparent nanocomposites with ultrathin, electrospun nylon-4,6 fiber reinforcement. *Advanced Materials*, *11*, 1362–1365.

Bonini, M., Rossi, S., Karlsson, G., Almgren, M., Lo Nostro, P., & Baglioni, P. (2006). Self-assembly of beta-cyclodextrin in water. Part 1. Cryo-TEM and dynamic and static light scattering. *Langmuir*, *22*, 1478–1484.

Challa, R., Ahuja, A., Ali, J., & Khar, R. K. (2005). Cyclodextrin in drug delivery: An updated review. *AAPS PharmScitech*, *6*. Article 43.

Choi, M. J., Ruktanonchai, U., Min, S. G., Chun, J. Y., & Soottitantawat, A. (2010). Physical characteristics of fish oil encapsulated by β-cyclodextrin using an aggregation method or polycarpolactone using an emulsion-diffusion method. *Food Chemistry*, *119*, 1694–1703.

Coleman, A. W., & Nicolis, I. (1992). An explanation of the abnormal solubility of β-cyclodextrin. *Journal of Inclusion Phenomena and Macrocyclic Chemistry*, *13*, 139–143.

Das, P., Mallick, A., Sarkar, D., & Chattopadhyay, N. (2008). Probe-induced self-aggregation of γ-cyclodextrin: Formation of extended nanotubular suprastructure. *Journal of Physical Chemistry C*, *112*, 9600–9603.

de Araujoa, D. R., Tsuneda, S. S., Ceredaa, C. M. S., Carvalho, F. D. G. F., Prete, P. S. C., Fernandes, S. A., et al. (2008). Development and pharmacological evaluation of ropivacaine-2-hydroxypropyl-β-cyclodextrin inclusion complex. *European Journal of Pharmaceutical Science*, *33*, 60–71.

Freville, J. C., Dollo, G., Le Corre, P., Chevanne, F., & Le Verge, R. (1996). Controlled systemic absorption and increased anesthetic effect of bupivacaine following epidural administration of bupivacaine-hydroxypropyl-beta-cyclodextrin complex. *Pharmaceutical Research*, *13*, 1576–1580.

González-Gaitano, G., Rodríguez, P., Isasi, J. R., Fuentes, M., Tardajos, G., & Sanchez, M. (2002). The aggregation of cyclodextrins as studied by photon correlation spectroscopy. *Journal of Inclusion Phenomenon*, *44*, 101–105.

He, Y., Fu, P., Shen, X., & Gao, H. (2008). Cyclodextrin-based aggregates and characterization by microscopy. *Micron*, *39*, 495–516.

Higuchi, T., & Connors, K. A. (1965). Phase solubility techniques. *Advances in Analytical Chemistry and Instrumentation*, *4*, 117–212.

Irie, T., & Uekama, K. (1997). Pharmaceutical applications of cyclodextrins. III. Toxicological issues and safety evaluation. *Journal of Pharmaceutical Science*, *86*, 147–162.

Job, P. (1928). Researches sur la formation de complexes mineraux en solution et sur leur stabilité. *Annali di Chimica Applicata*, *9*, 113–203.

Li, Z., Ren, J., Fane, G. A., Li, D. F., & Wong, F. S. (2006). Influence of solvent on the structure and performance of cellulose acetate membranes. *Journal of Membrane Science*, *279*, 601–607.

Loftsson, T., & Brewster, M. E. (1996). Pharmaceutical applications of cyclodextrins 1. Drug solubilisation and stabilization. *Journal of Pharmaceutical Science*, *85*, 1017–1025.

Loftsson, T., Hreindóttir, D., & Másson, M. (2007). The complexation efficiency. *Journal of Inclusion Phenomena and Macrocyclic Chemistry*, *57*, 545–552.

Loftsson, T., Jarho, P., Másson, M., & Sigurjonsdóttir, J. F. (2005). Cyclodextrins in drug delivery. *Expert Opinions in Drug Delivery*, *2*, 335–351.

Loftsson, T., Magnúsdósdottir, A., Másson, M., & Sigurjónsdóttir, J. F. (2002). Self-association and cyclodextrin solubilization of drugs. *Journal of Pharmaceutical Science*, *91*, 2307–2316.

Lopez, R. F. V., Collett, J. H., & Bentley, M. V. L. B. (2000). Influence of cyclodextrin complexation on the in vitro permeation and skin metabolism of dexamethasone. *International Journal of Pharmaceutics*, *200*, 127–132.

Maquart, F. X., Bellon, G., Gillery, P., Wegrowski, Y., & Borel, J. P. (1990). Stimulation of collagen synthesis in fibroblast cultures by a triterpene extracted from Centella asiatica. *Connective Tissue Research*, *24*, 107–120.

Maquart, F. X., Chastang, F., Simeon, A., Birembaut, P., Gillery, P., & Wegrowski, Y. (1999). Triterpenes from Centella asiatica stimulate extracellular matrix accumulation in rat experimental wounds. *European Journal of Dermatology*, *9*, 289–296.

Mele, A., Mendichi, R., & Selva, A. (1998). Non-covalent associations of cyclomaltooligosaccharides (cyclodextrins) with trans-β-carotene in water: Evidence for the formation of large aggregates by light scattering and NMR spectroscopy. *Carbohydrate Research*, *310*, 261–267.

Peppas, N. A., & Khare, A. R. (1993). Preparation structure and diffusional behavior of hydrogels in controlled release. *Advances in Drug Delivery Review*, *11*, 1–35.

Philip, L. R., & Peppas, N. A. (1987). A simple equation for description of solute release I. Fickian and non-fickian release from non-swellable devices in the form of slabs, spheres, cylinder or discs. *Journal of Controlled Release*, *5*, 23–36.

Pose-Vilarnovo, B., Perdomo-Lopez, I., Echezarreta-Lopez, M., Schroth-Pardo, P., Estrada, E., & Torres-Labandeira, J. J. (2001). Improvement of water solubility of sulfamathizole through its complexation with β- and hydroxypropyl-β-cyclodextrin: Characterization of the interaction in solution and in solid state. *European Journal of Pharmaceutical Science*, *13*, 325–331.

Pose-Vilarnovo, B., Rodriguez-Tenreiro, C., Santos, J. F. R., Vazquez-Doval, J., Concheiro, A., Alvarez-Lorenzo, C., et al. (2004). Modulating drug release with cyclodextrins in hydroxypropyl methlcellulose gels and tablets. *Journal of Controlled Release*, *94*, 351–363.

Rajewski, R. A., & Stella, V. J. (1996). Pharmaceutical applications of cyclodextrins. 2. In vivo drug delivery. *Journal of Pharmaceutical Science*, *85*, 1142–1169.

Romero, R. B., Leite, C. A. P., & Goncalves, M. D. C. (2009). The effect of the solvent on the morphology of cellulose acetate/montmorillonite nanocomposites. *Polymer*, *50*, 161–170.

Sangalli, M. E., Zema, L., Maroni, A., Foppoli, A., Giordano, F., & Gazzaniga, A. (2001). Influence of betacyclodextrin on the release of poorly soluble drugs from inert and hydrophilic heterogeneous polymeric matrices. *Biomaterials*, *22*, 2647–2651.

Shim, P. J., Park, J. H., Chang, M. S., Lim, M. J., Kim, D. H., Jung, Y. H., et al. (1996). Asiaticoside-mimetics as wound healing agent. *Bioorganic & Medicinal Chemistry Letters*, *6*, 2937–2940.

Shukla, A., Rasik, A. M., & Dhawan, B. N. (1999). Asiaticoside-induced elevation of antioxidant levels in healing wounds. *Phytotherapy Research*, *13*, 50–54.

Suguna, L., Sivakumar, P., & Chandrakasan, G. (1996). Effects of centella asiatica extract on dermal wound healing in rats. *Indian Journal of Experimental Biology*, *34*, 1208–1211.

Suwantong, O., Opanasopit, P., Ruktanonchai, U., & Supaphol, P. (2007). Electrospun cellulose acetate fiber mats containing curcumin and release characteristic of the herbal substance. *Polymer*, *48*, 7546–7557.

Suwantong, O., Ruktanonchai, U., & Supaphol, P. (2008). Electrospun cellulose acetate fiber mats containing asiaticoside or centella asiatica crude extract and the release characteristics of asiaticoside. *Polymer*, *49*, 4239–4247.

Suzuki, M., Tsutsui, M., & Ohmori, H. (1994). 2H NMR study of the self-assembly of an azo dye-cyclomaltooctaose (γ-cyclodextrin) complex. *Carbohydrate Research*, *261*, 223–230.

Taepaiboon, P., Rungsardthong, U., & Supaphol, P. (2007). Vitamin-loaded electrospun cellulose acetate nanofiber mats as transdermal and dermal therapeutic

agents of vitamin A acid and vitamin E. *European Journal of Pharmaceutics and Biopharmaceutics*, *67*, 387–397.

Thostenson, E. T., Ren, Z. F., & Chou, T. W. (2001). Advances in the science and technology of carbon nanotubes and their composites: A review. *Composite Science and Technology*, *61*, 1899–1912.

Tungprapa, S., Jangchud, I., & Supaphol, P. (2007). Release characteristics of four model drugs from drug loaded electrospun cellulose acetate fiber mats. *Polymer*, *48*, 5030–5041.

Valente, A. J. M., Polishchuk, A. Y., Burrows, H. D., & Lobo, V. M. M. (2005). Permeation of water as a tool for characterizing the effect of solvent, film thickness and water solubility in cellulose acetate membranes. *European Polymer Journal*, *41*, 275–281.

Verreck, G., Chun, I., Rosenblatt, J., Peeters, J., Dijck, A. V., Mensch, J., et al. (2003). Incorporation of drugs in an amorphous state into electrospun nanofibers composed of a water insoluble nonbiodegradable polymer. *Journal of Controlled Release*, *92*, 349–360.

Wang, F. J., Yang, Y. Y., Zhang, X. Z., Zhu, X., Chung, T. S., & Moochhala, S. (2002). Cellulose acetate membranes for transdermal delivery of scopamine base. *Materials Science and Engineering C*, *20*, 93–100.

Chiang Mai J. Sci. 2012; 39(2) : 231-245
http://it.science.cmu.ac.th/ejournal/
Contributed Paper

Effect of Degree of Acetylation on in Vitro Biocompatibility of Electrospun Cellulose Acetate-Based Fibrous Matrices

Pitt Supaphol*[a,b], Artphop Neamnark [a,b], Pattama Taepaiboon [a,b], and Prasit Pavasant [c]

[a] The Petroleum and Petrochemical College, Chulalongkorn University, Bangkok 10330, Thailand.
[b] The Center for Petroleum, Petrochemicals and Advanced Materials, Chulalongkorn University, Bangkok 10330, Thailand.
[c] Department of Anatomy, Faculty of Dentistry, Chulalongkorn University, Bangkok 10330, Thailand.
*Author for correspondence; e-mail: pitt.s@chula.ac.th

Received: 20 July 2011
Accepted: 20 December 2011

ABSTRACT

Ultrafine fibrous matrices of regenerated cellulose (RC) of varying degrees of acetylation were facilely prepared from alkaline hydrolysis of electrospun cellulose acetate (CA; acetyl content ≈ 40%) fiber mats. The alkaline treatment was carried out in 0.1 N NaOH solution in 4:1 v/v water/ethanol mixture at 25 ± 1°C for periods of up to 24 h, after the CA fiber mats had been thermally treated at 208 °C for 1 h. After having been treated in the NaOH solution for 10 min, 30 min, and 24 h, the resulting CA-based fibrous matrices exhibited the acetyl contents of about 24, 11, and 4%, respectively. Indirect cytotoxicity evaluation of these CA-based fibrous matrices against human fibroblasts (HFF) and human keratinocytes (HaCaT) indicated that they posed no threat to the cells. The direct culture of the cells on their surfaces suggested that these fibrous matrices only supported the short term culture of both types of cells (i.e., 1 d), while the neat and the 24 h-alkaline treated CA-based fibrous matrices exhibited marginally good support for the proliferation of HaCaT.

Keywords: Electrospinning, Cellulose acetate, Regenerated cellulose, Biocompatibility.

1. INTRODUCTION

Electrospinning has been a subject of intense research, due to its ability to produce ultrafine fibers, with diameters in the range of tens of nanometers to less than ten micrometers, that exhibit high surface area to volume/mass ratios [1,2]. The principle of the process is the use of electrical as opposed to mechanical force as the main driving force for fiber formation [1-6]. Morphology of the electrospun fibers depends on contributions from solution properties, process settings, and ambient conditions [1-6]. Due to the morphological uniqueness, the proposed uses of the electrospun fibers in the field of biomedical applications are, for examples, as carriers/substrates for enzyme encapsulation/

immobilization [7,8], carriers for drug delivery [9,10], and scaffolds for tissue regeneration [11-13].

Cellulose is one of the most common biopolymers on earth and is the primary structural component of cell walls of green plants [14]. Its usefulness has been known since the ancient time [14]. In the last decade, utilization of cellulose in biomedical applications was well documented [15-20]. Among these, many facets of biocompatibility were studied [15-18]. It has been proposed for uses as substrates/scaffolds for bone [16,18,19] and cartilage [20] tissue engineering. However, the fabrication of cellulose is hampered by its limited solubility in common solvents and its subservient to thermal degradation prior to melting. As a result, only a few reports on successful electrospinning of cellulose are available in the open literature [21-23]. Alternatively, ultrafine cellulose fibers can be obtained facilely from deacetylation of electrospun fibers of cellulose acetate (CA)- a cellulose derivative that is readily soluble in a number of organic solvents [24,25].

In the present contribution, ultrafine RC fiber mats were prepared from alkaline treatment of electrospun CA fiber mats. Various degrees of acetylation of the fiber mats were achieved by varying the treatment conditions. To fathom the possibility of using these CA-based membranes as topical wound dressing materials, biocompatibility of the native electrospun CA fiber mats and the ultrafine RC fiber mats of varying degrees of acetylation was assessed *in vitro* with human foreskin fibroblasts (HFF) and human keratinocytes (HaCaT).

2. EXPERIMENTAL DETAILS

2.1. Materials

Cellulose acetate (CA; white powder; M_w = 30,000 Da; degree of acetyl substitution ≈ 2.4; acetyl content = 39.7%) was purchased from Sigma-Aldrich (USA). Sodium hydroxide (NaOH) was purchased from Ajax Finechem (Australia) and hydrochloric acid (HCl) was from J.T. Baker (USA). Acetone (Carlo Erba, Italy), *N, N*-dimethylacetamide [DMAc, Labscan (Asia), Thailand], and ethanol [Labscan (Asia), Thailand] were used as-received.

2.2. Preparation of Electrospun CA Fiber Mats

The electrospinning of CA was carried out based on the method described in a published work by some of us and another colleague [26]. Briefly, a weighed amount of CA powder was dissolved in 2:1 v/v acetone/DMAc to obtain a CA solution at a fixed concentration of 17% w/v. Electrospinning of the solution was carried out using a Gamma High Voltage Research ES30P high voltage dc power supply as the power source, a flat-tipped 20-gauge stainless steel needle (OD = 0.91 mm) as the nozzle, and an aluminum foil wrapped around a home-made rotating metal drum (OD = 9 cm) as the fiber collection device. The electric field was 17.5 kV/15 cm, the rotational speed of the rotating drum was 60 ± 5 rpm, and the feed rate of the solutions was 1 mL h^{-1}. For 9 h of continuous electrospinning, the thicknesses of the CA fiber mats were 20-30 μm.

2.3. Thermal Treatment and Alkaline Treatment

The CA fiber mats were peeled off from the aluminum foil, sandwiched between two polytetrafluoroethylene (PTFE) sheets, and put in a hot-air oven at 208°C for 1 h [25]. They were then immersed in 0.1 N NaOH solution in 4:1 v/v water/ethanol mixture at room temperature (25 ± 1°C) for varying time intervals, ranging from 10 min

to 24 h. The alkaline-treated CA fiber mats were then rinsed in deionized (DI) water and kept in a desiccator prior to further uses.

2.4. Characterization

2.4.1. Physical characteristics

Morphological appearance of the neat, the heat-treated, and the alkaline-treated CA fiber mats was observed by a JEOL JSM-5200 scanning electron microscope (SEM). They were sputtered with a thin layer of gold using a JEOL JFC-1100E ion sputtering device prior to SEM observation.

2.4.2. Chemical functionalities and degree of deacetylation

Chemical functionalities of the neat and the alkaline-treated CA fiber mats were investigated by a Nicolet Nexus 670 Fourier-transform infrared spectroscope (4 cm^{-1} resolution with 4 scans over the wavenumber range of 400-4000 cm^{-1}). The degree of deacetylation (*%DD*) of the alkaline-treated CA fiber mats was evaluated by a titration method. Specifically, weighed samples of the CA fiber mats (2.8 cm in diameter) were immersed in 0.1 N of NaOH solution in 4:1 v/v water/ethanol mixture at the ratio of 1:1 w/v. After 10 min to 24 h of immersion, 5 mL of the NaOH solution was pipetted out and then titrated with 0.1 N HCl aqueous solution, with phenolphthalein being used to indicate the basicity-to-acidity crossover. The amount of the hydroxyl ions participated in the deacetylation reaction of CA could then be calculated from the amount of the titrant, which was used to calculate the *%DD*, i.e.

$$\%DD = \frac{m_i - m_f}{m_i} \times 100 , \quad (1)$$

where m_i and m_f are the moles of the acetyl groups in the CA fiber mats before and after the alkaline treatment.

2.4.3. Wide-angle X-ray diffraction studies

The crystalline nature of the neat, the heat-treated, and the alkaline-treated CA fiber mats was examined by a JEOL JDX 3530 wide-angle X-ray diffractometer (30 kV and 40 mA over the 2Theta range of 5 to 50°).

2.4.4. Physico-chemical characteristics

The water retention and the loss in the mass upon submersion in water of the neat and the alkaline-treated CA fiber mats were measured after their submersion in distilled water at 37°C for 24 h. If M_i denotes the initial mass of each fiber mat sample in its dry state and M and M_d are its masses after submersion in distilled water in its wet and dry states, respectively, the property values can be calculated as follows:

$$\text{Water retention (\%)} = \frac{M - M_d}{M_d} \times 100 , \quad (2)$$

$$\text{Mass loss (\%)} = \frac{M_i - M_d}{M_i} \times 100 . \quad (3)$$

2.5. Biological Evaluation

The potential for use of the neat and the alkaline-treated CA fiber mats as wound dressing materials was assessed by the indirect cytotoxicity evaluation and the direct cultures of mammalian cells onto their surfaces. Two types of cells were used: 1) human foreskin fibroblasts (HFF) and 2) immortalized non-tumorigenic human keratinocytes (HaCaT). The experiments were done in adaptation from previously-published protocols [12]. Briefly, either type of cells was first cultured in Dulbecco's modified Eagle's medium (DMEM; Sigma-Aldrich, USA), supplemented with fetal bovine serum (FBS; Biochrom, UK), L-glutamine (Invitrogen, USA), penicillin (Gibco®, Invitrogen, USA) and streptomycin (Gibco®, Invitrogen, USA). When the cells reached 80% confluence, they

were trypsinized and counted by a hemacytometer, prior to further uses.

The indirect cytotoxicity of the fibrous materials was assessed based on the method that was adapted from the ISO10993-5 standard test method. Briefly, the specimens (~ 14 mm in diameter), pre-washed with 70% ethanol for 30 min, were washed with autoclaved phosphate buffer saline (PBS) solution twice and once with the culture medium. Either type of cells was seeded in wells of a 24-well tissue-culture polystyrene plate (TCPS; Corning, USA) at 2×10^4 cells/well. After 24 h of attachment, the culture medium was replaced with serum-free medium (SFM; DMEM containing penicillin and streptomycin, but without FBS). Each of the specimens was then place into each well and both the cells and the specimen were incubated further for 1, 3, and 5 d. The extraction ratio was fixed at 10 mg mL^{-1}. After each specified time interval was reached, the medium in each well was removed. The viability of the cells was then quantified by 3-(4,5-dimethylthiazol-2-yl)-2,5-diphenyltetrazolium bromide (MTT) assay. The viabilities of the cells that had been cultured with fresh SFM were used as control.

For the direct cell culture studies, the well-washed specimens were placed in wells of 24-well TCPS. A stainless steel metal ring (12 mm in diameter) had been placed on top of each fiber mat specimen and 500 mL of the culture medium had been pipetted into each well, prior to the cell culturing. Subsequently, 2×10^4 cells/well of either type of cells were seeded onto each specimen and allowed to attach and proliferate for 1, 3, and 5 d. After rinsing the specimens with PBS twice to remove unattached cells, the viabilities of the cells were quantified by the MTT assay and the viabilities of the cells that had been cultured on TCPS were used as control. Lastly, the morphology of the cultured cells was investigated. The cell-cultured specimens were harvested and washed with PBS twice. After the cells had been fixed with 3% glutaraldehyde aqueous solution and washed with 0.2 M PBS aqueous solution, the specimens were dehydrated through a series of graded ethanol solutions and pure ethanol for 2 min and finally dried in air. Finally, they were observed by SEM.

2.6. Statistical Analysis

All the quantitative values were expressed as means ± standard deviation values. Statistical comparisons were performed using one-way ANOVA with SPSS 13.0 for Windows software (SPSS, USA). P values < 0.05 were considered statistically significant ($n = 3$).

3. RESULTS AND DISCUSSION

3.1. Morphology

The as-prepared 17% w/v CA solution in 2:1 v/v acetone/DMAc was electrospun under the electric field of 17.5 kV/15 cm for a fixed collection time of about 9 h [26]. A selected SEM image of the obtained fiber mats is shown in Figure 1a. The diameters of these individual fiber segments were determined to be 265 ± 39 nm ($n \geq 50$). Due to the fluffiness of the obtained fibrous matrices, further treatment in an alkaline aqueous solution would become a problem, as the materials could easily lose their physical integrity. Ma et al. [25] suggested that this shortcoming could be solved by thermally-treating the fiber mats at 208°C for 1 h. Figure 1b shows the morphology of the representative heat-treated fiber mat, which is obviously similar to that of the untreated precursor. The thermal treatment not only imparted the ease of handling to the fibrous matrices, but also helped

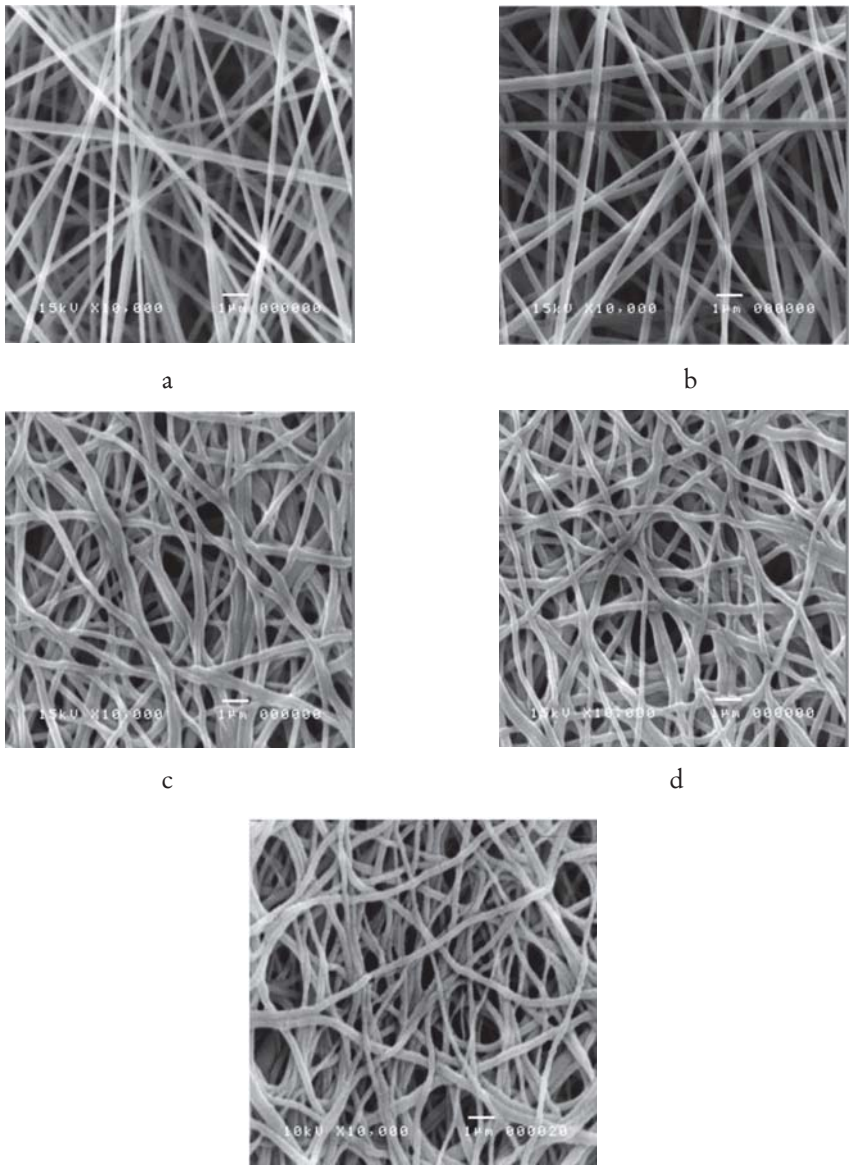


Figure 1. Selected scanning electron micrographs (magnification = 10,000x; scale bar = 1 μm) of electrospun fiber mats from 17% w/v CA solution in 2:1 v/v acetone/DMAc (a) before and (b) after heat treatment at 208°C for 1 h, including those of the thermally-treated fiber mats that had been submerged in 0.1 N NaOH solution in 4:1 v/v water/ethanol mixture at room temperature (25 ± 1°C) for (c) 10 min, (d) 30 min, and (e) 24 h. The electrospun CA fiber mats were fabricated under the electric field of 17.5 kV/15 cm for a fixed collection time of about 9 h.

maintain their physical integrity after having been submerged in 0.1 N NaOH solution in 4:1 v/v water/ethanol mixture at 25 ± 1°C for periods of up to 24 h. Figure 1c-e shows the morphology of the fiber mats after they had been submerged in the alkaline solution for 10 min, 30 min and 24 h, respectively. Apparently, the fibrous character of the alkaline-treated fiber mats was still intact, with no evidence of the individual fibers being destroyed. On the other hand, Son et al. [24] reported that, after being submerged in a potassium hydroxide (KOH) solution in ethanol for 30 min, obvious destruction of the CA fiber mats was evident.

3.2. Chemical Functionalities and *%DD*

The deacetylation reaction of the alkaline-treated CA fiber mats was followed qualitatively by FT-IR and quantitatively by titration. Figure 2 illustrates representative FT-IR spectra of a neat CA fiber mat and some of the CA fiber mats that had been submerged in the alkaline solution for 10 min, 30 min, and 24 h. For the neat CA fiber mat, a strong absorption peak centering at 1750 cm^{-1}, corresponding to the carbonyl groups (C=O) of the acetyl esters of CA, was evident. After 10 min of the alkaline treatment, the intensity of this peak decreased appreciably. Further increasing the alkaline treatment time resulted in a monotonous decrease in the intensity of the peak. The peak disappeared completely after submerging the mat in the NaOH solution for 24 h, thereby confirming the successful formation of RC fiber mats. In a similar manner, the presence of the peak centering at 1232 cm^{-1}, corresponding to the C-O stretching of the ester/ether groups of CA, decreased in its intensity upon submersion in the alkaline solution and even disappeared completely after 24 h of submersion in the alkaline solution. At 24 h of submersion in the NaOH solution, the presence of the peak

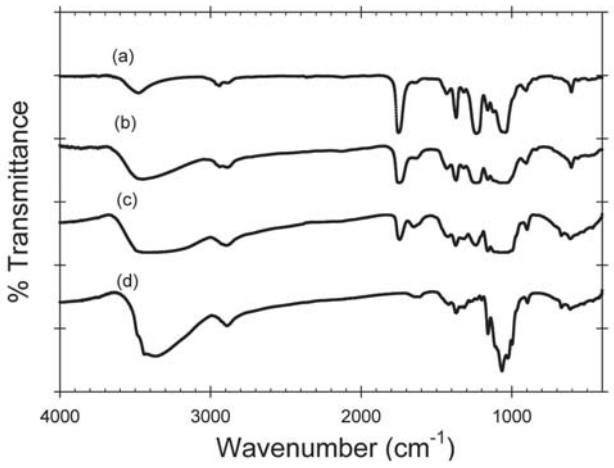


Figure 2. Representative FT-IR spectra of (a) a neat electrospun CA fiber mat and some of the thermally-treated fiber mats that had been submerged in 0.1 N NaOH solution in 4:1 v/v water/ethanol mixture at 25 ± 1°C for a period of (b) 10 min, (c) 30 min, and (d) 24 h.

centering at 1068 cm^{-1}, corresponding to the C-O stretching of the alcohol groups of cellulose, was clearly visible. Strikingly, the peak associated with the O-H stretching, centering at 3480 cm^{-1}, became more intense and broader for the alkaline-treated CA fiber mats, especially for the ones that had been submerged in the alkaline solution for 24 h.

The *%DD* values of all of the alkaline-treated CA fiber mats were determined by titration and the results are shown in Figure 3. It should be noted that the degree of acetyl substitution and the acetyl content of the as-received CA were 2.4 and 39.7%. The titration procedure was to quantify, in percentage, the amount of the acetyl groups that had been abstracted by the treatment with the NaOH solution. According to the obtained result, the *%DD* increased sharply from about 40% after 10 min of submersion in the alkaline solution to about 79% after 60 min of submersion. Further increase in the submersion time interval only resulted in a slight increase in the *%DD* to finally reach plateau values of about 88-90% after the CA fiber mats had been submerged in the alkaline solution for 7 to 24 h.

3.3. X-ray Diffraction

Figure 4 shows the X-ray diffraction patterns of the neat, the heat-treated, and some of the alkaline-treated CA fiber mats. For the neat CA fiber mat, two peaks at the 2Theta values of about 10.0 and 17.4° were observed. These peaks correspond respectively to the crystalline domains of CA and cellulose (ca. the acetyl content of the as-received CA was 39.7%). The intensity of these peaks increased appreciably after the thermal treatment, most likely a result of the increase in the mobility of the CA chains during the thermal treatment, hence the increase in the crystallinity of the crystalline domains. Kamide and Saito [27] reported a relationship between the glass transition temperatures (T_g, °C) and the degrees of

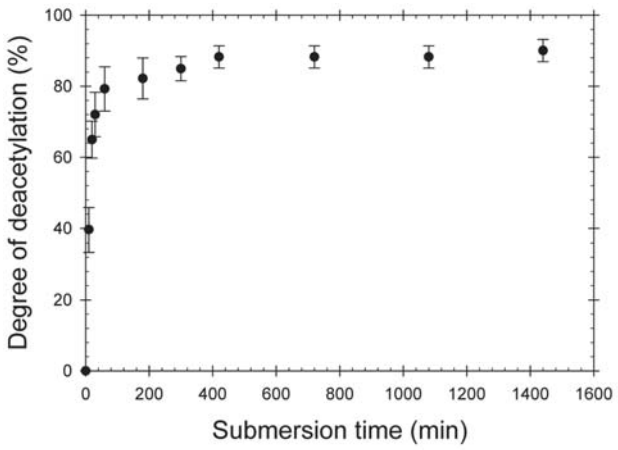


Figure 3. Degrees of deacetylation (*%DD*) of thermally-treated electrospun CA fiber mats that had been submerged in the NaOH solution as a function of submersion time (n = 5).

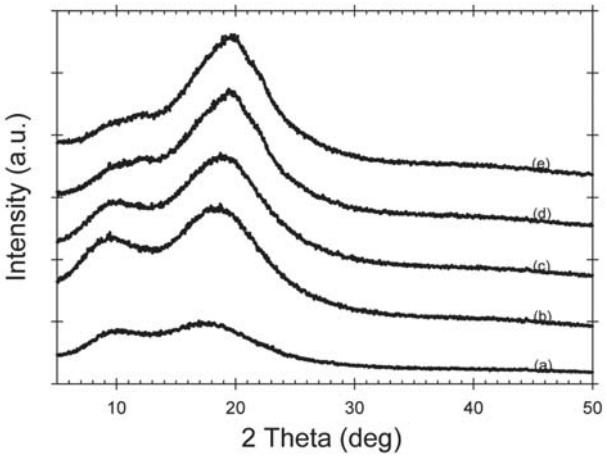


Figure 4. X-ray diffraction patterns of electrospun CA fiber mats (a) before and (b) after thermal treatment at 208°C for 1 h and those of the thermally-treated fiber mats that had been submerged in the NaOH solution for (c) 10 min, (d) 30 min, and (e) 24 h.

acetyl substitution ($z, \in [0,3]$) of CA, which was given as T_g = 249.9 - 20.3z. For z = 2.4, T_g of the as-received CA should be about 201°C. At the treatment temperature of 208°C, CA molecules should, therefore, have enough mobility to form more stable crystallites, hence the observed increase in the intensity of the crystalline peaks. The increase in the crystallinity of the thermally-treated CA would increase its stiffness and, at the same time, reduce the subservience to penetration by chemicals, hence an improvement of its physical integrity.

As for the alkaline-treated CA fiber mats, while the intensity of the low-angle peak decreased and shifted towards a higher 2Theta value with an increase in the treatment time interval, that of the high-angle peak increased and also shifted towards a higher 2Theta value. As the intensity of the high-angle peak increased with an increase in the alkaline treatment time, it becomes obvious that the decrease in the acetyl content along the CA chains was responsible for the observed increase in the crystallinity of the alkaline-treated CA fiber mats as well as the rearrangement of the crystalline packing into that of cellulose. The reappearance of the-OH groups, hence the occurrence of the hydrogen bonding, should be responsible for the observed increase in the crystallinity of the alkaline-treated CA fiber mats.

3.4. Physico-chemical Characteristics

The neat CA fiber mats and the CA fiber mats that had been treated with the alkaline solution for 10 min, 30 min, and 24 h were studied further. Based on Figure 3, the acetyl contents of these fibrous materials were estimated to be about 40, 24, 11, and 4%, respectively. These materials were tested for the water retention and the loss in the mass upon submersion in water for 24 h and the results are summarized in Table 1. The water retention decreased after the CA fiber mats underwent the alkaline treatment and the

Table 1. Water retention and the loss in the mass of thermally-treated electrospun CA fiber mats before and after submersion in the NaOH solution for 10 min, 30 min, and 24 h (n = 5).

Sample	Water retention (%)	Mass loss (%)
Neat	420 ± 19	0.6 ± 0.5
10 min of alkaline treatment	335 ± 13	1.0 ± 0.7
30 min of alkaline treatment	326 ± 25	1.1 ± 0.7
24 h of alkaline treatment	336 ± 16	1.4 ± 0.6

* These fiber mat samples had been submerged in distilled water at 37°C for 24 h.

variation in the submersion time did not have a strong influence on the property values. It should be noted that the retention of water in an ultrafine fibrous material originates from the absorption of water within the mass of the material and from the retention of water between inter-fibrous pores due to the capillary action. While the latter should increase when the CA fiber mats had been treated with the NaOH solution (i.e., due to the increase in the hydrophillicity), the fact that the water retention values of the alkaline-treated CA fiber mats were lower than that of the neat materials should be a result of the decrease in the absorbed amount of water within the mass of the matrix material. This, in turn, resulted from the fact that the CA fiber mats had to be thermally treated prior to being treated with the NaOH solution. The thermal treatment caused the crystallinity of the matrix material to increase, hence less amount of water to be absorbed. On the other hand, after the alkaline treatment, the loss in the mass of the fiber mats increased very slightly. It is well-known that cellulose undergoes alkaline degradation, the degradation occurs from the reducing ends of the molecule and produces water-soluble *D*-glucoisosaccharinic acid as a by-product [28].

3.5. Indirect Cytotoxicity Evaluation

The indirect cytotoxicity of the neat CA fiber mats and the CA fiber mats that had been treated with the alkaline solution for 10 min, 30 min, and 24 h were evaluated against HFF and HaCaT. Here, it is assumed that the viability of the cultured cells was proportional to the MTT absorbance. Figure 5 shows the viabilities of the cells that had been cultured in SFM both in the absence and in the presence of the fiber mat specimens for 1, 3, or 5 d were reported relatively to that of the cells that had been cultured in the absence of the specimens for 1 d. Evidently, the viabilities of both types of cells that had been cultured on the surface of TCPS, without or with the presence of the fiber mat specimens, increased monotonically with an increase in the cell culturing time. In fact, the viabilities of the cells, at any given cell culturing time point, were statistically the same, without or with the presence of the fiber mat specimens. The results indicate clearly that the proliferative ability of the cultured cells was unaffected, despite the presence of the fiber mat specimens in the culture medium of up to 5 d. In other words, these fibrous materials released no substances in the levels that would be harmful or pose any adverse effect to the growth in the number of the cells.

3.6. Cell Culture Studies

As previously mentioned, the acetyl contents of the neat CA fiber mats and

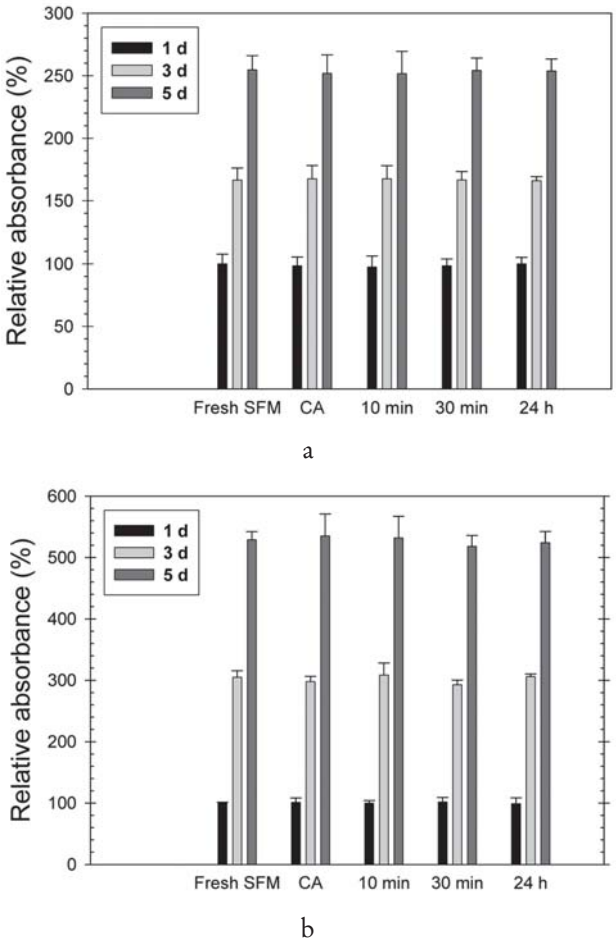


Figure 5. Indirect cytotoxicity evaluation of thermally-treated electrospun CA fiber mats before and after submersion in the NaOH solution for 10 min, 30 min, and 24 h, against (a) human foreskin fibroblasts (HFF) and (b) immortalized non-tumorigenic human keratinocytes (HaCaT) (n = 3). The fiber mat specimens were placed into the wells, that had been pre-cultured with the cells at 2×10^4 cells/well for 24 h, in serum-free medium (SFM) for a period of 1, 3, or 5 d at the extraction ratio of 10 mg mL^{-1}. The viabilities of the cells were reported in terms of the absorbance values relatively to that of the cells that had been cultured in the absence of the specimens for 1 d.

the CA fiber mats that had been treated with the alkaline solution for 10 min, 30 min, and 24 h were about 40, 24, 11, and 4%, respectively. These fibrous materials were tested further for *in vitro* biocompatibility with HFF and HaCaT. The cells were directly seeded and cultured on these fibrous matrices for 1, 3, and 5 d and those seeded and cultured on bare wells of TCPS were used as positive control. Again, the viability of the seeded and the cultured cells was proportional to the MTT absorbance.

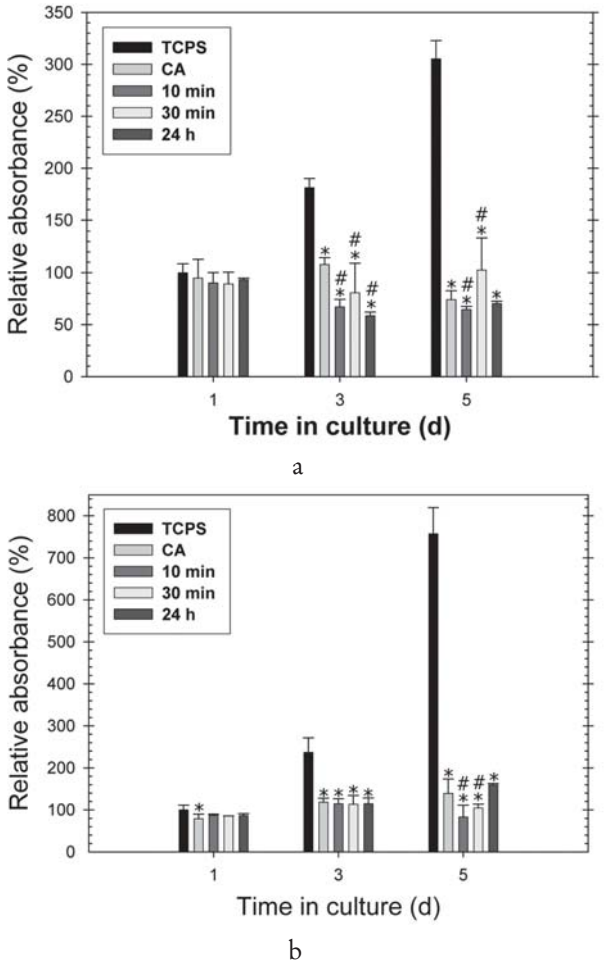


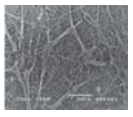
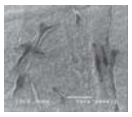
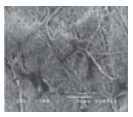
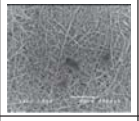
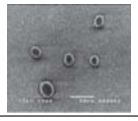
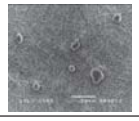
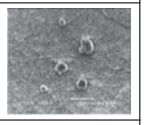
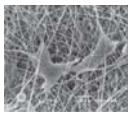
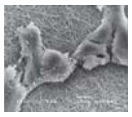
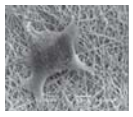
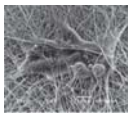
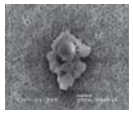
Figure 6. Attachment and proliferation of (a) HFF and (b) HaCaT that that had been seeded at 2×10^4 cells/well and cultured on tissue-culture polystyrene plate (TCPS, used as positive control) and thermally-treated electrospun CA fiber mats before and after submersion in the NaOH solution for 10 min, 30 min, and 24 h as a function of culturing time ($n = 5$). The viabilities of the cells were reported in terms of the absorbance values relatively to that of the cells that had been cultured on TCPS for 1 d. (*) $p < 0.05$ compared with TCPS at each specific time point and (#) $p < 0.05$ compared with CA at each specific time point.

Evidently, both types of cells adhered and proliferated well on the surface of TCPS. On day 1 of cell seeding, the viabilities of both types of cells that had been seeded on all of the fibrous matrices were not significantly different from those on TCPS, except for those of HaCaT that had been seeded on the neat CA fiber mats showing significantly lower values. On days 3 and 5, the viabilities of both types of cells that had

been cultured on all of the fibrous matrices were inferior to those on TCPS.

For HFF, the variation in the acetyl contents of the CA-based fibrous matrices did not pose strong effect on the viabilities of the cells cultured on them on day 1. Such an effect was seen when the cells had been grown for longer periods of time (i.e., 3 and 5 d). On day 3, only the neat CA fiber mats could support the growth of the cells particularly better than the alkaline-treated counterparts. On day 5, the viabilities of the cells grown on the CA fiber mats that had been treated with the alkaline solution for 30 min increased, while those on the neat CA counterparts decreased, causing the 30 min-alkaline treated CA fiber mats to be the better support for the growth of the cells. For HaCaT, the variation in the acetyl contents of the CA-based fibrous matrices did not affect the viabilities of the cells grown on them on days 1 and 3, despite the slight increase in the viabilities of the cells on day 3, when compared with those on day 1. On day 5, the viabilities of the cells grown on the neat CA fiber mats and the CA fiber mats that had been treated with the alkaline solution for 24 h, which showed equivalent values, increased slightly from day 3, those of the cells grown on the CA fiber mats that had been treated with the alkaline solution for 10 and 30 min decreased slightly.

Table 2. SEM images illustrating morphologies of HFF and HaCaT that had been grown on surfaces of thermally-treated electrospun CA fiber mats before and after submersion in the NaOH solution for 10 min, 30 min, and 24 h for 1 and 3 d.

Type of cells	Cell culturing time (d)	Type of CA-based fibrous matrices			
		CA	10 min	30 min	24 h
HFF*	1				
	3				
HaCaT**	1				
	3				

Magnification = *500x and **1500x

The morphologies of both HFF and HaCaT that had been seeded and cultured on the surfaces of the CA-based fibrous matrices are shown in Table 2. On day 1, both types of cells extended their cytoplasm over the surfaces of the fibrous matrices particularly well and even appeared in their normal cell shapes (i.e., spindle-like morphology for HFF and cobblestone morphology for HaCaT). On day 3, HFF on the neat CA fiber mat still appeared

expanded over the surface, but the extent of the cellular expansion was much decreased, when compared with the cells on day 1. HFF on the surfaces of the alkaline-treated CA fiber mats, on the other hand, were completely round. The change of the cell shape from spindle-like into round morphology, as the cell culturing time increased, suggested that the CA-based fibrous matrices are not supportive of the growth of human fibroblasts. This is in line with the observation reported by Sanchavanakit et al. [29] on bacterial cellulose fibrous membranes. Unlike HFF, HaCaT, on day 3 in their culture on the surfaces of all of the fibrous matrices, still retained their cobblestone morphology. However, the cells appeared to be more aggregated, especially those that had been cultured on the surfaces of the CA fiber mat that had been treated with the alkaline solution for 10 and 30 min. Despite the aggregation of the cells, the numbers of HaCaT on the surfaces of the CA fiber mat and the CA fiber mat that had been treated with the alkaline solution for 24 h increased from those on day 1. As reported by Sanchavanakit et al. [29], bacterial cellulose fibrous membranes showed good support for adhesion and proliferation of human keratinocytes.

4. CONCLUSIONS

FT-IR, titration, and X-ray diffraction confirmed partial removal of acetyl groups from the thermally-treated (208°C for 1 h) electrospun CA fiber mats upon submersion in 0.1 N NaOH solution in 4:1 v/v water/ethanol mixture at 25 ± 1°C. For the CA fiber mats that had been treated with the alkaline solution for 10 min, 30 min, and 24 h, the acetyl contents were about 24, 11, and 4%, respectively (cf. the acetyl content of about 40% for the as-received CA). The indirect cytotoxicity evaluation of the CA and the RC fibrous matrices against human fibroblasts (HFF) and human keratinocytes (HaCaT) indicated that these materials did not release any substance in the level that would be toxic or suppress the growth of both types of cells. Further evaluation with the direct culture of the cells on the materials revealed that these materials could only support the short term culture of both types of cells (i.e., 1 d) and only the neat CA fiber mats and the CA fiber mats that had been treated with the NaOH solution for 24 h showed marginally good support for the proliferation of the human keratinocytes. These results suggested the potential for use of the fibrous matrices as temporary dressings of skin wounds and this should be evaluated further *in vivo*.

5. ACKNOWLEDGMENTS

The authors acknowledge the partial support received from 1) The Thailand Research Fund (TRF, DBG5280015), 2) The Petroleum and Petrochemical College (PPC), Chulalongkorn University, and 3) Center for Petroleum, Petrochemicals, and Advanced Materials (CPPAM), Chulalongkorn University.

REFERENCES

[1] Doshi J. and Reneker D.H., Electrospinning process and applications of electrospun fibers, *J. Electrostat.*, 1995; **35**: 151-160.

[2] Reneker D.H. and Yarin A.L., Electrospinning jets and polymer nanofibers, *Polymer*, 2008; **49**: 2387-2425.

[3] Shim Y.M., Hohman M.M., Brenner M.P. and Rutledge G.C., Experimental characterization of electrospinning: The electrically forced jet and instabilities, *Polymer*, 2001; **42**: 9955-9967.

[4] Ding B., Kim H.Y., Lee H.C., Shao C.L., Lee D.R., Park S.J., Kwag G.B. and Choi K.J., Preparation and characterization of a nanoscale poly(vinyl alcohol) fiber aggregate produced by an electrospinning method, *J. Polym. Sci., B: Polym. Phys*., 2002; **40:** 1261-1268.

[5] Theron S.A., Zussman E. and Yarin A.L., Experimental investigation of the governing parameters in the electrospinning of polymer solutions, *Polymer,* 2004; **45**: 2017-2030.

[6] Zhang C., Yuan X., Wu L., Han Y. and Sheng J., Study on morphology of electrospun poly(vinyl alcohol) mats, *Eur. Polym. J*., 2005; 41: 423-432.

[7] Ren G., Xu X., Liu Q., Cheng J., Yuan X., Wu L. and Wan Y., Electrospun poly(vinyl alcohol)/ glucose oxidase biocomposite membranes for biosensor applications, *React. Funct. Polym*., 2006; **66**: 1559-1564.

[8] Ye P., Xu Z.K., Wu J., Innocent C. and Seta P., Nanofibrous poly (acrylonitrile-co-maleic acid) membranes functionalized with gelatin and chitosan for lipase immobilization, *Biomaterials*, 2006; **27**: 4169-4176.

[9] Zeng J., Yang L., Liang Q., Zhang X., Guan H., Xu X., Chen X. and Jing X., Influence of the drug compatibility with polymer solution on the release kinetics of electrospun fiber formulation, *J. Control. Release*, 2005; **105**: 43-51.

[10] Luong-Van E., Grøndahl L., Chua K.N., Leong K.W., Nurcombe V. and Cool S.M., Controlled release of heparin from poly(e-caprolactone) electrospun fibers, *Biomaterials*, 2006; **27**: 2042-2050.

[11] Chong E.J., Phan T.T., Lim I.J., Zhang Y.Z., Bay B.H., Ramakrishna S. and Lim C.T., Evaluation of electrospun PCL/gelatin nanofibrous scaffold for wound healing and layered dermal reconstitution, *Acta Biomater.,* 2007; **3**: 321-330.

[12] Wutticharoenmongkol P., Sanchavanakit N., Pavasant P. and Supaphol P., Preparation and characterization of novel bone scaffolds based on electrospun polycaprolactone fibers filled with nanoparticles, *Macromol. Biosci*., 2006, 6: 70-77; Wutticharoen mongkol P., Sanchavanakit N., Pavasant P. and Supaphol P., Novel bone scaffolds of electrospun polycaprolactone fibers filled with nanoparticles, *J. Nanosci. Nanotechnol*., 2006, 6: 514-522; Wutticharoenmongkol P., Pavasant P. and Supaphol P., Osteoblastic phenotype expression of MC3T3-E1 cultured on electrospun polycaprolactone fiber mats filled with hydroxyapatite nanoparticles, *Biomacromolecules*, 2007, **8**: 2602-2610.

[13] Suwantong O., Pavasant P. and Supaphol P., Electrospun zein fibrous membranes using glyoxal as cross-linking agent: Preparation, characterization and potential for use in biomedical applications, *Chiang Mai J. Sci.,* 2011, **38**: 56-70.

[14] Anonymous, Cellulose acetate, 2009; http://en.wikipedia.org/wiki/ Cellulose acetate.

[15] Miyamoto T., Takahashi S., Ito H., Inagaki H. and Noshiki Y., Tissue biocompatibility of cellulose and its derivatives, *J. Biomed. Mater. Res*., 1989; **23**: 125-133.

[16] Barbié C., Chauveaux D., Barthe X., Baquey C. and Poustis J., Biological behaviour of cellulosic materials after bone implantation: Preliminary results, *Clin. Mater*., 1990; **5**: 251-258.

[17] Mannhalter C., Biocompatibility of artificial surfaces such as cellulose and related materials, *Sens. Actuat., B: Chem.* 1993; **11**: 273-279.

[18] Martson M., Viljanto J., Hurme T. and Saukko P., Biocompatibility of cellulose sponge with bone, *Eur. Surg. Res*., 1998; **30**: 426-432.

[19] Barbosa M.A., Granja P.L., Barrias C.C. and Amaral I.F., Polysaccharides as scaffolds for bone regeneration, *ITBM-RBM*, 2005; **26**: 212-217.

[20] Muller F.A., Muller L., Hofmann I., Greil P., Wenzel M.M. and Staudenmaier R., Cellulose-based scaffold materials for cartilage tissue engineering, *Biomaterials,* 2006; **27**: 3955-3963.

[21] Kulpinski P., Cellulose nanofibers prepared by the N- methylmorpholine-N-oxide method, *J. Appl. Polym. Sci*., 2005; **98**: 1855-1859.

[22] Kim C.W., Frey M.W., Marquez M. and Joo Y.L., Preparation of submicron-scale, electrospun cellulose fibers via direct dissolution, *J. Polym. Sci.,B: Polym. Phys.,* 2005; **43**: 1673-1683.

[23] Kim C.W., Kim D.S., Kang S.Y., Marquez M. and Joo Y.L., Structural studies of electrospun cellulose nanofibers, *Polymer,* 2006; **47**: 5097-5107.

[24] Son W.K., Youk J.H., Lee T.S. and Park W.H., Electrospinning of ultrafine cellulose acetate fibers: Studies of a new solvent system and deacetylation of ultrafine cellulose acetate fiber, *J. Polym. Sci., B: Polym. Phys.,* 2004; **42**: 5-11.

[25] Ma Z., Kotaki M. and Ramakrishna S., Electrospun cellulose nanofiber as affinity membrane, *J. Membr. Sci.,* 2005; **265**: 115-123.

[26] Taepaiboon P., Rungsardthong U. and Supaphol P., Vitamin-loaded electrospun cellulose acetate nanofiber mats as transdermal and dermal therapeutic agents of vitamin A acid and vitamin E, *Eur. J. Pharm. Biopharm.,* 2007; **67**: 387-397.

[27] Kamide K. and Saito M., Thermal analysis of cellulose acetate solids with total degrees of substitution of 0.49, 1.75, 2.46, and 2.92, *Polym. J.,* 1985; **17**: 919-928.

[28] Mark H.F., Bikales N.M., Overberger C.G. and Menges G., Encyclopedia of Polymer Science and Engineering, New York, John Wiley and Sons, 1985.

[29] Sanchavanakit N., Sangrungraungroj W., Kaomongkolgit R., Banaprasert T., Pavasant P. and Phisalaphong M., Growth of human keratinocytes and fibroblasts on bacterial cellulose film, *Biotechnol. Prog.,* 2006; **22**: 1194-1199.

PREPARATION CHARACTERIZATION AND STUDY OF CRUDE BONE PROTEIN DELIVERY FORM GELATIN MICROSPHERES AND GELATIN MICROSPHERES INTEGRATED HYALURONAN-GELATIN BLENDED SCAFFOLD FOR BONE TISSUE REGERNATION

Parintorn Hariraksapitak,[1,a] Prasit Pavasant,[2] and Pitt Supaphol [1,*]

[1] The Petroleum and Petrochemical College, Chulalongkorn University, Bangkok 10330, Thailand
[2] Department of Anatomy, Faculty of Dentistry, Chulalongkorn University, Bangkok 10330, Thailand

ABSTRACT

This study aimed to develop a protein delivery HA-Gelatin blended scaffold for bone tissue regeneration. The designed scaffold was composed of gelatin microspheres as the part of integrated delivery device in which the crude bone protein (CBP) extracted from bone extracellular matrix was encapsulated. Gelatin microspheres were prepared with the thermal gelation in water-in-oil emulsion technique. Two types of gelatin (A and B) at different three pH which were physiologic (5.2 and 4.95 for type A and B respectively), 7.4, and 10.0 were specified as the preparative conditions and investigated for their influences on the microspheres properties. The results showed the effect of interaction between gelatin type and pH on microspheres size, zeta potential, swelling ability, and encapsulation of the CBP, but not on the CBP release characteristic. The significantly highest encapsulation of CBP (> 93%) was achieved in gelatin A, pH 10.0 and gelatin B, pH 4.95 microspheres. Astoundingly, the controlled release of CBP from any gelatin microspheres was not observed, implying that the anticipated ionic interaction between CBP and molecules of gelatin may not occur. However, the microspheres integrated composite scaffolds presented phase of sustained CBP release which suggests the essential influence of scaffold matrix on the release mechanism.

(**Key-words**: bone scaffolds; bone protein; gelatin microspheres; controlled release)

[a] On study leave from the Department of Conservative Dentistry, Faculty of Dentistry, Prince of Songkla University, Hatyai, Songkhla 90112, Thailand.

[*] Author to whom correspondence should be addressed (E-mail address: pitt.s@chula.ac.th)

1. INTRODUCTION

Tissue engineering is an approach to regenerate living tissue with an aim at establishing healthy tissue or organ for being a substitute of the damaged or the diseased tissue [1]. Progression in tissue engineering research since 1990 has been encouraging a reappraisal of the surgical approach for the treatment of trauma and degeneration of an individual [2]. Regarding dental practice, sufficient bone support is a major requirement to achieve favorable function and esthetic in the replacement of a losing tooth with a dental implant. Unfortunately, perfect bone structure is not always presented in most patients. Bone resorption easily occurs even in a simple tooth extraction case as the consequence of would heal process [3,4]. Prevention of the alveolar bone resorption caused by a tooth extraction has been of great concern, particularly through the principle of tissue engineering [5-8].

Basically, the fundamental of tissue engineering coalesces cell, supportive material termed “scaffold” and growth-inducing substance to promote three-dimensional tissue growth [9]. Scaffold, which is a three-dimensional construct, serves as a temporary territory for cells ingrowths. Ideal scaffold should perfectly imitate the extracellular matrix and provide the necessary support for cells to proliferate and maintain their differentiated function [10,11]. Scaffolds design was initially focused on their capabilities in supporting cell growth mostly at the physical and mechanical aspects. However, the design has been recently paradigmatically shifted to serve the function of a cellular guidance. This deliberation is in accordance with the concept of cellular guidance which has been extensively discussed and progressively revised as a new knowledge of the cell-material interaction in tissue regeneration [12,13]. Scaffolds have been designed as a route to transport biological factors for cell growth and differentiation and be able to guide and induce cell adhesion, proliferation, differentiation or even recruit the desired cells. The novel tissue engineering scaffold, therefore, can be considered as a special type of drug delivery apparatus [12], or as a drug delivery scaffold.

Drug delivery scaffold can be designed by the integration of a drug encapsulated delivery device into a designated scaffold. Such model has been broadly studied for their efficacy in controlled release and tissue engineering enhancement [14-17]. The drug delivery device itself has been designed in several profiles and configurations. However, most systems base on the encapsulation or entrapment of active substances in biocompatible polymeric devices [18]. Among numerous applicable drug delivery devices, Gelatin microspheres have been frequently studied with several therapeutic agents such as antihypertensive [19], signaling proteins like albumin [20], chondroitin 6-sulfate [21], bFGF [15], IGF and TGF-β [16], or even the plasmid DNA [17] can also be encapsulated in gelatin microspheres in which the release profiles was under control. These studies demonstrated satisfactory results of controlled release and tissue regeneration in animal test [21]. Gelatin microsphere apparently is a utility drug delivery device.

Gelatin is commonly used in pharmaceutical and medical application due to its biocompatibility and biodegradability. Structurally, gelatin is a heterogeneous mixture of single or multiple stranded polypeptides (and their oligomers) each of which contains about 300-4000 amino acids [22-24]. Molecules of gelatin are polyelectrolyte, presenting diverse isoelectric point (IEP) which are about 3-5 and 7-9 for the alkaline and acidic treated gelatin, respectively. Gelatin with different IEP

can be selectively used to from complex with the oppositely charged molecule like proteins, to be the polyion complexation which is quite stable and improbable to dissociate simultaneously. Polyion complexes thus are durable than bonding between low molecular weight electrolytes [22].

With an aim to regenerate bone in the dental socket, the crude bone protein (CBP) extracted from bone extracellular matrix is the material of interest. CBP evidently encompasses enormous active proteins and growth factors [25-29] which facilitates new bone formation [26,30]. Extraction of the crude bone protein with the intricate procedures does not obliterate bioactivities of those factors, and these presumptions initiate the plan to exploit CBP extracted from demineralized bone in regenerating bone tissue by applying the concept of the polyion complexation in achieving a degree of molecular interaction between gelatin microspheres and CBP.

This contribution proposes to fabricate a novel scaffold used for alveolar bone regeneration. On the basis of multi-functional scaffold, scaffold is designed and expected to function as not only a delivery device of the crude bone protein but also a supporting structure for the growth of bone cells. Concept of the polyion complexation is applied to achieve a degree of ionic-molecular interaction between the gelatin microspheres and crude bone protein. And it is also applied in fabricating a porous scaffold of which the polyelectolyte HA-gelatin blends are the materials of choice. The encapsulated gelatin microspheres are anticipated to be securely bound in the scaffold and provide controlled release of the crude bone protein in order to facilitate bone tissue regeneration.

2. EXPERIMENTAL SECTION

2.1. Materials

Gelatin from porcine skin (type A, Bloom no.170-180) was purchased form Fluka (Switzerland). Gelatin form bovine skin (type B, Bloom no.175-225) was purchased from Sigma Aldrich (USA). Hyaluronan (MW 1.35×10^6) was purchased from Coach Industries Inc (Japan). Albumin from bovine serum, tetramethylrhodamine conjugate (MW 66,000 Da) was purchased from Molecular Probes Inc (USA). Rhodamine protein label kit was purchased form Pierce (USA). Saturated Glutaraldehyde aqueous solution (5.6 M) was purchased from Fluka (Switzerland). 1-ethy-3-(3-dimethylaminopropyl)carbodiimide (EDC) was purchased form Fluka (Switzerland). Acetone (AR grade) was purchased from Lab-Scan (Thailand). All other chemical agents were of analytical grade and used without further purification.

2.2. Gelatin microspheres preparation

Gelatin microspheres were prepared by a thermal gelation technique with modification. In detail, 10 ml of 15% w/v gelatin (type A or B) aqueous solution was prepared at 40°C. In addition to the physiologic pH which is 5.2 or 4.95 for the gelatin type A or B respectively, pH of the gelatin solution was adjusted to 7.4 and 10.0 by the addition of 1N HCl or 1M NaOH with an aim to study the effects of pH and type of gelatin on behaviors of the as-prepared microspheres. Then, the solution was added dropwise into 200 ml of Soya oil preheated at 40°C under continuously stirring at 1,000 rpm with a homogenizer to form water-in-oil emulsion. After 10 min, temperature of the emulsion was reduced to be 4°C with an ice bath while stirring was continued for an additional 30 min to allow for

physically thermal gelation of the gelatin. Afterward, 200 ml of pre-cooled (4°C) acetone was added and stirred for the next 60 min in order to dehydrate and flocculate the coaceravate droplets. The microspheres were collected by filtration through a sintered glass filter (1 μm pores size) under vacuum, washed three times with 100 ml of cool (4°C) acetone to remove residual oil, and dried in air at room temperature over 24 h.

To crosslink the gelatin microspheres, 250 mg of the dry microspheres was suspended in 10 ml of acetone-water (2:1, v/v) containing 1% (w/v,~100mM) Glutaraldehyde solution and stirred at 4°C, 500 rpm for 1 h. The crosslinked microspheres were collected through a sintered glass filter and washed with precooled (4°C) acetone. Then, the crosslinked microspheres were suspended in 20 ml of 10 mM aqueous glycine solution containing Tween 80 (0.1 wt%), shaken at 37 °C, 50 rpm for 1 h to block the residual aldehyde groups of the unreacted glutaraldehyde. The crosslinked microspheres were then washed twice with 60 ml of the cool deionized water (4°C), with cool acetone, filtered, and eventually air-dried at room temperature for over 24 h.

2.3. Crude Bone Protein preparation

CBP was extracted from the bovine jaws bone. In particular, bone was initially washed and cleaned thoroughly in tap water and then sectioned into small pieces with a diamond disc driven by a rotor. Pieces of bones were further crushed into powder in liquid Nitrogen. Then, the as-prepared powder was immersed in 0.6 N HCl at 4°C and shaken continuously on an orbital shaker. After three days, the bony solution was centrifuged and the supernatant was collected, dialyzed for 48 h and lyophilized. The dry CBP was kept in desiccators until use.

2.4. Fluorescent labeling of Crude Bone Protein

Crude Bone Protein (CBP) was fluorescent-labeled with the 5-(and 6)-carboxytetramethylrhodamine, succinimidyl ester (NHS-Rhodamine). Briefly, 10 mg/ml of CBP solution was prepared with 50mM borate buffer, pH 8.5 and transferred to a reaction tube. Then, 10 mg/ml of NHS-Rhodamine in DMSO was added. The reaction solution was gently mixed well and incubated in the dark at room temperature for 1 hour. To remove the non-reacted NHS-Rhodamine, the reaction solution was filtered through a D-salt dextran desalting column using 10 mM phosphate buffered saline (PBS) with 0.15 M NaCl as a filtrating medium. The effluent solution was collected in 500-μl fraction. All fractions were subsequently detected by measuring the absorbance with spectrophotometer at 280 nm to identify the fraction containing NHS-Rhodamine-labeled CBP (hereafter, CBP-Rhod). The concentration of the CBP-Rhod existing in the selected fraction was further determined using spectrofluorometer (Cary Eclipse™) at 541 and 572 nm for the excitation and emission wavelength respectively, based on a BSA-Rhod (Molecular Probes™) standard curve over the concentration range 1-50 μg/ml (r^2=0.996). The CBP-Rhod fraction was stored at 4°C and protected from light until ready to use.

2.5. CBP-Rhod loading into gelatin microspheres

Crosslinked gelatin microspheres were loaded with CBP-Rhod by diffusion method. In particular, the aforementioned CBP-Rhod fraction was diluted with 10 mM PBS, 0.15 M NaCl, pH 7.2 to achieve the concentration ~700 μg/ml. Gelatin microspheres were immersed in the diluted CBP-Rhod solution to attain the loading dose of 4 μg CBP-Rhod per mg dried microspheres. The resulting mixture was vortexed for 1 h and incubated at 4°C for 24 h to let the CBP-Rhod infuse. The impregnated microspheres were frozen at -40°C for 24 h, lyophilized, and kept in the dark at 4°C until use.

2.6. Fabrication of porous composite hyaluronan-gelatin scaffolds

Porous composite hyaluronan (HA)-gelatin scaffolds were fabricated by the solvent casting and freeze-drying technique. Briefly, 2% (w/w) aqueous solution of a HA and gelatin mixture (1:1, w/w) was prepared at 50°C and left to cool down to room temperature. Then, in order to facilitate the blending of HA and gelatin, ionic strength of the mixture was adjusted by adding the equal amount of NaCl to HA (1:1, mole/equ) and being mixed up for 30 min. The resulting mixture became clearer and more translucent. To crosslink the polymers, calculated amount of EDC (1x to HA, mole/equ) was added and reacted under 200 rpm stirring at room temperature for 2 h. Afterward, the neat or the CBP-Rhod labeled microspheres were suspended in HA-gelatin mixture at 1% (w/w) concentration, which equals to 50% (w/w) of the polymer weight. The suspension was continuously stirred until the microspheres were well dispersed in the mixture and the then was cast in polypropylene discs at a constant weight, freezed at -40°C and lyophilized at -50°C. The samples were kept in desiccators until use.

2.7. Characterization

2.7.1. Size and morphology of gelatin microspheres and microspheres integrated HA-Gelatin scaffold

Gelatin microspheres were initially inspected under the computer connected Polarizing Optical Microscope (DMRXP, Leica) at 20x magnification. The images were recorded and further used to measure the diameters of the microspheres with the UTHSCSA Image Tool version 3.0 software. One hundred microspheres were measured for each preparative condition and the average values of their sizes were calculated. The data were also used to determine size distribution of the microspheres both before and after crosslinking with 100mM Glutaraldehyde. For the morphological study, gelatin microspheres and the as-prepared scaffolds were mounted on brass stubs, coated with gold using a JEOL JFC-1100 sputtering device, and observed for their microscopic morphology using JEOL JSM-5200 scanning electron microscopy (SEM).

2.7.2. Swelling ability of gelatin microsphere

Swelling ability was determined by the alteration of microspheres' size after water uptake. 20 mg of the dry crosslinked microspheres were incubated in 10 ml of 10 mM PBS with 0.15 M NaCl at 37°C for 24 h. Then, sizes of the swelling microspheres were examined with the same procedure as previously described in 2.7.1. One hundred microspheres of each preparative condition were

measured and the average diameters were calculated. The swelling ability was calculated according to the following equation:

$$\text{Swelling} = Ø_{swell} / Ø_{dry}$$

where $Ø_{swell}$ and $Ø_{dry}$ are the averaged diameter of the microspheres before and after incubation, respectively.

2.7.3. Zeta potential determination

Zeta potentials (or electrophoretic mobility) of the gelatin microspheres were determined using Zeta-Meter 3.0+ (Zeta-Meter, Inc., USA). Briefly, the suspension of 25 mg gelatin microspheres in 10 ml of deionized water was filled in an electrophoresis cell. Two electrodes were inserted into the cell and connected to the Zeat-Meter 3.0+ unit. Once the electrodes were energized, microspheres were aroused to move toward one electrode. A microsphere was observed under a microscope for its movement along a specific distance which was indicated by a built in grid. The zeta potential value was detected at a right time point when the microsphere moved to the end. Measurement was repeated 10 times for each preparative condition and the average values were calculated.

2.7.4. Actual loading of CBP-Rhod in gelatin microspheres

5 mg of Rhodamine-labeled gelatin microspheres were suspended in 1 ml of 10 mM PBS with 0.15 M NaCl in a 1.5 ml microcentrifuge tube. The tube was then placed in cool water and sonicated with the Sonicator (Vibracell™, Sonic, USA) at 20% amplitude. After 1 h, the suspension was centrifuged at 5,000 rpm for 5 min and the supernatant was collected. The actual amount of the CBP-Rhod in supernatant was determined using spectrofluorometer (Cary Eclipse™) by the same procedure done in the step of NHS-Rhodamine labeling (2.4). The experiment was carried out in triplicate and the results were presented in terms of Encapsulating efficiency of CBP-Rhod (EE) and Loading capacity of gelatin microspheres (LC), which were determined according to the following equation [31]:

$$\text{Encapsulating efficiency (\%)} = (\text{total } \mu g \text{ CBP-Rhod encapsulated} / \text{initial } \mu g \text{ CBP-Rhod loaded}) \times 100$$

$$\text{Loading capacity (\%)} = (\text{total mg CBP-Rhod encapsulated} / \text{total mg microspheres}) \times 100$$

2.7.5. In vitro CBP-Rhod release

In vitro release of CBP-Rhod from gelatin microspheres and the microspheres integrated HA-gelatin scaffold were investigated in buffer solution by a standard sampling-separation method. In the release assay, 5 mg of the CBP-loaded microspheres and one piece of the microspheres integrated HA-gelatin scaffold (circular shape with 10 mm in diameter and 2 mm in height), which contained 2.5 mg of gelatin microspheres, were separately immersed in 1 mL of 10 mM PBS with 0.15 M NaCl, and incubated in a shaking water bath (70 rpm) at 37°C. At a given time point, 500 µl of the buffer solution (hereafter, the sample solution) was withdrawn and an equal amount of fresh medium

was added in order to maintain a constant volume of the medium. The sample solution was centrifuged at 5000 rpm for 5 min at room temperature and the amount of CBP-Rhod in the sample solution was determined by spectrofluorometry at 541 and 572 nm for the excitation and emission respectively, as previously described. An average value was calculated at each time point. The experiment was done in triplicate.

2.7.6. Statistical analysis

Data were analyzed using the SPSS software version 14.0 for window. Initially, the normal distribution was assessed by the Shapiro-Wilk test. The normal distribution data, representing the homogeneity of the variances, shown by the Levene's test, were then investigated by the one-way analysis of variance (ANOVA) with the Tukey HSD post hoc multiple comparisons. Otherwise, the Dunnett T3 would be applied if the data did not exhibit the homogeneity of the variances. For the data of which the normal distribution was absent but the variance was homogeneous, the Kruskal-Wallis H was applied. To compare the means between 2 data groups, the students' unpaired t-test was used. The significant level was indicated at $p < 0.05$ in any case.

3. RESULTS AND DISCUSSION

3.1. Morphology of gelatin microspheres and microspheres integrated HA-Gelatin scaffold

The selected SEM images of the uncrosslinked gelatin microspheres are shown in Fig.1. As observed, the microspheres prepared at any given condition presented entirely spherical geometry with a smooth surface, on which the macroscopic pores were not detected. Aggregation of the various sizes microspheres into many small clusters was shown in all cases. In our opinion, such aggregation was caused by the direct contact between the adjacent particles once the solvent was expelled during microspheres preparation. The electrical charge on the surface of particles might be diminished in dry environment so that the electrostatic repulsive force was also weakened; as a consequence, repulsion among particles was unlikely illustrated.

Fig. 2 show the selected SEM images of internal architecture of the composite HA-gelatin scaffold. A well-defined porous structure and the inter-pore connectivity were observed throughout the bulk. The incorporated gelatin microspheres were extensively embedded into the wall of scaffold without deterioration of their geometry. Nevertheless, exceptional for the quite small particles, almost microspheres were not thoroughly submerged in thin walls of scaffold. This manifestation may be responsible for controlled release of the absorbed protein since the releasing medium could transport through the exposed microspheres differently from the one covered with walls of scaffold.

3.2. Effect of gelatin type and pH on size of the gelatin microspheres

Upon the preparation of gelatin microspheres by thermal gelation technique, the average size of particles depends on several manufacturing parameters, for instance, the type and dimension of stirrer, diameter of the vessel or container, volume ratio between aqueous and oil phases and their respective viscosities, stirring speed, and the surface tension between the two immiscible phases governed by type of the selected oil phase [32]. In this study, all parameters were identically controlled

in order to investigate the effect of gelatin type and pH on the microspheres size, and it was found that sizes of the as-prepared microspheres varied from ~4 to ~40 μm in which over 85% of the microspheres range between ~8 to ~25 μm (Fig. 3). For all given conditions, the size distributions presented a similar pattern of which the curves of normal distribution were observed.

The average sizes of the as-prepared gelatin microspheres at various conditions are presented in Fig. 4. Diameters of the uncrosslinked samples range between ~10 and ~20 μm for gelatin A microspheres, and between ~11 and ~ 23 μm for gelatin B microspheres. Average sizes of the microspheres were apparently in the same dimensional range for any preparative condition. However, when the data were statistically analyzed with the Univariate analysis of variance; test of between-subjects effects, sizes of the as-prepared microspheres were significantly different through the influence of the interaction between type of gelatin and pH. Effect of gelatin type or pH on microspheres size, therefore, can not be individually analyzed. The data were thus reorganized into six discrete groups and analyzed further with one-way ANOVA. The results presented that sizes of both gelatin A and B microspheres prepared at pH 7.4 and 10.0 are statistically the same, in contrast to the microspheres prepared at their physiologic pH at which gelatin A microspheres were significantly smaller than those of gelatin B. The effect of interaction between gelatin type and pH are thus limited at a certain condition, probably only at the physiologic pH.

Considering the crosslinked samples, only gelatin A microspheres prepared at its physiologic pH (5.2) presented a significant reduction in particle size comparing with the others which were ~11 and ~15 μm respectively. The difference in particle sizes might be due to the difference in crosslinking intensity of gelatin A from the others which was particularly favored at its physiologic pH, resulting in a denser network and smaller particle sizes [19]. Such observation was also detected in the size of swelling microspheres. Since the CBP was anticipated to be incorporated into gelatin microspheres by diffusion method, swelling ability of the microspheres was required to facilitate absorption of the CBP solution. The as-prepared microspheres illustrated ability to absorb and retain water as the hydrated swelling characteristic was remarkably observed in every study group (Fig. 5). With the crosslinking condition done in this study, the as-prepared microspheres could swell in water significantly at ~1.3 to 1.6 folds over their sizes in the dry state (Table 1). However, the difference of their swelling ability was not noticeably observed at any particular preparative condition.

The type of gelatin used and pH, thus, did not have a clear effect on the resulting size of the microspheres behaving in the uncrosslinked, crosslinked or swelling condition. The result of this study partially corresponded to that of Vandervoort and Ludwig in 2004 [19] which found that type of gelatin did not influence the resulting size of nanoparticle prepared by desolvation method where as the pH did.

3.3. Zeta potentials

The zeta potentials value of the microspheres was measured at all given conditions with an aim to study the influence driven from gelatin type and pH. The value would also be beneficial in the study of CBP loading and releasing through gelatin microspheres.

The zeta potentials of the microspheres at all given conditions were investigated with an aim to study the influence of gelatin type and pH on zeta potentials of the resulting microspheres. The impact of zeta potentials on CBP loading and releasing was also investigated

Zeta potentials values of the as-prepared microspheres are shown in Fig. 6.. Evidently, both gelatin A and B microspheres presented different zeta potentials values at different pH. In addition, those samples prepared with the same type of gelatin but at different pH also presented different zeta potentials values. Only the pH 10.0 at which statistic analysis was carried out due to the zeta potential values were so close as ~-54 and ~-58 mV for gelatin A and B microspheres, respectively in order to ensure the significance of difference. The analysis revealed their statistically different, therefore, both type of gelatin and pH do have significant influences on the zeta potential value of the microspheres obtained.

Since zeta potential is an indicator of charge density [21], the pH-induced disparity of zeta potential value can be explained with the isoelectric point (IEP), which factually is the pH at which net molecular charge and thus zeta potential is equal to zero. The IEP of gelatin A and B are ~9 and ~5, respectively [19,22], bringing about a different electrical charge of both gelatin types in function of the pH. The electrical charges of gelatin A and B are both positive at their physiologic pH since the pH was under IEP. At pH 7.4, gelatin A has a net positive charge by the under-IEP pH, while gelatin B is charged negatively by the over-IEP pH. And eventually at pH 10.0 which is over the IEP, they both present negative charge.

Concerning gelatin microspheres, the IEP of type A and B gelatin microspheres located somewhere in between pH 7.4-10.0 and pH 4.95-7.4, respectively (see Fig. 6). The IEP of the obtained microspheres corresponded to the theoretical IEP of gelatin precursor at any given pH. Therefore, the procedure of microspheres preparation used in this study, the thermal gelation in water-in-oil emulsion technique, does not affect the microspheres zeta potentials.

3.4. Loading of CBP in gelatin microspheres

Encapsulation of CBP into gelatin microspheres in this study was on the basis of polyion complexation. It was expected that a degree of molecular interaction was able to take place between bone proteins and gelatin microspheres of opposite charges [22]; as a consequence, a higher yield of the ionic complexes should result in higher encapsulation efficiency and loading capacity [1,22,23].

In order to overcome either the inactivity of bone protein from those procedures of microspheres preparation or the low loading yield of bone protein which was available in limited quantity, this study designed to incorporate CBP into the preformed empty gelatin microspheres by rehydrating the freeze-dried gelatin microspheres with a solution of the CBP-Rhod at 4°C for 24 h. Such condition should be favorable for the complete absorption [23]. The amount of CBP-Rhod that had been loaded in gelatin microspheres was reported as either the encapsulating efficiency (EE) or the loading capacity (LC) as shown in Table 2.

As observed, the EE of CBP-Rhod ranges highly between ~70 to ~ 90 % for both gelatin types. Comparatively, pH was deemed to influence on the EE with an opposing manner between gelatin A and B microspheres. The EE in groups of gelatin A microspheres was found to be

significantly highest at pH 10.0 in which the electrostatic charge was negative; whereas such statistically indifferent highest EE was also found in groups of gelatin B microspheres but at the physiologic pH in which the charge was positive (see also Fig. 6). Basing on the polyion complexation, this observation suggests the existence of both positively and negatively charged protein molecules in the crude bone extracts.

In addition, the encapsulation of CBP was not only influenced by the pH but also the gelatin type. The EE at pH 10.0 was found to be significantly different between gelatin A and B microspheres while the EE at pH 7.4 were insignificantly different. A disparity of zeta potential value due to pH change was not the only answer of the case as shown by the Univariate analysis of variance; test of between-subjects effects (data not shown) that the interaction between gelatin type and pH affect significantly to the EE and LC. As a consequence, both factors could not be separately considered.

Concerning the LC, the result ranges between ~ 280 to ~370 μg of the CBP-Rhod per 100 mg of microspheres. Reliance of the LC on type of gelatin and pH at any given condition was found to be identical with the EE. Therefore, the encapsulation of the CBP into microspheres evidently depends on both type of the gelatin and pH.

3.5. In vitro CBP-Rhod release

3.5.1. CBP-Rhod release form gelatin microspheres

The CBP-Rhod release form gelatin microspheres and the composite scaffolds were presented in term of CBP-Rhod cumulative releasing percentage from which the actual quantity of CBP-Rhod loaded in gelatin microspheres was calculated, as shown in Fig. 7.

The profiles of CBP-Rhod release form gelatin microspheres are apparently different from the composite scaffolds. Though the release profiles are similar at any given condition of either gelatin microspheres or the composite scaffolds, the amounts of CBP-Rhod release are remarkably different. In particular, the extremely high and low release is observed at the pH 10.0 of gelatin B and A microspheres respectively, where as those of the other conditions are quite the same. However, all profiles astoundingly illustrate the initial burst release of CBP-Rhod within the first hour which was about 73-96 %.

In order to study the CBP release kinetics, the semi-empirical equation based on a power-law expression was introduced as follows [33,34]

$$M_t/M_\infty = kt^n$$

where M_t/M_∞ is the fractional release of the CBP-Rhod, k is a constant concerning the structure and geometry of the releasing device and n is the releasing exponent indicating the mechanism of drug release. By using the least square method, the k and n can be detected from a profile in the plot of log M_t/M_∞ as a function of log t (min), as presented in Fig. 8 and Table 3.

From the log M_t/M_∞ - log t plot, The CBP-Rhod release profiles showed biphasic modulation characterized by an initial relatively rapid release period within the first 30 minutes followed by a slower release phase. The phase separation is indicated by the difference of the n value calculated as the slope of a straight line fitted to the profile with a satisfactory high correlation coefficient (see table xxx). The n values of all samples are close to zero particularly in phase 2 which is the slower release

phase, leading the factor "t^n" of the semi-empirical equation close to 1 at any time point. Comparatively, the results are much different form what have been theoretically identified as the n values of the monodispersed sphere are 0.43 and 0.85 for Fickian diffusion and the Case-II transport respectively, or 0.30 and 0.45 respectively for the mixture of multiple sizes microspheres [34,35]. The CBP-Rhod releases from gelatin microspheres, therefore, are constant and hardly depend on the time observed. The fast release implies that the anticipated polyion complexation between the CBP-Rhod and gelatin microspheres did not completely occur. This may be due to the molecule of Rhodamine which from the covalent amide bond to primary amine on the protein restricts the ionic interaction between the molecules of protein and gelatin.

3.5.2. CBP-Rhod release form composite scaffolds.

Comparing to the gelatin microspheres, the releases of CBP-Rhod from the composite scaffolds are slower and a period of sustained release is illustrated at any preparative condition. The amount of CBP-Rhod release within the first hour was approximately 36-50%. Interestingly, the extremely high and low release is also observed at scaffolds incorporated with pH 10.0 gelatin B and A microspheres respectively.

From the log M_t/M_∞ - log t plot, The CBP-Rhod release profiles showed three phases of release according to the calculated n values (see Fig. 8 and Table 3). Phase 1 correlated to an initial burst release of CBP-Rhod from the scaffolds within the first 30 min. The n values in this phase range from 0.37 to 0.62 which correlate to the theoretical value as mention earlier. Phase 2 corresponded to the sustained release of CBP-Rhod starting from 1 hour to 7 days. The n values of this slow release phase are much lesser than those in phase 1, but are in the same range as the n values of the initial burst CBP-Rhod release form gelatin microspheres. Phase 3, eventually, represented the CBP-Rhod release with an increasing rate from phase 2 but not faster than phase 1.

Considering the mechanism of CBP-Rhod release from the composite scaffolds, the initial burst release may be the combination of diffusion and dissolution release since the n values are in between 0.30 and 0.45[34,35] (except for gelatin B pH 7.4). Such observation is not found in case of CBP-Rhod release from gelatin microspheres. It is believed that CBP-Rhod might partially release into the HA-Gelatin blended solution in which the CBP-Rhod encapsulated gelatin microspheres were dispersed during the process of composite scaffolds fabrication. As a consequence, the releasing CBP-Rhod was also integrated in the mass of HA-Gelatin scaffolds. The initial burst release, therefore, may be the release from the scaffold matrix instead of the incorporated gelatin microspheres.

The mechanism of the sustained release in phase 2 may be the same as that of the initial burst release form gelatin microspheres, but occurs at a slower rate due to their comparable n values and lesser constant (k) values in most samples of the former case. This observation suggests that the sustained release concerns the release of CBP-Rhod from the incorporated gelatin microspheres exposing into porosities within scaffolds.

During phase 3 release, the degradation of HA-Gelatin scaffold might occur, as being observed during sampling, and induce the exposure of the underneath scaffold matrix including the gelatin microspheres which were previously submerged. The rate of CBP-Rhod release is thus higher,

but the mechanism can not be truly described regarding the theoretical n values because the mostly n values of phase 3 are lesser than the lower range of the theoretical n values. However, it is believed that phase 3 release is influenced by degradation and diffusive processes.

In this study, the difference in size between the gelatin microspheres was probably not large enough to result in a significantly different CBP-Rhod release rate [33,36]. However, the ongoing mechanism of the CBP controlled release can be the organization of a diffusion-erosion process contributed by the capability of water uptake into the gelatin microspheres and the ability of protein transportation through the scaffold. Microspheres formulation mainly controls the induction time necessary to achieve protein release while the composition of polymeric scaffold controls the release rate [37]. Therefore, a temporal and spatial control of signaling molecules may be obtained by the combination of the appropriated microspheres and scaffold formulations.

5. CONCLUSION

Type of gelatin and the preparative pH are the two factors that should be considerably controlled in the design of bone protein delivery scaffold which contains gelatin microspheres as an incorporated delivery device. Interaction between those two factors influences significantly on size of the as-prepared microspheres, surface charge or the zeta potential, swelling ability and encapsulation capability of the CBP. This effect, however, is not observed in the drug release studies. The ionic interaction between molecules of bone protein and gelatin in the microspheres was not large enough to provide sustained release of the CBP. Incorporation of the CBP loaded gelatin microspheres into HA-Gelatin blended scaffold create a complex environment and the synergistic functions between gelatin microspheres and scaffold in which controlled release was evidently presented.

ACKNOWLEDGMENTS

The authors acknowledged partial support received from (a) the National Center of Excellence for Petroleum, Petrochemicals, and Advanced Materials (NCE-PPAM), and (b) the Petroleum and Petrochemical College (PPC), Chulalongkorn University.

REFERENCES

1. Hoffman, A.S., Hydrogels for biomedical applications. Adv Drug Deliv Rev, 2002. **43**: p. 3-12.
2. Hollander, A.P. and P.V. Hatton, Biopolymer Methods in Tissue Engineering, ed. J.M. Walker. Vol. 1. 2004, Totowa, New Jersey: Humana Press.
3. Bodic, F., et al., Bone loss and teeth. Joint Bone Spine, 2005. **72**: p. 215-221.
4. Jahangiri, L., et al., Current perspectives in residual ridge remodeling and its clinical implications: A review. J Prosthet Dent, 1998. **80**: p. 244-237.
5. Wiesen, M. and R. Krrzis, Preservation of the alveolar ridge at implant sides. Periodontao Clin Investig, 1998. **20**: p. 17-20.
6. Hanne, E., et al., Preservation of alveolar ridge with hydroxyapatite-collagen implants in rats. J Prosthet Dent, 1998. **60**: p. 729-734.

7. Altundal, H. and O. Guvener, The effect of alendronate on resorption of the alveolar bone following tooth extraction. Int J Oral Maxillofac Surg, 2004. **33**: p. 286-293.
8. Yaffe, A., et al., Disposition of alendronate folllowing local delivery in a rat jaw. J Periodontol 1999, 1999. **70**: p. 893-895.
9. Langer, R. and J.P. Vacanti, Tissue engineering. Science, 1993. **260**: p. 920-926.
10. Hutmacher, D.W., Scaffolds in tissue engineering bone and cartilage. Biomaterials, 2000. **21**: p. 2529-2543.
11. Mikos, A.G., et al., Synthetic bioresorbable polymer scaffolds, in Biomaterials science: An introduction to materials in medicine, F.J. Schoen and J.E. Lemons, Editors. 2004, Elsevier Inc: California. p. 735-749.
12. Tessmar, J.K. and A.M. Gopferich., Matrices and scaffolds for protein delivery in tissue engineering. Adv Drug Deliv Rev, 2007. **59**(4-5): p. 274-291.
13. Causa, F., P.A. Netti, and L. Ambrosio, A multi-functional scaffold for tissue regeneration: The need to engineer a tissue analogue. Biomaterials, 2007. **28**: p. 5093-5099.
14. Lee, S.H. and H. Shin, Matrices and scaffolds for delivery of bioactive molecules in bone and cartilage tissue engineering. Adv Drug Deliv Rev, 2007. **59**: p. 339-359.
15. Kimura, Y., et al., Adipose tissue engineering based on human preadipocytes combined with gelatin microspheres containing basic fibroblast growth factor. Biomaterials, 2003. **24**: p. 2513-2521.
16. Holland, T.A., Y. Tabata, and A.G. Mikos, Dual growth factor delivery from degradable oligo(poly(ethylene glycol)fumurated) hydrogel scaffolds for cartilage tissue engineering. J Controlled Release, 2005. **101**: p. 111-125.
17. Kasper, F.K., et al., In vivo release of plasmid DNA from composites of oligo(poly(ethylene glycol)fumurated) and cationized gelatin microspheres. J Controlled Release, 2005. **107**: p. 547-561.
18. Baldwin, S.P. and W.M. Saltzma, Materials for protein delivery in tissue engineering. Adv Drug Deliv Rev, 1998. **33**: p. 71-86.
19. Vandervoort, J. and A. Ludwig, Preparation and evaluation of drug-loaded gelatin nanoparticles for topical ophthalmic use. Eur J Pharm Biopharm, 2004. **57**: p. 251-261.
20. Lee, M., et al., Modulation of protein delivery from modular polymer scaffolds. Biomaterials, 2007. **28**(10): p. 1862-1870.
21. Brown, K.E., et al., Gelatin/chondroitin 6-sulfate microspheres for the delivery of therapeutic proteins to the joint. Arthritis & Rheumatism, 1998. **41**(12): p. 2185-2195.
22. Young, S., et al., Gelatin as a delivery vehicle for the controlled release of bioactive molecules. J Controlled Release, 2005. **109**: p. 256-274.
23. Tabata, Y., et al., In vitro sorption and desorption of basic fibroblast growth factor from biodegradable hydrogels. Biomaterials, 1998. **19**: p. 1781-1789.
24. Chaplin, M., Water structure and science. http://www.lsbu.ac.uk/water/hygel.html, 2007.
25. Hauschka, P.V., et al., Growth factors in bone matrix, isolation of multiple types by affinity chromatography on heparin-sepharose. J Biol Chem, 1986. **261**(27): p. 12665-12674.

26. Somerman, M., et al., Identification of a bone matrix-derived chemotactic factor. Calcif Tissue Int, 1983. **35**: p. 481-485.
27. Hou, L.T., et al., Biological effects of cementum and bone extractss on human periodontal fibroblasts. . J periodontal, 2000. **71**: p. 1100-1109.
28. Syftestad, T.G. and A.I. Caplan, A fraction from extracts of demineralized adult bone stimulated the converison of mesenchymal cells into chondrocytes. Dev Biol, 1984. **104**: p. 348-356.
29. Cho, M.I., et al., In vitro formation of mineralized nodules by periodontal ligament cells form the rat. Calcif Tissue Int, 1992. **50**(459-467).
30. Urist, M.R., Bone: formation by autoinduction. Science, 1965. **150**: p. 893-899.
31. Freiberg, S. and X.X. Zhu, Polymer microspheres for controlled drug release. Int J Pharm, 2004. **282**: p. 1-18.
32. Arshady, R., Albumin microspheres and microcapsules: methodology of manufacturing techniques. J Controlled Release, 1990. **14**: p. 111-131.
33. Arifin, D.Y., L.Y. Lee, and C.-H. Wang, Mathematical modeling and simulation of drug release from microspheres: Implications to drug delivery systems. Adv Drug Deliv Rev, 2006. **58**: p. 1274-1325.
34. Ritger, P.L. and N.A. Peppas, A simple equation for description of solute release I. Fickian and Non-Fickian release from non-swellable deviecs in the form of slabs, spheres, cylinders or discs. J Controlled Release, 1987. **5**: p. 23-36.
35. Ritger, P.L. and N.A. Peppas, A simple equation for description of solute release II. Fickian and anomalous release from swellable devices. J Controlled Release, 1987. **5**(37-42).
36. Berkland, C., et al., Precise control of PLG microsphere size provides enhanced control of drug release rate. J Controlled Release, 2002. **82**: p. 137-147.
37. Ungaro, F., et al., Microshpere-integrated collagen scaffolds for tissue engineering: Effect of microsphere formulation and scaffold properties on protein release kinetics. J Controlled Release, 2006. **113**: p. 128-136.

CAPTION OF FIGURES

Figure 1 SEM images illustrating morphology of the gelatin microspheres prepared with gelatin type A at physiologic pH (5.2) (a), pH 7.4 (b), pH 10.0 (c) and gelatin type B at physiologic pH (4.95) (d), pH 7.4 (e), and pH 10.0 (f).

Figure 2 SEM images of the as-prepared microspheres integrated HA-gelatin scaffold illustrate thorough distribution of gelatin microspheres within the scaffold (a) and the embedded gelatin microspheres in the walls of scaffold's chamber (b), (b) is the magnified image of the selected area from (a).

Figure 3 Size distribution of the gelatin microspheres prepared with gelatin types A (a) and type B (b) at various pH (n = 100).

Figure 4 Particle sizes of the gelatin microspheres prepared with gelatin types A (a) and type B (b) at various pH and conditions (n = 100). a,b,c, *, 1,2,3 are significantly different at $p < 0.05$; One-Way ANOVA with Dunnett T3.

Figure 5 Images from Optical microscope illustrate morphology of uncrosslinked, dry gelatin microspheres (a) and crosslinked, wet and swelling gelatin microspheres (the samples were prepared with gelatin type A at pH 5.2).

Figure 6 Zeta potential values of the gelatin microspheres prepared with gelatin types A and B at various pH. * is significantly different at $p < 0.05$; Students' unpaired t-test.

Figure 7 CBP cumulative release (%) from gelatin microspheres (a) and microspheres integrated HA-Gel scaffolds (b).

Figure 8 Log M_t/M_∞ plotted as a function of log t (min) for CBP release from gelatin microspheres (a) and microspheres integrated HA-Gel scaffolds (b) at three releasing intervals (n1, n2, and n3).

CAPTION OF TABLES

Table 1 Swelling ratio of the gelatin microspheres prepared with gelatin types A (a) and type B (b) at various pH.

Table 2 Encapsulating efficiency of the CBP and Loading capacity of the gelatin microspheres. ^{a,b,c,d} are significantly different at $p < 0.05$; One-Way ANOVA with Tukey HSD (Mean ± SD, n=3)

Table 3 Constant (k), releasing exponent (n) and correlation coefficient (r^2) of CBP release from gelatin microspheres and microspheres integrated HA-Gel scaffolds at three releasing intervals (n1,n2, and n3). k and n values were calculated with the least squares method.

Development of polycaprolactone porous scaffold by combined solvent casting, particulate leaching and polymer leaching techniques for bone tissue engineering

Napaphat Thadavirul,[1] Prasit Pavasant,[2] and Pitt Supaphol [1,*]

[1] The Petroleum and Petrochemical College and The Center for Petroleum, Petrochemicals and Advanced Materials (C-PPAM), Chulalongkorn University, Bangkok 10330, Thailand

[2] Department of Anatomy, Faculty of Dentistry, Chulalongkorn University, Bangkok 10330, Thailand

One of the most common and straightforward technique to prepare porous scaffolds is the particulate leaching method, which involves the selective leaching of a mineral, usually sodium chloride salt or of an organic compound such as saccharose to generate the pores. One potential deficiency of the technique is lack of interconnectivity between pores. To improve the interconnectivity between pores, the scaffolds preparation methods has been proposed by combining solvent casting and salt particulate leaching with polymer leaching technique. In this study, sodium chloride and polyethylene glycol(PEG) will be used as water soluble porogens to forms porous polycaprolactone(PCL) scaffolds. The purpose of this study is to evaluate the feasibility of preparation method combining polymer and particulate leaching techniques for the preparation of highly interconnected three-dimensional polymeric porous scaffolds. The polymer scaffolds fabricated using this method demonstrated a highly open, interconnected porous structure than those made using the standard solvent casting/particle leaching technique. Scanning electron microscopic (SEM) images confirm that the scaffolds fabricated using this method have highly interconnected network, equal distribution, and uniform size of 378-435 μm pores. Mechanical properties, porosities, pore volume and water absorption capability were investigated. Moreover, the potential of use these scaffolds in bone tissue engineering application was evaluated in vitro with mouse calvaria-derived, pre-osteoblastic cells (MC3T3-E1). Indirect cytotoxicity evaluation revealed that scaffolds fabricated using this method released no substances at levels that were harmful to cells. Scanning electron microscopy observation showed the majority of the cells seeded on the surfaces of scaffolds at 3 days expanded over the area of the scaffolds which was the most expansion on the surface of scaffolds fabricated using this method. For mineralization, cells cultured on surfaces of PCL scaffolds fabricated using this method showed the higher mineral deposition than PCL scaffold fabricated using standard method.

Key-words: Scaffold, PCL, Solvent casting/Particulate leaching method, Polymer leaching method

[*] Authors to whom correspondence should be addressed: pitt.s@chula.ac.th (P. Supaphol)

1. Introduction

Several natural and synthetic polymers have been utilized for fabricating tissue engineering scaffolds. Requirements for these materials are that they must be inherently biocompatible, biodegradable, and highly cell adhesive. Additionally, they must have a porous, mechanically stable, and three-dimensional structure with facile manufacturing processes. The aliphatic polyesters such as polycaprolactone (PCL), poly lactic acid (PLA), polyglycolide (PGA), and its copolymers are the most extensively used for biodegradable scaffolds because of their excellent biocompatibility, biodegradability, and mechanical strength. These polymers which are biocompatible, biodegradable, and bioresorbable are approved by the Food and Drug Administration (FDA), and are easily processed into various structures of 3-dimensional matrices. [1, 2]

PCL is a semi-crystalline polyester which is degraded by hydrolysis of its ester linkages in physiological conditions such as in the human body. In particular it is especially interesting for the preparation of long term implant applications, owing to its degradation which is very slowly. It has an Food and Drug Administration (FDA) approval and is used as drug delivery devices, as sutures and as adhesion barriers. Due to their excellent biocompatibility, mechanical strength, the lack of toxicity, and low cost, PCL is one of the biodegradable polyesters which has attracted attention in the bone tissue engineering applications. [2-3]

Porous biodegradable scaffolds have been studied for the application as a three-dimensional template for initial cell attachment and subsequent tissue formation both in vitro and in vivo. Various tissues such as cartilage, bone, heart, valves, nerves, muscle, bladder, liver, etc. have been produced using the scaffolds. The scaffolds should be highly porous to allow cells to be seeded and to permit the facile invasion of blood vessels for the supply of nutrients to the transplanted cells. Scaffold architecture should permit cell intrusion, nutrient and waste product permeation, and new capillary network formation. Scaffold porosity is a fundamental characteristic for providing available space for cells to migrate and for vascularization of the tissue. Furthermore, the larger the surface available, the more cell interactions will arise. In general, the biological activity of a scaffold is determined by ligand density. Scaffold composition and porous fraction, that is the total surface of the structure exposed to cells, determine the ligand density. Highly specific surface areas allow for cell attachment and anchorage, and a high pore volume fraction enables cell growth, migration, and effective transportation of fluids and nutrients. Compatible to the structure of the tissue, scaffolds should be designed to have a high porosity, high surface area, a fully interconnected geometry, structural strength, and a specific three dimensional shape. [4-6]

Various techniques have been reported to prepare porous polymeric scaffold. A wide range of techniques commonly used in tissue engineering can generate scaffolds having a random structure with unpredictable pore sizes and reduced pore interconnections. Any variation in porosity within the 3D structure cannot be controlled, and mechanical strength, structural stability, and reproducibility are generally low. Among these techniques, solvent casting, freeze drying, phase inversion, fiber bonding, melt-based technologies, and high-pressure-based methods are

the most commonly used.[7] Porous polymers can be prepared by embedding soluble ingredients (porogens) into the polymer which upon removal, form pores in the polymer matrix. Nowadays in tissue engineering, solvent casting is often used in combination with other common methods in order to produce a 3D porous structure. Solvent casting in combination with particulate leaching has been used successfully to fabricate 3D scaffolds. Porogen agents commonly used in the field are: sodium chloride, ammonium bicarbonate, and glucose with different crystal sizes.[8-12]

The porogen leaching technique for solvent cast scaffold involves poring a polymer solution(e.g. PLA in chloroform) onto a bed of porogen: salt particles, paraffin microspheres or emulsion particles of defined size. The solvent is evaporated, resulting in the polymer solidifying around porogen particles. The entrapped porogen can then be leached out of the scaffold using numerous rinses of distilled water (NaCl) or organic solvent (paraffin), thus creating a defined pore structure. The leaching strategy has found applications in the creation of porous scaffolds for the growth of endothelial cells.[13] The scaffold's biochemical properties and architecture should support cell attachment, migration, growth, and ultimate tissue maturation.[14] An open and interconnected pore system within the three-dimensional (3D) structure is critical in ensuring proper nutrient and waste transport, tissue in-growth, vascularization, and eventually integration of the constructs with the host.[15] Due to their inherently high porosities and high interconnected pore networks, as well as wide variety of topographical features to encourage cellular adhesion, surface migration, and proliferation.

Blended polymers play an important role in developing a microporous-controlled delivery system. Usually, there are two types of polymers present in the blended membranes: one polymer is remained in the end-use, and another polymer is removed as a pore former to produce porous menbranes. Poly(ethylene glycol) (PEG) has been used as a main polymeric additive for membranes and a coating material for biomaterial application due to its specific properties i.e. water soluble polymeric additive. The pores in scaffolds can be created by leaching out water-soluble polymeric additive, PEG, using a solvent casting and polymer leaching method. [15-18]

To improve the interconnectivity between pores, the scaffolds preparation methods has been proposed by combining solvent casting and salt particulate leaching with polymer leaching technique. The purpose of this study is to evaluate the feasibility of preparation method combining polymer and particulate leaching techniques for the preparation of highly interconnected three-dimensional polymeric porous scaffolds.

2. Experimental Section

2.1. Materials. Polycaprolactone (PCL; 80,000 $gmol^{-1}$) were purchased from Sigma-Aldrich, USA. Polyethylene glycol (PEG; MW = 200, 600, and 1,000 $gmol^{-1}$) was purchased from Merck,Germany. Chloroform (Labscan; Asia, Thailand) was used as solvent for these polyesters. Sodium chloride (Ajax Finechem, Australia) was used as porogen. All other chemicals were of analytical reagent grade and used without further purification.

2.2. Preparation of PCL scaffolds. A solvent casting, polymer leaching and salt particulate leaching was used to prepare the scaffold. Briefly, the polymer solution was prepared by mixing the PCL pellet, PEG and chloroform in the concentration of 28% w/v, then the solution was stirred at room temperature for 2-3 hr, after that NaCl salt particles with size of 400-500 μm (polymer/NaCl = 1/30 w/w) were added. The mixture was then packed into Petri dishes and the cylindrical mold with the dimension of 1.2 mm in diameter and 0.8 mm in thickness. The molds were then placed in the hood overnight for solvent evaporation. After the time, the materials were immersed in deionized(DI) water for 48 hr with repeated change of DI water every 8 hr for leaching out the PEG and salt particles. Scaffolds were air-dried for 24 hr and vacuum-dried overnight. The salt-PEG leached PCL scaffolds have highly interconnectivity pores network. Prior to casting, each of the PCL and PCL-PEG blend solutions was characterized for its viscosity by using a Brookfield DV-III programmable viscometer. The measurement was carried out at room temperature (that is, 25±1 ℃).

2.3. Characterization of PCL scaffolds.

Microstructure observation. The morphology of the pores, their size, distribution and the interconnectivity between these pores of the porous scaffolds were observed by JEOL JSM-5200 scanning electron microscopy (SEM), Olympus SZH10 stereomicroscope, and Carl Zeiss Mirax desk visual slide microscope. One cylindrical scaffold was randomly selected from each group, cut with razor blade at the middle of the scaffold and mounted onto SEM stub. Cross sections of the scaffolds were coated with thin film of gold using JEOL JFC-1100E sputtering devices for 5 min prior to observation under SEM

Porosity, pore volume, and pore size. Porosity and pore volume of the scaffolds were measured gravimetrically according to the following equations:

$$Porosity\,(\%) = \left(1 - \frac{\rho\,\text{scaffold}}{\rho\,\text{polymer}}\right) x\,100$$

$$Pore\ volume = \left(\frac{1}{\rho\,\text{scaffold}} - \frac{1}{\rho\,\text{polymer}}\right) x\,100$$

where $\rho_{polymer}$ is the density of the polymer from which the scaffolds were fabricated and $\rho_{scaffold}$ is the apparent density of the scaffolds which was measured by a Sartorius YDK01 density measurement kit. Here, ρ_{PCL} was taken the value of 1.145 g cm^{-1}. Five specimens were measured for both the porosity and the pore volume and an average value for each property was calculated. On the other hand, pore size of the scaffolds was directly measured from SEM images, using a SemAfore Digital slow scan image recording system version 5.0 software. At least 30 pores for each of the cross- and the longitudinal sections (i.e., at least 60 pores in total) were measured and the average values for all of the scaffolds investigated were calculated.

Water absorption capability. The scaffold specimens, cut from the moldings that had been cast in the Petri dishes (circular shape with 15 mm in diameter and 3 mm in height), were first dried, weighed, and individually immersed in 10 mL of 10 mM phosphate buffer saline solution (PBS; pH 7.4)

at room temperature. At a given time point, the specimens were taken out, carefully placed on the glass for 5 sec to remove the excessive water and weighed immediately. The amount of water retained in the specimens was determined according to the following equation:

$$Water\ absorption(\%) = \frac{(Ww - Wd)}{Ww} \times 100$$

where W_d and W_w are the weight of the specimens before and after submersion in the medium, respectively. The experiment was carried out in pentuplicate and the measurements were carried out at different time intervals within a period of 14 d.

Water permeability. To obtain information about pore interconnection, flow resistance was evaluated by sealing the scaffolds between two rubber rings at the bottom of a measuring tube ending and filled with 10 cm of water. To keep the water level as even as possible during flow, the tube was communicating with a large diameter reservoir. Before each test, samples were preconditioned in water for 24 h. Flow resistance of scaffolds was then evaluated as the time needed for 10 ml of water to flow through the scaffold.

Compressive modulus. Compressive Modulus of the scaffolds were determined with a universal testing machine (Lloyd LRX, UK) using 500 N loaded cell in the dry state at room temperature, the both before and after degraded scaffolds at the different time interval were vertically compressed at the crosshead speed of 3 mm/min. The load was applied until the scaffolds were compressed to approximately 70% of their original thickness. The initial compressive modulus was determined as the slope of the linear portion of the stress strain curve at a compressive strain of 20%.

2.4. Biological characterization of PCL scaffolds.

Cell culture and cell seeding. Mouse fibroblasts (L929) and mouse calvaria-derived, pre-osteoblastic cells (MC3T3-E1) were used as reference cell lines. L929 were cultured as monolayer in Dulbecco's modified Eagle's medium (DMEM; Sigma-Aldrich, USA), supplemented with 10% fetal bovine serum (FBS; BIOCHROM AG), 1% L-glutamine (Invitrogen Corp.), and a 1% antibiotic and antimycotic formulation [containing penicillin G sodium, streptomycin sulfate, and amphotericin B (Invitrogen Corp., USA)]. MC3T3-E1 were cultured in Minimum Essential Medium (with Earle's Balanced Salts) (MEM; Hyclone, USA), supplemented by 10% fetal bovine serum (FBS; BIOCHROM AG, Germany), 1% L-glutamine (Invitrogen Corp., USA) and 1% antibiotic and antimycotic formulation [containing penicillin G sodium, streptomycin sulfate, and amphotericin B (Invitrogen Corp., USA)]. The medium was replaced every 2 days and the cultures were maintained at 37°C in a humidified atmosphere containing 5% CO_2.

Each scaffold was cut into circular discs (about 15 mm in diameter) and the disc specimens were placed in wells of a 24-well tissue-culture polystyrene plate (TCPS; Biokom Systems, Poland), and were later sterilized in 70% ethanol for 30 min. The specimens were then washed with autoclaved de-ionized water, PBS and subsequently immersed in MEM overnight. To ensure a complete contact between the specimens and the wells, the specimens were pressed with a metal ring (about 12 mm in diameter). MC3T3-E1 from the culture was trypsinized [0.25% trypsin containing 1 mM EDTA

(Invitrogen Crop., USA)] and counted by a hemacytometer (Hausser Scientific, USA). MC3T3-E1 were seeded at a density of about 60,000 cells/well for attachment study and 30,000 cells/well for proliferation study, on the scaffold specimens and empty wells of TCPS that were used as control. For indirect cytotoxicity, alkaline phosphatase activity, mineralization evaluations, MC3T3-E1 were seeded at a density of about 40,000 cells/well on the scaffold specimens and empty wells of TCPS. The culture was maintained in an incubator at 37°C in a humidified atmosphere containing 5% CO_2.

***Cytotoxicity evaluation*.** Two types of cells were used: 1) mouse calvaria-derived, pre-osteoblastic cells (MC3T3-E1) and 2) mouse fibroblasts (L929). Indirect cytotoxicity test was conducted on TCPS, salt leached PCL, salt-PEG 200 leached PCL, salt-PEG 600 leached PCL, and salt-PEG 1000 leached PCL. First, extraction media were prepared by immersing samples (about 15 mm in diameter) in a serum-free medium (SFM; containing DMEM, 1% L-glutamine, 1 % lactabumin, and 1% antibiotic and antimycotic formulation for L929 and containing MEM, 1% L-glutamine, 1 % lactabumin, and 1% antibiotic and antimycotic formulation for MC3T3-E1) for 1, 3, and 7 days. Each of these extraction media was used to evaluate the cytotoxicity of the scaffolds. L929 or MC3T3-E1 were separately cultured in wells of a 24-well culture plate in 10%serum-containing DMEM and MEM, respectively, for 16 h to allow cell attachment on the plate. Then, the cells were starved with SFM for 24 h, after which time the medium was replaced with an extraction medium. After 24 h of cell culturing in the extraction medium, 3-(4,5-dimethylthiazol-2-yl)-2,5-diphenyl-tetrazolium bromide (MTT) assay was carried out to quantify the amount of viable cells. The experiments were carried out in triplicate.

MTT Assay. The MTT assay is based on the reduction of the yellow tetrazolium salt to purple formazan crystals by dehydrogenase enzymes secreted from the mitochondria of metabolically active cells. The amount of purple formazan crystals formed is proportional to the number of viable cells. First, each culture medium was aspirated and replaced with 400 mL/well of MTT solution at 0.5 mg mL for a 24-well culture plate. Secondly, the plate was incubated for 30 minutes at 37 °C. The solution was then aspirated and 1 mL/well of dimethylsulfoxide (DMSO) containing 125 mL/well of glycine buffer (pH 10) was added to dissolve the formazan crystals. Finally, after 5 min of rotary agitation, the absorbance of the DMSO solution at 540 nm was measured using a Thermospectronic Genesis10 UV/Visible spectrophotometer.

Cell attachment and proliferation. Cell behavior such as adhesion and proliferation represent the initial phase of cell–scaffold communication that subsequently effect differentiation and mineralization. For attachment study, MC3T3-E1 was allowed to attach to TCPS, salt leached PCL, salt-PEG 200 leached PCL, salt-PEG 600 leached PCL, and salt-PEG 1000 leached PCL for 2, 4 and 6 h, respectively. Each sample was rinsed with PBS to remove unattached cells prior to morphological observation. Morphological appearance of the cells during attachment period was observed by SEM. For proliferation study, the viability of cells on the specimens was determined after 1, 2, and 3 day of cell culturing by DNA Quantification assay. The experiments were carried out in triplicate.

DNA Quantification Assay. The amount of DNA signifying the number of proliferated cells that had been cultured on each of the scaffolds for 1, 2, and 3 day was quantified by a DNA Quantification Kit (SigmaAldrich, USA). Briefly, the cultured cells were thoroughly washed twice with 400 µL of PBS. The cells were then lysed with 400 µL of a cell lysis buffer. The obtained suspension was centrifuged

for 10 min to precipitate the cell debris. The supernatant was pipetted out at 20 µL, which was later mixed with 2mL of 0.1 µg/mL Bisbenzimide H 33258 solution in 10X Fluorescent Assay Buffer. The fluorescent emission intensity of the obtained solution was then measured at 460 nm, after it had been excited at 360 nm, using the microplate reader.

***Morphological observation of cultured cells*.** After removal of the culture medium, the cell-cultured scaffold specimens were rinsed with PBS twice and the cells were then fixed with 3% glutaraldehyde solution, which was diluted from 50% glutaraldehyde solution (Sigma, USA) with PBS, at 500 µl/well. After 30 min, they were rinsed again with PBS. After cell fixation, the specimens were dehydrated in an ethanol solution of varying concentration (i.e. 30, 50, 70, 90, and 100%, respectively) for about 2 min at each concentration. The specimens were then dried in 100% hexamethyldisilazane (HMDS; Sigma, USA) for 5 min and later let dry in air after removal of HMDS. After completely dried, the specimens were mounted on an SEM stub, coated with gold, and observed by a JEOL JSM-5200 scanning electron microscope (SEM).

***Production of Alkaline Phosphatase of Cultured Cells*.** ALP activity of MC3T3-E1 was measured using Alkaline Phosphate Yellow Liquid. In this reaction, ALP catalyzes the hydrolysis of colorless organic phosphate ester substrate, *p*-nitrophenyl phosphate (pNPP) to a yellow product, p-nitrophenol, and phosphate. MC3T3-E1 was cultured on scaffold specimens for 3, 5, and 7 day to observe the production of alkaline phosphatase (ALP). The specimens were rinsed with PBS 2 times after removal of culture medium. Alkaline lysis buffer (10 mM Tris-HCl, 2 mM $MgCl_2$, 0.1% Triton-X100, pH 10) (100 µl/well) was added and the samples were scrapped and then frozen at -20°C for at least 30 min prior to the next step. An aqueous solution of 2 mg/ml *p*-nitrophenyl phosphate (pNPP; Zymed Laboratories, USA) mixed with 0.1 M amino propanol (10 µl/well) in 2 mM $MgCl_2$ (100 µl/well) having a pH of 10.5 was prepared and added into the specimens (110 µl/well). The specimens were incubated at 37°C for 15 min. The reaction was stopped by adding 900 µl /well of 50 mM NaOH and the extracted solution was transferred to a cuvette and placed in the UV-visible spectrophotometer, from which the absorbance at 410 nm was measured. The amount of ALP was then calculated against a standard curve. In order to calculate for the ALP activity, the amount of ALP had to be normalized by the amount of total protein synthesized. In the protein assay, the samples were treated in the same manner as the ALP assay up to the point was the specimens were frozen. After freezing, bicinchoninic acid (BCA; Pierce Biotechnology, USA) solution was added into the specimens. The specimens were incubated at 37°C for 15 min. The absorbance of the medium solution was then measured at 562 nm by the UV-visible spectrophotometer and the amount of the total protein was calculated against a standard curve.

***Mineralization analysis*.** Alizarin Red-S is a dye that binds selectively calcium salts and is widely used for mineral staining (the staining product i.e., an Alizarin Red S-calcium chelating product). The isolated osteoblastic cells were plated in 24-well plates at 40,000 cells/well and cultured in the culture medium. After 24 h, the cultures were treated with culture medium, with the supplement of 50 µg/ml ascorbic acid (Sigma, USA), 5 mM β-glycerophosphate (Sigma, USA), and 0.2 µg/ml dexamethasone (Sigma, USA), the medium was replaced every 2 days. After 14 days treatment, cells were washed with PBS and fixed with ice-cold absolute methanol for 10 min. Fixed cells were stained

with 1% Alizarin Red in deionized water (Sigma, USA) (pH 4.2) for 2-3 min. After removing alizarin red-S solution, the cells were rinsed with deionized water and dried at room temperature. The images of each culture were captured and the stain was extracted with the use of 10% cetylpyridinium chloride (Sigma, USA) in 10 mM sodium phosphate for 1 h and absorbance of the collected dye was read at 570 nm in spectrophotometer (Thermo Spectronics Genesis10 UV-visible spectrophotometer).

2.5. Statistical analysis. Values expressed as the mean ± standard deviation. Statistical analysis of different data groups was performed using One-Way Analysis of Variance (ANOVA) with the least-significant difference (LSD) test using SPSS software version 11.5. The values of *p* lower 0.05 were considered statistically significant.

3. Results

3.1. Preparetion of PCL scaffolds.

Table 1 show the viscosity of PCL solution and PEG-PCL blend solution in chloroform. The PCL solution was 1064 ± 15 cP on average while the PEG-PCL blend solution were in the range of 989 – 1106 cP on average.

3.2. Characterization of PCL scaffolds.

Microstructure Observation.

Figure 1 shows the stereomicroscope images of porous scaffolds formed by PCL, different types of PEG and NaCl salts in chloroform following NaCl and PEG leaching out in deionized water. Figure 2 and 3 show the visual slide microscope images of porous PCL scaffolds.

Fig. 4 and 5 show the SEM micrographs of microporous scaffolds formed by PCL/PEG blends by various types of PEG (PEG, MW = 200, 600, and 1,000) following by leaching in aqueous medium. The highly interconnected pores were formed in scaffolds after PEG was leached out, and corresponded to the transpaprent spots shown in stereomicroscope and visual slide microscope images. The size of pores in scaffolds prepared from PEG leached out were larger than that from no PEG leached out and more interconnected channels were distributed throughout the former ones. Well defined and interconnected pores, detected by optical microscope and SEM analysis of PCL scaffolds, resulted from the use of both salt and PEG. An irregular geometry of pores was obtained for NaCl leached and NaCl-PEG leached scaffolds. The pore dimensions of the obtained scaffolds ranges between 378 and 435 μm on average (n ≥ 30).

Porosity, Pore volume and Pore size.

As shown on table 2. , the porosity of scaffold showed the reverse trend with the density value. The porosity values of salt leached PCL scaffolds was 91.6% while the porosity values of the salt-PEG leached PCL scaffold were in the range of 91.2-92.6% on average (n=5).The density of scaffolds were in the range of 0.096-0.101.

Specially, the porosity increased from ∽ 91.6% for salt leached scaffold to ∽ 91.8% for salt-PEG 600 leached scaffold and 92.6% for salt-PEG 1000 leached scaffold, and pore volume increased from 9.6 cm^3g^{-1} for salt leached scaffold to 9.9 cm^3g^{-1} and 10.9 cm^3g^{-1} for salt-PEG 600 leached and salt-PEG1000 leached PCL scaffold . The pore volume increased with an increased the porosity.

***Water absorption capability*.**

Figure 6 illustrates the water absorption capabilities of the salt leached, salt-PEG 200 leached, salt-PEG 600 leached and salt-PEG 1000 leached PCL scaffolds in 0.1 M PBS at room temperature within 7 days. All salt-PEG leached PCL scaffolds showed a similar profile of the water absorption, the water absorption rate increased rapidly in the early 30 minute and maintained stable in 24 hr. While salt leached PCL scaffold showed a different profile of the water absorption, the water absorption rate slightly increased in the early 24 hr and maintained stable. Moreover, the water absorption capabilities of the PCL scaffolds were compared at 24 hr; it found that the salt leached PCL scaffold exhibited the lowest level of water absorption compared to the others.

Water permeability

Figure 7 show the flow resistance for the salt leached, salt-PEG 200 leached, salt-PEG 600 leached and salt-PEG 1000 leached PCL scaffolds. The flow resistance of salt leached PCL scaffold was in the range of 14.2-21.6 sec/10 ml (distance ∽ 15-50 cm). The flow resistance of salt-PEG 200 leached PCL scaffold was in the range of 11.1-15 sec/10 ml (distance ∽ 15-50 cm). The flow resistance of salt-PEG 600 leached PCL scaffold was in the range of 11.7-13.5 sec/10 ml (distance ∽ 15-50 cm). The flow resistance of salt-PEG 1000 leached PCL scaffold was in the range of 10.2-13.2 sec/10 ml (distance ∽ 15-50 cm).

***Compressive modulus*.**

The increase in the porosity of the scaffolds resulted in an decrease in compressive properties. The compressive modulus decreased from ∽ 88 kPa for the salt leached scaffold to 28, 42, and 49 for salt-PEG 200 leached, salt-PEG 600 leached, and salt-PEG 1000 leached PCL scaffold, respectively. The compressive modulus of the scaffolds was found to decrease as follow:

Salt leached > salt-PEG 1000 leached > salt-PEG 600 leached > salt-PEG 200 leached PCL scaffold.

3.3. Biological evaluation of neat and modified PLA fibrous scaffolds.

Indirect cytotoxicity evaluation.

Both mouse calvaria-derived preosteoblastic cells(MC3T3-E1) and mouse fibroblasts cells (L929) were used in the assessment. However we were interested in using the obtained scaffolds as potential bone scaffolds, it was mandatory to test the materials with L929 just to comply with the ISO10993-5 standard test method. For both types of cells, about 40,000 cells/well were seeded in empty wells of TCPS. Indirect cytotoxicity test was conducted on salt leached, salt-PEG 200 leached, salt-PEG 600 leached, and salt-PEG 1000 leached PCL scaffolds. Figure 8 a) and 8 b) show the viability of the cells obtained from MTT assay after the cells had been cultured with the 1, 3, 7 day-extraction media from scaffolds as compared with the fresh SFM(control TCPS). The viability of the cells was reported as the percentage with respect to that of the control. Evidently, the viability ratio of cells that had been cultured with all of extraction media (and with control TCPS) is greater than 80%. This results can be indicated that all types of PCL scaffolds released no substances at levels that were harmful to cells.

***Cell attachment and cell proliferation*.**

The biocompatility of PCL scaffolds was evaluated in the terms of their ability to promote the proliferation of the cells that had been allowed to attach on their surfaces. Figure 9 shows the

proliferation of MC3T3-E1 on the surface of TCPS and the PCL scaffolds on day 1-3 after cell culturing in terms of the viability of cells. The viability of cells on a scaffold could be quantified by Fluorescent emission intensity from the DNA Quantification test.

On day 1, the viability of cells on the salt-PEG leached scaffold was equivalent to that on TCPS while the viability of cell on the salt-PEG 200 leached, salt-PEG 600 leached, salt leached PCL scaffold was slightly lower than that on TCPS. On day 2, the viability of cell on the salt-PEG 1000 leached was equivalent to that on salt leached PCL scaffold. In comparison with TCPS the salt-PEG 200 leached scaffold was significantly lower. The proliferation of cells on salt-PEG 600 leached and salt-PEG 1000 leached PCL scaffold was significantly greater than that on TCPS and salt leached PCL scaffold on day 3.

***Cell Morphology*.**

Table 2 and 3 show selected SEM images (magnification = 3500X; scale bar = 5 μm) of MC3T3-E1 that were either seeded or cultured on the surfaces of glass, salt leached, salt-PEG 200 leached, salt-PEG 600 leached, salt-PEG 1000 leached PCL scaffolds at different time points.
According to these images, cell morphology and interaction between cells and the scaffolds can be visualized. At 2 h after cells seeding, the majority of cells on the glass surface was stilled rounded. At 4 h after cells seeding, the majority of cells on the glass surface started to extend their cytoplasm. At 6 h after cells seeding, the majority of cells showed evidence of the extension of their cytoplasm on the surface. For the cells that were seeded on the surface of various types of scaffolds, at 2 h after cells seeding, the majority of cells on surface was rounded. At 4 h after cells seeding, the majority of cells was remained round, but a closer examination around the edge of the cells revealed an evidence of filopodia. At 6 h after cells seeding, the majority of cells on the scaffolds were evidently expanded.

At 1, 2, and 3 days after cells seeding, the majority of the cells seeded on the surfaces of all types of scaffolds expanded over the area of the scaffolds which were the most expansion on the surface of salt-PEG 600 leached and salt-PEG 1000 leached PCL scaffolds.

***Alkaline Phosphatase (ALP) Activity*.**

Among the various biological functions of osteoblasts, secretion of alkaline phosphatase (ALP) is an important indicator determining the activity of the cells on a scaffold. The ALP activity of MC3T3-E1 that were cultured on PCL scaffolds, in comparison with that of TCPS, for 3, 5, and 7 days. The ALP activity of MC3T3-E1 on TCPS (i.e. controls), salt leached, salt-PEG 200 leached, salt-PEG 600 leached, salt-PEG 1000 leached PCL scaffolds were monitored at 3, 5 and 7 days in culture (see Figure 10). For all of PCL scaffolds investigated, the ALP activity on day 3 was lower than TCPS, while the ALP activity on day 5 was quite similar to TCPS. On day 7, the highest ALP activity of MC3T3-E1 was observed on the salt-PEG 1000 leached scaffold compared to TCPS, while the ALP activity of MC3T3-E1 on salt leached scaffold was lowest and lower than on TCPS.

***Mineralization*.**

Alizarin Red S staining was used to quantify the mineral deposition of MC3T3-E1 that were cultured on the surfaces of TCPS, salt leached, salt-PEG 200 leached, salt-PEG 600 leached, and salt-PEG 1000 leached PCL scaffolds for 14 days.

Figure11. shows photographic images of the stained specimens. The appearance of red on the stained product shows the presence of calcium. The quantitative analysis of the results shown in Figure 12. was carried out by elution of calcium deposition with cetylpyridinium chloride and spectrophotometically read at 570 nm. The results revealed that the mineral deposition of cells cultured in the (salt-PEG 600 leached and) salt-PEG 1000 leached PCL scaffold were significantly greater than that of the cells cultured on the salt leached PCL scaffolds and TCPS.

4. Discussion

The polarities of PCL and PEG were quite different, when mixing of both, PEG phase spontaneously and spherically dispersed in PCL phase in order to diminish the surface energy on the PCL-PEG interface.[16] Resulting that after the spherical PEG were leaching out, the interconnected pores network were formed in the salt-PEG leached PCL scaffolds.

A stereomicroscope, visual slide microscope and SEM were used to observe the pores, pores distribution and the interconnected pores network of the scaffolds. The effect of PEG leached out scaffolds is illustrated in Figure 1-5. Figure 1 is the stereomicroscope images of the PCL scaffolds. Highly porous PCL scaffold were obtained for all salt and salt-PEG leached PCL scaffolds. Figure 2 and 3 show the inner morphology of the scaffolds; the salt-PEG leached PCL scaffold show the highly porous with high interconnected network.

The PCL-PEG 1000 blend solution has the highest viscosity compared to PCL-PEG 200 and PCL-PEG 600 blend solution. On the other hand, base on Kamide's theory about particle growth during membrane formation,[15] since the molecular size of PEG MW = 200 and 600 g/mol would move with a larger diffusion velocity and higher collision frequency than PEG MW = 1000 g/mol would. This resulted in creating more uniform pore and interconnected pores by leaching PEG MW = 1000 g/mol out rather than leaching out PEG MW = 200 and 600 g/mol. Salt-PEG 600 leached and salt-PEG 1000 leached PCL scaffolds have better pores and interconnected pore distribution than salt-PEG 200 leached PCL scaffold. The distribution of pores in scaffolds prepared from PEG MW. 1000 g/mol was greatest and more interconnected networks were distributed throughout the scaffolds.

The salt-PEG leached PCL scaffolds show highly interconnectivity pores network in the scaffolds, which is not in case of the salt leached PCL scaffold. The pores of the salt-PEG leached scaffolds are interconnected and the inner surface of pores looks quite coarse. The developed interconnected pore network is likely to facilitate transporting nutrients and wastes for a facile cell growth and blood vessel invasion. The interconnected pores network and coarse surface are beneficial for all coherence and quick propagating of cell.

The interconnectivity and dimensions of the pores of the scaffolds affect not only the transport of nutrients into and wastes out of the cells through the pore structure of the scaffolds, but also other properties of the scaffolds. The porosity increased with increased the interconnectivity. According to the results in table 2, the greatest porosity, pore volume, and pore size values and the highest interconnectivity observed for salt-PEG 1000 leached PCL scaffolds are the obvious reasons for their greatest water absorption capability. The water absorption capability is an important property of a functional scaffold, as it allows the absorption and retention of wound exudates. In addition, the

passage of exudates through the pore structure provides a possibility for certain proteins which is one steps required for bone regeneration to be absorbed on the scaffold surface.[19-21]

At any distance, the flow resistance was significantly higher for salt leached PCL scaffold compared to salt-PEG 200 leached, salt-PEG 600 leached, and salt-PEG 1000 leached PCL scaffolds. Standard deviation of flow resistance was higher for salt-PEG 200 leached and salt-PEG 600 leached PCL scaffolds, to indicate a more irregular structure with non uniform distribution of interconnections between pores compared to salt-PEG 1000 leached PCL scaffold. The higher percentage of closed cells account for the higher flow resistance observed for the salt leached PCL scaffold.

The higher porosity (92.6% as opposed to 91.6%) of the scaffolds decreased compressive modulus from 88 to 49 kPa. The porosity is an important parameter of scaffolds, playing a significant role for cell proliferation and growth. The higher porosities can provide cells spacious surrounding for their propagation, but if porosities are too high,[22] it is very dificult for the scaffolds to maintain enough mechanical rigidity.[23] Although increased porosity facilitate bone ingrowth, the result is a reduction in meachanical properties, since this compromises the structural integrity of the scaffold, since this compromises the structural integrity of the scaffold.[24]

The biocompatibity of these PCL scaffolds as bone scaffolds was assessed by an indirect cytotoxicity evaluation with mouse fibroblastic cells (L929) and mouse calvaria-derived pre-osteoblastic cells (MC3T3-E1), based on the initial 40,000 cells/well of cells seeded. Even though we were interested in using the obtained scaffolds as potential bone scaffolds, it was mandatory to test the materials with L929 just to comply with the ISO10993-5 standard test method. The viability ratio of cells that had been cultured with all of extraction media (and with control TCPS) is greater than 80%. All of the obtained results clearly suggested that all types of the PLA fibrous scaffolds, released no substances at levels that were harmful to both types of cells. Similar to our results, Jie et al.[25] showed that the cytotoxicity of poly(D,L-lactide)/nano-hydroxyapatite composites was 79.6-82.6% and the cytotoxicity of these scaffolds was in grade I according to ISO10993-1, that means these kind of materials have very good cytocompatibility.

In comparison with TCPS, the viability of cell on the salt-PEG 200 leached, salt-PEG 600 leached, salt leached PCL scaffold was slightly lower on day 1 and the proliferation of cells on salt-PEG 600 leached and salt-PEG 1000 leached PCL scaffold was significantly greater on day 3. The lesser viability of cells in the attachment period on various types of the scaffolds in comparison with that on TCPS In contrast, the greater number of cells in the proliferation period on PCL scaffolds could be because of high porosity and high interconnectivity network of the PCL scaffolds though which the cells were able to penetrate into the scaffolds. As a result, higher porosity did not affect cell attachment, but resulted in increased cell proliferation, due to pore space increased with porosity and facilitated transport of oxygen and nutrients.[24,26]

ALP activity was measured to compare the effects of the scaffolds on osteoblastic differentiation by culturing MC3T3-E1 cells for 3, 5, and 7 days on PCL scaffolds. As shown in Figure 10, the ALP activities of the MC3T3-E1 cells cultured on the salt-PEG 1000 leached PCL scaffold was significantly higher than that on TCPS on day 7. When the culture was maintained up to 14 days, significantly

greater amount of calcium deposition was observed in the salt-PEG 1000 leached PCL scaffolds compared to the TCPS and salt leached PCL scaffolds, as determined by the alizarin red-S staining and the quantification of calcium deposition. Base on all results, the good in biocompatibility of the salt-PEG 1000 leached PCL scaffolds could be result from the high porosity and high interconnectivity network of PCL scaffolds that can permit cell intrusion, and permeation.

5.Conclusion

Three-dimensional PCL scaffolds with highly porous, and highly interconnectivity network can be prepared by our modified solvent casting, particulate leaching, and polymer leaching techniques using sodium chloride and polyethylene glycol(PEG) as a porogen. Scanning electron microscopic (SEM) and optical microscope images confirm that the scaffolds fabricated using this method have highly interconnected network, equal distribution, and uniform size of 400-500 μm pores. The greatest porosity, pore volume, and pore size values and the highest interconnectivity observed for salt-PEG 1000 leached PCL scaffolds are the obvious reasons for their greatest water absorption capability. The potential of use these scaffolds in bone tissue engineering application was evaluated in vitro with mouse calvaria-derived, pre-osteoblastic cells (MC3T3-E1). Indirect cytotoxicity evaluation revealed that scaffolds fabricated using this method released no substances at levels that were harmful to cells. Scanning electron microscopy observation showed the majority of the cells seeded on the surfaces of scaffolds at 3 days expanded over the area of the scaffolds which was the most expansion on the surface of scaffolds fabricated using this method. For mineralization, cells cultured on surfaces of PCL scaffolds fabricated using this method showed the highest mineral deposition. All of obtained results can be implied their potential for utilization as bone-scaffolding materials.

Acknowledgments. This research work was partial financial support received from 1) The Thailand Research Fund (TRF, grant no. DBG5280015 and a doctoral scholarship received from the Royal Golden Jubilee PhD Program), 2)the Petroleum and Petrochemical College (PPC), Chulalongkorn University, 3) the National Center of Excellence for Petroleum, Petrochemicals, and Advanced Materials, Thailand, and 4) Department of Anatomy, Faculty of Dentistry, Chulalongkorn University.

References and Notes

(1) Hyun, J. C; Tae, G. P. *Advanced Drug Delivery Reviews* **2007**, 59, 249-262.

(2) Woesz, A. *Virtual Prototyping & Bio Manufacturing in Medical Applications* **2008**, 9, 171-205

(3) Sinha, V.R.; Bansal, K.; Kaushik, R.; Kumiria, R.; Trehan, A. *International Journal of Pharmaceutics* **2004**, 278(1), 1-23

(4) Nam, Y. S; Park, T. G. *Biomed Mater Res* **1999**; 47 (1), 7-17

(5) Hutmacher D. W. *Biomater Sci Polym Ed* **2001**; 12 (1), 107-24

(6) Lee, J. H; Park, T. G; Park, H. S; Lee, D. S; Lee, Y. K; Yoon, S. C; Nam, J. *Biomaterials* **2003**, 24, 2773-2778

(7) Carletti, E.; Motta, A.; Migliaresi, C. *Methods in Molecular Biology*, 695, 17-39

(8) Kim, H.J.; Kim, U.J.; Leisk, G.G.; Bayan, C.; Georgakoudi, I.; Kaplan, D.L. *Macromol. Biosci*. **2007**, 7, 643-655

(9) Pattison, M.A.; Wurster, S.; Webster, T.J.; Haberstroh, K.M. *Biomaterials* **2005**, 25, 2491-2500

(10) Yoon, J.J.; Song, S.H.; Lee, S.S.; Park, T.G. *Biomaterials* **2004**, 25, 5613-5620

(11) Shin, M.; Abukawa, H.; Troulis, M.J.; Vacanti, J.P. *Biomed. Mater. Res. A*. **2008**, 84A, 702-709

(12) Sokolsky-Papkov, M.; Agashi, K.; Olaye, A.; Shakesheff, K.; Domb, A. J. *Advanced Drug Delivery Reviews* **2007**, 59, 187-206.

(13) Cao, Y.; Croll, T.; Lees, J.G; Tuch, B. E; Cooper-White, J.J. *Aust. J. Chem.* **2005**, 58 (10), 691-703

(14) Ekaputra, A. K; Prestwich, G. D; Cool, S. M; Hutmacher, D. W. *Biomacromolecules* **2008**, *9*, 2097-2103.

(15) Lin,W.J.; Lu, C.K, *Journal of Membrane Science* **2002**, 198, 109-118

(16) Lin, W.J.; Lee, H.G, *Journal of controlled Release* **2003**, 89, 179-187

(17) Kesting, R.E. *A Structural Perspective* **1985**

(18) Harris, J.M, *Biotechnical and Biomedical Applications* **1992**

(19) Yang, G.; Zhaang, H.F. *Journal of Membrane Science* **1999**, 161, 31

(20) Chuenjitkuntawown, B.; Inrung, W.; Damrongsri, D.; Mekaapiruk, K.; Supaphol, P.; Pavasant, P. *Journal of Biomedical Materials Research Part A* **2009**, 241-251

(21) Hariraksapitak, P.; Suwantong, O.; Pavasant, P.; Supaphol, P. *Polymer* **2008**, 49, 2678-2685

(22) Mikos, A.G.; Sarakinos, G.; Vacanti, J.P.; Langer, R.S.; Cima, L.G. United States Patent, 6,562,374, May 13, **2003**

(23) Yang, Q.; Chen, L.; Shen, X.Y.; Tan, Z.Q. *Journal of Macromolecular Science Part B: Physics* **2006**, 45, 1171-1181

(24) Karageorgiou, V.; Kaplan, D. *Biomaterials* **2005**, 26, 5474-5491

(25) Ren, J.; Zhao, P.; Ren, T.; Gu, S.; Pan, K. *J Mater Sci: Mater Med* **2008**, 19, 1075-1082

(26) Takahashi, Y.; Tabata, Y. J *Biomater Sci Polym Ed* **2004**, 15(1), 41-57

(27) Lee, H.; Park, T.G. *Design Principles in Biomaterials and scaffold*, 33, 580-593

(28) Desmet, T.; Morent, R.; Geyter, N.D.; Leys, C.; Schacht, E.; Dubruel, P. *Biomacromolecules* **2009**, 10(9), 2351-2378

(29) Lee, H.J.; Ahn, S.H.; Kim, G.H. *Chemistry of materials* **2011**, 10

(30) Draghi, L.; Resta, S.; Pirozzolo, M. G.; Tanzi, M. C. *Journal of Materials Science: Materials in Medicine* **2005, 16,** 1093 – 1097

(31) Stamatialis, D.F.; Papenburg, B.J.; Girones, M.; Saiful, S.; Bettahalli, S. N.M.; Schmitmeier, S.; Wessling, M. *Journal of Membrane Science* **2008**, 308, 1-34

(32) Lee, C.T.; Huang, C.P.; Lee, Y.D. *Biomacromolecules* **2006**, 7, 2200-2209

(33) Lim, Y.M.; Gwon, H.J.; Shin, J.; Jeun, J.P.; Nho, Y.C. *Journal of Industrial and Engineering Chemistry* **2008**, 14, 436-441

(34) Sarazin, P.; Roy, X.; Favis, B.D. *Biomaterials* **2004**, 25, 5965-5978

(35) Dorati, R.; Colonna, C.; Genta, I.; Modena, T.; Conti, B. *Polymer Degradation and Stability* **2010**,95, 694-701

(36) Rezwan, K.; Chen, Q.Z.; Blaker, J.J.; Boccacini, A.R. *Biomaterials* **2006**, 27, 3413-3431

(37) Wutticharoenmongkol, P.; Pavasant, P.; Supaphol, P. *Biomacromolecules* **2007**, 8, 2602-2610

(38) Lee, Y.H.; Lee, J.H.; An, I.G.; Kim, C.; Lee, D.S.; Lee, Y.K.; Nam, J.D. *Biomaterials* **2005**, 26, 3165-3172

(39) Shum, A.W.T.; Li, J.; Mak, A.F.T. *Polymer Degradation and Stability* **2005**, 87, 487-493

(40) Sombatmankhong, K.; Sanchavanakit, N.; Pavasant, P.; Supaphol, P. *Polymer* **2007**, 48, 1419-1427

(41) Sangsanoh, P.; Waleetorncheepsawat, S.; Suwantong, O.; Wuttcharoenmongkol. P.; Weeranantanapan, O.; Chuenjitbuntaworn, B.; Cheepsunthorn, P.; Pavasant, P.; Supaphol, P. *Biomacromolecules* **2007**, 8, 1587-1594

(42) Chuenjitbuntaworn, B.; Supaphol, P.; Pavasant, P.; Damrongsri, D. *Polym Int* **2010**, 59, 227-235

(43) Wutticharoenmongkol, P.; Sanchavanakit, N.; Pavasant, P.; Supaphol, P. *Journal of Nanoscience and Nanotechnology* **2006**, 6, 514-522

(44) Yang, Q.; Chen, L.; Shen, X.; Tan, Z. *Journal of Macromolecular Science Part B: Physics* **2006**, 45, 1171-1181

CAPTION OF FIGURES

Figure 1. Stereomicroscope images of (a) salt leached PCL scaffold (b) salt-PEG 200 leached PCL scaffold (c) salt-PEG 600 leached PCL scaffold (d) salt-PEG 1000 leached PCL scaffold

Figure 2. Visual slide microscope images at 5x magnification of (a) salt leached PCL scaffold (b) salt-PEG 200 leached PCL scaffold(c) salt-PEG 600 leached PCL scaffold (d) salt-PEG 1000 leached PCL scaffold

Figure 3. Visual slide microscope images at 10x magnification of (a) salt leached PCL scaffold (b) salt-PEG 200 leached PCL scaffold (c) salt-PEG 600 leached PCL scaffold (d) salt-PEG 1000 leached PCL scaffold

Figure 4. SEM images at 75x magnification illustrating the microstructures of the (a) salt leached PCL scaffold (b) salt-PEG 200 leached PCL scaffold(c) salt-PEG 600 leached PCL scaffold (d) salt-PEG 1000 leached PCL scaffold

Figure 5. SEM images at 200x magnification illustrating the microstructures of the (a) salt leached PCL scaffold (b) salt-PEG 200 leached PCL scaffold (c) salt-PEG 600 leached PCL scaffold (d) salt-PEG 1000 leached PCL scaffold

Figure 6. Water absorption capability of the salt leached and salt-PEG leached PCL scaffolds in 0.1 M PBS at room temperature within 7 days.

Figure 7. Flow resistance of the salt leached and salt-PEG leached PCL scaffolds

Figure 8. Indirect cytotoxic evaluation of PCL scaffolds based on viability of (a) mouse fibroblasts (L929) and (b) pre-osteoblast (MC3T3-E1) that had been cultured with the extraction media from each of these materials against the viability of the cells that had been cultured with the respective culture media for 1 day as a function of the incubation time of the extraction and the culture media of 1, 3, or 7 d. Statistical significance: $*p < 0.05$ compared with control and $^{\#}p < 0.05$ compared to the salt leached scaffolds at any given time point.

Figure 9. Proliferation of MC3T3-E1 that had been seeded or cultured on the surfaces of TCPS, the salt leached, and the salt-PEG leached PCL scaffolds for 1, 2, or 3d. Statistical significance: $*p < 0.05$ compared with control and $^{\#}p < 0.05$ compared to the salt leached PCL scaffolds at any given time p

Figure 10. Alkaline phosphatase (ALP) activity of MC3T3-E1 that were cultured on the surfaces of TCPS, the salt leached and the salt-PEG leached PCL scaffolds for 3, 5, or 7 d. Statistical significance: $*p < 0.05$ compared with control and $^{\#}p < 0.05$ compared to the salt leached PCL scaffolds at any given time p

Figure 11. Images of Alizarin Red-S staining for the mineralization in MC3T3-E1 for day 16 for (a) TCPS (b) salt leached PCL scaffold (c) salt-PEG 200 leached PCL scaffold (d) salt-PEG 600 leached PCL scaffold (e) salt-PEG 1000 leached PCL scaffold

Figure 12. Quantification of mineral deposition in MC3T3-E1 by the method of Alizarin Red-S staining. Statistical significance: $^{*}p < 0.05$ compared with control and $^{\#}p < 0.05$ compared to the salt leached PCL scaffolds at any given time point.

CAPTION OF TABLES

Table 1. Viscosity of PCL solution and PCL-PEG blend solutions

Table 2. Density, percentage of porosity, pore volume and pore size of the scaffolds
a,b,c,d are significantly different at $p < 0.05$ for an individual feature;
*one way ANOVA with Tukey HSD, n = 5 for porosity and pore volume, n = 30 for pore size.

Table3. Attachment of MC3T3-E1 that had been seeded or cultured on the surfaces of glass and the PCL scaffolds for 2, 4, or 6 h. Selected SEM images of cultured specimens, i.e., glass (i.e., control), salt leached PCL scaffold, salt-PEG 200 leached PCL scaffold, salt-PEG 600 leached PCL scaffold, and salt-PEG 1000 leached PCL scaffold at three different time points after MC3T3-E1 were seeded or cultured on their surfaces (magnification = 3500X; scale bar = 5 μm)

Table4. Proliferation of MC3T3-E1 that had been seeded or cultured on the surfaces of TCPS and the PCL scaffolds for 1, 2, or 3d. Selected SEM images of cultured specimens, i.e., glass (i.e., control), salt leached PCL scaffold, salt-PEG 200 leached PCL scaffold, salt-PEG 600 leached PCL scaffold, and salt-PEG 1000 leached PCL scaffold at three different time points after MC3T3-E1 were seeded or cultured on their surfaces (magnification = 3500X; scale bar = 5 μm).

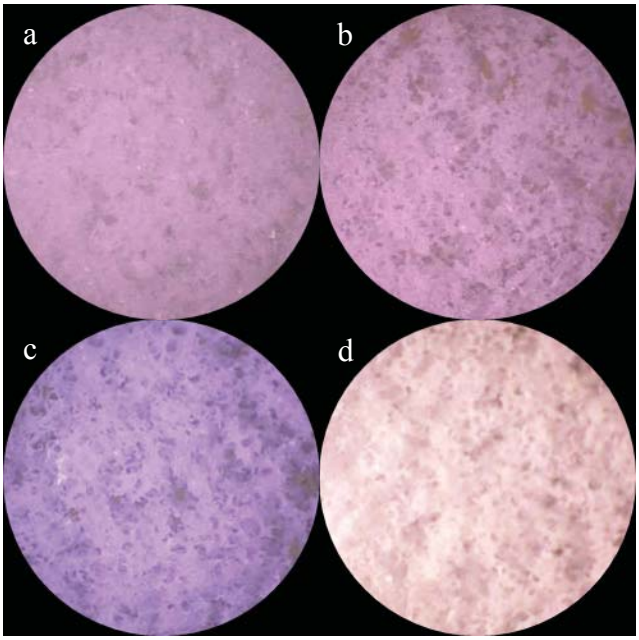


Figure 1. Stereomicroscope images of
(a) salt leached PCL scaffold (b) salt-PEG 200 leached PCL scaffold
(c) salt-PEG 600 leached PCL scaffold (d) salt-PEG 1000 leached PCL scaffold

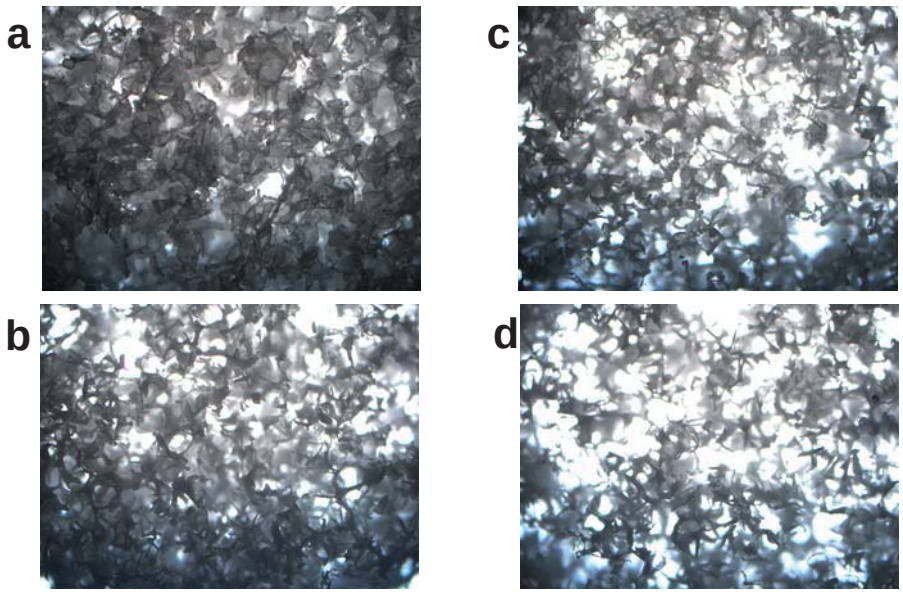


Figure 2. Visual slide microscope images at 5x magnification of
(a) salt leached PCL scaffold (b) salt-PEG 200 leached PCL scaffold
(c) salt-PEG 600 leached PCL scaffold (d) salt-PEG 1000 leached PCL scaffold

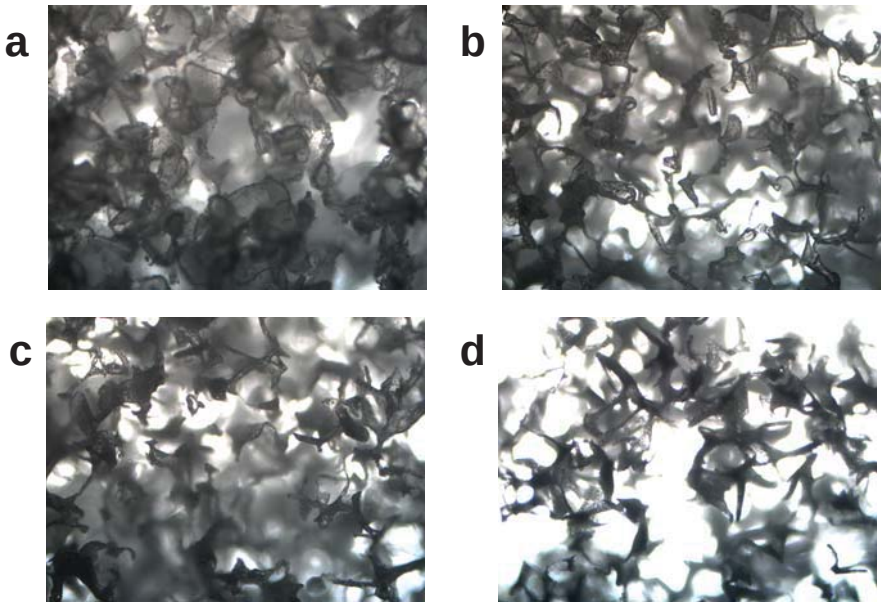


Figure 3. Visual slide microscope images at 10x magnification of
(a) salt leached PCL scaffold (b) salt-PEG 200 leached PCL scaffold
(c) salt-PEG 600 leached PCL scaffold (d) salt-PEG 1000 leached PCL scaffold

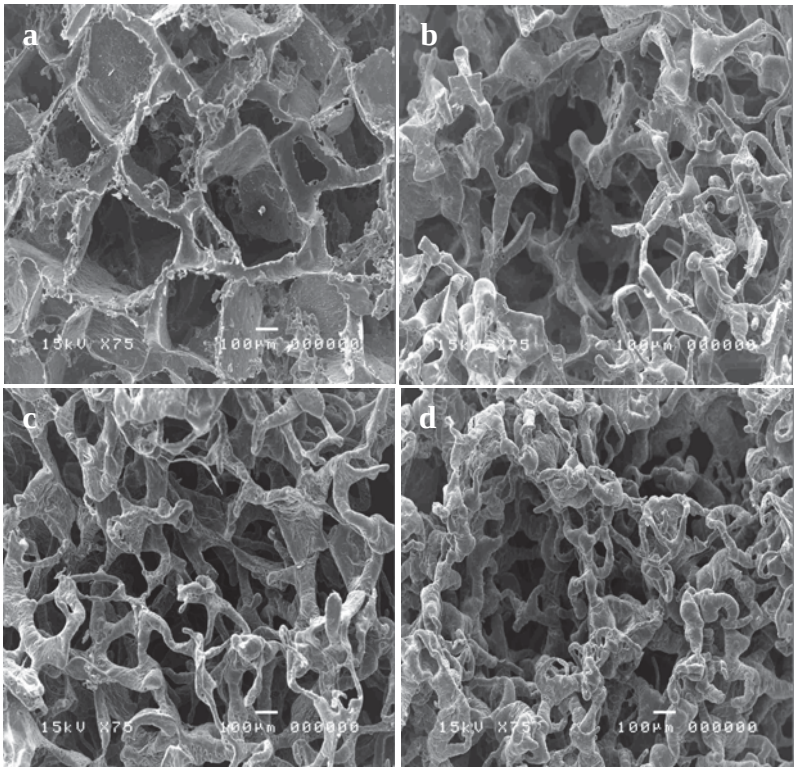


Figure 4. SEM images at 75x magnification illustrating the microstructures of the (a) salt leached PCL scaffold (b) salt-PEG 200 leached PCL scaffold (c) salt-PEG 600 leached PCL scaffold (d) salt-PEG 1000 leached PCL scaffold

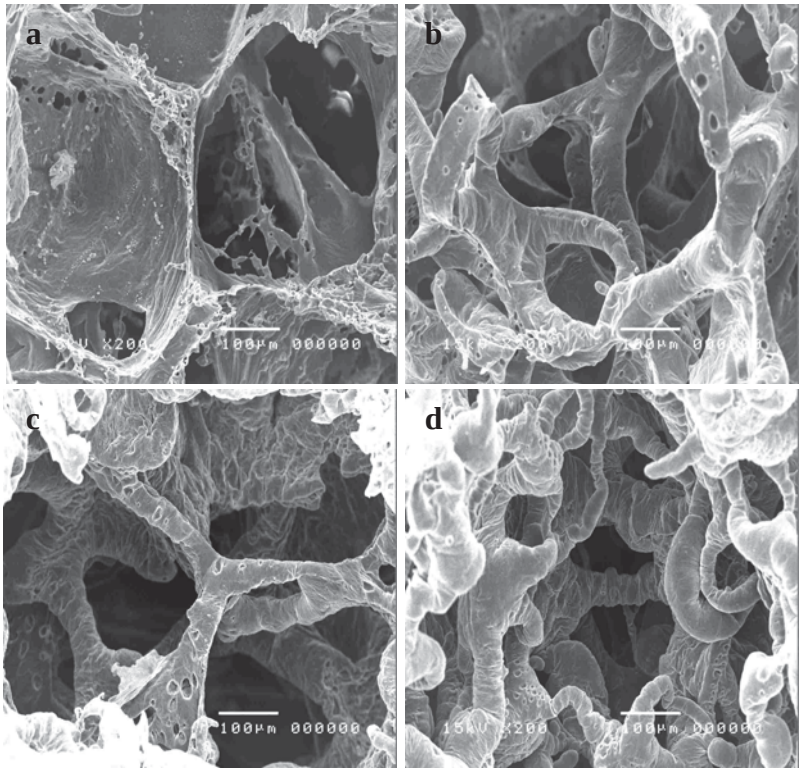
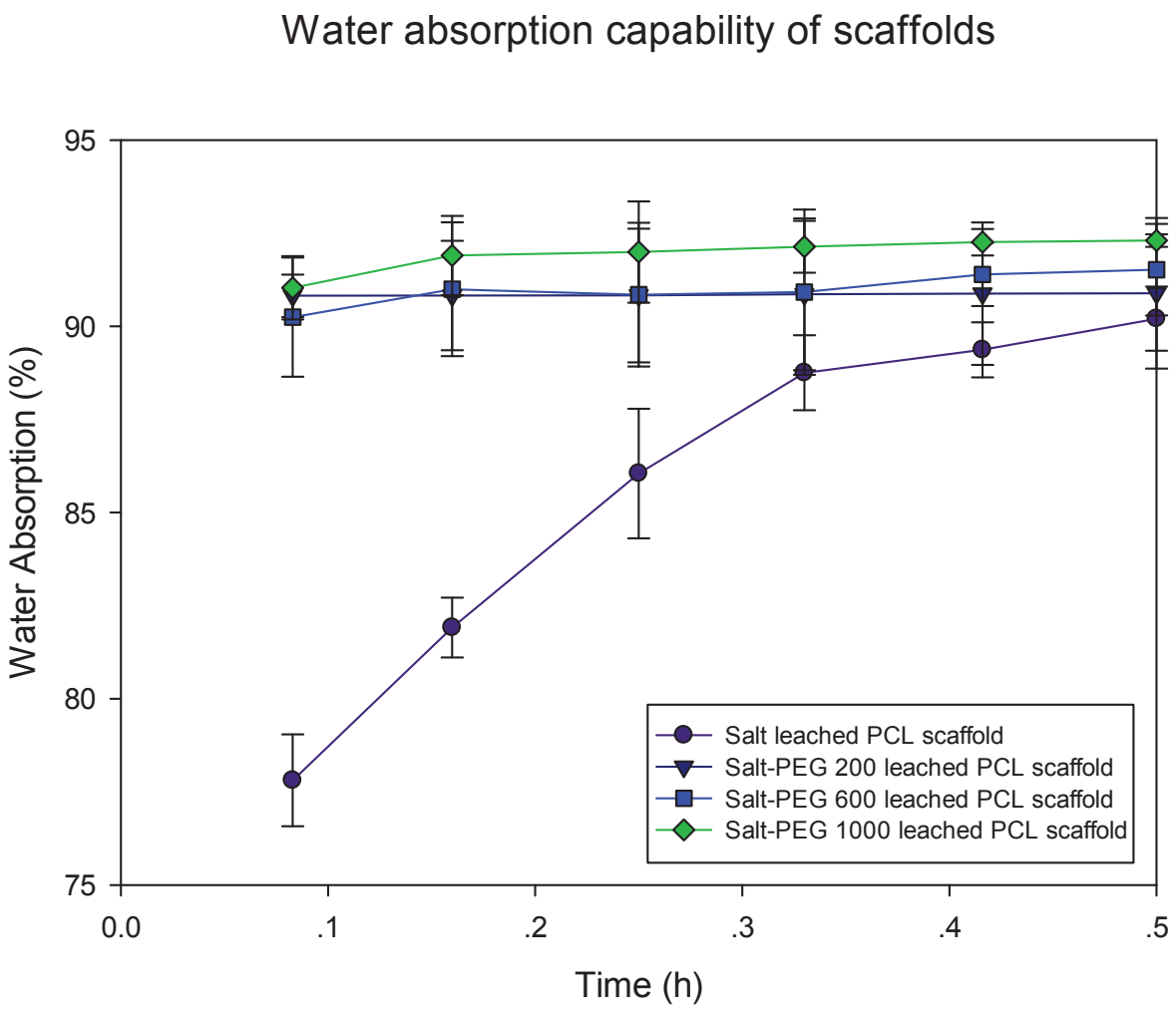
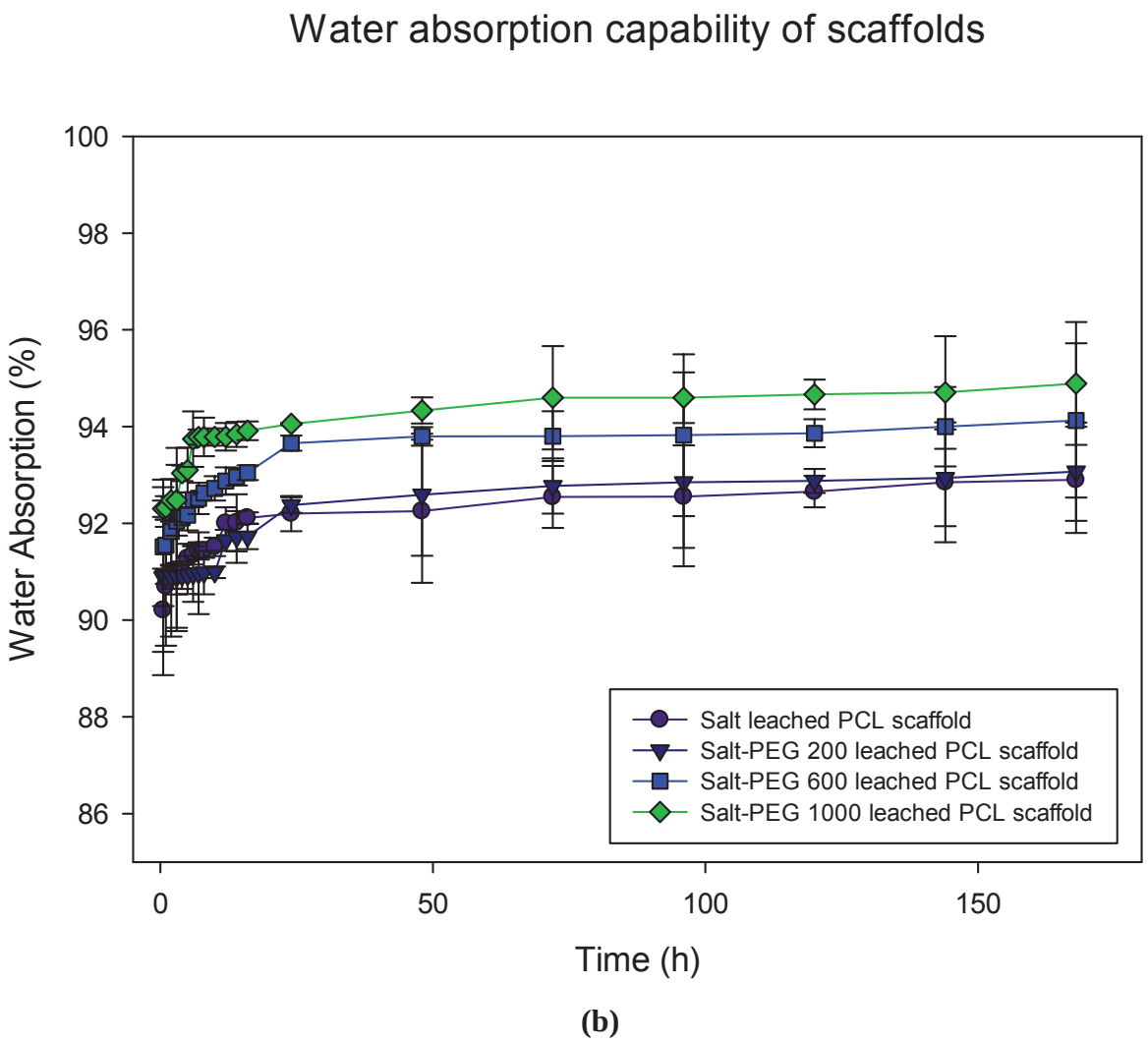


Figure 5. SEM images at 200x magnification illustrating the microstructures of the (a) salt leached PCL scaffold (b) salt-PEG 200 leached PCL scaffold (c) salt-PEG 600 leached PCL scaffold (d) salt-PEG 1000 leached PCL scaffold


Water absorption capability of scaffolds
Water Absorption (%)
95
90
85
80
75
0.0
.1
.2
.3
.4
.5
Time (h)
Salt leached PCL scaffold
Salt-PEG 200 leached PCL scaffold
Salt-PEG 600 leached PCL scaffold
Salt-PEG 1000 leached PCL scaffold

(a)



(b)

Figure 6. Water absorption capability of the salt leached and salt-PEG leached PCL scaffolds in 0.1 M PBS at room temperature within 7 days.

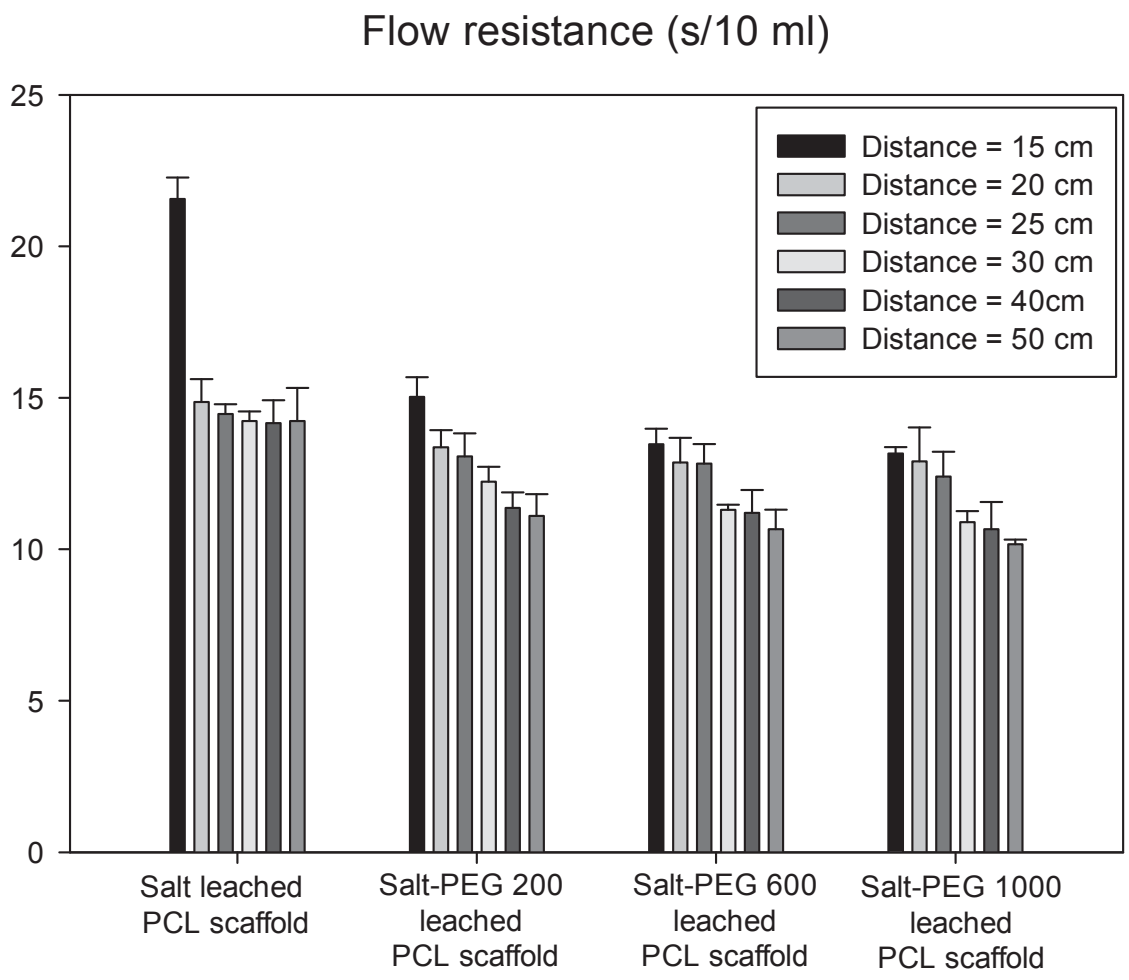
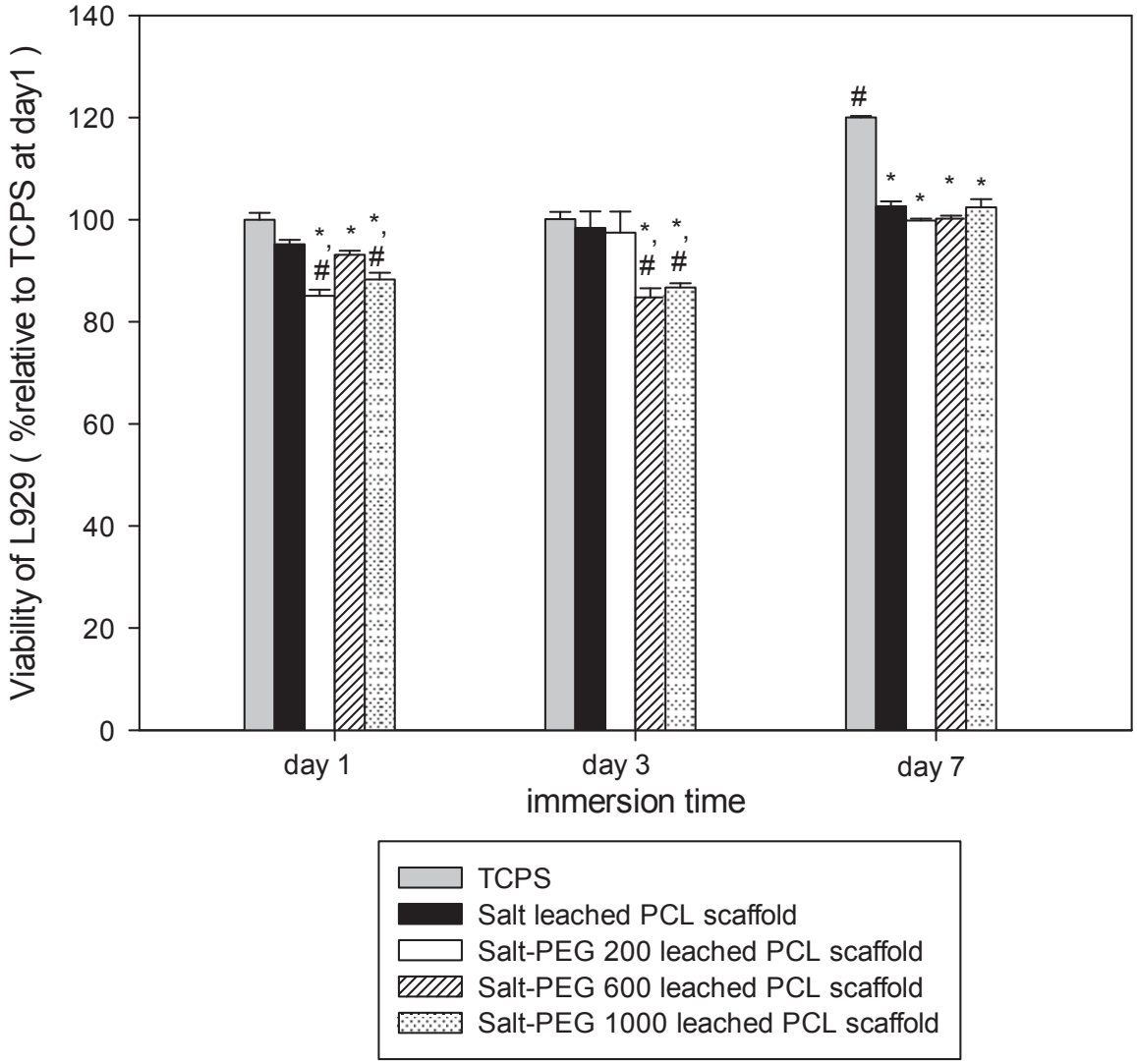
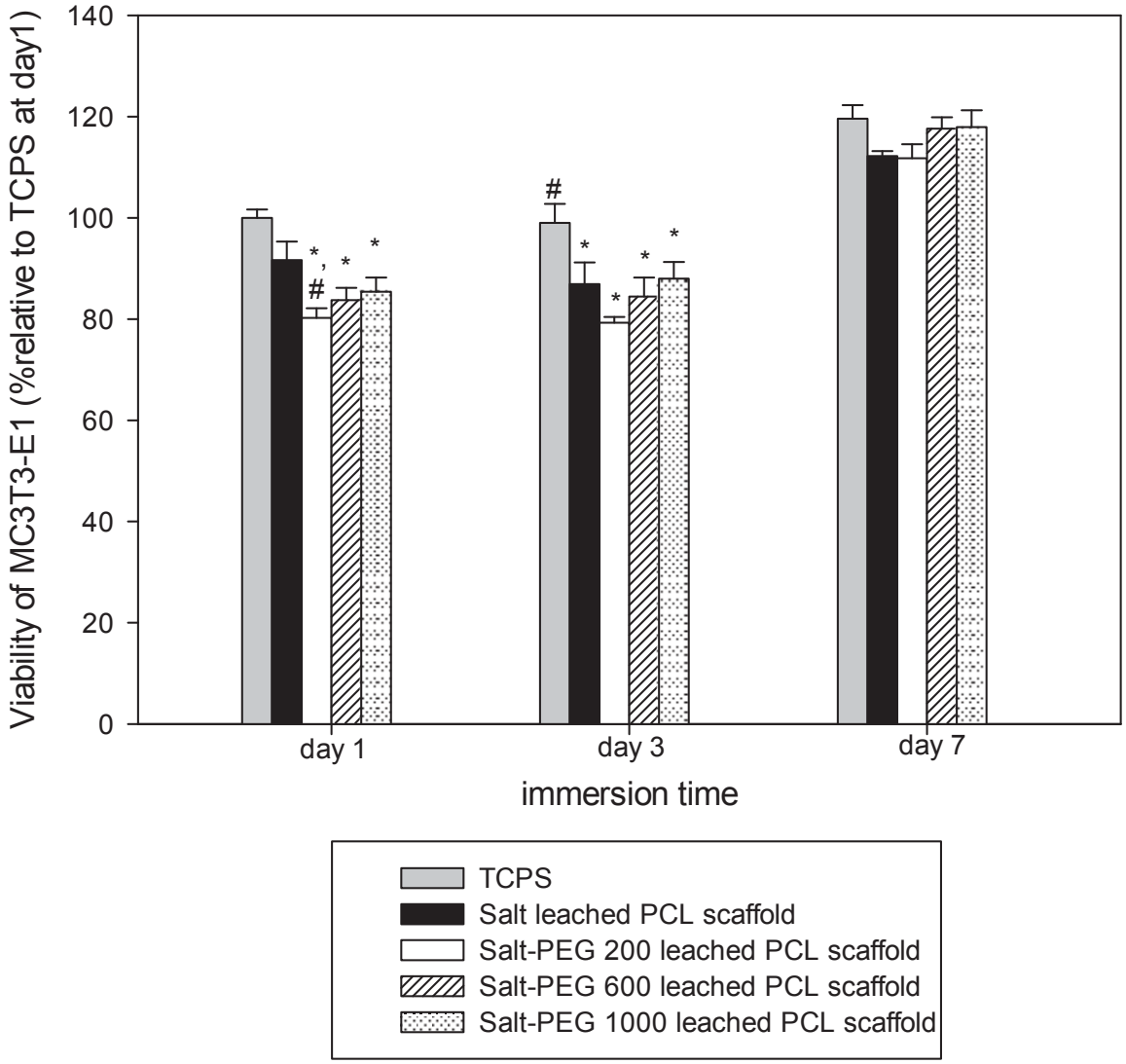


Figure 7. Flow resistance of the salt leached and salt-PEG leached PCL scaffolds


Viability of L929 (%relative to TCPS at day1)
140
120
100
80
60
40
20
0
day 1
day 3
day 7
immersion time
TCPS
Salt leached PCL scaffold
Salt-PEG 200 leached PCL scaffold
Salt-PEG 600 leached PCL scaffold
Salt-PEG 1000 leached PCL scaffold

(a)



(b)

Figure 8. Indirect cytotoxic evaluation of PCL scaffolds based on viability of (a) mouse fibroblasts (L929) and (b) pre-osteoblast (MC3T3-E1) that had been cultured with the extraction media from each of these materials against the viability of the cells that had been cultured with the respective culture media for 1 day as a function of the incubation time of the extraction and the culture media of 1, 3, or 7 d. Statistical significance: $^{*}p < 0.05$ compared with control and $^{\#}p < 0.05$ compared to the salt leached scaffolds at any given time point.

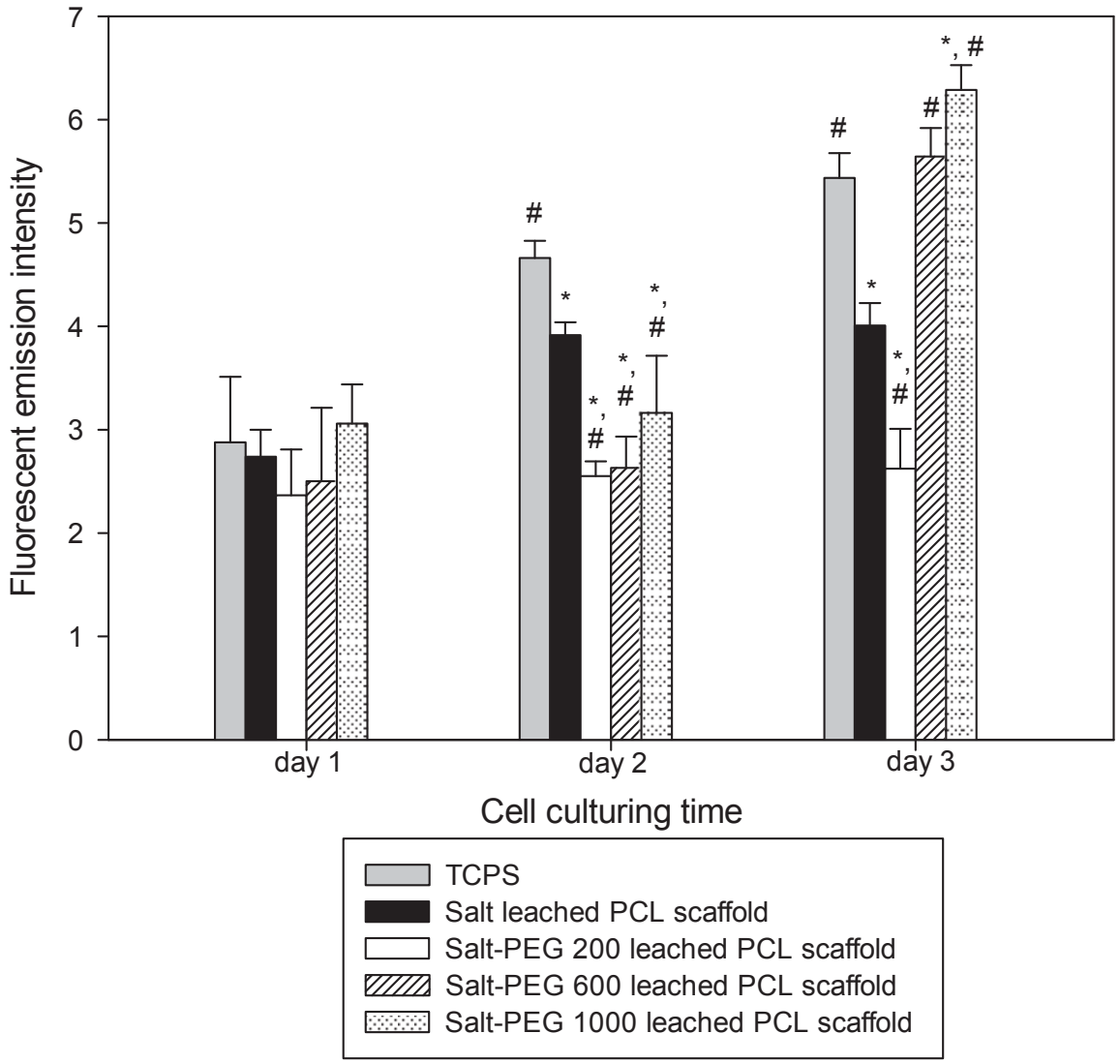


Figure 9. Proliferation of MC3T3-E1 that had been seeded or cultured on the surfaces of TCPS, the salt leached, and the salt-PEG leached PCL scaffolds for 1, 2, or 3d. Statistical significance: *$p < 0.05$ compared with control and $^{\#}p < 0.05$ compared to the salt leached PCL scaffolds at any given time p

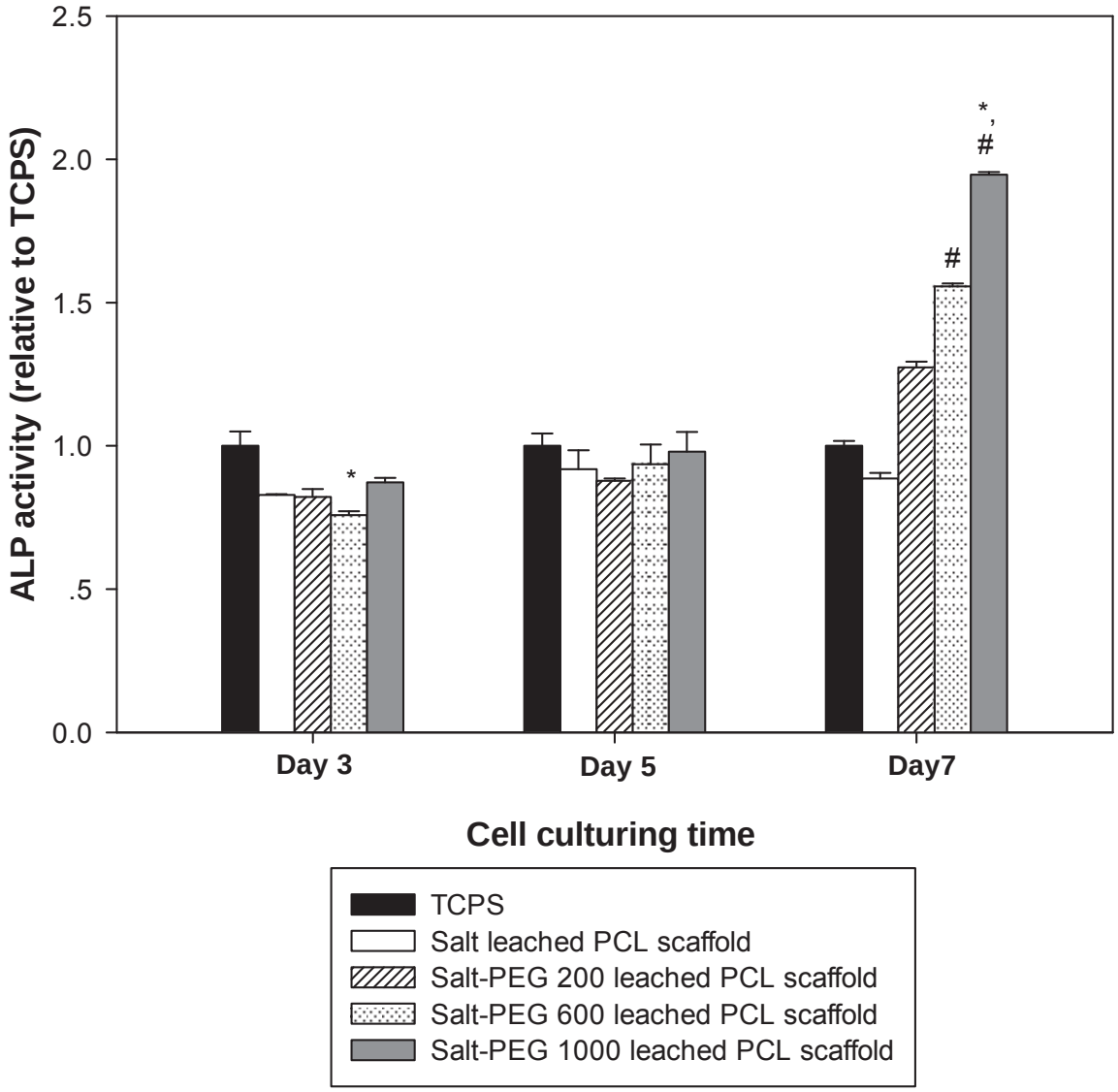


Figure 10. Alkaline phosphatase (ALP) activity of MC3T3-E1 that were cultured on the surfaces of TCPS, the salt leached and the salt-PEG leached PCL scaffolds for 3, 5, or 7 d. Statistical significance: $^{*}p < 0.05$ compared with control and $^{\#}p < 0.05$ compared to the salt leached PCL scaffolds at any given time p

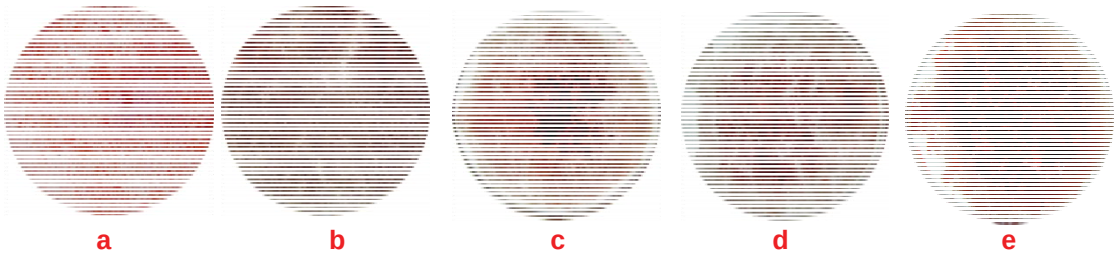


Figure 11. Images of Alizarin Red-S staining for the mineralization in MC3T3-E1 for day 16 for (a) TCPS (b) salt leached PCL scaffold (c) salt-PEG 200 leached PCL scaffold (d) salt-PEG 600 leached PCL scaffold (e) salt-PEG 1000 leached PCL scaffold

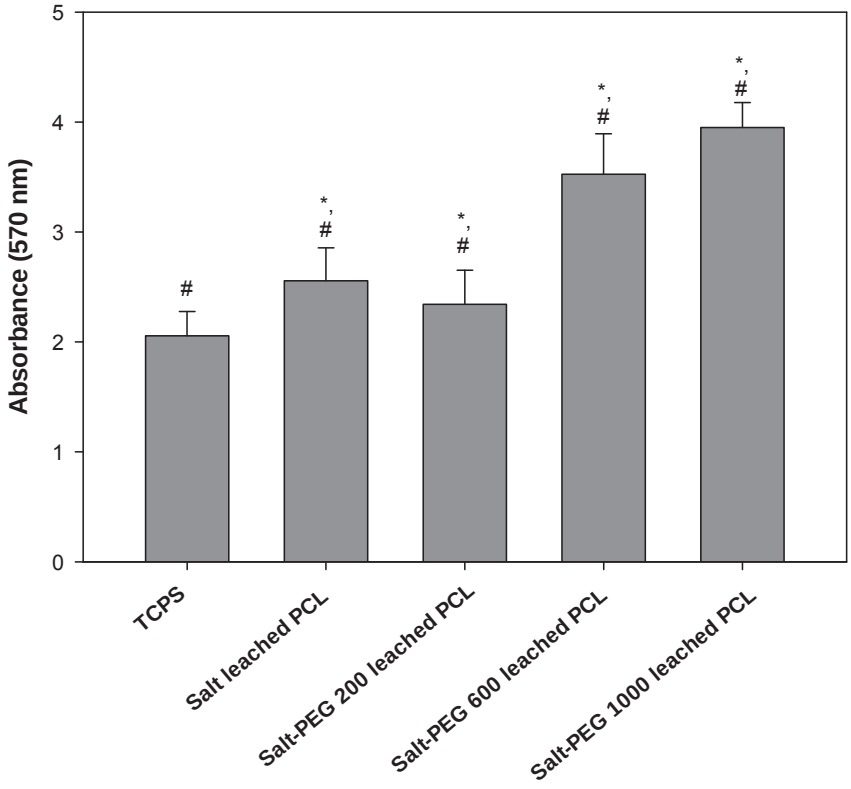


Figure 12. Quantification of mineral deposition in MC3T3-E1 by the method of Alizarin Red-S staining. Statistical significance: $^{*}p < 0.05$ compared with control and $^{\#}p < 0.05$ compared to the salt leached PCL scaffolds at any given time point.

	PCL solution	PCL-PEG 200 blend solution	PCL-PEG 600 blend solution	PCL-PEG 1000 blend solution
Viscosity (cP)	1064 ± 15	989 ± 25	1055 ± 35	1106 ± 27

Table 1. Viscosity of PCL solution and PCL-PEG blend solutions

Scaffolds	Density* (g/cm^3)	Porosity* (%)	Pore volume* (cm^3/g)	Pore size* (μm)	Compressive modulus (kPa)
Salt leached PCL scaffold	0.0961	91.60±0.52	9.56±0.61	421.27±34.18^b	88.46±15.38
Salt – PEG 200 leached PCL scaffold	0.1012^d	91.16±1.41^d	9.18±1.55	378.77±82.13^{a,c,d}	28.85±6.80
Salt – PEG 600 leached PCL scaffold	0.0935	91.83±0.61	9.87±0.82	423.07±40.83^b	42.95±7.85
Salt – PEG 1000 leached PCL scaffold	0.0852^b	92.56±0.43^b	10.90±0.68	434.13±36.74^b	49.98±8.04

Table 2. Density, percentage of porosity, pore volume and pore size of the scaffolds

a,b,c,d are significantly different at $p < 0.05$ for an individual feature;

*one way ANOVA with Tukey HSD, n = 5 for porosity and pore volume, n = 30 for pore size.

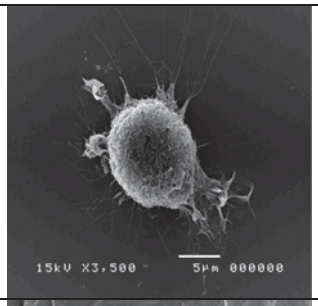
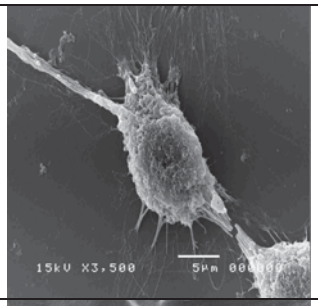
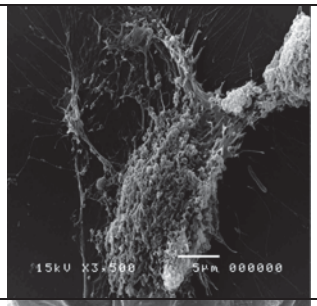
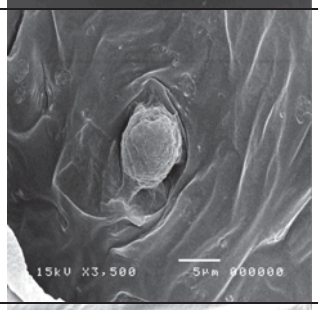
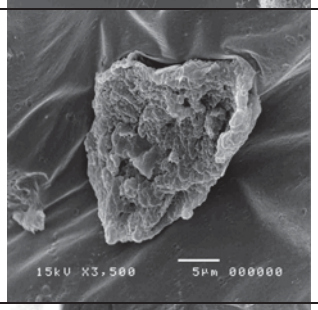
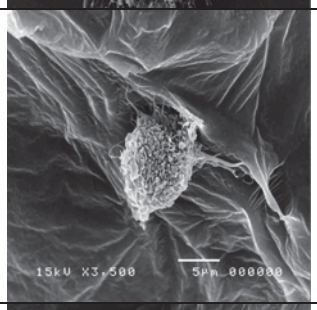
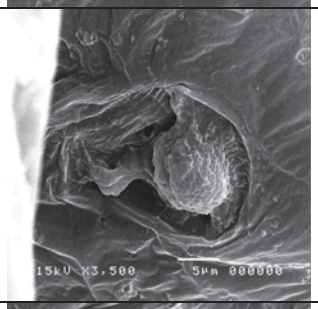
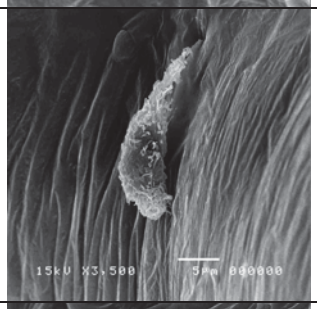
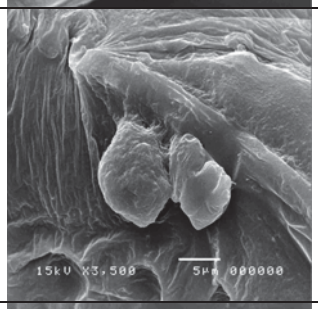
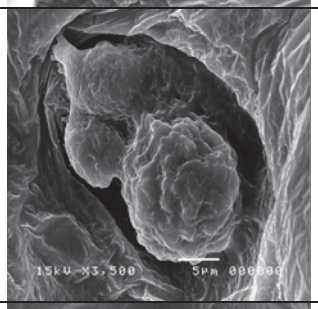
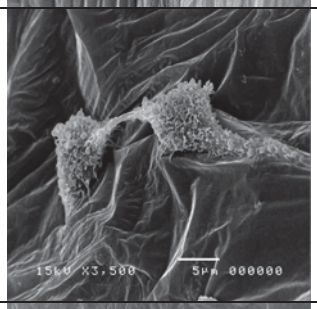
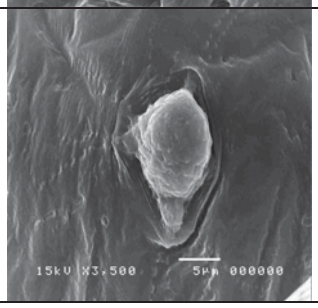
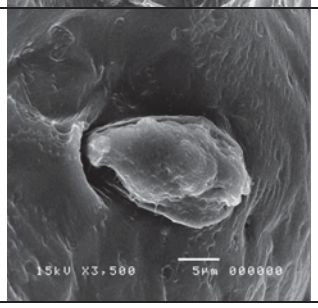
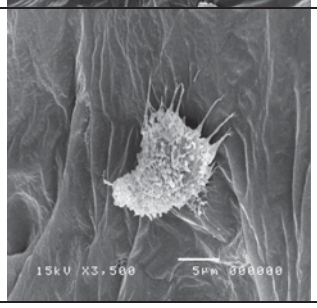
Substrate	Culturing time		
	2 hour	4 hour	6 hour
Glass			
Salt leached PCL scaffold			
Salt – PEG 200 leached PCL scaffold			
Salt – PEG 600 leached PCL scaffold			
Salt – PEG 1000 leached PCL scaffold			

Table3. Attachment of MC3T3-E1 that had been seeded or cultured on the surfaces of glass and the PCL scaffolds for 2, 4, or 6 h. Selected SEM images of cultured specimens, i.e., glass (i.e., control), salt leached PCL scaffold, salt-PEG 200 leached PCL scaffold, salt-PEG 600 leached PCL scaffold, and salt-PEG 1000 leached PCL scaffold at three different time points after MC3T3-E1 were seeded or cultured on their surfaces (magnification = 3500X; scale bar = 5 μm)

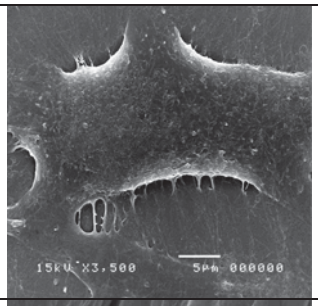
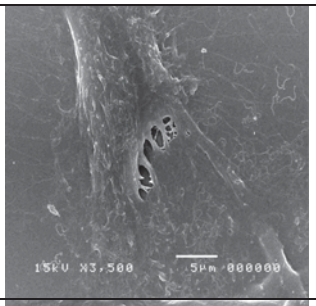
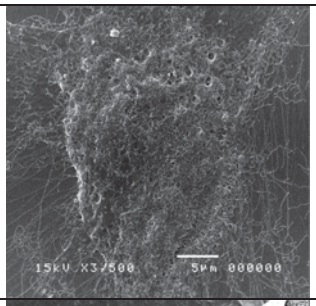
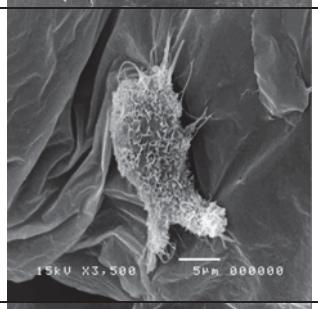
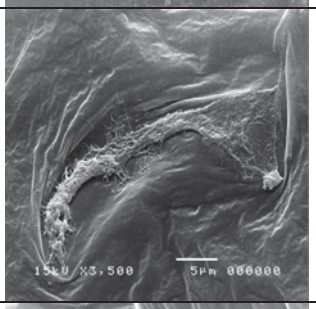
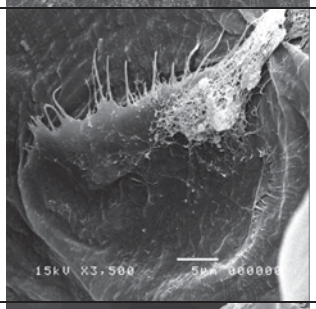
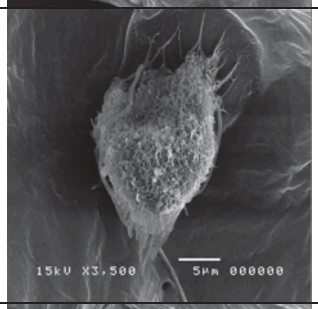
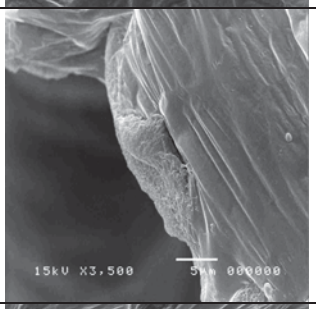
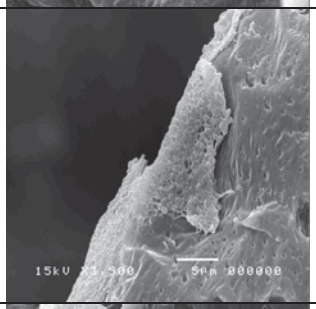
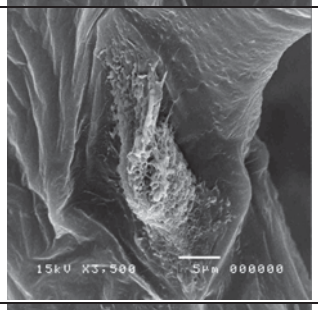
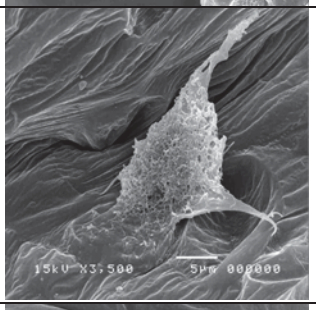
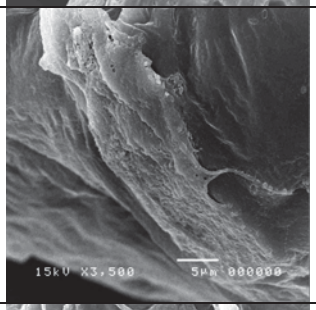
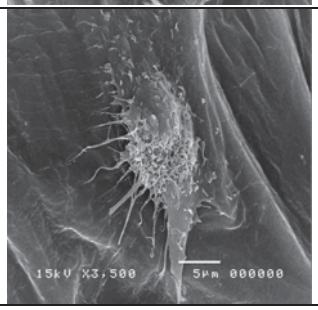
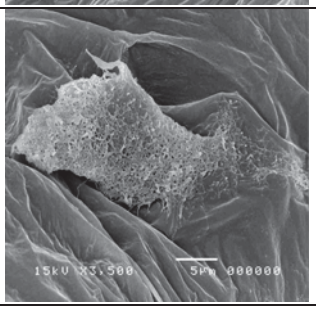
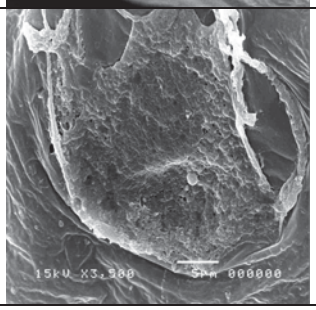
Substrate	Culturing time		
	1 day	2 day	3 day
Glass			
Salt leached PCL scaffold			
Salt – PEG 200 leached PCL scaffold			
Salt – PEG 600 leached PCL scaffold			
Salt – PEG 1000 leached PCL scaffold			

Table4. Proliferation of MC3T3-E1 that had been seeded or cultured on the surfaces of TCPS and the PCL scaffolds for 1, 2, or 3d. Selected SEM images of cultured specimens, i.e., glass (i.e., control), salt leached PCL scaffold, salt-PEG 200 leached PCL scaffold, salt-PEG 600 leached PCL scaffold, and salt-PEG 1000 leached PCL scaffold at three different time points after MC3T3-E1 were seeded or cultured on their surfaces (magnification = 3500X; scale bar = 5 μm).

Preparation and Properties of α-Chitin-Whisker-Reinforced Hyaluronan–Gelatin Nanocomposite Scaffolds

Parintorn Hariraksapitak,* Pitt Supaphol

Petroleum and Petrochemical College and Center for Petroleum, Petrochemicals, and Advanced Materials, Chulalongkorn University, Bangkok 10330, Thailand

Received 3 September 2009; accepted 8 January 2010
DOI 10.1002/app.32095
Published online 12 May 2010 in Wiley InterScience (www.interscience.wiley.com).

ABSTRACT: Tissue scaffolds made of naturally derived polymers present poor mechanical properties, which may limit their actual utilization in certain areas where high strength is a key criterion. This study was aimed at developing tissue scaffolds from a 50 : 50 w/w blend of hyaluronan (HA) and gelatin (Gel) that contained different amounts of acid-hydrolyzed α-chitin whiskers (CWs) by a freeze-drying method. The weight ratios of the CWs to the blend were 0–30%. These scaffolds were characterized for their physical, physicochemical, mechanical, and biological properties. Regardless of the CW content, the average pore size of the scaffolds ranged between 139 and 166 μm. The incorporation of 2% CWs in the HA–Gel scaffolds increased their tensile strength by about two times compared to those of the other groups of the scaffolds. Although the addition of 20–30% CWs in the scaffolds improved their thermal stability and resistance to biodegradation, the scaffolds with 10% CWs were the best for supporting the proliferation of cultured human osteosarcoma cells (SaOS-2). © 2010 Wiley Periodicals, Inc. J Appl Polym Sci 117: 3406–3418, 2010

Key words: biomaterials; nanocomposites

INTRODUCTION

The essence of tissue engineering is aimed at generating biological substitutes for lost or defective tissues. The process of tissue regeneration requires functional scaffolding materials to serve as templates for the attachment of cells and/or mediators for subsequent tissue development.[1,2] Scaffolds, in addition to being supportive frameworks, play important roles in the transportation of nutrients, metabolites, and regulatory molecules into and wastes out of cells. They can also be functionalized to provide specific signaling to the cells.[3] To achieve isomorphous tissue replacement, materials used for fabrication into scaffolds should be biocompatible and biodegradable. Synthetic polymers, such as polylactide, polyglycolide, and their respective copolymers, have been heavily explored because of their suitable chemistry and properties that can be tailored, such that the resulting scaffolds possess a controllable mechanical integrity and *in vivo* degradability.[4–7]

Alternatively, natural polymers, such as collagen, gelatin (Gel), and alginate, have equally been studied because of their inherent hydrophilicity and the presence of certain extracellular matrix (ECM)-like properties that provide a suitable environment for cell growth.[8,9] Notwithstanding, scaffolds made from natural polymers are mechanically weak; this limits their use as regenerating templates for semi-hard and hard tissues, such as cartilage and bones. This can be improved by several means, such as crosslinking,[10–13] blending,[14,15] and chemical modification.[16,17] Here, we used blending, crosslinking, and compositing means to arrive at functional bone scaffolds with improved physical, mechanical, and biological integrities. The natural materials used to fabricate the porous scaffolds were hyaluronan (HA) and Gel, and the reinforcing fillers used to prepare the HA/Gel nanocomposite scaffolds were nanocrystalline entities obtained from the acidic hydrolysis of chitin [i.e., α-chitin whiskers (CWs)]. Both the neat and the CW-reinforced HA/Gel scaffolds were fabricated by means of a freeze-drying technique,

Additional Supporting Information may be found in the online version of this article.

**Present address:* Department of Conservative Dentistry, Faculty of Dentistry, Prince of Songkla University, Hatyai, Songkhla 90112, Thailand.

Correspondence to: P. Supaphol (pitt.s@chula.ac.th).

Contract grant sponsor: Ratchadaphisek Somphot Endowment Fund (Chulalongkorn University).

Contract grant sponsor: Center for Petroleum, Petrochemicals, and Advanced Materials (Chulalongkorn University).

Contract grant sponsor: Petroleum and Petrochemical College (Chulalongkorn University).

Contract grant sponsor: Thailand Research Fund; contract grant number: DBG5280015.

© 2010 Wiley Periodicals, Inc.

and the obtained scaffolds were characterized for their mechanical, physicochemical, and biological properties.

HA, a linear polysaccharide, contains a repeating disaccharide unit of *N*-acetyl-D-glucosamine and glucuronic acid that is linked by a β-1,4-glycosidic bond, and the disaccharides are, in turn, linked by β-1,3-bonds to from a high-molecular-weight HA chain.[18] HA belongs to a group of polysaccharides found in the ECM of connective tissues of humans; hence, terms such as *connective tissue polysaccharides*, *mucopolysaccharides*, and *glycosaminoglycans* have been coined to represent the polymers in this group.[19] The functions of HA as an ECM component are plenty, with the most important ones as supporting frameworks for the attachment of cells and as a mediator for promoting cellular mobility, proliferation, and differentiation.[20] Because of its chemical specificity and long-chain nature, HA provides specific binding sites for numerous proteins, proteoglycans, and other biomolecules, such as growth factors.[8] Moreover, it is a major lubricating material found between bone joints.[21] On the basis of these reasons, the blending of HA with another biopolymer is a means of developing scaffolds with superior properties to those of the precursor materials.[14,22–24]

Gel is a natural biopolymer, prepared by the partial hydrolysis of collagens, the most abundant structural proteins found in various parts of animal and human tissues. Depending on the method by which the collagens are pretreated, two types of Gel can be produced.[25,26] Acidic treatment is appropriate for the un-fully-crosslinked collagens found in porcine or fish skins (i.e., type A Gel), whereas alkaline treatment is suitable for the more fully crosslinked collagens found in bovine hides (i.e., type B Gel). The resulting Gel products are different in both their molar mass and electrical properties from the ones obtained from the alkaline treatment, which possess a greater proportion of carboxyl groups, which render them negatively charged and lower their isoelectric points compared to those obtained from the acidic treatment.[25] Structurally, Gel is a heterogeneous mixture of single- or multiple-stranded polypeptides (and their oligomers), each of which contains about 300–4000 amino acid residues.[25,26] It has been studied extensively in the fields of controlled drug release and tissue engineering. The blending of chitosan, Gel, and HA in a certain proportion enhanced the resistance to enzymatic degradation and promoted fibroblastic migration and proliferation.[27] Similarly, scaffolds made from blends of Gel, chondroitin, and HA supported the differentiation of chondrocytes that had been cultured for 5 weeks particularly well.[28]

Chitin or poly(*N*-acetyl-D-glucosamine) is a high-molecular-weight polysaccharide predominantly found in the exoskeletons of arthropods and the internal flexible backbones of cephalopods. It is nontoxic, odorless, biocompatible with living tissues, and biodegradable.[29] CWs, nanocrystalline entities of chitin, have been successfully prepared from crab shells,[30] squid pens,[31] and tubes of *Riftia pachyptila* tube worms.[32] The commonly used hydrolytic condition for obtaining CWs is 3*N* hydrochloric acid (HCl) at boiling for 90 min under vigorous stirring.[30,32] CWs have been shown to be an effective reinforcing filler for many types of polymer matrices.[31–34] Nanocomposite films of poly(vinyl alcohol)/CWs and chitosan/CWs with or without heat treatment have been successfully prepared and reported.[33,34] The CW content ranged between 0 and 29.6% (by weight of the matrix materials). The tensile strengths of the nanocomposite films were found to increase compared to those of the corresponding neat films, with an initial increase in the CW content either leveling off or reaching a maximum value at a CW content of about 2.96%.[33,34] On the other hand, significant improvements were observed in the shear modulus of a CW-reinforced copolymer of styrene and butyl acrylate[31] and in the Young's modulus of CW-reinforced polycaprolactone.[32]

EXPERIMENTAL

Materials

Chitin powder (crab shells, α form, weight-average molecular weight = 4×10^5 g/mol) was purchased from Fluka (St. Gallen, Switzerland). Gel (porcine skin, type A, 170–180 bloom) was purchased form Fluka. HA (weight-average molecular weight = 1.4×10^6 g/mol) was purchased from Coach Industries (Osaka, Japan). 1-Ethyl-3-(3-dimethylaminopropyl)carbodiimide (EDC) was purchased form Fluka. HCl [37% (w/w), analytical-reagent grade] was purchased from Labscan Asia (Bangkok, Thailand). All other chemicals were analytical-reagent grade and were used without further purification.

Preparation of the CWs

CWs were prepared by the acid hydrolysis of chitin powder with 3*N* HCl at 120°C for 6 h under vigorous stirring and refluxing. The ratio of HCl to chitin powder was 30 mL/g. After acid hydrolysis, the obtained CW suspensions were diluted with distilled water and were then centrifuged at 10000 rpm for 5 min and decanted in triplicate. The suspensions were then transferred to dialysis bags and dialyzed in running water for 2 h and later in distilled water for 2 days. The dispersion of CWs was completed by a 5-min ultrasonification treatment for every 40 mL aliquot. The solid fraction of the as-prepared CW

suspensions was gravimetrically determined to be 1.43 wt % on average. The CW suspensions were stored at 4°C before further use.

Preparation of the neat HA–Gel scaffolds and the CW-reinforced HA–Gel scaffolds

An equal mass of HA and Gel powder was first mixed and dissolved in deionized (DI) water at 50°C to obtain a blend solution of the polymers (i.e., HA–Gel) at a fixed concentration of 2 wt %. The blend solution was left to cool to room temperature before various amounts of the as-prepared CW suspensions were added to the solution. The six different mass ratios between the CWs and HA–Gel were 0, 2, 5, 10, 20, and 30% (w/w). The mixtures were continuously stirred until they were fully homogenized. To crosslink HA–Gel, 1 mmol of EDC was added, and the mixtures were further stirred for 2 h at room temperature. Volumes of the mixtures were poured into polypropylene dishes to obtain molding specimens of two different shapes and dimensions (i.e., cylindrical and disc shapes), frozen at −40°C for 24 h, and lyophilized at −50°C for another 24 h. The obtained cylindrical scaffolds were about 10 mm in diameter and 2 mm in height, whereas the disc-shaped scaffolds were about 1 mm in thickness; these were later cut into a desired shape and size for the mechanical property assessment. The as-prepared scaffold specimens were kept in a desiccator before further use.

Characterization

Microstructure observation and pore size determination

One cylindrical scaffold was randomly selected from each group of the scaffolds. It was cut into pieces along both the longitudinal and the transverse directions. The cut pieces were mounted on copper stubs, coated with gold with a JEOL JFC-1100 sputtering device (Tokyo, Japan) and observed for their microscopic structure with a JEOL JSM-5200 scanning electron microscope. To determine the dimensions of the pores, 50 pores for each of the cross sections and the longitudinal sections (i.e., 100 pores in total) were directly measured from the scanning electron microscopy (SEM) images with The University of Texas Health Science Center at San Antonio (UTHSCSA) Image Tool version 3.0 software. The average values for all of the specimens investigated were calculated and reported.

Mechanical properties

For the tensile mechanical integrity, specimens ($50 \times 5 \times 1$ mm^3) were cut from the disc-shaped scaffolds. The mechanical integrity of the specimens, measured in their dry state, in terms of the tensile strength, Young's modulus, and elongation at break was assessed with a Lloyd LRX-Plus universal testing machine (West Sussex, UK) with a 10-N load cell at room temperature (26 ± 2°C). The gauge length was 30 mm, and the crosshead speed was 10 mm/min. The measurements were carried out in pentuplicate for each group of the scaffolds.

Water-retention capacity

Cylindrical scaffolds, in their dry state, were weighed and then individually immersed in DI water at room temperature. At a given time point, the specimens were taken out, blotted on a glass plate, which was set at about 45° from a horizontal baseline for 5 s to remove excessive water, and immediately weighed. The amount of water retained in the specimens was determined according to the following equation:

$$\text{Water retention}(\%) = [(W_w - W_d)/W_w] \times 100; \quad (1)$$

where W_d and W_w are the weights of the specimens before and after submersion in the water, respectively. The measurements for each group of the scaffolds were carried out in pentuplicate at different time intervals within a period of 24 h.

In vitro degradation

The *in vitro* degradation study of the scaffolds was carried under three conditions. In the first, cylindrical scaffolds were individually immersed in a 10 m*M* phosphate buffer saline (PBS) solution (pH 7.4) at room temperature without shaking for 24 h. Under the other two conditions, they were individually immersed in either PBS or bacterial collagenase at a concentration of 373 ng/mL at 37°C under shaking (70 rpm) for 24 h. After the specified time, the specimens were removed from the media, frozen at −40°C for 24 h, and lyophilized at −50°C for another 24 h. The degradability of the specimens was then quantified according to the following equation:

$$\text{Degradability}(\%) = W_t/W_i \times 100; \quad (2)$$

where W_i is the initial dry weight of the specimens and W_t is the dry weight of the specimens after each respective *in vitro* degradation assay. The measurements for each group of the scaffolds were carried out in triplicate.

Infrared (IR) spectroscopy and thermal analyses

A Thermo Nicolet Nexus 670 Fourier transform infrared (FTIR) spectrophotometer (Madison, WI)

was used to investigate the chemical functionalities of the as-prepared scaffolds by the KBr disk method. One cylindrical scaffold was randomly selected from each group of scaffolds and subsequently subjected to FTIR scanning over 32 scans at a resolution of 4 cm^{-1}. The thermal stability of the selected cylindrical scaffold specimens was assessed in terms of their degradation temperature with a PerkinElmer TGA-7 thermogravimetric analyzer (Waltham, MA) over a temperature range of 30–600°C at a heating rate of 10°C/min under a nitrogen atmosphere. The weights of the specimens ranged between 3 and 5 mg. A PerkinElmer DSC-7 differential scanning calorimeter (Waltham, MA) was used to determine the glass-transition temperature (T_g) of the scaffold specimens over a temperature range of 25–80°C at a heating rate of 10°C/min. The specimens, weighing around 5–6 mg, were subjected to a preheating run to erase their thermal history before the test.

Biological evaluation

Cell culture

Human osteosarcoma cells (SaOS-2) were cultured as a monolayer in α-minimum essential medium (α-MEM; Sigma–Aldrich, St. Louis, MO), supplemented by 10% fetal bovine serum (Biochrom, Cambridge, UK), 1% L-glutamine (Invitrogen, Carlsbad, CA), and a 1% antibiotic and antimycotic formulation containing penicillin G sodium, streptomycin sulfate, and amphotericin B (Invitrogen). The cells were maintained at 37°C in a 95% humidified atmosphere containing 5% CO_2 and passaged once every 3–4 days.

Cytotoxicity evaluation

Only the cylindrical scaffolds containing 0 and 30% CWs were used in these studies. The cytotoxicity of the scaffolds was evaluated by the indirect method with SaOS-2 as the reference cells. First, the extraction media were prepared by immersion of the scaffold specimens in 500 μL of serum-free medium (SFM; containing MEM, 1% L-glutamine, 1% lactabumin, and a 1% antibiotic and antimycotic formulation) for 24 h. Each of these extraction media was later used in the indirect cytotoxicity evaluation. SaOS-2 were cultured in wells of a 24-well culture plate at 4×10^4 cells/well in serum-containing MEM for 16 h to allow attachment of the cells to the plate. The cells were then starved with SFM for 24 h, after which time, the medium was replaced with an extraction medium. After 24 h of cell culturing in the extraction medium, a 3-(4,5-dimethylthiazol-2-yl)-2,5-diphenyl tetrazolium bromide (MTT) assay (see details in the Supporting Information) was carried out to determine the viability of the cells. The experiment was carried out in quadruplicate.

Cell attachment and cell proliferation

A primary evaluation for cell attachment was carried out by a direct morphological observation of SaOS-2 cells that had been seeded on the surface of the scaffold specimens. Only the cylindrical scaffolds containing 30% CWs were used in the study. Specifically, the cylindrical scaffold specimens were put in wells of a 24-well culture plate and sterilized with 1 mL of 70% ethanol for 30 min. They were then washed with sterilized DI water twice and later immersed in α-MEM overnight. SaOS-2 cells were then seeded on the surfaces of the specimens at 4×10^4 cells/specimen in a minimum volume of the culture medium and were allowed to attach on the surfaces for 3 h before the addition of 1.5 mL/well of the culture medium. The cells were cultivated at 37°C in a humidified atmosphere containing 5% CO_2 for 1 and 7 days, after which time, the morphology of the cultured cells was observed by SEM. After the removal of the culture medium, the cell-cultured scaffold specimens were rinsed with PBS twice, and the cells were fixed with a 3% glutaraldehyde solution, which was diluted from a 50% glutaraldehyde solution (Electron Microscopy Science, Hatfield, PA) with PBS for 30 min. The specimens were then dehydrated in graded ethanolic solutions (i.e., 30, 50, 70, and 90%) and in pure ethanol for about 2 min each. They were further dried in 100% hexamethyldisilazane (Sigma-Aldrich) for 5 min, dried in air after the removal of hexamethyldisilazane, mounted on SEM stubs, coated with gold, and finally, observed by SEM. The examinations were performed on three randomly selected scaffold specimens.

To quantify the viability of the attached and the proliferated cells, SaOS-2 cells had first been seeded or cultured on each of the four randomly selected specimens from each group of the scaffolds for 1, 24, 48, and 72 h before they were evaluated by the MTT assay at each time point. Only the cylindrical scaffolds were used in this study.

Statistical analysis

Data were analyzed with SPSS software version 14.0 for Windows (SPSS, Chicago, IL). Initially, the normal distribution was assessed by the Shapiro–Wilk test. The normal distribution data, representing the homogeneity of the variances, shown by the Levene's test, were then investigated by a one-way analysis of variance (ANOVA) with the Tukey HSD *post hoc* multiple comparisons. Otherwise, the Dunnett T3 was applied if the data did not exhibit the homogeneity of the variances. For the data of which the

normal distribution was absent but the variance was homogeneous, the Kruskal–Wallis H was applied. To compare the means between two data groups, the Student unpaired t test was used. The significant level was indicated at $p < 0.05$ in any case.

RESULTS AND DISCUSSION

Characterization of the CWs

The dialyzed CWs exhibited colloidal behavior in water. Protonation of the amino groups of chitin under acidic conditions induced positive charges (NH_3^+) on the surface of the CWs, which generated electrostatic repulsion among the nanocrystallites.[30] However, protonation of amino groups was not complete on all of the CW particles; hence, the hydrogen bonding associated with the free amino groups on the CWs caused them to aggregate. The representative TEM image of the as-prepared CWs, which were prepared from a dilute suspension, is illustrated in Figure 1. It was evident that the CWs were present as individual and partially aggregated entities. The aggregation of the CWs was facilitated by the increase in the pH of the suspension during dialysis, hence, the deprotonation of some of the protonated amino groups that occurred during the acid hydrolysis to prepare the CWs. According to the TEM results, the as-prepared CWs were present as slender rods with sharp points on both ends. The lengths (L's) and widths (d's) of these rods were 255 ± 56 and 31 ± 6 nm, respectively, with an L/d ratio of about 8. The histograms illustrating the distribution of the lengths and the widths of the as-prepared CWs, as shown in the Supporting Information, indicated that over 50% of the CWs exhibited lengths and the widths in the range 203–277 and 27–35 nm, respectively. These dimensions compared well with the reported values for CWs obtained from crab shells (L = 50–300 nm and d = 6–8 nm,[30] L = 100–600 nm and d = 4–40 nm,[35] and L = 100–650 nm and d = 10–80 nm[36]).

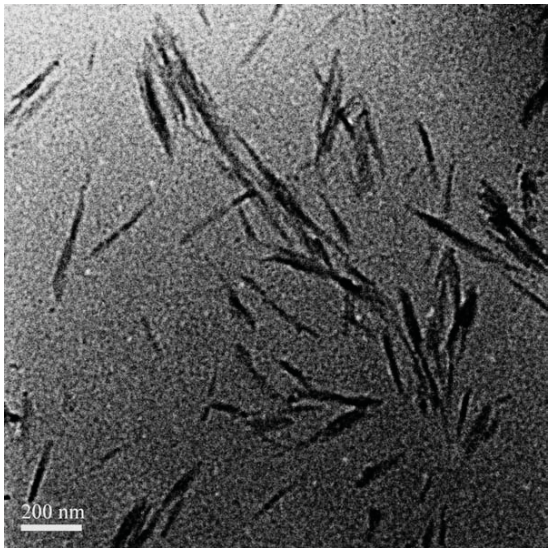


Figure 1 Representative TEM image of CWs prepared from a diluted suspension of acid-hydrolyzed chitin powder from crab shells.

Characterization of the CW-reinforced HA–Gel scaffolds

Physical characteristics

Representative photographic images of the as-prepared cylindrical scaffolds are shown in the Supporting Information. These scaffolds were extremely light in weight because of their highly porous nature. The color of these scaffolds ranged from the pure white of the neat HA–Gel scaffolds to the light brown of the 30% (w/w) CW-reinforced HA–Gel scaffolds. The brown color resulted from the presence of the CWs dispersing within the mass of the scaffolds. Representative SEM images illustrating the microstructure of the as-prepared scaffolds viewed on the surface perpendicular to the transverse direction (i.e., the surface of the transverse sections) are shown in Figure 2, whereas those illustrating the microstructure of the scaffolds viewed on the surface perpendicular to the longitudinal direction (i.e., the surface of the longitudinal sections) are shown in the Supporting Information. All of the scaffolds exhibited a well-defined porous structure, and regardless of the surface under consideration, the interpore connectivity was discernible throughout the bulk of the scaffolds. For a given group of the scaffolds, no significant difference in terms of the morphology of the pore structure was observed between the two sections. This was in exception to the one that contained 30% CWs, which showed a disruption in its microstructure when viewed on the surface of the longitudinal sections. The dimensions of the pores observed in these SEM images were determined and analyzed and are reported in Table I.

The size of the pores for all of the scaffolds in both the transverse and the longitudinal sections ranged between 92 and 230 μm, with the average value ranging between 139 and 166 μm. An increase in the content of the CWs did not have a significant effect on the pore dimensions. A comparison of the pore dimensions that were observed in the two sections for each group of the scaffolds was evaluated statistically, and there was no difference, except for those observed for the neat HA–Gel sample group. With an average pore size smaller than 200 μm, the transportation of nutrients and oxygen and the ingrowth of new blood vessels into the inner pores of the scaffolds were somewhat restricted. The lack of

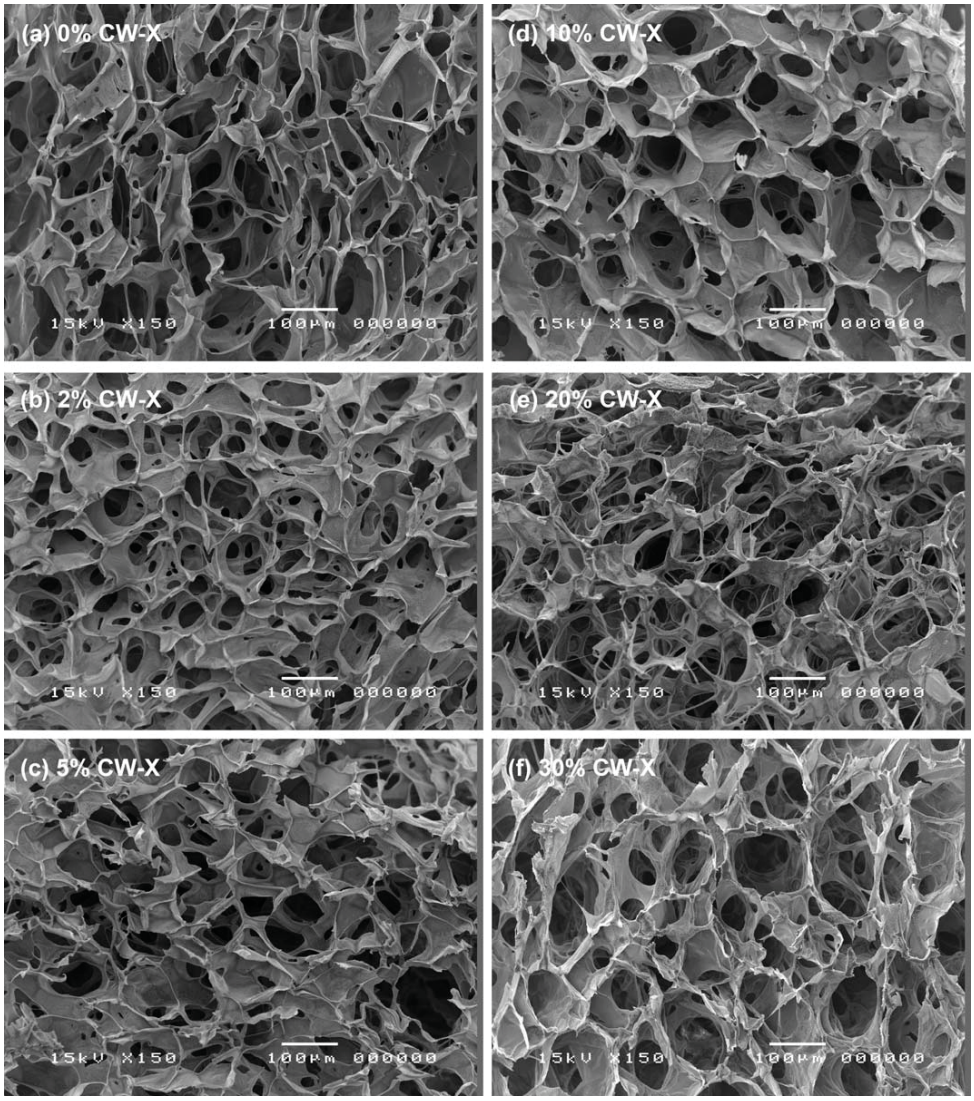


Figure 2 Representative SEM images illustrating the microstructures of the (a) neat HA–Gel scaffolds and CW-reinforced HA–Gel scaffolds containing (b) 2, (c) 5, (d) 10, (e) 20, and (f) 30% (w/w) CWs (viewed on surfaces perpendicular to the longitudinal direction, i.e., transverse surfaces).

TABLE I
Dimensions of the Pores of the Neat HA–Gel Scaffolds and the CW-Reinforced HA–Gel Scaffolds Observed on the Surfaces of Both Transverse and Longitudinal Sections

	Pore size (μm)			
	Transverse sections		Longitudinal sections	
Specimen	Range (Minimum − Maximum)	Average (Mean ± Standard deviation)	Range (Minimum − Maximum)	Average (Mean ± Standard deviation)
0% CW	92.3–208.8	140.9 ± 21.8^{a}	112.8–231.4	165.8 ± 27.7^{a}
2% CW	114.4–182.0	139.4 ± 16.0^{b}	108.4–182.1	145.4 ± 15.3^{b}
5% CW	104.1–224.5	153.2 ± 23.9^{c}	110.6–171.1	142.7 ± 13.8^{c}
10% CW	118.0–202.3	158.9 ± 19.1^{d}	104.3–205.4	162.8 ± 23.6^{d}
20% CW	113.5–200.5	151.4 ± 19.3^{e}	105.8–181.0	143.9 ± 17.2^{e}
30% CW	108.5–184.4	155.4 ± 15.7^{f}	97.2–231.3	149.0 ± 25.1^{f}

Superscript letters indicate comparisons only between sections of a given group of specimens at $p < 0.05$ (one-way ANOVA with Tukey HSD, $n = 50$).

TABLE II
Mechanical Properties of the Neat HA–Gel Scaffolds and the CW-Reinforced HA–Gel Scaffolds

Specimen	Modulus of elasticity (MPa)	Elongation at break (%)	Tensile strength (MPa)
0% CW	0.99 ± 0.10[a]	53.48 ± 10.69[a]	0.52 ± 0.06[a]
2% CW	14.10 ± 2.23[b]	28.35 ± 6.16[b]	1.03 ± 0.09[b]
5% CW	19.96 ± 3.64[b]	06.36 ± 1.42[c]	0.53 ± 0.15[a,c]
10% CW	12.46 ± 2.00[b]	11.63 ± 4.15[c,d]	0.48 ± 0.19[a,c]
20% CW	07.10 ± 0.93[c]	16.07 ± 0.96[b,d]	0.47 ± 0.06[a]
30% CW	11.96 ± 0.47[b]	16.03 ± 3.40[b,d]	0.72 ± 0.08[c]

Superscript letters indicate comparisons between groups of specimens for a single property at $p < 0.05$ (one-way ANOVA with Dunnett T3, $n = 5$).

ample oxygen supply leads to a medical condition known as *hypoxia*, which is suitable for the regeneration of cartilage but certainly not bone.[37,38] To obtain scaffolds with larger pore dimensions, the cooling rate associated with the freezing of the HA–Gel solution or the HA–Gel/CWs suspensions before the subsequent sublimation of the ice crystals needs to be decreased further because it is a known fact that a fast cooling rate induces the formation of tiny ice crystals, hence, the small pore dimensions.[39,40]

Mechanical properties

Mechanical properties, expressed in terms of the modulus of elasticity, elongation at break, and tensile strength, of the as-prepared scaffolds were evaluated, and the results are summarized in Table II. Statistical analysis indicated that inclusion of the CWs in amounts of 2–30% in the HA–Gel scaffolds resulted in a significant increase in the modulus of elasticity from that of the neat scaffolds. Nevertheless, the property values among the various groups of the CW-reinforced HA–Gel scaffolds were not statistically different, except for the one containing 20% CWs, which showed significantly lower values. For the elongation at break, the neat HA–Gel scaffolds exhibited significantly greater values over all of the reinforced samples, which statistically showed equivalent values among themselves. With regard to the tensile strength, it was obvious that the HA–Gel scaffolds that contained 2% CWs exhibited the property values that were significantly greater than those of the other groups of samples, which, among themselves, showed equivalent values. The result agreed well with the report of Sriupayo et al.,[34] who found that the greatest tensile strength of CW-reinforced chitosan films was observed at a CW content of 2.96% and an increase in the CW content resulted in a reduction in the property values. To put it into perspective, the modulus of elasticity and the tensile strength values of the scaffolds containing 2% CWs were much lower than those of bone, which are 16.4 GPa and 117.4 MPa, respectively, on average.[41]

Water absorption and *in vitro* degradability

The ability of the neat and CW-reinforced HA–Gel scaffolds to absorb water at room temperature within 24 h is graphically shown in Figure 3. All groups of the scaffolds demonstrated comparable water absorption within the first 60 min, which accounted for more than about 95% of their total wet weights. The values were as high as that of a superabsorbent.[42] The results were similar to those reported by Park et al.[43] on collagen–HA sponges. Such a great tendency to absorb a great amount of water is characteristic of a hydrogel material, such as HA and Gel, which are very hydrophilic in nature.[9] With the absorbed water, the interior of a scaffold becomes a hydrated environment, which facilitates the process of tissue regeneration by protecting cells and their products, such as secreted ECM. Furthermore, the hydrated environment facilitates the transportation of nutrients into and wastes out of the cells.[24] According to Figure 3, all groups of the scaffolds exhibited similar water absorption values and equivalent profiles; that is, the property values decreased gradually with increasing submersion time. The absorption of water in a given group of the scaffolds reached a maximum only after having been submerged in DI water for 15 min, and the inclusion of the CWs within the scaffolds did not strongly influence the water absorption. This was due to the inherent hydrophilicity of all of the compositions, the interconnectivity of the pore structures, and the similarity in the pore dimensions of all of the scaffolds, which facilitated the capillary

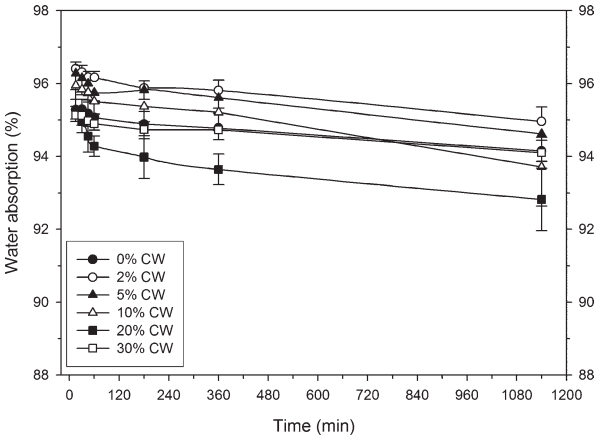


Figure 3 Ability of the neat HA–Gel scaffolds and the CW-reinforced HA–Gel scaffolds to absorb DI water (shown as the amount of water absorbed) at room temperature as a function of the submersion time.

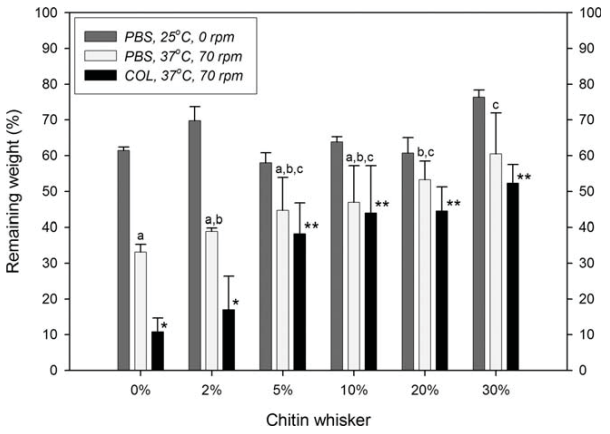


Figure 4 Degradability of the neat HA–Gel scaffolds and the CW-reinforced HA–Gel scaffolds (shown as the remaining weights of the scaffolds) in a PBS solution under static conditions (at 25°C without agitation) or dynamic conditions (at 37°C with agitation at 70 rpm) and in an aqueous solution of collagenase (COL) (at 37°C with agitation at 70 rpm) as a function of the CW content for the total observation period of 24 h. $^{a,b,c,*}p < 0.05$ (one-way ANOVA with Tukey HSD, $n = 4$).

action and, hence, the rapid adsorption of water.[42] The observed decrease in the amounts of water absorbed as the immersion time increased might have been due to the fact that the scaffolds began to disintegrate or partially dissolve, which diminished their capacity to imbibe both free and bound water.[24,43]

Despite the many benefits of the high water absorption of a scaffold, certain drawbacks should also be considered, such as weakening and acceleration due the to degradation of the scaffold.[24] The degradation of a scaffold occurs mainly by either a physical or chemical pathway. The physical pathway involves dissolution and hydrolysis, whereas the chemical pathway involves enzymatic cleavage in the presence of a suitable enzyme.[9] Here, we investigated the dissolution and hydrolytic degradation of the scaffolds in PBS over a submersion period of 24 h under both static conditions at room temperature and dynamic conditions, that is, by means of a shaking water bath at 70 rpm and 37°C. The enzymatic degradation of the scaffolds was also investigated in 373 ng/mL of bacterial collagenase, which represented a model concentration of tissue collagenase in the synovial fluid of the patients with osteoarthritis.[44,45] The investigation was carried out in the shaking water bath at 70 rpm and 37°C for 24 h. The results of these studies are graphically shown in Figure 4.

Figure 4 shows the remaining weights of the scaffolds after submersion in PBS or collagenase (COL) solution for 24 h. Upon submersion in PBS under the static conditions at room temperature, the remaining weights of the scaffolds were about 58–76% of their original dry weights, with no significant difference among all groups of the scaffolds. Under the dynamic conditions, on the other hand, the remaining weights, for a given group of the scaffolds, were significantly lower than those observed under the static conditions. The enhancement in the weight loss was obviously due to the added energy from the agitation, which increased the kinetic energy of the system. In addition, the thermal degradation of the HA molecules could occur to a certain extent at 37°C.[18] These could have been factors contributing to the observed values of the remaining weights of the scaffolds at 33–60% of the original dry weights of the scaffolds. The incorporation of CWs in the amounts of 20–30% in the HA–Gel scaffolds enhanced the resistance to degradation under the dynamic conditions compared with the neat scaffolds. Although a trend was observed for the relationship between the remaining weights of the scaffolds and the CW content, statistical analysis among the scaffolds that contained 5–30% CWs did not show a significant difference in their property values.

In the collagenase medium, the degradation of the scaffolds was noticeably enhanced as the remaining weights, for a given group of the scaffolds, were the lowest. Regardless of the CW content, the values were in the range 11–52% of the original dry weights of the scaffolds. In addition to the agitation and the hypothetical thermal degradation of HA, the scission of Gel peptide bonds at glycine subunits by the enzyme was the main contributing factor.[43] The presence of the CWs at levels of 5% or more significantly enhanced the stability to degradation of the scaffolds in the presence of the enzyme. Such an enhancement could have been due to the interaction between the CWs and the HA–Gel matrix molecules, which reduced the enzyme accessibility.[46]

IR spectroscopy analysis

Figure 5 illustrates FTIR spectra of the neat and CW-reinforced HA–Gel scaffolds over the wave-number range 3500–500 cm^{-1}. Those of the constituting materials are also shown for comparison. The absorption peaks at 1656, 1547, 1450, and 1237 cm^{-1}, characteristic of amide bonds (CO—NH), were observed in the spectrum of Gel,[43,47,48] whereas those at 1412 and 1076 cm^{-1}, corresponding to carboxylate salts (symmetric stretching) and ester bonds, respectively, were observed in the spectrum of HA, of which repeating units comprised glucuronic acid and acetylglucosamine. The spectrum of the CWs should have been similar to that of HA because both of them were polysaccharides. Being crystalline entities, however, the CWs presented sharper and more intense signals at certain positions,[49] particularly at 1076 (ester bonds), 1378

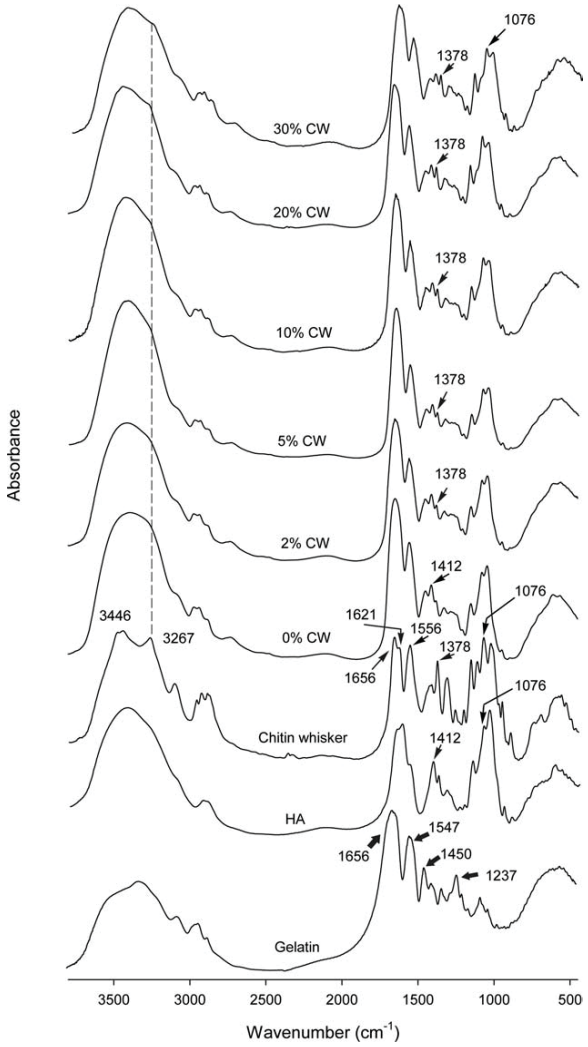


Figure 5 IR spectra of the Gel, HA, CWs, and corresponding scaffolds.

(carboxylate salts), and 3267 and 3446 cm^{-1} (hydroxyl groups).[48] Additionally, the CWs exhibited characteristic amide I peaks at 1621 and 1656 cm^{-1} and the amide II peak at 1556 cm^{-1}.[35,47] The peak at 1621 cm^{-1} was only specific to CWs, whereas that at 1656 cm^{-1}, representing the stretching of hydrogen bonds between carbonyl groups and the neighboring amine groups of intrachains, could also be found for the amide bonds of a protein.[49]

For the neat HA–Gel scaffolds, the peaks at 1650, 1550, 1412, and 1076 cm^{-1} were discernible. Crosslinking with EDC generated both the amide and the ester linkages in the structure of the blends.[50] The amide bonds were formed between the carboxyl groups of Gel and/or of the glucuronic acid in HA and the amino groups of Gel. The ester bonds, on the other hand, were formed between the carboxyl

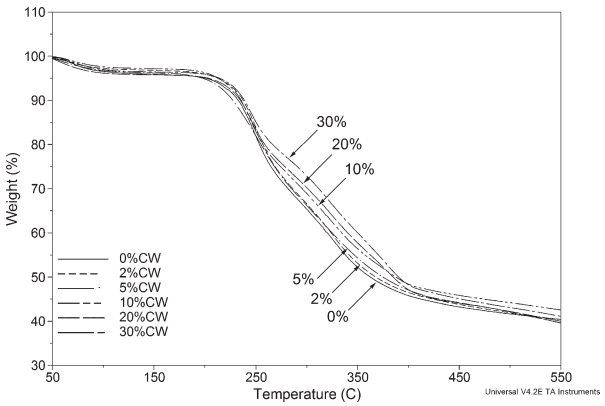


Figure 6 Thermogravimetric analysis thermograms (10°C/min in a nitrogen atmosphere) of the neat HA–Gel scaffolds and the CW-reinforced HA–Gel scaffolds.

groups and the hydroxyl groups of Gel and/or of HA.[51,52] For the scaffolds that contained CWs, the presence of the CWs were confirmed by the presence of characteristic peaks at 1378 and 1076 cm^{-1} and the absorption shoulder at 3267 cm^{-1}, and the intensities of these peaks and the shoulder were found to increase with an increase in the content of the CWs.

Thermal characteristics

Figure 6 shows thermogravimetric analysis thermograms of the as-prepared scaffolds. All samples exhibited similar profiles of weight change. Table III summarizes the values of the temperatures at which the losses in the weight of the scaffolds reached 5, 25, and 50% (on the basis of their original weights). Apparently, at temperatures lower than 200°C, the loss in the weight of all of the scaffolds, except for the ones containing 5% CWs, was less than 5%, with no particular relationship with the CW content. At temperatures around 210–230°C, the loss in the weight increased abruptly to reach maximum values at temperatures around 245–250°C, as indicated by the positions of the peaks of the corresponding

TABLE III
Temperatures at Which 5, 25, and 50% Mass Losses Were Reached (T-5%, T-25%, and T-50%, respectively) for the Neat HA–Gel scaffolds and the CW-Reinforced HA–Gel Scaffolds and Residual Weights at 550°C

Specimen	T-5% (°C)	T-25% (°C)	T-50% (°C)	Residue at 550°C (wt %)
0% CW	200.6	264.9	362.6	40.4
2% CW	212.6	269.0	368.0	39.6
5% CW	194.4	268.4	375.0	39.6
10% CW	213.3	274.2	387.8	42.5
20% CW	203.3	278.5	385.0	40.0
30% CW	214.4	290.7	390.5	41.1

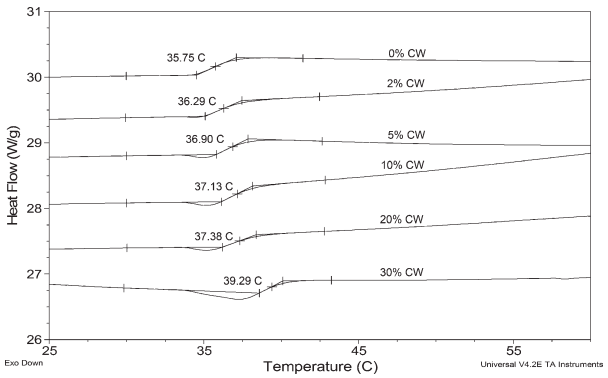


Figure 7 Differential scanning calorimetry thermograms (10°C/min in a nitrogen atmosphere) of the neat HA–Gel scaffolds and the CW-reinforced HA–Gel scaffolds. Their T_g's are illustrated.

derivative curves (not shown). As the temperatures increased to around 260–360°C, the loss in the weight of the different groups of the scaffolds became most noticeably different and inversely related to the CW content within the scaffolds. Careful consideration of the results revealed that the temperatures required for the scaffolds that contained 10–30% CWs to reach 25 and 50% of the weight loss were significantly greater than those of the neat scaffolds and the ones containing 2 and 5% CWs. This demonstrated that reinforcing the scaffolds with 10–30% CWs enhanced the thermal stability of the resulting scaffolds. Notwithstanding, such enhancement was only reflected in a limited temperature range, that is, 260–360°C, as the residual weights of all of the scaffolds at 550°C were comparable.

Figure 7 shows the differential scanning calorimetry thermograms of the as-prepared scaffolds. The range of the temperature was chosen such that it revealed the glass transitions of the materials. Apparently, the neat HA–Gel scaffolds exhibited the T_g at about 35.8°C. With the addition and increasing amount of the CWs, T_g was found to increase from that of the neat materials to 36.3°C at 2% CWs and finally to 39.3°C at 30% CWs. With the T_g values of the HA–Gel scaffolds that contained 5–30% CWs in the range 36.9–39.3°C, the enhancement in the resistance to biodegradation of the corresponding scaffolds by collagenase, as previously shown, could have been, at least partly, due to the observed increase in the T_g values from that of the neat materials. The increased T_g values that were close to or greater than the physiological temperature of 37°C should have resulted in less mobility of the matrix molecules and, thus, the lower tendency for conformational change. However, because the T_g values of these scaffolds were measured in their dry state, the actual values in the physiological environment (i.e., wet conditions) should be much less because of the plasticizing effect from absorbed water molecules. Nevertheless, the marked increase in the T_g values for the scaffolds that contained 5–30% CWs coincided with the observed improvement in the resistance to enzymatic degradation of these scaffolds.

Cytotoxicity and *in vitro* response of bone cells

We first investigated the cytotoxicity of the as-prepared scaffolds. The assessment was carried out on the basis of the indirect cytotoxicity assay, in which the extraction media from the neat and the 30% CW-reinforced HA–Gel scaffolds were used to incubate SaOS-2 osteosarcoma cells for 24 h. The viability of the cells, determined spectrophotometrically at 570 nm, was compared with that of the cells that had been incubated with SFM for the same period of time. The results are shown in Table IV. Evidently, the viability of the cells that were cultured with either the extraction media from the neat scaffolds or the SFM was statistically the same, a result indicating that the neat HA–Gel scaffolds were biocompatible with the bone cells. Nevertheless, the viability of the cells decreased significantly when they were cultured with the extraction media form the scaffolds that contained 30% CWs. This result suggests that the presence of the CWs (at 30%) had an adverse effect on cell viability. Further evaluation by the direct culturing of the cells onto the scaffolds was then carried out to confirm whether they were toxic to the cells.

Figure 8 shows representative SEM images in various magnifications of SaOS-2 cells that were cultured on the surfaces of the 30% CW-reinforced HA–Gel scaffolds for 1 or 7 days. On day 1, the cells attached well to the surfaces of the scaffolds. The majority of the cells exhibited evidence of cytoplasmic process in the form of filopodia over the

TABLE IV
Indirect Cytotoxicity Evaluation of the Neat HA–Gel Scaffolds and the 30% CW-Reinforced HA–Gel Scaffolds on the Basis of the Viability of Human Osteosarcoma Cells (SaOS-2)

	Absorbance at 570 nm		
Sample	Control	0% CW	30% CW
1	0.575	0.524	0.465
2	0.508	0.536	0.410
3	0.537	0.487	0.409
4	0.540	0.569	0.428
Average	0.540 ± 0.027	0.529 ± 0.034	0.428 ± 0.026*

* At $p < 0.05$ (one-way ANOVA with Tukey HSD, $n = 4$).

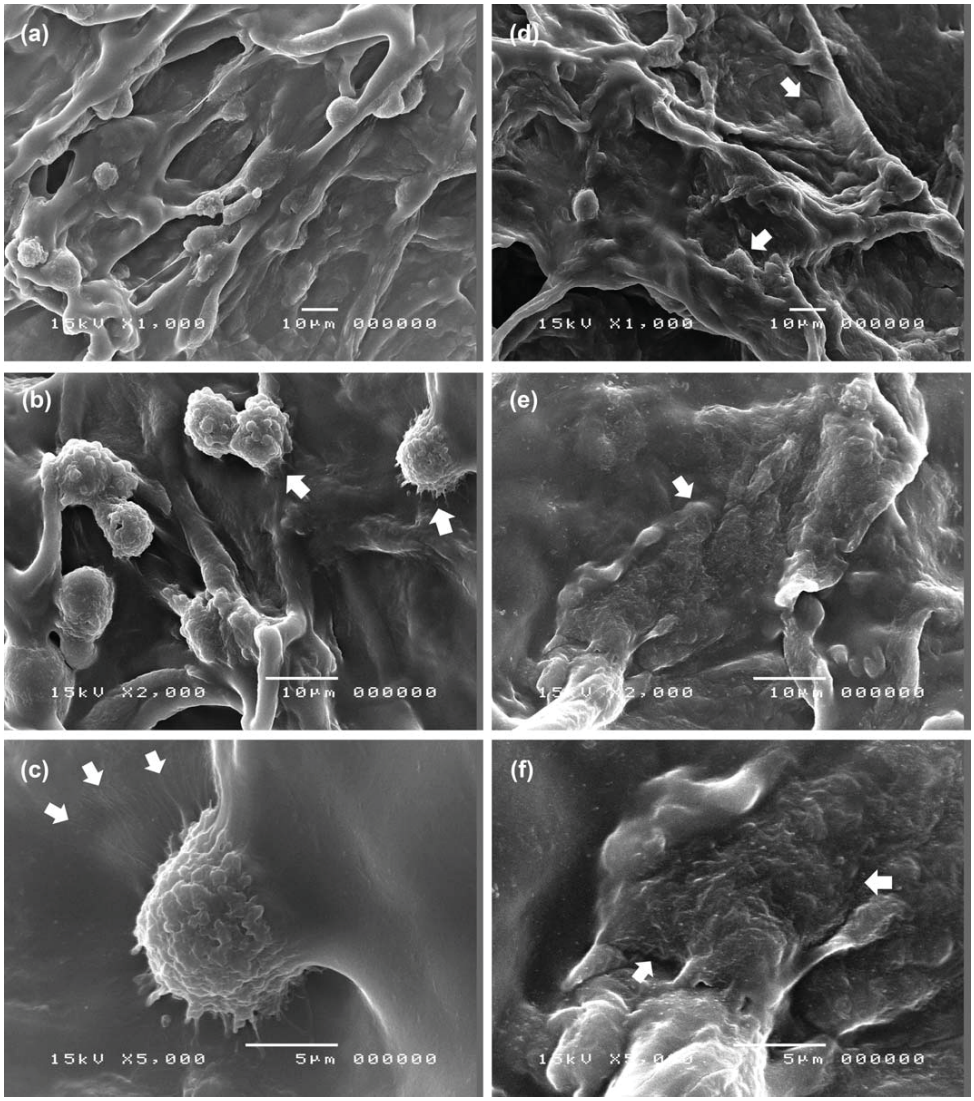


Figure 8 Representative SEM images at different magnifications [(a,d) 1000, (b,e) 2000, and (c,f) 5000×] illustrating the morphology and behavior of SaOS-2 cultured on the surfaces of 30% CW-reinforced HA–Gel scaffolds for (a–c) 1 and (d–f) 7 days. White arrows show (b,c) the cytoplasmic process of the cells and (d–f) cells that fused into the underlying surfaces of the scaffolds.

surfaces [see Fig. 8(b,c), as indicated by arrows]. The observation of cytoplasmic expansion indicated a good initial response of the cells to the as-prepared scaffolds, which influenced the subsequent cellular processes of proliferation and differentiation.[53] On day 7, the morphology of the cells changed from the rather well-defined round shape observed on day 1 to fully expanded and even fused to the underlying surfaces of the scaffolds [see Fig. 8(d–f), as indicated by arrows]. Such an observation confirmed the preference of the cells to the surfaces, as they adhered and spread well over the surfaces. Despite the fact that the indirect cytotoxicity evaluation of the studied scaffolds produced a poor result, the observation of the bone cells that appeared to attach and expanded well over their surfaces indicated the applicability of the scaffolds for bone cell culture.

To investigate the effect of CW content on the proliferation of bone cells, the viability of SaOS-2 cells that were cultured on the neat and CW-reinforced HA–Gel scaffolds for 1, 24, 48, and 72 h was evaluated by the MTT assay. The results are graphically shown in Figure 9. At 1 h after cell seeding, the viability of the adherent cells on the surfaces of the scaffolds was either as good as or better than that on the tissue culture plate. At 24 h after cell culturing, only the cells that had been cultured on the surfaces of the 10% CW-reinforced HA–Gel scaffolds showed viability greater than the other groups of the scaffolds and the tissue culture plate. At 48 and 72 h

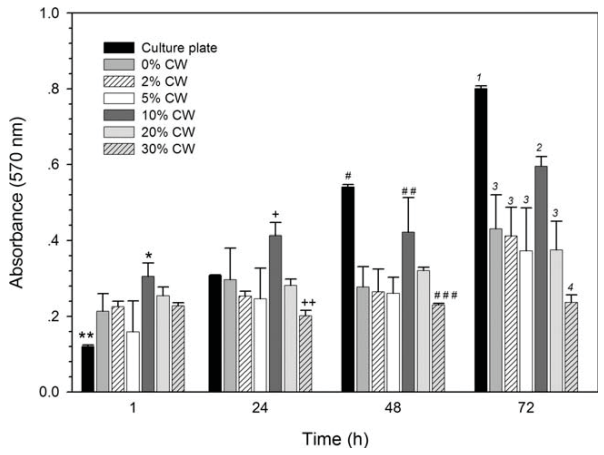


Figure 9 Viability of SaOS-2 cultured on the surfaces of the neat HA–Gel scaffolds and the CW-reinforced HA–Gel scaffolds. $^{*,+,\#,1}p < 0.05$ (one-way ANOVA with Tukey HSD, $n = 4$).

after cell culturing, the viability of the cells on the tissue culture plate was significantly greater than that of those cultured on the surfaces of the scaffolds. Among the various groups of the scaffolds, the ones containing 10% CWs, again, exhibited the greatest viability of the cultured bone cells. It has been suggested that the presence of HA is not always positive in regulating the functions of cells.[54] Liu et al.[27] reported that HA–Gel–chitosan ternary blend films with a weight content of HA of 0.31% significantly promoted the attachment, migration, and proliferation of fibroblasts better than those with weight contents of HA of 1.56 and 3.11%. On the basis of these negative reports, the composition of HA within the scaffolds could be reduced to establish a much better positive environment for cell culture. Notwithstanding, among the various groups of the scaffolds, the ones that contained 10% CWs showed the most promising results for the attachment and proliferation of the bone cells.

CONCLUSIONS

CW-reinforced HA–Gel nanocomposite scaffolds were successfully fabricated by the freeze-drying method. The variation in the amount of the incorporated CWs did not have an obvious effect on the morphology of the internal structure of the scaffolds. Nevertheless, the characteristics of the as-prepared scaffolds could be regulated through the variation in the amount of the incorporated CWs so that the optimal balance among their physicochemical, mechanical, and biological properties could be achieved. A high proportion of incorporated CWs was found to enhance the thermal stability and the resistance to biodegradation, whereas a rather low proportion of the CWs increased the tensile strength and enhanced the biocompatibility in terms of the attachment and proliferation of the cultured human osteosarcoma cells of the resulting scaffolds. Although the scaffolds that contained 10% CWs showed great promise as substrates for bone cell culture, their actual utilization could be limited to a low-stress-bearing area, such as the socket of a dental root.

The authors thank Prasit Pavasant (Faculty of Dentistry, Chulalongkorn University) for access to the cell culture facility and Tanom Bunaprasert (Faculty of Medicine, Chulalongkorn University) for fruitful discussion.

References

1. Rezwan, J. K.; Chen, Q. Z.; Blanker, J. J.; Boccaccini, A. R. Biomaterials 2006, 27, 3413.
2. Griffith, L. G. Acta Mater 2000, 48, 263.
3. Vunjak-Novakovic, G. In Culture of Cells for Tissue Engineering; Vunjak-Novakovic, G.; Freshney, R. I., Eds.; Wiley: Hoboken, NJ, 2006; p 132.
4. Mathew, H. W. T. In Polymeric Biomaterials; Dumitriu, S., Ed.; Marcel Dekker: New York, 2002; p 168.
5. Mercier, N. R.; Costantino, H. R.; Tracyc, M. A.; Bonassar, L. J. Biomaterials 2005, 26, 1945.
6. Wu, L.; Ding, J. Biomaterials 2004, 25, 5821.
7. Wu, C. S.; Liao, H. T. Polymer 2005, 46, 10017.
8. Alberts, B.; Johnson, A.; Lewis, J.; Raff, M.; Roberts, K.; Walter, P. Molecular Biology of the Cell, 4th ed.; Garland Science: New York, 2002.
9. Drury, L. J.; Mooney, D. J. Biomaterials 2003, 24, 4337.
10. Lee, K. Y.; Rowley, J. A.; Eiselt, P.; Moy, E. M.; Bouhadir, K. H.; Mooney, D. J. Macromolecules 2000, 33, 4291.
11. Shu, X. Z.; Liu, Y.; Palumbo, F.; Prestwich, G. D. Biomaterials 2003, 24, 3825.
12. Segura, T.; Anderson, B. C.; Chung, P. H.; Webber, R. E.; Shull, K. R.; Shea, L. D. Biomaterials 2005, 26, 359.
13. Liu, Y.; Shu, X. Z.; Prestwich, G. D. Biomaterials 2005, 26, 4737.
14. Liu, L. S.; Thompson, A. Y.; Heidaran, M. A.; Poser, J. W.; Spiro, R. C. Biomaterials 1999, 20, 1097.
15. Wong, M.; Siegrist, M.; Wang, X.; Hunziker, E. J Orthop Res 2001, 19, 493.
16. Prestwich, G. D.; Marecak, D. M.; Marecek, J. F.; Vercruysse, K. P.; Ziebell, M. R. J Controlled Release 1998, 53, 93.
17. Shu, X. Z.; Liu, Y.; Palumbo, F. S.; Luo, Y.; Prestwich, G. D. Biomaterials 2004, 25, 1339.
18. Lapcik, L. J.; Lapcik, L.; Smedt, S. D.; Demeester, J.; Chabrecek, P. Chem Rev 1998, 98, 2663.
19. Mano, J. F.; Silva, G. A.; Azevedo, H. S.; Malafaya, P. B.; Sousa, R. A.; Silva, S. S.; Boesel, L. F.; Oliveira, J. M.; Santos, T. C.; Marques, A. P.; Neves, N. M.; Reis, R. L. J R Soc Interface 2007, 4, 999.
20. Kikuchi, T.; Yamada, H.; Fujikawa, K. Osteoarthr Cartil 2001, 9, 351.
21. Mikos, A. G.; Lu, L.; Temenoff, J. S.; Tessmar, J. K. In Biomaterials Science: An Introduction to Materials in Medicine, 2nd ed.; Schoen, F. J.; Lemons, J. E., Eds.; Elsevier: New York, 2004; p 735.
22. Oerther, S.; Payan, E.; Lapicque, F.; Presle, N.; Hubert, P.; Muller, S.; Netter, P.; Lapicque, F. Biochim Biophys Acta Gen Subj 1999, 1426, 185.
23. Oerther, S.; Le Gall, H.; Payan, E.; Lapicque, F.; Presle, N.; Hubert, P.; Dexheimer, J.; Netter, P.; Lapicque, F. Biotechnol Bioeng 1998, 63, 206.

24. Hoffman, A. S. Adv Drug Delivery Rev 2002, 43, 3.
25. Young, S.; Wong, M.; Tabata, Y.; Mikos, A. G. J Controlled Release 2005, 109, 256.
26. Tabata, Y.; Nagano, A.; Muniruzzaman, M.; Ikada, Y. Biomaterials 1998, 19, 1781.
27. Liu, H.; Yin, Y.; Yao, K.; Ma, D.; Cui, L.; Cao, Y. Biomaterials 2004, 25, 3523.
28. Chang, C. H.; Liu, H. C.; Lin, C. C.; Chou, C. H.; Lin, F. H. Biomaterials 2003, 24, 4853.
29. Ravi Kumar, M. N. V. React Funct Polym 2000, 46, 1.
30. Revol, J. F.; Marchessault, R. H. Int J Biol Macromol 1993, 15, 329.
31. Paillet, M.; Dufresne, A. Macromolecules 2001, 34, 6527.
32. Morin, A.; Dufresne, A. Macromolecules 2002, 35, 2190.
33. Sriupayo, J.; Supaphol, P.; Blackwell, J.; Rujiravanit, R. Polymer 2005, 46, 5637.
34. Sriupayo, J.; Supaphol, P.; Blackwell, J.; Rujiravanit, R. Carbohydr Polym 2005, 62, 130.
35. Nair, K. G.; Dufresne, A. Biomacromolecules 2003, 4, 657.
36. Lu, Y.; Weng, L.; Zhang, L. Biomacromolecules 2004, 5, 1046.
37. Boyan, B. D.; Hummert, T. W.; Dean, D. D.; Schwartz, Z. Biomaterials 1996, 17, 137.
38. Karageorgiou, V.; Kaplan, D. Biomaterials 2005, 26, 5474.
39. Kang, H. W.; Tabata, Y.; Ikada, Y. Biomaterials 1999, 20, 1339.
40. Shapiro, L.; Cohen, S. Biomaterials 1997, 18, 583.
41. Currey, J. J Theor Biol 2004, 231, 569.
42. Park, H.; Park, K. In Hydrogels and Biodegradable Polymers for Bioapplications; Ottenbrite, R. M.; Huang, S. J.; Park, K., Eds.; American Chemical Society: Washington, DC, 1994; p 1.
43. Park, S. N.; Park, J. C.; Kim, H. O.; Song, M. J.; Suh, H. Biomaterials 2002, 23, 1205.
44. Maeda, S.; Sawai, T.; Uzuki, M.; Takahashi, Y.; Omoto, H.; Seki, M.; Sakurai, M. Ann Rheum Dis 1995, 54, 970.
45. Holland, T. A.; Tabata, Y.; Mikos, A. G. J Controlled Release 2005, 101, 111.
46. Vizarova, K.; Bakos, D.; Rehakova, M.; Perikova, M.; Panakova, E.; Koller, J. Biomaterials 1995, 16, 1217.
47. Magoshi, J.; Mizuide, M.; Magoshi, Y. J Polym Sci Polym Phys Ed 1979, 17, 515.
48. Coates, J. In Encyclopedia of Analytical Chemistry; Meyers, R. A., Ed.; Wiley: Chichester, England, 2000; p 10815.
49. Rinaudo, M. Prog Polym Sci 2006, 31, 603.
50. Prestwich, G. D. Biomaterials from Chemically-Modified Hyaluronan. http://www.glycoforum.gr.jp/science/hyaluronan/HA18/HA18E.html (accessed Jan 2010).
51. Sannino, A.; Papada, S.; Madaghiele, M.; Maffezzoli, A.; Ambrosio, L.; Nicolais, L. Polymer 2005, 46, 11206.
52. Tomihata, K.; Ikada, Y. J Biomed Mater Res 1997, 37, 243.
53. Anselme, K. Biomaterials 2000, 21, 667.
54. Stern, R.; Asari, A. A.; Sugahara, K. N. Eur J Cell Biol 2006, 85, 699.

ACS APPLIED MATERIALS & INTERFACES

Research Article

www.acsami.org

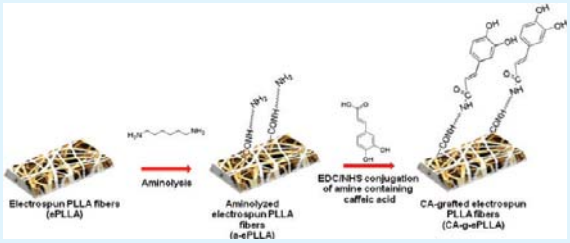
Preparation and Characterization of Caffeic Acid-Grafted Electrospun Poly(L-Lactic Acid) Fiber Mats for Biomedical Applications

Piyachat Chuysinuan,[†] Prasit Pavasant,[‡] and Pitt Supaphol*[,†]

[†]The Petroleum Petrochemical College, The Center of Excellence on Petrochemical and Materials Technology, [‡]Department of Anatomy, Faculty of Dentistry, Chulalongkorn University, Bangkok 10330, Thailand

Supporting Information

ABSTRACT: Caffeic acid (CA) was chemically immobilized onto the surfaces of the individual electrospun poly(L-lactic acid) (PLLA) fibers to enhance the hydrophilicity and impart the antioxidant activity to the obtained fibrous membranes. This was done in two sequential steps. First, amino groups were covalently introduced onto the surfaces through the reaction with 1,6-hexamethylenediamine (HMD). In the second step, the amino moieties reacted with CA, which had been preactivated sequentially with 1-ethyl-3-(3-dimethylaminopropyl)carbodiimide (EDC) and *N*-hydroxysuccinimide (NHS). The success of the reactions was confirmed by the ninhydrin assay and X-ray photoelectron spectroscopic analysis (XPS). Indirect cytotoxicity evaluation with murine dermal fibroblasts (L929) and human dermal fibroblasts (HDFa) revealed that the neat and the modified PLLA fibrous matrices released no substances in the levels that were harmful to the cells. Direct culturing of HDFa on these fibrous substrates indicated that they supported the proliferation of the cells on days 2 and 3 very well and that the CA-immobilized substrates exhibited the highest cell viability. Lastly, the antioxidant activity of the CA-immobilized substrates, as revealed by the 1,1-diphenyl-2-picryldrazyl (DPPH) radical scavenging assay, was as high as 88% on average.



KEYWORDS: *electrospinning, poly(L-lactic acid), immobilization, caffeic acid, antioxidant, radical scavanging*

INTRODUCTION

Electrospinning is a simple and an efficient method for fabricating ultrafine fibers, the diameters of which range from a few micrometers down to tens of nanometers. Typically, an ultrafine stream of a polymeric liquid (solution or melt) is continuously drawn from the conical apex of its droplet by electrical forces and deposits randomly as a nonwoven fabric on a collection device.[1,2] This is driven mainly by the Coulombic repulsive force between charges of the same polarity in the polymer liquid as well as the electrical force exerting on the charges by the electric field, which acts to destabilize the partially spherical droplet of the polymer liquid at the tip of the capillary to finally form a droplet of a conical shape. By increasing the strength of the electric field above a threshold value (which varies from one system to the next), the ultrafine stream of the polymeric liquid is drawn out from the tip of the cone, as previously mentioned.[1,2]

Poly(L-lactic acid) (PLLA) is a biodegradable aliphatic polyester, the monomer of which, i.e., L-lactic acid or L-2-hydroxypropionic acid, is produced from a fermentation process of sugar or other related raw materials.[3] The monomer then undergoes condensation polymerization into a high-molecular-weight PLLA or condensation dimerization into L-lactide, which is further processed into a high-molecular-weight PLLA by ring-opening polymerization.[3] Due to its inherent biocompatibility, PLLA has been used extensively in medicine as surgical sutures (normally as a copolymer thread with glycolic acid)[4] and suture anchors.[5] PLLA can be fabricated into fibrous matrices by electrospinning.[6−14] Various solvent systems have been used to prepare electrospinnable PLLA solutions, some of which are chloroform,[6] 3:2 w/w methylene chloride/*N*,*N*′-dimethylformamide (DMF),[7] 1,1,1,3,3,3-hexafluoro-2-propanol (HFIP),[8] chloroform, dichloromethane (DCM), or tetrahydrofuran (THF),[9] 9:1 v/v DCM/DMF,[10] 3:1 v/v chloroform/acetone,[11] 7:3 v/v DCM/THF,[12,13] and 7:3 v/v DCM/DMF.[14]

Approved by the U.S. Food and Drug Administration (US-FDA) for various clinical applications in humans,[15] applicability of electrospun PLLA fibrous matrices in biomedicine is an obvious choice. Kenawy et al.[6] were the first group to report the use of electrospun fibrous matrices of poly(lactic acid) (PLA) and its blend with poly(ethylene-co-vinyl acetate) (PEVA) to incorporate an anti-infection drug, tetracycline hydrochloride, and to study the release of the drug therefrom. Although the PLA matrices showed a burst release of the drug, the PLA/PEVA blend counterparts showed a prolonged release characteristic. A burst release was also observed for a cephamycin antibiotic drug, cefoxitin, from electrospun fibrous poly(D,L-lactic acid) (PDLA) matrices containing the drug.[7] Development of an antibacterial bandage based on electrospun

Received: March 6, 2012
Accepted: May 12, 2012
Published: May 12, 2012

 © 2012 American Chemical Society

PLLA fibrous matrices containing silver nanoparticles was reported by Xu et al.[10] Li et al.,[11] on the other hand, developed a biosensor assembly based on electrospun PLA fibrous matrices that contained biotin. Though dispersed inhomogeneously within the mass of the PLA fibers, the incorporated biotin could immobilize streptavidin, which subsequently bound with biotinylated nucleic acid probes for the detection of a synthetic *E. coli* DNA. Finally, uses of electrospun PLLA fibrous matrices as substrates for cell/tissue culture were demonstrated on a number of different cell types, e.g., preosteoblastic and Schwann cells.[8,12,13]

Previously, our group developed electrospun PLLA fiber matrices containing gallic acid or 3,4,5-trihydroxybenzoic acid, a natural phenolic acid indigenous to a variety of plants, and reported the release characteristic of the substance therefrom.[14] In addition to its anticarcinogenic, antifungal, anti-inflammatory, and antityrosinase activities, gallic acid is one of the most potent antioxidants in its class.[16,17] It was found that the cumulative amount of the substance released from the gallic acid-loaded PLLA fiber mats was greatest in the normal saline, followed respectively by those in the citrate-phosphate and the acetate buffer and that the free radical scavenging activity of the as-loaded and the as-released gallic acid remained active.[14] Another compound of natural origins exhibiting a strong antioxidant activity is caffeic acid (CA) or 3-(3,4-dihydroxyphenyl)-2-propenoic acid.[18−20] As a key intermediate in the biosynthesis of lignin, it can be found in all plants. Other biochemical activities of CA are anticarcinogenic, anti-inflammatory, and antimutagenic activities.[19−21]

Here, it is of our interest to apply CA as the active therapeutic agent and electrospun PLLA fibrous matrices as substrates. However, to fabricate CA-incorporated PLLA fibrous matrices from a PLLA solution containing CA could lead to easy leaching of the substance into a liquid medium.[14] To prolong the therapeutic effect of the substance, covalent immobilization of CA onto the surfaces of the individual PLLA fibers would be a logical choice. Among the various chemical pathways, grafting of CA onto an aliphatic polyester, such as PLLA and polycaprolactone (PCL), can be done in two sequential steps.[22,23] First, some of the ester groups on the surfaces of electrospun PLLA fibers are reacted with 1,6-hexamethylenediamine (HMD), resulting in the introduction of the more reactive amino groups on the surfaces. Second, the carboxylic acid moiety of CA is activated successively with 1-ethyl-3-(3-dimethylaminopropyl)carbodiimide (EDC) and *N*-hydroxysuccinimide (NHS), prior to being reacted with an amino group on the surface of an aminolyzed PLLA fiber. The introduction of the amino groups was assessed spectrophotometrically by the ninhydrin assay, while the presence of CA was by X-ray photoelectron spectroscopy (XPS). Biocompatibility of the surface-modified PLLA fibrous matrices was evaluated with live cultures with murine and human dermal fibroblasts. Lastly, the antioxidant activity of the CA-grafted PLLA fibrous matrices was evaluated based on the 1,1-diphenyl-2-picrylhydrazyl (DPPH) free radical scavenging assay.

EXPERIMENTAL SECTION

Materials. PLLA (M_n = 80 000 g mol^{-1}), CA, HMD, EDC, and NHS were purchased from Sigma-Aldrich (USA). DCM (Carlo Erba, Italy), DMF [Lab-Scan (Asia), Thailand], and ethanol [Lab-Scan (Asia), Thailand] were of analytical reagent grade and used without further purification.

Preparation of Electrospun PLLA Fiber Mats. Electrospinning of PLLA was carried out based on a previously published method.[14] Briefly, 10% w/v PLLA solution in 7:3 v/v DCM/DMF was fed into a glass syringe fitted with a blunt 20-gauge stainless steel hypodermic needle (OD = 0.91 mm), used as the nozzle. An aluminum sheet wrapped around a homemade rotating cylinder (width and diameter ≈ 15 cm; rotational speed ≈ 50 rpm) was used as the collector. The solution was charged with a Gamma High Voltage Research D-ES30PN/M692 at a fixed electric field of 20 kV/18 cm. After the solution had been electrospun continuously for 18 h, the thicknesses of the obtained fiber mats were measured to be 120 ± 15 μm.

Surface Modification of Electrospun PLLA Fiber Mats. Aminolysis of the PLLA fiber mats was carried out based on a previously published method,[22] with slight modification. Specifically, the fiber mats had been washed in an ethanolic aqueous solution (1:1 v/v) for 2 to 3 h, prior to being washed with a large quantity of deionized (DI) water. The aminolysis was then carried out by immersing the fiber mats in a HMD/isopropanol (IPA) solution of varying concentrations (i.e., 0.02, 0.04, 0.06, and 0.08 g mL^{-1}) for varying periods of the reaction time (i.e., 5, 10, 15, 20, and 30 min) at 50 °C. The aminolyzed PLLA fiber mats (hereafter, a-ePLLA) had been rinsed in DI water for 24 h at room temperature to remove unreacted HMD, prior to being dried in vacuo at room temperature until of a constant mass. Activation of CA was done based on a previously published method,[23] with slight modification. Specifically, 250 mg of CA, a priori dissolved in 10 mL of ethanolic aqueous solution (1:1 v/v), was reacted with 169 mg of EDC and later with 102 mg of NHS. The mixture was stirred in an ice−water bath for 1 h to finally obtain a solution of the activated CA. The aminolyzed PLLA fiber mats were subsequently immersed into the activated CA solution and stirred in the ice−water bath for 30 min. After 24 h of the reaction time at room temperature, the CA-grafted PLLA fiber mats (CA-g-ePLLA) were washed thoroughly with ethanol several times and finally dried in vacuo at room temperature.

Materials Characterization. The free amino (NH_2) groups on the surfaces of the neat and the modified PLLA fiber mats were quantified by ninhydrin or 2,2-dihydroxyindane-1,3-dione assay.[22] The fiber mat samples were first immersed in 1 M ninhydrin/ethanol solution for 1 min, transferred into a glass tube, and then heated at 80 °C for 15 min to accelerate the reaction between ninhydrin and the NH_2 groups that might be present on the surfaces of the fiber mat samples. If there were enough NH_2 groups on the surfaces, they would turn blue. Upon complete evaporation of the adsorbed ethanol, 1,4-dioxane was added to dissolve the fiber mat samples. IPA was subsequently added to stabilize the blue compound. The absorbance of the obtained solutions were read at 538 nm using a Shimadzu UV-2550 ultraviolet−visible (UV−vis) spectrophotometer and the concentrations of the NH_2 groups in the sample solutions were calculated from a standard calibration curve of HMD solutions in 1,4-dioxane/IPA (1:1 v/v) (see Figure I in the Supporting Information).

Surface elemental chemistry of the neat and the modified PLLA fiber mats was analyzed by a Thermo Fisher Scientific Thetaprobe X-ray photoelectron spectroscope (XPS).[24] Monochromatic Al Kα X-ray was employed for the analysis of one spot on each sample with a photoelectron emission angle of 50° (with respect to the surface normal). The analytical area was approximately 400 μm × 400 μm, and the maximal analytical depth was in the range of ∼4−8 nm. A few eV Ar^+ ions, generated by an electron flood gun, were used for charge compensation. Electron and ion beams were focused and steered toward the analytical area. Further correction was made based on adventitious C 1s at 285 eV, using the manufacturer's standard software. Survey spectra were acquired for surface composition analysis with sensitivity factors from Scofield library.

The amounts of the immobilized CA on the surfaces of the CA-g-ePLLA specimens were also investigated. Specimens (circular disk; ∼2.8 cm in diameter; cut from randomly selected areas of three different fiber mats) were individually dissolved in 10 mL of 7:3 v/v DCM/DMF solution. The absorbance of the sample solutions was spectrophotometrically read at 243 nm and the concentrations of the immobilized CA were calculated from a standard calibration curve of

CA solutions in 7:3 v/v DCM/DMF (see Figure II in the Supporting Information).

Static water contact angles of the neat and the modified PLLA fiber mats were measured at room temperature using a Krüss DSA 100 drop shape analyzer,[25] equipped with a Gilmont syringe and a 24-gauge flat-tipped needle. Five droplets of distilled water (10 μL) were placed randomly at different positions on each sample. The projected images of the droplets, after they had been settled on the surfaces until of no noticeable change in their shapes, were analyzed for the contact angles.

Morphological appearance and size of the individual fibers of the neat and the modified PLLA fiber mats were examined by a JEOL JSM 5410LV scanning electron microscope (SEM). At least 100 readings of the fiber diameters from various SEM images were analyzed using SemAphore 4.0 software.

Mechanical properties in terms of stress at maximum load, strain at maximum load, Young's modulus, and elongation at break of the neat and the modified PLLA fiber mats were tested on a Lloyd LRX universal testing machine (gauge length = mm and crosshead speed = 100 mm min^{-1}). The specimens were cut into a rectangular shape (10 mm ×100 mm). The measurements were carried out on ten different specimens.

Biological Evaluation. Murine dermal fibroblasts (L929) and human dermal fibroblasts (HDFa) were used as reference cells. L929 and HDFa were cultured as monolayer in Dulbecco's modified Eagle's medium (DMEM; Sigma-Aldrich, USA), supplemented with 10% fetal bovine serum (FBS; Biochrom, UK), 1% L-glutamine (Invitrogen, USA), and a 1% antibiotic and antimycotic formulation [containing penicillin G sodium, streptomycin sulfate, and amphotericin B (Invitrogen, USA)]. The medium was replaced on every other day and the cultures were maintained at 37 °C in a humidified atmosphere containing 5% CO_2.

In the indirect cytotoxicity evaluation, the fiber mat specimens were assessed using a procedure adapted from the ISO10993−5 standard test method. First, extraction media were prepared by immersing the fiber mat specimens (∼15 mm in diameter) in a serum-free medium (SFM; containing DMEM, 1% L-glutamine, 1% lactabumin, and 1% antibiotic and antimycotic formulation) for 1, 2, or 3 d in an incubator at the extraction ratio of 20 mg/mL. L929 or HDFa (∼40 000 cells/well) were separately cultured in wells of a 24-well tissue-culture polystyrene plate (TCPS; Biokom, Poland) in 10% serum-containing DMEM for 16 h to allow cell attachment onto the well surface. After starving the cells with SFM for 24 h, the medium was replaced with 0.5 mL of an extraction medium and the cells were reincubated for another 24 h. The viability of the cells cultured with each of the extraction media and the fresh SFM that had been preincubated for an equivalent time interval (i.e., control) was determined with 3-(4,5-dimethylthiazol-2-yl)-2,5-diphenyl-tetrazolium bromide (MTT) assay.

The MTT assay is based on the reduction of the yellow tetrazolium salt to purple formazan crystals by dehydrogenase enzymes secreted from the mitochondria of metabolically active cells. The amount of formazan crystals is supposedly proportional to the number of viable cells. First, each specimen was incubated at 37 °C with 300 μL/well of MTT solution at 0.5 mg mL^{-1}, without phenol red. After 30 min of incubation, the MTT solution was removed. A buffer solution containing dimethylsulfoxide (DMSO; 900 μL/well) and glycine buffer (pH 10; 125 μL/well) was added into the wells to dissolve the formazan crystals. After 10 min of agitation, the solutions were measured for their absorbance at 540 nm, using a Thermospectronic Genesis10 UV−visible spectrophotometer.

In the cell attachment and the cell proliferation studies, only HDFa were used. Specimens (∼15 mm in diameter) were placed in wells of a 24-well TCPS and subsequently sterilized in 70% ethanol for 1 h. The specimens, after having been washed successively with autoclaved deionized water and phosphate saline solution (PBS), were immersed in DMEM overnight. A stainless steel ring (∼12 mm in diameter) was placed on top of each specimen to ensure its complete contact to the bottom of the well. HDFa (∼40,000 cells/well) were seeded on the fiber mat specimens and empty wells of TCPS (i.e., control) and incubated at 37 °C in a humidified atmosphere containing 5% CO_2. In the attachment study, the cells had been allowed to attach onto the substrates for 2, 4, or 18 h, prior to being quantified for their viability by the MTT assay. Prior to the measurement, each cell-plated specimen had to be rinsed with PBS to remove unattached cells. In the proliferation study, the cells had been allowed to attach onto the substrates for 16 h, prior to being quantified for their viability by the MTT assay on days 1, 2, and 3 after cell culturing.

The morphology of the cells at some time points was observed by SEM. After removal of the culture medium, each cell-cultured specimen was rinsed twice with PBS and the cells were fixed with 3% glutaraldehyde solution [diluted from 50% glutaraldehyde solution (Sigma-Aldrich, USA) with PBS] at 500 μL/well. After 30 min, the specimen was rinsed again with PBS and underwent dehydration with ethanolic aqueous solutions of varying concentrations (i.e., 30, 50, 70, and 90 vol %) and pure ethanol for ∼2 min each. It was then dried in hexamethyldisilazane (HMDS; Sigma-Aldrich, USA) for 5 min and finally in air. The specimens were then observed by a JEOL JSM-5200 scanning electron microscope (SEM). The morphology of the cells that had been seeded or cultured on glass substrates (12 mm in diameter; Menzel, Germany) was used as positive control.

Protein Adsorption. Specimens (∼15 mm in diameter) were placed in wells of a 24-well TCPS. A stainless steel ring (∼12 mm in diameter) was placed on top of each specimen to ensure its complete contact to the bottom of the well. A solution of type I collagen in PBS (0.1 mg·mL^{-1} for 0.5 mL) was then added to each well. After 2, 4, 24, 48, and 72 h of immersion, each specimen was thoroughly rinse with DI water to remove excess collagen. The amount of adsorbed collagen on each specimen was carried out by first immersing the specimen in 2 mL of 1% w/v sodium dodecyl sulfate (SDS) aqueous solution for 30 min. The concentration of the dissolved collagen was then quantified by BCA protein assay kit (Thermo Fisher Scientific, USA). Specifically, 25 μL of each of the dissolved collagen sample solutions had been pipetted into a 96-well TCPS, before the BCA working solution of 200 μL was added. The plate was sealed and incubated at 60 °C for 30 min. The absorbance measurements were taken at 562 nm at room temperature. The collagen concentration was calculated from a standard calibration curve (see Figure III in the Supporting Information).

Antioxidant Activity. The antioxidative activity of CA after it had been grafted onto the surfaces of the PLLA fiber mats was assessed by the DPPH assay. The procedure was carried out based on a previously published method,[14,26] with slight modification. Specifically, each specimen (∼2.8 cm in diameter) was dissolved in 10 mL of 7:3 v/v DCM/DMF solution. The sample solution was then diluted with 10 mL methanol. After that, 3 mL of an ethanolic solution of DPPH (100 μM) was added into 1 mL of the sample solution. The mixture had been incubated at room temperature in darkness for 30 min, prior to being spectrophotometrically read at 517 nm. The neat fiber mat specimens were used as internal control and the amount of the immobilized CA participated in scavenging activity of the DPPH radical species could be quantified against a standard curve of CA (see Figure IV in the Supporting Information). The antioxidant activity (% AA) was then expressed as the percentage of the absorbance value of the DPPH radical species that was decreased in comparison with that of the control condition (i.e., the testing solution without the addition of the dissolved specimens), according to the following equation

$$\%AA = \frac{(A_{control} - A_{sample})}{A_{control}} \times 100 \quad (1)$$

where $A_{control}$ and A_{sample} represent the absorbance values of the blank and the sample solutions, respectively.

Statistical Analysis. All values were presented as the means ± standard deviations. Statistical analysis between two data sets was performed using One-Way Analysis of Variance (ANOVA) and Scheffe's post hoc test in SPSS (SPSS, USA). The values of p lower than 0.05 were considered statistically significant.

RESULTS AND DISCUSSION

The purpose of chemical immobilization of CA onto the surfaces of the individual electrospun PLLA fibers is 2-fold. The

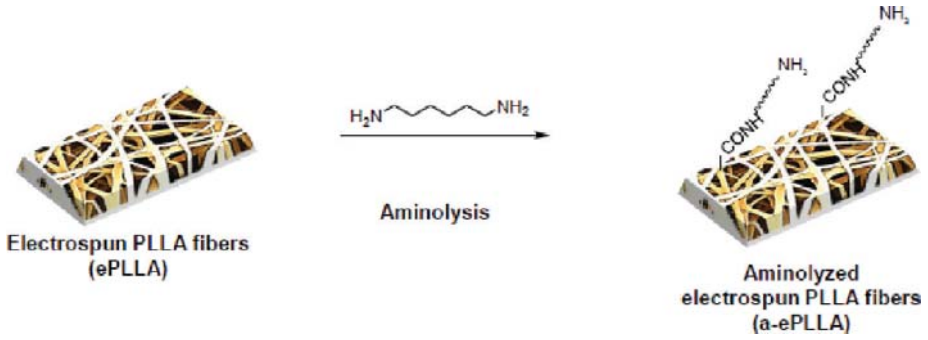


Figure 1. Aminolysis of the electrospun PLLA fiber surfaces through the reaction with 1,6-hexamethylenediamine (HMD).

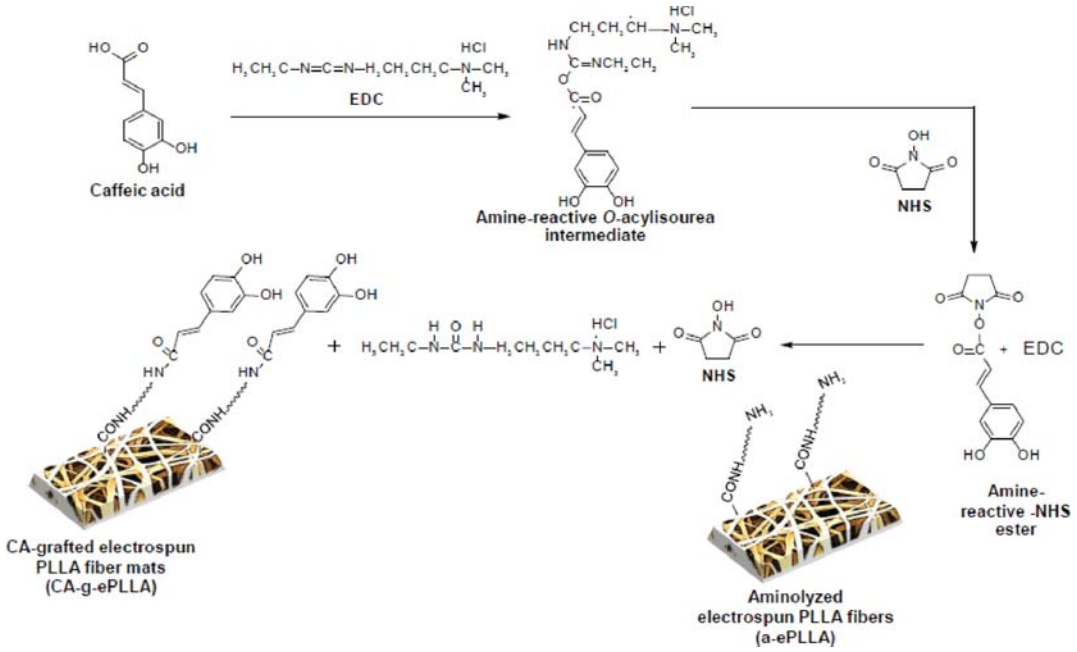


Figure 2. Chemical pathway detailing the conjugation reaction of CA with an amino moiety ($-NH_2$) on the aminolyzed electrospun PLLA fiber (a-ePLLA) surfaces via conjugating agents.

first is to increase the hydrophilicity of the surfaces, as the hydroxyl moieties of CA are more hydrophilic than the ester linkages indigenous to PLLA. Second, it is aimed at imparting the antioxidant activity to the modified PLLA fibrous matrices, as this activity is deemed important for an active wound dressing. According to the reaction schemes shown in Figures 1 and 2, the grafting of CA onto the surfaces of the individual electrospun PLLA fibers can be done in two sequential steps. In the first step, amino groups were covalently introduced onto the surfaces of the individual electrospun PLLA fibers through the reaction with HMD to obtain the aminolyzed PLLA fiber mats (a-ePLLA). Here, an amino moiety ($-NH_2$) of HMD would react with an ester linkage ($-COO-$) of PLLA to from the amide linkage ($-CONH-$), whereas the other amino moiety would be left available for further reaction. In the second step, the CA-grafted PLLA fiber mats (CA-g-ePLLA) were obtained through the reaction between CA, the carboxylic acid moiety ($-COOH$) of which had been activated sequentially with EDC and NHS, and the other amino moiety of HMD, which had been introduced on the surfaces of the a-ePLLA in the first step.

Characterization of Neat and Modified PLLA Fibrous Matrices. *Quantification of Free Amino Groups.* Quantification of the amino moieties that had been introduced on the surface of the a-ePLLA was evaluated with the ninhydrin assay. A number of factors would influence the amounts of the amino groups that would be introduced on the surface of the a-ePLLA. Some of these are the initial concentration of HMD, the reaction time, and the reaction temperature. Here, only the effects of the HMD concentration (see Table 1) and the reaction time (see Table 2) were studied. Within the

Table 1. Surface Density of $-NH_2$ Groups on the a-ePLLA as a Function of HMD Concentration at a Fixed Reaction Time of 10 Min[a]

HMD concentration (g mL^{-1})	surface density of -NH_2 ($\times 10^{-7}$ mol cm^{-2})
0.02	0.82 ± 0.06
0.04	1.20 ± 0.03
0.06	1.65 ± 0.05
0.08	1.96 ± 0.04

[a]The reaction temperature was fixed at 50 °C.

Table 2. Surface Density of $-NH_2$ Groups on the a-ePLLA as a Function of Reaction Time at a Fixed HMD Concentration of 0.04 g mL^{-1}[a]

reaction time (min)	surface density of $-NH_2$ ($\times 10^{-7}$ mol cm^{-2})
5	0.76 ± 0.04
10	1.20 ± 0.03
15	1.77 ± 0.07
20	1.82 ± 0.06
30	3.10 ± 0.04

[a]The reaction temperature was fixed at 50 °C.

investigated ranges of the HMD concentrations and the reaction times, the density of the amino groups was an increasing function of both independent parameters. Nevertheless, treating the neat PLLA fibrous membranes at a high HMD concentration and/or a long reaction time would jeopardize both the physical and the mechanical integrity of the modified fibrous membranes. As the aminolytic condition becomes harsher (i.e., a result of the increased HMD concentration, increased reaction time, etc.), increasing numbers of ester linkages would be cleaved and the carboxylic acid chain ends would react with HMD, resulting in greater numbers of shorter PLLA chains and this occurs from the surface in. Here, the optimized aminolytic condition that resulted in the a-ePLLA that did not disintegrate while undergoing further reaction and/or evaluation is 0.04 g mL^{-1} of HMD/IPA solution at 50 °C for 10 min. At this condition, the surface density of the introduced amino groups was 0.120 ± 0.003 μmol cm^{-2}.

Elemental Composition of Surfaces and Quantification of Immobilized CA. XPS was used to examine the chemical composition at the surfaces of the neat and the modified PLLA fibrous matrices. Quantitative analysis of the obtained results is shown in Table 3. As expected, no nitrogen-based moieties

Table 3. Percentages of Area under the Peaks of High-Resolution C 1s, O 1s, and N 1s XPS Spectra, Including the Ratios of the Percentages of the Area under the Peaks O 1s/C 1s, N 1S/C 1s, and N 1s/O 1s, of the Neat and the Modified PLLA Fibrous Matrices

sample	C 1s	O 1s	N 1s	O 1s/C 1s	N 1s/C 1s	N 1s/O 1s
ePLLA	61.1	38.9	0	0.6367	0	0
a-ePLLA	64.4	34.8	0.8	0.5404	0.0125	0.0230
CA-g-ePLLA	60.6	39.0	0.4	0.6436	0.0066	0.0103

were observed on the surfaces of the neat PLLA fibrous membranes (i.e., the ePLLA). This was evidenced by the nonexistence of the N 1s spectra. In addition, the ratio between the surface oxygen atoms and the surface carbon atoms (i.e., O 1s/C 1s) was about 0.64. For the a-ePLLA, this ratio decreased to about 0.54 and, at the same time, surface nitrogen atoms could then be detected. This is because aminolysis introduced both the carbon and the nitrogen atoms on the fiber surfaces. For the CA-g-ePLLA, the O 1s/C 1s ratio increased again to about 0.64. This is because the grafting of CA introduced both the carbon and the oxygen atoms on the fiber surfaces. This resulted in the simultaneous decrease in the number of surface nitrogen atoms, as evidenced by the decrease in the N 1s/C 1s and the N 1s/O 1s ratios from those of the a-ePLLA.

The surface density of the immobilized CA on the CA-g-ePLLA was quantified spectrophotometrically to be 6.2 ± 0.2 μg cm^{-2} or 0.034 ± 0.003 μmol cm^{-2} (based on the projection area of the specimens and note that M_w of CA = 180.16 g·mol^{-1}) (n = 5). This implies that about 28% of the amino groups on the surface of the a-ePLLA participated in the immobilization reaction with CA. When calculated based on the actual weights of the specimens, the amount of the immobilized CA on the CA-g-ePLLA was 1.13 ± 0.03 μg mg^{-1} or 0.0063 ± 0.0006 μmol mg^{-1}. To see whether the as-grafted CA could be released from the CA-g-ePLLA or not, a separate experiment was carried out. Here, the CA-g-ePLLA specimens (~2.8 mm in diameter) were immersed in PBS at 37 °C for periods of 1, 3, and 7 days. After each time point, a sample solution was withdrawn and spectrophotometrically read at 243 nm. The obtained results confirmed nonexistence of CA in the sample solutions. This clearly implies that there was no physical adsorption of CA on the surfaces of a-ePLLA and that the cleavage of the amide linkages could not occur in PBS.

Wettability and Morphology. Static contact angles of water droplets on the surfaces of the neat and the modified PLLA fibrous membranes were used to assess the hydrophilicity of these surfaces. Such values for the neat PLLA fibrous matrices were 104.8° ± 0.3°. The surfaces became much more hydrophilic after the aminolytic treatment in 0.04 g mL^{-1} of HMD/IPA solution at 50 °C for 10 min (i.e., the water contact angles = 83.3° ± 0.4°). The hydrophilicity of the surfaces increased even more after CA having been grafted onto the surfaces of the a-ePLLA (i.e., the water contact angles = 55.5° ± 0.5°). The wettability of a surface depends not only on the chemical modification of the surface, but on the typographical nature of it as well. For an electrospun fibrous membrane, the wettability of its surface depends on the topography, the size, the arrangement,[25] and the surface chemistry of the individual, underlying fibers.[22] To ascertain that the increase in the hydrophilicity of the modified PLLA fibrous membranes over that of the neat ones was not due to any change in their surface topography, the morphology of the neat and the modified PLLA fibrous membranes was investigated (see Figure 3). Evidently, there is no obvious discrepancy in the morphology of the modified fibers from that of the neat ones, as the surface of all of these individual fibers was smooth. Nonetheless, the diameters of the modified fibers (i.e., ~850 and ~920 nm on average after the aminolysis and the grafting of CA, respectively) were generally greater than those of the neat ones (i.e., ~620 nm on average). The increase in the electrospun fiber diameters after a surface modification was also reported on electrospun poly(D,L-lactic acid) (PDLLA) fibers that had been grafted with chitosan.[27] Recently, It has been demonstrated that an increase in the size of the individual fibers increased the hydrophobicity of the electrospun fibrous membranes.[25] Thus, the increase in the hydrophilicity of the modified PLLA fibrous membranes over that of the neat materials was certainly not due to the change in the size of these individual fibers.

Mechanical Integrity. The mechanical properties of the ePLLA and the CA-g-ePLLA were investigated. The stress at maximum load and the Young's modulus of the ePLLA were 3.6 ± 0.2 and 351 ± 5 MPa, respectively, whereas the strain at maximum load and the strain at break of the materials were 75.6 ± 4.6 and 87.7 ± 4.6%, respectively. On the other hand, the stress at maximum load and the Young's modulus of the CA-g-ePLLA were 0.89 ± 0.29 and 154 ± 14 MPa, respectively, whereas the strain at maximum load and the strain at break of the materials were 2.2 ± 0.2 and 5.8 ± 0.5%, respectively. Upon

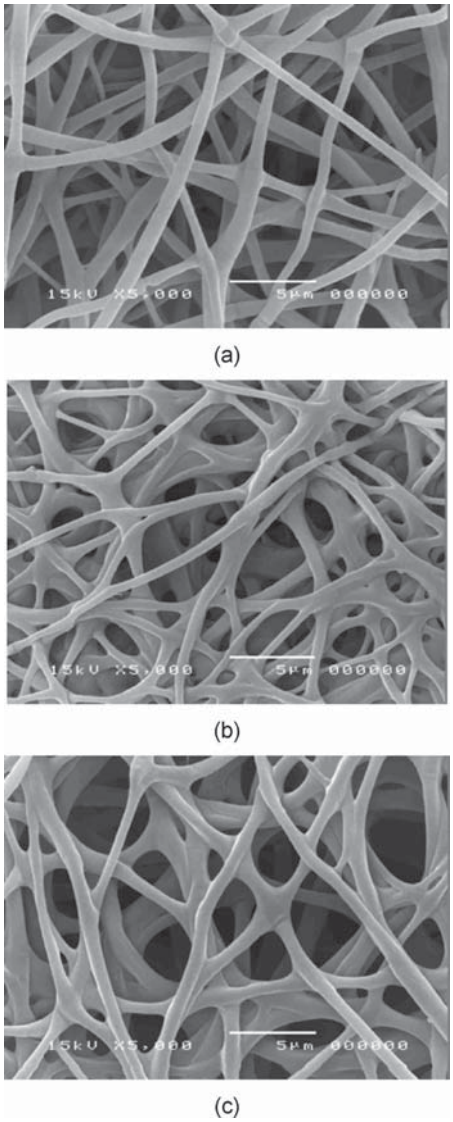


Figure 3. Representative SEM images (scale bar = 5 μm and magnification = 5000×) illustrating morphology of (a) neat electrospun PLLA fibers (ePLLA) and the one that had been modified by (b) aminolysis (0.04 g mL^{-1} of HMD/IPA solution at 50 °C for 10 min; a-ePLLA) and subsequently by (c) grafting with caffeic acid (CA) that had been a priori activated successively with EDC and NHS (CA-g-ePLLA). The size of these fibers were determined to be 618 ± 92, 854 ± 181, and 918 ± 186 nm, respectively.

the aminolysis and the EDC/NHS conjugation of CA onto the ePLLA surfaces, both the stiffness and the extensibility of the CA-g-ePLLA decreased significantly.

Biological Evaluation of Neat and Modified PLLA Fibrous Matrices. *Indirect Cytotoxicity Evaluation.* The potential for use of the neat and the modified PLLA fibrous membranes in biomedical applications was first assessed by the indirect cytotoxicity evaluation assay, using L929 and HDFa as reference cells. In the assessment, the extraction media were prepared by immersing each fiber mat sample in SFM for different periods of up to 3 days. The viability of the cells that had been cultured with each of these media, in comparison with that of the cells that had been cultured with the fresh SFM that had been preincubated for similar periods of time, for 1 day is shown in Figure 4. The viability of the cells that had been cultured with the fresh SFM that had been preincubated for 1 d

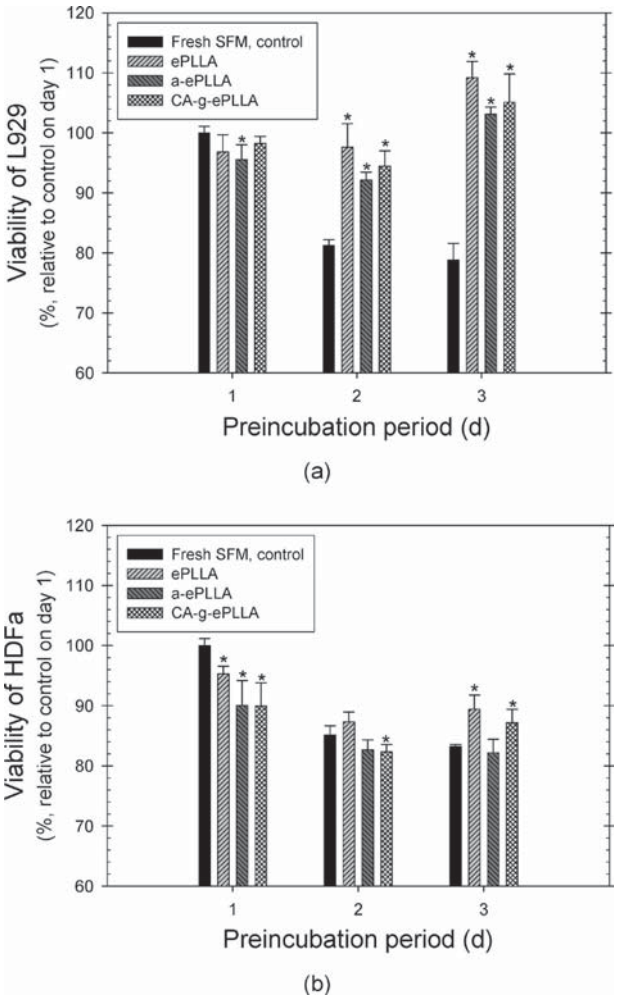


Figure 4. Indirect cytotoxic evaluation of ePLLA, a-ePLLA, and CA-g-ePLLA based on viabilities of (a) murine dermal fibroblasts (L929) and (b) human dermal fibroblasts (HDFa) that had been cultured with the extraction media from these materials against the viabilities of the cells that had been cultured withthe respective serum-free media for 1 day as a function of the preincubation period of 1, 2, or 3 days. *p < 0.05: compared with the control group at any given time point.

was used as the basis to obtain the relative viabilities shown in the figure. For both cell types, the viability of the cells that had been cultured with the fresh SFM was found to decrease with an increase in the preincubation period, which may be due to the increase in the dissolved CO_2 level upon the prolonged incubation. Notwithstanding, the viabilities of either cell type were greater than ∼80% on average. For L929 that had been cultured with the extraction media from both the neat and the modified PLLA fibrous matrices, the viabilities of the cells showed increasing trends, with the values ranging from ∼92 to ∼109% on average. For HDFa on the other hand, decreasing trends were observed, with the values ranging from ∼82 to ∼95% on average. Because the viabilities were greater than ∼80%, the obtained results indicated nontoxicity of all of the fibrous matrices, as none of the materials released substances in the levels that were detrimental to the cells.

Cell attachment and Cell Proliferation. All of the fibrous matrices were evaluated further for their potential for use as wound dressing materials. For this, HDFa were directly seeded or cultured on their surfaces in order to assess the ability of the materials in supporting the attachment and the proliferation of the cells. The viabilities of the cells that had been grown on the surfaces of TCPS at 2 h after cell seeding (for the attachment assay) and on day 1 after cell culturing (for the proliferation assay) were used as the bases to obtain the relative viabilities shown in Figure 5. For the attachment assay, the viability of the

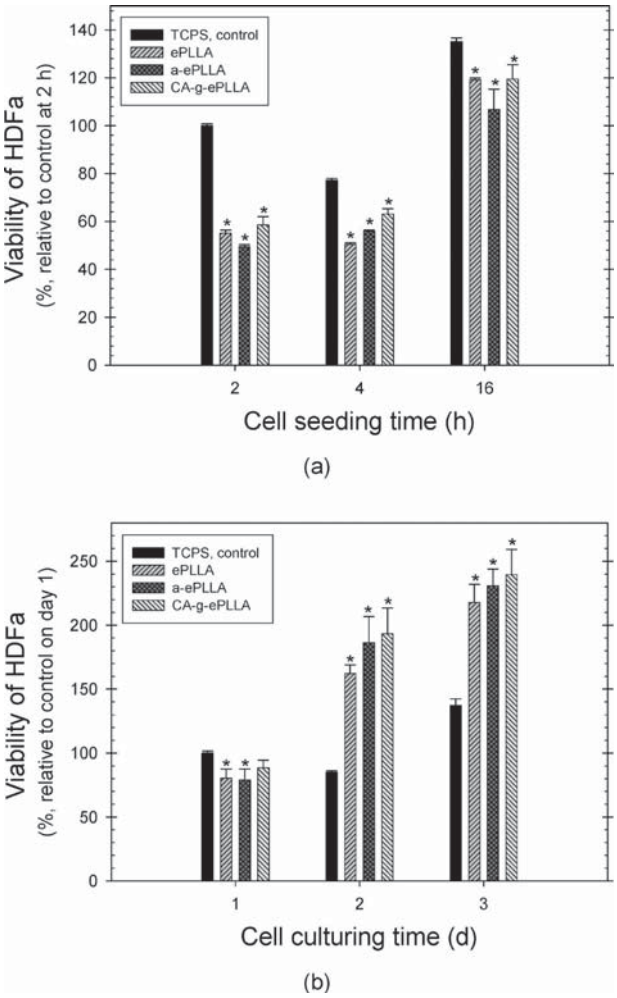


Figure 5. (a) Attachment and (b) proliferation based on viabilities of HDFa that had been seeded or cultured on the surfaces of ePLLA, a-ePLLA, and CA-g-ePLLA in comparison with those of the cells that had been seeded or cultured on the surface of tissue-culture polystyrene plate (TCPS) as a function of the cell seeding or cell culturing time. $*p < 0.05$: compared with the control group at any given time point.

attached cells on the surface of TCPS at 4 h was lower than that at 2 h, whereas that of the attached cells at 16 h was greater. At any given time point, the viabilities of the attached cells on all of the fibrous matrices were lower than that on the control surface. At 2 and 4 h after cell seeding, the ability to support the attachment of the cells for a given type of the fibrous matrices was not of statistical difference. At 16 h, however, the viabilities of the cells attached on all types of the fibrous matrices increased tremendously to approach that of the cells that could adhere onto the control surface. Noticeably, the CA-g-ePLLA were better than the a-ePLLA in supporting the attachment of HDFa at any given time point. On day 1 after cell culturing, the viabilities of the cells on all of the fibrous matrices were still inferior to that of the cells on TCPS. Interestingly, the profiling of viabilities was similar to that observed at 16 h after cell seeding. This result could be interpreted that at least 24 h was required for HDFa to completely adhere to these surfaces. Significant increase in the proliferation of the cultured cells on all types of the fibrous matrices was observed on days 2 and 3 after cell culturing. Though not statistically significant, the ability of the CA-g-ePLLA in supporting the proliferation of HDFa was better than that of the a-ePLLA, which in turn was better than that of the ePLLA.

The inferiority of all of the fibrous matrices to TCPS in supporting the attachment of HDFa could be due to the lesser numbers of cells that were able to attach on the rougher and more hydrophobic surfaces of the fibrous matrices in comparison with the smoother and more hydrophilic surface of TCPS. Surfaces of different degrees of hydrophilicity (or hydrophobicity) would influence different types and amounts of proteins to adsorb. Even though a rough surface of the fibrous matrices possesses a greater specific surface area than a smoother surface of TCPS, the types and amounts of the proteins that are adsorbed on the smooth and hydrophilic surface of TCPS may mediate the adherence of the cells much better than do those adsorbed on the rough and hydrophobic surface of the fibrous matrices. The flat surface of TCPS also ensures that the adsorbed proteins are readily accessible to the cells. Unlike the flat surface of TCPS, only a limited part of the adsorbed proteins on the rough surface is accessible to the cells. Furthermore, the kinetics of the protein adsorption on the surfaces of different characters (i.e., different surface topographies, different effective surface areas, different surface wetting phenomena, etc.) play important roles in regulating the different time intervals for which the proteins require to adsorb in the amounts that are effective for mediating cellular behavior. Here, it is logical to hypothesize that a much longer time is needed for a much greater amount of proteins required to adsorb on the surfaces of the fibers to have a mediating effect to the cultured cells. Hence, on days 2 and 3, we see much greater increase in the proliferation of the cells grown on all types of the fibrous matrices and such an increase should be a result of the greater surface areas of the fibrous substrates. Among the three types of the fibrous matrices, the CA-g-ePLLA were the best in supporting the attachment and the proliferation of HDFa (i.e., based on the average values of the viabilities shown in Figure 5). Because the surface of the CA-g-ePLLA was more hydrophilic than those of the ePLLA and the a-ePLLA, the greater adsorption of proteins on their surface should be the main reason.

Here, a separate experiment was carried out to quantify the amounts of a model protein that were able to adsorb onto the surfaces of the ePLLA and the CA-g-ePLLA. Type I collagen was used as the model protein. The amounts of the adsorbed proteins were reported at various immersion time points and the results are shown in Figure 6. Obviously, increasing the immersion time in the protein solution caused the amount of the absorbed protein to increase, except for the CA-g-ePLLA at 48 and 72 h that showed equivalent values (suggesting that the maximal adsorption was already reached at these time points). Regardless of the time points investigated, the adsorption of

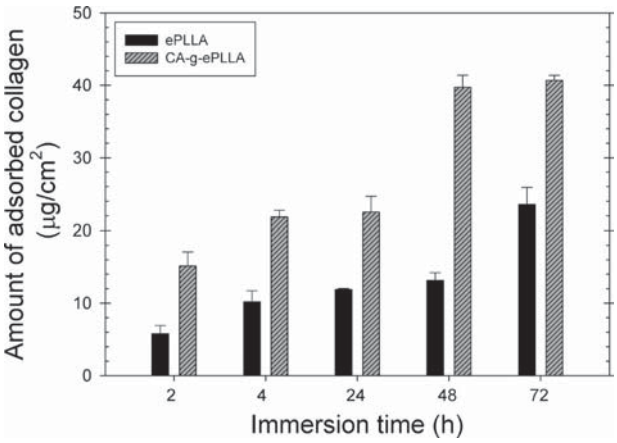


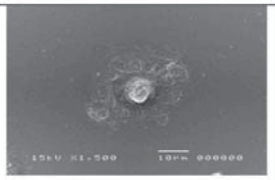
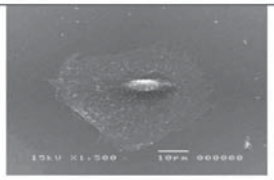
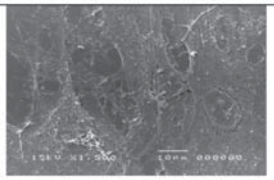
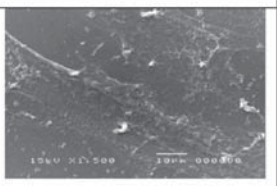
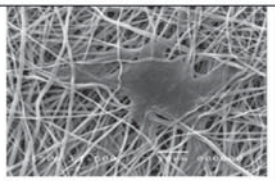
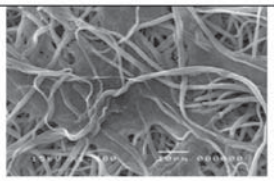
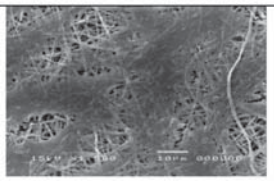
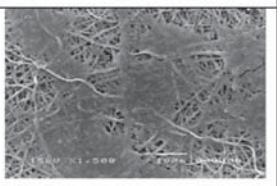
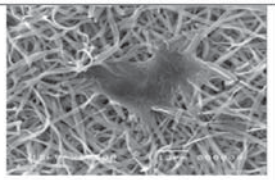
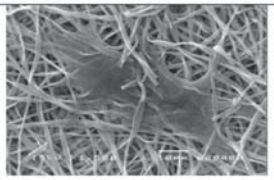
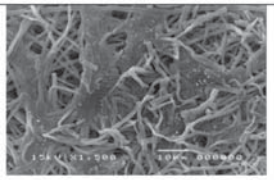
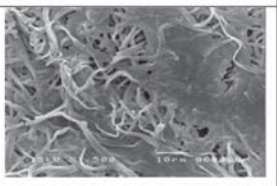
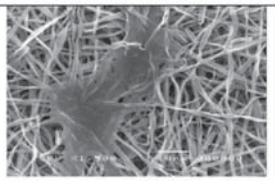
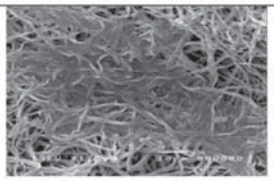
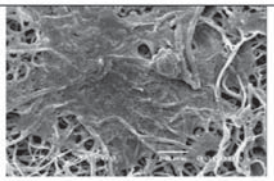
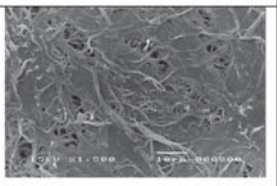
Figure 6. Areal amounts of type I collagen adsorbed on the surfaces of ePLLA and CA-g-ePLLA (i.e., the adsorbed amounts divided by the projection area of the specimens) at various immersion time points. All data sets at any given time point were significantly different (*p < 0.05).

type I collagen on the e-PLLA was in the range of 5.8−23.6 $\mu g \cdot cm^{-2}$ on average (based on the projection area of the specimens), which corresponded to 1.2−7.7 $\mu g \cdot mg^{-1}$ on average (based on the actual weights of the specimens) (n = 5). Significantly greater values were observed for the CA-g-ePLLA over the range of 15.1−40.7 $\mu g\ cm^{-2}$ or 2.8−8.6 $\mu g\ mg^{-1}$ on average. Evidently, the greater hydrophilicity of the CA-g-ePLLA should be responsible for the greater amounts of type I collagen adsorbed on their surfaces.

Cell Morphology. The morphology of HDFa that had been seeded or cultured on the surfaces of the neat and the modified PLLA fibrous membranes was also investigated. Here, glass was used as the control substrate instead of TCPS because of the ease of taking the specimens for SEM observation. Representative SEM images are shown in Table 4. At 2 h after cell seeding, the majority of the cells on the glass surface was still round, while, at 4 h, the evidence of cytoplasmic process was already observed. The full cytoplasmic expansion of the cells on the glass substrate was realized after they had been cultured on the surface for 1 and 3 d. At 4 h after cell seeding, the majority of the cells on the surfaces of the ePLLA and the a-ePLLA was rather round, whereas that on the surface of the CA-g-ePLLA was more expanded. The full cytoplasmic expansion of the cells grown on these fibrous substrates was observed at 4 h after cell seeding, particularly for that of the cells grown on the CA-g-ePLLA. On day 1 after cell culturing, HDFa, in their fully expanded form, covered about 80% or more on the surfaces of all of the fibrous substrates. On day 3, the cell-covered areas were evidently increased, especially for that observed on the CA-g-ePLLA. The obtained results clearly confirmed the preference of HDFa toward the CA-g-ePLLA surface.

Antioxidant Activity of CA-g-ePLLA. The antioxidant activity of the CA-g-ePLLA was determined by the DPPH assay. DPPH• is a stable free radical, exhibiting a characteristic UV absorption at 517 nm, and has been extensively used to

Table 4. Representative SEM Images (magnification = 1500×; scale bar = 10 μm) of Cultured HDFa on Glass, ePLLA, a-ePLLA, and CA-g-ePLLA at Four Different Time Points after Cell Seeding or Cell Culturing

Material	Cell seeding/culturing time point			
	2 h	4 h	1 d	3 d
Glass (control)				
ePLLA				
a-ePLLA				
CA-g-ePLLA				

dx.doi.org/10.1021/am300404v | *ACS Appl. Mater. Interfaces* 2012, 4, 3031−3040

evaluate the antioxidant activity of a variety of substances.[14,28−30] CA, which can act as a donor of an H-atom or an electron in a similar manner to gallic acid, can transform DPPH• into its reduced form DPPH•-H.[31] The antioxidant activity of CA, as the grafted species on the surface of the PLLA fibers, was determined to be 88.4 ± 1.3% (n = 5). The result confirmed that CA still retains its free radical scavenging ability, even though its mobility was limited because of its chemical immobilization onto the surface of the PLLA fibers. Interestingly, the amount of the as-grafted CA on the surfaces of the individual fibers of the CA-g-ePLLA that participated in the scavenging activity of the DPPH radical species was determined to be 2.73 ± 0.10 $\mu g \cdot cm^{-2}$ (based on the projection area of the specimens) or 0.49 ± 0.17 $\mu g\ mg^{-1}$ (based on the actual weights of the specimens) or about 44% (based on the amount of the immobilized CA).

CONCLUSION

Electrospun PLLA fiber mats, with the average fiber diameter of about 620 nm, were prepared from 10% w/v PLLA solution in 7:3 v/v DCM/DMF. The surfaces of the individual PLLA fibers were successfully modified by CA via a two-step grafting procedure and the reactions were confirmed by the ninhydrin assay and XPS. Amino groups were introduced first on the fiber surface and the optimal condition was 0.04 g mL^{-1} of HMD/IPA solution at 50 °C for 10 min, resulting in the surface density of the introduced amino groups of (1.20 ± 0.03) × 10^{-7} mol cm^{-2}. After this step, the wettability of the fiber mat surface improved significantly, as the water contact angles reduced from those of the neat PLLA fiber mats (i.e., 104.8° ± 0.3°) to 83.3° ± 0.4°. The wettability of the fiber mat surface improved even further after the chemical immobilization of CA (with the water contact angles being 55.5° ± 0.5°). Such the chemical modifications caused the fiber diameters to increase to ∼850 and ∼920 nm on average after the aminolysis and the grafting of CA, respectively. In the indirect cytotoxicity assay, none of the fibrous materials released substances in the levels that were detrimental to the cells. In the direct cell culturing assay, all of the fibrous matrices showed very good support for the proliferation of HDFa on days 2 and 3 after cell culturing, with the CA-modified fibrous substrates being the best. Lastly, the antioxidant activity of the grafted CA moieties on the PLLA fibers was determined to be 88.4 ± 1.3%.

ASSOCIATED CONTENT

Supporting Information

Additional graphs: calibration curves (Figure I−IV) and an additional result (Figure V). This material is available free of charge via the Internet at http://pubs.acs.org.

AUTHOR INFORMATION

Corresponding Author

*E-mail: pitt.s@chula.ac.th.

Notes

The authors declare no competing financial interest.

ACKNOWLEDGMENTS

This project was supported in part by (1) the "Integrated Innovation Academic Center: IIAC", Chulalongkorn University Centenary Academic Development Project, Chulalongkorn University, (2) the Center of Excellence on Petrochemical and Materials Technology, Chulalongkorn University, and (3) the Petroleum and Petrochemical College, Chulalongkorn University. P.C. acknowledges her doctoral scholarship received from the Development and Promotion of Science and Technology Talents (DPST) Project, the Institute for the Promotion of Teaching Science and Technology. Additional financial support from The Thailand Research Fund (TRF, Grant DBG5280015) to procure some of the chemicals used in this work is greatly acknowledged.

REFERENCES

(1) Reneker, D. H.; Yarin, A. L. *Polymer* **2008**, *49*, 2387−2425.
(2) Bhardwaj, N.; Kundu, S. C. *Biotechnol. Adv.* **2010**, *28*, 325−347.
(3) Södergard, A.; Stolt, M. *Prog. Polym. Sci.* **2002**, *27*, 1123−1163.
(4) Gupta, B.; Revagade, N.; Hilborn, J. *Prog. Polym. Sci.* **2007**, *32*, 455−482.
(5) Purcell, D. B.; Rudzki, J. R.; Wright, R. W. *Oper. Tech. Sports Med.* **2004**, *12*, 180−187.
(6) Kenawy, E. R.; Bowlin, G. L.; Mansfield, K.; Layman, J.; Simpson, D. G.; Sanders, E. H.; Wnek, G. E. *J. Controlled Release* **2002**, *81*, 57−64.
(7) Zong, X.; Kim, K.; Fang, D.; Ran, S.; Hsiao, B. S.; Chu, B. *Polymer* **2002**, *43*, 4403−4412.
(8) Badami, A. S.; Kreke, M. R.; Thompson, M. S.; Riffle, J. S.; Goldstein, A. S. *Biomaterials* **2006**, *27*, 596−606.
(9) Peesan, M.; Rujiravanit, R.; Supaphol, P. *J. Biomater. Sci. − Polym. Ed.* **2006**, *17*, 547−565.
(10) Xu, X.; Yang, Q.; Wang, Y.; Yu, H.; Chen, X.; Jing, X. *Eur. Polym. J.* **2006**, *42*, 2081−2087.
(11) Li, D.; Frey, M. W.; Baeumner, A. J. *J. Membr. Sci.* **2006**, *279*, 354−363.
(12) Sangsanoh, P.; Waleetorncheepsawat, S.; Suwantong, O.; Wutticharoenmongkol, P.; Weeranantanapan, O.; Chuenjitkuntaworn, B.; Cheepsunthorn, P.; Pavasant, P.; Supaphol, P. *Biomacromolecules* **2007**, *8*, 1587−1594.
(13) Chuenjitkuntaworn, B.; Supaphol, P.; Pavasant, P.; Damrongsri, D. *Polym. Int.* **2010**, *59*, 227−235.
(14) Chuysinuan, P.; Chimnoi, N.; Techasakul, S.; Supaphol, P. *Macromol. Chem. Phys.* **2009**, *210*, 814−822.
(15) Yaszemski, M. J.; Payne, R. G.; Hayes, W. C.; Langer, R.; Mikos, A. G. *Biomaterials* **1996**, *17*, 175−185.
(16) Kim, Y. J. *Biol. Pharm. Bull.* **2007**, *66*, 1052−1055.
(17) Kim, J. H.; Kang, N. J.; Lee, B. K.; Lee, K. W.; Lee, H. J. *Mutat. Res.−Fund. Mol. Mech. Mutagen.* **2008**, *638*, 175−183.
(18) Olthof, M. R.; Hollman, P. C. H.; Katan, M. B. *J. Nutr.* **2001**, *131*, 66−71.
(19) Feng, R. T.; Ni, H. M.; Wang, S. Y.; Tourkova, I. L.; Shurin, M. R.; Harada, H.; Yin, X. M. *J. Biol. Chem.* **2007**, *282*, 13468−13476.
(20) Dastmalchi, K.; Dorman, H. T. D.; Oinonen, P. P.; Darwis, Y.; Laakso, I.; Hiltunen, R. *LWT-Food Sci. Technol.* **2008**, *41*, 391−400.
(21) Elegir, G.; Kindl, A.; Sadocco, P.; Orlandi, M. *Enzyme Microb. Technol.* **2008**, *43*, 84−92.
(22) Mattanavee, W.; Suwantong, O.; Puthong, S.; Bunaprasert, T.; Hoven, V. P.; Supaphol, P. *ACS Appl. Mater. Interfaces* **2009**, *1*, 1076−1085.
(23) Pasanphan, W.; Chirachanchai, S. *Carbohyd. Polym.* **2008**, *72*, 169−177.
(24) Kampalanonwat, P.; Supaphol, P. *Ind. Eng. Chem. Res.* **2011**, *50*, 11912−11921.
(25) K-hasuwan, P.; Pavasant, P.; Supaphol, P. *Langmuir* **2011**, *27*, 10938−10946.
(26) Re, R.; Pellegrini, N.; Proteggente, A.; Pannala, A.; Yang, M.; Rice-Evans, C. *Free Radical Biol. Med.* **1999**, *26*, 1231−1237.
(27) Cui, W.; Li, X.; Xie, C.; Chen, J.; Zou, J.; Weng, J. *Polymer* **2010**, *51*, 2320−2328.
(28) Tabata, H.; Katsube, T.; Tsuma, T.; Ohta, Y.; Imawaka, N.; Utsumi, T. *Food Chem.* **2008**, *109*, 64−71.
(29) Kubola, J.; Siriamornpun, S. *Food Chem.* **2008**, *110*, 881−890.

(30) Bozin, B.; Mimica-Dukic, N.; Samojlik, I.; Goran, A.; Igic, R. *Food Chem.* **2008**, *111*, 925−929.
(31) Yen, G.-C.; Duh, P.-D.; Tsai, H.-L. *Food Chem.* **2002**, *79*, 307−313.

Langmuir

ARTICLE

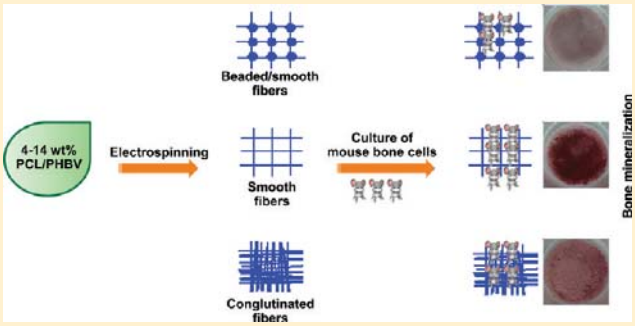
pubs.acs.org/Langmuir

Effect of the Surface Topography of Electrospun Poly(ε-caprolactone)/Poly(3-hydroxybuterate-*co*-3-hydroxyvalerate) Fibrous Substrates on Cultured Bone Cell Behavior

Prae-ravee K-hasuwan,[†,‡] Prasit Pavasant,[§] and Pitt Supaphol*[,†,‡]

[†]The Petroleum and Petrochemical College, [‡]The Center for Petroleum, Petrochemicals, and Advanced Materials, and [§]Department of Anatomy, Faculty of Dentistry, Chulalongkorn University, Bangkok 10330, Thailand

ABSTRACT: The use of electrospun fibrous matrices as substrates for cell/tissue culture has usually been confined to those consisting of smooth fibers. Here, we demonstrated that in vitro responses of mouse-calvaria-derived preosteoblastic cells (MC3T3-E1) that had been cultured on electrospun fibrous substrates made from blend solutions of 50/50 w/w poly(ε-caprolactone) (PCL) and poly(3-hydroxybutyrate-*co*-3-hydroxyvalerate) (PHBV) of varying concentrations, ranging from 4 to 14 wt %, depended strongly on the topography of the individual fibers. As the concentration of the blend solutions increased from 4 to 14 wt %, the topography of the individual fibers changed from discrete beads/smooth fibers to beaded fibers/smooth fibers and finally to smooth fibers, and the average diameter of the individual, smooth fibers increased from ∼0.4 to ∼1.8 μm. The results clearly showed that MC3T3-E1 preferred the smooth hydrophilic surface of the fibrous substrate from 10 wt % PCL/PHBV solution because the cells appeared to attach, proliferate, and differentiate on the surface of this substrate particularly well.



INTRODUCTION

The replacement of a large bone defect (i.e., a defect with a size that is beyond the ability of the bone tissue to self-regenerate) requires the use of a scaffold with a 3D porous structure that favors the infiltration of bone cells and new blood vessels.[1−3] The material used in the fabrication of the scaffold should be biocompatible and exhibit a rate of degradation that is comparable to that of the neotissue. It should also exhibit mechanical properties that are suitable for maintaining the integrity of the replaced site throughout the course of the healing process. Furthermore, a high porosity and the suitability of the topography and chemical functionality of the surface of the scaffold are important factors determining its effectiveness when it is in contact with biological entities in the replaced site.[1−3]

Among various types of scaffolds, the ones exhibiting a fibrous architecture resembling the fibrillar structure of the natural extracellular matrix (ECM) of the connective tissues showed much better support for the attachment and proliferation of cultured bone cells when compared to those of smoother surfaces (e.g., films).[4] Various techniques that have been used to fabricate fibrous substrates are, for examples, phase separation, melt blowing, and electrospinning.[4−6] Low tooling costs, technical simplicity, and numerous unique characteristics of the obtained fibrous materials (e.g., small diameters of the individual fibers ranging from tens of nanometers to a few micrometers, the interconnected porous structure of the obtained matrices, and vast possibilities for surface functionalization) make electrospinning one of the most commonly utilized fabrication methods of fibrous matrices for biomedical applications.[4−9] However, the use of fibrous matrices as substrates for cell/tissue culture has thus far been confined to those consisting mainly of smooth individual fibers.[2,4−6,8,9] It is known that the morphology of individual electrospun fibers is most affected by the variation in the concentration, and hence the shear viscosity, of the spinning solutions.[10] As the shear viscosity increases, the morphology of the obtained products would change from discrete droplets to beaded fibers and finally to smooth fibers of varying cross-sectional shapes (i.e., round, ribbonlike, etc.). Additionally, the size of the individual fibers (for beaded and smooth fibers) increases monotonically with an increase in the shear viscosity of the spinning solutions.[10] Because beads have usually been considered to be defects of the fibers (i.e., for beaded fibers), proposed uses of the electrospun products in biomedical applications have been confined to those consisting of smooth fibers.[4−9] The main objective of the present work is therefore to investigate the biological response of mouse-calvaria-derived preosteoblastic cells (MC3T3-E1) that are cultured on electrospun fibrous substrates with varying surface topographies of the individual fibers.

Among the various biocompatible and biodegradable materials that have been fabricated into bone scaffolds, poly-

Received: June 16, 2011
Revised: July 25, 2011
Published: July 26, 2011

ACS Publications © 2011 American Chemical Society

(ε-caprolactone) (PCL), poly(3-hydroxybutyrate-*co*-3-hydroxyvalerate) (PHBV), their blends, and the blends of each of them with another biocompatible and biodegradable polymer (e.g., poly(3-hydroxybutyrate) (PHB), polylactide (PLA), etc.), and their composites with an osteoconductive material (e.g., hydroxyapatite (HAp)) have been shown to provide very good support for the attachment, proliferation, and differentiation of cultured bone cells.[4,11−14] PCL, a U.S. Food and Drug Administration (USFDA)-approved material for craniofacial indications, is a synthetic semicrystalline aliphatic polyester with low glass transition and melting temperatures.[4,11,15] The popularity of PCL as a bone scaffolding material stems from its solubility in a wide range of common organic solvents, its nontoxic biodegradation products, and the degradation rate that is suitable for harboring bone regeneration.[15,16] Various forms of PCL, such as electrospun fibrous substrates,[4] particulate-leached porous scaffolds,[11] centrifugation-induced porous scaffolds,[17] spiral-structured porous scaffolds,[18] and porous scaffolds made by the precision-extruding deposition (PED) method,[19] have been shown to provide good support for bone regeneration in vitro and/or in vivo. On the other hand, PHBV, the most common copolymeric variant of PHB, is a semicrystalline aliphatic polyester produced naturally in certain strains of bacteria.[12,20−22] PHB is ideal to be used in vivo because its biodegradation product, D,L-β-hydroxybutyrate (HB), is a normal component of blood and tissues.[23] Notwithstanding, PHBV is most commonly utilized mainly because of the presence of the hydroxyvalerate comonomeric unit that reduces the crystallinity and, simultaneously, improves flexibility and processability.[22] PHBV in various physical forms, such as electrospun fibrous substrates[12] and particulate-leached porous scaffolds,[24] has been shown to provide good support for the growths of various cell types, including osteoblasts, fibroblasts, Schwann cells, epithelial cells, and ovine chondrocytes.

In this work, fibrous matrices of varying surface topographies of the individual fibers were prepared by electrospinning from the blend solutions of 50/50 w/w PCL/PHBV in a mixture of chloroform and *N*,*N*-dimethylformamide (DMF). This was achieved by varying the concentration of the solutions (i.e., between 4 and 14 wt %). The effect of the solution concentration on the morphology of the individual fibers as well as the morphology, mechanical integrity, and the physicochemical properties of the obtained fibrous matrices was examined in comparison with those of the fibers obtained from solutions of the individual polymeric constituents. The potential for the use of these fibrous matrices as bone scaffolds was assessed in vitro with MC3T3-E1 in terms of the attachment, proliferation, alkaline phosphatase (ALP) activity, and mineralization.

EXPERIMENTAL SECTION

Materials. Poly(ε-caprolactone) (PCL, M_w = 80 000 g·mol^{-1}) and poly(3-hydroxybutyrate-*co*-3-hydroxyvalerate) (PHBV, M_w = 680 000 g·mol^{-1}) were purchased from Sigma-Aldrich, USA. *N*,*N*-Dimethylformamide (DMF), dichloromethane (DCM), and chloroform were purchased from Labscan (Asia), Thailand. All other chemicals were analytical reagent grade and used without further purification.

Preparation of Fibrous Substrates. Blend solutions of 50/50 w/w PCL/PHBV of varying concentrations ranging from 4 to 14 wt % were prepared in 80/20 v/v chloroform/DMF at room temperature (25 ± 1 °C). PCL solution at 12 wt % was prepared in 50/50 v/v DCM/DMF at room temperature, and PHBV solution at 14 wt % was prepared in chloroform at 50 °C.[25] The electrospinning of these solutions was carried out using a typical method. Briefly, each of the solutions was contained in a glass syringe, the open end of which was connected to a gauge-20 stainless steel needle (o.d. = 0.91 mm), used as the nozzle. An aluminum (Al) sheet wrapped around a rotating drum (width and o.d. of the drum ∼15 cm; rotational speed ∼50 rpm) was employed as a collector. The distance from the tip of the needle to the outer surface of the Al sheet was set at 10 cm. A Gamma High-Voltage Research D-ES30PN/M692 power supply was used to generate a high dc potential (i.e., 21 kV for the blend and PCL solutions and 12 kV for the PHBV solution). The emitting electrode (+) of the power supply was attached to the needle, and the grounding electrode was attached to the collector. A Kd Scientific syringe pump was used to maintain the feed rate of the solution at ∼1 mL·h^{-1}. The solutions were electrospun consecutively for ∼10 h.

Characterization. The viscosities of the polymer solutions were measured by a Brookfield DVIII Ultra rheometer at room temperature and 20 rpm rotational speed of the spindle (n = 5).

The surface topographies and sizes of the individual fibers as well as those of the beads (in the case of the beaded fibers) of the obtained fibrous substrates were analyzed by a JEOL JSM-5410LV scanning electron microscope (SEM). For each sample, the sizes of the individual fibers (and beads, where applicable) were measured from various positions of at least five different SEM images by SemAphore 4.0 software ($n \geq 50$). Additionally, the thicknesses of the fibrous substrates were measured by a Mitutoyo digital micrometer (n = 5).

The chemical integrity of the obtained fibers was identified by a Nicolet NEXUS407 Fourier transform infrared spectrometer in attenuated total reflection mode (ATR-FTIR), at a resolution of 4 cm^{-1} over a wavenumber range of 4000 to 400 cm^{-1}.

Static water contact angles of the obtained fibrous substrates were measured with a Krüss DSA 100 drop shape analysis system. Ten droplets of distilled water (10 μL) were placed randomly at different positions on each sample. The projected images of the droplets, after they had been allowed to stay on the substrates until no further change in their shapes was observed, were analyzed for the contact angles, and the data were averaged.

The mechanical integrity, in terms of the tensile strength and Young's modulus, of the obtained fibrous substrates (rectangular shape, 10 mm × 100 mm) was assessed using a Lloyd LRX universal testing machine (gauge length = 50 mm and crosshead speed = 20 mm·min^{-1}) (n = 5).

The true densities of the obtained fibrous substrates ($\rho_{scaffold}$) were measured on ∼1 g samples using a Quantachrome Ultrapycnometer-1000 gas pycnometer (n = 5). On the basis of the obtained data, the porosities and pore volumes of the matrices can be calculated from the following expressions, respectively: $(1 - (\rho_{scaffold}/\rho_{polymer})) \times 100$ and $(1/\rho_{scaffold} - 1/\rho_{polymer})$, where $\rho_{polymer}$ represents the bulk density of the polymeric constituent(s). Here, ρ_{PCL}, ρ_{PHBV}, and $\rho_{PCL/PHBV(50/50\ w/w)}$ were taken as 1.145, 1.250, and 1.198 g·cm^{-3}, respectively.

Cell Culturing. Mouse-calvaria-derived preosteoblastic cells (MC3T3-E1; ATCC CRL-2593) were cultured in minimum essential medium with Earle's Balanced Salts (MEM; HyClone, USA), supplemented by 10% fetal bovine serum (FBS; Biochrom, U.K.), 1% L-glutamine (Invitrogen, USA), and a 1% antibiotic and antimycotic formulation (containing penicillin G sodium, streptomycin sulfate, and amphotericin B; Invitrogen, USA). The medium was replaced every other day, and the cultures were maintained at 37 °C in a humidified atmosphere containing 5% CO_2. Fibrous substrate specimens (circular discs, ∼15 mm in diameter) were placed in wells of a 24-well tissue-culture polystyrene plate (TCPS; Corning, USA) and subsequently sterilized in 70% ethanol for 90 min. The specimens were then washed with autoclaved deionized water and then immersed in MEM overnight. A metal ring (∼12 mm in diameter) was placed on top of each specimen to ensure good contact of the specimen with the bottom of each well.

MC3T3-E1 from the cultures were trypsinized (0.25% trypsin containing 1 mM ethylenediaminetetraacetic acid (EDTA); Invitrogen, USA), counted by a Hausser Scientific hemacytometer, and seeded at ~40 000 cells cm^{-2} on each of the specimens and the empty wells of a TCPS (i.e., positive control).

In the attachment and the proliferation studies, cells were cultured in the same media as mentioned above. For other studies, cells were cultured in MEM supplemented by 2% FBS, 1% L-glutamine, and 1% antibiotic and antimycotic during the first 3 days, after which they were cultured in the same medium but with the addition of an osteogenic supplement (i.e., 5 mM glycerol-2-phosphate disodium salt hydrate (β-glycerophosphate; Sigma-Aldrich, USA) and 50 $\mu g \cdot mL^{-1}$ L-ascorbic acid (Sigma-Aldrich, USA)).

Cell Attachment and Cell Proliferation. The cells were allowed to attach to the fibrous substrate specimens and empty wells of a TCPS for 2, 4, and 6 h in the attachment study ($n = 4$). At each time point, the number of attached cells was quantified by a 3-(4,5-dimethylthiazol-2-yl)-2,5-diphenyl-tetrazolium bromide (MTT; Sigma-Aldrich, USA) assay. Additionally, the cells were first allowed to attach to the specimens and empty wells of a TCPS for 16 h and then were measured at 24 h. The number of proliferated cells was also determined by MTT assay on days 1, 2, and 3 after cell culturing ($n = 4$). The appearance of the cells during the attachment and proliferation periods was characterized by SEM (discussed later).

Quantification of Viable Cells (MTT Assay). MTT assay is a cell quantification method that measures the activity of mitochondria in their ability to reduce a tetrazolium-based compound, MTT, to a purplish formazan product. The amount of purplish formazan product is proportional to the number of viable cells. Each cell-cultured specimen was incubated at 37 °C for 30 min with MTT solution, and the formazan product was then dissolved in a mixture of dimethylsulfoxide (DMSO; Carlo Erba, Italy; 900 μL/well) and glycine buffer (pH 10; 125 μL/well). The absorbance of the supernatant was evaluated with a Thermospectronic Genesis10 UV−visible spectrophotometer at 570 nm. The observed UV absorbance values were converted to the number of cells using predetermined standard calibration curves.

Morphological Observation of Cultured Cells. Each cell-cultured specimen, after the removal of the culture medium, was rinsed with PBS twice, and the cells were then fixed with 3% glutaraldehyde solution (Electron Microscopy Science, USA) at 500 μL/well for 30 min. The specimen was rinsed again with PBS and dehydrated in ethanolic aqueous solutions of varying concentrations (i.e., 30, 50, 70, and 90 vol %) and in pure ethanol for ~2 min each. It was dried in 100% haxamethyldisilazane (HMDS; Sigma-Aldrich, USA) for 5 min and subsequently in air. The specimens were then observed by SEM, and the morphology of the cells that had been cultured on glass substrates (12 mm in diameter; Menzel, Germany) was used as a positive control.

Alkaline Phosphatase (ALP) Analysis. MC3T3-E1 were cultured on the fibrous substrate specimens and the empty wells of a TCPS for 3 and 7 days to determine the ALP activity ($n = 4$). Each specimen, after the removal of the culture medium, was rinsed with PBS. Alkaline lysis buffer (10 mM Tris-HCl, 2 mM $MgCl_2$, 0.1% Triton-X 100, pH 10) (100 μL/well) was added, and the specimen was scrapped, sonicated, and then frozen at −20 °C for ~30 min. An aqueous solution of 2 $mg \cdot mL^{-1}$ *p*-nitrophenyl phosphate (PNPP; Invitrogen, USA) mixed with 0.1 M aminopropanol (10 μL/well) in 2 mM $MgCl_2$ (100 μM/well) was added to the specimen, which was then incubated at 37 °C for 30 min. An aqueous solution of NaOH (50 nM at 0.9 mL/well) was added, and the extracted solution was measured spectrophotometrically at 410 nm. The amount of ALP was calculated against a predetermined standard curve and then normalized by the total protein content. For the protein assay, each specimen was treated in the same manner as in the ALP assay up to the point where it was frozen. A bicinchoninic acid (BCA; Pierce Biotechnology, USA) solution was then added to the specimen and incubated at 37 °C for 30 min. The absorbance of the medium solution was finally measured spectrophotometrically at 562 nm, and the amount of total proteins was calculated against a predetermined standard curve.

Mineralization Analysis. Calcium deposition was investigated by Alizarin Red-S (Sigma-Aldrich, USA) staining. MC3T3-E1 had been cultured on the fibrous substrate specimens and empty wells of a TCPS for 14 days ($n = 4$), after which the cells were fixed with cold methanol for 10 min, washed with deionized water, and immersed in 1% Alizarin Red-S solution in a mixture of 0.4 mL ammonium hydroxide/40 mL water for 3 min. Each stained specimen was washed several times with deionized water and air dried at room temperature. The stained specimen was photographed, and the redness, signifying the amount of calcium deposition, was quantified by destaining with 10% cetylpyridinium chloride monohydrate (Sigma-Aldrich, USA) in 10 mM sodium phosphate at room temperature for 15 min and spectrophotometrically read at 570 nm.

Statistical Analysis. All values were presented as means ± standard deviations. The significance between two data sets was determined by one-way ANOVA analysis using the *t* test for all analyses, except for the attachment, proliferation, and ALP activity analytical studies. Scheffe's test was applied to the three studies. The statistical significance was accepted at a 0.05 confidence level.

RESULTS AND DISCUSSION

Characterization of Polymer Solutions and Fibrous Substrates. As previously mentioned, the shear viscosity poses a strong influence on the morphology of the individual electrospun fibers.[10] Prior to electrospinning, the PCL/PHBV solutions were measured for the shear viscosities (Table 1). As the total concentration of the blend solutions increased from 4 to 14 wt %, the shear viscosity increased from ~290 to ~580 mPa·s. Electrospinning of these solutions was carried out under an electric field of 21 kV/10 cm. (See Figure 1 for the representative SEM images of the obtained products.) At 4 wt %, a combination of discrete beads (~16 μm on average) and smooth fibers (~0.4 μm on average) was obtained. At 6 and 8 wt %, a combination of beaded and smooth fibers was evident. At these concentrations, the sizes of the beads were in the range of 2.6−3.4 μm on average and those of the fibers were in the range of 0.5−0.6 μm on average. The densities of the beads that were observed on the electrospun products from 4 to 8 wt % PCL/PHBV solutions were 1420, 3480, and 3020 beads·mm^{-2}, on average. Between 10 and 14 wt %, only smooth fibers were generated. The size of these fibers increased from ~0.8 μm on average at 10 wt % to ~1.8 μm on average at 14 wt %. It should be mentioned at this point that the blend composition of 50/50 w/w between PCL and PHBV was chosen on the basis of preliminary results, which showed that the fibers that had been obtained from other blend compositions were very nonuniform (results not shown). This may arise from the immiscibility of the two polymers (later discussion).

From these SEM images, the individual fibers in all of the fibrous substrates were randomly aligned, and they appeared to conglutinate to one another at touching points. Although the random alignment related directly to the slow rotational speed of the collection device used during fiber collection, the partial conglutination was due to the rather short collection distance and hence incomplete evaporation of the solvent from the jet segments during their flights to the collector.[10] Electrospinning of

Table 1. Viscosities of PCL/PHBV, PCL, and PHBV Solutions and Physical, Physico-Chemical, and Mechanical Characteristics of the Obtained Electrospun Fibrous Substrates

sample	viscosity (mPa·s)	fiber diameter (μm)	bead size (μm)	bead density (beads·mm^{-2})	thickness (μm)	water contact angle (deg)	tensile strength (MPa)	Young's modulus (MPa)	elongation at break (%)
4% PCL/PHBV	292 ± 3	0.44 ± 0.09	15.56 ± 0.95	1420 ± 130	93 ± 7	121 ± 2	0.98 ± 0.06	162.1 ± 4.6	1.4 ± 0.2
6% PCL/PHBV	343 ± 4	0.51 ± 0.03	2.57 ± 0.34	3480 ± 190	98 ± 3	117 ± 1	1.21 ± 0.38	145.6 ± 3.7	2.3 ± 0.6
8% PCL/PHBV	371 ± 3	0.58 ± 0.02	3.36 ± 0.23	3020 ± 330	109 ± 4	106 ± 3	1.58 ± 0.17	139.2 ± 3.8	2.8 ± 0.4
10% PCL/PHBV	434 ± 5	0.77 ± 0.02			117 ± 5	85 ± 2	1.84 ± 0.09	112.3 ± 1.9	4.3 ± 0.7
12% PCL/PHBV	528 ± 5	1.08 ± 0.06			113 ± 6	90 ± 1	1.87 ± 0.11	108.8 ± 2.2	4.5 ± 0.5
14% PCL/PHBV	581 ± 7	1.79 ± 0.05			110 ± 5	99 ± 1	1.95 ± 0.26	102.7 ± 2.6	4.9 ± 0.2
12% PCL	451 ± 3	0.96 ± 0.04			121 ± 2	103 ± 1	2.41 ± 0.36	82.4 ± 5.6	5.7 ± 0.8
14% PHBV	621 ± 2	2.19 ± 0.07			92 ± 4	115 ± 3	1.79 ± 0.13	126.7 ± 7.1	3.8 ± 0.3

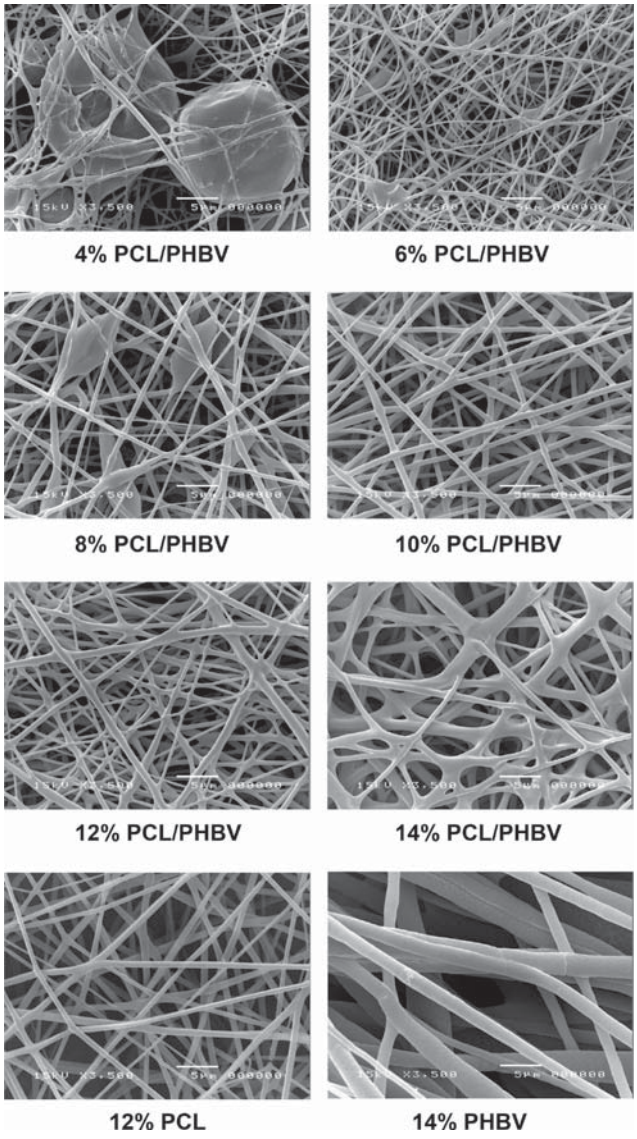


Figure 1. Representative SEM images (scale bar = 5 μm and magnification = 3500×) of the electrospun fibrous substrates from 4 to 14 wt % PCL/PHBV, 12 wt % PCL, and 14 wt % PHBV solutions.

the neat PCL and PHBV solutions was also carried out for comparison (Figure 1). The obtained fibers shared essentially

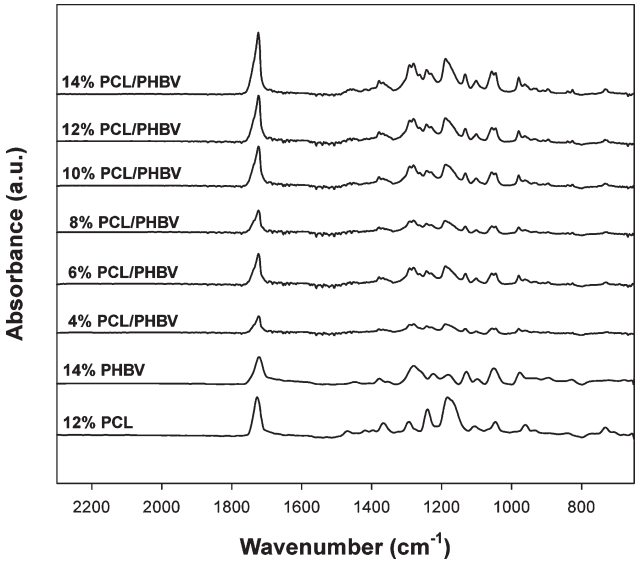


Figure 2. ATR-FTIR spectra of the obtained electrospun fibrous substrates.

the same features as those obtained from the 10−14 wt % PCL/PHBV solutions. The sizes of these fibers were ∼1.0 and ∼2.2 μm on average, respectively. Upon consecutive spinning for ∼10 h, the thicknesses of the blend fibrous substrates ranged between ∼90 and ∼110 μm on average whereas those of the PCL and the PHBV counterparts were ∼120 and ∼90 μm on average, respectively. The actual sizes of the fibers and beads, where applicable, are also summarized in Table 1.

The chemical integrity of the PCL/PHBV fibers was investigated by ATR-FTIR (Figure 2). Those of the neat PCL and PHBV counterparts are also shown for comparison. The absorption peak, centered at around 1724 cm^{-1} and belonging to the stretching vibrations associated with the crystalline conformations of the carbonyl ester (C═O),[26] was evident in all of the IR spectra. For the blend fibers, the way in which this peak increased in its intensity with an increase in the total concentration of the solutions is indicative of the increase in the total crystallinity. Referring to Figure 2, because all of the characteristic peaks of the neat polymers can be observed in the IR spectra of the blend fibers, the existence of both PCL and PHBV components within the blend fibers was confirmed. Furthermore, because no peak shifts or new absorption peaks were observed for the blend fibers, it is expected that specific interactions between PCL and PHBV

Table 2. True Densities, Porosities, and Pore Volumes of the Obtained Electrospun Fibrous Substrates

sample	true density, $\rho_{scaffold}$ ($\times 10^{-2}$ g·cm^{-3})	porosity (%)	pore volume (cm^3·g^{-1})
4% PCL/PHBV	2.30 ± 0.26	98.1 ± 0.5	42.6 ± 3.2
6% PCL/PHBV	2.61 ± 0.15	97.8 ± 0.3	33.2 ± 2.5
8% PCL/PHBV	2.86 ± 0.54	97.6 ± 0.7	34.1 ± 3.0
10% PCL/PHBV	3.19 ± 0.23	97.3 ± 0.4	30.5 ± 1.7
12% PCL/PHBV	3.57 ± 0.39	97.0 ± 0.7	27.2 ± 1.7
14% PCL/PHBV	3.93 ± 0.38	96.7 ± 0.6	24.6 ± 2.4
12% PCL	4.69 ± 0.11	95.9 ± 0.4	20.6 ± 2.1
14% PHBV	2.13 ± 0.17	98.3 ± 0.2	46.1 ± 2.6

molecules were inexistent. Qiu et al.[27] showed that solvent-cast PCL/PHBV blend films exhibited distinctive and unchanged glass-transition and melting temperatures of either component, which is indicative of an immiscible polymer blend.

The physico-chemistry, in terms of static water contact angles, of all of the fibrous substrates was investigated (Table 1). When the size of the plated water droplet is much greater than that of the underlying fibers of a fibrous substrate, both the size and the topography of the underlying individual fibers play important roles in controlling the contact angle of the water droplet.[28,29] For the beaded fibers, as the size of the beads decreased (corresponding to the increase in the solution concentration), the water contact angle was found to increase, hence leading to a decrease in the wettability.[28] As the beads disappeared completely (i.e., smooth fibers), a sudden decrease in the water contact angles and hence a sudden increase in the wettability was observed.[28] For the smooth fibers, an increase in the sizes of the fibers was responsible for the observed increase in the water contact angles and hence the decrease in the wettability.[29]

Here, as the total concentration of the PCL/PHBV solutions increased from 4 to 8 wt %, the average water contact angle of the obtained beaded fibers decreased from ~121 to ~106°. A sharp drop in the average water contact angle was observed when only the smooth fibers were the main products at 10 wt %, but as the concentration of the blend solutions increased from 10 to 14 wt %, the average water contact angle of the obtained smooth fibers increased again from ~85 to ~99°. Evidently, the wettability of the fibrous substrate that had been obtained from the 10 wt % blend solution was the greatest. On the basis of the SEM images of the PCL/PHBV fibrous substrates in Figure 1, it can be postulated that the smoother the surface of the fibrous substrates, the greater the wettability. For comparison, the average water contact angles of the PCL and PHBV fibrous substrates were ~103 and ~115°, respectively.

The mechanical integrity in terms of the tensile strength, Young's modulus, and elongation at break of the fibrous substrates is also investigated (Table 1). For the blend fibrous substrates, the tensile strength and the elongation at break values were found to increase (i.e., from ~0.98 to ~1.95 MPa on average for the tensile strength and from ~1.4 to ~4.9% on average for the elongation at break), whereas that of the Young's modulus was found to decrease (i.e., from ~162 to ~103 MPa on average), with an increase in the total concentration of the PCL/PHBV solutions from 4 to 14 wt %. Interestingly, the neat PCL fibrous substrates exhibited the greatest values of the tensile strength and elongation at the break (i.e., ~2.41 MPa and ~5.7% on average, respectively,) and at the same time they had the lowest value of the Young's modulus (i.e., ~82.4 MPa on average). The property values of the neat PHBV fibrous substrates, on the other hand, were relatively moderate (Table 1).

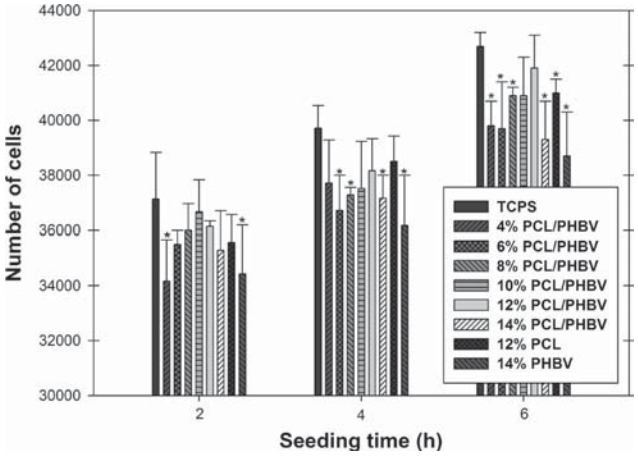


Figure 3. Attachment of MC3T3-E1 that were seeded onto the surfaces of TCPS and various types of fibrous substrates as a function of the cell seeding time. *Significance at $p < 0.05$ with respect to TCPS.

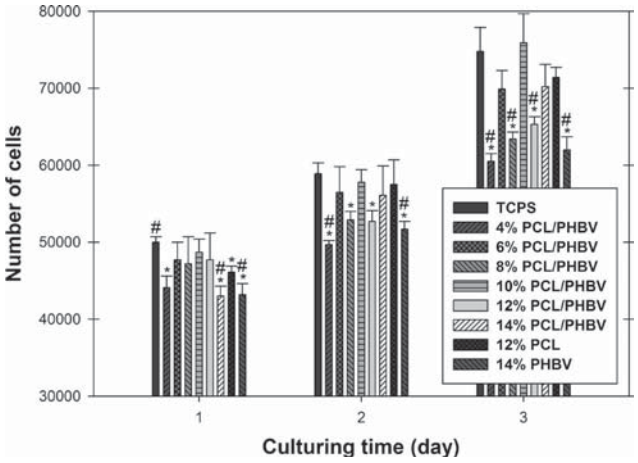


Figure 4. Proliferation of MC3T3-E1 that were cultured on the surfaces of TCPS and various types of fibrous substrates as a function of the cell culturing time. *Significance at $p < 0.05$ with respect to TCPS. #Significance at $p < 0.05$ with respect to the fibrous substrate from 12 wt % PCL solution.

The true densities, porosities, and pore volumes of the obtained fibrous substrates were investigated (Table 2). For the blend fibrous substrates, the true density was found to increase (i.e., from ~2.3 × 10^{-2} to ~3.9 × 10^{-2} g·cm^{-3} on average), and those of the porosity and the pore volume were found to decrease (i.e., from ~98.1 to ~96.7% on average for the porosity and from ~42.6 to ~24.6 cm^3·g^{-1} on average for the pore volume), with an increase in the total concentration of the PCL/PHBV solutions from 4 to 14 wt %. The results imply that as the total concentration of the blend solutions increased the packing of the underlying fibers also increased. Among all of the fibrous substrates investigated, those made of PCL exhibited the lowest porosity and those made of PHBV were the greatest (Table 2).

Cell Attachment and Cell Proliferation. Quantitative analysis for the adherence of MC3T3-E1 after having been seeded on the surfaces of TCPS and all types of fibrous substrates for 2, 4,

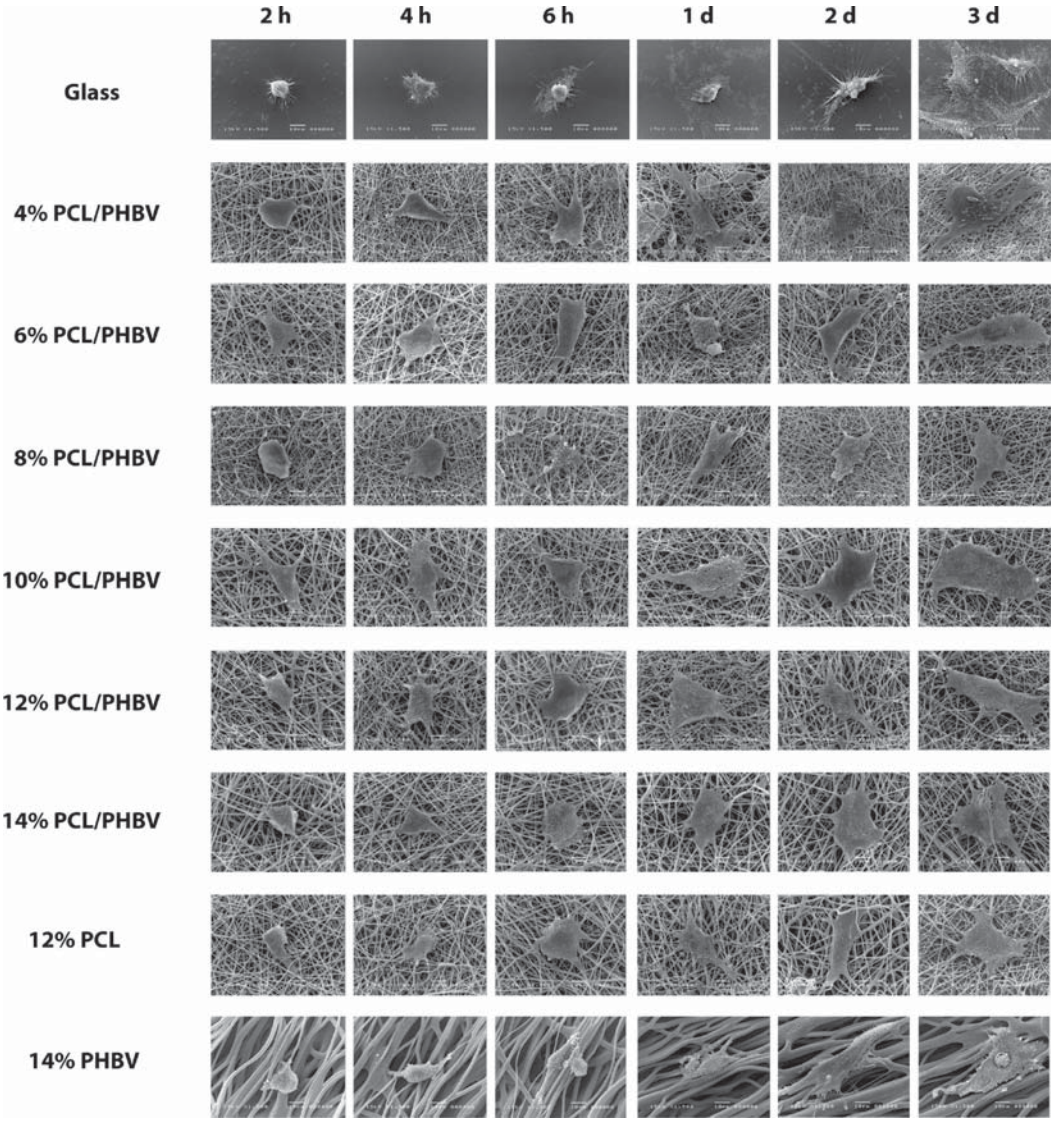


Figure 5. Representative SEM images (scale bar = 10 μm and magnification = 1500×) of MC3T3-E1 that were seeded/cultured on the surfaces of a glass substrate (control) and various types of fibrous substrates at various time points.

and 6 h is shown in Figure 3. For any given type of substrate, the number of cells increased with an increase in the cell seeding time. At 2 h, the numbers of cells on the surfaces of almost all types of fibrous substrates, except for those of the substrates from 4 wt % PCL/PHBV and 14 wt % PHBV solutions that exhibited significantly lower values, were equivalent to that on TCPS. At 4 h, the numbers of cells on the surfaces of the fibrous substrates from 4, 10, and 12 wt % PCL/PHBV and 12 wt % PCL solutions were equivalent to that on TCPS. At 6 h, only the numbers of cells on the surfaces of the fibrous substrates from 10 and 12 wt % PCL/PHBV solutions were equivalent to that on TCPS. Among the various types of fibrous substrates, those from 10 and 12 wt % PCL/PHBV and 12 wt % PCL solutions, regardless of the cell seeding time, appeared to support the attachment of the investigated bone cells slightly better than did the others.

A quantitative analysis of the proliferation of MC3T3-E1 after having been cultured on the surfaces of TCPS and all types of fibrous substrates for 1−3 days is shown in Figure 4. For any given type of substrate, the number of cells increased with an increase in the cell culturing time. On day 1, the numbers of cells on the surfaces of fibrous substrates from 6 to 12 wt % PCL/PHBV were equivalent to that on TCPS. On days 2 and 3, the numbers of cells on the surfaces of fibrous substrates from 6, 10, and 14 wt % PCL/PHBV and 12 wt % PCL solutions were equivalent to that on TCPS. Nevertheless, the average number of cells proliferated on the surface of the fibrous substrate from 10 wt % PCL/PHBV solution was greater than those on the surfaces of the other types of fibrous substrates. Particularly on day 3, the average number of cells on the surface of the fibrous substrate from 10 wt % PCL/PHBV solution was significantly greater than that of the fibrous substrate from 12 wt % PCL and slightly greater than that on TCPS.

Though not totally relevant, Kumbar et al.[30] demonstrated that the biological response of human skin fibroblasts (hSF) that had been cultured on the surfaces of poly(lactic acid-*co*-glycolic acid) (PLAGA) fibrous substrates was, in many respects, fiber-size-dependent. Specifically, the PLAGA fibrous substrates with the diameters of the underlying fibers ranging from 250 to

1200 nm showed significantly greater support for the proliferation and the expression of collagen III of the cultured hSF than the matrices with lower or larger fiber diameters. However, no particular trends were observed for the production of collagen I and elastin with the variation in fiber diameter.[30] Khang et al.[31] prepared poly(L-lactide-*co*-glycolide) (PLGA) films with chemogradient wettability by a corona treatment and found that fibroblasts adhered, spread, and grew particularly better onto positions with moderate hydrophilicity (i.e., a water contact angle of ~55°). On the basis of these studies,[30,31] both the size of the underlying fibers and hence the wettability of a fibrous substrate should play important roles in mediating the cell behavior. Here, the mouse bone cells appeared to attach and proliferate well on the surface of the fibrous substrate from 10 wt % PCL/PHBV solution, which exhibited the lowest water contact angle of ~85° on average.

Because the adsorption of proteins is influenced by the hydrophilicity/hydrophobicity of a surface, a surface with a certain water contact angle would favor the adsorption of certain proteins, which may or may not act as cellular mediators. Additionally, it is hypothesized that both the size and the topography of the underlying fibers of a fibrous substrate may directly influence the organization of organelles within the attached cells. Different organizations of the organelles may result in different chemosignaling pathways that directly influence the cell behavior. Although the effect of different surface topographies on the wettability, adsorption of proteins, and responses of the cultured bone cells should be a subject of thorough investigation, the effect of different organizations of organelles, in response to different surface topographies, on certain behaviors of the cultured bone cells can be rationalized from an existing published report.[32] In an attempt to investigate the effect of fiber alignment on the responses of MG63 human osteosarcoma cells that had been cultured on the surfaces of randomly aligned and well-aligned poly(L-lactic acid) (PLLA) fibrous substrates, Wang et al.[32] found that the cells on the well-aligned fibrous substrate elongated their cytoplasms along the fiber axis but appeared to attach, proliferate, and differentiate better on the randomly aligned fibrous substrate. This exemplifies the importance of the surface topography of a scaffold in cellular behavior.

Selected SEM images illustrating the morphologies of MC3T3-E1 that had been cultured on the surfaces of glass and all types of fibrous substrates for various time intervals are shown in Figure 5. At 2 h after cell seeding, most of the cells on almost all types of the fibrous substrates were still round, except for those on the surfaces of the fibrous substrates from 6 wt % PCL/PHBV, 10 wt % PCL/PHBV, and 12 wt % PCL solutions that showed a slight expansion of their cytoplasms. At this time point, the cells on the control glass substrate were also still round, but a cytoplasmic process in the form of filopodia was clearly visible. At 4 and 6 h after cell seeding, the cells on all types of substrates became more expanded. Interestingly, the cells on the fibrous substrate from 14 wt % PHBV solution were very small, and because of the large size of the individual fibers, the cells appeared to elongate their cytoplasms along the fiber axis. On days 1 and 2 after cell culturing, the cells, in their expanded morphology, proliferated well to cover ~30 to ~40% of the surfaces on almost all types of fibrous substrates. On day 3, full expansion of the cells on all types of substrates was seen. Strikingly, most of the cells expansion was observed for the cells on the fibrous substrate from 10 wt % PCL/PHBV solution, which proliferated to cover

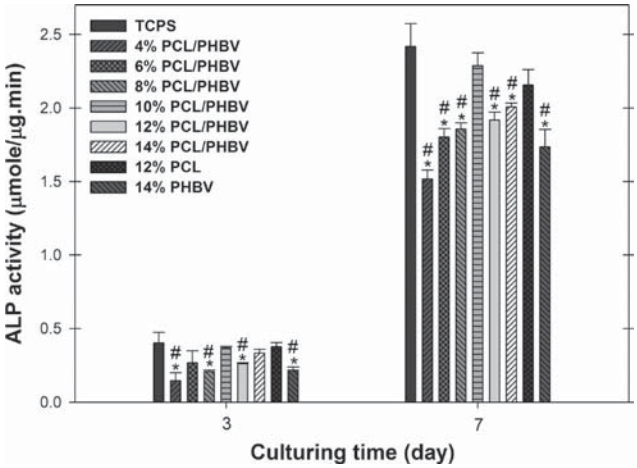


Figure 6. ALP activity of MC3T3-E1 that was cultured on the surfaces of TCPS and various types of fibrous substrates at various given time points after cell culturing. *Significance at $p < 0.05$ with respect to TCPS. #Significance at $p < 0.05$ with respect to the fibrous substrate from 12 wt % PCL solution.

~70% of the surface. Noticeably, the cells on the fibrous substrate from 14 wt % PHBV solution grew in size but still exhibited the elongation of their cytoplasms along the fiber axis. On the basis of the results shown in Figure 5, the fibrous substrate from 10 wt % PCL/PHBV solution was clearly the best among the investigated fibrous substrates for supporting the growth of MC3T3-E1.

Alkaline Phosphatase (ALP) Activity. The expression of ALP from MC3T3-E1 that had been cultured on TCPS and all types of fibrous substrates for 3 and 7 days is shown in Figure 6. On day 3, the ALP activities of the cells that had been grown on the surfaces of TCPS and the fibrous substrates from 6, 10, and 14 wt % PCL/PHBV and 12 wt % PCL solutions were statistically the same, which appeared to be greater than that of cells on the rest of the fibrous substrates. On day 7, increases in the ALP activity from that observed on day 3 of the cells that had been grown on all types of substrates were evident. Strikingly, only the cells that had been grown on the surfaces of the fibrous substrates from 10 wt % PCL/PHBV and 12 wt % PCL solutions exhibited ALP activity at levels that are statistically equivalent to those that had been grown on TCPS, whereas the cells that had been grown on the surfaces of all other types of fibrous substrates had much lower values. Because ALP is usually secreted from normal bone cells during the early matrix formation and maturation period and is triggered by cellular contacts (when the cells reach confluence) and/or by the expression of ample amounts of early matrix proteins (e.g., type I collagen, fibronectin, and/or TGF-β1),[4,33] it is logical to note that the fibrous substrates from 10 wt % PCL/PHBV and 12 wt % PCL solutions were both able to up-regulate the ALP production of MC3T3-E1 much better than the rest of the fibrous substrates. Between the two types of the fibrous substrates, the one from 10 wt % PCL/PHBV solution was able to support the ALP production of the cells slightly better than the one from the 12 wt % PCL solution (on the basis of the average values of the obtained results).

Mineralization. The ability to promote bone formation is the most important characteristic of a bone scaffold. Here, photographic images of Alizarin Red S staining of MC3T3-E1 that had been cultured on TCPS and all types of fibrous substrates for 14

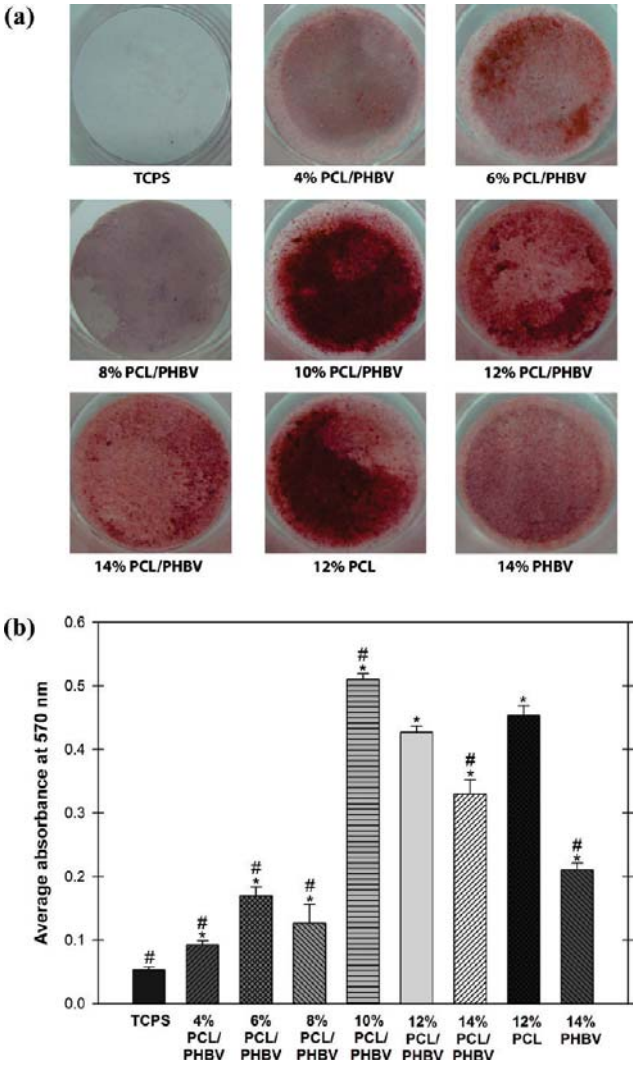


Figure 7. Alizarin Red S staining for the mineralization of MC3T3-E1 on day 14 after being cultured on the surfaces of TCPS and various types of fibrous substrates: (a) photographic images of the stained specimens and (b) the corresponding quantitative analyses. *Significance at $p < 0.05$ with respect to TCPS. #Significance at $p < 0.05$ with respect to the fibrous substrate from 12 wt % PCL solution.

days, along with their quantitative analyses, are shown in Figure 7. Because of the presence of calcium ions in the mineralized tissues, the staining product with Alizarin Red S appeared red. According to the obtained results, the cells that had been cultured on all types of the fibrous substrates stained positively for calcium deposition along with those that had been cultured on the fibrous substrate from 10 wt % PCL/PHBV solution exhibiting the greatest intensity, followed by those that had been cultured on the fibrous substrate from 12 wt % PCL solution. Interestingly, despite the high attachment, high proliferation, and high expression of ALP for the cells that had been grown on TCPS, mineralization of the cells on this control surface on day 14 was the lowest.

All of the obtained results emphasize the importance of a thorough investigation for the efficacy of a bone scaffold because the mineralization of the bone cells does not rely solely on the ability of the scaffold to promoting the attachment, the proliferation, and/or the secretion of ALP of the cells. The obtained results also imply that both the topography (i.e., patterning and/or roughness) and the physicochemical characteristic (i.e., hydrophilicity/hydrophobicity) of the surface of a scaffold are important factors in determining the efficacy of the scaffolds. To this end, it should also be emphasized that before a scaffold that has been evaluated as positive for promoting infiltration, attachment, proliferation, and differentiation of the target cells in vitro can be used in vivo, it should also be tested for inflammatory reactions because it has recently been demonstrated that the in vitro inflammatory response of a scaffold by macrophages is also surface-topography-dependent.[34]

CONCLUDING REMARKS

The fibrous substrates with different morphologies of the individual fibers were prepared from solutions of 50/50 w/w PCL/PHBV in 80/20 v/v chloroform/DMF by electrospinning. As the concentration of the solutions increased from 4 to 14 wt %, the topography of the individual fibers changed from discrete beads/smooth fibers to beaded fibers/smooth fibers and finally to smooth fibers, and the size of the individual fibers increased from ~0.4 to ~1.8 μm on average. Among the various fibrous substrates, the one prepared from 10 wt % PCL/PHBV solution exhibited the lowest static water contact angles of ~85° on average. Likely because of the smoothness of the obtained fibrous substrate and the lowest water contact angles of its surface, the fibrous substrate from 10 wt % PCL/PHBV solution, with an average fiber diameter of ~0.8 μm, was the best at promoting the attachment, proliferation, and differentiation of the cultured mouse bone cells (MC3T3-E1). This type of fibrous matrix could be used as scaffolding substrates for calvarial defects.

AUTHOR INFORMATION

Corresponding Author

*Postal address: The Petroleum and Petrochemical College, Chulalongkorn University, Soi Chula 12, Phyathai Road, Pathumwan, Bangkok 10330, Thailand. Tel: +66-2-218-4131. Fax: +66-2-215-4459. E-mail: pitt.s@chula.ac.th.

ACKNOWLEDGMENT

We acknowledge partial financial support received from (1) The Thailand Research Fund (TRF, grant no. DBG5280015), (2) The Institute for the Promotion of Teaching Science and Technology (IPST, for the DPST scholarship of P.K.), (3) The Petroleum and Petrochemical College (PPC), Chulalongkorn University, and (4) the Center for Petroleum, Petrochemicals, and Advanced Materials (CPPAM), Chulalongkorn University.

REFERENCES

(1) Thomson, R. C.; Wake, M. C.; Yaszemski, M. J.; Mikos, A. G. *Adv. Polym. Sci.* **1995**, *122*, 245–274.

(2) Tuzlakoglu, K.; Bolgen, N.; Salgado, A. J.; Gomes, M. E. *J. Mater. Sci. Mater. Med.* **2005**, *16*, 1099–1104.

(3) Kenar, H.; Torun Köse, G.; Hasirci, V. *Biomaterials* **2006**, *27*, 885–895.

(4) (a) Wutticharoenmongkol, P.; Sanchavanakit, N.; Pavasant, P.; Supaphol, P. *Macromol. Biosci.* **2006**, *6*, 70–77. (b) Wutticharoenmongkol, P.; Sanchavanakit, N.; Pavasant, P.; Supaphol, P. *J. Nanosci. Nanotechnol.*

2006, *6*, 514–522. (c) Wutticharoenmongkol, P.; Pavasant, P.; Supaphol, P. *Biomacromolecules* **2007**, *8*, 2602–2610.
(5) Zhang, Y.; Lim, C. T.; Ramakrishna, S.; Huang, Z. M. *J. Mater. Sci. Mater. Med.* **2005**, *16*, 933–946.
(6) Li, W. J.; Laurencin, C. T.; Caterson, E. J.; Tuan, R. S.; Ko, F. K. *J. Biomed. Mater. Res., Part A* **2002**, *60*, 613–621.
(7) (a) Taepaiboon, P.; Rungsardthong, U.; Supaphol, P. *Nanotechnology* **2006**, *17*, 2317–2329. (b) Taepaiboon, P.; Rungsardthong, U.; Supaphol, P. *Eur. J. Pharm. Biopharm.* **2007**, *67*, 387–397. (c) Suwantong, O.; Opanasopit, P.; Ruktanonchai, U.; Supaphol, P. *Polymer* **2007**, *48*, 7546–7557. (d) Rujitanaroj, P.; Pimpha, N.; Supaphol, P. *Polymer* **2008**, *49*, 4723–4732.
(8) Noh, H. K.; Lee, S. W.; Kim, J. M.; Oh, J. E.; Kim, K. H.; Chung, C. P.; Choi, S. C.; Park, W. H.; Min, B. M. *Biomaterials* **2006**, *27*, 3934–3944.
(9) Kenawy, E. R.; Layman, J. M.; Watkins, J. R.; Bowlin, G. L.; Matthews, J. A.; Simpson, D. G.; Wnek, G. E. *Biomaterials* **2003**, *24*, 907–913.
(10) (a) Deitzel, J. M.; Kleinmeyer, J.; Harris, D.; Beck Tan, N. C. *Polymer* **2001**, *42*, 261–272. (b) Mit-uppatham, C.; Nithitanakul, M.; Supaphol, P. *Macromol. Chem. Phys.* **2004**, *205*, 2327–2338. (c) Supaphol, P.; Chuangchote, S. *J. Appl. Polym. Sci.* **2008**, *108*, 969–978.
(11) Chuenjitkuntaworn, B.; Inrung, W.; Damrongsri, D.; Mekaapiruk, K.; Supaphol, P.; Pavasant, P. *J. Biomed. Mater. Res.* **2010**, *94A*, 241–251.
(12) (a) Sombatmankhong, K.; Suwantong, O.; Waleetorncheepsawat, S.; Supaphol, P. *J. Polym. Sci., Polym. Phys.* **2006**, *44*, 2923–2933. (b) Sombatmankhong, K.; Sanchavanakit, N.; Pavasant, P.; Supaphol, P. *Polymer* **2007**, *48*, 1419–1427. (c) Suwantong, O.; Waleetorncheepsawat, S.; Sanchavanakit, N.; Pavasant, P.; Cheepsunthorn, P.; Bunaprasert, T.; Supaphol, P. *Int. J. Biol. Macromol.* **2007**, *40*, 217–223.
(13) Ito, Y.; Hasuda, H.; Kamitakahara, M.; Ohtsuki, C.; Tanihara, M.; Kang, I. K.; Kwon, O. H. *J. Biosci. Bioeng.* **2005**, *100*, 43–49.
(14) Ndreu, A.; Nikkola, L.; Ylikauppila, H.; Ashammakhi, N.; Hasirci, V. *Nanomedicine* **2008**, *3*, 45–60.
(15) Yeo, A.; Rai, B.; Sju, E.; Cheong, J. J.; Teoh, S. H. *J. Biomed. Mater. Res.* **2008**, *84A*, 208–218.
(16) Bölgen, N.; Menceloğlu, Y. Z.; Acatay, K.; Vargel, I.; Pişkin, E. *J. Biomater. Sci., Polym. Ed.* **2005**, *16*, 1537–1555.
(17) Oh, S. H.; Park, I. K.; Kim, J. M.; Lee, J. H. *Biomaterials* **2007**, *28*, 1664–1671.
(18) Wang, J.; Valmikinathan, C. M.; Liu, W.; Laurencin, C. T.; Yu, X. *J. Biomed. Mater. Res.* **2010**, *93A*, 753–762.
(19) Shor, L.; Güçeri, S.; Chang, R.; Gordon, J.; Kang, Q.; Hartsock, L.; An, Y.; Sun, W. *Biofabrication* **2009**, *1*, 015003.
(20) Holmes, P. A. *Phys. Technol.* **1985**, *16*, 32–36.
(21) Gassner, F.; Owen, A. J. *Polym. Int.* **1996**, *39*, 215–219.
(22) Sudesh, K.; Abe, H.; Doi, Y. *Prog. Polym. Sci.* **2000**, *25*, 1503–1555.
(23) Cheng, S.; Chen, G. Q.; Leski, M.; Zou, B.; Wang, Y.; Wu, Q. *Biomaterials* **2006**, *27*, 3758.
(24) Rivard, C. H.; Chaput, C.; Rhalmi, S.; Selmani, A. *Ann. Chir.* **1996**, *50*, 651–658.
(25) Sangsanoh, P.; Waleetorncheepsawat, S.; Suwantong, O.; Wutticharoenmongkol, P.; Weeranantanapan, O.; Chuenjitbuntaworn, B.; Cheepsunthorn, P.; Pavasant, P.; Supaphol, P. *Biomacromolecules* **2007**, *8*, 1587–1594.
(26) (a) Varnell, D. F.; Runt, J. P.; Coleman, M. M. *Macromolecules* **1981**, *14*, 1350–1356. (b) Rohindra, D. R.; Khurma, J. R. *South Pac. J. Nat. Sci.* **2007**, *9*, 53–60. (c) Ai, J.; Chorbani, F.; Heidari, K, S.; Biazar, E. *Int. J. Nano Dim.* **2011**, *1*, 241–251.
(27) Qiu, Z.; Yang, W.; Ikehara, T; Nishi, T. *Polymer* **2005**, *46*, 11814–11819.
(28) Yoon, Y. I.; Moon, H. S.; Lyoo, W. S.; Lee, T. S.; Park, W. H. *J. Colloid Interface Sci.* **2008**, *320*, 91–95.
(29) Tong, H. W.; Wang, M.; Lu, W. W. *J. Biomater. Sci., Polym. Ed.*, DOI: 10.1163/092050611X560708.
(30) Kumbar, S. G.; Nukavarapu, S. P.; James, R.; Nair, L. S.; Laurencin, C. T. *Biomaterials* **2008**, *29*, 4100–4107.
(31) Khang, G.; Lee, S. J.; Lee, J. H.; Kim, Y. S.; Lee, H. B. *Biomed. Mater. Eng.* **1999**, *9*, 179–187.
(32) Wang, B.; Cai, Q.; Zhang, S.; Yang, X.; Deng, X. *J. Mech. Behav. Biomed. Mater.* **2011**, *4*, 600–609.
(33) Choi, J. Y.; Lee, B. H.; Song, K. B; Park, R. W.; Kim, I. S.; Sohn, K. Y.; Jo, J. S.; Ryoo, H. M. *J. Cell. Biochem.* **1996**, *61*, 609–618.
(34) Saino, E.; Focarete, M. L.; Gualandi, C.; Emanuele, E.; Cornaglia, A. I.; Imbriani, M.; Visai, L. *Biomacromolecules* **2011**, *12*, 1900–1911.

Comparison of isolation techniques for bone marrow derived canine mesenchymal stem cells (MSCs) and the effects of MSCs loaded onto polycarpolactone hydroxyapatite scaffold on non-union bone healing

Chalika Wangdee [a], Kumpanart Soontornvipart [a], Prasit Pavasant [b], Pitt Supaphol [c], Sasijaras Tantrajak[a], Mongkol Techakumphu [d], Wijit Banlunara [e], Theerawat Tharasanit [d,*]

[a] *Department of Veterinary Surgery,* [d]*Department of Obstetrics, Gynaecology and Reproduction,* [e]*Department of Pathology, Faculty of Veterinary Science, Chulalongkorn University, Bangkok 10330, Thailand*

[b] *Department of Anatomy, Faculty of Dentistry, Chulalongkorn University, Bangkok 10330, Thailand*

[c] *The Petroleum and Petrochemical College, Chulalongkorn University, Bangkok 10330, Thailand*

* Corresponding author. Tel.: +662 2189644

E-mail address: Theerawat.t@chula.ac.th

Abstract

Mesenchymal stem cells (MSCs) have increasingly become an attractive aspect for tissue engineering. However, limitation of cell numbers at isolation and culture has restricted the clinical exploitations. Bone marrow contents were collected from 7 dogs and then submitted to 3 different MSC isolation techniques (direct plating, red blood cell lysis treatment and gradient density). The number of cells, expression of MSC markers and in vitro differentiation obtained from each technique were examined. In order to study in vivo osteogenic capability of derived MSCs, non-union ulna lesions (n=3) were firstly induced by transplantation of a composite of polycarpolactone/ hydroxyapatite (PCL/HA) scaffold onto 'experimentally induced' a critical-size ulna bone defect. The MSCs were then injected into the lesions. The non-union sites were examined by radiography, angiography and histology at 2, 4, 6, 8 and 12 weeks after MSC injection.

Gradient density (1.08 ± 0.92) and RBC lysis (0.94 ± 0.55) techniques yielded higher numbers ($x10^6$) of putative MSCs on day 7 of culture compared with direct plating technique (0.26 ± 0.28). A large proportion of isolated MSCs, irrespective the isolation techniques expressed all MSC markers used (CD 44, CD 90). For all MSC transplanted dogs, neither radiological changes at scaffold-ulna interface nor callus formation was observed. At 16 weeks after MSC injection, the angiogram indicated an increased neovascularization. This was confirmed by the histological finding that there was an improvement of vascularization within the thicker fibrous tissue surrounded the scaffold.

It is concluded that gradient density and RBC lysis treatment are suitable MSC isolation techniques in terms of the numbers of cells obtained and also their MSC properties. However,

the potential use of these MSCs following injection to non-union bone site was compromised possibly caused by a lack of osteogenic stimulation.

Keywords: bone marrow, mesenchymal stem cells, dogs, polycarpolactone/ hydroxyapatite (PCL/HA) scaffold, non-union bone

1. Introduction

In dogs with impaired bone healing, the incidence of long bone non-union is 3.4% and the most common site of non-union (40-60%) is often associated with the radius and/or ulna. [1] The etiology of a non-union may involve multiple factors including a poor blood supply to the affected area, poor apposition of fractured bone-end, motion at the fracture site, large fracture gap, pathological fractures, foreign bodies, large quantities of necrotic bone, infection and non-justified corticosteroid therapy.[2, 3] For treatment of non-union bone, autologous bone graft is the gold standard that leads to bone union through osteogenecity, osteoconductivity and osteoinductivity. However, it carries with it a high risk of fracture and infection, pain at the donor site and limited cancellous bone.[4] Such shortcomings can be addressed by bone tissue engineering, an interdisciplinary field that applies principles of bioengineering, material science and life science to develop biological substitutes that restore, maintain, and improve tissue function.[5]

Stem cells are anticipated to serve as a powerful tool for tissue engineering in human and veterinary medicine.[6, 7] Mesenchymal stem cells (MSCs) are able to self-renew and differentiate into mesodermal lineage such as bone, cartilage and adipose tissues.[8] They also can potentially transdifferentiate into other cell lineages.[9] Canine MSCs have been demonstrated to have potential for cell-based therapy for bone and soft tissue regeneration.[10-12] Although bone marrow is the major accessible and enriched source of MSCs, the numbers of MSCs obtained from bone marrow is generally insufficient for transplantation since the population of MSCs has been reported to range about 0.001 to 0.01% of bone marrow mononuclear cells in rodents and felines. [13, 14] This therefore highlights the importance of the isolation technique for MSCs. Because the specific markers for bone marrow derived MSCs have yet to be identified, the characterization of

MSCs usually relies upon the traditional MSC properties. These include plastic adherence, expression of some surface markers such as CD 90, CD 105 and Stro-1, while lacking the expression of hemopoietic stem cell marker (CD 34) [15, 16]. More importantly, these cells have a capability to differentiate into mesodermal lineages including bone, cartilage and adipose tissue [17] or transdifferentiate into other cell lineages such as neuron [18]. In dog, direct plating of bone marrow aspirate is frequently used for bone marrow derived MSCs. However, no such information about comparison of the technique for MSC isolation has been reported. It is therefore important to standardize the MSC isolation technique in order to increase the cell homogeneity of the MSCs population, thereby improving efficiency for bone regeneration.[19]

Scaffold, a three-dimensional porous structure with interconnection between pores, allows cell attachment that can replace defective bone. Polycaprolactone (PCL) is a biodegradable synthetic polymer [20, 21] with advantages over other polymeric materials for bone formation and remodeling phase, including good biocompatibility, higher and prolonged mechanical strength, more stability in ambient conditions, and a slower biodegradation rate. [22, 23] Hydroxyapatite (HA) ($Ca_{10}[PO_4]_6[OH]_2$) is known as a ceramic of choice for bone tissue engineering because its chemical and crystal properties resemble to the mineral component of bone tissue, giving it to have an excellent biocompatibility [24-26], osteoconductive capacity and also ability to bind directly to host bone. [27] The combination of PCL and HA synergistically improves mechanical properties, osteoconductivity and osteointegrative potentials of the scaffold. [24-26] The objectives of this study were to compare the effects of isolation techniques on derivation of bone marrow MSCs and characteristics and also to examine the effect of MSC transplantation on bone healing of an experimentally ‘induced’ non-union ulna bone defect in dogs.

2. Materials and methods

All chemicals used in this study were purchased from Sigma Aldrich, St. Louis, USA, unless otherwise specified.

2.1 Collection and isolation of canine bone marrow derived mesenchymal stem cells

This study was approved by the Committee for the Ethical Care of Animals of the Chulalongkorn University. Seven mature dogs, mixed breeds, weighed between 10 to 15 kg were enrolled in this study. All dogs were physically examined and remained health entirely the experiment. Routine blood analysis was performed preoperatively. Acepromazine 0.02 mg/kg and morphine 0.5 mg/kg were administered intramuscularly, and the anesthesia was induced with propofol (Fresenius Kabi, Austria GmbH, Graz, Austria) and maintained with isoflurane in 100% oxygen. Cefazolin (25 mg/kg) was administered intravenously as prophylactic antibiotic. Epidural anesthesia using 0.5% bupivacaine (1 mg/kg) combined with morphine (0.1 mg/kg) was additionally performed to relief pain sensation caused by bone marrow aspiration procedure. Fifteen milliliters of bone marrow were harvested from the iliac crest of each dog with a heparinized syringe.

The bone marrow aspirate (15 ml) was equally divided into 3 aliquots, and each aliquot of 5 ml bone marrow was then submitted to one of the following isolation techniques: 1) direct plating, 2) red blood cell lysis treatment and 3) gradient density.

2.1.1 Direct plating

Direct plating was performed by adding bone marrow aspirate directly into a 10 cm Petri-dish (BD-Falcon^{TM}, Franklin Lake, NJ, USA) containing with 7 ml of MSC culture medium. After 24 of culture, the attached cells were washed with Dulbecco's phosphate buffered saline

without calcium and magnesium (DPBS, Invitrogen, Carlsbad, CA, USA) for 2-3 times, and the fresh MSC medium was then added.

2.1.2 Red blood cell lysis treatment

Red blood cell lysis buffer (8.3 g/L ammonium chloride in 0.01 M Tris-HCl buffer, pH 7.5 $\pm$ 0.2) was used to eliminate the contaminated red blood cells (RBC) in the bone marrow aspirate. The RBC lysis buffer was mixed at a ratio of 1: 1 with bone marrow aspirate and then incubated at room temperature (approximately 25-26^{o}C) for 5 min. The mixture was then centrifuged at 1000 rpm for 5 min. After the supernatant was discarded, the pellet was resuspended with MSC medium, and the isolated cells were cultured in MSC culture medium. The non-attached cells were washed out in the following day.

2.1.3 Gradient density

Bone marrow aspirate (5 ml) was gently layered onto a histopaque® 1077 (density 1.077 $\pm$0.001) in a 15 ml conical tube (BD-Falcon^{TM}, Franklin Lake, NJ, USA). The centrifugation was performed at 26^{o}C and 400g for 30 min, and the interface containing mononuclear cells was then collected. The presumptive MSCs were washed with MSC culture medium for two times prior to culture.

2.2 Culture of bone marrow derived mesenchymal stem cells

Following MSC isolation (day 0) as previously described, the isolated cells were allowed to attach to the culture plate for 24 h prior to washing with DPBS. These cultured cells were assigned as primary cells at passage 0 (P_0). MSC culture medium was composed of a low-glucose Dulbecco's modified Eagle's medium (low glucose DMEM) supplemented with 10% (v/v) fetal bovine serum (FBS, Invitrogen), 2 mM L-glutamine (Invitrogen, Carlsbad, USA), 100 unit/ml penicillin G, 100 µg/ml streptomycin, 40µg/ml gentamicin and 5 µg/ml amphotericin B.

Subculture of MSCs was performed after treating the cells with 0.05% (w/v) trypsin-EDTA (Invitrogen). The disaggregated cells were then centrifuged and split into new Petri-dish at a ratio of 1:3. Putative MSCs at passages 3 (P_3) were used for flow cytometric analysis in order to examine the expression of cell-surface antigens and also for *in vitro* differentiation. In all cases, the culture condition was performed at 37^{o}C in a humidified condition of 5 % CO_2 in air.

2.3 Assessing the characteristics of canine mesenchymal stem cells

2.3.1 Flow cytometry

The examination of MSCs was performed as essentially described by Tharasanit et al. (2011). Canine MSCs at the 3rd passages from a total of 5 dogs (Dog no. 1, 4, 6, 7 and 8) were immunologically examined for surface markers. These makers included the positive (CD 44, CD 90) and negative (CD 34) makers. The MSCs were first dissociated from the Petri dishes with Trypsin- EDTA and then centrifuged. A total of 200,000 to 300,000 cells were used for immunolabeling. Rat monoclonal anti-canine CD 90 (AbD serotec, Kidlington, UK) with rabbit anti-rat FITC secondary antibodies and monoclonal anti-canine CD44 antibody conjugated with allophycocyanin (APC) (R&D system, Minneapolis, USA) were used as MSC positive markers. A rat monoclonal anti-canine CD 34 antibody conjugated with fluorescein isothiocyanate (FITC) was used as the negative MSC marker. Fluorescently-labeled MSCs were washed and fixed with 1% (w/v) paraformaldehyde in PBS and stored at 4°C in the dark until analysis. Non-staining MSCs and MSCs labeled with only the secondary antibody were used as controls. At least 20,000 MSCs were analyzed by flow cytometry.

2.3.2 *In vitro* bone differentiation of MSCs

Canine bone marrow derived MSCs at passage 3 from four dogs were simultaneously induced to osteogenic lineage (each dog represented one replicate). Osteogenic differentiation was performed as essentially described by Bosch et al. (2006) with minor modifications. The MSCs were first cultured to reach approximately 80% confluence, the osteogenic medium containing MSC medium supplemented with 0.1 μM dexamethasone, 50 μM ascorbic acid, 10 mM β-glycerophosphate (Merck, Darmstadt, Germany) was then added into the culture dish. The *in vitro* bone differentiation was performed for 21 days. Von Kossa staining was used to detect deposition of calcium phosphate indicating *de novo* bone formation.

2.3.3 Scaffold preparation and MSC transplantation

PCL/HA composite scaffolds were prepared as previously described [28]. The scaffold were cut into 10x5x25 millimeters and sterilized with 100% (v/v) absolute ethanol for 1 h. The scaffolds were washed thoroughly with sterilized distilled water and then DPBS to remove the ethanol.

Anesthesia and surgical procedures were performed as similar as previously described. Brachial plexus block using 0.5% bupivacaine (1.3 mg/kg) was additionally performed prior bilateral ulnar osteotomy to reduce pain. A total of 3 dogs were induced bilateral ulnar non-union (n=6) by cutting the mid-shaft of the ulnar bone (2.5 cm) using an oscillating saw. The osteotomized sites were implanted with the PCL/HA composite scaffold to improve bone stability. After the operation, all forelimbs were applied with modified Robert Jone bandages reinforced with thermoplastic splint (Vet-lite, Bangkok, Thailand). All dogs also received 5 mg/kg enrofloxacin (Bayer, Bangkok, Thailand) and 4 mg/kg carprofen (Pfizer, Bangkok, Thailand) orally for 7 days after implantation. All dogs demonstrated for bone non-union during 12 weeks after scaffold implantation. For transplantation, autologous MSCs were subcultured to

185 passage 4 as previously described. After trypsinization, approximately $10x10^6$ cells/ml were
186 loaded into a syringe containing with minimum volume (0.5 ml) of DMEM supplemented with
187 1% (v/v) FBS. Three MSC transplanted sites (proximal, middle and distal parts of the PCL/HA
188 scaffold implant) were injected via a 23 G indwelling intravenous catheter with MSCs under a
189 fluoroscope (Philips healthcare, Eindhoven, the Netherlands).

190 2.4 Examination of bone formation

191 2.4.1 Radiography

192 The lateral radiographs were taken immediately at 2, 4, 6, 8, 10 and 12 weeks post-
193 operation in all dogs. Bone healing was evaluated using radiographic scoring system previously
194 described [29] as shown in table 1. Bone union was justified grading from 0 to 3 at the proximal
195 and distal of implanted material. In addition, the new bone formation was scored 0 to 4.

196 2.4.2 Angiography

197 Fluoroscopic angiography was performed in two experimental dogs at 12 weeks before
198 MSC injection (dog no. 1, 2) and 16 weeks after MSC injection (dog no.1) in order to observe
199 blood vessels at an implantation site. Anesthesia and surgical procedures were performed as
200 previously described. The 23 G intravenous catheter connected with an extension tube was
201 inserted into the axillary vein and the radiographic contrast medium (iohexol, Omnipaque®, G E
202 healthcare, Buckinghamshire, UK) was slowly administrated in order to observe the presence of
203 the blood vessel at the MSC transplanted site using fluoroscopy.

204 2.4.3 Histological examination of MSCs loaded scaffold

205 The biopsy was performed both before (n=2) and after MSC transplantation (n=2) at 12
206 and 20 weeks post-transplantation. The biopsy samples were fixed with 10% (v/v) buffered
207 formalin, and the fixed samples were embedded in paraffin and processed following guideline

for a routine histological procedure. The sections were stained with hematoxylin & eosin (H&E) and examined for neovascularization and bone formation under a light microscope. Occasionally, Masson's trichrome staining was additionally performed to detect the presence of collagen fibers.

3. Statistical analysis

Values are present as means ± standard deviation (SD). Efficacy for different MSC isolation techniques on the number of isolated MSCs, viability and expression of MSC markers were compared by one-way analysis of variance (ANOVA) and post-hoc analysis with the least significant difference (LSD). Angiographs and histological findings were descriptively analyzed. The differences in radiographic scores at 2, 4, 6 and 8 weeks post MSC transplantation were evaluated using Kruskal-Wallis one way analysis and Mann-Whitney U test. In all cases, statistical analysis was performed using SPSS statistical program (version 17.0). P values <0.05 were considered statistically significant.

4. Results

Following MSC isolation, putative MSCs were attached onto Petri-dish. These MSCs irrespective the MSC isolation techniques demonstrated a typical MSC morphology (figure 1 A-C). There were several cell types including thin spindle shaped, typical fibroblast-like, and mantle cells. On day 7 after MSC isolation, the total number of MSCs obtained from a 5-ml of bone marrow aspirate was ranged from 0.35×10^6 to 2.8×10^6, 0.04×10^6 to $1.43\times$, 0.03×10^6 to 0.75×10^6 for gradient density, RBC lysis treatment and direct plating, respectively (Table 2). The gradient density techniques significantly increased the numbers of isolated MSCs when

compared with direct plating technique ($P<0.05$), while cell yields obtained from this gradient density was efficiently comparable to RBC lysis treatment ($P>0.05$).

Cell-surface antigen profiles of canine MSCs was ascertained after immunolabeling with canine-specific/cross-reacted monoclonal antibodies and examined with a flow cytometer. Ranges and averages of percentage of cells positive for CD 44, CD 90 and CD34 are shown in table 2. Canine MSCs at passage 3 highly expressed CD 44 (95.66-99.89) and rarely expressed CD 34 in all cases (table 2). Furthermore, the cultured MSCs demonstrated to have capability to differentiate into osteogenic lineage as they positively stained with Von Kossa following osteogenic induction (figure 2).

Following MSC transplantation into non-union sites, all three dogs could walk properly within 24 hours after surgery. Neither radiological changes at scaffold-ulna interface nor callus formation was presented at the implant sites of PCL/HA alone (figure 3A) and PCL/HA combined with MSCs (figure 3B) at 2, 4, 6, 8 and 12 weeks post-operatively. The density of the implant grafts was comparable to soft tissue density. The radiographic scores was 0 in all cases.

Fluoroscopic angiography indicated the presence of blood vessels within the PCL/HA scaffolds at 12 weeks after implantation (figure 4A). These blood vessels descriptively appeared to increase when examined at 16 weeks after MSC injection (figure 4B). This result was in an accordance with histology of the host-PCL/HA transplanted sites that neovascularization was observed in PCL/HA both with and without MSC injection. However, no such osteoid formation was observed in the histological sections. The transplanted PCL/HA scaffolds was filled with loose and unorganized connective tissue (figure 5A) but the thickness of the fibrous tissues and the number of small blood vessels were likely to increase at 20 weeks after MSCs injection (figure 5B). The fibrous tissue was mainly comprised of the spindle cells with extensive collagen

253 deposition which was confirmed by Masson's trichrome staining (Figure 5B). Interestingly, we
254 also found a number of multinucleated gaint cells and lymphocytes within the scaffolds
255 indicating the inflammatory response.
256
257 **Discussion**
258 In the present study, we demonstrated that bone marrow derived canine MSCs could be
259 enriched by treating the bone marrow aspirate prior to culture, and these harvested cells were
260 highly expressed MSC markers (CD 44 and CD 90) and had a potential to differentiate into
261 osteogenic lineage in vitro. However, the de novo bone formation following transplantation of
262 the MSCs into PCL/HA scaffold was compromised.
263 Bone marrow was considered as a primary source of MSCs but only 0.001 to 0.01% of
264 bone marrow mononuclear cells in rodents and felines were identified as MSCs [13, 14]. In addition,
265 no consensus makers have been defined as conclusive markers for canine MSCs and thus the
266 ability of cells that can adhere onto plastic Petri-dish is often used.[30] In the current study, we first
267 examined the different techniques to enrich MSCs from bone marrow aspirate and found that
268 gradient density significantly increased the numbers of isolated MSC on day 7 of culture when
269 compared with direct plating technique ($P<0.05$, table 2). It had become clear that the presence
270 of RBC in the culture dish negatively affected on the number of harvested MSCs probably
271 because the RBC may compromise the MSCs to settle and adhere to the Petri-dish.[31] In addition,
272 excessive RBC lysis during culture may cause the release of free hemoglobin that can induce
273 cellular stress and apoptosis [32, 33]. Although the efficacy of the gradient density was similar to
274 that of RBC lysis treatment ($P>0.05$), the RBC lysis buffer treatment is preferable for clinical use
275 since it requires less time-consuming and inexpensive. This technique may also be beneficial for

initial growth of the isolated MSCs due to the platelet derived growth factor secreted from the remaining platelets following RBC lysis. [30] In addition to the effect of isolation techniques on MSC derivation, the numbers of MSCs isolated were considerably variable among donors, irrespective the isolation techniques used. This result was in an agreement to the facts that the number of bone marrow MSCs significantly decreases with increased age and poor health status [34-37], while the cells obtained from young donors grew more rapidly.[38] However, there was no effect of isolation techniques on the expression of MSC makers (CD 40 and CD 90) and also in vitro differentiation, suggesting that MSC properties could be maintained using the current culture system. However, study on the effect of long term culture of these MSCs on MSC proliferation activity and also differentiation capability remains elusive. This aspect is important given that the large numbers of cells would be required for cell/tissue engineering. [6]

To date, several attempts have been made on transplantation of MSC into long-bone defects. [3, 13, 39, 40] However, the de novo bone formation following transplant has been unsuccessful [13] especially in dog that has a slower bone turnover rate compared with mouse. [41] Furthermore, the injured bone site often becomes ischemic due to the excessive vascular destruction [42] A combination of osteopotential cell and biolodegradable scaffold is one of the most successful strategies in bone tissue engineering. Our previous data suggested that PLC/HA composite scaffold demonstrated as a promising approach for promoting new bone formation when transplanted to calvarial defect in mouse. [43] In order to minimize the risk of ischemic lesion, we therefore first transplanted the PCL/HA scaffold to the large bone lesion allowing the neovascularization within the scaffold before MSC transplantation. After 12 week of PCL/HA scaffold transplant, no bone formation was found but the fluoroscopy indicated the neovascularization within the scaffold (figure 4A). However, no osteogenic differentiation was

observed following MSC transplant into the vascularized scaffolds. From this result, it has become clear that implanted site of scaffold and species employed plays an important role for bone regeneration (i.e. cortical versus cancellous bone) [44]. Furthermore, a large size and slow degradable PCL-HA scaffolds may also create an unfavorable environment for bone formation [45-47]. In this study, several multinucleated giant cells in the PLC/HA scaffold indicated chronic reactions due to the foreign body response. Similar tissue reaction was previously reported.[48-50]. Although the scaffolds used in this study were contaminated with copper (probably from hydroxyapatite ceramic) as we further we analyzed the scaffold using energy dispersive x-ray (SEM/EDX) analysis (unpublished data), the failure for osteogenesis of transplanted MSCs in the scaffold was probably not caused by the cell cytotoxicity of the contaminated copper. There was a good evidence of fibrovascular tissue infiltration with an extent matrix deposition throughout the entire PCL/HA scaffold, and injection of MSCs into the scaffold seemed to increase the thickening size of the fibroblastic mass and vascularization (figure 5B). In fact, several factors are critical for bone tissue engineering, the main hallmark remains to be the sufficient osteogenic factors to stimulate de novo bone differentiation of the transplanted MSCs [2]. Several growth factors and pathways have been demonstrated to be necessary for bone development. [51] For example, bone morphologic protein-2 (BMP-2) increased osteocalcin release from MSCs promoting and healing response and induced chondrogenic and osteogenic differentiation of human bone marrow MSCs [52-54] and also promoted the new bone formation in femoral defects in rats [40] and increased the local population of cells and the connective tissue progenitors in a canine femur defect model with the combination of MSCs. [55]

In conclusion, this study revealed that MSCs can be derived from bone marrow. These MSCs could further enrich by treating bone marrow aspirate with gradient density and red blood

cell lysis treatment. Although these MSCs highly expressed the MSC markers and also retained the differentiation potentials, the bone differentiation following implantation was compromised. Further novel strategy in particular the combination of tissue engineering and osteogenic substances that can create a proper environment for de novo bone formation remain to be studied.

Conflict of interest statement

None of the authors of this paper has a financial or personal relationship with other people or organizations that could inappropriately influence or bias the content of the paper.

Acknowledgments

This project was financially supported by the Thailand Research Fund (DBG 5280015). We also would like to thank Supranee Buranapraditkun for technical support on flow cytometry analysis.

References

Table 1 Radiographic scoring system for evaluation of bone healing.[39]

	Score	Description
Bone formation	0	No new bone; graft approximates density of soft tissue
		Minimal new bone composed mostly of noncontiguous
	1	Areas of minimal density
		New bone present as mostly contiguous areas of normal
	2	Density and fills approximately 50% of the defect
		New bone present as mostly contiguous areas of normal
	3	Density and fills approximately 51-95% of the defect

	4	New bone a solid contiguous mass that fills > 95% of the defect
Bone union	0	No contact between new bone and noninvolved adjacent normal bone
	1	Partial bridge (< 50%) from new bone to adjacent normal bone
	2	Partial bridge (> 50%) from new bone to adjacent normal bone
	3	Complete bridge from new bone to adjacent normal bone

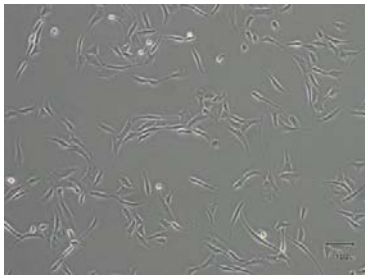
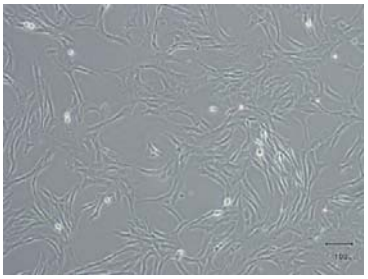
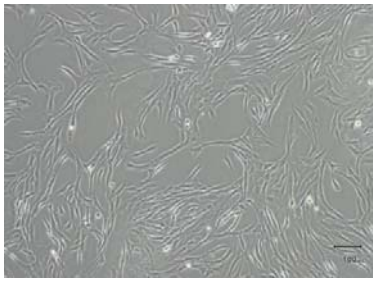
340

341 **Table 2** Mean ± SD (range) of total number of MSCS on day 7 and the proportion of MSCs
342 (passage 3) positive to cell surface markers. The MSCs were isolated from bone marrow using
343 three different techniques.

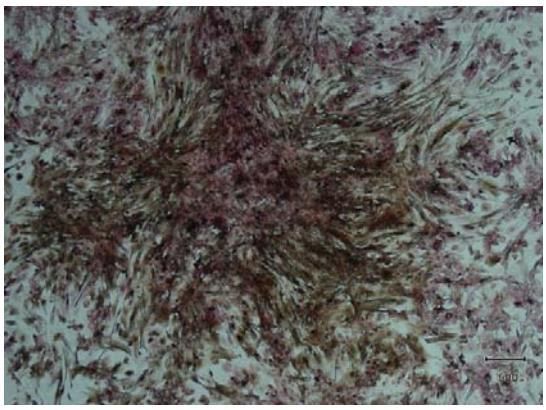
	Total cell number ($x10^6$)	Cell surface markers		
		CD 44	CD 90	CD 34
Whole aspiration	0.26 ± 0.28^{a} (0.03-0.75)	98.74+1.73 (95.66-99.59)	95.84+3.05 (91.93-99.15)	0.018+0.03 (0-0.01)
RBC lysis treatment	$0.94 \pm 0.55^{a,b}$ (0.04-1.43)	99.28+0.82 (99.18-99.89)	93.48+10.76 (74.3-99.21)	0.014+0.03 (0-0.06)
Gradient	1.08 ± 0.92^{b} (0.35-2.8)	99.2+0.96 (99.02-99.89)	93.62+6.65 (82.53-98.88)	0.012+0.027 (0-0.06)

344

345 **Figure 1** Morphology of canine MSCs derived from bone marrow using direct plating (A), RBC
346 lysis treatment (B) and gradient density (C).
347

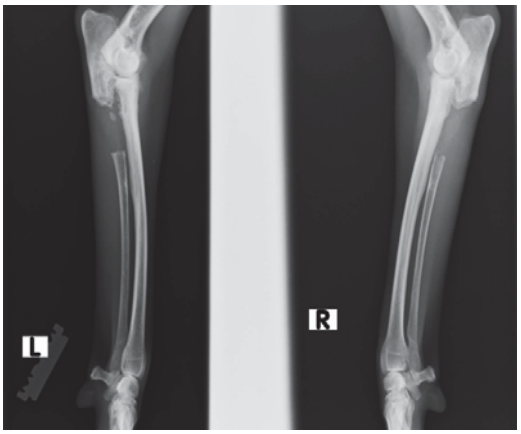
348 **A**  **B**  **C** 

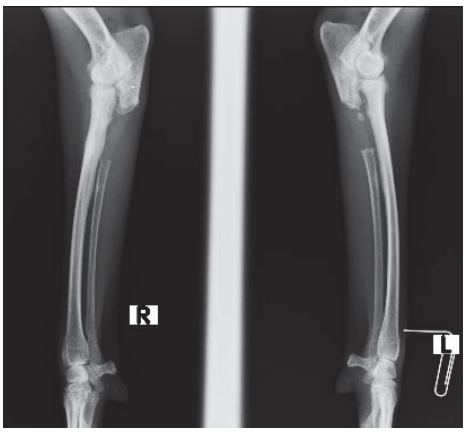
349 **Figure 2** An example of canine bone marrow MSCs that were induced to differentiate into
350 osteogenic lineage as they were positive to Von Kossa staining
351



352

353 **Figure 3** Radiographs demonstrating canine ulnar segment defect with PCL/HA alone (A) or
354 PCL/HA combined with MSCs at 12 weeks (B) postoperatively. Note that no *de novo* bone
355 formation was observed.
356

357 A 

B 

358 **Figure 4** Fluoroscopic angiography at 12 weeks (A) after PCL/HA scaffold implant and at 16
359 weeks after MSC injection (B). The increased blood vessels were observed at the implantation
360 site after BMSC injection.

361

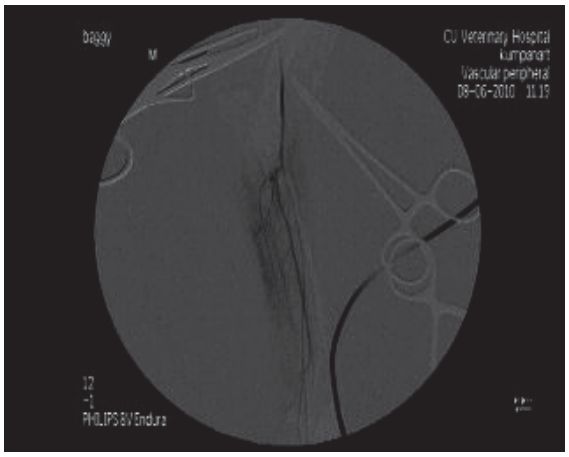
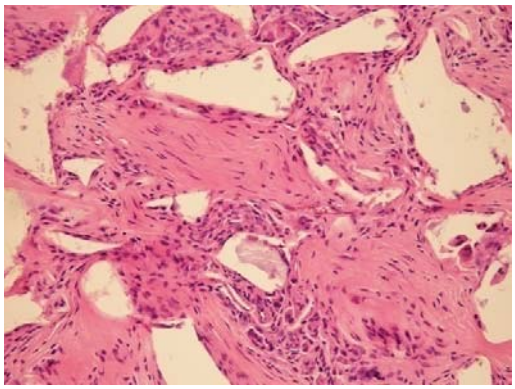
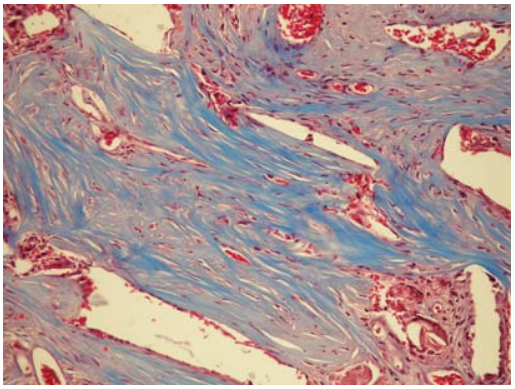
362 A  B 

Figure 5 Histology of PCL/HA implanted site at 12 weeks after surgery (A) and at 20 weeks after MSC injection (B) indicates the newly formation of capillaries and arterioles. Masson's trichrome staining (B) indicates that the thickening of fibrous tissue mainly constructed by an extensive collagen fibers.

A  B 

References

1. Bartels KE. Nonunion. *Vet Clin North Am Small Anim Pract*. 1987;17:799-809.

2. Calori GM, Mazza E, Colombo M, Ripamonti C, Tagliabue L. Treatment of long bone non-unions with polytherapy: indications and clinical results. *Injury*. 2011;42:587-590.

3. Vertenten G, Gasthuys F, Cornelissen M, Schacht E, Vlaminck L. Enhancing bone healing and regeneration: present and future perspectives in veterinary orthopaedics. *Vet Comp Orthop Traumatol*. 2010;23:153-162.

4. Lee HB, Chung Y.S., Heo SY, Kim NS. Augmentation of bone healing of nonunion fracture using stem cell based tissue engineering in a dog: a case report. *Veterinarni Medicina*. 2009;54:198-203.

5. Langer R, Vacanti JP. Tissue engineering. *Science*. 1993;260:920-926.

6. Barry FP, Murphy JM. Mesenchymal stem cells: clinical applications and biological characterization. *Int J Biochem Cell Biol*. 2004;36:568-584.

7. Ribitsch I, Burk J, Delling U, et al. Basic Science and Clinical Application of Stem Cells in Veterinary Medicine. *Adv Biochem Eng Biotechnol*. 2010;123:219-263.

8. Zuk PA, Zhu M, Ashjian P, et al. Human adipose tissue is a source of multipotent stem cells. *Mol Biol Cell*. 2002;13:4279-4295.

9. Alaminos M, Perez-Kohler B, Garzon I, et al. Transdifferentiation potentiality of human Wharton's jelly stem cells towards vascular endothelial cells. *J Cell Physiol*. 2010;223:640-647.

397 10. Kraus KH, Kirker-Head C. Mesenchymal stem cells and bone regeneration. *Vet Surg*.
398 2006;35:232-242.

399 11. Jang BJ, Byeon YE, Lim JH, et al. Implantation of canine umbilical cord blood-derived
400 mesenchymal stem cells mixed with beta-tricalcium phosphate enhances osteogenesis in bone
401 defect model dogs. *J Vet Sci*. 2008;9:387-393.

402 12. Zucconi E, Vieira NM, Bueno DF, et al. Mesenchymal stem cells derived from canine
403 umbilical cord vein--a novel source for cell therapy studies. *Stem Cells Dev*. 2010;19:395-402.

404 13. Kadiyala S, Jaiswal N, Bruder SP. Culture-Expanded, Bone Marrow-Derived Mesenchymal
405 Stem Cells Can Regenerate a Critical-Sized Segmental Bone Defect. *Tissue Engineering*.
406 1997;3:173-185.

407 14. Martin DR, Cox NR, Hathcock TL, Niemeyer GP, Baker HJ. Isolation and characterization
408 of multipotential mesenchymal stem cells from feline bone marrow. *Exp Hematol*. 2002;30:879-
409 886.

410 15. Dominici M, Le Blanc K, Mueller I, et al. Minimal criteria for defining multipotent
411 mesenchymal stromal cells. The International Society for Cellular Therapy position statement.
412 *Cytotherapy*. 2006;8:315-317.

413 16. Wagner W, Wein F, Seckinger A, et al. Comparative characteristics of mesenchymal stem
414 cells from human bone marrow, adipose tissue, and umbilical cord blood. *Exp Hematol*.
415 2005;33:1402-1416.

416 17. Bosch P, Pratt SL, Stice SL. Isolation, characterization, gene modification, and nuclear
417 reprogramming of porcine mesenchymal stem cells. *Biol Reprod*. 2006;74:46-57.

418 18. Krabbe C, Zimmer J, Meyer M. Neural transdifferentiation of mesenchymal stem cells--a
419 critical review. *APMIS*. 2005;113:831-844.

420 19. Roberts SJ, Howard D, Buttery LD, Shakesheff KM. Clinical applications of musculoskeletal
421 tissue engineering. *Br Med Bull*. 2008;86:7-22.

422 20. Williams JM, Adewunmi A, Schek RM, et al. Bone tissue engineering using
423 polycaprolactone scaffolds fabricated via selective laser sintering. *Biomaterials*. 2005;26:4817-
424 4827.

425 21. Amato I, Ciapetti G, Pagani S, et al. Expression of cell adhesion receptors in human
426 osteoblasts cultured on biofunctionalized poly-(epsilon-caprolactone) surfaces. *Biomaterials*.
427 2007;28:3668-3678.

428 22. Gunatillake PA, Adhikari R. Biodegradable synthetic polymers for tissue engineering. *Eur*
429 *Cell Mater*. 2003;5:1-16; discussion 16.

430 23. Shor L, Guceri S, Wen X, Gandhi M, Sun W. Fabrication of three-dimensional
431 polycaprolactone/hydroxyapatite tissue scaffolds and osteoblast-scaffold interactions in vitro.
432 *Biomaterials*. 2007;28:5291-5297.

433 24. Di Silvio L, Dalby MJ, Bonfield W. Osteoblast behaviour on HA/PE composite surfaces with
434 different HA volumes. *Biomaterials*. 2002;23:101-107.

435 25. Wang M. Composite scaffolds for bone tissue engineering. *American Journal of*
436 *Biochemistry and Biotechnology*. 2006;2:80-84.

437 26. Neuendorf RE, Saiz E, Tomsia AP, Ritchie RO. Adhesion between biodegradable polymers
438 and hydroxyapatite: Relevance to synthetic bone-like materials and tissue engineering scaffolds.
439 *Acta Biomater*. 2008;4:1288-1296.

440 27. Hutmacher DW, Schantz JT, Lam CX, Tan KC, Lim TC. State of the art and future
441 directions of scaffold-based bone engineering from a biomaterials perspective. *J Tissue Eng*
442 *Regen Med*. 2007;1:245-260.

443 28. Wutticharoenmongkol P, Pavasant P, Supaphol P. Osteoblastic phenotype expression of
444 MC3T3-E1 cultured on electrospun polycaprolactone fiber mats filled with hydroxyapatite
445 nanoparticles. *Biomacromolecules*. 2007;8:2602-2610.

446 29. Johnson KD, August A, Sciadini MF, Smith C. Evaluation of ground cortical autograft as a
447 bone graft material in a new canine bilateral segmental long bone defect model. *J Orthop*
448 *Trauma*. 1996;10:28-36.

449 30. Horn P, Bork S, Diehlmann A, et al. Isolation of human mesenchymal stromal cells is more
450 efficient by red blood cell lysis. *Cytotherapy*. 2008;10:676-685.

451 31. Horn P, Bork S, Wagner W. Standardized isolation of human mesenchymal stromal cells
452 with red blood cell lysis. *Methods Mol Biol*. 2011;698:23-35.

453 32. Kumar S, Bandyopadhyay U. Free heme toxicity and its detoxification systems in human.
454 *Toxicol Lett*. 2005;157:175-188.

455 33. Meguro T, Chen B, Parent AD, Zhang JH. Caspase inhibitors attenuate oxyhemoglobin-
456 induced apoptosis in endothelial cells. *Stroke*. 2001;32:561-566.

457 34. Egrise D, Martin D, Vienne A, Neve P, Schoutens A. The number of fibroblastic colonies
458 formed from bone marrow is decreased and the in vitro proliferation rate of trabecular bone cells
459 increased in aged rats. *Bone*. 1992;13:355-361.

460 35. Dodson SA, Bernard GW, Kenney EB, Carranza FA. In vitro comparison of aged and young
461 osteogenic and hemopoietic bone marrow stem cells and their derivative colonies. *J Periodontol*.
462 1996;67:184-196.

463 36. Rao MS, Mattson MP. Stem cells and aging: expanding the possibilities. *Mech Ageing Dev*.
464 2001;122:713-734.

465 37. Bobis S, Jarocha D, Majka M. Mesenchymal stem cells: characteristics and clinical
466 applications. *Folia Histochem Cytobiol*. 2006;44:215-230.

467 38. Musina RA, Bekchanova ES, Sukhikh GT. Comparison of mesenchymal stem cells obtained
468 from different human tissues. *Bull Exp Biol Med*. 2005;139:504-509.

469 39. Johnson KD, Frierson KE, Keller TS, et al. Porous ceramics as bone graft substitutes in long
470 bone defects: a biomechanical, histological, and radiographic analysis. *J Orthop Res*.
471 1996;14:351-369.

472 40. Burastero G, Scarfi S, Ferraris C, et al. The association of human mesenchymal stem cells
473 with BMP-7 improves bone regeneration of critical-size segmental bone defects in athymic rats.
474 *Bone*. 2010;47:117-126.

475 41. Cook SD, Baffes GC, Wolfe MW, Sampath TK, Rueger DC. Recombinant human bone
476 morphogenetic protein-7 induces healing in a canine long-bone segmental defect model. *Clin*
477 *Orthop Relat Res*. 1994;(301):302-312.

478 42. McCartney WT, MacDonald JB. Incidence of non-union in long bone fracture in 233 cats.
479 *Intern J Apply Res Vet Med*. 2006;4:209-212.

480 43. Chuenjitkuntaworn B, Inrung W, Damrongsri D, Mekaapiruk K, Supaphol P, Pavasant P.
481 Polycaprolactone/hydroxyapatite composite scaffolds: preparation, characterization, and in vitro
482 and in vivo biological responses of human primary bone cells. *J Biomed Mater Res A*.
483 2010;94:241-251.

484 44. Dickson G, Buchanan F, Marsh D, Harkin-Jones E, Little U, McCaigue M. Orthopaedic
485 tissue engineering and bone regeneration. *Technol Health Care*. 2007;15:57-67.

486 45. Bostman O, Hirvensalo E, Makinen J, Rokkanen P. Foreign-body reactions to fracture
487 fixation implants of biodegradable synthetic polymers. *J Bone Joint Surg Br*. 1990;72:592-596.

488 46. Bergsma EJ, Rozema FR, Bos RR, de Bruijn WC. Foreign body reactions to resorbable
489 poly(L-lactide) bone plates and screws used for the fixation of unstable zygomatic fractures. *J*
490 *Oral Maxillofac Surg*. 1993;51:666-670.

491 47. Prokop A, Jubel A, Helling HJ, et al. Soft tissue reactions of different biodegradable
492 polylactide implants. *Biomaterials*. 2004;25:259-267.

493 48. Linder L, Lundskog J. Incorporation of stainless steel, titanium and Vitallium in bone. *Injury*.
494 1975;6:277-285.

495 49. Volker W, Dorszewski A, Unruh V, Robenek H, Breithardt G, Buddecke E. Copper-induced
496 inflammatory reactions of rat carotid arteries mimic restenosis/arteriosclerosis-like neointima
497 formation. *Atherosclerosis*. 1997;130:29-36.

498 50. Tindel NL, Marcillo AE, Tay BK, Bunge RP, Eismont FJ. The effect of surgically implanted
499 bullet fragments on the spinal cord in a rabbit model. *J Bone Joint Surg Am*. 2001;83-A:884-890.

500 51. Lin GL, Hankenson KD. Integration of BMP, Wnt, and notch signaling pathways in
501 osteoblast differentiation. *J Cell Biochem*. 2011;112:3491-3501.

502 52. Schmitt JM, Hwang K, Winn SR, Hollinger JO. Bone morphogenetic proteins: an update on
503 basic biology and clinical relevance. *J Orthop Res*. 1999;17:269-278.

504 53. Cheng H, Jiang W, Phillips FM, et al. Osteogenic activity of the fourteen types of human
505 bone morphogenetic proteins (BMPs). *J Bone Joint Surg Am*. 2003;85-A:1544-1552.

506 54. Shen B, Wei A, Whittaker S, et al. The role of BMP-7 in chondrogenic and osteogenic
507 differentiation of human bone marrow multipotent mesenchymal stromal cells in vitro. *J Cell*
508 *Biochem*. 2010;109:406-416.

509 55. Takigami H, Kumagai K, Latson L, et al. Bone formation following OP-1 implantation is
510 improved by addition of autogenous bone marrow cells in a canine femur defect model. *J Orthop*
511 *Res*. 2007;25:1333-1342.

512

The effects of mesenchymal stem cells combined with polycapolactone/hydroxyapatite composite scaffold on the healing of ulnar defect in dogs

Author names: Sasijaras Tantrajak[1]
Prasit Pavasant[2]
Pitt Supaphol[3]
Chalika Wangdee [1]
Chanin Kalpravidh[1]
Wijit Banlunara [4]
Mongkol Techakumphu[5]
Kumpanart Soontornvipart [1]
Theerawat Tharasanit [5]*

Author's addresses:

[1] *Department of Veterinary Surgery,* [4]*Department of Pathology,* [5]*Department of Obstetrics, Gynaecology and Reproduction, Faculty of Veterinary Science, Chulalongkorn University, Bangkok 10330, Thailand*

[2] *Department of Anatomy, Faculty of Dentistry, Chulalongkorn University, Bangkok 10330, Thailand*

[3] *The Petroleum and Petrochemical College, Chulalongkorn University, Bangkok 10330, Thailand*

Correspondence: Theerawat Tharasanit
Department of Obstetrics, Gynaecology and Reproduction,
Chulalongkorn University, Faculty of Veterinary Science,
Bangkok 10330, Thailand
Tel: + 66 2 218 9644

Fax: +66 2 252 0738

E-mail address: Theerawat.t@chula.ac.th

Abstract

Bone tissue engineering using biodegradable scaffolds combined with mesenchymal stem cells (MSCs) has increasingly become a promising alternative treatment for extensive bone defects. This study aimed at investigating the interaction between canine bone marrow derived MSCs and polycaprolactone/hydroxyapatite (PCL/HA) scaffolds followed by an *in vivo* evaluation of the efficacy of MSC loaded PCL/HA scaffolds on the healing of critical-sized ulnar defect. The MSCs from 4 dogs were collected by bone marrow aspiration and then cultured in vitro. Expression of cell surface antigen (CD 44 and CD 90) and in vitro differentiation were used to characterize the properties of canine MSCs. Following MSC loading into PCL/HA scaffold, the viability, proliferative activity and in vitro bone differentiation of the MSCs were evaluated.

Viability assay demonstrated that the majority of cells remained viable on day 1 after MSC seeding. This was in accordance to the significant increased total protein concentrations observed between day 1 and 5 and day 3 and 5 after seeding ($P<0.05$). The presence of nuclei and adhered MSCs to the scaffold surface as evaluated by DAPI staining and scanning electron microscopy also indicated the MSC and scaffold compatibility. Furthermore, the loaded MSCs were capable of bone differentiation. Despite the promising *in vitro* results, neither new bone nor callus formation was observed in defects transplanted with PCL/HA alone or MSC-loaded PCL/HA scaffolds. Defects in both groups were filled with fibrovascular tissue and remnants of the scaffold. It is concluded that PCL/HA scaffolds demonstrate a good biocompatibility to the canine MSCs. However, neither bone nor callus

formation was observed in canine ulnar defects implanted with MSCs loaded PCL/HA. Further study for mechanism controlling the fate of MSCs after transplantation is required.

Introduction

Extensive bone defect is one of the most common problems in veterinary orthopedics which can be resulted from congenital malformations, traumatic injury, osteomyelitis and bone tumor. Natural bone healing mechanism alone may not be able to regenerate sufficient amount of bone tissue to fill up the large defect consequently result in delayed or nonunion. Therefore, proper surgical intervention and bone healing enhancement are necessary when dealing with such defects (Drosse et al., 2008). Autogenous cancellous bone is considered as the most effective bone graft material (Keating and McQueen, 2001; Griffon, 2005). However, the limited amount of graft available, donor site morbidity and prolonged surgical time are the major drawbacks of autogenous cancellous graft.

The combination of biomaterial scaffolds and mesenchymal stem cells (MSC) is one of the most promising strategies for bone tissue engineering and cellular delivery (Salgado et al., 2004; Sharma et al., 2005; Necas et al., 2008). Hydroxyapatite (HA) ($Ca_{10}[PO_4]_6[OH]_2$) is known as a ceramic of choice for bone tissue engineering because it has excellent biocompatibility due to the chemical and crystal properties resemblance to the mineral component of bone tissue. HA possesses both osteoconductive capacity and ability to bind directly to host bone. Polycaprolactone (PCL) is a biodegradable synthetic polymer which has been extensively investigated as a scaffold for bone tissue engineering (Williams et al., 2005; Amato et al., 2007; Guarino et al., 2008; Porter et al., 2009). PCL is a semi-crystalline hydrophobic polymer which belongs to an aliphatic polyester family. PCL offers advantages over others polymeric materials including, good biocompatibility, higher and prolonged mechanical strength, more stable in ambient condition, and slower biodegradation rate which is suitable for bone formation and remodeling phase (Shor et al., 2007; Gunatillake and

Adhikari, 2003).Several *in vivo* studies have been conducted which demonstrated the promising outcomes of the use of PCL scaffolds for bone tissue engineering application (Rohner et al., 2003; Williams et al., 2005; Oh et al. 2007; Savarino et al., 2007; Dupont et al. 2010). Combining HA with PCL PCL-based scaffold helps improve mechanical properties, osteoconductive and osteointegrative potential (Silvio et al., 2002; Wang, 2006; Neuendorf et al., 2008). Numerous earlier studies in rodent models suggested that the biodegradable PCL/HA composite scaffolds are good candidates for bone tissue engineering (Azevedo et al., 2003; Ciapetti et al., 2003; Wutticharoenmongkol et al., 2006; Wutticharoenmongkol et al., 2007; Yu et al., 2009).

To promote bone healing after transplantation the biodegradable scaffold, cellular compartment of the bone tissue engineering is also important. Mesenchymal stem cell (MSC) is one of the adult stem cells which possess the two remarkable characterizations including the self-renewal capacity and the ability to differentiate along mesenchymal lineage such as 4steoblast, chondroblast and adipocyte under an appropriate condition (Pittinger et al., 1999). MSCs reside in various tissues such as bone marrow, adipose tissue, skin, periosteum and placenta (Toma et al., 2001; Tondreau et al., 2004; Miao et al., 2006; Bunnel et al., 2007). Bone marrow is considered as a primary source of MSCs for bone engineering application due to the ease of harvesting and isolating procedure (Tuan et al., 2002). Martin and his colleagues (2002) demonstrated the frequency of feline MSCs in bone marrow mononuclear cell fraction in the range 1 in 4.7 to 5.9 x 10^5 cells which is closely to the frequency of other species (Pittinger, 1999; Wexler et al., 2003). Due to a very small number of MSCs resided in the bone marrow, isolation, cultivation and expansion *ex vivo* are requisite prior seeding them onto the scaffold (Robert et al., 2008).

This study aimed to investigate the interaction between canine mesenchymal stem cells and PCL/HA scaffolds with respect to cell viability, adhesion and morphology,

proliferative capacity and the ability to differentiate into osteogenic lineage. In addition, in vitro bone formation following transplantation of canine MSCs combined with PCL/HA scaffolds were also tested in critical size defects of ulnar bone.

Materials and Methods

All chemicals used in this study were purchased from Sigma Aldrich, St. Louis, USA, unless otherwise specified.

2.1 Scaffolds

PCL/HA composites scaffolds used in this study were prepared as previously described (Wutticharoenmongkol et al., 2006). Scaffolds were prepared from Polycaprolactone (PCL; Aldrich, USA; *M*w = 80,000 $g \cdot mol^{-1}$) incorporated with 40% w/w HA powder by solvent casting and particular leaching technique. Sucrose with diameter around 400–500 μm was used as the porogen to create the interconnected network. The scaffold porosity was in the range of 85-87%. PCL/HA composite scaffolds were cut into 5 x 5 x 5 mm and 10 x 5 x 25 mm for *in vitro* and *in vivo* studies, respectively. The scaffolds were sterilized with 100% (v/v) absolute ethanol for 1 hour and washed thoroughly with steriled distilled water and DPBS to remove residual ethanol. The scaffolds were preconditioned in culture medium for 2 hours prior to seeding procedure.

2.2 Animals

All protocols used in this study were approved by the Committee for the Ethical Care of Animals of the Chulalongkorn University. Seven mongrel dogs were enrolled in this study with various sexes (male=2, female=5), body weights were ranging from 12 to 16 kg. In each dog, a 2.5 cm bilateral ulnar ostectomy was performed to create critical sized defects. One dog had to undergo the second operation in order to get the total of 15 defect sites. Complete blood counts and blood chemical profiles were also examined prior surgery. Acepromazine

maleate (0.02 mg/kg) (Vetranquil™, Ceva Sante animal, Libourne, France) combined with morphine sulphate (0.5 mg/kg) (Food and drug administration, Bangkok, Thailand) were used as the premedication drugs which administered intramuscularly. General anesthesia was induced with 4-6 mg/kg propofol (Fresenius Kabi Austria GmbH, Graz, Austria) intravenously and then maintained with an inhalation anesthesia using isoflurane in 100% oxygen via the rebreathing anesthetic circuit. Cefazolin (250 mg/ml) 25 mg/kg was administered intravenously as the prophylactic antibiotic. Additionally, brachial plexus nerve block using 0.5% bupivacaine (1 mg/kg) was performed to minimize pain sensation (Skarda and Tranquilli, 2007) that may occur during ulnar ostectomy.

2.3 MSCs isolation and culture expansion

The bone marrow contents (5-10 ml) from 4 dogs were collected using a 18 G needle connecting to a 5 ml heparinized syringe. To remove an excessive RBC, 5 ml of red blood cell lysing buffer (8.3 g/L ammonium chloride in 0.01 M Tris-HCl buffer pH 7.5 $\pm$ 0.2; Sigma-Aldrich, USA) was added into 5 ml aspirated bone marrow in a 15 ml sterile plastic tube (BD Falcon™, Becton Dickinson, Thailand). The solution was gently mixed followed by centrifugation at 1000 rpm for 5 minutes at 26 ˚C. The supernatant was discarded and the pellet was resuspended with 1 ml of MSC culture medium containing low-glucose Dulbecco's modified Eagle's medium (low glucose DMEM; Sigma, USA.) supplemented with 10% (v/v) fetal bovine serum (FBS) (Invitrogen, Carlsbad, USA), 2 mM L-glutamine, 100 unit/ml penicillin G, 100 µg/ml streptomycin and 5 µg/ml amphotericin B. Cells were plated in 100 mm tissue culture dish (BD Falcon™, Thailand) in 6 ml of culture medium. The initial seeding density was approximately between 50-60% confluences. The culture plate was gently mixed before incubated at 37^{o}C in a humidified condition of 5% CO_2.

2.4 Characterization of canine mesenchymal stem cells

2.4.1 Flow cytometry

149 The examination of MSCs was performed as essentially described by Tharasanit et al.
150 (2011). Canine MSCs at the 3rd passages from a total of 4 dogs were immunologically
151 examined for surface markers. These makers included the positive (CD 44, CD 90) and
152 negative (CD 34) makers. The MSCs were first dissociated from the Petri dishes with
153 Trypsin- EDTA and then centrifuged. A total of 200,000 to 300,000 cells were used for
154 immunolabeling. Rat monoclonal anti-canine CD 90 (AbD serotec, Kidlington, UK) with
155 rabbit anti-rat FITC secondary antibodies and monoclonal anti-canine CD44 antibody
156 conjugated with allophycocyanin (APC) (R&D system, Minneapolis, USA) were used as
157 MSC positive markers. A rat monoclonal anti-canine CD 34 antibody conjugated with
158 fluorescein isothiocyanate (FITC) was used as the negative MSC marker. Fluorescently-
159 labeled MSCs were washed and fixed with 1% (w/v) paraformaldehyde in PBS and stored at
160 4°C in the dark until analysis. Non-staining MSCs and MSCs labeled with only the secondary
161 antibody were used as controls. At least 20,000 MSCs were analyzed by flow cytometry.

162 2.4.2 *In vitro* bone differentiation of MSCs

163 Canine bone marrow derived MSCs at passage 3 from four dogs were simultaneously
164 induced to osteogenic lineage (each dog represented one replicate). Osteogenic differentiation
165 was performed as essentially described by Bosch et al. (2006) with minor modifications. The
166 MSCs were first cultured to reach approximately 80% confluence, the osteogenic medium
167 containing MSC medium supplemented with 0.1 μM dexamethasone, 50 μM ascorbic acid,
168 10 mM β-glycerophosphate (Merck, Darmstadt, Germany) was then added into the culture
169 dish. The *in vitro* bone differentiation was performed for 21 days. Von Kossa staining was
170 used to detect deposition of calcium phosphate indicating *de novo* bone formation.

171 **2.5 *In vitro* assay for MSC and scaffold interaction**

172

For *in vitro* study of biocompatibility of MSC and the scaffold, PCL/HA scaffolds were seeded with canine MSCs at a density of 100,000 cells/scaffold. The loaded scaffolds were incubated at 37˚C in a humidified condition of 5% CO_2 in air After 45 min of incubation, a 5-ml of culture medium was added to cover the entire scaffold.

2.5.1 Scanning electron microscopy

Scanning electron microscope (SEM) was performed to illustrate MSC morphology and the ability to attach on the PCL/HA scaffold on day 1, 3 and 5 after seeding. Briefly, the loaded PCL/HA scaffolds were washed twice with PBS (pH 7.2) and fixed with ice-cold 3% glutaraldehyde for 30 min. Then, the scaffolds were dehydrated with serial ethanol dilutions (30%, 50%, 70%, 90% and 100% (v/v) ethanol, respectively) for 2 min at each concentration. Finally, the scaffolds were soaked with Hexamethyldisilazane (HMDS) for 5 min and allow to air dried overnight at room temperature, so that HMDS was evaporated from the scaffolds before coating with gold. The SEM was performed using a JSM-5410LV scanning electron microscope (JEOL, Japan).

2.5.2 MSC viability and proliferative capacity

After 1 day of seeding, MSC-loaded scaffolds were cut into thin sections for evaluation of canine MSC viability. The viability assay was performed by dual fluorescent staining method using calcein AM and ethidium homodimer. A bright green fluorescence from calcein AM demonstrated the presence of active esterase enzyme activity while cell plasma membrane disrupted cells (dead cells) exhibited red fluorescent color. For MSC proliferation evaluation, PCL/HA scaffolds were seeded with canine at a density of 50,000 cells per scaffold. The proliferative capacity was qualitatively analyzed based on the serial fluorescent images of canine MSCs staining with 4', 6-diamidino-2-phenylindole dihydrochloride (DAPI; Roche, Germany) in conjunction with a quantitative analysis of the total protein content by the bicinchoninic acid (BCA) protein assay kit (Pierce

198 Biotechnology, USA). For DAPI fluorescence staining, the loaded PCL/HA scaffolds were
199 fixed at day 1, 2 and 4 of incubation with 3.7% formaldehyde. MSC loaded-PCL/HA scaffold
200 were then stained with DAPI (1:1000) for 10 min and observed under Zeiss Axio Observer
201 fluorescence microscope (Carl Zeiss, Germany) at a wavelength of 380 nm. The total protein
202 quantification of MSC-loaded PCL/HA construct was determined on day 1, 3 and 5 after
203 seeding. The BCA assay is a colorimetric detection and quantification of total protein in the
204 cell/scaffold construct by measuring the purple water-soluble product resulting from the
205 chelation of BCA and Cu^{+1}. Briefly, the working solution was prepared by mixing Reagent A
206 and reagent B in the ratio of 50:1. Then the loaded PCL/HA scaffolds were washed twice
207 with PBS to eliminate the contaminated protein from the culture medium and chopped with a
208 shaped scissors into small pieces before adding 200 µl of 2% sodium dodecly sulfate in a 1
209 ml of microcentrifuge tube. Mixed thoroughly by vortexing for 1 min and centrifuged at 5000
210 rpm for 1 min. A 50 µm of the supernatant was transferred into new 1 ml of microcentrifuge
211 tube then added 1 ml of working solution, mixed thoroughly by vortexing, and incubated at
212 37ºC for 30 min. Finally, 80 µl of the final solution was pipetted into a 24-well plate and
213 measured the absorbance at 562 nm wavelength using an absorbance microplate reader
214 (ELx800^{TM}; Biotek, Vermont). All data were collected and analyzed by microplate data
215 collection and analysis Software (Gen5^{TM}; Biotek, Vermont) with the reference to bovine
216 serum albumin.

217 **Osteogenic differentiation of MSC within PCL/HA scaffold**

218 The ability of canine MSCs to differentiate into an osteoblastic lineage on PCL/HA
219 scaffold was investigated by seeding MSCs at a density of 50,000 cells onto the PCL/HA
220 scaffold size 5 x 5 x 5 mm. The MSC loaded PCL/HA scaffold treated with the bone
221 induction medium on day 3 of culture, and differentiation was confirmed by using Alizarin
222 Red staining on day 14 of induction.

223 **2.6 Effect of PCL/HA and MSCs on bone healing of critical- size ulnar defects**

224 To perform bilateral ulnar ostectomy, dogs were anaesthetized as mentioned above. A
225 10 cm incision was made through the skin and subcutaneous tissue over the caudolateral
226 aspect of the ulna. The bilateral 2.5 cm ulnar ostectomy was performed using an oscillating
227 saw. No internal fixation was used in this study due to the canine model is mechanically
228 stability without further fixation as the radius is the major load-bearing structure in the canine
229 forelimb. In this study, defects on the left ulnae were implanted with the corticocancellous
230 autografts to serve as a control group (n=7) while defects on the right ulnae were randomly
231 implanted with PCL/HA composite scaffold alone (n=4) or PCL/HA combined with canine
232 MSCs (n=4). After the operation, all forelimbs were applied with modified Robert Jone
233 bandages reinforced with thermoplastic splints (Vet-lite, BEC, Thailand) for 2 weeks. The
234 dogs were received 5 mg/kg enrofloxacin (Baytril; Bayer, USA) and 4 mg/kg carprofen
235 (Rimadly; Pfizer, USA) orally twice a day for 7 days after implantation.

236 2.6.1 Examination of bone healing by Radiographic examination

237 The craniocaudal (CrCd) radiographs were taken immediately after operation and at 2,
238 4, 6, 8 weeks postoperatively. Bone healing was evaluated and scored by 3 radiologists in a
239 blinded fashion using the radiographic scoring system described by Jones et al. (2008) (Table
240 4)

241 2.6.2 histological analysis of PCL/HA scaffold implant

242 At the 8 weeks after implantation, biopsy was performed to verify the formation of
243 bone following transplantation. The sites of biopsy included the middle portion of the implant
244 and the host bone-implant interface. The sample was fixed in 10% (v/v) formalin and
245 processed as a routine histological procedure as described elsewhere. The samples were
246 sectioned and stained with hematoxylin and eosin (H&E).

247

248 **Table 1** Radiographic scoring system for bone healing evaluation (Jones et al., 2008)

Description	Radiographic score
No change from immediate postoperative appearance	0
A slight increase in radiodensity distinguishable from the graft	1
Recognizable increase in radiodensity, bridging of one cortex with new bone formation to the graft	2
Bridging of at least one cortex with material of nonuniform radiodensity, early incorporation of the graft suggested by obscurity of graft borders	3
Defect bridged on both medial and lateral sides with bone of uniform radiodensity, cut ends of the cortex still visible, graft and new bone not easy to differentiate	4
Same as grade 3, with at least one of four cortices obscured by new bone	5
Defect bridged by uniform new bone, cut ends of cortex no longer distinguishable, graft no longer visible	6

249

250 **Statistical analysis**

251 For total protein concentrations, Leven test was used to assess the homogeneity of
252 variance among the groups and all data was analyzed using analysis of Variance (ANOVA)
253 to determine the difference in protein concentrations between day 1, 3 and 5 after seeding.
254 Significance was defined when a p value was less than 0.05.

255 For radiographic scores which were nonparametric data, Kruskal-Wallis one-way
256 analysis of variance was used to determine the difference in healing efficacy of the implants
257 at 2, 4, 6 and 8 weeks postoperatively. Significance was defined as a p value less than or
258 equal to 0.05.

Result

At 24 hours after plating, adherent cells demonstrated heterogeneous morphology including a fibroblastic-like cell, polygonal cell and round cell. Non-adherent cells were removed by changing the culture medium and cells were distributed more homogeneous population of spindle-shaped cells was mainly observed (Fig. 2). The total number of adherent cells on day 7 of culture was 1.327×10^6 cells and the percentages viability was 98.64.

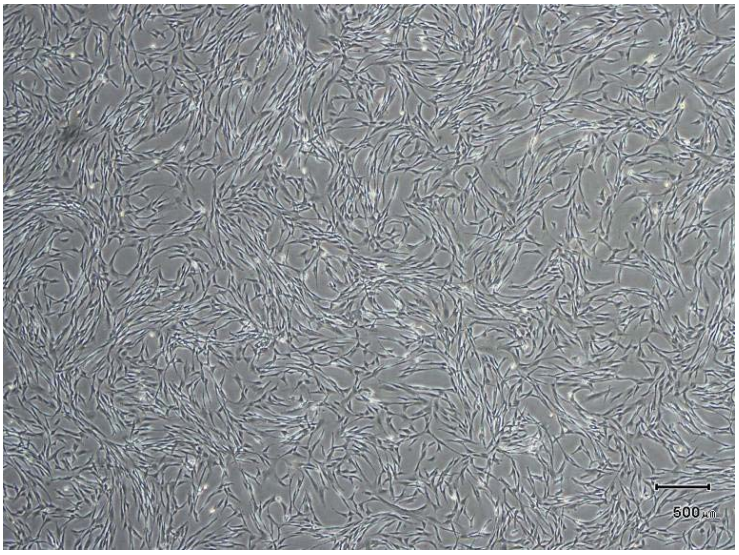


Figure 1 Canine bone marrow derived mesenchymal stem cells at passage 1 on day 3 of culture (100 X magnification, 500 µm scale bar)

The percentage of cells positive for each CD was demonstrated in table 5. The percentage of CD 44 expressed by canine MSCs at passage 3 was more than 97% while the percentage of CD 90-positive cells was more than 93%. In addition, less than 1% of MSC population expressed CD 34.

Canine MSCs at passage 3 were subjected to demonstrate the mesenchymal differentiation capacity with the specific condition according to the cell type. Histochemical special staining was performed in order to verify each differentiation on day 21 after induction. Von Kossa, Oil Red O and Alcian blue staining were used to confirm osteoblastic, adipogenic and chondrogenic differentiation, respectively. Under an osteogenic condition (Figure 4), the former spindle-shaped cells gradually transformed into polygonal, cuboidal, osteoblast-like cells extending their long processes connecting to each other to form a cellular network and started to synthesize the extracellular matrix that was positive to Von Kossa (Figure 5A) and Alizarin Red (Figure 5B). For adipogenic differentiation, thin fibroblastic cells became oval to round-shaped cells with large cytoplasm containing lipid vacuoles stained positively with Oil Red O (Figure 6). Finally, chondrogenic differentiation was achieved by culturing canine MSCs in a pellet cultural system combining with a special chondrogenic induction medium. MSCs were slowly aggregated and developed into a small round nodule within the first week of induction. The nodule was positively stained with Alcian blue indicated the presence of glycosaminoglycans at 3 weeks of induction.

Table 2 The percentage of canine MSCs positive for CD 44, CD 90 and CD 34 determined by flow cytometry at passage 3

		Markers		
Dog	**Passage**	**CD34**	**CD44**	**CD90**
Dog 1	3	0	99.82	99.21
Dog 2	3	0	99.89	98.02
Dog 3	3	0	99.95	93.52
Dog 4	3	0.06	97.91	96.92

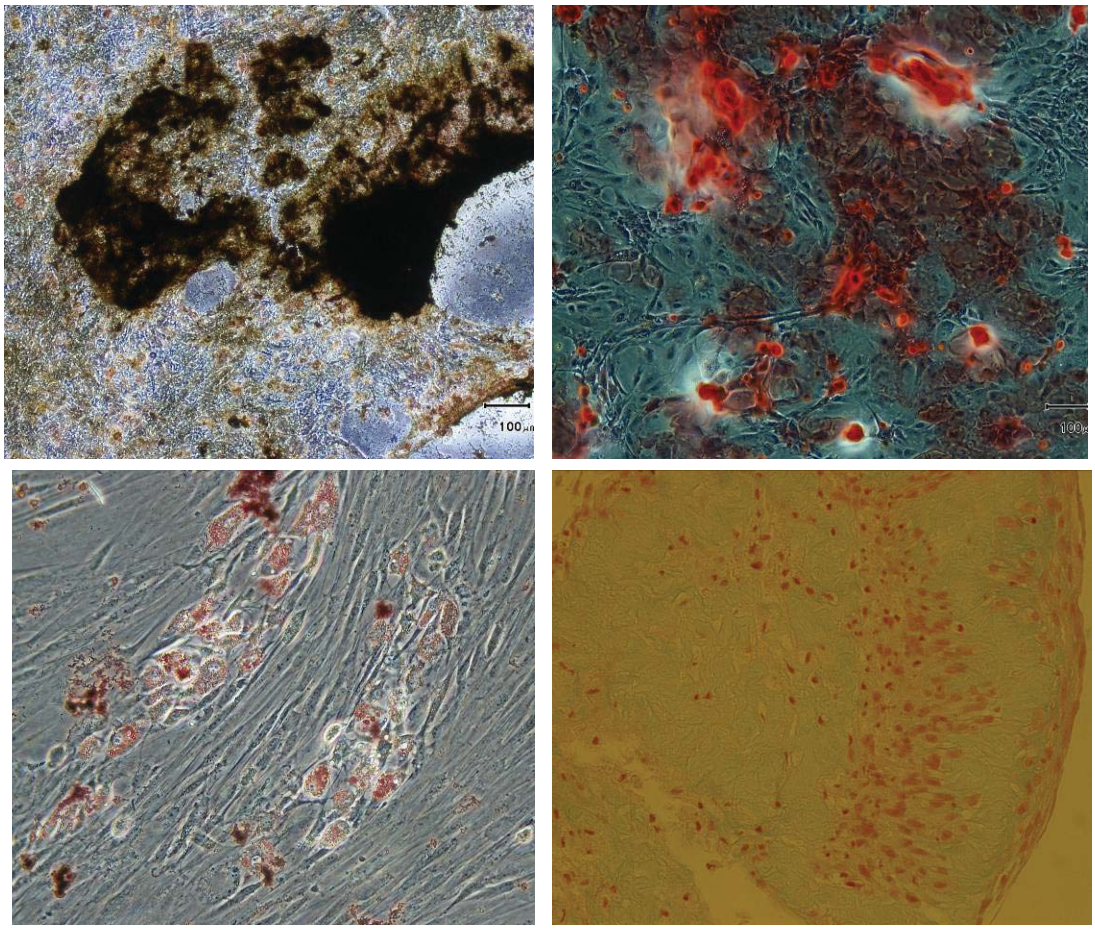


Figure 2 Von Kossa Alizarin Red and Oil Red O staining were used to validate the differentiation capacity of canine MSC into the osteogenic lineage

In vitro studies of canine MSCs behavior on PCL/HA composite scaffold was evaluated in terms of MSC attachment, morphology, the ability to growth and proliferation within the scaffold. The combination of calcein AM and ethidium homodimer fluorescence staining was used to assess MSC viability. A green fluorescence from calcein AM represented the viable MSCs while a red fluorescence indicated the non-viable cells (Figure 8). On day 1 after seeding, a mixed population of viable and non-viable canine MSCs was observed. The majority of the cells exhibited green calcein fluorescence with a small number of cells was labeled with red fluorescence. In addition, MSCs were found throughout the sample represented a good cell distribution within the scaffold.

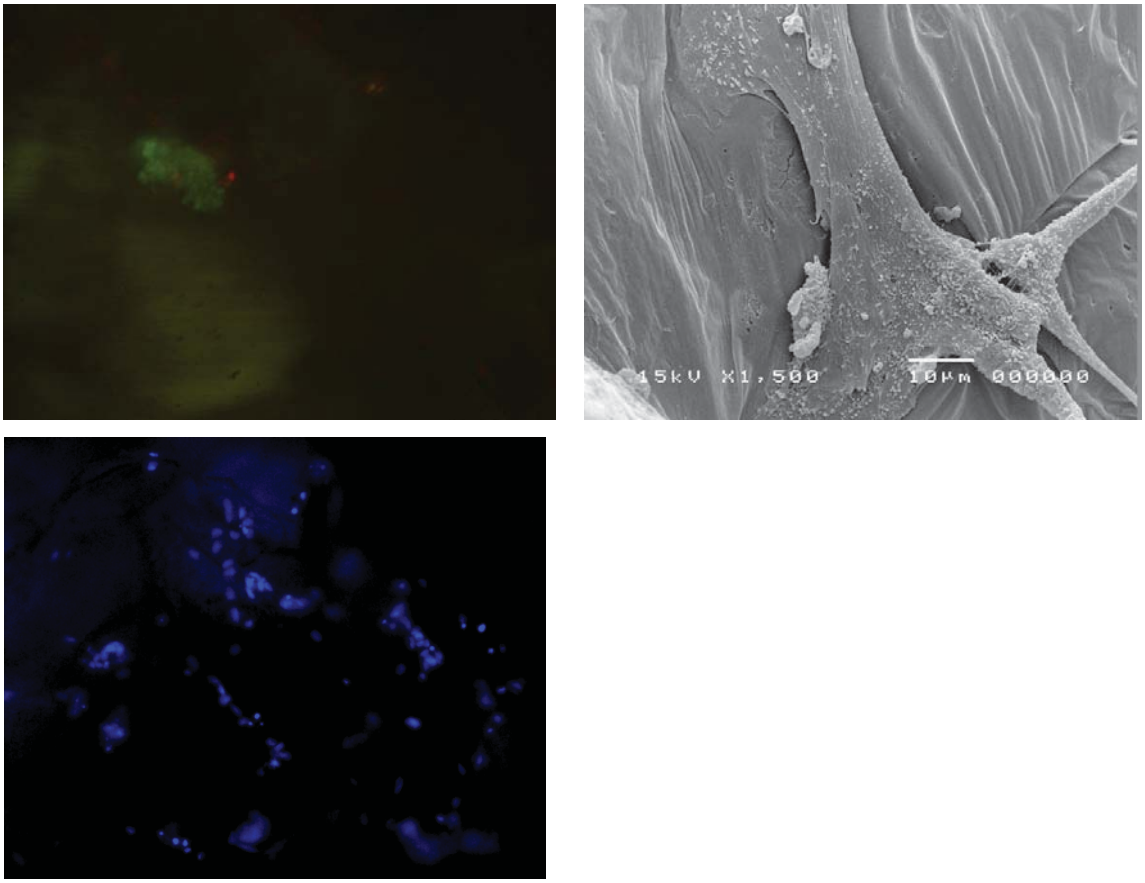


Figure 3 Photomicrographs indicating viability of MSCs within the scaffold. A: viability of canine MSCs 12 hours after seeding and B: SEM image of canine MSCs attached and expanded the cellular process onto the scaffold (3 days after MSC seeding), c: fluorescent analysis of canine MSC proliferation using DAPI nuclear staining

Canine MSC attachment and morphology was observed by SEM on day 1, 3 and 5 after seeding. On day 1 after seeding, MSCs appeared as flat cells spreading onto the surface of scaffold with finger-like projection of cell membrane (filopodia) adhered to the scaffold (Fig 9A). MSCs became more spread and elongated with an enlargement of adhesive areas

between cells and scaffold on day 3 of seeding. In addition, on day 3, more cells were observed and appeared to form small cell clusters with an intercellular connection (Fig 9B).

The proliferation of canine MSCs within PCL/HA scaffold was determined by qualitative comparison of serial DAPI fluorescent images on day1 (Figure 10A and B), 2 (Figure 10C and D) and 4 (Figure 10 E and F) after seeding. An increase MSC population was observed by an increase in DAPI-stained nuclei density over time. The quantitative analysis of the protein content was conducted to evaluate MSC growth and proliferation within PCL/HA scaffold using the BCA protein assay. The amount of protein (μg/ml) in each samples were calculated from the absorbance of the sample solution measured at a wavelength of 562 nm with reference to the standard protein (Table 6). The total protein concentration of MSC-loaded PCL/HA scaffold on day 1, 3 and 5 was 523±15.27, 626.67±71.12 and 861.67±127.16 μg/ml, respectively. A significant differences were found between protein content of PCL/HA alone and MSC-loaded PCL/HA scaffold at all time points. A significant increase in total protein concentration of MSC-loaded PCL/HA scaffold were observed between day 1 and day 5 and day 3 and day 5 ($p<0.05$). However, no significant difference was found between day 1 and 3 (Figure 11). Notably, the color of the sample solution was changed from green to purple in the proportion to the protein concentration in the scaffold (Figure 12).

To confirm an osteogenic differentiation potential of canine MSCs after seeding on PCL/HA scaffold, Alizarin Red staining was performed on day 14 of induction. Positive Alizarin Red staining was observed in both PCL/HA scaffolds alone and MSC-loaded PCL/HA scaffolds. After washed the samples several time with PBS, only PCL/HA scaffolds that combined with canine MSCs were still remained positive to Alizarin Red suggested the presence of calcium deposition within scaffolds.

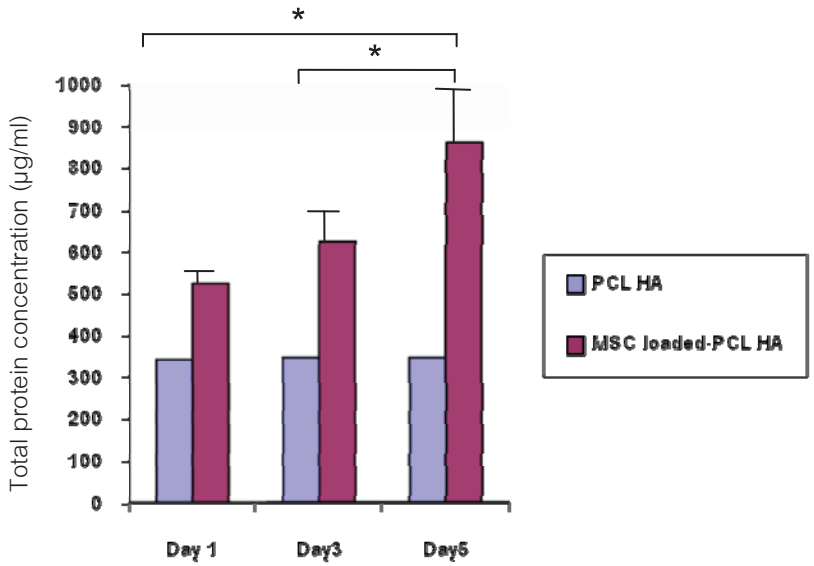


Figure 4 Quantitative measurement of total protein concentrations of PCL/HA and MSC loaded-PCL/HA scaffolds on day 1, 3 and 5 of culture. *Significant increase in protein concentration was observed ($p<0.05$)**.**

The craniocaudal radiographs of the defects were taken immediately and at 2, 4, 6 and 8 week postoperatively (Fig. 13A, B, C and D) illustrated the progressive bone healing of the ulnar defect that treated with corticocancellous bone graft (group 1). Slightly new bone formation was visible during the first 4 weeks postoperatively. At 6week, the bone bridge formation between graft and host bone was evident at the distal part of the defect. By 8 weeks postoperatively, the bone bridging was clearly observed on both side of cortices. An increase in radiodensity of the graft-host bone interfaces with time demonstrated a progressive healing of the defect. Neither new bone nor callus formation was observed in the defect site treated with PCL/HA alone (group 2) (Figure 14A, B, C and D) and MSC-loaded PCL/HA (group 3) (Figure 15A, B, C and D) at any time point. A slightly increase in radiodensity was observed within the implant site in both groups. There were statistically significant differences ($p<0.05$) in radiographic score between group 1, 2 and 3 at 6 weeks and between group 1 and 2 and group 1 and 3 at 8 weeks postoperatively. No significant differences in radiographic score were detected between treatment groups at 2 and 4 weeks postoperatively ($p>0.05$)



Figure 5 Radiographs of canine ulnar segmental defects treated with the autogenous cancellous bone graft (A-D) and PCL/HA scaffold implant (E-H) at (A, E) 2 weeks; (B, F) 4 weeks; (C, G) 6 weeks and (D, H) 8 weeks postoperatively

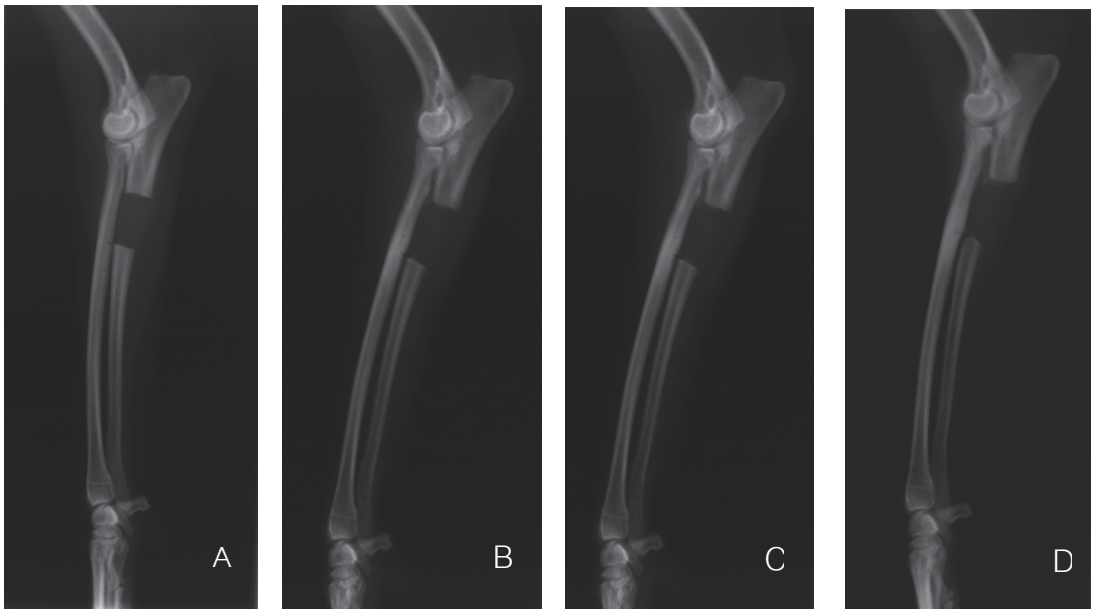


Figure 6 Radiographs of canine ulnar segmental defects treated with MSC-loaded PCL/HA scaffold at (A) 2 weeks; (B) 4 weeks; (C) 6 weeks and (D) 8 weeks postoperatively

Histopathology of the defect implanted with autogenous cancellous bone graft (group 1) showed a good incorporation between the graft and host bone (Figure 16A) with the osteoid formation and new bone formation along the graft-host bone junction. The longitudinal section of the graft revealed the re-establishment of vascular supply within the marrow cavity (Figure 16B). In group 2, the incorporation of the PCL/HA scaffold and host bone was mainly achieved by fibrocartilaginous tissue with minimal osteoid formation (Figure 17A). The defect site was filled with loose and unorganized connective tissue with new vascular ingrowth. There were still some remnants of the scaffold which sloughed off during the histological preparation (Figure 17B). Finally, in group 3, more fibrovascular tissue was observed in the defect, which implanted with MSC-loaded PCL/HA scaffold compared with PCL/HA group (Figure 18). The fibrous tissue is mainly comprised of spindle-shaped cells with extensive collagen deposition confirmed by Masson's Trichrome staining (Figure 19). It is notable that numerous of multinucleated giant cells were found

adjacent to remnants of the scaffold indicating a chronic inflammation with foreign body giant cell response to the scaffold.

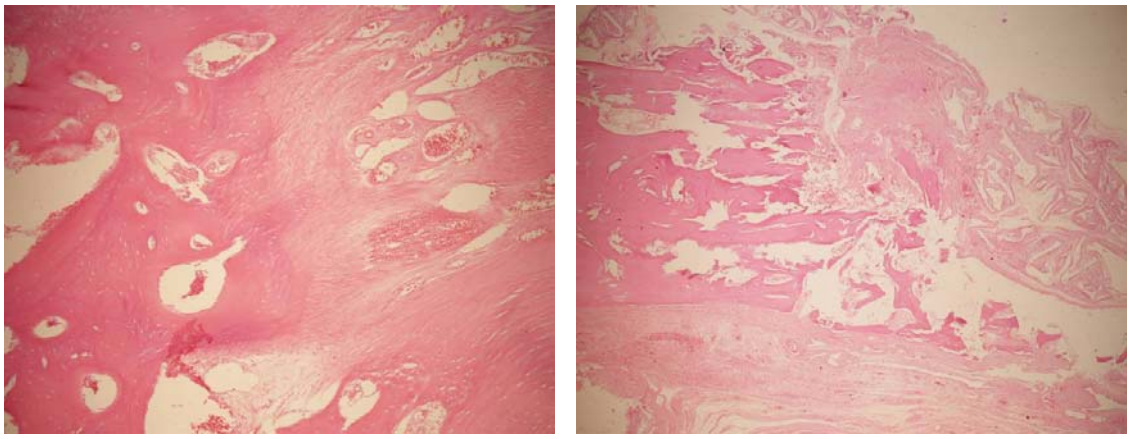


Figure 7 Histological sections of an ulnar defect implanted with cancellous bone graft (A) and with PCL/HA scaffold (B) at 8 week postoperatively. The junction between host bone (HB) and the graft (CB) and scaffold (PCL/HA)

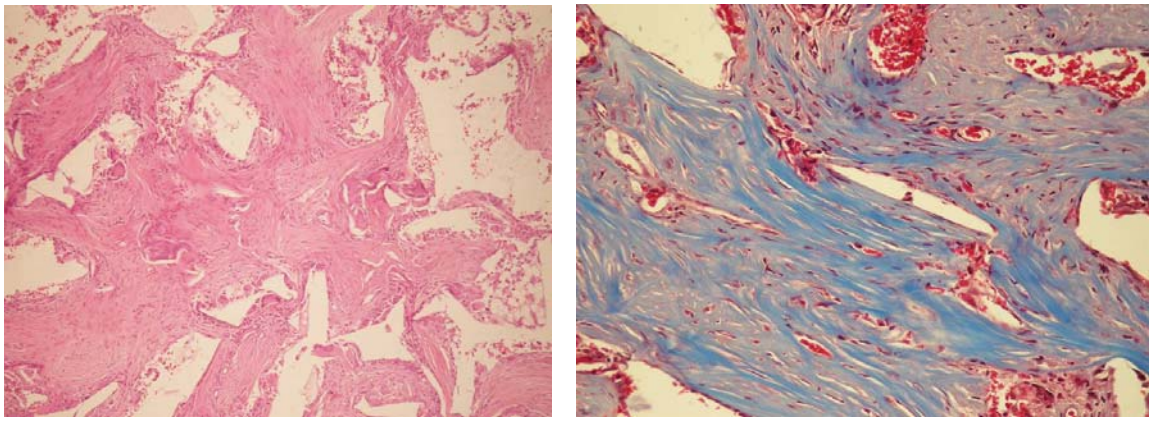


Figure 8 Histological sections of an ulnar defect implanted with MSC-loaded PCL/HA scaffold at 8 week postoperatively. A: H&E staining and Masson's trichrome staining (B)

Discussion

Implantation of biological bone substitutes is one of the promising bone tissue engineering strategies for treatment of extensive bone defects. Mesenchymal stem cell in combination with polymer/ceramic composite scaffold has been widely investigated as an alternative to autogenous cancellous bone graft. In this study, we successfully isolated canine MSCs from bone marrow and identified these cells according to the multipotent human MSCs characterization which recently proposed by International Society for Cellular Therapy (Dominici et al., 2006). Then, we investigated the interaction between canine MSCs and PCL/HA composite scaffold in terms of cell viability, proliferative capacity and ability to differentiate into osteoblast. Finally, we evaluated the efficacy of canine MSCs combined with PCL/HA composite scaffold in comparison with PCL/HA alone and autogenous on the healing of ulnar critical sized defects in dog.

MSCs reside in various adult tissues such as bone marrow, adipose tissue, skin, periosteum and placenta (Tuan et al., 2002). These cells are responsible for regulating tissue homeostasis, repair and regeneration. Although MSCs originated from various tissue sources possess similar phenotypic expression, significant difference in cell proliferation and multilineage differentiation potentials are observed. In this study, bone marrow was chosen as a source of MSCs because it is easy to assess and can be aspirated in large volume. Moreover, MSCs derived from bone marrow and synovium are superior to periosteum-, adipogenic- and skeletal muscle- derived MSCs with regard to self renewal, expansion and differentiation potential (Sakaguchi et al., 2005). Canine MSCs were harvested from the bone marrow samples aspirated from the dorsal iliac crest of 4 dogs. Red blood cell lysing buffer was added to enrich the initial MSC population by eliminating the contaminated red blood cells before culture. Canine MSCs used in the present study were isolated by their ability to adhere to the polystyrene plastic plate and subsequently subcultured when cells reached 80-90% confluence. Owing to the absence of MSC specific antigen marker, at least three

minimum criteria were required to characterize MSCs are as follows: the ability to adhere to plastic surface, the expression of cell surface antigen and the capacity to differentiate along the mesenchymal lineage (Dominici et al., 2006). The isolated cells exhibited classical spindle shaped morphology and expressed high levels of MSC markers inculding CD 44 and CD 90. The flow cytometric analysis of cell surface protein revealed more than 94% of the isolated cells were positive for both CD 44 and CD 90 which corresponding with previous study (Kern et al., 2006; Jung et al., 2008). No expression of CD34 was observed which indicated no contamination of hematopoietic stem cells was found in the culture. And finally, these isolated cells were capable of differentiation into a mesenchymal lineage when cultured in a proper condition.

Due to the major concern in the survival and proliferative capacity of cells within the large scaffold constructs, an *in vitro* study of canine MSCs behavior was performed on 3D PCL/HA scaffolds. Dual fluorescence viability assay using calcein AM and ethidium homodimer was performed to determine the MSC viability within PCL/HA scaffold. This assay allows the simultaneous visualization of viable and dead cells within the scaffold (Decherchi et al., 1997). Calcein AM is a hydrophobic compound which can diffuse through intact cell membrane of viable cells and subsequently hydrolyze intracellular esterase result in calcein, a green fluorescence, retained in the cytoplasm. In contrast to calcein AM, ethidium homodimer can penetrate only damaged cell membranes and bind to DNA of the dead cells result in emission of red fluorescence. From dual viability assay, an intense green fluorescence was mainly observed through the entire scaffold indicated the majority of canine MSCs remained viable on day 1 after seeding. A small number of dead cells were found in the outer part of the scaffold and became more prominent in the middle of the scaffold. This may be due to the diffuse limitation of oxygen and nutrient caused by the scaffold thickness. Moreover, all MSC loaded-scaffolds were cultured under a static condition may even hinder

514 the fluid transportation result in an accumulation of waste products within the scaffold. To
515 overcome these problems, dynamic culture conditions such as a spinner flask, orbital shaker
516 or perfusion system has been used since the approach can improve cell viability, uniform
517 distribution and subsequently increase in extracellular matrix deposition (Yeatts and Fisher,
518 2011). Nerurkar et al. (2011) suggested that the dynamic culture condition using orbital
519 shaker enhanced MSC infiltration and collagen deposition on electrospun PCL nanofibrous
520 scaffold. Additionally, transient shaking culture significantly improved MSC distribution,
521 provided favorable condition for chondrogenic differentiation and increased
522 glycosaminoglycans accumulation within the scaffold. The results from SEM images showed
523 that canine MCSs adhered favorably to PCL/HA scaffold. Cells exhibited flat morphology
524 with filopodia projected from cell body and attached to the scaffold surface. Filopodia are
525 protrusion of cell membrane which play an important role in the formation of adhesive
526 connection between cell and the extracellular matrix (Yang et al., 2010). The attached cells
527 became more elongated in shaped with an enlargement of focal adhesion suggested growth
528 and maturation of canine MSCs in PCL/HA scaffold over time. MSC proliferative capacity
529 on 3D PCL/HA scaffold was evidenced by comparison of serial DAPI fluorescence images.
530 DAPI is a DNA-specific dye which has been commonly used for DNA detection and
531 visualization. This dye binds specifically to A-T base pair in DNA sequence results in
532 formation of the DAPI-DNA complex which exhibits a blue fluorescence emission under a
533 fluorescence microscope. An increase in DAPI stained nuclei was observed over time
534 reflected the proliferative capacity of the loaded MSCs. Notably, the background interference
535 was observed during the fluorescent microscopical analysis of the loaded scaffold in both
536 dual viability assay and DAPI fluorescent staining. It is thought that the autofluorescence
537 emission of the polymers caused by an aromatic and aliphatic ester bond when excited with
538 green or blue wavelength. Moreover, the fluorescent interference is even more exaggerated

due to the light scattering caused by the thickness of the polymer and its porous nature. To avoid these interferences, a thin section of the sample can diminish light scattering and minimize over all autofluorescence from polymer or using other fluorescent probe that can be excited and emits in the different wavelength. Jaafar et al. (2011) applied the use of Sudan Black B (SB) as an autofluorescence quencher for 4 types of polymer, including polyglycerol sebacate, polyurethane, polylactice-co-caprolactone, and polylactic acid-co-glycolic acid. SB is a lysochrome diazo dye which has been commonly used as a neutral triglyceride and lipid staining. Reduction of an overall background interference was based on two mechanisms, the light absorption capacity of SB and the ability to modify the surface of the polymers. No interaction between SB and fluorescently labeled cells was observed.

Despite the promising result from the visual DAPI fluorescence image analysis, the uncertainty of the outcome may occur due to the subjective evaluation of these images. Therefore, the BCA protein assay was performed in order to quantify proliferative capacity of canine MSCs after seeded onto the scaffold (Sachana and Hargreaves, 2007). The assay is based on the ability of the peptide bonds in protein to reduce Cu^{+2} into Cu^{+1} and the chelation of Cu^{+1} with BCA result in purple-colored products that can be measured with spectrophotometer. The total protein concentration are calculated from the optical density of each the samples at a wavelength of 562 nm with respect to the standard curve. Significant increases in the protein concentration were observed between day 1 and day 5 and day 3 and day 5 ($p<0.05$). An increase in the absorbance of the loaded PCL/HA is correlated with the greater amount of the protein concentration in the sample indicated the growth and proliferative capacity of canine MSCs resided in the scaffold. As expected, there was no significant difference in protein concentration was found between day 1 and day 3. These may result from the physical adaptation of cells to the change in environment. Moreover, the newly seeded cells may also require time to adjust and adhere onto the new surface condition

and subsequently reformation of the intercellular connection which necessary for optimal cell proliferation. And finally, the present *in vitro* study demonstrated the ability of canine MSCs to differentiate into an osteogenic lineage after seeded onto 3D PCL/HA scaffold as evidenced by Alizarin staining on day 14 of induction.

As the combination of osteopotential cell and biolodegradable scaffold is one of the most successful strategies in bone tissue engineering and the use of PLC/HA composite scaffold fabricated by solvent casting and particular leaching techniques has been demonstrated as a promising approach for promoting new bone formation (Chuenjitkuntaworn et al., 2010). This study was performed as a further investigation using canine model in order to evaluate the efficacy of PCL/HA and MSC-loaded PCL/HA on the healing of ulnar critical size defects. Key (1934) has defined the ulnar critical sized defect as a segmental defect that larger than 1 to 1.5 times of the diameter of the shaft of the bone. All dogs were able to stand and ambulate on day 1 and 2 after surgery, respectively. Defects in PCL/HA group were healed with fibrous connective tissue consisted of long spindle-shaped fibroblastic cells and collagen fiber as an extracellular matrix. The presence of capillaries within the graft sites suggested that PCL/HA scaffolds can support the ingrowth of vascular tissue. Similar results were obtained in the group that treated with MSC-loaded PCL/HA scaffold, however, Mason's trichrome staining suggested that more collagen deposition was found when compared to PCL/HA group. Although there was a good evidence of fibrovascular tissue infiltration with an extent matrix deposition throughout the entire PCL/HA scaffold, no osteogenic differentiation was observed. In contrast to the promising result in a calvarial defect of mouse (Chuenjitkuntaworn et al., 2010) neither new bone nor callus formation was observed in defects treated with PCL/HA alone or MSC-loaded PCL/HA scaffold. Several possible reasons could explain for this inconsistency. It is believed that larger animal possesses bone regenerative capacity to a lesser extent than small animal.

589 Moreover, the physiological differences between dog and mouse with regard to the slower
590 bone turnover rate lower basal metabolic rate and longer lifespan in dog may contribute to
591 different bone healing result (Cook et. al., 1994). The variation in size, location and the
592 mechanical environment of the defects may impact on the biological response to the scaffold.
593 PCL/HA scaffolds used in the present study were not only larger in size but also thicker in
594 dimension than the previous study. This may cause a massive release of the degradation
595 product, caproic acid, from the scaffold and subsequently creating an unfavorable
596 environment for bone regeneration (Böstmann et al. 1990; Bergsma et al., 1995; Prokop et
597 al., 2004). And finally, the major consideration was given to the different types of bone
598 defect (flat bone versus long bone), the loading condition of the bone (non-loading calvarial
599 versus loading ulnar bone). A calvarial defect is considered as a non-weight-bearing model
600 which experiences lesser mechanical interference than a long bone model. Therefore, a
601 calvarial bone defect may provide more favorable environment for new bone regeneration
602 than an ulnar bone defect in a biomechanical aspects.

603 Canine ulna defect model has been extensively used as a study model to evaluate the
604 efficacy of biomaterials in bone tissue engineering application because no fixation is required
605 as the radius is the major load-bearing bone of the forearm and the interosseous ligament
606 between the radius and the ulna was remained intact. Moreover, the ulnar ostectomy
607 procedure can be done on both sides simultaneously, thus reducing the number of animal
608 used in the study (Salkeld et al., 2001; Paskalev et al., 2006; Jones et al., 2008). Several
609 successful results have been reported using a canine ulnar model without fixation (Heiple et
610 al., 1963; Nillson et. al., 1986; Cook et al., 1994; Salkeld et al., 2001; Paskalev et al., 2006;
611 Jones et al., 2008). However, there might be some mechanical interference between defect
612 sites causing an unfavorable condition for mesenchymal stem cells to differentiate into

613 osteoblastic cells. To overcome this problem, intramedullary pins or plates and screws may
614 use to stabilize canine ulnar defect in order to optimize the new bone formation.

615 Last but not least, histological analysis demonstrated the presence of numerous
616 multinucleated giant cells within defect sites that implanted with PCL/HA and MSC-loaded
617 PCL/HA scaffold. These giant cells appeared adjacent to remnants of the scaffold which
618 reflected chronic inflammation with foreign body response. For this reason, scaffold
619 samples were sent to identify the contamination using scanning electron microscope with
620 energy dispersive x-ray (SEM/EDX) analysis. The result of the SEM/EDX analysis showed
621 that the scaffolds were contaminated with copper (Cu) from hydroxyapatite ceramic. Thus,
622 chronic inflammation with foreign body giant cell response from copper contamination may
623 result in an impaired new bone formation at defect site. Similar tissue reaction was reported
624 by Linder and Lundskog (1975), Völker et al. (1997), Tindel et al. (2001) and Saitoh et al.
625 (2010). Saitoh and his group investigated an in vivo tissue response to three different metal
626 particles including copper, nickel and titanium by subcutaneous implantation in mouse. One
627 week after implantation, subcutaneous tissue was excised for evaluation of tissue reaction
628 using histological and transmission electron microscopic analysis. The result of this study
629 showed that copper particles caused the highest degree of inflammation. Similar result was
630 observed in the study of Linder and Lundskog that compared the reaction of bone to copper,
631 stainless steel, titanium and vitallium.

632

633 **Conclusions**

634 The present study was conducted in order to investigate the *in vitro* interaction
635 between canine MSCs and PCL/HA composite scaffolds by seeding cells onto the scaffold
636 and observed for cell behaviors with respect to cell viability, cell attachment and
637 morphology, the proliferative capacity and the ability to differentiate into osteogenic lineage.

The *in vitro* study demonstrated a good biocompatibility between canine MSCs and PCL/HA scaffolds. From dual fluorescence viability assay showed that the majority of seeded cells emitted green fluorescence indicating most of cells remained viable on day 1 after seeding. Similarly the result from SEM analysis revealed that canine MSCs adhered favorably onto PCL/HA scaffold. Cells already attached on the scaffold with flat morphology and filopodia projection within day 1 of seeding. More cell numbers were observed with formation of cell cluster in some area of scaffold suggested that canine MSCs were able to growth and maturation after seeding. To confirm the proliferative capacity of the seeded cell, serial DAPI florescent image analysis combined with BCA protein assay were performed. A progressive increase in DAPI-stained cells was observed under a fluorescent microscope on day 1, 2 and 4 after seeding which collated to an increase in total protein concentration on day 1 (523.33±15.27), day 3 (626.67±71.12) and day 5 (861.67±127.16) after seeding. Moreover, a significant increase ($p<0.05$) in protein concentration was observed between day 1 and 5 and day 3 and 5 of seeding. And finally, the ability of canine MSCs to differentiate into osteoblats were confirmed by Alizarin Red staining on day 14 of osteogenic induction. The present *in vitro* study concluded that there was a good interaction between canine MSCs and PCL/HA scaffold.

Despite a promising result from an *in vitro* study, neither bone nor callus formation was observed in canine ulnar defects that implanted with PCL/HA and PCL/HA scaffolds. Defects in these two groups were healed with fibrovascular tissue which infiltrated through the pore of the scaffold. Surprisingly, numerous of multinucleated giant cells were found indicating chronic inflammation with foreign body giant cell response due to the presence of remnants of PCL/HA scaffold.

663 **References**

664 Amato, H., Ciapetti, G., Pagani, S., Marletta, G., Satriano, C., Baldini, N. and Granchi, D.
665 2007. Expression of cell adhesion receptors in human osteoblasts cultured on
666 biofunctionalized poly-(ε-caprolactone) surfaces. Biomaterials 28: 3668-3678.

667 Azevedo, M. C., Reis, R. L., Claase, M. B., Grijpma, D. W. and Feijen. J. 2003.
668 Development and properties of polycaprolactone/hydroxyapatite composite
669 biomaterials. J. Mater. Sci. Mater. Med. 14(2): 103-107.

670 Ashton, B. A., Allen, T. D., Howlett, C. R., Eaglesom, C. C., Hattori, A. and Owen, M.
671 1980. Formation of bone and cartilage by marrow stromal cells in diffusion chambers
672 *in vivo*. Clin. Orthop. 151: 294-307.

673 Bergsma, E. J., Rozema, F. R., Bos, R. M. and Brujn, W. 1993. Foreign body reactions to
674 resorbable poly(L-lactide) bone plate and screws used for the fixation of unstable
675 zygomztic fractures. J. Maxillofac. Surg. 51: 666-670.

676 Bosch, P., Pratt, S.L. and Stice, S.L. 2006. Isolation, characterization, gene modification, and
677 nuclear reprogramming of porcine mesenchymal stem cells. Biol Reprod.74: 46-57.

678 Böstmann, O., Hirvensalo, E., Mäkinen, J. and Rokkanen, P. 1990. Foreign body reactions
679 to fracture fixation implants of biodegradable synthetic polymers. J. Bone Jt. Surg.
680 B72:592.

681 Breuls, R. G. M., Jiya, T. U. and Smit, T. H. 2008. Scaffold stiffness influences cell
682 behavior: opportunities for skeletal tissue engineering. Open Orthop. J. 2: 103-109.

683 Bunnel, B. A., Flaat, M., Gagliardu, C., Patel, B. and Ripoll, C. 2007. Adipose-derived stem
684 cells: Isolation, expansion and differentiation. Bull. Exp. Biol. Med. 140(1): 138-143.

685 Calandrelli, L., Immirzi, B., Malinconico, M. and Luessenheide, S. 2004. Natural and
686 synthetic hydroxyapatite filled PCL: mechanical properties and biocompatibility
687 analysis. J. Bioact. Compat. Polym. 19: 301-313.

688 Ciapetti, G., Ambrosio, L., Savarino, L., Granchi, D., Cenni, E., Baldini, N., Pagani, S.,
689 Guizzardi, S., Causa, F. and Guinti, A. 2003. Osteoblast growth and function in
690 porous poly ε-caprolactone matrices for bone repair: a preliminary study. Biomaterial.
691 24: 3815-3824.

692 Chen, B. and Sun, K. 2005. Mechanical and dynamic viscoelastic properties of
693 hydroxyapatite reinforced poly(ε-caprolactone). Polym. Test. 24: 978-982.

694 Chuenjitkuntaworn, B., Inrung, W., Mekaapiruk, K., Damrongsri, D., Supaphol, P. and
695 Pavasant, P. 2010. Polycaprolactone/hydroxyapatite composite scaffolds:
696 preparation, characterization and in vitro and in vivo biological responses of
697 human primary bone cells. J. Biomed. Mat. Res. A 94(1): 241-251.

698 Cook, S. D., Baffes, G .C, Wolfe, M. W., Sampath, T. K. and Rueger, D. C. 1994.
699 Recombinant human bone morphogenetic protein-7 induces healing in a canine long-
700 bone segmental defect model. Clin. Orthop. Related Res. 301: 302-312.

701 Cornell, C. N. 1999. Osteoconductive materials and their role as substitutes for autogenous
702 bone grafts. Orthop. Clin. North Am. 30: 592-600.

703 Decherchi, P, Cochard, P. and Gauthier, P. 1997. Dual staining assessment of
704 Schwann cell viability within whole peripheral nerves using calcein-AM and
705 ethidium homodimer. J. Neurosci. Meth. 71: 205–213.

Dickson, G., Buchsnan, F., Marsh, D., Harkin-Jones, E., Little, U. and McCaigue, M.
2007. Orthopedic tissue engineering and bone regeneration. Technology and Health
Care 15: 57-67.

Dominici, M., Le Blanc, K., Mueller, I., Slaper-Cortenbach, I., Marini, F. C. Krause, D. S.,
Deans, R. J., Keating, A., Prockop D. J. and Horwitz, E. M. (2006) Minimal criteria
for defining multipotent mesenchymal stromal cells. The International Society for

Cellular Therapy position statement. Cytotherapy 8(4): 315-317.

Drosse, I., Volkmer, E., Capanna, R., Biase, P. D., Mutschler, W. and Schieker, M. 2008. Tissue engineering for bone defect healing: An update on a multi-component approach. Injury, Int. J. care Injured 39S2: S9-S20.

Dupont, K. M., Sharma, K., Stevens, H. Y., Boerckel, J D., Garcia, A. J. and Guldberg, R. E. 2010. Human stem cell delivery for treatment of large segmental bone defects. Proceedings of the National Academy of Sciences 107(8): 3305-3310.

Fabbri, P., Bondioli, F., Messori, M., Baetoli, C., Dinucci, D. and Chillini, F. 2010. Porous scaffolds of polycaprolactone reinforced with *in situ* generated hydroxyapatite for bone tissue engineering. J. Mater. Sci. Mater. Med. 21(1): 343-351.

Jaafar I. H., LeBlon, C. E., Wei, M., Ou-Yang, D. and Coulter, L. P. 2011. Improving fluorescence imaging of biological cells on biochemical polymers. Acta Biomat. 7: 1588-1598.

Giancotti, F. G. 1999. Integrin signaling. Science 285: 1028-1032.

Griffon, D. J. 2005. Fracture healing. In A. L. Johnson, J. E. F. Houlton and R. Vannini (eds.), AO Principles of fracture management in the dog and cat, pp.73-98. Davos Platz, Switzerland. AO publishing.

Guarino, V., Causa, F., Taddei, P., di Foggia, M., Ciapetti, G., Martini, D., Fagnano, C., Baldini, N. and Ambrosio, L. 2008. Polylactic acid fibre-reinforced polycaprolactone scaffolds for bone tissue engineering. Biomater. 29(27):
3662-3670.

Gunatillake, P. A. and Adhikari, R. 2003. Biodegradable synthetic polymers for tissue engineering. Eur. Cells Mater. 5:1-16.

Heiple, K. G., Chase, S. W. and Herdon, C. H. 1963. A comparative study of the healing

process following different types of bone transplantation. J. Bone Joint Surg. Am. 45:1593-1616.

Heng, B. C., Bezerra, P. P., Meng, Q. R., Chin, D. W., Koh, L. B., Zhang, H., Preiser, P. R., Boey, F. Y. and Venkatraman, S. S. 2010. Adhesion, proliferation, and gene expression profile of human umbilical vein endothelial cells cultured on bilayered polyelectrolyte coatings composed of glycosaminoglycans. Biointer. Phases 5(3): 53-62.

Heo, S. J., Kim, S. E., Hyun, Y. T., Kim, D. H., Lee, H. M., Shin, J. W., Hwang, Y. M. and Shin, J. W. 2007. Biodegradable composite of poly ε-caprolactone/ hydroxyapatite 3-D scaffolds for bone tissue engineering. In F. Ibrahim, N. A. Abu Osman, J. Usman and N. A. Kadri (eds.), Proceedings of the International Federation for Medical and Biological Engineering, pp. 672-675. Berlin: Springer.

Hulbert, S. F., Young, F. A. and Mathews, R. S. 1970. Potential of ceramic materials as permanently implantable skeletal prostheses. J. Biomed. Mater. Res. 4(3): 433-456.

Hutmacher, D. W. 2000. Scaffolds in tissue engineering bone and cartilage. Biomaterials. 21: 2529-2543.

Hutmacher, D. W., Schantz, J. T., Lam, C. X. F., Tan, K. C. and Lim, T. C. 2007. State of the art and future directions of scaffold-based bone engineering from a biomaterials perspective. J. Tissue Eng. Regen. Med. 1: 245-260.

Jones, C. B., Sabatino, C. T., Badura, J. M., Sietsema, D. L. and Marotta, J. S. 2008. Improved healing efficacy in canine ulnar segmental defects with increasing recombinant human bone morphogenetic protein-2/allograft ratios. J. Orthop. Trauma. 22(8): 550-559.

Karageorgiou, V. and Kaplan, D. 2005. Porosity of 3D biomaterial scaffolds and

osteogensis. Biomaterials 26: 5474-5491.

Keating, J. F. and McQueen, M. M. 2001. Substitutes for autogenous bone graft in orthopaedic trauma. J. Bone Joint Surg. Br. 82-B: 3-8.

Kern, S., Eichler, H., Stoeve, J., Klüter, H. and Bieback, K. 2006. Comparative analysis of mesenchymal stem cells from bone marrow, umbilical cord blood, or adipose tissue. Stem cells 24: 1294-1301.

Key, J. A. 1934. The effect of a local calcium depot on osteogenesis and healing of fractures. J. Bone Joint Surg. Am. 16: 176-184.

Khan, Y., Yaszemski, M. J., Miko, A. G. and Laurencin, C. T. 2008. Tissue engineering of bone: Material and matrix consideration. J. Bone Joint Surg. Am. 90: 36-42.

Kraus, K. H. and Kirker-head, C. 2006. Mesenchymal stem cell and bone regeneration. Vet . Surg. 35: 232-242.

Kuboki, Y., Takita, H., Kobayashi, D., Tsuruga, E., Inoue, M., Murata, M., Nagai, M., Dohi, N. and Ogushi, H. 1998. BMP-induced osteogensis on the surface of hydroxyapatite with geometrically feasible and nonfeasible structures: topology of osteogensis. J. Biomed. Mater. Res. 39(2): 190-199.

Langer, R. and Vacanti, J. P. 1993. Tissue engineering. Science. 260: 920-926.

Lui, X. and Ma, X. 2004. Polymeric scaffolds for bone tissue engineering. Ann. Biomed. Eng. 32(3): 477-486.

Martin, D. R., Cox, N. R., Hathcock, T. L., Neimeyer, G. P. and Baker, H. J. 2002. Isolation and characterization of multipotential mesenchymal stem cells from feline bone marrow. Exp. Hematol. 30(8): 879-886.

Martinez, S. A. and Walker, T. 1999. Bone graft. Vet. Clin. North Ame. Small Ani. Pract. 29(5): 1207-1213.

Meyer, U. and Wiesmann, H. P. 2006. Bone and Cartilage Engineering. Berlin: Springer.

Miao, Z., Jin, J., Chen, L., Zhu, J., Huang, W., Zhao, J., Qian, H. and Zhang, X. 2006. Isolation of mesenchymal stem cells from human placenta: Comparison with human bone marrow mesenchymal stem cells. Cell Biol. Int. 30: 681-687.

Mistry, A. S. and Mikos, A. G. 2005. Tissue engineering strategies for bone regeneration. Adv. Biochem. Engin./Biotechnol. 94: 1-22.

706 Moore, W. R., Graves, S. E. and Bain, G. I. 2001. Synthetic bone graft substitutes. ANZ. J.
707 Surg. 71: 354-361.

708 Mygind, T., Stiehler, M., Baatrup, A., Li, H., Zou, X., Flyvbjerg, A., Kassem, M. and
709 Bünger, C. 2007. Mesenchymal stem cell ingrowth and differentiation on coralline
710 hydroxyapatite scaffolds. Biomaterials 28: 1036-1047.

711 Nilsson, O. S., Urist, M. R., Dawson, E. G., Schmalzried, T. P. and Finerman, G. A. M. 1986.
712 Bone repair induced by bone morphogenetic protein in ulnar defects in dogs. J. Bone
713 Joint Surg. Br. 68(4): 635-642.

714 Necas, A., Planka, L., Srnec, R., Rauser, P., Urbanova, L., Lorenzova, J., Crha, M. Jancar, J.
715 and Gal, P. 2008. Biomaterials and stem cells in the treatment of articular cartilage,
716 meniscal, physeal, bone ligament and tendinous defects. Acta. Vet. Brno. 77: 277-
717 284.

718 Nerurkar, N. L., Sen, S., Baker, B. M., Elliott, D. M. and Mauck, R. L. 2011. Dynamic
719 culture enhances stem cell infiltration and modulates extracellular matrix production
720 on aligned electrospun nanofibrous scaffolds. Acta Biomater. 7: 485-491.

721 Neuendorf, R. E., Saiz, E., Tomsia, A. P.and Ritchie, R. O. 2008. Adhesion between
722 biodegradable polemers and hydroxyapatite: relevance to synthetic bone-like
723 materials and tissue engineering scaffolds. Acta Biomater. 4(5): 1288-1296.

724 Oh, S., Oh, N., Appleford, M. and Ong, J. L. 2006. Bioceramics for tissue engineering
725 applications – a review. Am. J. Biochem. Biotechnol. 2(2): 49-56.

726 Oh, S. H., Park, I. K., Kim, J. m. and Lee, J. H. 2007. In vitro and in vivo characteristics of
727 PCL scaffolds with pore size gradient fabricated by a centrifugation method.
728 Biomaterials. 28: 1664-1671.
729 Park, S. A., Lee, S. H. and Kim, W. D. 2010. Fabrication of porous
730 polycaprolactone/hydroxyapatite (PCL/HA) blend scaffolds using a 3D plotting
731 system for bone tissue engineering. Bioprocess. Biosyst. Eng. DOI: 10.1007/s00449-
732 010-0499-2.
733 Paskalev, M., Krastev, S., Mechkarski, S. V., Philipov, J. and Dyakova, S. V. 2006.
734 Experimental study on guided bone regeneration in canine segmental ulnar defects.
735 Bulg. J. Vet. Med. 9(4): 281-291.
736 Pittenger, M. F., Mackay, A. M., Beck, S. C., Jaiswal, R. K., Douglas, R., Mosca, J. D.,
737 Moorman, M. A., Simonetti, W., Crgig, S. and Marshak, D. R. 1999. Multilineage
738 potential of adult human mesenchymal stem cells. Science. 284:143-144.
739 Porter, J. R., Ruckh, T. T. and Popat, K. C. 2009. Bone tissue engineering: a review in bone
740 biomimetics and drug delivery strategies. Biotechnol. Prog. 25(6): 1539-1560.
741 Prokop, A., Jubel, A., Helling, H. J., Eibach, T., Peters, C., Baldus, S. E. and Rehm, K. E.
742 2004. Soft tissue reactions of different biodegradable polylactide implants.
743 Biomaterials 25: 259-267.
744 Rai, B., Ho, K. H., Lei, Y., Teo, C. J., Yacob, K. B., Chen, F. Ng, F. ans Teoh, S. H. 2007.
745 Polycaprolactone-20% tricalcium phosphate scaffolds in combination with platelet-
746 rich plasma for the treatment of critical-sized defects of the mandible: a pilot study. J.
747 Oral Maxillofac. Surg. 65: 2195-2205.
748 Remedios, A. 1999. Bone and bone healing. 1999. Vet. Clin. North Am. Small Anim.
749 Pract. 29(5): 1029-1044.

750 Rezwan, K., Chen, Q. Z., Blaker, J. J. and Boccaccini, A. B. 2006. Biodegradable and
751 bioactive porous polymer/inorganic composite scaffolds for bone tissue
752 engineering. Biomaterials 27: 3413-3431.
753 Roberts, S. J., Howard, D., Buttery, L. D. and Shakesheff, K. M. 2008. Clinical
754 applications of musculoskeletal tissue engineering. British Medical Bulletin.
755 86: 7-22.
756 Rohner, D., Hutmacher, D., See, P., Cheng, T. K., Yeow, V., Yong, T. S., Teik, L. S. and
757 Hammer, B. 2002. Reconstruction of craniofacial defects with bone-marrow-
758 coated polycaprolactone scaffolds: an animal study in the Yorkshire pig.
759 Proceedings of the 12th Singapore General Hospital Annual Scientific Meeting.
760 11(1): 32-39.
761 Rohner, D., Hutmacher, D., Cheng, T. K., Oberholzer, M. and Hammer, B. 2003. *In vivo*
762 efficacy of bone-marrow-coated polycaprolactone scaffolds for the reconstruction of
763 orbital defects in the pig. J. Biomed. Mater. Res. Part B: Appl. Biomater. 66B: 574-
764 580.
765 Sachana, M. and Hargreaves, A. J. 2007. Toxicological testing: *in vivo* and *in vitro*
766 Model. In: R. C. Gupta (ed.), Veterinary toxicology: basic and clinical principles. pp.
767 51-66. California. Elsevier.
768 Sachlos, E. and Czernuszka, J. T. 2003. Making tissue engineering scaffold work.
769 Review on the application of solid freeform fabrication technology to the ptoduction
770 of tissue engineering scaffolds. Eur. Cell and Mater. 5: 29-40.
771 Sakaguchi, Y., Sekiya, I., Yagishita, K., and Muneta, T. 2005. Comparison of human
772 stem cells derived from various mesenchymal tissues. Arthritis Rheum. 52(8): 2521-
773 2529.
774 Salgado, A. J., Gomes, M. E. and Reis, R. L. 2004. Tissue engineering of mineralized

775 tissue: the essential element. In: Learning from nature how to design new
776 implantable biomaterial. Dordrecht: Kluwer academic publishers. 205-222.
777 Salkeld, S. L., Patron, L. P., Barrack, R. L. and Cook S. D. 2001. The Effect of osteogenic
778 Protein-1 on the healing of segmental bone defects treated with autograft or allograft
779 bone. J. Bone Joint Surg. Am. 83-A (6): 803 – 816.
780 Samuelson, D. A. 2007. Cartilage and bone. In: T. Merchant (ed.), Textbook of
781 veterinary histology, pp. 100-129. Missouri: Sauders.
782 Savarino, L., Baldini, N., Greco, M., Capitani, O., Pinna, S., Valentini, S., Lombrado, B.,
783 Esposito, M. T., Pastore, L., Ambrosio, L., Battista, S., Causa, F., Zeppetelli, S.,
784 Guarino, V. and Netti, P. A. 2007. The performance of poly-ε-caprolcatone scaffolds
785 in a rabbit femur model with and without autologous stromal cells and BMP-4.
786 Biomaterials 28: 3101-3109.
787 Schuckert, K. H., Joop, S. and Teoh, S. W. 2009. Mandibular defect reconstruction
788 using three-dimensional polycaprolactone scaffold in combination with platelet-rich
789 plasma and recombinant human bone morphogenetic protein-2: *De novo* synthesis of
790 bone in a single case. Tissue Eng. Part A 15(3): 493-499.
791 Sfeir, C., Ho, L., Doll, B. A., Azari, K. and Hollinger, J. O. 2005. Fracture Healing. In: J.
792 R. Lieberman and G. E. Friedlaender (eds.), Bone Regeneration and Repair, pp. 21-
793 44. New Jersey: Humana.
794 Sharma, P., Cartmell, S. and El Haj A. J. 2005. Applications of Cell Immobilization
795 Biotechnology. Dordrecht: Springer. 153-166.
796 Shor, L., Güceri, S., Wen, X., Gandhi, M. and Sun, W. 2007. Fabrication of three-
797 dimensional polycaprolactone/hydroxyapatite tissue scaffolds and osteoblast-scaffold
798 interactions in vitro. Biomaterials 28: 5291-5297.

799 Silvio, L. D., Dalby, M. J. and Bonfield, W. 2002. Osteoblast behavior on HA/PE composite
800 surfaces with different HA volume. Biomaterials 23: 101-107.
801 Skarda, R. T. and Tranquilli, W. J. 2007. Local and regional anesthetic and analgesic
802 techniques: dogs. In: W. J. Tranquilli, J. C. Thurmon and K. A. Grimm. (eds.), Lump
803 and Jones' veterinary anesthesia and analgesia, 4th ed. pp. 561-594. Iowa: Blackwell.
804 Tabata. Y. 2009. Biomaterial technology for tissue engineering applications. J. R. Soc.:
805 Interface. 6: S311-324.
806 Tondreau, T., Lagneaux, L., Dejeneffe, M., Delforge, A., Massy, M., Mortier, C. and Bron,
807 D. 2004. Isolation of BM mesenchymal stem cells by plastic adhesion or negative
808 selection: phenotype, proliferation kinetics and differentiation potential.
809 Cytotherapy 6(4): 372- 379.
810 Toma, J, G., Akhavan, M., Femandes, K. J. L., Barnabé-Heider, F., Scdikot, A., Kaplan, D.
811 R. and Miller, F. D. 2001. Isolation of multipotent adult stem cells from the dermis of
812 mammalian skin. Nature cell biol. 3: 778-784.
813 Tuan, R. S., Boland, G. and Tuli, R. 2002. Adult mesenchymal stem cells and cell-based
814 tissue engineering. Arthr. Res. Ther. 5(1): 32-45.
815 Van den Bogert, C., Van Kernebeek, G., Leij, L. D. and Kroom,. 1986. Inhibition of
816 mitochondrial protein synthesis leads to proliferation arrest in the G_1-phase of the cell
817 cycle. Cancer Lett. 32(1): 41-5.
818 Wang, M. 2006. Composite scaffolds for bone tissue engineering. Am. J. Biochem.
819 Biotechnol. 2(2): 80-84.
820 Williams, J. M., Adewunmi, A., Schek, R. M., Flanagan, C. L., Krebsbach, P. H., Feinberg,
821 S. E., Hollister, S. J. and Das, S. 2005. Bone tissue engineering using
822 polycaprolactone scaffolds fabricated via selective laser sintering. Biomaterials 26:
823 4817-4827.

824 Wexler, S. A., Donaldson, C., Denning-Kendall P., Rice, C., Bradley, B. and Hows, J. M.
825 2003. Adult bone marrow is a rich source of human mesenchymal “stem” cells but
826 umbilical cord and mobilized adult blood are not. Br. J, Haemato. 121: 368-374.
827 Wutticharoenmongkol, P., Sanchavanakit, N., Pavasant, P. and Supaphol, Pitt. 2006.
828 Novel bone scaffolds of electrospun polycaprolactone fibers filled with nanoparticles.
829 J. nanosci. Nanotechnol. 6: 514-522.
830 Wutticharoenmongkol, P., Pavasant, P. and Supaphol, P. 2007. Osteoblast phenotype
831 expression of MC3T3-E1 cultured on electrospun polycaprolactone fiber mats
832 filled with hydroxyapatite nanoparticles. Biomacromolecules. 8: 2602-2610.
833 Yang, C., Huang, L., Shen, T. and Yeh, J. A. 2010. Cell adhesion, morphology and
834 biochemistry on nanotopographic oxidized silicon surface. Eur. Cell Mater. 20: 415-
835 430.
836 Yeatts, A. B. and Fisher, J. P. 2011. Bone tissue engineering bioreactors: dynamic
837 culture and the influence of shear stress. Bone. 48(2): 171-181.
838 Yu, H., Wooley, P. H. and Yang, S. 2009. Biocompatibility of polycaprolactone-
839 hydroxyapatite composite on mouse bone marrow-derived osteoblasts and endothelail
840 cells. J. Orthop. Res. 4: 5-13.
841

Differentiation potentials of canine bone marrow mesenchymal stem cells

Author's name: Theerawat Tharasanit[1]*,
Nawapen Phutikanit[1],
Chalika Wangdee[2],
Kumpanart Soontornvipart[2],
Sasijaras Tantrajak[2],
Theerayuth Kaewamatawong[3],
Junpen Suwimonteerabutr[1],
Pitt Supaphol[4]
Mongkol Techakumphu[1]

Address: [1]Department of Obstetrics, Gynaecology and Reproduction, [2] Department of Surgery, [3]Department of Pathology, Faculty of Veterinary Science, Chulalongkorn University, Bangkok 10330, Thailand
[4]The Petroleum and Petrochemical College, Chulalongkorn University, Bangkok 10330, Thailand

Correspondence: Theerawat Tharasanit
Department of Obstetrics, Gynaecology and Reproduction Faculty of Veterinary Science, Chulalongkorn University, Bangkok 10330, Thailand

Tel: +662 2189644
Fax: +66 2520738
Email address: Theerawat.t@chula.ac.th

Abstract

Mesenchymal stem cells (MSCs) are multipotent cells that have characteristics of self-renewal and differentiation into various specific cell types, in particular mesodermal lineages. This study aimed at isolating, identifying and examining the differential capability of canine MSCs. Bone marrow aspirates were obtained from 4 dogs. Putative MSCs were then cultured in MSC medium and subpassaged. At the 3rd to 5th passages, MSCs were examined for their morphology and doubling time. Two cell lines were examined for the expression of CD 34, CD 44 and CD 90, using flow cytometry. The *in vitro* differentiation of these MSCs into mesodermal lineages (bone, cartilage and adipose tissues) and ectodermal lineage (neuron) was performed using osteogenic, chondrogenic, adopogenic and neurogenic media, respectively. Histological examinations (Von Kossa and Alcial blue staining) and mRNA expressions (GLA and COL1A1) were used to examine the bone and cartilage differentiation, while Oil red O staining was used to determine adipogenic differentiation.

Plastic-adhered MSCs had high potential for cell division, with a mean doubling time of 35.4 ± 9.3 h. These fibroblast-like MSCs expressed MSCs markers (CD 44 and CD 90), while fewer than 5% of these MSCs were tested positive to a hemopoietic stem cell marker (CD34). Based on the histological examinations and gene expressions, these cells demonstrated the ability to differentiate into bone, cartilage and adipose tissues. In conclusion, MSCs can be isolated from canine bone marrow and these cells are capable of *in vitro* differentiation into specific mesodermal lineages.

Keywords: Bone marrow; canine; mesenchymal stem cells

บทคัดย่อ

ประสิทธิภาพการเจริญเปลี่ยนแปลงของเซลล์ต้นกำเนิดมีเซนไคม์จากสุนัข

ธีรวัฒน์ ธาราศานิต[1] นวเพ็ญ ภูติกนิษฐ์[1] ชาลิกา หวังดี[2] กัมปนาท สุนทรวิภาต[2] ศศิจรัส ตันตระจักร์[2]*

ธีระยุทธ แก้วอมตะวงค์[3] จันเพ็ญ สุวิมลธีระบุตร[1] พิชญ์ ศุภผล มงคล เตชะกำพุ[1]

เซลล์ต้นกำเนิดมีเซนไคม์ (MSCs) เป็นเซลล์ที่มีความสามารถในการเจริญเพิ่มจำนวนได้เองและสามารถพัฒนาเป็นเซลล์จำเพาะหลายชนิดโดยเฉพาะเซลล์ในกลุ่มเนื้อเยื่อชั้นกลาง การศึกษาครั้งนี้มีวัตถุประสงค์เพื่อศึกษาวิธีการเก็บ การพิสูจน์ และการตรวจสอบคุณสมบัติการเจริญเปลี่ยนแปลงของเซลล์ต้นกำเนิดมีเซนไคม์ของสุนัข ภายหลังการเก็บของเหลวจากไขกระดูกสุนัข ทำการเลี้ยงเซลล์เพื่อเพิ่มจำนวนและทำการตรวจลักษณะรูปร่างและอัตราเร็วของการเพิ่มจำนวนเซลล์เป็นสองเท่า จากนั้นทำการตรวจการแสดงออกของโปรตีนบนผิวเซลล์ชนิด CD 34 CD 44 CD 90 ด้วยเทคนิคโฟลวไซโตเมตรี และตรวจคุณสมบัติของเซลล์ในการเจริญเปลี่ยนแปลงเป็นเซลล์ในกลุ่มเนื้อเยื่อชั้นกลาง (กระดูก กระดูกอ่อน และ ไขมัน) และเนื้อเยื่อชั้นนอก (เซลล์ประสาท) ใช้เทคนิคทางจุลวิทยาร่วมกับการย้อมสี Von Kossa และ Alcial blue รวมถึงการ

แสดงออกของ mRNA ต่อยีน GLA และ COL1A1 ในการตรวจวินิจฉัยกระดูกและกระดูกอ่อน ตามลำดับ และใช้ Oil Red O ในการตรวจเนื้อเยื่อไขมัน

เซลล์ MSCs ที่เกาะบนจานเพาะเลี้ยงพลาสติกมีคุณสมบัติในการแบ่งตัวโดยมีค่าเฉลี่ยของระยะเวลาการเพิ่มจำนวนเป็นสองเท่า เท่ากับ 35.4± 9.3 ชั่วโมง เซลล์ MSCs มีลักษณะคล้ายเซลล์ไฟโบรบลาส ให้ผลบวกต่อการแสดงออกของโปรตีนจำเพาะต่อเซลล์ MSC (CD 44 และ CD 90) ในขณะที่เซลล์จำนวนน้อยกว่าร้อยละ 5 ให้ผลบวกต่อเซลล์ต้นกำเนิดเลือด (CD 34) จากการตรวจคุณสมบัติของเซลล์ด้วยเทคนิคทางจุลวิทยาและการแสดงออกของยีน พบว่าเซลล์เหล่านี้สามารถเจริญพัฒนาเป็นเซลล์กระดูก กระดูกอ่อน และ เซลล์ไขมันได้ การศึกษาครั้งนี้สรุปว่าเซลล์ MSCs ที่เจาะเก็บจากไขกระดูกสุนัขมีความสามารถในการเจริญพัฒนาในจานเพาะเลี้ยงให้เป็นเซลล์ในกลุ่มเนื่อเยื่อชั้นกลางได้

คำสำคัญ: ไขกระดูก สุนัข เซลล์ต้นกำเนิดมีเซนไคม์

[1]ภาควิชาสูติศาสตร์ เธนุเวชวิทยาและวิทยาการสืบพันธุ์ [2]ภาควิชาศัลยศาสตร์ [3]ภาควิชาพยาธิวิทยา คณะสัตวแพทยศาสตร์ จุฬาลงกรณ์มหาวิทยาลัย กรุงเทพฯ 10330

*** ผู้รับผิดชอบบทความ** Email: theerawat.t@chula.ac.th

Introduction

Stem cells have been intensively studied over the past two decades because these cells have the remarkable potential to develop into various specific cell lineages upon being cultured in appropriated conditions. Because of this, they have been considered as a powerful tool for cell- or tissue-based engineering in human and veterinary medicine (Bongso et al., 2008; Barry et al., 2004; Ribitsch et al., 2010). Stem cells are different from other cell types by two important characteristics (Wobus and Boheler, 2005), as they have the capability of self-renewal, while maintaining themselves in an undifferentiated stage. In specific condition, these quiescent stem cells, however, differentiate into specific cell types or tissues with special functions such as cardiomyocyte (Jing et al., 2008; Mayorga et al., 2009), bone (Barry and Murphy, 2004), cartilage (Kavalkovich et al., 2002) and neuron (Trzaska et al., 2007; Kim et al., 2009).

Stem cells are usually classified into three types (viz. embryonic, induced-pluripotent and adult stem cells), according to their origins and production techniques. Embryonic stem (ES) cells are pluripotent-specialized cells that are isolated form an inner cell mass of blastocyst-stage embryos (Evans and Kaufman, 1981; Martin, 1981). Induced-pluripotent stem cells (iPS) are also pluripotent stem cells that can be derived from genetic modification of non-pluripotent somatic cells (Takahashi and Yamanaka, 2006). Although these two types of ES cells are capable of unlimited cell division and differentiation into all three germ layers (endoderm, ectoderm and mesoderm), their clinical exploitation has been obscured by the possibility of tumorogenesis after transplantation *in vivo* (Erdo et al., 2003; Reubinoff et al., 2000; Arnhold et al., 2000). In contrast to the ES cells, adult stem cells have less ability of self-renewal, and their differentiation usually occurs within a cell lineage from which

they originated. For example, mesenchymal stem cells (MSCs) can only differentiate into mesodermal lineages, such as bone, cartilage and adipose tissues (Zuk et al., 2002). Interestingly, although these cells have been described as multipotent stem cells as differential potentials are essentially restricted to only mesodermal lineages, a recent report showed that they also have a potential to differentiate into other cell lineages, such as endoderm and ecdoderm origins (a process referred to as transdifferentiation) (Alaminos et al., 2010).

To date, host-specific MSCs are highly desired in regenerative medicine because they can be logically isolated and propagated from many tissue origins, such as bone marrow and adipose tissue. Canine MSCs have been demonstrated to have the potential for use in cell-based therapy, particularly for bone and soft tissue regeneration (Jung et al., 2009; Zucconi et al., 2010; Jang et al., 2008; Hiyama et al., 2008; Kraus and Kirker-Headm, 2006). It is commonly accepted that the identification of MSCs relies on the expressions of positive (Stro-1, CD 90, CD 105, CD 44, CD 73) and negative markers (i.e., markers for hemopoietic cells: CD 34 and 45). In dogs, only the attachment property of MSCs to plastic culture dishes is commonly-accepted method for the selection of canine MSCs, while the use of MSC markers for identification varies from one laboratory to the next.

The present study is aimed at evaluating the isolation and the identification techniques for canine mesenchymal stem cells (MSCs) that are derived from bone marrow aspirates and studying their differentiation potentials.

Materials and Methods

All chemicals were purchased from Sigma-Aldrich, St Louis, USA, unless otherwise specified.

Isolation of mesenchymal stem cells from bone marrow aspirates

Bone marrow aspirates were obtained from 4 healthy dogs. The procedure for obtaining these aspirates was reviewed and approved by the Ethical Committee for Animal Use, Faculty of Veterinary Science, Chulalongkorn University (accession no. 0931055). In brief, the animals were premedicated intramuscularly with 0.1 mg/ml Acepromacine maleate (Vetranquil™; Ceva Sante animal, Libourne, France) and 0.25 mg/kg morphine sulphate (Food and Drug Administration, Bangkok, Thailand). After 15-20 mins, anesthesia was induced intravenously with 4 mg/kg propofol (Fresenius Kabi Austria GmbH, Graz, Austria). The bone marrow contents were collected from either the humorous or iliac crest into a 10-ml heparinized syringe (containing 1000 IU heparin). The bone marrow aspirates were then transported to the laboratory (at 26 °C) and processed within 4 h after bone marrow aspiration. Upon arrival, bone marrow aspirates were first layered onto gradient density (Histopaque®-1077 density 1.077 g/ml) and centrifuged at 26 °C and 400*g* for 30 min. The mononuclear cells at the interface between each of the bone marrow aspirates and Histopaque® were used. Occasionally, the remaining red blood cells were mixed and incubated with an equal volume of red blood cell lysis buffer for 5 mins. The mixture was then centrifuged and resuspended with 1 ml of culture medium.

Culture of canine bone marrow mesenchymal stem cells

Following MSC isolation, presumptive MSCs were seeded into a 100 mm-Petri dishes (BD-Falcon™, Franklin Lake, NJ, USA), containing low glucose

158 Dulbecco's modified Eagle's medium (DMEM) supplemented with 10% (v/v) fetal
159 bovine serum (Invitrogen, Carlsbad, USA), 2 mM L-glutamine, 100 IU/ml penicillin
160 and 100 µg/ml streptomycin. Non-adherent cells were removed by washing the
161 culture dishes with Dulbecco's phosphate buffered saline (DPBS; Invitrogen) and the
162 culture medium was changed every 2-3 d. Adherent cells were cultured (passage 0)
163 until they reached approximately 70-80% confluence. To sub-passage, the adherent
164 cells were washed twice with DPBS and then digested with 0.125 % trypsin-EDTA
165 (Gibco^{TM}, Invitrogen) for 2 mins and the enzyme was inactivated with an excessive
166 amount of fetal bovine serum in DMEM. The cell suspension was then centrifuged at
167 4 °C and 1000 rpm for 5 mins. If cryo-preservation of cells were needed, a freezing
168 medium containing 10% (v/v) dimethylsulphoxide (DMSO, Sigma-Aldrich) and 90%
169 (v/v) fetal bovine serum was added to the cells. The equilibrated cell suspension was
170 added into a 1-ml cryovial (Corning, USA). The freezing rate was controlled at 1
171 °C/min using a cryobox.
172
173 *Cell morphology and population doubling time*
174 MSCs were daily examined for cell morphology at 100 and 200x
175 magnification using a phase contrast microscope (CKX41, Shinjuku, Olympus). At
176 the 3rd passage, the MSCs were plated into a 12-well plate at 20,000 cells/cm^2
177 (approximately, 40-50% confluence). The MSCs were then trypsinized with trypsin-
178 EDTA, and the total number of cells in each culture well was counted using a
179 hemocytometer at 24 h interval for 3 consecutive days. The doubling time was
180 calculated using the equation, ln(2)/growth rate, whereas the growth rate refers to the
181 number of doublings that occurred per unit of time.
182

Flow cytometry analysis

Canine MSCs at the 3rd passage were immunologically examined for the surface markers of MSCs. Because there is no universal marker that is specific to MSCs, identification of MSCs therefore relied on both positive and negative markers. To perform flow cytometry, the MSCs were first dissociated from the Petri dishes with Trypsin-EDTA and then centrifuged. A total of 200,000 to 300,000 cells were stained with each respective antibody. Rat monoclonal anti-canine CD 34 conjugated with Fluorescein isothiocyanate (FITC) (a marker for hemopoietic stem cells) was used as the negative MSC marker. Rat monoclonal anti-canine CD 90 (AbD serotec, Kidlington, UK) with Rabbit anti-rat FITC secondary antibody and monoclonal anti-canine CD44 conjugated with Allophycocyanin (APC) (R&D system, Minneapolis, USA) were used as MSC positive markers. Fluorescently-labeled MSCs were finally washed once, fixed with 1% (w/v) paraformaldehyde in PBS and stored in the dark at 4 °C until analysis. Non-staining MSCs and MSCs labeled with only the secondary antibody were used as controls. At least 20, 000 MSCs were used to test the presence of each cell surface marker, using flow cytometry (BD Biosciences, Franklin Lakes, USA).

Differentiation of MSCs

The MSCs derived from the canine bone marrow at the 3rd-5th passages from 2 dogs were used to demonstrate their differentiation potentials. MSCs were induced to differentiate into bone, cartilage and adipose tissues according to the methods as previously described (Bosch et al., 2006), with some modifications. For bone differentiation, MSCs were first sub-cultured to reach approximately 80% confluence, and the bone induction medium consisting of DMEM supplemented with 10% (v/v)

208 FCS, 100 nM dexamethasone, 50 ng/ml ascorbic acid and 10 mM β-glycerophosphate
209 was added into the Petri dishes. The bone induction medium was changed every 2-3 d.
210 A three-dimensional culture system was used to induce cartilage differentiation.
211 MSCs were dissociated and then transferred to a 15-mL cornical tube (BD Falcon^{TM},
212 Becton Dickinson, Franklin Lake, NJ, USA). After centrifugation, aggregated cells
213 were re-suspended with the cartilage induction medium containing DMEM, 10 ng/ml
214 TGF-β1, 100 nM dexamethasone and 50 ng/ml ascorbic acid 2-phosphate. The
215 medium was changed every 2-3 d. The adipose tissue differentiation was performed
216 with monolayer MSCs, as previously described (Zuk et al., 2002). The MSCs were
217 treated with 4 cycles of adipogenic induction and maintenance (each cycle consists 3
218 d of adipogenic induction and 2 d of adipogenic maintenance). The adipogenic
219 induction medium consisted of DMEM 10% (v/v) FCS, 0.1 mg/ml human
220 recombinant insulin, 10 mM sodium pyruvate, 1 mM methyl isobutylxanthine
221 (IBMX), 0.2 mM indomethacin and 1 μM dexamethasone. Adipogenic maintenance
222 was prepared in a similar manner to adipogenic induction, but without IBMX,
223 dexamethasone and indomethacin. Neurogenic induction was performed with DMEM
224 supplemented with 200 μM butylated hydroxyanisole, 25 mM KCl, 2mM valproic
225 acid, 10 μM forskolin, 1μM hydrocortisone, 5 μg/ml Insulin and 2% (v/v) DMSO.
226
227 *Assessment of MSC differentiation*
228 After the fixation of MSC-derived bone tissues in 4% (w/v)
229 paraformaldehyde, the tissues were embedded in paraffin for histological analysis.
230 The histological sections of the tissues were stained with Von Kossa and Alcian blue
231 to detect the deposition of calcium phosphate and glycosaminoglycans enriched-
232 matrix, indicating the successful differentiation of MSCs into bone and cartilage

tissues, respectively. The presence of adipogenesis was confirmed by Oil Red O staining which detects intracellular neutral triglycerides and lipids. In addition, alkaline phosphatase activity was also examined on day 3 of bone differentiation using leukocyte alkaline phosphatase kit (86R) following manufacturer's instruction.

Reverse transcription polymerase chain reaction (RT-PCR)

Total RNA was extracted from undifferentiated MSCs that were cultured in monolayer and differentiated cell pellets collected on D9 and D21 of differentiation using Absolutely RNA® Nanoprep Kit (Stratagene, Agilent Technologies, USA). The contaminating genomic DNA was removed during the purification steps by DNase I treatment according to the manufacturer's instructions. Total RNA was eluted from the purification column with sterile distilled water and was quantified using a NanoDrop® 1000 spectophotometer (Thermo Scientific, USA). Gene-specific oligonucleotide primers were synthesized by BioDesign Co., Ltd. (Bangkok, Thailand). Two target genes reported to be involved in osteogenic lineage differentiation, i.e., collagen type I alpha I (COL1A1) and bone γ-carboxyglutamate protein (GLA), were selected for this experiment. A housekeeping gene, i.e., glyceraldehype 3-phosphate dehydrogenase (GAPDH), was included as the internal control and reference. Oligonucleotide sequences, PCR product size, Genebank accession number and references of primers are shown in Table 1.

cDNA was synthesized from an aliquot of 150 to 200 ng of total RNA using random hexamer primers and Omniscript® Reverse Transcription Kit (Qiagen, Hilden, Germany). One microliter of RT reaction was mixed with 12.5 μL of GoTaq® Green Master Mix (Promega, WI, USA), 6.25 μM each of forward- and reverse primers, and sterile distilled water to reach the final volume of 25 μL. PCR was carried out on an

Amplitronyx™6 thermocycler machine (Nyxtechnik, CA, USA). The suitable cycle condition was determined and applied for each primer pair as follows: GAPDH, 94°C for 2 mins, followed by 30 cycles of 94 °C for 30 s, 55 °C for 30 s, 72 °C for 45 s, plus the final extension at 72 °C for 5 mins; COL1A1 and GLA, 94 °C for 1 min, followed by 30 cycles of 94 °C for 30 s, 58 °C for 30 s, 72 °C for 1 min, plus the final extension at 72 °C for 10 mins. PCR products were analyzed by electrophoresis on 2% ethidium bromide incorporated-agarose gels in Tris-Boric-EDTA (TBE) buffer. The images of agarose gels were taken using GeneFlash Gel Documentation (Syngene, Synoptic Ltd., Frederick, USA) and the calculation of relative intensity of target gene mRNA expression signal utilizing the expression intensity of GAPDH as the reference was carried out using the Scion Imaging program (Beta 4.0.3; Scion Corporation, MD)

Results

Fibroblastic-like cells were isolated from canine bone marrow (Figure 1). These cells adhered to the culture dish by 24 h of culture. At passage 3, putative MSCs were cultured and analyzed for expression of MSC surface markers and population doubling time. These MSCs were expressed mesenchymal stem cells markers (CD 44 and CD 90) and also negative to hemopoietic stem cells marker (CD 34). Two canine MSCs (dog 3 and dog 4) strongly expressed CD 44 (99.9% and 86.7%) and CD 90 (92.5%, and 95.3%), respectively (Figure 2). However, the growth rates of MSCs (population doubling time) were found to be different among putative MSCs from different dogs (46.1, 24.2, 38.8 and 32.4 h).

We further demonstrated that these cells were also capable of differentiation into mesodermal lineages including bone, cartilage and adipose tissues. Alkaline

phosphatase activity was present as early as day 3 of bone differentiation (Figure 3D). The MSCs treated with bone differentiation medium were aggregated into a small mass (Figure 3C). After 21 days of differentiation, differentiated MSCs were essentially positive to Oil red O, Alcial blue and Von kossa as indicators of fat, cartilage and bone formation respectively (Figure 3 A, B and E). In addition, MSCs were also transdifferentiated into multiple-process neuron-like cells soon after treating MSCs with neurogenic medium (Figure 3F).

COL1A1 and GLA expression was detected in undifferentiated MSCs. The early stage of differentiation up-regulated the genes as seen in the increment of relative signal intensity on D9 post culture. COL1A1 mRNA increased continuously on D21 post differentiation, while the expression of GLA gene dropped below the starting point (Figure 4).

Discussion

In the current study, we successfully isolated well-defined mesenchymal stem cells derived from canine bone marrow. These specialized cells are classified as multipotent stem cells because they have the capability of differentiation into mesodermal lineage. MSCs have been isolated from many tissue of the body such as bone marrow (Wagner et al., 2005; Kern et al., 2006), adipose tissue (Zuk et al., 2002), umbilical cord (Lee et al., 2004; Koch et al., 2007) and dental pulp (Jo et al., 2007; Waddington et al., 2008). In dog, the data in regard to the isolation, characterization and clinical use of canine MSCs has been limited. Until recently, canine MSCs have been isolated from bone marrow (Csaki et al., 2007; Jafarian et al., 2008), adipose tissue (Neupane et al., 2008; Vieira et al., 2010) and umbilical cord (Seo et al., 2009). Because there is no specific marker for the identification of canine

MSCs, the isolation and identification technique has therefore been different among laboratory. MSCs from many species demonstrate antigen specific on cell membrane such as CD 29, CD 44, CD 90, CD 105 and Stro-1 (Csaki et al., 2007, Bosnakovski et al., 2005, Martin et al., 2002; Rho et al., 2009; Meirelles and Nardi, 2009). In the current study, only canine antibodies were proven a good candidate for MSC isolation when compared with antibodies from other animals such as anti-mouse Stro-1 and anti-human CD 105 (unpublished data), suggesting the specificity of canine surface antigen. This phenomenon is one of the hallmarks affecting the exploitation of MSCs for clinical use since MSCs are located in the bone marrow with a mixed population of cells and it has been estimated that there are only 0.0001-0.01% MSCs in the nucleated cells of bone marrow aspirate (Pittenger et al., 1999). Most investigators have been isolated MSC using their capacity to adhere to a plastic culture dish. However, macrophages, endothelial cells, lymphocytes, and smooth muscle cells can also adhere to culture plate and therefore contaminate the MSC preparations. The isolation, identification and purification of canine MSCs recently become an important issue for the clinical use of MSCs. Although legal regulation use of canine MSCs has yet to be discussed, the minimum requirements for clinical use MSCs have been announced for human (Dominici et al., 2006). Human MSCs must demonstrate the fibroblast-like morphology and have ability to adhere to a plastic culture dish, positively express ($\geq$ 95%) cell surface receptors (e.g. CD 29, CD 44, CD 73, CD 105, CD 106, Stro-1, etc.) and negatively express ($\leq$ 2%) the hematopoietic lineage markers (e.g. c-Kit, CD 14, CD 34, CD 45). More importantly, these cells must show a capability of differentiation into mesodermal lineage (bone, cartilage and adipose tissues). In the current study, we found that MSCs, at least under our conditions, were already committed to differentiate into bone and cartilage as they prematurely

expressed GLA and COL1A1 (early markers for bone and cartilage differentiation) prior to differentiation induction. It is also possible that the MSCs used in this study had spontaneous differentiation during culture. Until recently, study of pathways regulating the bone and cartilage differentiation of canine bone marrow MSCs is still required in order to improve the efficiency of in vitro bone and cartilage differentiation for cell- or tissue-based engineering. Volk et al. (2005) reported that canine MSCs can be efficiently differentiated into bone using bone morphologic protein 2 (BMP-2) which is similar to other species (Li et al., 2007). In addition to the differential capability into mesodermal lineage, transdifferentiation of MSCs to neuron-like cells has been believed to hold a great promise in cell treatment therapy (Zipori, 2004; Krabbe et al., 2005; Bongso et al., 2008). However, this transdifferentiation of MSCs into neuron-like cells has been contradictory especially the toxic effect of DMSO on actin microfilament during differentiation (Lu et al., 2004; Neuhuber et al, 2004). Interestingly, it has been shown that MSCs expressed neuronal specific genes, even though they were not treated with neuronal differentiation medium (Yamaguchi et al., 2004; Kamishina et al., 2006). In this study, we only recorded morphological changes of canine MSCs after neuronal differentiation. The 'true' capability of canine MSCs in neuron differentiation has yet to be examined in the prospective study.

In conclusion, our study demonstrates that canine mesenchymal stem cells can be isolated from bone marrow, and these MSCs are capable of differentiation into specific mesodermal linage (bone, cartilage and adipose tissue) following passages and *in vitro* differentiation.

Acknowledgement

This work was financially supported by the Innovation Center for Veterinary Science, Faculty of Veterinary Science, Chulalongkorn University, Chulalongkorn University Centenary Academic Development Project, the Thailand Research Fund MRG5380153, TRF-DBG5280015, TRF Senior Research Scholars RTA-5080010 and the national Research University Project of CHE and The Rajadaphiseksomphot Endowment Fund (HR1166I).

References

Alaminos, M., Pérez-Köhler, B., Garzón, I., García-Honduvilla, N., Romero, B., Campos, A. and Buján, J. 2010. Transdifferentiation potentiality of human Wharton's jelly stem cells towards vascular endothelial cells. J Cell Physiol. 223: 640-647.

Arnhold, S., Lenartz, D., Kruttwig, K., Klinz, F.J., Kolossov, E., Hescheler, J., Sturm, V., Andressen, C. and Addicks, K. 2000. Differentiation of green fluorescent protein-labeled embryonic stem cell-derived neural precursor cells into Thy-1-positive neurons and glia after transplantation into adult rat striatum. J Neurosurg 93: 1026-1032.

Barry, F.P. and Murphy, J.M. 2004. Mesenchymal stem cells: clinical applications and biological characterization. Int J Biochem Cell Biol. 36: 568-584.

Bongso, A., Fong, C.Y. and Gauthaman, K. 2008. Taking stem cells to the clinic: Major challenges. J Cell Biochem. 105: 1352-1360.

382

383 Bosch, P., Pratt, S.L. and Stice, S.L. 2006. Isolation, characterization, gene
384 modification, and nuclear reprogramming of porcine mesenchymal stem cells. Biol
385 Reprod.74: 46-57.

386

387 Bosnakovski, D., Mizuno, M., Kim, G., Takagi, S., Okumura, M. and Fujinaga, T.
388 2005. Isolation and multilineage differentiation of bovine bone marrow mesenchymal
389 stem cells. Cell Tissue Res. 319: 243-253.

390

391 Csaki, C., Matis, U., Mobasheri, A., Ye, H. and Shakibaei, M. 2007. Chondrogenesis,
392 osteogenesis and adipogenesis of canine mesenchymal stem cells: a biochemical,
393 morphological and ultrastructural study. Histochem Cell Biol. 128: 507-520.

394

395 Dominici, M., Le Blanc, K., Mueller, I., Slaper-Cortenbach, I., Marini, F.C., Krause,
396 D.S., Deans, R.J., Keating, A., Prockop, D.J. and Horwitz, E.M. 2006. Minimal
397 criteria for defining multipotent mesenchymal stromal cells. The International Society
398 for Cellular Therapy position statement. Cytotherapy 8: 315-317.

399

400 Erdo, F., Buhrle, C., Blunk, J., Hoehn, M., Xia, Y., Fleischmann, B., Föcking, M.,
401 Küstermann, E., Kolossov, E., Hescheler, J., Hossmann, K.A. and Trapp, T. 2003.
402 Host-dependent tumorigenesis of embryonic stem cell transplantation in experimental
403 stroke. J Cereb Blood Flow Metab 23: 780-785.

404

405 Evans, M.J. and Kaufman, M.H. 1981. Establishment in culture of pluripotential cells
406 from mouse embryos. Nature 292: 154-156.

Hiyama, A., Mochida, J., Iwashina, T., Omi, H., Watanabe, T., Serigano, K., Tamura, F. and Sakai, D. 2008. Transplantation of mesenchymal stem cells in a canine disc degeneration model. J Orthop Res. 26: 589-600.

Jafarian, M., Eslaminejad, M.B., Khojasteh, A., Mashhadi Abbas, F., Dehghan, M.M., Hassanizadeh, R. and Houshmand, B. 2008. Marrow-derived mesenchymal stem cells-directed bone regeneration in the dog mandible: a comparison between biphasic calcium phosphate and natural bone mineral. Oral Surg Oral Med Oral Pathol Oral Radiol Endod. 105: 14-24.

Jang, B.J., Byeon, Y.E., Lim, J.H., Ryu, H.H., Kim, W.H., Koyama, Y., Kikuchi, M., Kang, K.S. and Kweon, O.K. 2008. Implantation of canine umbilical cord blood-derived mesenchymal stem cells mixed with beta-tricalcium phosphate enhances osteogenesis in bone defect model dogs. J Vet Sci. 9: 387-393.

Jing, D., Parikh, A., Canty, J.M. Jr and Tzanakakis, E.S. 2008. Stem cells for heart cell therapies.Tissue Eng Part B Rev. 14: 393-406.

Jo, Y.Y., Lee, H.J., Kook, S.Y., Choung, H.W., Park, J.Y., Chung, J.H., Choung, Y.H., Kim, E.S., Yang, H.C. and Choung, P.H. 2007. Isolation and characterization of postnatal stem cells from human dental tissues. Tissue Eng. 13(4): 767-773.

Jung, D.I., Ha, J., Kang, B.T., Kim, J.W., Quan, F.S., Lee, J.H., Woo, E.J., Park, H.M. 2009.A comparison of autologous and allogenic bone marrow-derived mesenchymal stem cell transplantation in canine spinal cord injury. J Neurol Sci. 285: 67-77.

Kamishina, H., Deng, J., Oji, T., Cheeseman, J.A. and Clemmons, R.M. 2006. Expression of neural markers on bone marrow-derived canine mesenchymal stem cells. Am J Vet Res. 67: 1921-1928.

Kavalkovich, K.W., Boynton, R.E., Murphy, J.M. and Barry, F. 2002. Chondrogenic differentiation of human mesenchymal stem cells within an alginate layer culture system. In Vitro Cell Dev Biol Anim. 38: 457-466.

Kern, S., Eichler, H., Stoeve, J., Klüter, H. and Bieback, K. 2006. Comparative analysis of mesenchymal stem cells from bone marrow, umbilical cord blood, or adipose tissue.Stem Cells. 24: 1294-1301.

Kim, N.R., Kang, S.K., Ahn, H.H., Kwon, S.W., Park, W.S., Kim, K.S., Kim, S.S., Jung, H.J., Choi, S.U. and Ahn, J.H, Kim, K.R. 2009. Discovery of a new and efficient small molecule for neuronal differentiation from mesenchymal stem cell. J Med Chem. 52: 7931-7933.

Koch, T.G., Heerkens, T., Thomsen, P.D. and Betts, D.H. 2007. Isolation of mesenchymal stem cells from equine umbilical cord blood. BMC Biotechnol. 7: 26.

455 Krabbe, C., Zimmer, J. and Meyer, M. 2005. Neural transdifferentiation of
456 mesenchymal stem cells--a critical review. APMIS. 113: 831-844.
457
458 Kraus, K.H., and Kirker-Headm C. 2006. Mesenchymal stem cells and bone
459 regeneration. Vet Surg. 35:232-242.
460 Lee, O.K., Kuo, T.K., Chen, W.M., Lee, K.D., Hsieh, S.L. and Chen, T.H. 2004.
461 Isolation of multipotent mesenchymal stem cells from umbilical cord blood. Blood.
462 103: 1669-1675.
463
464 Li, H., Dai, K., Tang, T., Zhang, X., Yan, M. and Lou, J. 2007. Bone regeneration by
465 implantation of adipose-derived stromal cells expressing BMP-2. Biochem Biophys
466 Res Commun. 356: 836-342.
467
468 Lu, P., Blesch, A. and Tuszynski, M.H. 2004. Induction of bone marrow stromal cells
469 to neurons: differentiation, transdifferentiation, or artifact? J Neurosci Res. 77: 174-
470 191.
471
472 Martin, D.R., Cox, N.R., Hathcock, T.L., Niemeyer, G.P. and Baker, H.J. 2002.
473 Isolation and characterization of multipotential mesenchymal stem cells from feline
474 bone marrow. Exp Hematol. 30: 879-886.
475
476 Martin, G.R. 1981. Isolation of a pluripotent cell line from early mouse embryos
477 cultured in medium conditioned by teratocarcinoma stem cells. Proc. Natl. Acad. Sci.
478 USA. 78: 7634-7638.
479

Mayorga, M., Finan, A. and Penn, M. 2009. Pre-transplantation specification of stem cells to cardiac lineage for regeneration of cardiac tissue. Stem Cell Rev. 5: 51-60.

Meirelles, Lda S. and Nardi, N.B. 2009. Methodology, biology and clinical applications of mesenchymal stem cells. Front Biosci. 14: 4281-4298.

Neuhuber, B., Gallo, G., Howard, L., Kostura, L., Mackay, A. and Fischer, I. 2004 Reevaluation of in vitro differentiation protocols for bone marrow stromal cells: disruption of actin cytoskeleton induces rapid morphological changes and mimics neuronal phenotype. Neurosci Res. 77: 192-204.

Neupane, M., Chang, C.C., Kiupel, M. and Yuzbasiyan-Gurkan, V. 2008. Isolation and characterization of canine adipose-derived mesenchymal stem cells. Tissue Eng Part A. 14:1007-1015.

Pittenger, M.F., Mackay, A.M., Beck, S.C., Jaiswal, R.K., Douglas, R., Mosca, J.D., Moorman, M.A., Simonetti, D.W., Craig, S. and Marshak, D.R. 1999. Multilineage potential of adult human mesenchymal stem cells. Science. 284: 143-147.

Reubinoff, B.E., Pera, M.F., Fong, C.Y., Trounson, A. and Bongso, A. 2000. Embryonic stem cell lines from human blastocysts: somatic differentiation in vitro. Nat Biotechnol 18: 399–404.

Rho, G.J., Kumar, B.M. and Balasubramanian, S.S. 2009. Porcine mesenchymal stem cells--current technological status and future perspective. Front Biosci.14: 3942-3961.

505

506 Ribitsch, I., Burk, J., Delling, U., Geißler, C., Gittel, C., Jülke, H. and Brehm, W.
507 2010. Basic Science and Clinical Application of Stem Cells in Veterinary Medicine.
508 Adv Biochem Eng Biotechnol. 123: 219-263.

509 Seo, M.S., Jeong, Y.H., Park, J.R., Park, S.B., Rho, K.H., Kim, H.S., Yu, K.R, Lee,
510 S,H., Jung, J.W., Lee, Y.S. and Kang, K.S. 2009. Isolation and characterization of
511 canine umbilical cord blood-derived mesenchymal stem cells. J Vet Sci. 10: 181-187.

512

513 Takahashi, K., and Yamanaka, S. 2006. Induction of pluripotent stem cells from
514 mouse embryonic and adult fibroblast cultures by defined factors. Cell 126, 663-676.

515

516 Trzaska, K.A., Kuzhikandathil, E.V. and Rameshwar, P. 2007. Specification of a
517 dopaminergic phenotype from adult human mesenchymal stem cells. Stem Cells. 25:
518 2797-2808.

519

520 Vieira, N.M., Brandalise, V., Zucconi, E., Secco, M., Strauss, B.E. and Zatz, M. 2010
521 Isolation, characterization, and differentiation potential of canine adipose-derived
522 stem cells.Cell Transplant. 19: 279-289.

523

524 Volk, S.W., Diefenderfer, D.L., Christopher, S.A., Haskins, M.E. and Leboy, P.S.
525 2005. Effects of osteogenic inducers on cultures of canine mesenchymal stem cells.
526 Am J Vet Res. 66: 1729-1737.

527

528 Waddington, R.J., Youde, S.J., Lee, C.P. and Sloan, A.J. 2009. Isolation of distinct
529 progenitor stem cell populations from dental pulp. Cells Tissues Organs. 189: 268-
530 274.
531
532 Wagner, W., Wein, F., Seckinger, A., Frankhauser, M., Wirkner, U., Krause, U.,
533 Blake, J., Schwager, C., Eckstein, V., Ansorge, W., Ho, A.D. 2005. Comparative
534 characteristics of mesenchymal stem cells from human bone marrow, adipose tissue,
535 and umbilical cord blood. Exp Hematol. 33: 1402-1416.
536
537 Wobus, A.M. and Boheler, K.R. 1999. Embryonic Stem Cells as Developmental
538 Model in vitro. Cells Tissues Organs. 165: 129-130.
539
540 Yamaguchi, S., Kuroda, S., Kobayashi, H., Shichinohe, H., Yano, S., Hida, K.,
541 Shinpo, K., Kikuchi, S. and Iwasaki, Y. 2006. The effects of neuronal induction on
542 gene expressionprofile in bone marrow stromal cells (BMSC)--a preliminary study
543 using microarray analysis. Brain Res. 1087: 15-27.
544
545 Zipori, D. 2004. Mesenchymal stem cells: harnessing cell plasticity to tissue and
546 organ repair. Blood Cells Mol Dis. 33:211-215.
547
548 Zucconi, E., Vieira, N.M., Bueno, D.F., Secco, M., Jazedje, T., Ambrosio, C.E.,
549 Passos-Bueno, M.R., Miglino, M.A. and Zatz, M. 2010. Mesenchymal stem cells
550 derived from canine umbilical cord vein--a novel source for cell therapy studies. Stem
551 Cells Dev. 19: 395-402.
552

553 Zuk, P.A., Zhu, M., Ashjian, P., De Ugarte, D.A., Huang, J.I., Mizuno, H., Alfonso,
554 Z.C., Fraser, J.K., Benhaim, P. and Hedrick, M.H. 2002. Human adipose tissue is a
555 source of multipotent stem cells. Mol Biol Cell. 13: 4279-4295.

556

557

558

559 **Table 1** Oligonucleotide primers used in this study

Gene	Sequences	Size (bp)	Accession number	Reference
COL1A1	(F) 5'-CAC CTC AGGAGA AGG CTC AC–3'	123	NM_001003090.1	Min-Soo et al. (2009)
	(R) 5'-ATG TTC TCG ATC TGC TGG CT–3'			
GLA	(F) 5'-GTG GTG CAA CCT TCG TGT C-3'	131	XM_547536.2	Min-Soo et al. (2009)
	(R) 5'-GCT CGC ATA CTT CCC TCT TG-3'			
GAPDH	(F) 5'-GGA GAA AGC TGC CAA ATA TG-3'	191	AB038241	Sano et al. 2005
	(R) 5'-CAG GAA ATG AGC TTG ACA AAG TGG-3'			

560

561

562

563

564

565

566

567

568

569

570

571

572

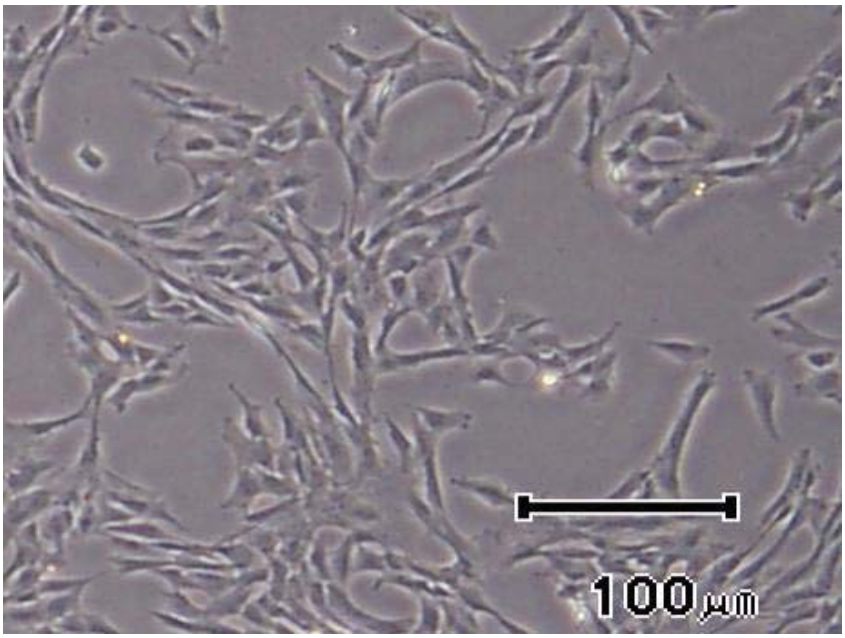
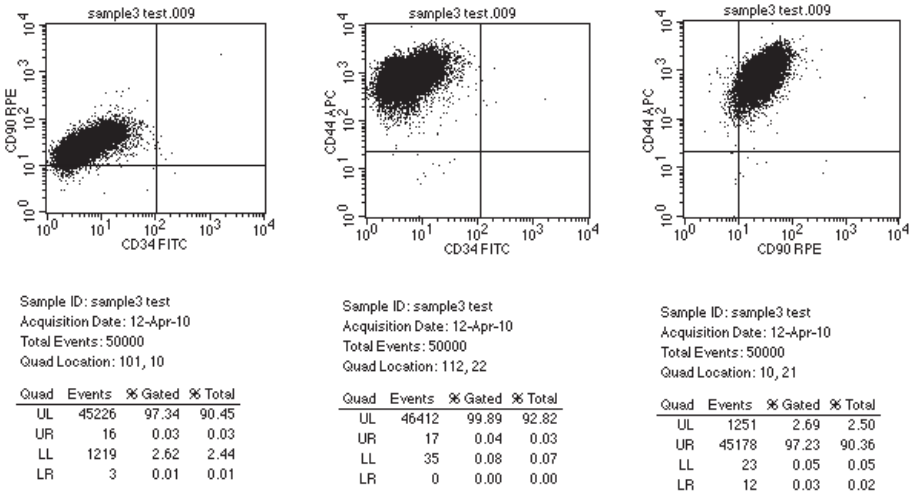


Figure 1 Fibroblastic-like mesenchymal stem cells derived from bone marrow aspirate



Sample ID: sample3 test
Acquisition Date: 12-Apr-10
Total Events: 50000
Quad Location: 101, 10

Quad	Events	% Gated	% Total
UL	45226	97.34	90.45
UR	16	0.03	0.03
LL	1219	2.62	2.44
LR	3	0.01	0.01

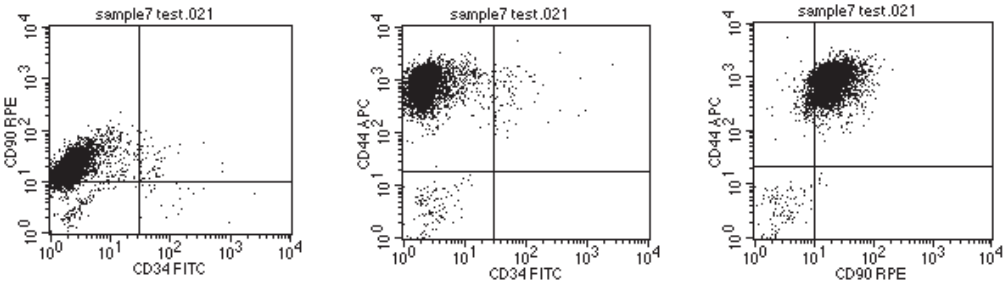
Sample ID: sample3 test
Acquisition Date: 12-Apr-10
Total Events: 50000
Quad Location: 112, 22

Quad	Events	% Gated	% Total
UL	46412	99.89	92.82
UR	17	0.04	0.03
LL	35	0.08	0.07
LR	0	0.00	0.00

Sample ID: sample3 test
Acquisition Date: 12-Apr-10
Total Events: 50000
Quad Location: 10, 21

Quad	Events	% Gated	% Total
UL	1251	2.69	2.50
UR	45178	97.23	90.36
LL	23	0.05	0.05
LR	12	0.03	0.02

607



Sample ID: sample7 test
Acquisition Date: 19-Mar-10
Total Events: 20000
Quad Location: 30, 10

Quad	Events	% Gated	% Total
UL	12763	86.73	63.81
UR	230	1.56	1.15
LL	1641	11.15	8.21
LR	82	0.56	0.41

Sample ID: sample7 test
Acquisition Date: 19-Mar-10
Total Events: 20000
Quad Location: 30, 17

Quad	Events	% Gated	% Total
UL	14019	95.26	70.09
UR	303	2.06	1.52
LL	388	2.64	1.94
LR	6	0.04	0.03

Sample ID: sample7 test
Acquisition Date: 19-Mar-10
Total Events: 20000
Quad Location: 10, 22

Quad	Events	% Gated	% Total
UL	1610	10.94	8.05
UR	12711	86.38	63.55
LL	366	2.49	1.83
LR	29	0.20	0.14

608

609 **Figure 2** Expressions of CD 34, CD 44 and CD 90 in canine MSCs. Samples from

610 dog 3 (upper panel) and dog 4 (lower panel) were analyzed by flow cytometry.

611

612

613

614

615

616

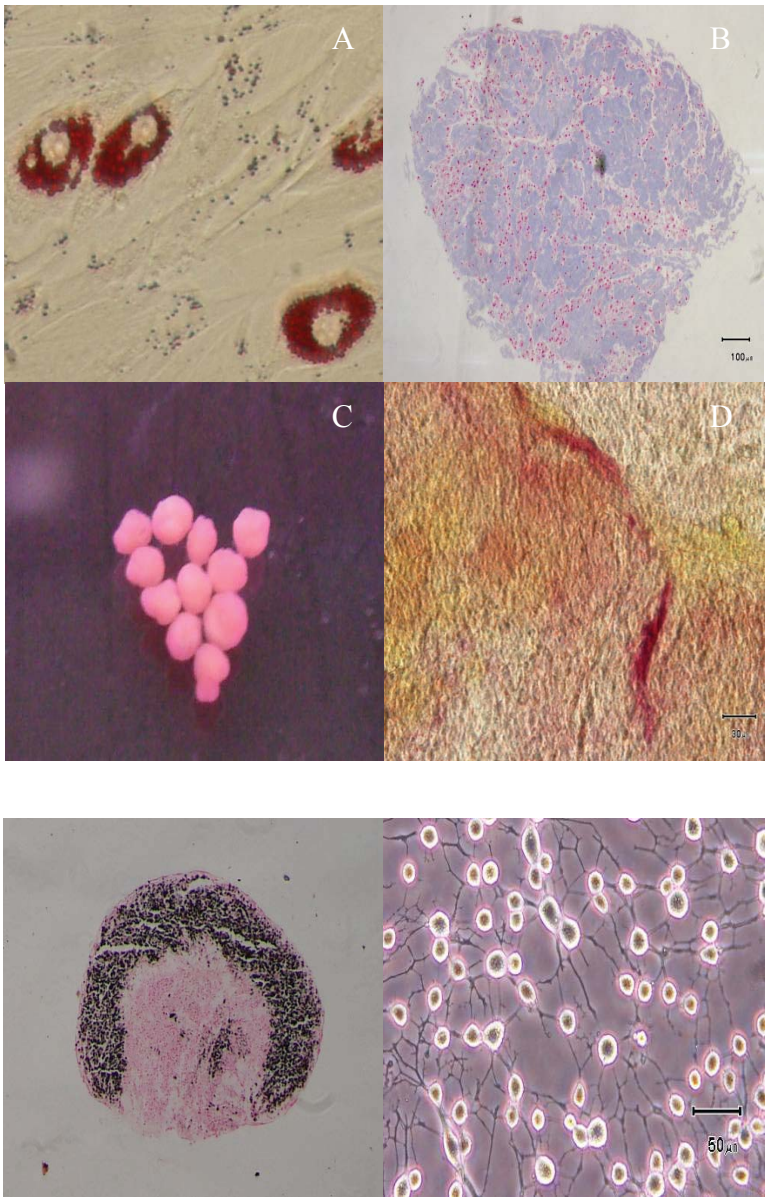


Figure 3 differentiation potential of canine mesenchymal stem cell (A) adipose tissue; cartilage (B) bone (C and E) and neuron-like cells (F). Adipocytic cells accumulated with neutral lipids as shown by oil red O staining. Cartilagenous and bone tissues were confirmed by the presence of glucosaminoglycan enriched matrix, calcium phosphate and alkaline phosphatase activity (D) using Alcial blue, Von kossa and leukocyte alkaline phosphatase kit, respectively.

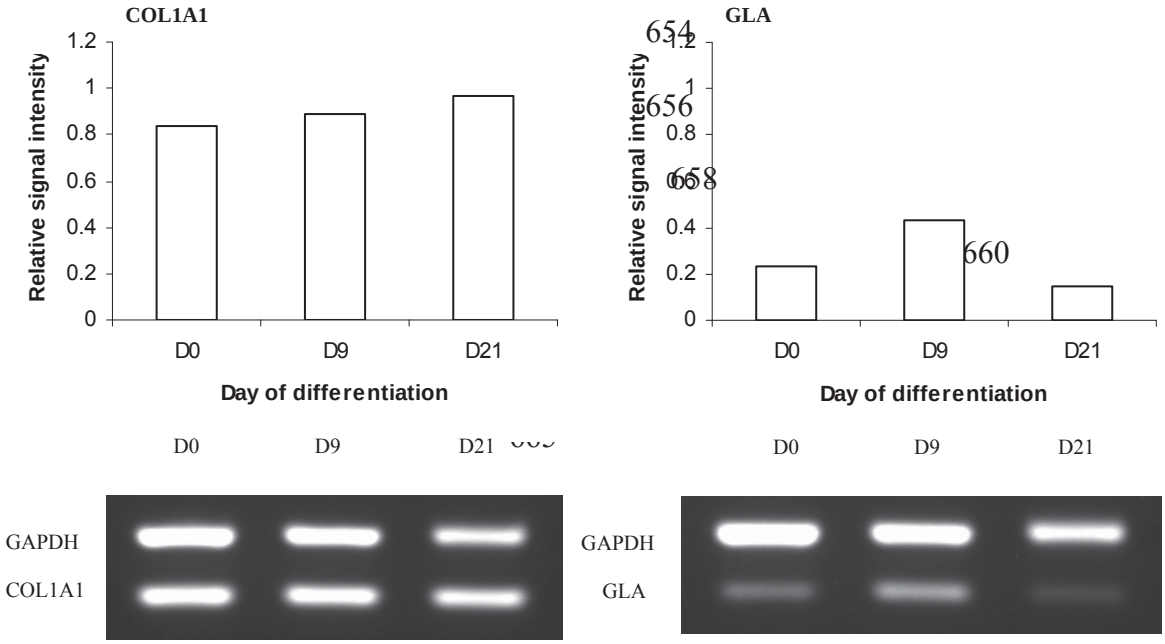


Figure 4 Relative signal intensity of COL1A1 and GLA expression compared with GAPDH expression on D0, D9 and D21 of dog MSCs bone differentiation *in vitro*.

Synthesis of Protein-incorporated Hydroxyapatite Particles for Biomedical Applications

Prae-ravee K-hasuwan[1], Neeranut Kuanchertchoo[2], Pitt Supaphol[1]

[1]*The Petroleum and Petrochemical college,Chulalongkorn University,Bangkok,10330,Thailand*
[2]*Department of Material Technology,Ramkhamhaeng University,Bangkok,10240,Thailand*

Protein-incorporated hydroxyapatite particles were successfully synthesized by a co-precipitation method using ovalbumin as a model protein. Different amounts of ovalbumin (1 g and 3 g/1000 ml distilled water) were used to examine the incorporation capacity within hydroxyapatite particles. The hydroxyapatite particulate samples were characterized by means of X-ray diffraction, transmission electron microscopy, scanning electron microscopy, Fourier transform infrared spectroscopy, thermogravimetric analysis, Barrett-Joyner-Halenda gas sorption, and particle size distribution analysis. It was found that all of the particulate samples had a typical hydroxyapatite crystalline phase and a rod-like shape (5-8 nm in length and 20-30 nm in diameter) with a narrow particle size distribution, suggesting the agglomeration of small crystallites. Although the particle morphologies were similar, the incorporation capacities and the average pore sizes were different, depending on the incorporated amounts of ovalbumin. The incorporated ovalbumin content and the average pore diameter increased with an increase in the initial amount of added ovalbumin. Therefore, these materials may be useful for controlled release of proteins in biomedical applications.

THE EFFECT OF MESENCHYMAL STEM CELLS COMBINED WITH POLYCAPROLACTONE/HYDROXYAPATITE COMPOSITE SCAFFOLD ON THE HEALING OF ULNAR DEFECT IN DOGS

Sasijaras Tantrajak*[1], Chanin Kalpravidh[1], Theerawat Tharasanit[1], Mongkol Techakumphu[1], Kumpanart Soontornvipart[1], Chalika Wangdee[1], Prasit Pavasant[2] and Pitt Supaphol[3]
[1]Faculty of Veterinary Science, [2]Faculty of Dentistry, [3]Faculty of Sciences. Chulalongkorn University, Bangkok 10330, Thailand

Introduction

Extensive bone defect is one of the major problem in veterinary orthopedics. Natural bone healing alone is not sufficient to repair such defect which may result in bone nonunion. Therefore, bone tissue engineering has been introduced as an alternative approach for treating large segmental defect[1]. Tissue implantation strategy using mesenchymal stem cells (MSCs) combined with a scaffold is commonly used to enhance bone repair[2]. The aims of this study were to examine the interaction between canine MSCs and polycaprolactone/hydroxyapatite (PCL/HA) scaffold (*in vitro* study) and to examine the effect of MSCs combined with PCL/HA on the healing of ulnar defects in dogs (*in vivo* study)



Fig. 1: Bone marrow aspiration from dorsal iliac crest

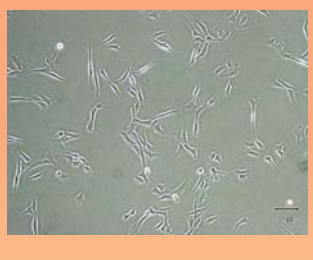


Fig. 2: Canine MSCs Day 9, passage 1

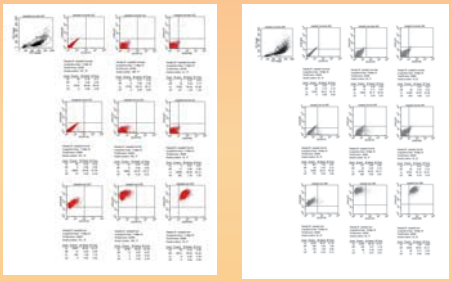


Fig. 3: Examples of flow cytometric analysis of isolated canine MSCs in the 3rd and 5th passages (CD 34, 44, 90)

Materials and methods

All study protocols were approved by the Committee for the Ethical Care of Animals of the Chulalongkorn University.

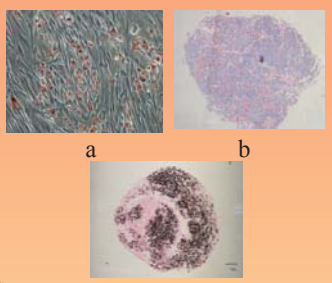
Putative canine MSCs were harvested via bone marrow aspiration. They were then cultured in vitro and characterized by morphology, expression of MSC markers (CD 44 and 90) and in vitro differentiation before seeding into PCL/HA.

Results and discussions

The isolated cells from bone marrow exhibited fibroblast-like morphology, ability to adherence to plastic surface, expression of specific surface antigen and ability to differentiation. The bone remodeling/healing after MSC transplantation is being studied.



Fig. 4: fluorescent staining of MSCs 12 hours after seeding (green=viable cells; red=dead cells)



a b c

Fig. 5: multilineage Differentiation (a: adipose tissue; b:cartilage and c: bone

Acknowledgements

This project was supported by the Thailand Research Fund (DBG5280015) and the 90th anniversary of Chulalongkorn University fund. The scaffolds used in the study were generously provided from the Faculty of dentistry.

References

1. Meyer, U. and Wiesmann, H. P. 2006. Bone and Cartilage Engineering. Germany: Springer.
2. Salgado, A. et. al. 2004. In: Learning from nature how to design new implantable biomaterial. 205-222.

Development of Bone Scaffolds for Applications in Dentistry and Animal Care

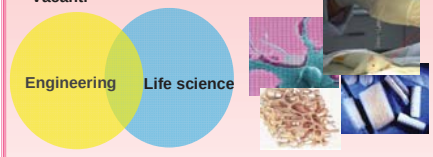
Pitt Supaphol,[a] Prasit Pavasant,[b] Mongkol Techakumphu,[c] Kumpanart Soontornvipart,[d] Keskanya Subbalekha,[e] and Theerawat Tharasanit [c]

[a]*The Petroleum and Petrochemical College, Chulalongkorn University, Soi Chula 12, Phyathai Road, Pathumwan, Bangkok 10330, Thailand.*
[b]*Department of Anatomy, Faculty of Dentistry, Chulalongkorn University, 34 Henry Dunant Road, Pathumwan, Bangkok 10330, Thailand.*
[c]*Department of Obstetrics, Gynaecology and Reproduction, Faculty of Veterinary Science, Chulalongkorn University, Henry Dunant Road, Pathumwan, Bangkok 10330, Thailand.*
[d]*Department of Surgery, Faculty of Veterinary Science, Chulalongkorn University, Henry Dunant Road, Pathumwan, Bangkok 10330, Thailand.*
[e]*Department of Oral and Maxillofacial Surgery, Faculty of Dentistry, Chulalongkorn University, 34 Henry Dunant Road, Pathumwan, Bangkok 10330,Thailand.*
(E-mail address: pitt.s@chula.ac.th)

Introduction

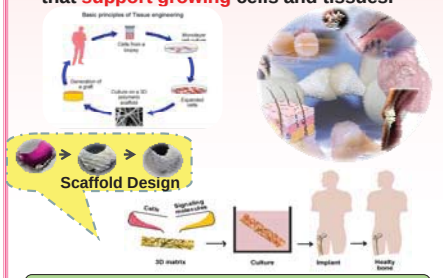
Tissue Engineering

- **"An interdisciplinary field that applies the principles of engineering and life science toward the development of biological substitutes that restore, maintain, or improve tissue function." Langer and Vacanti**



Scaffold

Scaffolds are three dimensional structures that support growing cells and tissues.



Adult stem cells: Mesenchymal stem cells

- **Bone marrow**, cytoskeleton muscle, adipose tissue, dental pulp, umbilical cord etc.,



- **Why mesenchymal stem cells (MSCs)?**
  - MSCs can be isolated from many tissues: bone marrow, cytoskeleton muscle, adipose tissue, dental pulp, umbilical cord etc.
  - Cells are rare (0.001-0.01% of total population of nucleated cells in BM)
  - Differential capability: specific lineage and plasticity
  - High potential of clinical use:
    - ❑Low tissue reaction, homing, non-tumorogenesis



Objectives

- To investigate the potential of Polycaprolactone(PCL) and Polycaprolactone(PCL) /Hydroxyapatite(HAp) scaffolds to be used as bone scaffolds
- To compare the isolation techniques and differentiation potentials of canine mesenchymal stem cells derived from bone marrow and adipose tissue
- To examine the effect of canine mesenchymal stem cells combined with polycaprolcatone/hydroxyapatite composite scaffold on the healing of ulnar defects in dogs (*in vivo* study)

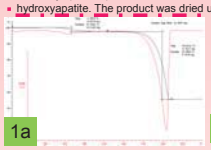
Experiment

- •Comparative Study of Mesoporous Protein-encapsulated Hydroxyapatite for Biomedical Applications
- •Development of Hydroxyapatite as Carriers in Polycarpolactone Scaffolds for Bone Tissue Engineering
- •Preparation of Crude Bone Protein into Silica Microsphere/Polycaprolactone (PCL) Scaffold for Bone Cell Developments
- •Surface-Modified Electrospun Polycaprolactone Fibrous Membranes Modified with Gelatin, Bovine Serum Albumin or Crude Bone Protein Extract and Their Potential for Use as Bone Scaffolds
- •Isolation, identification and culture of canine mesenchymal stem cells derived from bone marrow and adipose tissue
- •The effect of mesenchymal stem cells combined with polycaprolactone/hydroxyapatite composite scaffold on the healing of ulnar defect in dogs
- •Electrospun asiaticoside/HPβCD complex-loaded cellulose acetate fiber mats and Their Potential for Use as Bone Scaffolds

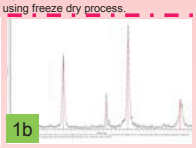
Results and Discussion

Comparative Study of Mesoporous Protein-encapsulated Hydroxyapatite for Biomedical Applications

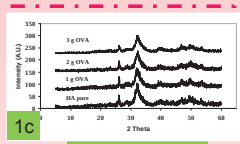
• Hydroxyapatite was prepared from CaO which obtained from calcination of egg shell. CaO was dissolved in 1 M HNO_3 to prepared clear solution. Phosphoric acid was added to make Ca/P ratio stoichiometry (1.67). Water was boiled before adding to the reaction in order to prevent CO_2 dissolved. Tris (hydroxymethyl) aminomethane was applied to control pH near neutrality (7.2-9.4). The reaction was performed under air condition. Ovalbumin was added for co-precipitating with hydroxyapatite. The product was dried using freeze dry process.



Thermogram of egg shell with heating rate 10ºC/min up to 1000 ºC



XRD pattern of egg shell calcined at 1000 ºC

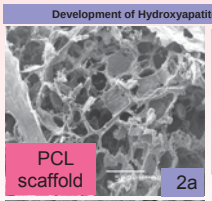


XRD pattern of HA-OVA prepared at pH 7

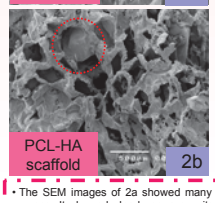
•Egg shell was starting material to prepared CaO. Thermogravimetric analysis was used to estimate calcinations temperature as show in Fig. 1a). The phase of product after calcination was examined using XRD. Results from TGA show that the temperature for calcinations was 820 °C but the reaction is reversible. So, temperature must be increased to 1000 °C to convert to CaO completely. XRD pattern of CaO product was shown in Fig 1b).

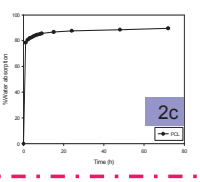
•Hydroxyapatite synthesized with pH 7 was characterized using XRD. The XRD pattern show characteristic peaks of hydroxyapatite without other impurities (Fig. 1c).

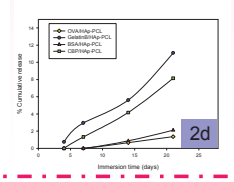
Development of Hydroxyapatite as Carriers in Polycarpolactone Scaffolds for Bone Tissue Engineering



Scaffolds	Density (g/cm^3)	Porosity (%)	Pore volume (cm^3/g)	Pore size (μm)
PCL	0.1139	90.05	7.91	347.07 ± 42.19





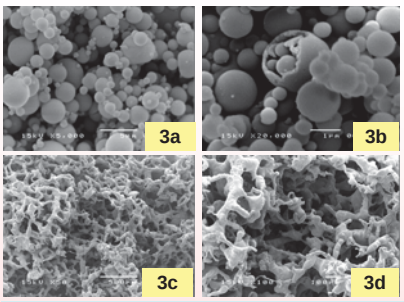


• The SEM images of 2a showed many square units occurring from the shape of NaCl porogens used in the fabricating process. It showed clearly square units due to neat PCL scaffold whereas 2b exhibited the lost square because HAps embedded in the PCL scaffold.

•Figure 2c illustrates the water absorption capabilities of the PCL scaffolds in 0.1 M PBS at room temperature within 3 days (72 h). The water absorption rate was rapidly increased in the early 24 hours and maintained stable.

•The release of proteins from HAp-PCL scaffolds were investigated by immersing HAp-PCL scaffolds into *in vitro* culturing environment, 10% MEM (containing MEM, 10% FBS, 1% L-glutamine, 1% antibiotic). All samples were incubated in a shaking water bath (70 rpm) at 37 ºC for 21 days. The result shows gelatin and CBP started to before day 7 whereas OVA and BSA release after day 7. The amount of released proteins gradually increased time dependently. This result correspond to the work done by proteins releasing from HAp particles, however, protein release from scaffold spends a longer time due to different media. It is different in ionic strength, in MEM shows higher ionic strength. High ionic strength should promote aggregation of protein and retard release.

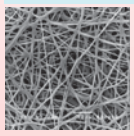
Preparation of Crude Bone Protein into Silica Microsphere/Polycaprolactone (PCL) Scaffold for Bone Cell Developments

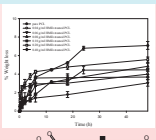


•**Figure 3a and 3b** demonstrated the SEM images of synthesized silica microspheres with sol-gel technique at different magnifications. These images showed the spherical particle with smooth surface and particle size around 0.3 to 4 microns.

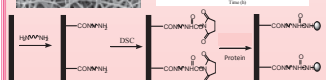
•**Figure 3c and 3d** demonstrated the SEM images microstructure of the as-prepared scaffolds. The SEM images showed the homogeneous porous feature of scaffold and the pore size is around 50 to 400 microns.

Surface-Modified Electrospun Polycaprolactone Fibrous Membranes Modified with Gelatin, Bovine Serum Albumin or Crude Bone Protein Extract and Their Potential for Use as Bone Scaffolds





Material	density ($x10^{-3}g/cm^3$)	porosity (%)	pore volume (cm^3/g)	Contact angle (θ)
PCL pure	4.69 ± 0.44	95.91 ± 0.38	20.62 ± 2.07	123.7 ± 0.1
aminolyzed PCL	4.25 ± 0.97	96.29 ± 0.85	23.63 ± 5.28	115.3 ± 0.2
activated PCL	4.14 ± 0.57	96.39 ± 0.50	23.64 ± 3.07	118.7 ± 0.3
gelatin A immobilized PCL	3.75 ± 0.59	96.72 ± 0.51	26.33 ± 4.52	95.5 ± 1.1
gelatin B immobilized PCL	3.59 ± 0.88	96.86 ± 0.77	28.15 ± 6.17	94.4 ± 2.1
BSA immobilized PCL	3.85 ± 0.74	96.64 ± 0.65	25.88 ± 4.97	97.5 ± 2.0
CBP immobilized PCL	4.58 ± 0.93	96.00 ± 0.81	21.64 ± 4.35	48.5 ± 1.8



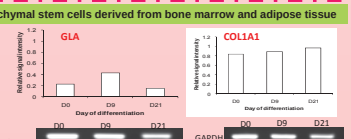
•Amino groups can be covalently introduced onto the surface of the electrospun PCL fibrous scaffolds by reaction with 1,6-hexamethylenediamine (HMD), One amino group (NH_2) of HMD reacts with an ester group (—COO—) of PCL to form the amide linkage (—CONH—), while another amino group which is unreacted and free can be used as active sites through which biomolecules (i.e;proteins) can be bonded to the surface using *N, N'*-disuccinimidyl carbonate (DSC) as a coupling agent.

•CBP immobilized PCL scaffold has largest decrease of contact angle as compared with the neat PCL scaffold (control). This means that immobilization of gelatin crude bone protein can most improve the hydrophilicity of the surface.

Isolation, identification and culture of canine mesenchymal stem cells derived from bone marrow and adipose tissue



Canine bone marrow and adipose tissue mesenchymal stem cells are spindle and fibroblastic-like cells.



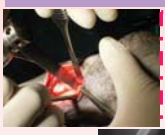
Results and Discussion

Isolation, identification and culture of canine mesenchymal stem cells derived from bone marrow and adipose tissue

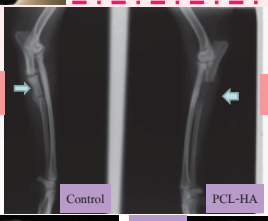


•The experiments showed that MSC derived from bone marrow and adipose tissue can be isolated and cultured and expresses cell-surface antigen markers of MSCs. These abilities provide the opportunity to compare the differential potentiality to multiple cell lineages.

The effect of mesenchymal stem cells combined with polycaprolactone/hydroxyapatite composite scaffold on the healing of ulnar defect in dogs



•The dogs were randomly divided into 2 groups:
Group 1: received PCL/HA without MSC
Group 2: received PCL/HA with MSC
•The contralateral ulna was implant with corticocancellous bone graft to serve as the control.





•MSCs can be isolated from bone marrow and adipose tissue of dogs.
•These MSCs have a unique characteristic of MS C (self-renewal and differentiation).
•In vitro/in vivo study (fate of MSCs) is required before clinical application.

Electrospun asiaticoside/HPβCD complex-loaded cellulose acetate fiber mats and Their Potential for Use as Bone Scaffolds

Type of materials	Electrospun fiber mats
Containing 10 wt.% AC (Asiaticoside)	
Containing 10%w/w AC/HPβCD at the mixing ratio of 1:0.5	
Containing 10%w/w AC/HPβCD at the mixing ratio of 1:1	
Containing 10%w/w AC/HPβCD at the mixing ratio of 1:2	

Conclusion

•**Polymer-ceramic (Hydroxyapatite or Silica) composites** may be extremely prospective bone substitute material mainly through evidence with its given biocompatibility towards bone and demonstrated continuity between living bone and the composites. The composites are implanted into rectangular bone defect created by operation at the load-bearing area in dog.

•**The expected results** are that the polymer-ceramic composite living bone complex should have been proven to have sufficient flexibility. The strain pattern on the surface of composite implant should develop quite similar to that of natural cortical bone. These characteristics suggest that it achieves normal skeletal function in the points of biomechanical properties in vivo.

Acknowledgments

•Thailand Research Fund (TRF) (through a Strategic Basic Research grant: DBG5280015)

•The National Center of Excellence for Petroleum, Petrochemicals, and Advanced Materials (NCE-PPAM)

References

•Chuenjitkuntaworn, B., Inrung, W., Mekaapiruk, K., Damrongsri, D., Supaphol, P. and Pavasant, P. 2009. Polycaprolactone/hydroxyapatite composite scaffolds: preparation, characterization and in vitro and in vivo biological responses of human primary bone cells. J. Biomed. Mat. Res. Part A. (accepted)
•Choong, C., Triffitt, J.T., and Cui, Z.F. (2004). Polycaprolactone scaffolds for bone tissue engineering: effects of a calcium phosphate coating layer on osteogenic cells. Food and bioproducts processing, 82(C2), 117-125